1996 ANNUAL TROPICAL CYCLONE REPORT

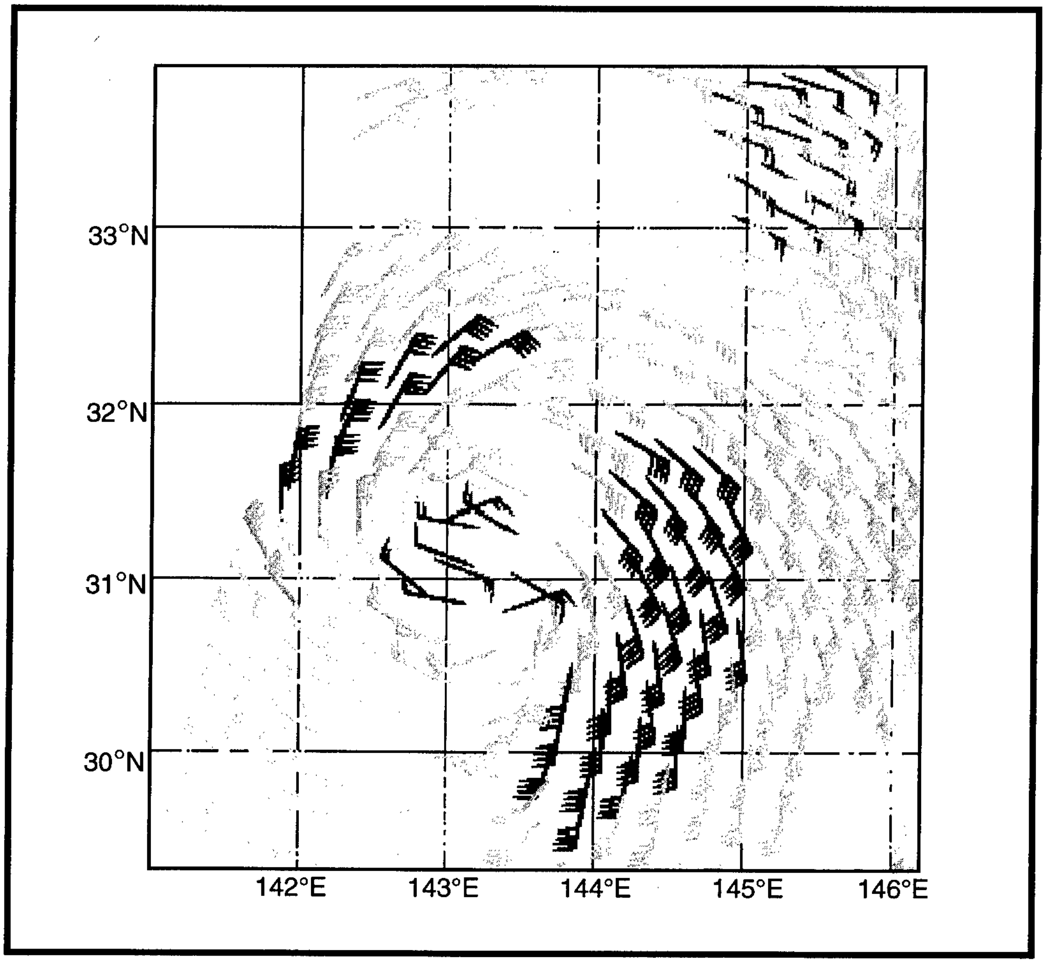

JOINT TYPHOON WARNING CENTER
GUAM, MARIANA ISLANDS

The 1996 Annual Tropical Cyclone Report is dedicated to:
Captain Christopher T. Nicklas, USAF
1967 to 1997

FRONT COVER: Vectors describe Typhoon Orson's (19W) surface wind field at approximately 01000Z September 1996. An automated algorithm, using the European Remote Sensing Satellite -1 (ERS-1) synthetic aperture radar (scatterometer) data, estimates these vectors which can be used to determine the radii of gale-force winds surrounding the typhoon. Although these data have proven invaluable, they are limited by the algorithm's inability to resolve scalar wind speeds above 50 knots and the wind direction 180 degree ambiguities.

U. S. NAVAL PACIFIC METEOROLOGY AND OCEANOGRAPHY CENTER WEST
JOINT TYPHOON WARNING CENTER
PSC 455, BOX 12
FPO AP 96540-0051

C. P. DILLON

CAPTAIN, UNITED STATES NAVY
COMMANDING OFFICER

MARK J. ANDREWS

LIEUTENANT COLONEL, UNITED STATES AIR FORCE
DIRECTOR, JOINT TYPHOON WARNING CENTER

Work on this report was supported in part by
the Office of Naval Research Grant N00014-96-1-0744

STAFF

JOINT TYPHOON WARNING CENTER

	LCDR	ERIC J. TREHUBENKO	USN	TDO, DEPUTY DIRECTOR
*	LCDR	MICHAEL D. ANGOVE	USN	TDO, DEPUTY DIRECTOR
	LCDR	KENNETH A. MALMQUIST	USN	TDO
**	LCDR	STACY R. STEWART	USNR	TDO
	LT	MICHAEL S. KALAFSKY	USN	TDO
*	LT	STEVEN P. DUARTE	USN	TDO
	CAPT	CARL A. McELROY	USAF	TDO
	CAPT	CHRISTOPHER T. NICKLAS	USAF	TDO
*	CAPT	PAUL H. LEWIS	USAF	TDO, STATISTICS OFFICER
	AG2	DARIN L. WARD	USN	LPO, GRAPHICS
	AG3	JOHN E. UROGI	USN	TDA
*	AG3	ROBERT M. GIGUERE	USN	TDA, STATISTICS
*	AG3	ANDRES G. GRANT	USN	TDA, GRAPHICS
	AGAN	JESSICA REZA	USN	TDA, STATISTICS
	AG3	CAROL A. GILL	USN	TDA
*	SRA	DAVID J. CORREA JR.	USAF	TDA
*	SRA	TIMOTHY C. WILLIAMS	USAF	TDA
*	SRA	CLARKE P. WILSON	USAF	TDA
	SRA	SAMUEL R. PUGH	USAF	TDA
*	SRA	JEFFREY L. WILKERSON	USAF	TDA
	SRA	DIONNE M. TIRSCHEL	USAF	TDA
	A1C	MARSHA D. BOGLE	USAF	TDA
	A1C	JASON R. DOBBINS	USAF	TDA

36 OSS/OSJ

	MAJ	ROGER T. EDSON	USAF	TECHNIQUE DEVELOPMENT
	CAPT	RICHARD A. ANSTETT	USAF	TDO, OIC USPACOM SAT NETWORK
*	CAPT	JOHN A. RUPP	USAF	TDO, OIC USPACOM SAT NETWORK
	MSGT	TIMOTHY R. CRUME	USAF	SAT FORECASTER, NCOIC
	TSGT	SHIRLEY A. BROWN	USAF	CHIEF INFORMATION MANAGEMENT
	TSGT	ZEFANIAS E. EBARLE	USAF	SAT FORECASTER
	TSGT	HARRY F. LIND	USAF	SAT FORECASTER
	TSGT	DENNIS W. MILLER	USAF	SAT FORECASTER
	SSGT	MERRYRUTH I. DEOCARIZA	USAF	SAT FORECASTER
	SSGT	LINDA R. HAM	USAF	SAT FORECASTER
	SSGT	TERRY L. MEST	USAF	SAT FORECASTER
	SSGT	BRUCE W. WOFFORD	USAF	SAT FORECASTER
	SRA	SEAN M. McDUNN	USAF	DATA DEVELOPMENT

ATCR STAFF

CAPT	GARY B. KUBAT	USAF	TDO, EDITOR, BEST TRACK OFFICER
CAPT	WILLIAM J. CARLE	USAF	TDO, STATISTICS OFFICER
MR	FRANK H. WELLS	USN	TECHNICAL EDITOR
AG1	PAUL G. SANCHEZ	USN	LPO, GRAPHICS
AG2	BRYAN Y. HONG	USN	TDA, GRAPHICS
AG3	CHRISTOPHER CROSS	USN	TDA, GRAPHICS
A1C	MATHEW A. BOYD	USAF	TDA, GRAPHICS

UNIVERSITY OF GUAM / JTWC RESEARCH LIAISON

DR	MARK A. LANDER	TROPICAL CYCLONE RESEARCH, TECHNICAL WRITING
MR	CHARLES P. GUARD	TROPICAL CYCLONE RESEARCH, TECHNICAL WRITING

* TRANSFERRED DURING 1996
** ACTIVE DUTY TRAINING

FOREWORD

The Annual Tropical Cyclone Report is prepared by the staff of the Joint Typhoon Warning Center (JTWC), a combined Air Force/Navy organization operating under the command of the Commanding Officer, U.S. Naval Pacific Meteorology and Oceanography Center West (NAVPACMETOCCEN WEST)/Joint Typhoon Warning Center, Guam. The JTWC was founded 1 May 1959 when the U.S. Commander-in-Chief Pacific (USCINCPAC) forces directed that a single tropical cyclone warning center be established for the western North Pacific region. The operations of JTWC are guided by USCINCPAC Instruction 3140.1W.

The mission of JTWC is multifaceted and includes:

1. Continuous monitoring of all tropical weather activity in the Northern and Southern Hemispheres, from 180° east longitude westward to the east coast of Africa, and the prompt issuance of appropriate advisories and alerts when tropical cyclone development is anticipated.

2. Issuance of warnings on all significant tropical cyclones in the above area of responsibility.

3. Determination of requirements for tropical cyclone reconnaissance and assignment of appropriate priorities.

4. Post-storm analysis of significant tropical cyclones occurring within the western North Pacific and North Indian Oceans.

5. Cooperation with the Naval Research Laboratory, Monterey, California on evaluation of tropical cyclone models and forecast aids, and the development of new techniques to support forecast requirements.

Special thanks to: the men and women of the Alternate Joint Typhoon Warning Center for standing in for JTWC as needed; Fleet Numerical Meteorology and Oceanography Center (FNMOC) for their operational support; the Naval Research Laboratory for its dedicated research; the Air Force Global Weather Central (AFGWC) and National Oceanic and Atmospheric Administration (NOAA) National Environmental Satellite, Data, and Information Service (NESDIS) for satellite support; the 36th Communications Squadron's Defense Meteorological Satellite Program (DMSP) Site 18 at Nimitz Hill, Guam; and the Operations and Equipment Support departments of NAVPACMETOCCEN WEST, Guam for their high quality support; all the men and women of the ships and facilities ashore throughout the JTWC area of responsibility (AOR), and especially on Guam, who took the observations that became the basis for our analyses, forecasts and post-analyses; CDR Lester E. Carr III and Dr. Russell L. Elsberry for their efforts at the Naval Postgraduate School and publication of the Systematic and Integrated Approach to Tropical Cyclone Track Forecasting Part II ; the personnel at the Navy Publications and Printing Service Branch Office, Guam; Dr. Robert F. Abbey Jr. and the Office of Naval Research for their support to the University of Guam (UOG) for the Research Liaisons to JTWC; the UOG Research Liaisons for their contributions to this publication; Dr. Mark A. Lander for his training efforts, suggestions and valuable insights, and Mr. Charles P. Guard for his support and data collection efforts; Dr. Jeff D. Hawkins, Chris S. Veldon, Samuel Chang and Roger Weldon for their tireless efforts to get the most possible out of remote sensing technologies; Capt Carl Davis for his assistance in obtaining the satellite imagery for the northern Indian Ocean tropical cyclones; Mr. John "Jack" Beven for his efforts to include ground truth in his Weekly Tropical Cyclone Summaries; Mr. Charles R. "Buck" Sampson, Sally A. Calvert, Rosemary Lande, Mike D. Frost, Mugur Georgescu, Daren H. Grant, and Ann J. Schrader for their support and continued development of the Automated Tropical Cyclone Forecasting (ATCF) system; and, AG2 Bryan Y. Hong, AG3 Chris Cross, and A1C Matthew A. Boyd for their excellent desktop publishing and graphics assistance.

EXECUTIVE SUMMARY

The 1996 tropical cyclone season was spectacular. During the western North Pacific (WNP) season there was a near record number of significant tropical cyclones (TCs) -- 43 compared to the 1964 record of 44; 40% above average. Of these, 21 reached typhoon intensity -- the most typhoons in one season since 1972. Additionally, six reached super-typhoon intensity -- two above average. The north Indian Ocean (NIO) also experienced an active season with eight significant TCs -- 60% above average!

The Southern Hemisphere had an average season with 28 significant TCs, although the start of the 1997 season (coincident with the latter half of the 1996 Northern Hemisphere season) was more active than normal.

Despite the high ops tempo induced by an extremely active season, warning support to U.S. assets afield and afloat was superb. Warning verification statistics indicate JTWC was on par with the best season on record in terms of warning skill. The average 1996 forecast errors of 105 nm, 178 nm and 272 nm at 24-, 48- and 72-hour positions, respectively, were second only to 1994.

The JTWC continued to use and assist in the advancement of new technologies for the analysis and forecast of TCs during 1996. Satellite-measured observations of atmospheric winds from the ocean surface to the upper troposphere significantly contributed to earlier diagnosis of TC genesis and wind field definition. Examples include scatterometry-derived winds provided by the European Space Agency Remote Sensing Satellite (ERS-1&2), water vapor-, infrared-, and visible-derived drift wind vectors provided by the University of Wisconsin, and the Defense Meteorological Satellite Program's Special Sensor Microwave Imager-derived wind speed measurements.

Over 9500 satellite-based TC fixes were provided by the USPACOM Meteorological Satellite Network to support warnings in JTWC's Area of Responsibility (AOR), the bulk of which were provided by the JTWC Satellite Operations section. A new satellite-interpretation technique for TCs undergoing extratropical transition was developed in-house and used by the Network during 1996. Also developed during 1996 was systematic methodology to establish TC positions based on microwave imagery, and a new satellite-derived position code number criteria scheme.

The excellent error statistics of 1996 can in part be contributed to continued application of the Systematic and Integrated Approach to Tropical Cyclone Forecasting, developed by CDR Lester E. Carr III and Dr. Russell L. Elsberry of the Naval Postgraduate School. Also of note was the operational implementation of the Geophysical Fluid Dynamics - Navy (GFDN) model. GFDN is a slightly modified version of the model used by the National Hurricane Center for Atlantic TCs, and it provides guidance on selected TCs of tropical-storm or higher intensity throughout JTWC's AOR.

Another significant contribution to our overall error statistics has been the hard work and dedication of the "JTWC" team, consisting of Air Force and Navy officer, enlisted, and civilian personnel. Despite limited manning resources, JTWC met its mission objectives with flying colors. Unfortunately, with additional taskings such as the BRAC-directed move of the JTWC to Pearl Harbor in early 1999, the ability to support the production of a document such as this has been dramatically reduced. A significant reduction of scope in future Annual Tropical Cyclone Reports is planned, unless we hear differently from you, the reader.

TABLE OF CONTENTS

1. OPERATIONAL PROCEDURES

1.1 GENERAL

The Joint Typhoon Warning Center (JTWC) provides a variety of routine products and services to the organizations within its area of responsibility (AOR) as prescribed by USCINCPACINST 3140.1W. JTWC issues the following products:

1.1.1 SIGNIFICANT TROPICAL WEATHER ADVISORY — Issued daily, or more frequently as needed, to describe all tropical disturbances and their potential for further development during the advisory period. Separate bulletins are issued for the Western Pacific and the Indian Oceans.

1.1.2 TROPICAL CYCLONE FORMATION ALERT — Issued in a specified area when synoptic, satellite, or other germane data indicate development of a significant tropical cyclone is likely within 24 hours.

1.1.3 TROPICAL CYCLONE/ TROPICAL DEPRESSION WARNING — Issued periodically throughout each day to provide forecasts of position, intensity, and wind distribution for tropical cyclones in JTWC's AOR.

1.1.4 PROGNOSTIC REASONING MESSAGE — Issued with warnings for tropical storms, typhoons, and super typhoons in the western North Pacific to discuss the rationale for the content of the specific JTWC warning.

1.1.5 PRODUCT CHANGES — The contents and availability of the above JTWC products are set forth in USCINCPACINST 3140.1W. Changes to USCINCPACINST 3140.1W and JTWC products and services are proposed and discussed at the annual U.S. Pacific Command (PACOM) Tropical Cyclone Conference.

1.2 DATA SOURCES

1.2.1 COMPUTER PRODUCTS — Numerical and statistical guidance are available from the USN Fleet Numerical Meteorology and Oceanography Center (FNMOC) at Monterey, California. FNMOC supplies JTWC with analyses and prognoses from the Navy Operational Global Atmospheric Prediction System (NOGAPS) via NIPRNET communication (refer also to section 1.3.5, TESS(3)). NOGAPS products routinely disseminated to JTWC include: surface pressure and winds, upper-air winds, deep-layer-mean winds, geopotential height and height change, and sea-surface temperature. These products are based on the 00Z and 12Z synoptic times, and atmospheric components are available at all standard levels. These products, along with selected ones from the (U.S.) National Center for Environmental Prediction (NCEP), the European Centre for Medium-Range Weather Forecasts (ECMWF), and the Japanese Meteorological Agency (JMA) are received as electronic files via networked computers, and by computer modem connections on government and commercial telephone lines as a backup method for the network. Additionally, selected computer generated products are received via the PC-Based Weather Facsimile (PCGRAFAX) System.

1.2.2 CONVENTIONAL DATA — These data sets are comprised of land and shipboard surface observations, enroute meteorological observations from commercial and military aircraft (AIREPS) recorded within six hours of synoptic times, and cloud-motion winds derived from satellite data. The conventional data are manually and computer plotted, and manually analyzed in the tropics for the surface/gradient and 200-mb levels. These

analyses are prepared twice daily from 00Z and 12Z synoptic data.

1.2.3 SATELLITE RECONNAISSANCE — Meteorological satellite imagery recorded at USAF/USN ground sites and USN ships supply day and night coverage in JTWC's AOR. Interpretation of this satellite data provides tropical cyclone positions and estimates of current and forecast intensities (Dvorak, 1984). The USAF tactical satellite sites and Air Force Global Weather Central (AFGWC) currently receive and analyze Special Sensor Microwave/Imager (SSM/I) data to provide locations of tropical cyclones when the low-level center is obscured by higher clouds, and estimates of 35-kt (18-m/sec) wind radii near tropical cyclones.

Data from satellites — Defense Meteorological Satellite Program (DMSP), National Oceanographic and Atmospheric Administration (NOAA), (Japanese) Geostationary Meteorological Satellite (GMS), and (European Geostationary) Meteorological Satellite (METEOSAT) — provide the foundation for reconnaissance.

Use of satellite reconnaissance is discussed further in section 2.3 Satellite Reconnaissance Summary.

Additionally, scatterometry data from the European Remote Sensing (ERS)-1 satellite also provide valuable insight as to the distribution of low-level winds around tropical cyclones. This year's cover shows a scatterometer pass over Typhoon Orson (19W) from the ERS-1 satellite. When remotely sensed data of this quality became available, JTWC immediately began using it to supplement other available data. Evolution of algorithms and display of scatterometer data has occurred rapidly over the past few years and JTWC has been fortunate to have access to this leading edge technology.

JTWC retrieves scatterometry data on a routine basis from web sites on the NIPRNET/Internet maintained by the Naval Oceanographic Office (NAVOCEANO), the Oceanic Sciences Branch of NOAA, and FNMOC. The scatterometry data available at these sites provide information on tropical cyclone position and low-level winds surrounding a tropical cyclone. Heavy-rain contamination near a tropical cyclone's center limits the usefulness of intensity estimation. In addition to determining positions and wind distribution around tropical cyclones, JTWC also uses scatterometry data to refine the twice daily manual analyses of the surface/gradient-level wind flow and atmospheric structure.

Scatterometry algorithms are discussed further in Chapter 7.

1.2.4 RADAR RECONNAISSANCE — Land-based radar observations are used to position tropical cyclones. Once a well-defined tropical cyclone moves within range of land-based radar sites, radar reports are invaluable for determination of position, movement, and, in the case of Doppler radar, storm structure and wind information. JTWC's use of radar reports during 1996 is discussed in section 2.4 Radar Reconnaissance Summary.

1.2.5 AIRCRAFT RECONNAISSANCE — Until the summer of 1987, dedicated aircraft reconnaissance was used routinely to locate and determine the wind structure of tropical cyclones. Now, aircraft fixes are only rarely available from transiting jet aircraft or from weather-reconnaissance aircraft involved in research missions. No aircraft fixes were available in 1996.

1.2.6 DRIFTING METEOROLOGICAL BUOYS — In 1989, the Commander, Naval Meteorology and Oceanography Command (COMNAVMETOCCOM) put the Integrated Drifting Buoy Plan into action to meet

USCINCPACFLT requirements that included tropical cyclone warning support. In 1996, 30 drifting buoys were deployed in the western North Pacific by a NAVOCEANO-contracted C-130 aircraft. Of the 30 buoys, 24 were Compact Meteorological and Oceanographic Drifters (CMOD) with temperature and pressure sensors and six were Wind Speed and Direction (WSD) with wind speed and direction, temperature and pressure. The buoys were evenly split by type over two deployments — the first in June, followed by the second in September. The purpose of the split deployment was to overlap the expected three-month lifespans of the CMOD buoys in order to provide continuous coverage during the peak of the western North Pacific tropical cyclone season.

1.2.7 AUTOMATED METEOROLOGICAL OBSERVING STATIONS (AMOS) — Through a cooperative effort between COMNAVMETOCCOM, the Department of the Interior, and NOAA/NWS to increase data availability for tropical analysis and forecasting, a network of 20 AMOS stations is being installed in the Micronesian Islands (see Tables 1-1 and 1-2). Previous to this effort, two sites were installed in the Northern Mariana Islands at Saipan and Rota through a joint venture between the Navy and NOAA/NWS. The site at Saipan relocated to Tinian in 1992. Since September of 1991, the capability to transmit data via Service ARGOS and NOAA polar-orbiting satellites has been available as a backup to regular data transmission to the Geostationary Operational Environmental Satellite (GOES) West, and more recently for sites to the west of Guam, to the GMS. Upgrades to existing sites are also being accomplished as opportunities arise to enable access to Service ARGOS. JTWC receives data from all AMOS sites via the AWN under the KWBC bulletin headers SMPW01, SIPW01 and SNPW01 (SXMY10 for Tinian and Rota).

1.3 TELECOMMUNICATIONS

Telecommunications support for the NPMOCW/JTWC is provided by the Naval ComputerTelecommunications Area Master Station, Western Pacific (NTWP) and their Base Communications Department. The NPMOCW/JTWC telecommunications link to NTWP is a new fiber-optic cable which incorporates stand-by redundancy features. Connectivity includes "switched" secure and non-secure voice, facsimile, data services, and dedicated audio and digital circuits to NTWP. Telecommunications connectivity and the basic system configurations which are available to JTWC follow.

1.3.1 AUTOMATED DIGITAL NETWORK (AUTODIN) — AUTODIN currently supports the message requirements for JTWC, with the process of converting to the new Defense Messaging System (DMS) in progress. A personal computer (PC) system running the "Gateguard" software application provides transmit and receive message capabilities. Secure connectivity is provided by a dial-up Secure Telephone Unit-III path with NTWP.

The Gateguard system is used to access the AUTODIN/DMS network for dissemination of warnings, alerts, related bulletins, and messages to Department of Defense (DoD) and U.S. Government installations. Message recipients can retransmit these messages for further dissemination using the Navy Fleet Broadcasts, Coast Guard continuous wave (CW) Morse code, and text to voice broadcasts.

AUTODIN/DMS messages are also relayed via commercial telecommunications routes for delivery to non-DoD users. Inbound message traffic for JTWC is received via AUTODIN/DMS addressed to NAVPACMETOCCEN WEST GU/JTWC.

Table 1-1 AUTOMATED METEOROLOGICAL OBSERVING STATIONS SUMMARY

Site	Location		Call sign	ID#	System	Installed
Saipan*	15.2°N	145.7°E	15D151D2	-----	ARC	1986
Rota	14.2°N	145.2°E	15D16448	91221	ARC	1987
Faraulep**	8.1°N	144.6°E	FARP2	52005	C-MAN/ARGOS	1988
Enewetak	11.4°N	162.3°E	ENIP2	91251	C-MAN/ARGOS	1989
Ujae***	8.9°N	165.7°E	UJAP2	91365	C-MAN	1989
Pagan	18.1°N	145.8°E	PAGP2	91222	C-MAN/ARGOS	1990
Kosrae	5.4°N	163.0°E	KOSP2	91355	C-MAN/ARGOS	1990
Mili	6.1°N	172.1°E	MILP2	91377	C-MAN	1990
Oroluk	7.6°N	155.2°E	ORKP2	91343	C-MAN	1991
Pingelap	6.2°N	160.7°E	PIGP2	91352	C-MAN/ARGOS	1991
Ulul	8.4°N	149.4°E	NA	91328	C-MAN/ARGOS	1992
Tinian*	15.0°N	145.6°E	15D151D2	91231	ARC	1992
Satawan	6.1°N	153.8°E	SATP2	91338	C-MAN/ARGOS	1993
Ulithi	9.9°N	139.7°E	NA	91204	C-MAN/ARGOS	1995
Ngulu	8.3°N	137.5°E	NA	91411	C-MAN/ARGOS	1995
Ebon	4.6°N	168.7°E	NA	91442	C-MAN/ARGOS	1996
Maloelap	8.7°N	171.2°E	NA	91374	C-MAN/ARGOS	1996

* Saipan site relocated to Tinian and commissioned on 1 June 1992.
** The prototype site on Faraulep was destroyed on 28 November 1991 by Super Typhoon Owen.
*** Ujae site was destroyed on 18 November 1992 by Super Typhoon Gay.

ARC = Automated Remote Collection system (via GOES West)
C-MAN = Coastal-Marine Automated Network (via GOES West or GMS)
ARGOS = Service ARGOS data collection (via NOAA's TIROS-N)

Table 1-2 PROPOSED AUTOMATED METEOROLOGICAL OBSERVING STATIONS

Site	Location		Installation	Delayed
Pulusuk	6.5°N	149.5°E	1993	Yes*
Faraulep	8.6°N	144.6°E	1994	Yes
Eauripik	6.7°N	143.0°E	1994	Yes
Utirik	11.2°N	169.7°E	1994	Yes
Satawal	7.4°N	147.0°E	1995	Yes
Ujelang	9.8°N	161.0°E	1995	Yes
Maug	20.0°N	145.2°E	1996	Yes

* Runway construction

1.3.2 AUTOMATED WEATHER NETWORK (AWN) — The AWN provides weather data over the Pacific Meteorological Data System (PACMEDS). JTWC uses two PC systems which run the Windows based WINDS/AWNCOM software application package to interface with a dedicated 1.2 kb/sec (kilo-bits per second) PACMEDS circuit. These PC systems provide JTWC the PACMEDS transmit and receive capabilities needed to effectively store and manipulate large volumes of alphanumeric meteorological data available from reporting stations throughout JTWC's AOR. The AWN also allows JTWC access to data which are available on the Global Telecommunications System (GTS). JTWC's AWN station identifier is PGTW.

1.3.3 AUTOMATED WEATHER DISTRIBUTION SYSTEM (AWDS) — The AWDS consists of two dual-monitor workstations which communicate with a UNIX based communications/data server via a private Local Area Network (LAN). The server's data connectivity is provided by two dedicated long-haul data circuits. The AWDS provides JTWC with additional transmit and receive access to alphanumeric AWN data at Tinker AFB using a dedicated 9.6 kb/sec circuit. Access to satellite imagery and computer graphics from Air Force Global Weather Center (AFGWC) is provided by another dedicated 9.6 kb/sec circuit.

AWDS current configuration was upgraded in 1996 to include improved workstation performance, and integration into NPMOCW's LAN backbone which has access to the Defense Information Systems Network's (DISN), this and the NIPRNET connectivity should allow JTWC to send and receive products among other AWDS systems. Send e-mail requests to jtops@npmocw.navy.mil for more information.

1.3.4 DEFENSE SWITCHED NETWORK (DSN) — DSN is a worldwide, general purpose, switched telecommunications network for the DoD. The network provides a rapid and vital voice and data link for JTWC to communicate tropical cyclone information with DoD installations and civilian agencies.

JTWC utilizes DSN to access DSN-based users, FTS2000, SprintNET networks for commercial or non-DoD based users, and local commercial long distance carriers for voice and data requirements.

The DSN and commercial telephone numbers for JTWC are 349-5240 or 349-4224. The commercial area code is 671 and the DSN Pacific area code is 315.

1.3.5 TACTICAL ENVIRONMENTAL SUPPORT SYSTEM (3) (TESS(3)) — The TESS(3) is connected by NIPRNET to FNMOC. NIPRNET connectivity is provided by a dedicated virtual-switched data services 56 kb/sec packet switched-data link. FNMOC's supercomputer generated gridded fields are pushed to the TESS(3) using NIPRNET, allowing for local value added tailoring of analyses and prognoses. The TESS(3) provides connectivity through NIPRNET to all COMNAVMETOCCOM Centers worldwide.

1.3.6 NIPRNET—DISN's NIPRNET has replaced the DDN MILNET computer communications network, providing a much needed boost in throughput speed for the transfer of large data and image files. NIPRNET has links or gateways to the non-DoD Internet, allowing data to be pulled and pushed from Internet based World Wide Web (WWW) and File Transfer Protocol (FTP) servers. This capability has enhanced JTWC's ability to exchange data with the Internet-based research community.

The JTWC's products are currently available to users of the DISN based Secret IP Router Network (SIPRNET) using WWW browser software. The JTWC's SIPRNET web site address can be obtained by contacting JTWC's Operations Officer. The JTWC's unclassified NIPRNET/Internet web site address is http://www.npmocw.navy.mil. The JTWC's Internet e-mail server's IP address is 192.231.128.1 and the e-mail address is jtops@npmocw.navy.mil.

1.3.7 TELEPHONE FACSIMILE— TELEFAX provides the capability to rapidly scan and transmit, or receive, documents over commercial telephone lines or DSN. TELEFAX is used to disseminate tropical cyclone advisories and warnings to key agencies on Guam and, in special situations, to DoD, other U.S. Government agencies, and the other Micronesian Islands. Inbound documents for JTWC are received at 349-6143, 349-6101, or 349-4032 (commercial area code 671, or DSN Pacific area code 315).

1.3.8 LOCAL USER TERMINAL (LUT) — JTWC uses a LUT, provided by the Naval Oceanographic Office, as the primary means of receiving real-time data from drifting meteorological buoys and ARGOS-equipped AMOS via the polar-orbiting TIROS-N satellites.

1.4 DATA DISPLAYS

1.4.1 AUTOMATED TROPICAL CYCLONE FORECAST (ATCF) SYSTEM — The ATCF is an advanced software program that assists the Typhoon Duty Officer (TDO) in the preparation, formatting, and dissemination of JTWC's products. It cuts message preparation time and reduces the number of corrections. The ATCF automatically displays: the working and objective best tracks; forecasts of track, intensity, and wind distribution; and, information from computer generated forecast aids and products from other agencies. It also computes the myriad of statistics calculated by JTWC. Links have been established through the LAN to the NAVPACMETOCCEN WEST Operations watch team to facilitate the generation of tropical cyclone warning graphics for the fleet facsimile broadcasts, for NAVPACMETOCCEN WEST's local metwatch program, and for warning products for Micronesia. A module permits satellite reconnaissance fixes to be input from 36 OSS/OSJ into the LAN.

1.4.2 TESS(3) receives, processes, stores, displays and prints copies of FNMOC data and environmental products. It also ingests and displays satellite imagery from the Naval Meteorological Data Receiver-Recorder Set (SMQ-11) and other TESS(3) sets worldwide.

1.4.3 AWDS functions are similar to those of the TESS(3), but the environmental products and satellite global data base imagery are produced by AFGWC.

1.4.4 NAVAL OCEANOGRAPHIC DATA DISTRIBUTION SYSTEM (NODDS) — NODDS is a personal computer (PC)-based system that uses a telephone modem to download, store and display environmental and satellite products from FNMOC.

1.4.5 NAVAL SATELLITE DISPLAY SYSTEM - GEOSTATIONARY (NSDS-G) — The NSDS-G is NAVPACMETOCCEN WEST's primary geostationary imagery processing and display system. It can be used to process high resolution geostationary imagery for analysis of tropical cyclone positions and intensity estimates for the Western Pacific Ocean should the Meteorological Imagery, Data Display, and Analysis System (MIDDAS - see Chapter 2) and Mark IVB (see Chapter 2 also) fail.

1.4.6 PC-BASED WEATHER FACSIMILE (PCGRAFAX) SYSTEM — PCGRAFAX is a microcomputer-based system that receives, stores and displays analog and digital facsimile products that are transmitted over high frequency (HF) radio.

1.4.7 SATELLITE WEATHER DATA IMAGING SYSTEM (SWDIS) — The SWDIS (also known as the M-1000) is a PC-based system that interfaces with the LAN to retrieve, store, and display various products such as: geostationary-satellite imagery from other NSDS-G sites at Rota (Spain), Pearl Harbor (Hawaii), or Norfolk (Virginia), scatterometer data from NAVOCEANO and NOAA, and composites of global geostationary-satellite imagery from the Internet. The SWDIS has proven instrumental in providing METEOSAT reduced-resolution coverage of tropical cyclones over the western Indian Ocean as well as long time-series animations of water-vapor imagery.

1.5 ANALYSES

The JTWC TDO routinely performs manual streamline analyses of composite surface/gradient-level (3000 ft (914 m)) and upper-tropospheric (centered on the 200-mb level) data for 00Z and 12Z daily. Computer analyses of the surface, 925-, 850-, 700-, 500-, 400-, and 200-mb levels, deep-layer-mean winds, frontal boundaries depiction, 1000-200 mb/400-200 mb/and 700-400 mb wind shear, 500-mb and 700-mb 24-hour height change, and a variety of other meteorological displays come from the 00Z and 12Z FNMOC data bases. Additional sectional charts at intermediate synoptic times and auxiliary charts, such as station-time plot diagrams, time-height cross-section charts and pressure-change charts, are analyzed during periods of significant tropical cyclone activity.

1.6 FORECAST PROCEDURES

This section first introduces the Systematic and Integrated Approach to TC Track Forecasting by Carr and Elsberry (1994), referred to hereafter as the "Systematic Approach" and then provides JTWC's basic approach to track, intensity and wind radii forecasting.

1.6.1 THE SYSTEMATIC APPROACH — JTWC began applying the Systematic Approach (Figure 1.1) in 1994. The basic premise of this approach is that forecasters can improve upon dynamical track forecasts generated by numerical models and other objective guidance if the forecasters are equipped with:

1) a meteorological knowledge base of conceptual models that organizes a wide array of scenarios into a relatively few recurring, dynamically-related situations; and

2) a knowledge base of numerical-model TC-forecast traits and objective-aid traits within the different recurring situations that is organized around the meteorological knowledge base.

1.6.1.1 General Concepts — *Track, intensity, and size components of a TC forecast are dynamically interdependent.*

1) TC motion affects intensity and how a TC intensifies can affect its motion.

2) TC size affects propagation relative to environmental steering. A large TC may significantly modify its environment. Thus, the present size of a TC and any subsequent changes in size can affect motion.

3) TC size may affect intensity indirectly through changes induced on TC motion.

1.6.1.2 Key Motion Concepts — *TC motion results from a variety of causes.*

1) Environmental Steering — To a first approximation, TC's go where the winds of

the large scale environment blow them (i.e., TCs are a "cork in the stream").

2) TC Propagation — The motion of TCs usually departs in a minor, but not insignificant way from the steering provided by the large scale environment.

3) TC-Environment Interaction — In certain situations, the circulation of the TC interacts with the environment in such a way as to significantly alter the structure of the environment, thus modifying the environmental steering winds which are a primary source of TC motion.

1.6.1.3 Knowledge Base Framework

1.6.1.3.1 Environment Structure — Structure is classified in terms of a large-scale synoptic PATTERN and two or more synoptic REGIONs within the pattern that tend to produce characteristic directions and speeds of steering flow for a TC located therein. Four patterns with six associated regions are recognized by the Systematic Approach. JTWC notes that not all tropical cyclones fit "neatly" into these patterns/regions at all times and that hybrids and transitions between patterns occur. These patterns/regions are briefly described below.

1.6.1.3.1.1 Patterns — There are four primary patterns:

Standard Pattern (S) (Figure 1.2)

1) most frequently occurring pattern in the WNP; and,

2) key feature is roughly zonally-oriented subtropical ridge (STR) anticyclones.

Poleward-Oriented Pattern (P) (Figure 1.3)

1) second highest frequency of occurrence in the WNP;

2) key feature is a ridge (anticyclone) that extends from the STR deep into the tropics and interrupts the tropical easterlies;

3) usually has SW-to-NE axis orientation; and,

4) usually produces strong poleward steering on its west and poleward side.

Monsoon Gyre (G) (Figure 1.4)

1) only occurs during June-November period;

2) key feature is a particularly large and deep monsoonal circulation (thus, "monsoon

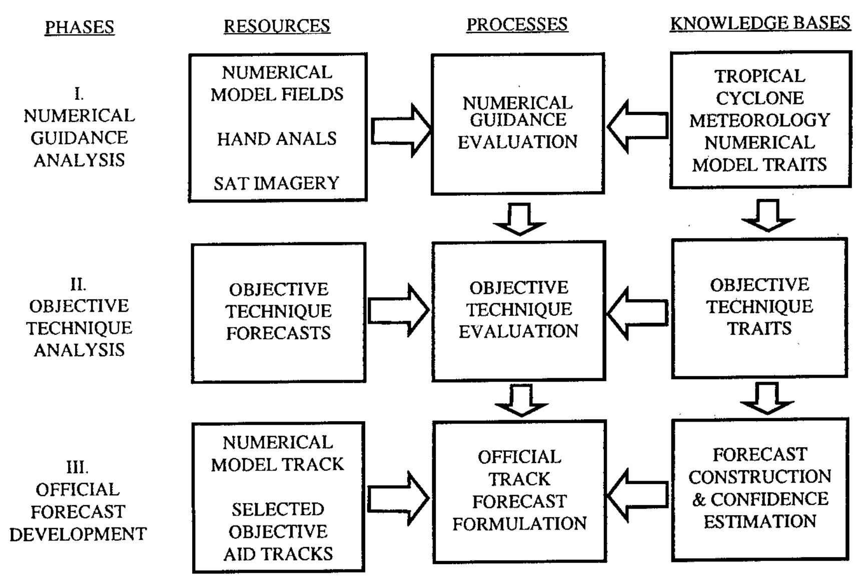

Figure 1.1 Systematic Approach Flowchart

gyre"); and,

3) usually situated between a zonally-oriented STR anticyclone to the NW and a meridionally-oriented anticyclone on its eastern periphery.

Multiple TC (M) (Figure 1.5)

1) key feature is more than one TC with a large break in the STR in the vicinity of the two TCs;

2) the TCs are oriented approximately east-west (i.e., zonally-oriented TCs);

3) the TCs must be far enough apart to preclude significant mutual advection, but close enough to preclude the development of ridging between them (typically greater than 10°, but less than about 25°);

4) the average latitude of the two TCs must be sufficiently close to the latitude of the STR axis (no more than about 10° equatorward or 5° poleward) so that regions of poleward/equatorward flow are established, which affect TC motion and intensification; and,

5) there are three subsets of the "M" pattern which describe varying degrees of interaction between the two cyclones.

1.6.1.3.1.2 Regions. There are six primary regions associated with the four patterns:

Dominant Subtropical Ridge (DR) — the area of tropical easterlies equatorward of the STR axis, except near any break in the STR;

Weakened Subtropical Ridge (WR) — the area of weaker southeasterly winds in the vicinity of a break in the STR;

Accelerating Midlatitude Westerlies (AW) — the area of eastward and poleward steering extending east from a break in the STR;

Poleward Oriented (PO) - the area of poleward steering west of the ridge feature in the "P" and "G" Patterns;

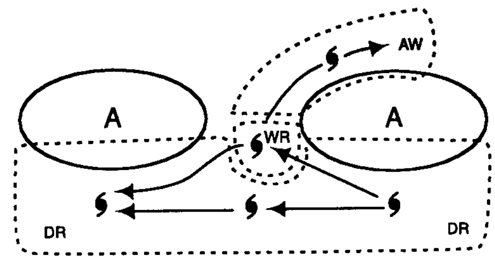

Figure 1.2 Standard Pattern

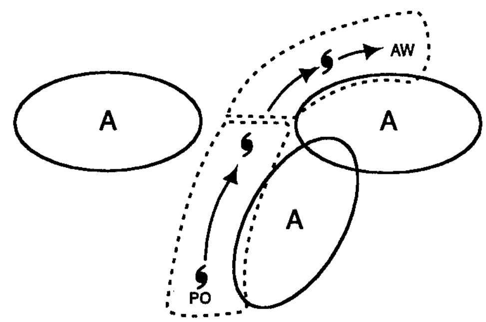

Figure 1.3 Poleward Oriented Pattern

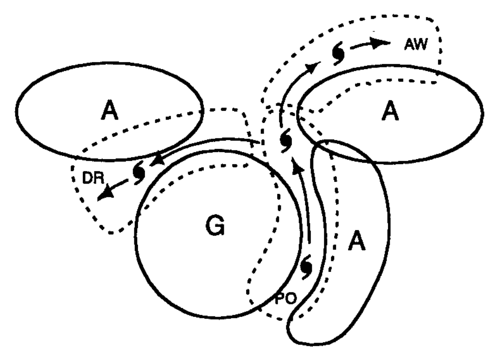

Figure 1.4 Gyre Pattern

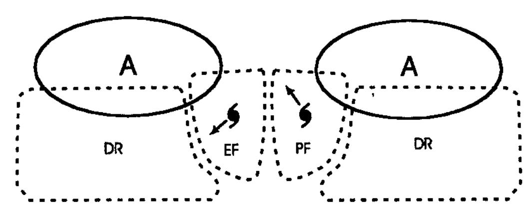

Figure 1.5 Multiple TC Pattern

LEGEND FOR FIGURES:

→ = CHARACTERISTIC TC TRACK	G = GYRE
- - = REGIONAL BOUNDARY	WR = WEAKENED RIDGE
DR = DOMINANT RIDGE	EF = EQUATORIAL FLOW
A = ANTICYCLONE	PF = POLEWARD FLOW
AW = ACCELERATING WESTERLIES	PO = POLEWARD ORIENTED

Multiple TC Poleward Flow (PF) — created in the region of the eastern TC of a "M" Pattern as a result of the gradient between the western TC and the STR circulation to the east; and,

Multiple TC Equatorward Flow (EF) — created in the region of the western TC of a "M" Pattern as a result of the gradient between the eastern TC and the STR circulation to the west.

1.6.1.3.1.3 Nomenclature. — JTWC makes routine use of the aforementioned Patterns and Regions of the Systematic Approach. In order to quickly transcribe this information, a short-hand contraction standard has developed. By utilizing the one-letter contraction of a pattern and the two-letter contraction of an associated region (e.g., S/DR) an effective method of quickly and accurately describing Systematic Approach concepts in writing exists.

1.6.1.3.2 TC Structure. — TC structure consists of an INTENSITY that is based on the maximum wind speed near the center of the TC, and a SIZE that is based on some measure of the extent of the TC windfield. TC intensity is related to steering level and TC size is related to propagation and environment modification.

1.6.1.3.3 Transitional Mechanism. — These mechanisms act to change the structure of the environment (pattern/region) and fall into two categories:

1) TC-Environment Transformations. The TC and the environment may interact, resulting in a change in environmental structure (pattern/region) and thus the direction/speed of the associated steering flow. In addition, TC-environment transformations may result in a change to TC structure. Recognized TC-environment transformations are listed below (refer to Carr and Elsberry (1994) for a more thorough treatment):

- *Beta Effect Propagation*
- *Vertical Wind Shear*
- *Ridge Modification by TC*
- *Monsoon Gyre - TC Interaction*
- *TC Interaction (Direct (DTI), Semi-direct (STI), and Indirect (ITI)) (Figure 1.6)*

2) Environmental Effects. These also result in changes to the structure of the environment (pattern/region) surrounding the TC, but do not depend on, are or largely independent of, the presence of the TC. Recognized environmental effects are listed below (refer to Carr and Elsberry (1994) for thorough treatment):

- *Advection by Environment*
- *Monsoon Gyre Formation*
- *Monsoon Gyre Dissipation*
- *Subtropical Ridge Modulation (by mid-latitude troughs)*

TC movement, intensification, and size evolution are closely linked, therefore, an "ideal TC forecast approach" may be defined as a fully integrated solution for the time evolution of the 3-dimensional TC circulation. TC track, intensity and size forecasts are then to be considered as three partial representations of the total forecast solution.

1.6.2 BASIC APPROACH TO FORECASTING

1.6.2.1 Initial Positioning — The warning position is the best estimate of the center of the surface circulation at synoptic time. It is estimated from an analysis of all fix information received from one hour before to one and one-half hours after that synoptic time. The analysis is aided by a computer-generated objective best-track scheme that weights fix information based on its statistical accuracy. The TDO includes synoptic observations and other information to adjust the position, testing consistency with the past direction, speed of movement and the influence of the different scales of motions. If the fix data are not

a DTI

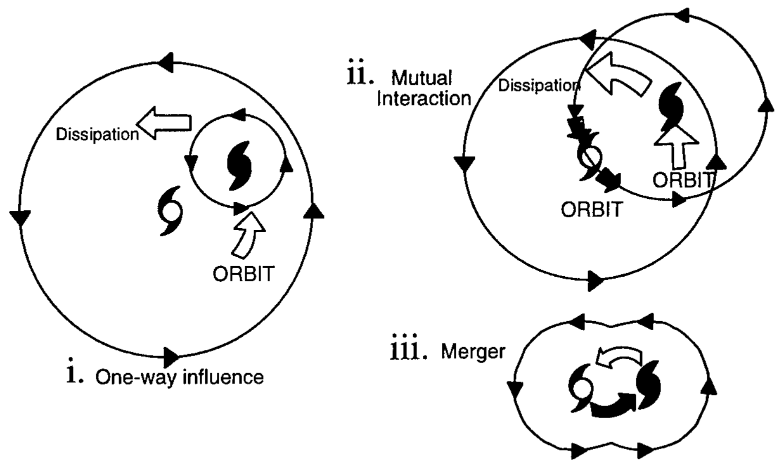

b STI

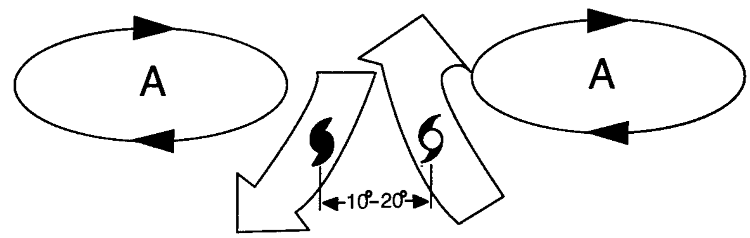

c ITI

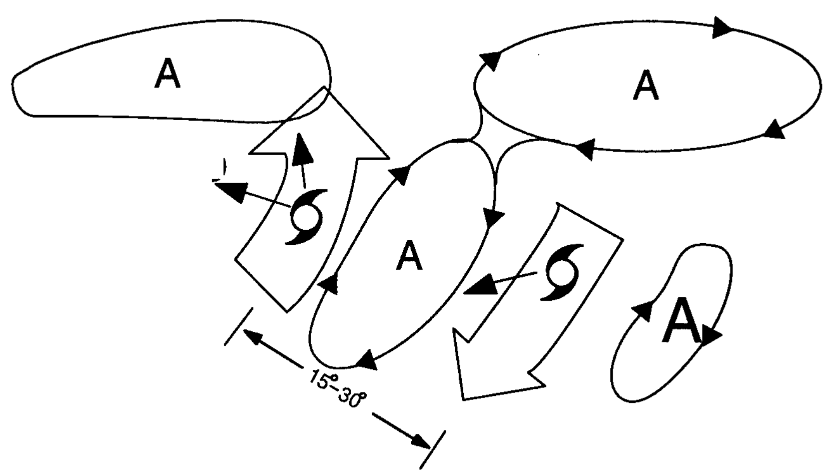

Figure 1-6 Tropical Cyclone Interaction: (a) Direct TC Interaction (DTI) is composed of three types — (i) one-way influence, (ii) mutual interaction, and (iii) merger — (b) Semi-Direct TC Interaction (STI), (c) and Indirect TC Interaction (ITI).

available due to reconnaissance-platform malfunction or communication problems, or are considered unrepresentative, synoptic data and/or extrapolation from previous fixes are used.

1.6.2.2 Track Forecasting — In preparing the JTWC official forecast, the TDO evaluates a wide variety of information and employs Systematic Approach methodology. The JTWC uses a standardized, three-phase tropical cyclone motion-forecasting process to improve forecast accuracy and forecast-to-forecast consistency. Figure 1.1 depicts the three phases and inputs to the Systematic Approach outlined below.

1.6.2.2.1 Numerical Guidance Analysis Phase — NOGAPS analyses and prognoses at various levels are evaluated for position, development, and movement of not only the tropical cyclone, but also relevant synoptic features such as:

1) subtropical ridge circulations;

2) midlatitude short/long-wave troughs and associated weaknesses in the subtropical ridge;

3) monsoon surges;

4) influences of cyclonic cells in the tropical upper-tropospheric trough (TUTT);

5) other tropical cyclones; and,

6) the distribution of sea-surface temperature.

The TDO determines into which pattern/region the tropical cyclone falls, and what environmental influences and transitional mechanisms are indicated in the model fields. The process outlined above permits the TDO to develop an initial impression of the environmental steering influences to which the tropical cyclone is, and will be, subjected to as depicted by NOGAPS. The NOGAPS analyses are then compared to the manually-plotted and analyzed charts prepared by the TDA and TDO, and to the latest satellite imagery, in order to determine how well the NOGAPS-initialization process has conformed to the available synoptic data, and how well the resultant analysis fields agree with the synoptic situation inferred from the imagery. Finally, the TDO compares both the computer- and manually-analyzed charts to monthly climatology in order to make a preliminary determination of to what degree the tropical cyclone is, and will continue to be, subject to a climatological or nonclimatological synoptic environment. Noting latitudinal and longitudinal displacements of subtropical ridge and long-wave midlatitude features is of particular importance, and will partially determine the relative weights given to climatologically- or dynamically-based objective forecast guidance.

1.6.2.2.2. Objective Techniques Analysis Phase — By applying the guidance of the Systematic Approach, the TDO can relate the latest set of guidance given by JTWC's suite of objective techniques with the NOGAPS model prognoses and currently observed meteorological conditions. Performance characteristics for many of the objective techniques within the synoptic patterns/regions outlined in section 1.6.1.3.1.1 have been determined. Estimating the likely biases of each of the objective technique forecasts of TC track, intensity, and size given the current meteorological situation, the TDO eliminates those which are most likely inappropriate. The TDO also determines the degree to which the current situation is considered to be, and will continue to be, climatological by comparing the forecasts of the climatology-based objective techniques, dynamically-based techniques, and past motion of the present storm. Additionally, the spread of the set of objective forecasts, when plotted, is used to provide a measure of the predictability of subsequent motion, and the advisability of including a moderate-probability alternate forecast scenario in the prognostic reasoning message or warning (outside the western North Pacific).

The directional spread of the plotted objective techniques is typically small well before or well after recurvature (providing high forecast confidence), and is typically large near the decision point of recurvature or non-recurvature, or during a quasi-stationary or erratic-movement phase. A large spread increases the likelihood of alternate forecast scenarios.

1.6.2.2.3. Forecast Development Phase — The TDO then constructs the JTWC official forecast giving due consideration to:

1) interpretation of the TC-environment scenario depicted by numerical model guidance;

2) known properties of individual objective techniques given the present synoptic situation or geographic location;

3) the extent to which the synoptic situation is, and is expected to remain, climatological; and,

4) past statistical performance of the various objective techniques on the current storm.

The following guidance for weighting the objective techniques is applied:

1) weight persistence strongly in the first 12 to 24 hours of the forecast period;

2) use conceptual models of recurring, dynamically-related meteorological patterns with the traits of the numerical and objective-aid guidance associated with the specific synoptic situation; and,

3) give significant weight to the last JTWC forecast at all forecast times, unless there is significant evidence to warrant departure (also consider the latest forecasts from regional warning centers, as applicable).

1.6.3 INTENSITY FORECASTING — The empirically derived Dvorak (1984) technique is used as a first guess for the intensity forecast. The TDO then adjusts the forecast after evaluating climatology and the synoptic situation. An interactive conditional-climatology scheme allows the TDO to define a situation similar to the system being forecast in terms of location, time of year, current intensity, and intensity trend. Synoptic influences such as the location of major troughs and ridges, and the position and intensity of the TUTT all play a large part in intensifying or weakening a tropical cyclone. JTWC incorporates a checklist into the intensity-forecast procedure. Such criteria as upper-level outflow patterns, neutral points, sea-surface temperatures, enhanced monsoonal or cross-equatorial flow, and vertical wind shear are evaluated for their tendency to enhance or inhibit normal development, and are incorporated into the intensity-forecast process. In addition to climatology and synoptic influences, the first guess is modified for interactions with land, with other tropical cyclones, and with extratropical features. Climatological and statistical methods are also used to assess the potential for rapid intensification (Mundell, 1990).

1.6.4 WIND-RADII FORECASTING — Since the loss of dedicated aircraft reconnaissance in 1987, JTWC has turned to other data sources for determining the radii of winds around tropical cyclones. The determination of wind-radii forecasts is a three-step process:

1) Low-level satellite drift winds, scatterometer and microwave imager 35-kt wind-speed analysis (see Chapter 2), and synoptic data are used to derive the current wind distribution.

2) The first guess of the radii is then determined from statistically-derived empirical wind-radii models. The JTWC currently uses three models: the Tsui model, the Huntley model, and the Martin-Holland model. The latter model uses satellite-derived parameters to determine the size and shape of the wind profile associated with a particular tropical cyclone. The Martin-Holland model also incorporates latitude and speed of motion to produce an asymmetrical wind distribution. These models provide wind-distribution

analyses and forecasts that are primarily influenced by the intensity forecasts. The analyses are then adjusted based on the actual analysis from step 1), and the forecasts are adjusted appropriately.

3) Finally, synoptic considerations, such as the interaction of the cyclone with mid-latitude high pressure cells, are used to fine-tune the forecast wind radii.

1.6.5 EXTRATROPICAL TRANSITION — When a tropical cyclone moves into the mid-latitudes, it often enters an environment that is detrimental to the maintenance of the tropical cyclone's structure and energy-producing mechanisms. The effects of cooler sea-surface temperatures, cooler and dryer environmental air, and strong vertical wind shear all act to convert the tropical cyclone into an extratropical cyclone. JTWC indicates this conversion process is occurring by stating the tropical cyclone is "becoming extratropical." JTWC will indicate the conversion is expected to be complete by stating the system has become "extratropical." When a tropical cyclone is forecast to become extratropical, JTWC coordinates the transfer of responsibility with NAVPACMETOCCEN WEST which assumes warning responsibility for the extratropical system.

1.6.6 TRANSFER OF WARNING RESPONSIBILITY — JTWC coordinates the transfer of warning responsibility for tropical cyclones entering or exiting its AOR. For tropical cyclones crossing 180°E longitude in the North Pacific Ocean, JTWC coordinates with the Central Pacific Hurricane Center (CPHC), Honolulu via NAVPACMETOCCEN, Pearl Harbor, Hawaii. For tropical cyclones crossing 180°E longitude in the South Pacific Ocean, JTWC coordinates with NAVPACMETOCCEN, which has responsibility for the eastern South Pacific. Whenever a tropical cyclone threatens Guam, files are electronically transferred from JTWC to the Alternate Joint Typhoon Warning Center (AJTWC) collocated with NAVPACMETOCCEN. In the event that JTWC should become incapacitated, the AJTWC assumes JTWC's functions. Assistance in determining satellite reconnaissance requirements, and in obtaining the resultant data, is provided by the weather unit supporting the 15th Air Base Wing, Hickam AFB, Hawaii.

2. RECONNAISSANCE AND FIXES

2.1 GENERAL

JTWC depends primarily on two reconnaissance platforms, satellite and radar, to provide necessary, accurate and timely meteorological information in support of advisories, alerts and warnings. When available, synoptic and aircraft reconnaissance data are also used to supplement the above. As in past years, optimal use of all available reconnaissance resources to support JTWC's products remains a primary concern. Weighing the specific capabilities and limitations of each reconnaissance platform and the tropical cyclone's threat to life and property both afloat and ashore continues to be an important factor in careful product preparation.

2.2 RECONNAISSANCE AVAILABILITY

2.2.1 SATELLITE — Interpretation of satellite imagery by analysts at Air Force/Navy tactical sites and on Navy ships yields tropical cyclone positions, estimates of the current intensity and 24-hr forecast intensity. Additional positioning and surface wind field estimation information are available for analysis from DMSP SSM/I data and the ERS-2 and NSCAT scatterometers.

2.2.2 RADAR — Interpretation of land-based radar, which remotely senses and maps precipitation within tropical cyclones, provides positions in the proximity (usually within 175 nm (325 km)) of radar sites in Kwajalein, Guam, Japan, South Korea, China, Taiwan, Philippine Islands, Hong Kong, Thailand and Australia. Where Doppler radars are located, such as the Weather Surveillance Radar-1988 Doppler (WSR-88D) on Guam and Okinawa, measurements of radial velocity are also available, and observations of the tropical cyclone's horizontal velocity field and wind structure integrated in the vertical are possible.

2.2.3 AIRCRAFT — No weather reconnaissance aircraft fixes were received at JTWC in 1996.

2.2.4 SYNOPTIC — JTWC also determines tropical cyclone positions based on analysis of conventional surface/gradient-level synoptic data. These positions are an important supplement to fixes derived from remote sensing platforms, and become most valuable in situations where satellite, radar, and aircraft fixes are unavailable or are considered unrepresentative.

2.3 SATELLITE RECONNAISSANCE SUMMARY

Per USCINCPAC INSTRUCTION 3140.1W , the Pacific Air Force (PACAF) has primary responsibility for providing tropical cyclone reconnaissance for the U.S. Pacific Command (USPACOM). The Commanding Officer, NAVPACMETOCCEN WEST/JTWC, tasks all reconnaissance requirements, and the Officer In Charge (OIC) of the USPACOM Satellite Reconnaissance Network (hereafter referred to as Network) is delegated the authority to manage Network support to JTWC. However, operational control of radar and satellite readout sites engaged in tropical cyclone reconnaissance remains in normal command channels. The OIC of the Network and the personnel of Satellite Operations (SATOPS) are members of the 36 OSS/OSJ, and are collocated with JTWC at Nimitz Hill, Guam. The network sites are listed in Table 2-1.

Direct readout Network sites provide coverage of the tropical western North Pacific, South China Sea, and south central Indian Ocean using DMSP and NOAA TIROS polar orbiting satellites. PACAF Instruction 15-102 requires each network site to perform a minimum of two fixes per tropical cyclone per day if the tropical cyclone is within a site's coverage. Network

direct readout site coverage is augmented by other sources of satellite based reconnaissance.

Air Force Global Weather Central (AFGWC) provides AOR-wide coverage to

Table 2-1 USPACOM SATELLITE RECONNAISSANCE NETWORK SITES

UNIT	ICAO
15 OSS/OSW, Hickam AFB, Hawaii	PHIK
18 OSS/OSW, Kadena AB, Japan	RODN
607 COS/DOW, Yongsan Garrison Republic of Korea	RKSY
Air Force Global Weather Central, Offutt AFB, Nebraska	KGWC
NPMOD DGAR, Diego Garcia	FJDG

JTWC using recorded smooth DMSP and NOAA TIROS imagery. This imagery is recorded and stored on the satellites for later relay to a command readout site, which in turn passes the data via satellite to AFGWC. Civilian contractors for the Army at Kwajalein Atoll provide additional polar orbiting satellite based tropical cyclone surveillance in the Marshall Islands and east of 180°W as needed. The NOAA/NESDIS Satellite Applications Branch at Suitland, Maryland (ICAO identifier KWBC) also performs tropical cyclone fix and intensity analysis over the JTWC AOR using METEOSAT and GMS geostationary platforms.

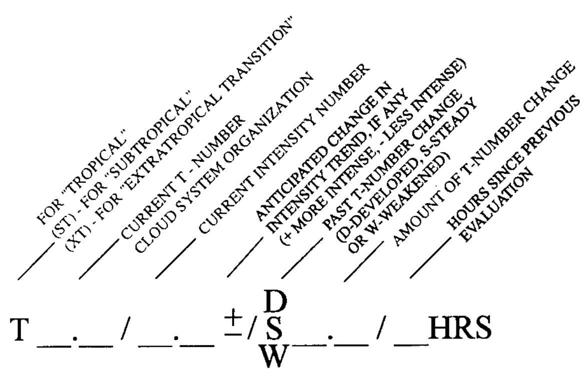

Example: T 3.5 / 4.5+ /W1.5 / 24 HRS

Figure 2-1 Dvorak code for communicating estimates of current and forecast intensity derived from satellite data. In the example, the current "T-number" is 3.5, but the current intensity is 4.5. The cloud system has weakened by 1.5 "T-numbers" since the evaluation conducted 24 hours earlier. The plus (+) symbol indicates an expected reversal of the weakening trend or very little further weakening of the tropical cyclone during the next 24-hour period.

The Network provides tropical cyclone positions and intensity estimates once JTWC issues either a TCFA or a warning. An example of the Dvorak code is shown in Figure 2-1. Each satellite-derived tropical cyclone position is assigned a Position Code Number (PCN) (Arnold and Olsen, 1974), which is a statistical estimate of fix position accuracy. The PCN is determined by 1) the availablility of visible landmarks in the image that can be used as references for precise gridding, and 2) the degree of organization of the tropical cyclone's cloud system (Table 2-2)

Once a tropical cyclone reaches an intensity of 50 kt (26 m/sec), AFGWC and Nimitz Hill SATOPS analyze the 35-kt (18-m/sec) wind distribution surrounding the tropical cyclone based on microwave satellite imagery.

Table 2-2 POSITION CODE NUMBER (PCN)

PCN	CENTER DETERMINATION/GRIDDING METHOD
1	EYE/GEOGRAPHY
2	EYE/EPHEMERIS
3	WELL DEFINED CIRCULATION CENTER/GEOGRAPHY
4	WELL DEFINED CIRCULATION CENTER/EPHEMERIS
5	POORLY DEFINED CIRCULATION CENTER/GEOGRAPHY
6	POORLY DEFINED CIRCULATION CENTER/EPHEMERIS

SATOPS provides three-hourly positions and six-hourly intensity estimates for all tropical cyclones in TCFA or warning status. Current intensity estimates are made using the Dvorak technique for both visible and enhanced infrared imagery. The standard relationship between tropical cyclone "T-number", maximum sustained surface wind speed, and minimum sea-level pressure (Atkinson and Holliday, 1977) for the Pacific is shown in Table 2-3. Subtropical cyclone intensity estimates are made using the Hebert and Poteat (1975) technique. Intensity estimates of tropical cyclones undergoing extratropical transition are made

using the Miller and Lander (1997) technique described in section 2.3.3.

SATOPS at Nimitz Hill uses hourly full disk GMS imagery to observe 70% of the JTWC AOR from 80°E to 180°W (Figure 2-2). Images are remapped to a Mercator projection

Table 2-3 ESTIMATED MAXIMUM SUSTAINED WIND SPEED (KT) AS A FUNCTION OF DVORAK CURRENT AND FORECAST INTENSITY NUMBER AND MINIMUM SEA-LEVEL PRESSURE (MSLP)

T-NUMBER	ESTIMATED WIND SPEED-KT	(M/SEC)	MSLP (MB) (PACIFIC)
0.0	<25	<(13)	- - - -
0.5	25	(13)	- - - -
1.0	25	(13)	- - - -
1.5	25	(13)	- - - -
2.0	30	(15)	1000
2.5	35	(18)	997
3.0	45	(23)	991
3.5	55	(28)	984
4.0	65	(33)	976
4.5	77	(40)	966
5.0	90	(46)	954
5.5	102	(53)	941
6.0	115	(59)	927
6.5	127	(65)	914
7.0	140	(72)	898
7.5	155	(80)	879
8.0	170	(87)	858

to enhance imagery limb coverage at 80°E - 100°E. Animated geostationary imagery is a valuable tool for determining the location and motion of tropical cyclones. Animated water vapor channel imagery is useful for observing environmental synoptic features that affect tropical cyclone development and movement.

SATOPS has access to polar and geostationary data on both the Air Force Mark IVB workstation and the MIDDAS. The MIDDAS consists of a network of three DEC Vax 3400s running advanced graphics software, with two large screen workstations. The Mark IVB is the SATOPS backup satellite data analysis system with the ability to ingest and process both polar and geostationary satellite data, and display imagery on one large screen workstation. The Mark IVB also acts as a front end for the MIDDAS which has no independent receiver/antenna. Both the MIDDAS and the Mark IVB can display NOAA Advanced Very High Resolution Radiometer (AVHRR), DMSP Operational Linescan System (OLS) and Special Sensor Microwave/Imager (SSM/I), and also geostationary visible, infrared and water vapor channel imagery. The MIDDAS can display NOAA TIROS Operational Vertical Sounder (TOVS) data, and the Mark IVB can display DMSP SSM/T1 and SSM/T2 sounder data.

NOAA TIROS AVHRR imagery provides five channels of imagery — visible, near and middle IR, and two in the far IR channels. DMSP OLS provides imagery in two channels — visible/near IR (commonly referred as broadband visible), and far IR. TOVS includes the High Resolution Infrared Radiation Sounder/2 (HIRS/2), the Microwave Sounding Unit (MSU), and the Stratospheric Sounding Unit (SSU).

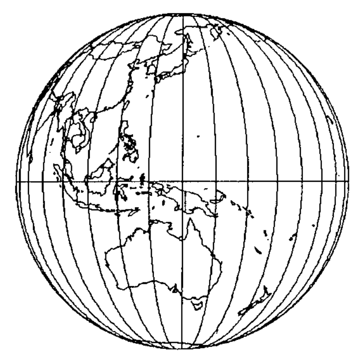

Figure 2-2 GMS Full Disk Coverage

2.3.1 SATELLITE PLATFORM SUMMARY— Figure 2-3 shows the operational status of polar orbiting spacecraft. Imagery was received from two DMSP and two NOAA satellites during 1996. Both of the F-10 and F-11 OLS imagers are in standby mode and only SSM/I imagery was provided, while F-12 provided only OLS imagery. Only F-13 provided both OLS and SSM/I imagery. NOAA-12 and NOAA-14 were operational throughout the year, with fully functional AVHRR imagers .

2.3.2 STATISTICAL SUMMARY—Satellite-based tropical cyclone positions and intensities were the primary input for JTWC's warnings, accounting for 91% of all fixes. The Network and other agencies provided JTWC with 10,360 fixes — 5,568 western North Pacific, 629 northern Indian Ocean, 2,539 Southern Hemisphere, and 1,624 for circulations which did not develop into significant tropical cyclones. JTWC SATOPS provided 7,601 of the fixes. A comparison of satellite fixes to corresponding best track positions is shown in Table 2-4.

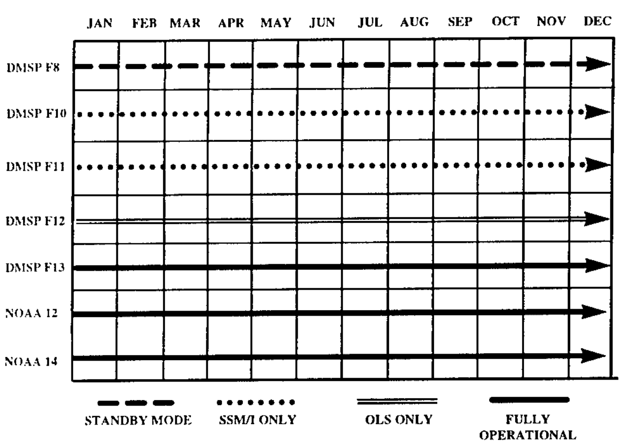

Figure 2-3 Polar orbiting spacecraft status for 1996

2.3.3 APPLICATION OF NEW TECHNIQUES AND TECHNOLOGY— SATOPS uses animated geostationary imagery, multispectral display capability, and microwave imagery to assign fix codes to each tropical cyclone pattern and sensor type (see Table 2-5) (Crume and Lander, 1997). These fix codes will be compared to best track positions to reexamine JTWC's use of the current PCNs after sufficient data are collected. The goal is to give the TDO a better statistical value for each satellite-derived fix position based on the use of current sensors. Many of our current sensors were not operational during the original PCN study.

In addition, SATOPS developed an XT technique (Miller and Lander, 1997a) to better estimate the intensity of tropical cyclones undergoing extratropical transition — a weakness in the current Dvorak technique. The Dvorak T numbers appear to drop too fast when such systems

Table 2-4 MEAN DEVIATION (NM) OF ALL DMSP NETWORK DERIVED TROPICAL CYCLONE POSITIONS FROM JTWC BEST TRACK POSITIONS (NUMBER OF CASES IN PARENTHESES)

PCN	1986-1995 AVERAGE		1996 AVERAGE	
WESTERN NORTH PACIFIC OCEAN				
1&2	13.9	(7239)	11.4	(1,155)
3&4	23.7	(6714)	26.9	(813)
5&6	41.2	(16,793)	54.7	(2,698)
Totals	30.9	(30,746)	39.2	(4,666)
NORTH INDIAN OCEAN				
1&2	12.8	(164)	15.3	(7)
3&4	31.9	(151)	25.3	(70)
5&6	39.2	(1,364)	53.9	(459)
Totals	36.0	(1,679)	49.7	(536)
WESTERN SOUTH PACIFIC AND SOUTH INDIAN OCEAN				
1&2	15.7	(2,514)	11.2	(337)
3&4	25.9	(2,004)	24.7	(338)
5&6	36.5	(9,209)	35.9	(1,379)
Totals	31.1	(13,727)	30.0	(2,054)

lose their persistent central convection, while synoptic data indicate the low-level circulations still contain winds greater than what is indicated by the T numbers. The XT technique should be applied during intensity analysis when a tropical cyclone:

1) loses one half or more of its persistent central convection;

2) maintains its forward motion, or accelerates; or,

3) when it undergoes compound or complex transition.

The XT technique should be applied as soon as appropriate to avoid an artificial intensity minima and discontinued after extratropical transition is complete. Transition is defined as complete when the system has progressed poleward of the polar jet maximum or when water-

vapor imagery clearly indicates the core of the system has become very dry. After extratropical transition is complete, the intensity estimation technique of Smigielski and Mogil (1992) for midlatitude cyclones is more appropriate.

Satellite imagery features measured with the XT technique are:

1) Arc length of the primary outer cloud band not connected with the circulation center.

2) organizational extent of the low-level circulation.

3) existence of deep convection between the outer cloud band and the circulation center.

4) translational speed of the system. (Refer also to Figure 2-4.)

Table 2-6 shows the wind intensities associated with each XT number, which are on the same wind scale as Atkinson and Holliday (1977).

Work is underway at SATOPS to establish methodology for determining tropical cyclone center positions from SSM/I imagery (Miller and Lander, 1997b). SATOPS produced 511 SSM/I-based fixes in 1996 with the MISTIC. Timeliness and number of SSM/I-based fixes should continue to improve with the network

Table 2-5 POSITION CODE NIMBER (PCN) CRITERIA AND FIX CODES FOR TC LOW-LEVEL CIRCULATION CENTERS (CCs) FROM SATELLITE (NOTE 1)

PCN	PCN	Definitions	Sensor /technique type and fix code					
Grid by Geography (note 2)	Grid by Ephemeris (note 2)		IR	Vis	Both	SSM/I only (note 3)	Vis/IR & SSM/I (note 3)	Anmtn (note 4)
1	2	**EYE**						
		Eye within CDO, geometric center (regular/round, any diameter) (note 5)	1	2	3	4	S	A
		Small eye (irregular/ragged, diameter < 30 nm on long axis) (note 5)	5	6	7	8	S	A
3	4	**WELL DEFINED**						
		Eye(ragged/irregular, diameter > 30 nm center more than 1/2 enclosed by wall cloud) (note 5)	9	10	11	12	S	A
		Tightly curved band/banding type eye (band curves at least 1/2 distance around center, diameter ≤ 90 nm)	13	14	15	16	S	A
		Exposed low-level CC	17	18	19	20	S	A
		Small CDO (round with well defined edges, positioned near geometric center, diameter ≤ 80 nm)		21	22	23	S	A
		Small embedded center (diameter ≤ 80 nm)	24		25	26	S	A
		Large CDO (with clear indications of shearing, low-level cloud lines, or overshooting tops, that bias low-level center position away from the geometric center, diameter > 80 nm)		27	28	29	S	A
		Any CDO or Embedded Center with low-level CC clearly visible on co-registered SSM/I (note 6)	30	31	32	33	S	

Table 2-5 (CONTINUED)

5	6	**POORLY DEFINED CC**						
		Large eye (ragged/irregular, diameter > 30 nm on long axis, more than 1/2 enclosed by wall cloud)	34	35	36	37	S	A
		Spiral banding systems (convective curvature) not classifiable as banding eye or tightly curved band	38	39	40	41	S	A
		Large CDO	42	43	44	45	S	A
		Embedded center positioned with IR	46					A
		Partially exposed low-level centers with CC less than 1/2 exposed	47	48	49	50	S	A
		Cloud minimum wedge/cold comma	51	52	53	54	S	A
		Central cold cover	55	56	57	58	S	A
		Cirrus outflow (upper-level outflow provides the only circulation parameters)	59	60	61	62	S	A
		Poorly organized low-level center evident only in high resolution animation (Vis/IR or both)	63					
		All others	64	65	66	67	S	A
		Monsoon depressions or multiple cloud clusters, positioned using any of the following methods:	Any combination of Vis , IR/EIR, and SSM/I					
		Circle method	68					
		Conservative feature	69					
		Animation	70					
		Extrapolation	71					

Note 1: Use the following steps to determine the PCN and Fix Code:

a. Based on the analysis of the circulation parameters, determine a TC low-level CC position.

b. Go to Table 2-5, then to the definitions column. Choose a PCN based on the cloud pattern, discrete measurements, as necessary, and/or technique used to determine the position.

c. Move across to the Fix Code columns, and based on the sensor(s) used, select a fix code.

Note 2: Odd PCNs (1, 3, 5) are gridded with geography, the low-level CC being within 10 degrees (600 nm) of the geographic feature used for gridding. Even PCNs (2, 4, 6) are gridded with ephemeris, or the low-level CC is not within 10 degrees (600 nm) of the geographic feature used for gridding.

Note 3: Append "S" to the numerical fix code entry to indicate Special Sensor Microwave Imager (SSM/I) and visible and/or IR data was used in determining the low-level CC (i.e. 18S). (DMSP) fixes only. For the purposes of this fix code, SSM/I (S) and Animation (A) are mutually exclusive.

Note 4: Append "A" to the numerical fix code entry to indicate animation was used in determining the low-level CC (e.g. 11A). Geostationary fixes only. For the purposes of this fix code, SSM/I (S) and Animation (A) are mutually exclusive.

Note 5: For fix code entries 1-9, encode 01-09.

Note 6: In order to use SSM/I data to position low-level CCs, you must be able to correct the navigation/gridding and interrogate the SSM/I imagery directly for latitude/longitude (DMSP fixes only).

using DMSPs F10 and F11 (SSM/I-only) on the Mark IVB. The recently successful F14 launch should also enhance JTWC's use of the microwave products during 1997.

Mark IVB Network sites received the new software Build 7 during 1996. Also installed

Table 2-6 XT - INTENSITIES

77 KT	= XT 4.5	T 4.5
65 KT	= XT 4.0	T 4.0
55 KT	= XT 3.5	T 3.5
45 KT	= XT 3.0	T 3.0
35 KT	= XT 2.5	T 2.5
30 KT	= XT 2.0	T 2.0
25 KT	= XT 1.0	T 1.5
20 KT	= XT 0.0	T 1.0

was a patch which allows navigation of SSM/I imagery and the ability to overlay SSM/I and OLS imagery. In addition, installation of the Mark IVB Satellite Imagery Dissemination System (SIDS) was completed at Kadena AB and Nimitz Hill SATOPS. SIDS generates satellite imagery products from the Mark IVB, and makes them available to geographically separated units via modem dial-up or LAN/Server connections.

2.3.4 FUTURE OF SATELLITE RECONNAISSANCE — SATOPS remains committed to improving the support provided to JTWC and the USPACOM tropical cyclone warning system. The most significant METSAT improvement anticipated in 1997 is the summer launch of the Chinese geostationary satellite, Feng Yun. With a subpoint at 105°E, this satellite will offer a field of view over the Indian Ocean extending to the east coast of Africa (Figure 2-5). Network sites in the western Pacific should be able to access real time imagery from both GMS-5 and Feng Yun-2B. This opportunity will also provide JTWC with total geostationary satellite coverage of its AOR for the first time.

HQ PACAF/DOW and the Mark IVB depot-support team are exploring a means to send

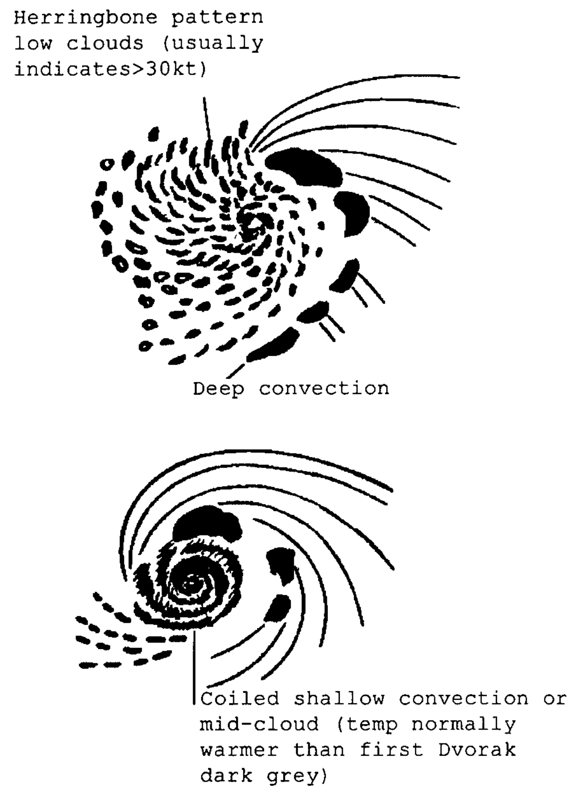

Figure 2-4 Two examples of cloud features analyzed with the XT Technique.

DMSP high resolution and SSM/I imagery to JTWC after the Base Realignment and Closure (BRAC) mandated relocation to Pearl Harbor, Hawaii (planned for January, 1999). Transmission of Feng Yun 2 geostationary data to Pearl Harbor is being addressed since this satellite will orbit below the horizon at Hawaii preventing line of sight communication.

Figure 2-5 Geostationary coverage from 105°E

Mark IVB software Build 8 will introduce a more user-friendly menu and the ability to generate common image files, such as bitmaps, GIF or TIFF files, from received satellite imagery. Installation of the DMSP Image Generating System (DIGS) on the MISTIC II workstation allows SATOPS to save SSM/I imagery in TIFF files.

AFGWC recently implemented a new capability to use geostationary data from METEOSAT, GMS, and GOES to provide additional fix support. In addition, DMSP F-14 was launched in April 1997 in anticipation of DMSP F-12's failure and should provide valuable data. A Dvorak-like technique is under development to determine tropical cyclone intensity from SSM/I imagery.

2.4 RADAR RECONNAISSANCE SUMMARY

Of the 43 significant tropical cyclones in the western North Pacific during 1996, 17 passed within range of land-based radar with sufficient precipitation and organization to be fixed. A total of 691 land-based radar fixes were logged at JTWC. As defined by the World Meteorological Organization (WMO), the accuracy of these fixes falls within three categories: good [within 10 km (5 nm)], fair [within 10 - 30 km (5 - 16 nm)], and poor [within 30 - 50 km (16 - 27 nm)]. Of the 691 radar fixes encoded in this manner, 182 were good, 239 fair, and 270 poor. The radar network provided timely and accurate fixes which allowed JTWC to better track and forecast tropical cyclone movement. In addition to fixes, the Guam and Okinawa WSR-88D radars supplied meteorologists with a look into the vertical and horizontal structure of precipitation and winds in tropical cyclones passing nearby.

In the Southern Hemisphere, 50 radar reports were logged for tropical cyclones. No radar fixes were received for the North Indian Ocean.

2.5 TROPICAL CYCLONE FIX DATA

Table 2-7a delineates the number of fixes per platform for each individual tropical cyclone for the western North Pacific. Totals and percentages are also indicated. Similar information is provided for the North Indian Ocean in Table 2-7b, and for the South Pacific and South Indian Ocean in Table 2-7c.

Table 2-7a WESTERN NORTH PACIFIC OCEAN FIX PLATFORM SUMMARY FOR 1996

TROPICAL CYCLONE		SATELLITE	SCATTEROMETER	RADAR	SYNOPTIC	AIRCRAFT	TOTAL
01W	TD	53	0	0	0	0	53
02W	TS ANN	162	0	5	3	0	170
03W	TD	11	0	0	0	0	11
04W	TY BART	241	8	7	0	0	256
05W	TS CAM	90	2	0	1	0	93
06W	TY DAN	174	3	9	0	0	186
07W	STY EVE	253	1	88	11	0	353
08W	TY FRANKIE	85	0	0	5	0	90
09W	TY GLORIA	122	0	37	8	0	167
10W	STY HERB	268	1	25	8	0	302
11W	TS IAN	53	0	0	0	0	53
12W	TY JOY	183	1	0	0	0	184
13W	TY KIRK	348	2	220	5	0	575
14W	TS LISA	48	0	9	2	0	59
15W	TD	57	1	0	0	0	58
16W	TS MARTY	20	1	0	6	0	27
17W	TD	16	0	0	0	0	16
18W	TY NIKI	142	1	3	4	0	150
19W	TY ORSON	321	3	0	0	0	324
20W	TY PIPER	97	2	0	0	0	99
21W	TD	26	0	0	0	0	26
22W	TS RICK	68	2	0	0	0	70
23W	STY SALLY	148	1	16	1	0	166
24W	TS	68	0	0	3	0	71
25W	TY TOM	165	3	0	3	0	171
26W	STY VIOLET	222	5	21	1	0	249
27W	TY WILLIE	81	0	13	5	0	99
28W	STY YATES	230	1	46	0	0	277
29W	TY ZANE	243	2	153	1	0	399
30W	TS ABEL	153	4	0	5	0	162
31W	TD	91	0	0	0	0	91
32W	TY BETH	209	3	10	2	0	224
33W	TY CARLO	171	3	0	1	0	175
34W	TD	19	2	0	3	0	24
35W	TS	31	1	0	4	0	36
36W	STY DALE	189	7	23	0	0	219
37W	TS ERNIE	234	1	6	8	0	249
38W	TS	50	0	0	0	0	50
39W	TD	18	2	0	5	0	25
40W	TD	83	4	0	2	0	89
41W	TD	57	1	0	0	0	58
42W	TY FERN	216	4	0	6	0	226
43W	TS GREG	52	1	0	0	0	53
Totals		5,568	73	691	103	0	6,435
Percentage of Total		87%	1%	11%	1%	0%	100%

Table 2-7b NORTH INDIAN OCEAN FIX PLATFORM SUMMARY FOR 1996

TROPICAL CYCLONE	SATELLITE	SCATTEROMETER	RADAR	SYNOPTIC	AIRCRAFT	TOTAL
01B	54	1	0	0	0	55
02A	10	1	0	0	0	11
03B	96	0	0	6	0	102
04A	25	0	0	0	0	25
05A	85	3	0	16	0	104
06B	114	1	0	2	0	117
07B	87	0	0	1	0	88
08B	158	2	0	1	0	161
Totals	629	8	0	26	0	663
Percentage of Total	95%	1%	0%	4%	0%	100%

Table 2-7c SOUTH PACIFIC AND SOUTH INDIAN OCEAN FIX PLATFORM SUMMARY FOR 1996

TROPICAL CYCLONE	SATELLITE	SCATTEROMETER	RADAR	SYNOPTIC	AIRCRAFT	TOTAL
01S DARYL/AGNIELLE	185	1	0	0	0	186
02S EMMA	168	2	0	0	0	170
03S FRANK	144	1	13	1	0	159
04S GERTIE	97	1	5	1	0	104
05P BARRY	76	0	2	0	0	78
06S BONITA	81	1	0	3	0	85
07S HUBERT/CORYNA	71	1	0	0	0	72
08P YASI	33	0	0	0	0	33
09P CELESTE	76	0	5	2	0	83
10P JACOB	175	0	0	4	0	179
11S ISOBEL	66	1	0	0	0	67
12S ----	64	0	0	0	0	64
13P DENNIS	128	1	2	0	0	131
14S DOLORESSE	44	3	0	0	0	47
15S ----	28	1	2	0	0	31
16S EDWIDGE	61	1	0	0	0	62
17S FLOSSY	47	0	0	0	0	47
18S KIRSTY	98	0	11	1	0	110
19P ETHEL	93	1	9	1	0	104
20P ZAKA	13	0	0	0	0	13
21P ATU	57	1	1	2	0	61
22S GUYLIANNE	47	2	0	0	0	49
23P BETI	144	4	0	9	0	157
24S HANSELLA	56	4	0	0	0	60
25S OLIVIA	138	2	0	0	0	140
26S ITELLE	118	3	0	0	0	121
27S ----	110	0	0	0	0	110
28S JENNA	121	0	0	0	0	121
Totals	2,539	31	50	24	0	2,644
Percentage of Total	96%	1%	2%	1%	0%	100%

3. SUMMARY OF WESTERN NORTH PACIFIC AND NORTH INDIAN OCEAN TROPICAL CYCLONES

3.1 WESTERN NORTH PACIFIC OCEAN TROPICAL CYCLONES

The year of 1996 was busy for the Joint Typhoon Warning Center (JTWC), with a near record number of significant tropical cyclones (TCs) occurring in the western North Pacific (WNP) (Table 3-1); 43 versus 44 which was the record set in 1964 (Table 3-2). This number was almost 40% higher than the climatological average of 31 significant TCs in the WNP for the 37-year period 1959-1995. The year of 1996 included six super typhoons, 15 lesser typhoons, 12 tropical storms and 10 tropical depressions. The calendar-year total of 33 TCs of at least tropical-storm intensity was 5 above the long-term average (Figure 3-1). The calendar-year total of 21 typhoons

Table 3-1 WESTERN NORTH PACIFIC SIGNIFICANT TROPICAL CYCLONES FOR 1996

TROPICAL CYCLONE		PERIOD OF WARNING	NUMBER OF WARNINGS ISSUED	ESTIMATED MAXIMUM SURFACE WINDS KT	(M/SEC)	ESTIMATED MSLP (MB)
01W	TD	29 FEB - 01 MAR	7	30	(15)	1000
02W	TS ANN	02 APR - 09 APR	27	40	(21)	994
03W	TD	25 APR - 26 APR	4	25	(13)	1002
04W	TY BART	09 MAY - 18 MAY	39	125	(64)	916
05W	TS CAM	18 MAY - 24 MAY	22	60	(31)	980
06W	TY DAN	05 JUL - 12 JUL	30	75	(39)	967
07W	STY EVE	13 JUL - 20 JUL	27	140	(72)	898
08W	TY FRANKIE	21 JUL - 24 JUL	14	90	(46)	954
09W	TY GLORIA	22 JUL - 27 JUL	22	90	(46)	954
10W	STY HERB	23 JUL - 01 AUG	38	140	(72)	898
11W	TS IAN	28 JUL - 31 JUL	10	40	(21)	994
12W	TY JOY	29 JUL - 05 AUG	28	75	(39)	967
13W	TY KIRK	03 AUG - 16 AUG	51	95	(49)	949
14W	TS LISA	05 AUG - 07 AUG	8	40	(21)	994
15W	TD	12 AUG - 16 AUG	9	30	(15)	1000
16W	TS MARTY	13 AUG - 14 AUG	3	50	(26)	987
17W	TD	14 AUG	2	30	(15)	1000
18W	TY NIKI	18 AUG - 23 AUG	21	95	(49)	949
19W	TY ORSON	21 AUG - 03 SEP	51	115	(69)	927
20W	TY PIPER	23 AUG - 26 AUG	14	65	(33)	976
21W	TD	26 AUG - 27 AUG	4	25	(13)	1002
22W	TS RICK	28 AUG - 31 AUG	10	35	(18)	997
23W	STY SALLY	05 SEP - 09 SEP	19	140	(72)	898
24W	TS	09 SEP - 14 SEP	16	45	(23)	991
25W	TY TOM	11 SEP - 20 SEP	35	75	(39)	957
26W	STY VIOLET	11 SEP - 23 SEP	44	130	(67)	910
27W	TY WILLIE	17 SEP - 23 SEP	22	65	(33)	976
28W	STY YATES	22 SEP - 01 OCT	37	130	(67)	910
29W	TY ZANE	24 SEP - 03 OCT	39	110	(57)	933
30W	TS ABEL	11 OCT - 17 OCT	21	50	(26)	987
31W	TD	13 OCT - 17 OCT	13	25	(13)	1002
32W	TY BETH	13 OCT - 21 OCT	33	90	(46)	954
33W	TY CARLO	21 OCT - 26 OCT	24	105	(54)	938
34W	TD	29 OCT - 30 OCT	4	30	(15)	1000
35W	TS	02 NOV - 03 NOV	6	40	(21)	994
36W	STY DALE	04 NOV - 13 NOV	39	140	(72)	898
37W	TS ERNIE	04 NOV - 17 NOV	48	50	(26)	987
38W	TS	06 NOV - 08 NOV	5	50	(26)	992
39W	TD	08 NOV - 09 NOV	3	30	(15)	1000
40W	TD	25-27 NOV/29-01 DEC	15	25	(13)	1002
41W	TD	14 DEC - 20 DEC	13	30	(15)	1000
42W	TY FERN	21 DEC - 30 DEC	35	80	(41)	963
43W	TS GREG	24 DEC - 27 DEC	10	45	(23)	991

was 3 above the long term average. Six of the typhoons became super typhoons, two over the climatological average (Figure 3-2).

Thirty-one of the 43 significant TCs in the WNP during 1996 originated in the low-latitude monsoon trough or near-equatorial trough. Eleven — Dan (06W), Eve (07W), Joy (12W), Tropical Depression (TD) 15W, TD 17W, Piper (20W), TD 21W, Rick (22W), TD 23W, Carlo (33W), and Tropical Storm 38W — formed at relatively high latitude in association with cold-core cyclonic vortices (cells) in the tropical upper-tropospheric trough (TUTT). There were no significant TCs in the WNP during 1996 which originated east of the international date line. Historically, about one TC per year numbered/named by the Central Pacific Hurricane Center or the National Hurricane Center moves into the WNP.

Table 3-2 DISTRIBUTION OF WESTERN NORTH PACIFIC TROPICAL CYCLONES FOR 1959 - 1996

YEAR	JAN	FEB	MAR	APR	MAY	JUN	JUL	AUG	SEP	OCT	NOV	DEC	TOTALS
1959	0	1	1	1	0	1	3	8	9	3	2	2	31
	000	010	010	100	000	001	111	512	423	210	200	200	17 7 7
1960	1	0	1	1	1	3	3	9	5	4	1	1	30
	001	000	001	100	010	210	210	810	041	400	100	100	19 8 3
1961	1	1	1	1	4	6	5	7	6	7	2	1	42
	010	010	100	010	211	114	320	313	510	322	101	100	20 11 11
1962	0	1	0	1	3	0	8	8	7	5	4	2	39
	000	010	000	100	201	000	512	701	313	311	301	020	24 6 9
1963	0	0	1	1	0	4	5	4	4	6	0	3	28
	000	000	001	100	000	310	311	301	220	510	000	210	19 6 3
1964	0	0	0	0	3	2	8	8	8	7	6	2	44
	000	000	000	000	201	200	611	350	521	331	420	101	26 13 5
1965	2	2	1	1	2	4	6	7	9	3	2	1	40
	110	020	010	100	101	310	411	322	531	201	110	010	21 13 6
1966	0	0	0	1	2	1	4	9	10	4	5	2	38
	000	000	000	100	200	100	310	531	532	112	122	101	20 10 8
1967	1	0	2	1	1	1	8	10	8	4	4	1	41
	010	000	110	100	010	100	332	343	530	211	400	010	20 15 6
1968	0	1	0	1	0	4	3	8	4	6	4	0	31
	000	001	000	100	000	202	120	341	400	510	400	000	20 7 4
1969	1	0	1	1	0	0	3	3	6	5	2	1	23
	100	000	010	100	000	000	210	210	204	410	110	010	13 6 4
1970	0	1	0	0	0	2	3	7	4	6	4	0	27
	000	100	000	000	000	110	021	421	220	321	130	000	12 12 3
1971	1	0	1	2	5	2	8	5	7	4	2	0	37
	010	000	010	200	230	200	620	311	511	310	110	000	24 11 2
1972	1	0	1	0	0	4	5	5	6	5	2	3	32
	100	000	001	000	000	220	410	320	411	410	200	210	22 8 2
1973	0	0	0	0	0	0	7	6	3	4	3	0	23
	000	000	000	000	000	000	430	231	201	400	030	000	12 9 2
1974	1	0	1	1	1	4	5	7	5	4	4	2	35
	010	000	010	010	100	121	230	232	320	400	220	020	15 17 3
1975	1	0	0	1	0	0	1	6	5	6	3	2	25
	100	000	000	001	000	000	010	411	410	321	210	002	14 6 5
1976	1	1	0	2	2	2	4	4	5	0	2	2	25
	100	010	000	110	200	200	220	130	410	000	110	020	14 11 0
1977	0	0	1	0	1	1	4	2	5	4	2	1	21
	000	000	010	000	001	010	301	020	230	310	200	100	11 8 2
1978	1	0	0	1	0	3	4	8	4	7	4	0	32
	010	000	000	100	000	030	310	341	310	412	121	000	15 13 4
1979	1	0	1	1	2	0	5	4	6	3	2	3	28
	100	000	100	100	011	000	221	202	330	210	110	111	14 9 5
1980	0	0	1	1	4	1	5	3	7	4	1	1	28
	000	000	001	010	220	010	311	201	511	220	100	010	15 9 4
1981	0	0	1	1	1	2	5	8	4	2	3	2	29
	000	000	100	010	010	200	230	251	400	110	210	200	16 12 1
1982	0	0	3	0	1	3	4	5	6	4	1	1	28
	000	000	210	000	100	120	220	500	321	301	100	100	19 7 2
1983	0	0	0	0	0	1	3	6	3	5	5	2	25
	000	000	000	000	000	010	300	231	111	320	320	020	12 11 2

TABLE CONTINUED ON TOP OF NEXT PAGE

Table 3-2 (CONTINUED FROM PREVIOUS PAGE)

YEAR	JAN	FEB	MAR	APR	MAY	JUN	JUL	AUG	SEP	OCT	NOV	DEC	TOTALS
1984	0	0	0	0	0	2	5	7	4	8	3	1	30
	000	000	000	000	000	020	410	232	130	521	300	100	16 11 3
1985	2	0	0	0	1	3	1	7	5	5	1	2	27
	020	000	000	000	100	201	100	520	320	410	010	110	17 9 1
1986	0	1	0	1	2	2	2	5	2	5	4	3	27
	000	100	000	100	110	110	200	410	200	320	220	210	19 8 0
1987	1	0	0	1	0	2	4	4	7	2	3	1	25
	100	000	000	010	000	110	400	310	511	200	120	100	18 6 1
1988	1	0	0	0	1	3	2	5	8	4	2	1	27
	100	000	000	000	100	111	110	230	260	400	200	010	14 12 1
1989	1	0	0	1	2	2	6	8	4	6	3	2	35
	010	000	000	100	200	110	231	332	220	600	300	101	21 10 4
1990	1	0	0	1	2	4	4	5	5	5	4	1	31
	100	000	000	010	110	211	220	500	410	230	310	100	21 9 1
1991	0	0	2	1	1	1	4	8	6	3	6	0	32
	000	000	110	010	100	100	400	332	420	300	330	000	20 10 2
1992	1	1	0	0	0	3	4	8	5	6	5	0	33
	100	010	000	000	000	210	220	440	410	510	311	000	21 11 1
1993	0	0	2	2	1	2	5	8	5	6	4	3	38
	000	000	011	002	010	101	320	611	410	321	112	300	21 9 8
1994	1	0	1	0	2	2	9	9	8	7	0	2	41
	001	000	100	000	101	020	342	630	440	511	000	110	21 15 5
1995	1	0	0	0	1	2	3	7	7	8	2	3	34
	001	000	000	000	010	020	210	421	412	512	020	012	15 11 8
1996	0	1	0	2	2	0	7	10	7	5	6	3	43
	000	001	000	011	110	000	610	433	610	212	132	111	21 12 10
(1959-1995)													
MEAN	0.6	0.3	0.6	0.8	1.3	2.2	4.7	6.6	5.9	4.9	3.0	1.5	31.4
CASES	22	10	23	27	46	79	168	238	212	177	107	54	1163

The criteria used in Table 3-2 are as follows:
1) If a tropical cyclone was first warned on during the last two days of a particular month and continued into the next month for longer than two days, then that system was attributed to the second month.
2) If a tropical cyclone was warned on prior to the last two days of a month, it was attributed to the first month, regardless of how long the system lasted.
3) If a tropical cyclone began on the last day of the month and ended on the first day of the next month, that system was attributed to the first month. However, if a tropical cyclone began on the last day of the month and continued into the next month for only two days, then it was attributed to the second month.

Table 3-2 Legend

Total for the month/year → 43

Typhoons, Tropical Storms, Tropical Depressions → 21 12 10

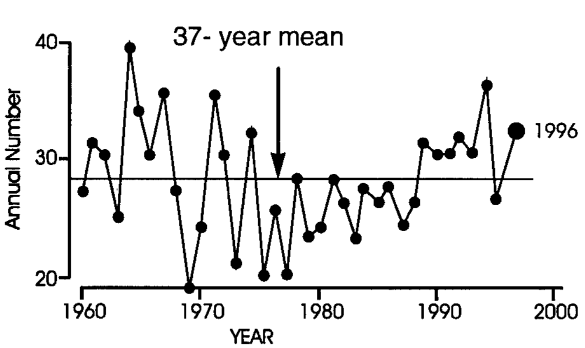

Figure 3-1 Tropical cyclones of tropical storm or greater intensity in the western North Pacific (1960-1996)

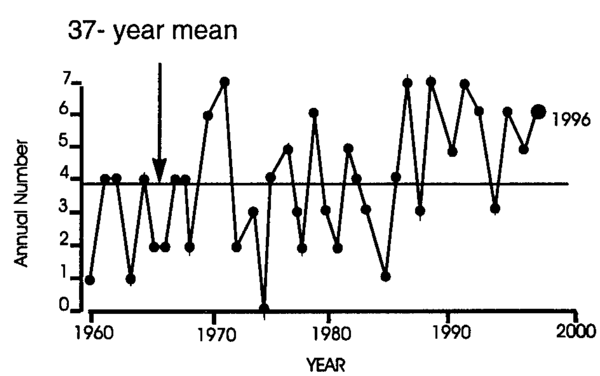

Figure 3-2 Number of western North Pacific super typhoons (1960-1996).

The 1996 year was a continuation of a weak cold phase of the El Niño/Southern Oscillation (ENSO) which began during 1995. Large-scale atmospheric and oceanic circulation anomalies during 1996 were generally as expected for a weak cold phase of ENSO (sometimes referred to as La Niña, or El Viejo). For example, the sea-surface temperature (SST) along the equator in the central and eastern Pacific was colder than normal (Figure 3-3), the Southern Oscillation Index (SOI) was positive (Figure 3-3), and low-level easterly wind anomalies persisted in the low latitudes of the WNP (Figure 3-4).

The annual mean genesis location of TCs which form in the WNP is related to the status of ENSO: it tends to be east of normal during El Niño years and west of normal during El Viejo years. Consistent with the TC distribution associated with a cold phase of ENSO, the annual mean genesis location during 1996 was west of normal (Figure 3-5a), as it was during 1995. It was also slightly north of normal. A breakdown of the genesis locations of all 1996 WNP TCs (Figure 3-5b) shows that most formed between 120°E and 160°E. Only five formed east of 160°E, while ten — six more than normal — formed in the

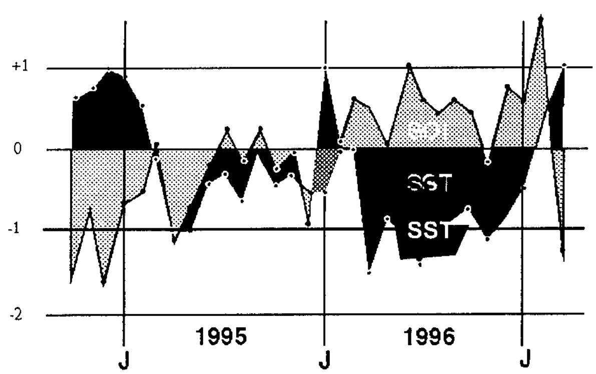

Figure 3-3 Anomalies from the monthly mean for eastern equatorial Pacific Ocean sea-surface temperature (hatched) in degrees Celsius and the Southern Oscillation Index (SOI) (shaded) for the period 1995 through 1996. (Adapted from Climate Prediction Center, 1996).

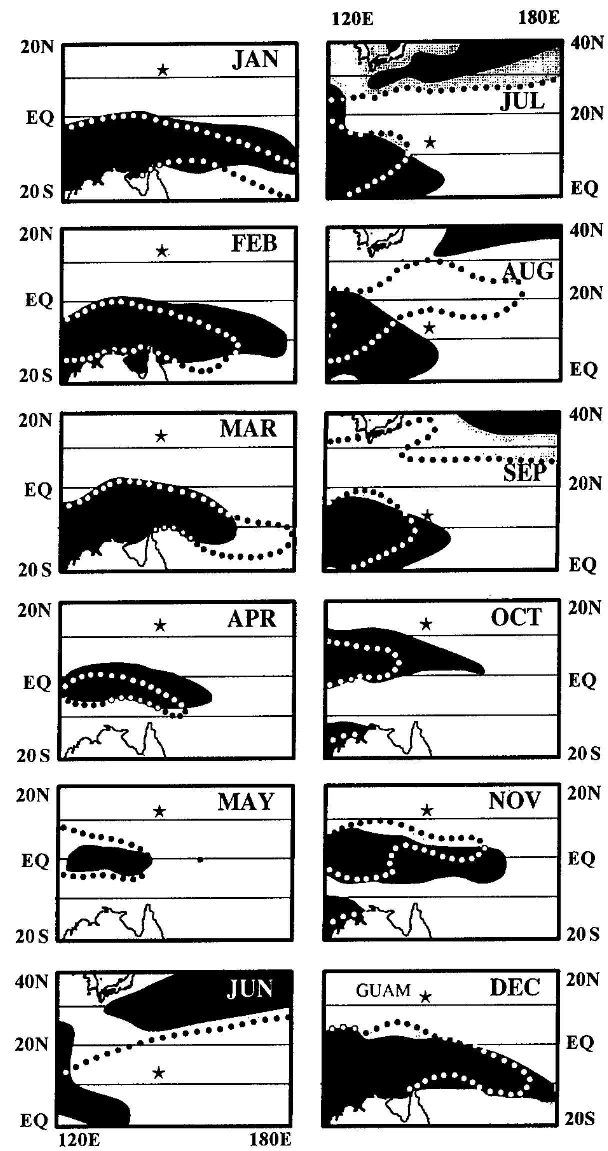

Figure 3-4 Comparison between climatological (black) and analyzed (shaded) mean monthly winds with a westerly component for the WNP in 1996. For June, July and August the area of coverage is shifted northward to include the subtropics. For reference, the star indicates the location of Guam. The outline of Australia appears in the lower left of each panel except for June, July and August and September where the Korean peninsula and Japan appear in the upper left. The climatology is adapted from Sadler, et al. (1987). The 1996 monthly mean winds were adapted from the Climate Prediction Center (1996).

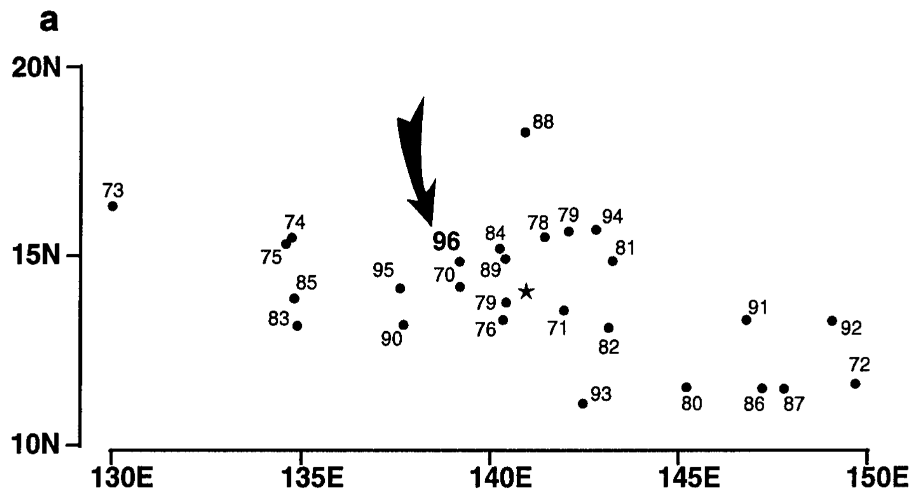

Figure 3-5a Mean annual genesis locations for the period 1970-1996. 1996's location is indicated by the arrow. The star lies at the intersection of the 27-year average latitude and longitude of genesis. For statistical purposes, genesis is defined as the first 25-kt (13-m/sec) intensity on the best track.

South China Sea, contributing to the westward displacement of the annual mean genesis location. Only one TC formed east of 160°E and south of 20°N in a region designated on Figure 3-5b as the "El Niño" box. The annual number of TCs which form in the "El Niño" box is much greater during El Niño years than during El Viejo years (Lander, 1994). During El Viejo years the few TCs which form east of 160°E tend to occur north of 20°N and are often associated with TUTT cells.

During June through October of 1996, low-level easterly wind flow was unusually persistent in the low latitudes of the WNP (Figure 3-4), and the normal southwest monsoon of the Philippine Sea (with its episodic extensions further eastward) was replaced by mean monthly easterly flow. Corresponding anomalies in the upper troposphere consisted of westerly wind anomalies over the low latitudes of the WNP. Similar large-scale wind anomalies dominated the low latitudes of the WNP during 1995, and may have been related

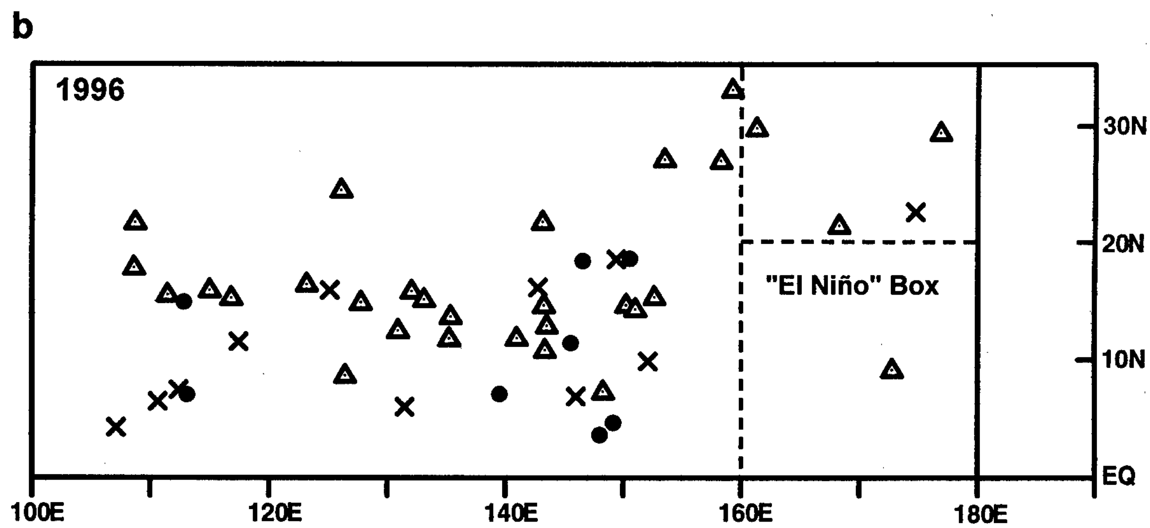

Figure 3-5b Point of formation of significant tropical cyclones in 1996 as indicated by the initial intensity of 25 kt (13 m/sec) on the best track. The symbols indicate: solid dots = 01 January to 15 July; open triangles = 16 July to 15 October; and, X = 16 October to 31 December.

to a westward displacement of the mean genesis location during that year. Despite similar wind anomalies in low latitudes, there were far more TCs during 1996 than during 1995. Some factors suggested for the enhanced number of TCs during 1996 include:

1) a high number of TUTT-cell related TCs during 1996;

2) an unusual eastward penetration of the monsoon trough at high latitudes during August of 1996 (Figure 3-6); and,

3) a return of near-normal monsoonal westerlies during November and December.

The most distinctive characteristic of the WNP TC distribution during 1996 was the large number of TUTT-cell related TCs. Eleven (26%) of the 43 significant TCs in the WNP during 1996 formed in association with TUTT cells. TUTT-cell related TC genesis is described in detail in Joy's (12W) summary.

Another distinctive characteristic of the TC distribution during 1996 was the formation of several TCs at high latitude in association with a displacement of the monsoon trough during August well to the north of normal. A northward-displaced monsoon trough was the site of the development of Kirk (13W), Orson (19W), Piper (20W), and Rick (22W), and TDs 15W, 17W, and 23W. Some of these TCs (e.g., Piper (20W) and Rick (22W)) also formed in association with TUTT cells.

During November and December of 1996, monsoonal westerlies returned to a near-normal distribution. Two episodes of strong low-level equatorial westerly winds (sometimes referred to as equatorial westerly wind bursts) occurred, one during early November and the other during the latter half of December. The November westerly wind burst was associated with the development of the late-season TCs

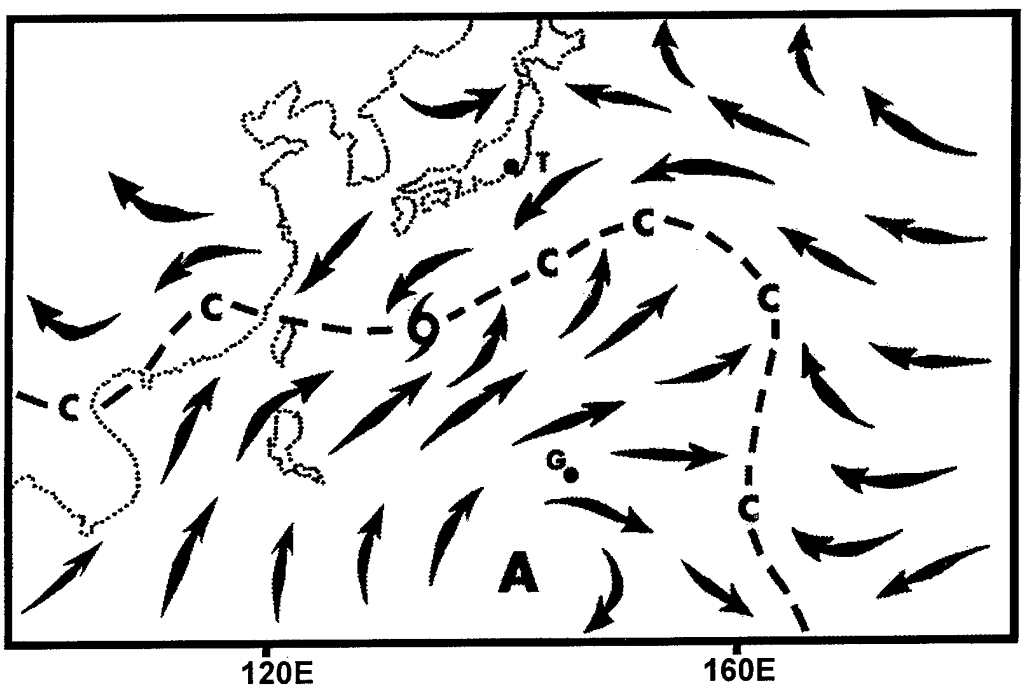

Figure 3-6 Schematic illustration of the low-level circulation pattern which dominated the WNP during August. Arrow indicates wind direction, dashed line indicates the axis of the monsoon trough, C indicates LLCCs, A = anticyclone center, G = Guam, and T = Tokyo. A TC is shown located along the trough axis.

Dale (36W) and Ernie (37W). December's episode of strong equatorial westerly wind was associated with the development of five TCs — two in the Northern Hemisphere (Fern (42W) and Greg (43W)), and three in the Southern Hemisphere (Ophelia (11S), Phil (12P), and Fergus (13P)).

The tracks of the TCs which formed in the WNP during 1996 indicate an above-normal number of TCs (10) in the South China Sea (SCS), and an above-normal number (12) of north-oriented tracks (which includes the three "S" tracks as a specific type of north-oriented motion). Of the 43 TCs, nine (21%) were straight runners, eight (19%) were recurvers, twelve (28%) moved on north-oriented tracks, and fourteen (32%) were designated as "other". Of the twelve TCs which moved on north-oriented tracks during 1995, three underwent "S" motion. Ten of the fourteen "other" TCs remained in or near the SCS. The three "S" tracks occurred in association with a northward-displaced monsoon trough during August.

In summary, a chronology of all the TC activity in the JTWC AOR during 1996 is provided in Figure 3-7. Composite best tracks for the WNP TCs are provided for the periods: 01 January to 08 August (Figure 3-8a), 09 August to 07 October (Figure 3-8b), and 08 October to 31 December (Figure 3-8c). Table 3-3 includes: a climatology of typhoons, and tropical storms/typhoon for the WNP for the periods 1945-1959 and 1960-1996. Table 3-4 is a summary of the TCFA's for the WNP for the period 1976-1996.

Table 3-3 WESTERN NORTH PACIFIC TROPICAL CYCLONES

TYPHOONS (1945-1959)

	JAN	FEB	MAR	APR	MAY	JUN	JUL	AUG	SEP	OCT	NOV	DEC	TOTALS
MEAN	0.3	0.1	0.3	0.4	0.7	1	2.9	3.1	3.3	2.4	2	0.9	16.4
CASES	5	1	4	6	10	15	29	46	49	36	30	14	245

TYPHOONS (1960-1996)

	JAN	FEB	MAR	APR	MAY	JUN	JUL	AUG	SEP	OCT	NOV	DEC	TOTALS
MEAN	0.3	0.1	0.2	0.4	0.7	1	2.8	3.4	3.4	3.2	1.7	0.7	17.9
CASES	10	2	8	15	26	38	104	126	126	120	62	25	662

TROPICAL STORMS AND TYPHOONS (1945-1996)

	JAN	FEB	MAR	APR	MAY	JUN	JUL	AUG	SEP	OCT	NOV	DEC	TOTALS
MEAN	0.4	0.1	0.5	0.5	0.8	1.6	2.9	4	4.2	3.3	2.7	1.2	22.2
CASES	6	2	7	8	11	22	44	60	64	49	41	18	332

TROPICAL STORMS AND TYPHOONS (1960-1996)

	JAN	FEB	MAR	APR	MAY	JUN	JUL	AUG	SEP	OCT	NOV	DEC	TOTALS
MEAN	0.5	0.2	0.5	0.6	1.1	1.8	4.3	5.6	5.1	4.3	2.7	1.2	28
CASES	19	9	17	23	41	67	159	208	189	159	100	46	1037

Table 3-4 TROPICAL CYCLONE FORMATION ALERTS FOR THE WESTERN NORTH PACIFIC OCEAN FOR 1976-1996

YEAR	INITIAL TCFAS	TROPICAL CYCLONES WITH TCFAS	TOTAL TROPICAL CYCLONES	PROBABILITY OF TCFA WITHOUT WARNING*	PROBABILITY OF TCFA BEFORE WARNING
1976	34	25	25	26%	100%
1977	26	20	21	23%	95%
1978	32	27	32	16%	84%
1979	27	23	28	15%	82%
1980	37	28	28	24%	100%
1981	29	28	29	3%	96%
1982	36	26	28	28%	93%
1983	31	25	25	19%	100%
1984	37	30	30	19%	100%
1985	39	26	27	33%	96%
1986	38	27	27	29%	100%
1987	31	24	25	23%	96%
1988	33	26	27	21%	96%
1989	51	32	35	37%	91%
1990	33	30	31	9%	97%
1991	37	29	31	22%	94%
1992	36	32	32	20%	100%
1993	50	35	38	30%	92%
1994	50	40	40	20%	100%
1995	54	33	35	39%	94%
1996	41	39	43	5%	91%
(1976-1996)					
MEAN:	37	29	30	22%	97%
TOTALS:	782	605	637		

* Percentage of initial TCFA's not followed by warnings.

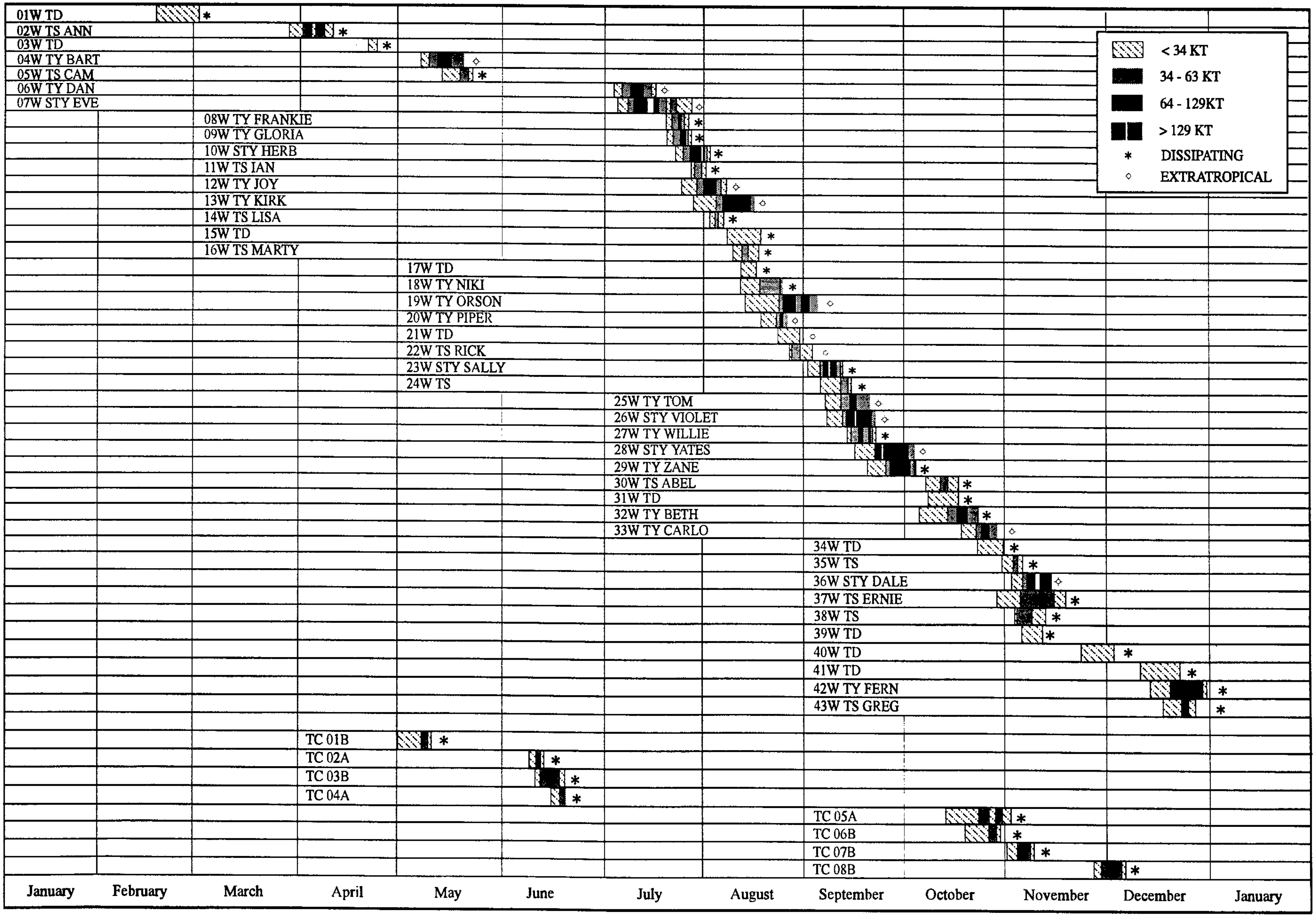

Figure 3-7 Chronology of western North Pacific and North Indian Ocean tropical cyclones for 1996.

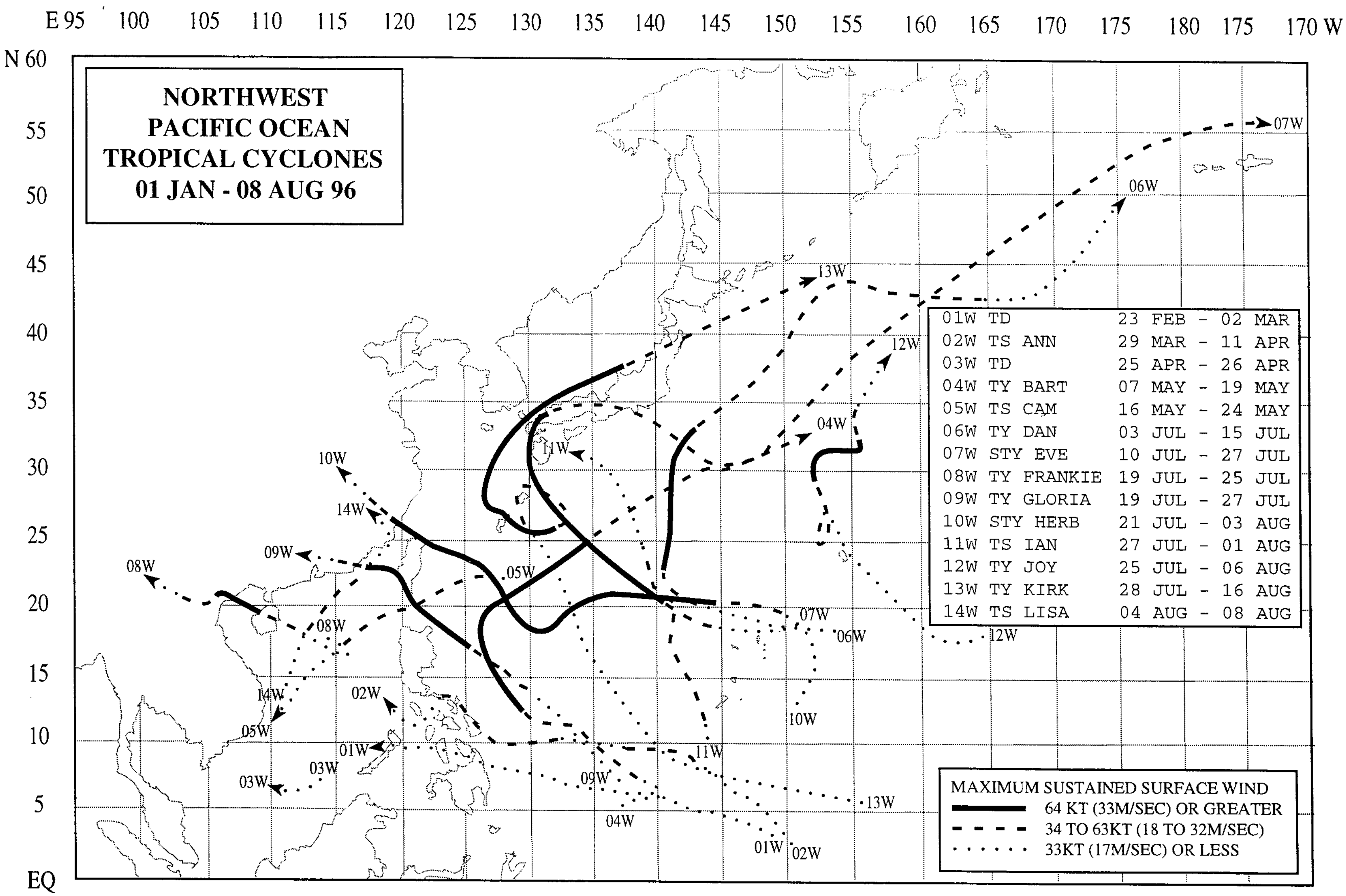

Figure 3-8a Composite best tracks for the western North Pacific Ocean tropical cyclones for the period 01 January to 08 August 1996

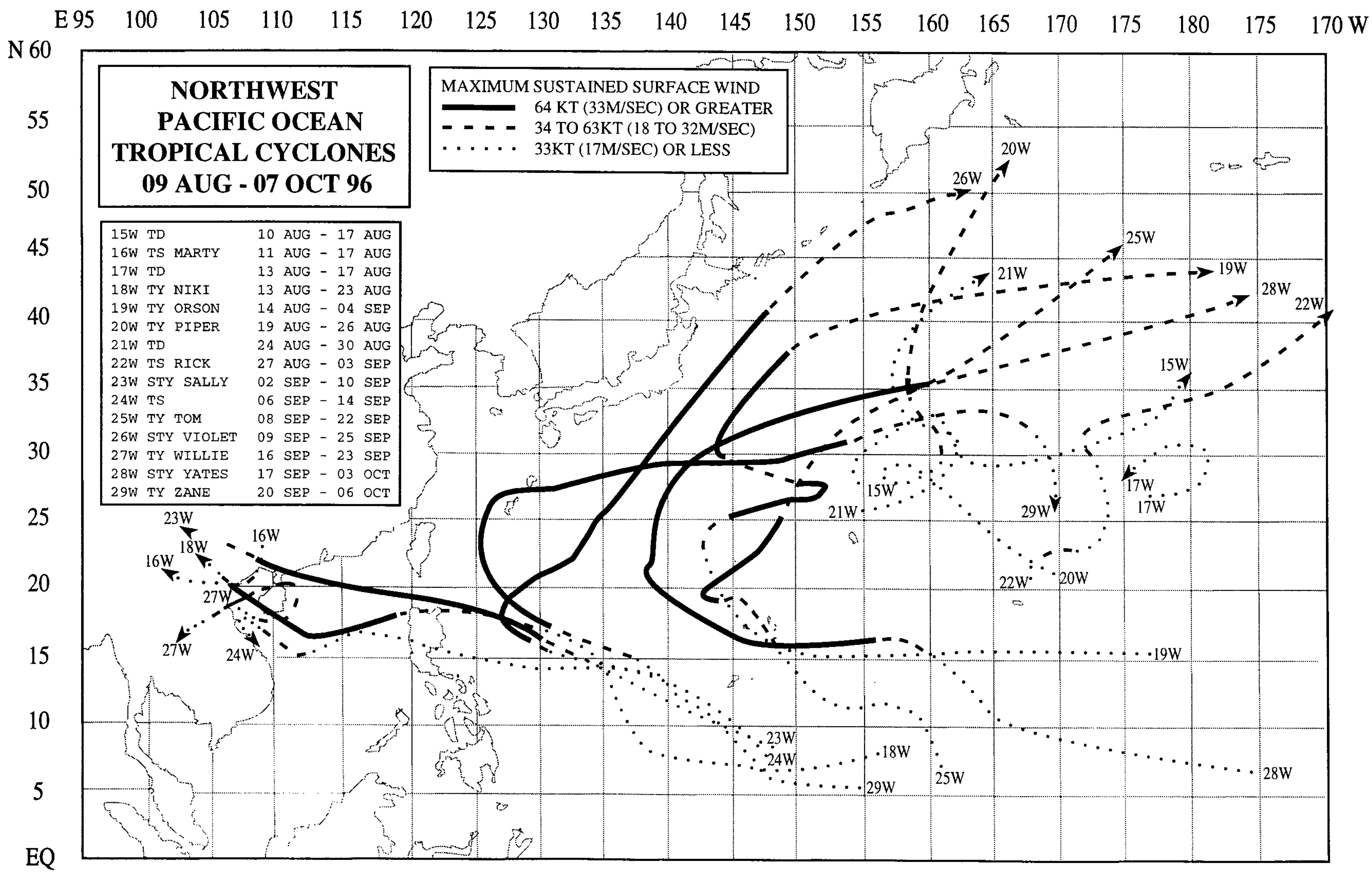

Figure 3-8b Composite best tracks for the western North Pacific Ocean tropical cyclones for the period 09 August to 07 October 1996

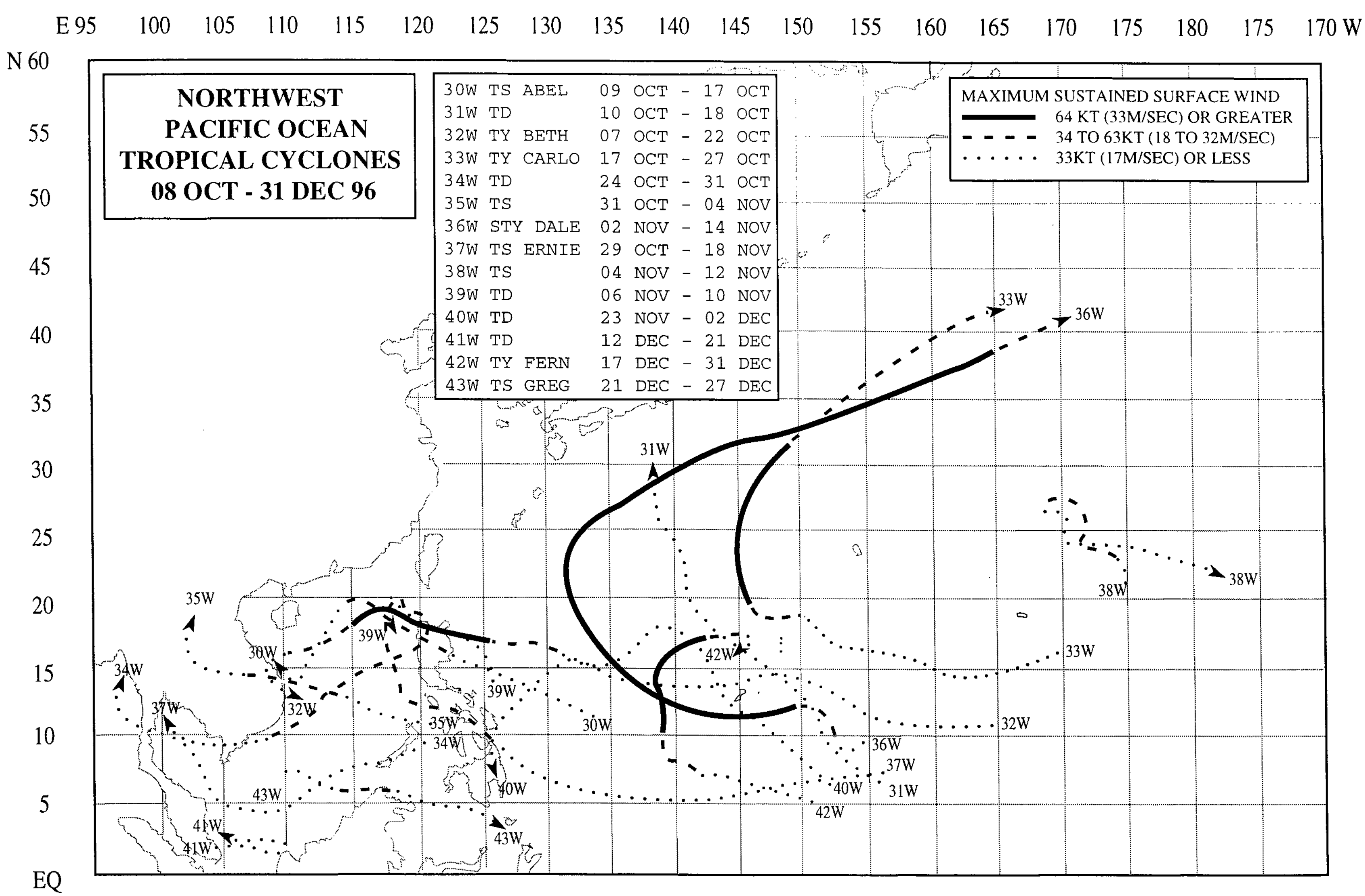

Figure 3-8c Composite best tracks for the western North Pacific Ocean tropical cyclones for the period 08 October to 31 December 1996

3.1.1 MONTHLY ACTIVITY SUMMARY

JANUARY

There were no significant TCs in the western North Pacific basin during January 1996.

FEBRUARY

For only the fourth time since 1970, a significant TC formed in the WNP during February. Toward the end of the month, **Tropical Depression (TD) 01W** formed south of Guam. It developed in a temporary near-equatorial trough over the Caroline Islands, associated with a short-lived westerly wind burst. Tropical Depression 01W moved to the west-northwest, failed to mature, and on the last day of the month it moved into the Philippine archipelago just north of Mindanao.

MARCH

During the first two days of March, TD 01W completed its passage over the Philippines, entered the SCS and dissipated. For most of the rest of March, the WNP was relatively clear, while several TCs originated within the western South Pacific (WSP). At the end of March, the WSP became quiet, and a broad, persistent area of deep convection extended westward from Hawaii to central Micronesia. On the last two days of March, the tropical disturbance which became Ann (02W) originated at low latitudes southeast of Guam.

APRIL

Two TCs — **Tropical Storm (TS) Ann (02W)** and **TD 03W** — were active during April. During the first week of April, Ann became the first named TC of 1996. After becoming a tropical storm while south of Guam, Ann moved westward along 10°N and made landfall in the central Philippines. On 11 April, Ann dissipated over the eastern SCS. The remainder of April was quiet until the last week when an area of persistent deep convection northwest of Borneo became Tropical Depression 03W. TD 03W had a very short life (30 hours).

MAY

During the first week of May, the tropics of the WNP were dominated by low-level easterly wind flow accompanied by westerly wind flow aloft. A zonally-oriented band of convection stretched east-west across Micronesia south of 10°N. By the end of the first week, an area of deep convection began to organize in the western Caroline Islands as monsoonal low-level westerly winds penetrated into the WNP eastward to 140°E and south of 5°N. This area of deep convection became **Typhoon Bart (04W)**, the first typhoon of 1996. Initially moving toward the Philippines, it turned to the north and remained at sea. Undergoing a period of rapid intensification, Bart became a very intense typhoon, peaking at 125 kt (64 m/sec) on 14 May. A day later, the intense typhoon recurved to the northeast, and on 19 May it became extratropical near 30°N 152°E.

As Bart was recurving, cloudiness began to increase in the southwesterly monsoon flow across the SCS and extended east-northeastward toward Bart. Most of the deep convection associated with this monsoon flow was located within the SCS in the form of a large ensemble of mesoscale convective systems (MCSs) which were associated with a weak low-level cyclonic circulation, and extensive cirrus outflow indicative of anticyclonic outflow aloft. These structural attributes are typical of a monsoon depression. The deep convection of this monsoon depression consolidated, and the system became **TS Cam (05W)**. Cam moved toward the east-northeast for its entire life. While at peak intensity, it passed through the Luzon Strait and then slowly weakened as it drifted eastward into the Philippine Sea and dissipated.

JUNE

There were no significant TCs in the WNP during June as amounts of deep convection were below normal, low-level winds were anomalously easterly and upper-level winds were anomalously westerly (Climate Prediction Center (CPC), 1996). While several tropical disturbances developed during the month, a

combination of stronger-than-normal low-level easterly flow with stronger-than normal upper-level westerly flow created an environment of strong vertical shear which was unfavorable for TC formation and development. Since 1959, only five other years have had no significant TCs during June.

JULY

July was a busy month in the WNP with a total of eight TCs. Early in the month, the southwest monsoon remained inactive in the WNP with large-scale wind anomalies similar to those of June. The first two TCs of the month, **Typhoon Dan (06W)** and **Super Typhoon Eve (07W)**, formed in association with TUTT cells. Typical of TC genesis in association with TUTT cells, Dan and Eve formed at relatively high latitude (Dan at 24°N, and Eve at 20°N), and both formed in low-level easterly flow. On 15 July, Eve underwent a period of explosive intensification and reached a peak of 140 kt (72 m/sec), becoming the first super typhoon in the WNP during 1996. The first TC of the year to make landfall as a typhoon, Eve passed through the northern Ryukyu Islands and made landfall in southern Japan.

In the middle of July, the monsoon began to move eastward as the axis of the monsoon trough extended into Micronesia. Extensive amounts of deep convection formed in an east-west band extending across the WNP from the coast of Southeast Asia to the Marshall Islands. By 21 July, this cloud band had consolidated into three distinct cloud clusters, all of which became named TCs — from west to east: **Typhoon Frankie (08W)**, **Typhoon Gloria (09W)**, and **Super Typhoon Herb (10W)**. Frankie originated from a monsoon depression in the SCS. It became a typhoon in the Gulf of Tonkin and went ashore in Vietnam late on 23 July. While Frankie was developing in the SCS, a monsoon depression in the Philippine Sea became Gloria. Gloria moved northwestward, became a typhoon, and affected Luzon, Taiwan, and eastern China. During the early phases of its development, Gloria formed a very large Central Cold Cover (CCC) with a near-record cloud-top temperature of -100°C. As Frankie and Gloria moved westward, Herb formed and became the easternmost of three tropical cyclones simultaneously active along the monsoon trough. Herb became a super typhoon when east of Taiwan. A very intense TC, it was also very large — the largest TC in terms of the mean radius to its outermost closed isobar in the WNP during 1996. Herb made landfall in the southern Ryukyu Islands, Taiwan, and mainland China. Significant property damage and loss of life were attributed to Herb in these areas. On Taiwan, a brand new NEXRAD WSR-88D took a direct hit from Herb, and was severely damaged. As Herb moved westward toward Taiwan, **TS Ian (11W)** formed near Guam at the end of the monsoon trough and then moved on a north-northwestward track while embedded within the peripheral southerly flow on the eastern side of the very large Super Typhoon Herb (10W). Ian appeared to be adversely affected by Herb's upper-level outflow, and did not intensify above 40 kt (21 m/sec).

At the end of July, as Herb moved westward, a TUTT cell generated a tropical disturbance in the eastern part of the WNP basin near 20°N 165°E. This tropical disturbance became **Typhoon Joy (12W)**. Joy did not become a typhoon until 01 August when it had moved to nearly 30°N. Also by the end of July, a new monsoon trough began to form at low latitudes in Micronesia, replacing the monsoon trough which moved with Herb into China. The monsoon depression which became **Typhoon Kirk (13W)** formed south of Guam in late July, but did not become a named TC until the first week of August.

AUGUST

August was also a very busy month, with eight TCs developing during the month, and four of the July TCs — Ian (11W), Herb (10W), Joy (12W), and Kirk (12W) — carrying over into the early part of the month. On 01 August, Ian dissipated south of Japan. Herb dissipated over eastern China on 03 August.

Joy, which developed near 20°N 165°E in the last week of July, reached typhoon intensity on 01 August. It moved on a north-oriented track and merged with a frontal cloud band on 06 August. Typhoon Kirk (13W), the last of the TCs originating during July, developed from a monsoon depression at low latitude, and did not significantly intensify until reaching 27°N on 05 August. The typhoon moved on a complex north-oriented track which saw it undergo an unusual clockwise loop before passing directly over Okinawa where it took a full 12 hours for its 70-nm (130-km) diameter eye to pass. Kirk recurved near Okinawa, intensified to its peak of 95 kt (49 m/sec), moved to the northeast, and made landfall in Kyushu on 14 August.

During the period 04-17 August (as the large slow-moving Kirk tracked northward, executed its clockwise loop, and recurved), four relatively weak TCs formed elsewhere in the WNP. **TS Lisa (14W)** was the first TC to form during August. It originated from a monsoon depression in the SCS. Moving northeastward, the system attained only 40 kt (21 m/sec); and late on 06 August it made landfall west of Taiwan in east central China. On 12 August, **TD 15W** developed in the subtropics at a time when the monsoon trough was displaced far to the north of normal. Although it was located along the axis of this northward-displaced monsoon trough, the structure of the very small TD 15W was influenced by a northward-displaced TUTT, and an upper-level cut-off low to the east of Japan. The system dissipated over water on 17 August. **TS Marty (16W)** originated as a tropical disturbance in the monsoon trough over land in southwestern China. This disturbance moved southward into the Gulf of Tonkin and intensified to a tropical storm on 13 August. The system then turned more to the west and, after a short path over water, it made landfall about 60 nm (110 km) south of Hanoi. Marty was reported to have severely impacted Vietnamese fishing boats in the Gulf of Tonkin where 125 people were reported killed and another 107 missing. **TD 17W** formed to the east-southeast of TD 15W at the eastern end of the northward-displaced monsoon trough. This TD tracked eastward across the international date line, then doubled back and crossed the date line again. On 17 August after a short life and a short track, TD 17W dissipated over water near 27°N 177°E.

During the middle of August, as TDs 15W and 17W developed along the axis of a monsoon trough which was displaced to a higher-than-normal latitude, a ridge of high pressure to its south produced easterly low-level winds across the deep tropics of the WNP. Within these low-latitude easterly winds, several tropical disturbances formed. The tropical disturbance which became **Typhoon Niki (18W)** can be traced to a small ensemble of MCSs which appeared in the eastern Caroline Islands on 13 August. This disturbance moved westward and slowly developed. It became a tropical storm after it crossed 130°E and before it crossed Luzon. Niki did not become a typhoon until it was in the SCS. The typhoon passed over the southern tip of Hainan Island, crossed the Gulf of Tonkin, and made landfall in northern Vietnam. The tropical disturbance which became **Typhoon Orson (19W)** developed within a very complex circulation pattern that can best be described as the early stages of the breakdown of the high-latitude monsoon trough within which Kirk (13W), TD 15W, and TD 17W were located. When the pre-Orson tropical disturbance formed on 15 August, Kirk (13W) was moving eastward over northern Honshu (and becoming extratropical), and TDs 15W and 17W were dissipating at high latitude (30°N) and east of 160°E. For the next four days, the pre-Orson tropical disturbance tracked westward along 15°N. On 19 August, it turned northward and intensified. Orson had a complex history, including two periods of intensification, the formation of a very large eye, and a highly erratic track.

When Orson became a typhoon while moving east-northeastward at 25°N, the monsoon trough became reestablished at a high latitude. The final three TCs of August developed at high latitude in this monsoon trough, and were also associated with TUTT cells. **Typhoon Piper (20W)** was another of the TCs of 1996 which originated in association with a TUTT cell. It was a very small TC — easily

the smallest typhoon in the WNP during 1996. Developing at a relatively high latitude to the east of Orson (19W), Piper was located at the eastern end of a high-latitude reverse-oriented monsoon trough. Typical of TCs associated with a reverse-oriented monsoon trough, Piper moved on a north-oriented "S"-shaped track. On 26 August, the typhoon accelerated toward the north-northeast and was absorbed into a frontal cloud band east of the Kamchatka peninsula. On 24 August, the weak low-level circulation which became **TD 21W** developed east of Orson and west of Piper. Sandwiched between these two TCs, TD 21W remained weak while in an environment of westerly vertical wind shear. After moving on a north-oriented "S"-shaped track, the system dissipated over water near 42°N 163°E early on 30 August. **TS Rick (22W)** formed after Piper and TD 21W moved out of the high-latitude monsoon trough on their north-oriented "S"-shaped tracks. The tropical disturbance which became Rick was located between Orson (19W) and a well-defined TUTT cell. In addition to its association with a TUTT cell, Rick also became part of the monsoon trough. Located at the eastern end of the high-latitude monsoon trough, it moved on a north-oriented "S"-shaped track. On 31 August, the system entered the accelerating westerlies regime north of the subtropical ridge, and by 03 September it dissipated north of 40°N and east of the international date line.

SEPTEMBER

TC activity in the WNP during September continued at a fast pace, with no break from the high levels of TC activity of July and August. The month produced seven TCs, including six typhoons (half of which became super typhoons). As the month began, two TCs — Rick and Orson — were still active from August. Rick dissipated on 03 September, and Orson became extratropical on 04 September.

As the long-lived Orson recurved at the beginning of September, the unusual monsoon flow pattern of August gave way to a pattern more in line with climatology: the maximum cloud zone and the axis of the monsoon trough became established from the Philippines east-southeastward into Micronesia. Five TCs — Sally (23W), TS 24W, Tom (25W), Violet (26W), and Willie (27W) — formed in this monsoon trough. This very active monsoon trough moved northward, and became reverse oriented. By the final week of September, it had migrated to a relatively high latitude as TCs Tom (25W) and Violet (26W) carried the trough with them out of the tropics. As this monsoon trough exited the tropics, yet another monsoon trough formed at low latitudes, and was the site of development for the next two TCs in the WNP: Yates (28W) and Zane (29W).

Super Typhoon Sally (23W) was the first significant TC to form during September. Forming southwest of Guam, Sally moved on a relatively steady west-northwest straight-moving track. It became a super typhoon while moving through the Luzon Strait, and later, though weaker, it made landfall in southwestern China where it caused extensive damage and considerable loss of life. **TS 24W** (unnamed) began as a tropical disturbance located near Guam. By the morning of 09 September this disturbance became a large monsoon depression in the Philippine Sea. The system moved westward, crossed Luzon and entered the SCS. On 14 September, it moved into the Gulf of Tonkin where it dissipated. The upgrade to a tropical storm was based upon a post analysis of synoptic data which indicated that the sustained winds reached a peak of 45 kt (23 m/sec) when the TC was in the SCS.

The next two September TCs — **Typhoon Tom (25W)** and **Super Typhoon Violet (26W)** — moved in tandem along spatially-proximate recurving tracks. Although both TCs had very large circulations, their approximate 1100-nm (2050-km) separation distance was too far apart for the TCs to exhibit binary interaction. When Tom reached its peak intensity of 75 kt (39 m/sec) on 16 September, it had an unusual structure featuring a "pin-hole" eye in a small central cloud mass surrounded by extensive peripheral rain bands within a large outer wind field. By contrast, Violet (located to the west of Tom) had a size similar to Tom, and yet the structure of its core

could not have been more different: Violet's eye began small, but then became very large with a diameter on the order of 75 nm (140 km). Violet was responsible for killing seven people and injuring 44 others in southeastern Japan.

While the circulation of the large TCs Tom and Violet dominated much of the WNP, a small TC — **TS Willie (27W)** — developed in the Gulf of Tonkin. Never more than 90 nm (170 km) from shore, Willie circumnavigated Hainan Island while undergoing a counter-clockwise loop. Willie was a small TC, and was part of a three-TC outbreak along the monsoon trough, with the larger TCs Tom and Violet to its northeast. At one point, Tom, Violet, Willie and a subtropical (ST) low existed simultaneously along the trough axis. Due to the relative motions of these TCs (and the ST low), the trough axis became reverse oriented.

The tendency of the monsoon trough of the WNP to form and then migrate northward lends itself to a natural segregation of TCs into "families" with the commonality among the TCs within each "family" being that they were associated with the same monsoon trough. The five-TC sequence of early September — Sally, TS 24W, Tom, Violet, and Willie —all had in common an origin within the same monsoon trough. By late September, this monsoon trough moved northward, became reverse oriented, and migrated to higher latitude as TCs Tom and Violet carried it with them out of the tropics. As this monsoon trough exited the tropics, a new monsoon trough formed at low latitudes, and was the site of development for the next two TCs in the WNP: **Super Typhoon Yates (28W)** and **Zane (29W)**. Like Tom and Violet before them, the final two September TCs — Yates and Zane — developed in the same monsoon trough, at approximately the same time, and recurved simultaneously along similarly shaped and spatially-proximate tracks. Yates and Zane had motion characteristics suggestive of semi-direct and indirect TC interaction. The mutual anticyclonic orbit of Yates and Zane during the period 23 to 26 September (manifested in a south-of-west track for Yates) are typical of indirect TC interaction. The periods of mutual cyclonic orbit at the beginning and at the end of the tracks is consistent with semi-direct TC interaction. It is often difficult to differentiate between semi-direct and direct TC interaction, but one clue is often the separation distance. True mutual interaction of two TCs usually occurs when the TCs are within 780 nm (1450 km) of each other. Yates and Zane were at this threshold, and it is possible that they may have interacted directly, especially at the end of their tracks when the cyclonic orbit increased rapidly.

OCTOBER

At the beginning of October, Yates and Zane recurved and moved into the midlatitudes. During this time, for about one week, the low latitudes of the WNP became relatively free of deep convection, and there was a break in TC activity. By the end of the first week of October, amounts of deep convection began to increase in the low latitudes of the WNP, and winds throughout most of Micronesia became light and variable in association with the establishment of yet another monsoon trough. Renewed deep convection (loosely organized into discrete ensembles of MCSs) was located in an east-west zone across the low latitudes of the WNP. The first three TCs of October—Abel, TD 31W, and Typhoon Beth — developed in this cloud band over the span of three days. **TS Abel (30W)** originated from a monsoon depression in the Philippine Sea, crossed Luzon, and became a tropical storm in the SCS. Forced to move southwestward by the northeast monsoon, it dissipated over water while approaching the coast of southern Vietnam. Moving toward the northwest, **TD 31W** exhibited a shear-type cloud pattern for all of its life. On 17 October, the deep convection associated with TD 31W decreased in amount and became sheared well to the east of the LLCC as the system dissipated over water. The tropical disturbance which became **Typhoon Beth (32W)** was first detected in the eastern Caroline Islands. For a week, it developed very slowly, and while passing over Guam, it produced a thunderstorm with a spectacular display of cloud-to-ground lightning (an unusual event in the maritime tropics). On 16 October, Beth

became a typhoon in the Philippine Sea. The typhoon passed over Luzon where loss of life was reported. Encountering the northeast monsoon in the South China Sea, it turned to the southwest, weakened, and made landfall in central Vietnam.

On 17 October, three TCs were active in the western part of the WNP: Abel (in the South China Sea), TD 31W (east-southeast of Okinawa), and Beth (32W) (near the coast of Luzon). Elsewhere in the tropics of the WNP, amounts of deep convection were below normal and the low-level wind was predominantly from the east. The only area of deep convection considered to have a potential for TC formation was associated with a TUTT cell which was centered near 17°N 168°E. **Typhoon Carlo (33W)** formed in association with this TUTT cell. Water-vapor imagery provided detailed information on the evolution of upper-level winds, clouds, and moisture for this event. Carlo reached its peak intensity of 105 kt (54 m/sec) while moving northward after reaching its apparent "point of recurvature": a typical behavioral characteristic of TCs which move on a north-oriented track. Accelerating to a speed of 30 kt (55 km/hr), Carlo was absorbed into the frontal cloud band of an intense extratropical low on 27 October.

In late October, TC development shifted to the SCS. On 25 October, **TD 34W** developed just west of the Visayan Islands of the Philippines. This small and weak TC moved to the west-southwest, and as it approached the Malay peninsula, it turned toward the northwest. TD 34W passed through the Gulf of Thailand, moved across the Isthmus of Kra into the Bay of Bengal, and then dissipated over southern Myanmar on 31 October. On the last day of the month, the monsoon depression which became **TS 35W** formed over the Philippines at nearly the same location at which TD 34W originated. It did not become a tropical storm until early November. As a monsoon depression, TS 35W was a larger system than TD 34W. It moved across the SCS and made landfall in central Vietnam. The upgrade to tropical storm intensity was based upon post analysis of ships reports and satellite imagery.

NOVEMBER

From late October through the first day of November, the tropics of the WNP (except the SCS) was dominated by easterly low-level wind and upper-level westerly wind. Deep convection was disorganized and widely scattered. On 02 November (the same day that TS 35W became a tropical storm in the SCS), the amount of deep convection in the low latitudes of the WNP began to increase in association with lowering pressure throughout Micronesia. This was accompanied by the onset of a near-equatorial trough along 5°N. On 03 November, the deep convection consolidated into two distinct clusters: one centered near 8°N 150°E (which became Super Typhoon Dale (36W)), and the other centered near 7°N 138°E (which became TS Ernie (37W)). **Super Typhoon Dale (36W)** became a large and very intense typhoon with an extensive area of monsoon gales to its south and southwest. The equatorial westerly wind burst that preceded Dale's formation was accompanied by extremely low sea-level pressure reports along the equator. Passing 110 nm (205 km) south of Guam late on 07 November, the typhoon generated phenomenal seas and surf which pounded the island for three days. Dale recurved, and on 14 November, it transitioned into an intense extratropical cyclone. **TS Ernie (37W)** originated from a westward moving tropical disturbance first noted on 29 October in the eastern Caroline Islands. For several days the pre-Ernie tropical disturbance moved westward before showing signs of development on 03 November. The system became a tropical storm only a few hours before making landfall in northern Mindanao. Ernie crossed the Philippines and entered the SCS where it reached its peak intensity of 50 kt (26 m/sec). While undergoing a clockwise loop west of Luzon, the system merged with TD 39W, and later moved toward the west-southwest in association with a surge in the northeast monsoon to its north. On 18 November, the weakened TC dissipated in the Gulf of Thailand.

The rest of the November TCs were weak. **TS 38W** (unnamed) — the third unnamed TC of 1996 in the WNP — developed

from an unusually late-in-the-year TUTT cell located northeast of Dale. For nearly eight days (04-12 November), the system moved erratically. The TC dissipated on 12 November when it was located near 22°N 179°W, approximately 180 nm (335 km) east of where it formed late on 04 November. Late on 06 November, a tropical disturbance formed between Dale and Ernie as they were moving toward the west. This disturbance became **TD 39W**. Located within 200 nm (370 km) of one another, TD 39W and Ernie underwent a binary interaction that ended in merger. On 10 November, the weakened TD 39W was absorbed into the circulation of Ernie.

After Dale recurved, and Ernie and TD 39W moved into the SCS, the WNP experienced a break in TC activity associated with rising sea-level pressure (SLP) and light winds at low latitude. After a week-long lull, and although low-latitude SLP remained high, an extensive area of deep convection formed in Micronesia. On 23 November, this area of deep convection evolved into a large monsoon depression centered near Chuuk. Moving northwestward toward Guam, this monsoon depression became **TD 40W**. The depression moved as far north as 18°N, where it ran into a region of enhanced northeasterly low-level flow. The system then became sheared, began to drift toward the southwest, and interacted with some MCSs along its path. The weakened TC dissipated over Mindanao on 02 December.

DECEMBER

After the demise of TD 40W over the southern Philippines on 02 December, activity subsided in the WNP until 10 December when an area of deep convection formed in the SCS. On 13 December, synoptic data indicated that a weak low-level circulation center (LLCC) was located at low latitude east of the Malay peninsula in association with the deep convection in the region. The LLCC moved eastward and became **TD 41W** on 14 December. The depression moved eastward toward Borneo, then on December 16, as it neared the northwest coast of Borneo, it doubled back and moved westward. The TC continued westward and dissipated on 21 December when located approximately 90 nm (165 km) from where it formed.

During mid-December, amounts of deep convection began to increase across Indonesia and eastward along the equator to near 160°E associated with a developing equatorial westerly wind burst (WWB). The WWB gradually strengthened and westerly winds increased to 40 kt (21 m/sec) with gusts to 50 kt (26 m/sec) extending from Indonesia to 155°E. The band of strong low-level westerly winds persisted between the axes of twin low-latitude monsoon troughs. A total of five TCs — two in the Northern Hemisphere (Fern (42W) and Greg (43W)), and three in the Southern Hemisphere (Ophelia (11S), Phil (12P), and Fergus (13P)) — formed along the respective monsoon trough axis.

Typhoon Fern (42W) formed southeast of Guam at low latitude in association with a Southern Hemisphere twin, Fergus (13P). Fern moved west-northwestward, and turned to the north on Christmas Day when it was located just west of Yap. Fern attained its maximum intensity of 80 kt (41 m/sec) on 26 December. The weakening typhoon dissipated 150 nm (280 km) northeast of Saipan on the last day of the month.

The final WNP TC of 1996, **TS Greg (43W)**, developed in the SCS mid-way between Vietnam and Borneo. Greg moved eastward at low latitude for its entire life, apparently steered by the strong westerly winds associated with the intense WWB to its south. The TC reached its peak intensity of 45 kt (23 m/sec) on Christmas Day, and the next morning made landfall in an unusual location: the northern tip of Borneo near the city of Kota Kinabalu in the East Malaysian State of Sabah. Greg was responsible for loss of life and extensive damage to property in Sabah. At least 124 lives were reported lost with another 100 reported missing primarily due to flooding from torrential rains. Greg continued its unusual east-southeastward motion and dissipated on 27 December at 3°N in the eastern Celebes Sea.

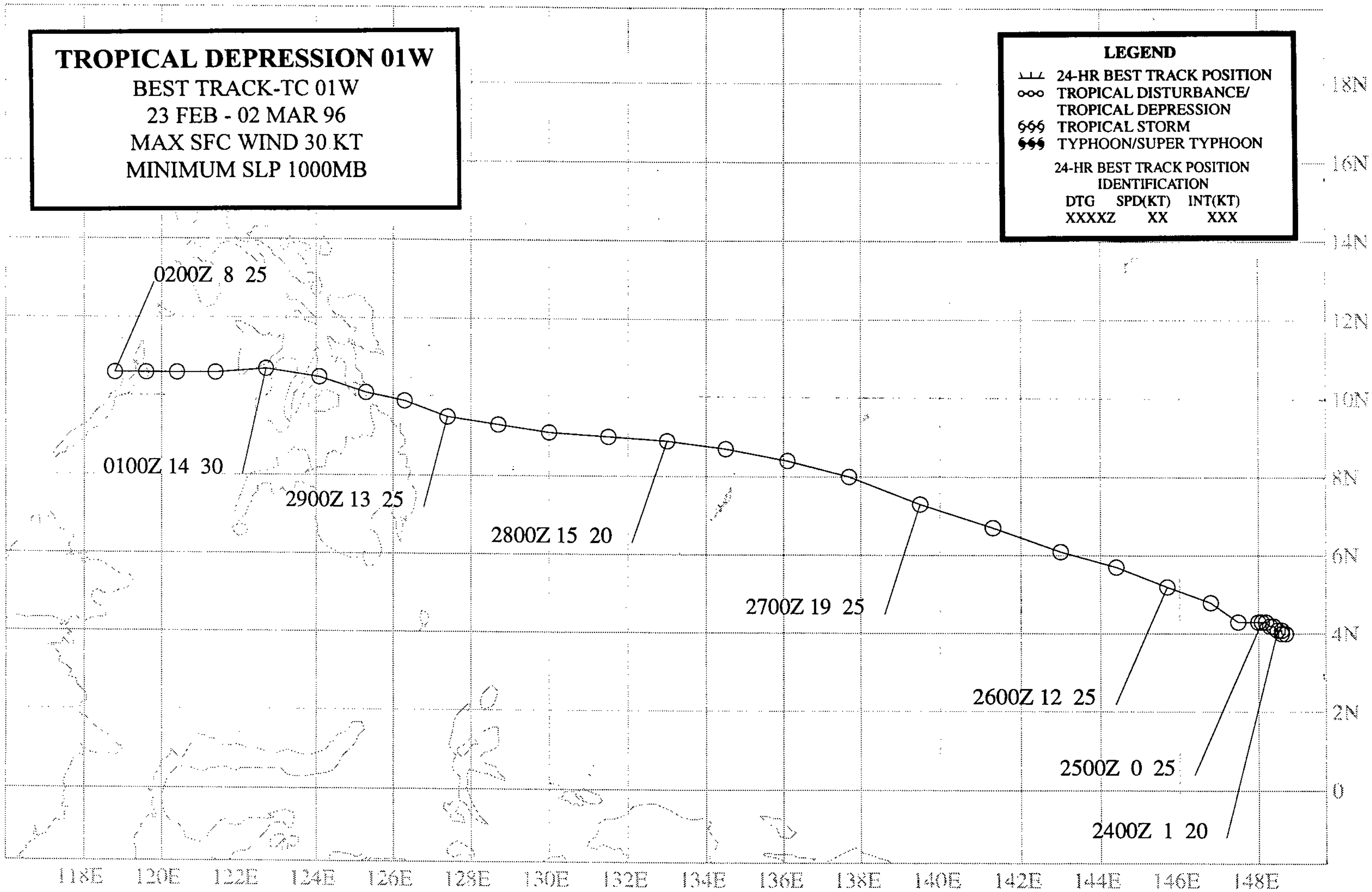

TROPICAL DEPRESSION 01W
BEST TRACK-TC 01W
23 FEB - 02 MAR 96
MAX SFC WIND 30 KT
MINIMUM SLP 1000MB
LEGEND
24-HR BEST TRACK POSITION
TROPICAL DISTURBANCE/
TROPICAL DEPRESSION
TROPICAL STORM
TYPHOON/SUPER TYPHOON
24-HR BEST TRACK POSITION
IDENTIFICATION
DTG SPD(KT) INT(KT)
XXXXZ XX XXX
0200Z 8 25
0100Z 14 30
2900Z 13 25
2800Z 15 20
2700Z 19 25
2600Z 12 25
2500Z 0 25
2400Z 1 20
18N
16N
14N
12N
10N
8N
6N
4N
2N
0
118E
120E
122E
124E
126E
128E
130E
132E
134E
136E
138E
140E
142E
144E
146E
148E

TROPICAL DEPRESSION 01W

The first significant tropical cyclone (TC) of 1996 in the western North Pacific (WNP), Tropical Depression (TD) 01W formed at low latitude in a near-equatorial trough associated with a surge in the monsoonal westerlies (i.e., a westerly wind burst). The tropical disturbance which became TD 01W was first mentioned on the 230600Z February Significant Tropical Weather Advisory when satellite imagery indicated that deep convection was becoming organized on the northeastern end of a monsoonal cloud band along the equator (Figure 3-01-1a). After deep convection along the equator collapsed, a weak TC consolidated in the Northern Hemisphere, and moved westward toward the Philippines (Figure 3-01-1b). Two formation alerts (one at 281300Z and the other at 290430Z) were issued prior to the first warning valid at 290600Z February. The first warning indicated that the intensity of TD 01W was 30 kt (15 m/sec). Although forecast to slowly intensify while crossing the Visayan Island group of the central Philippines, TD 01W remained at 30 kt (Figure 3-01-1c), and then weakened as it approached the South China Sea. The final warning was issued at 011800Z March. No reports of damage or injuries were received.

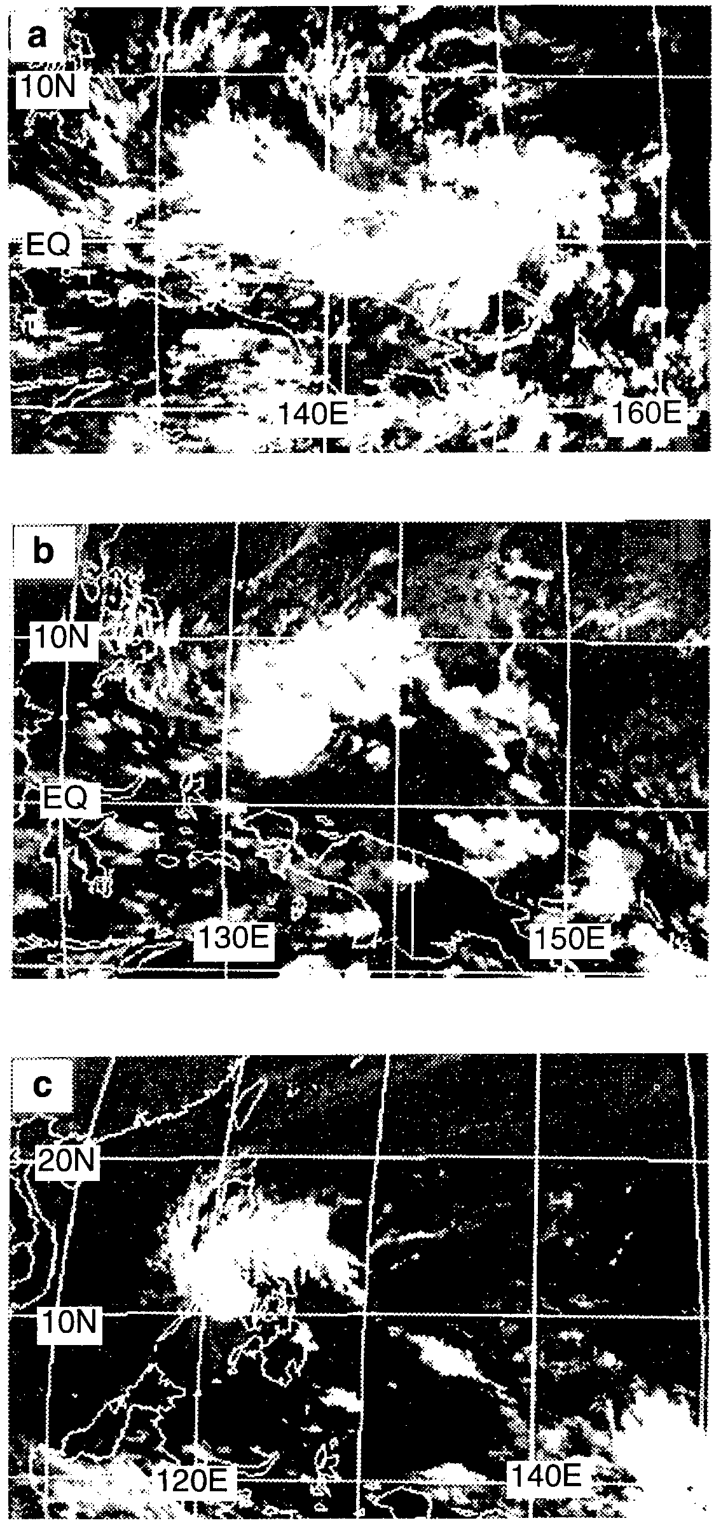

Figure 3-01-1 (a) The tropical disturbance which became TD 01W originated at the northeastern end of a monsoonal cloud band located along the equator. (b) After the equatorial deep convection collapsed, an area of deep convection consolidated at low latitude in the Philippine Sea. (c) TD 01W crosses the central Philippines at its peak intensity of 30 kt (15 m/sec) (Infrared GMS satellite imagery at 240531Z February, 261831Z February, and 010031Z March respectively).

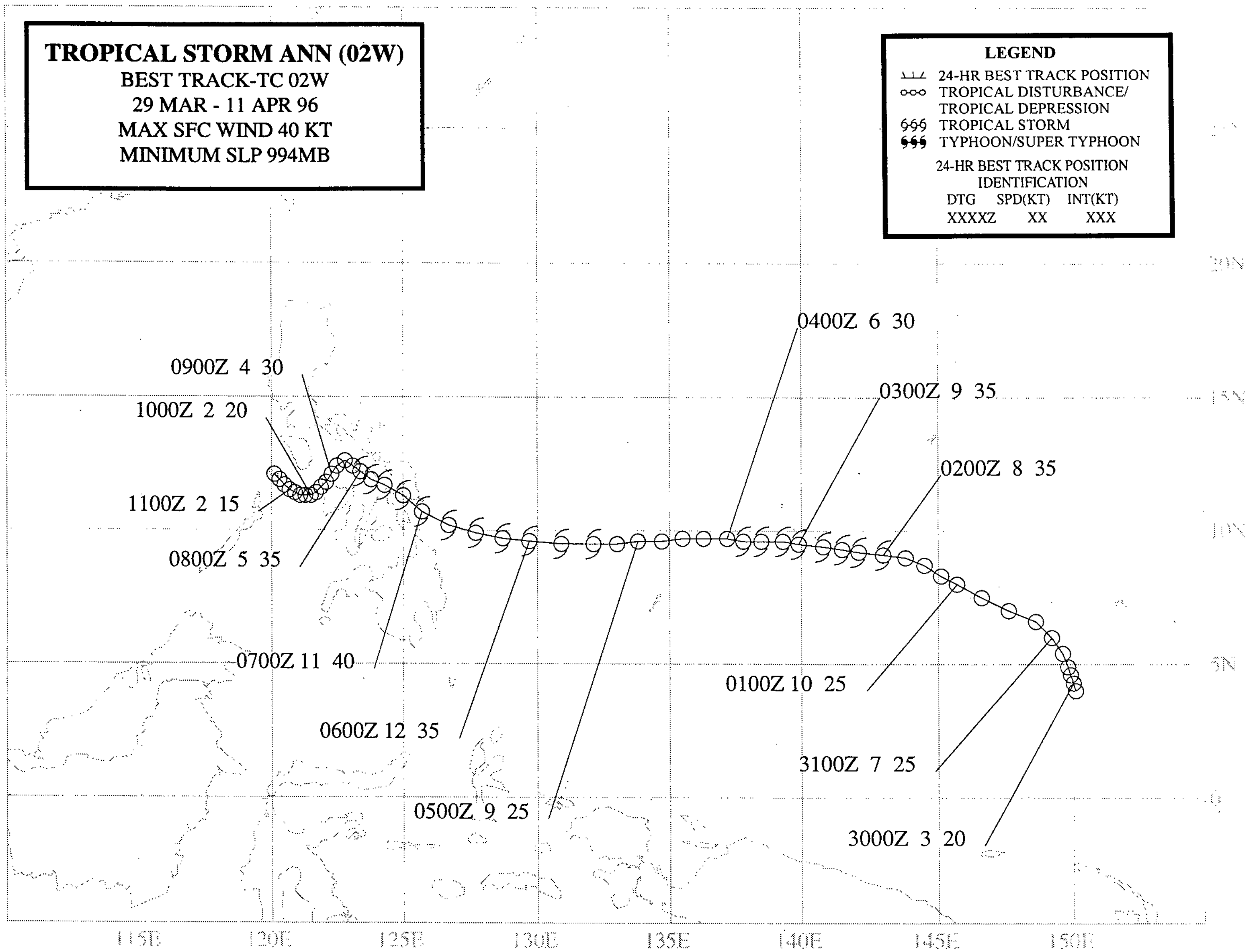

TROPICAL STORM ANN (02W)
BEST TRACK-TC 02W
29 MAR - 11 APR 96
MAX SFC WIND 40 KT
MINIMUM SLP 994MB
LEGEND
24-HR BEST TRACK POSITION
TROPICAL DISTURBANCE/
TROPICAL DEPRESSION
TROPICAL STORM
TYPHOON/SUPER TYPHOON
24-HR BEST TRACK POSITION
IDENTIFICATION
DTG SPD(KT) INT(KT)
XXXXZ XX XXX
0400Z 6 30
0900Z 4 30
0300Z 9 35
1000Z 2 20
0200Z 8 35
1100Z 2 15
0800Z 5 35
0700Z 11 40
0100Z 10 25
0600Z 12 35
3100Z 7 25
0500Z 9 25
3000Z 3 20
20N
15N
10N
5N
0
115E
120E
125E
130E
135E
140E
145E
150E

TROPICAL STORM ANN (02W)

I. HIGHLIGHTS

The first named TC of 1996 in the WNP, Ann formed in the Eastern Caroline Islands. While moving westward, Ann had two peaks of intensity, one while southwest of Guam, and the other as it went ashore in the Philippines. Deep convection associated with Ann deposited as much as five inches of rain in 24 hours on parts of Guam — the value of the monthly average rainfall for this dry-season month.

II. TRACK AND INTENSITY

The tropical disturbance that became Ann was first mentioned on the 280600Z March Significant Tropical Weather Advisory. Comments on this advisory included:

" ... An area of convection is located [in the Caroline Island group]. The area is located in a near equatorial trough with strong easterly trades to the north, while animated visible satellite imagery shows winds with a weak westerly component between the trough and the equator ..."

This disturbance moved steadily northwestward and fluctuations in the amount and organization of its deep convection prompted the JTWC to issue three Tropical Cyclone Formation Alerts (TCFA) prior to the first warning. The first TCFA was issued valid at 302000Z March when its deep convection became better organized. The second TCFA was issued, valid at 312000Z, when the disturbance failed to become better organized, but it was determined that conditions were still favorable for intensification. A third TCFA followed, valid at 012000Z April.

The first warning on Tropical Depression (TD) 02W was released, valid at 020000Z, when microwave imagery defined the low-level circulation and indicated the cyclone possessed wind speeds of 25 kt (13 m/sec). TD 02W was upgraded to Tropical Storm Ann 24 hours later based upon intensity estimates of 35 kt (18 m/sec) from both conventional satellite (i.e., infrared and visible) and microwave imagery. Ann was downgraded to a tropical depression at 040000Z when it became less organized in satellite imagery. A final warning was issued at 041200Z when it was thought that Ann was dissipating over water. The system was soon regenerated to TD 02W on the warning valid at 050000Z when the organization of its deep convection improved (Figure 3-02-1). On the warning valid at 050600Z, TD 02W was once again upgraded to Tropical Storm Ann. Traveling almost due westward along 10°N, Ann remained at minimal tropical-storm intensity until just before it passed through the Philippine archipelago where, at 061800Z, it reached its peak intensity of 40 kt (21 m/sec). Entering the central Philippines, Ann slowed its forward speed and dissipated as a significant tropical cyclone before it could cross into the South China Sea. The final warning was issued valid at 091200Z.

III. DISCUSSION

a. *Position inaccuracies*

During the five day period 010000Z through 060000Z April, the warning position (based primarily on satellite fixes) was displaced 90 to 120 nm (165 to 220 km) to the north of the final best track. The final best track for this period was placed further to the south after a careful re-examination of the synoptic data, coupled with a re-evaluation of the satellite imagery. It is not uncommon for the working best track of poorly defined, westward moving TCs at low latitude to be relocated southward in a final analysis (see the summary of Tropical Storm 35W).

b. *Ann's southern twin?*

As Ann moved westward toward the Philippines along 10°N, a Southern Hemisphere TC — Olivia (25S) — moved westward in near symmetry along 10°S (Figure 3-02-1). Although Ann and Olivia (25S) did not form as classical TC twins as described by Lander (1990), they were, for a short period, situated in near symmetry with respect to the equator as they both moved to the west along their respective near-equatorial trough axes. Ann later dissipated over the Philippines while Olivia recurved in the South Indian Ocean.

IV. IMPACT

No reports of damage or injuries were received. On the positive side, the peripheral rainbands of Ann contributed some much-needed dry-season rainfall to parts of the island of Guam.

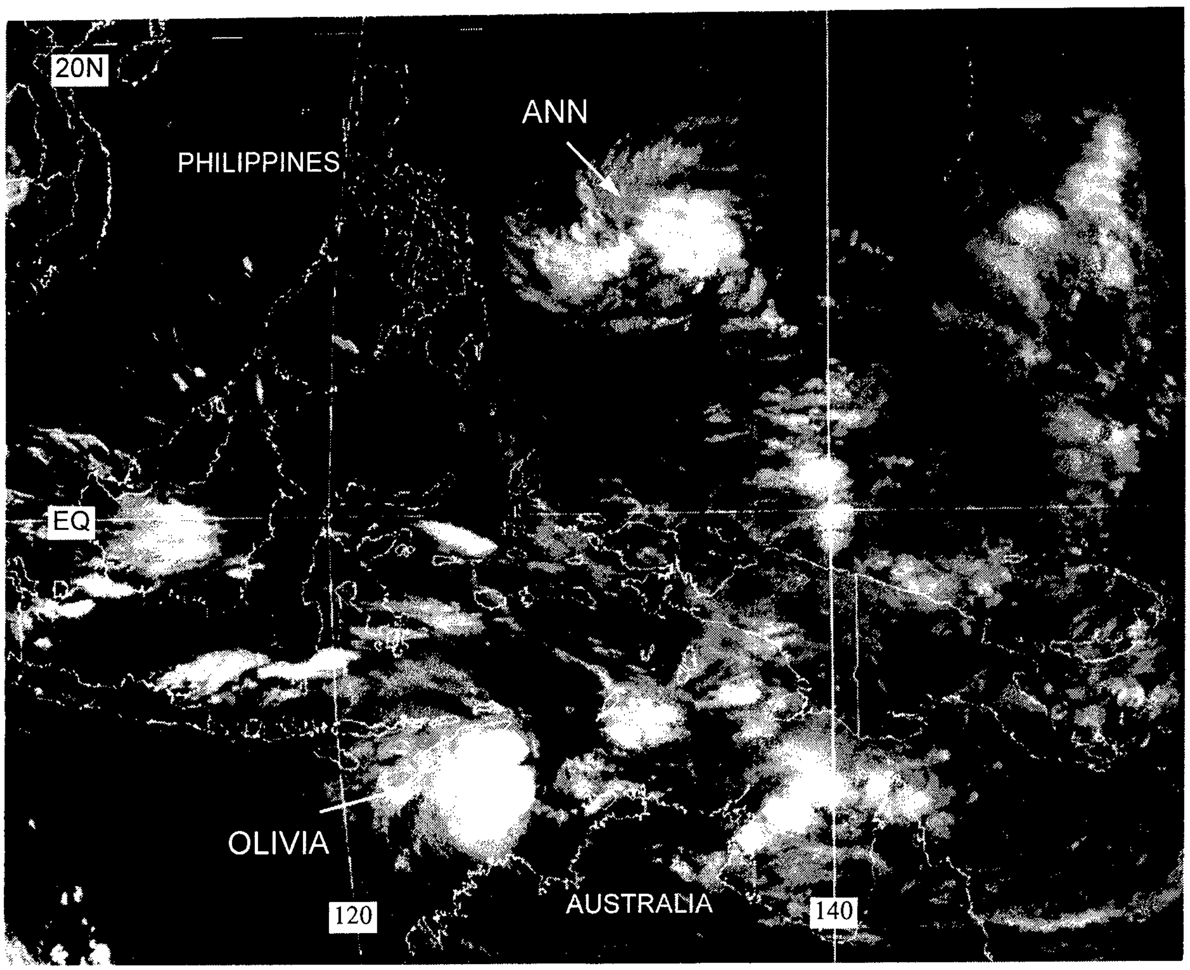

Figure 3-02-1 Tropical Storm Ann moves westward toward the Philippines in near symmetry with the westward moving TC Olivia (25S) (042224Z April infrared GMS imagery).

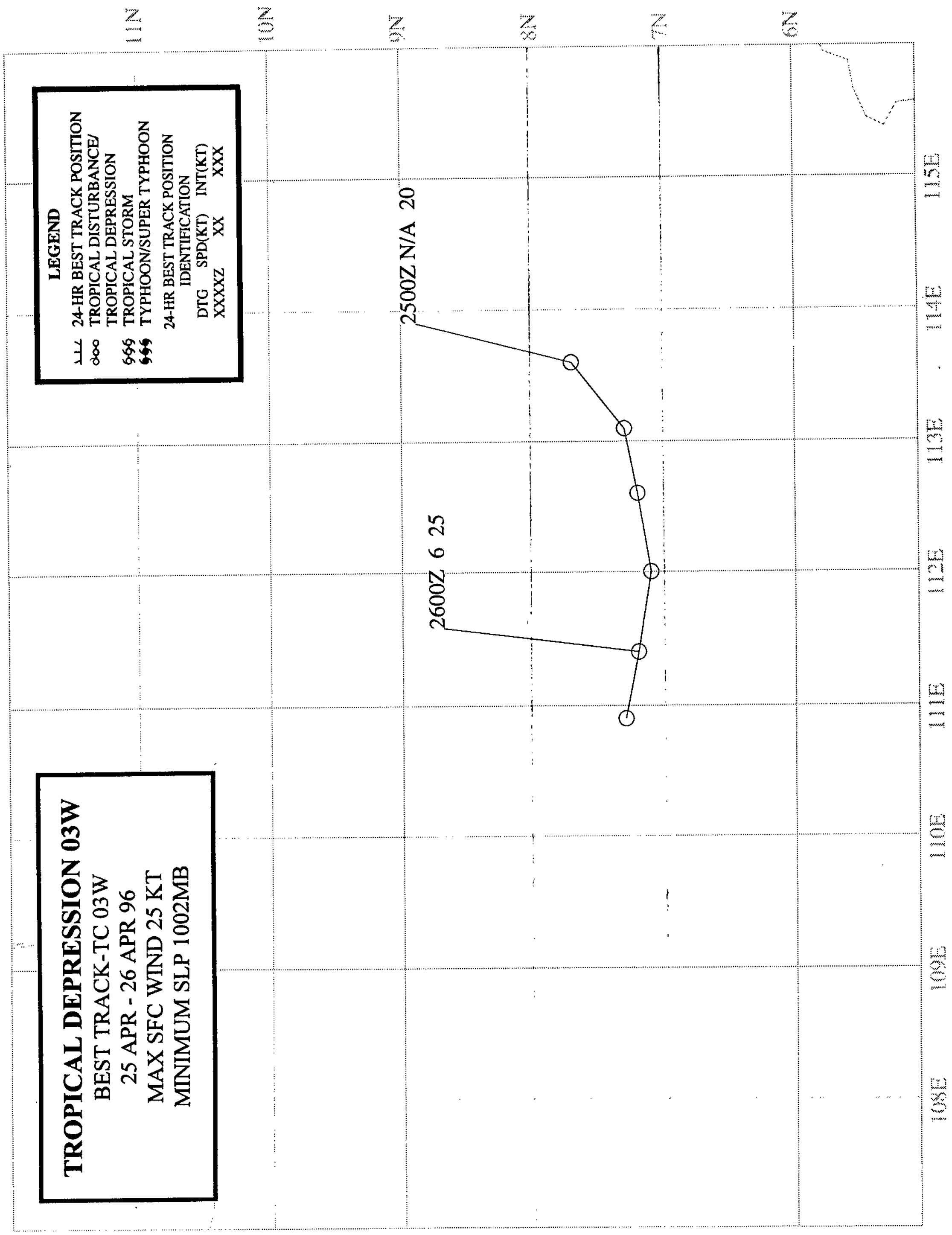
TROPICAL DEPRESSION 03W
BEST TRACK-TC 03W
25 APR - 26 APR 96
MAX SFC WIND 25 KT
MINIMUM SLP 1002MB
LEGEND
24-HR BEST TRACK POSITION
TROPICAL DISTURBANCE/
TROPICAL DEPRESSION
TROPICAL STORM
TYPHOON/SUPER TYPHOON
24-HR BEST TRACK POSITION
IDENTIFICATION
DTG SPD(KT) INT(KT)
XXXXZ XX XXX
2500Z N/A 20
2600Z 6 25
11N
10N
9N
8N
7N
6N
108E
109E
110E
111E
112E
113E
114E
115E

TROPICAL DEPRESSION 03W

Short-lived Tropical Depression (TD) 03W was first mentioned on the 250600Z April Significant Tropical Weather Advisory when satellite imagery and synoptic data showed that a low-level circulation center (LLCC) was associated with an area of persistent deep convection northwest of Borneo (Figure 3-03-1). As the persistent deep convection became better organized, and SSM/I-derived wind speeds of 30 kt (15 m/sec) were observed north and west of the LLCC, the JTWC issued a Tropical Cyclone Formation Alert, valid at 250900Z. Ship reports and satellite intensity estimates indicating wind speeds of 25 kt (15 m/sec) near the LLCC prompted the JTWC to issue the first warning on TD 03W, valid at 251200Z. TD 03W was short-lived, however, and the final warning was issued, valid at 260900Z, when the deep convection became disorganized.

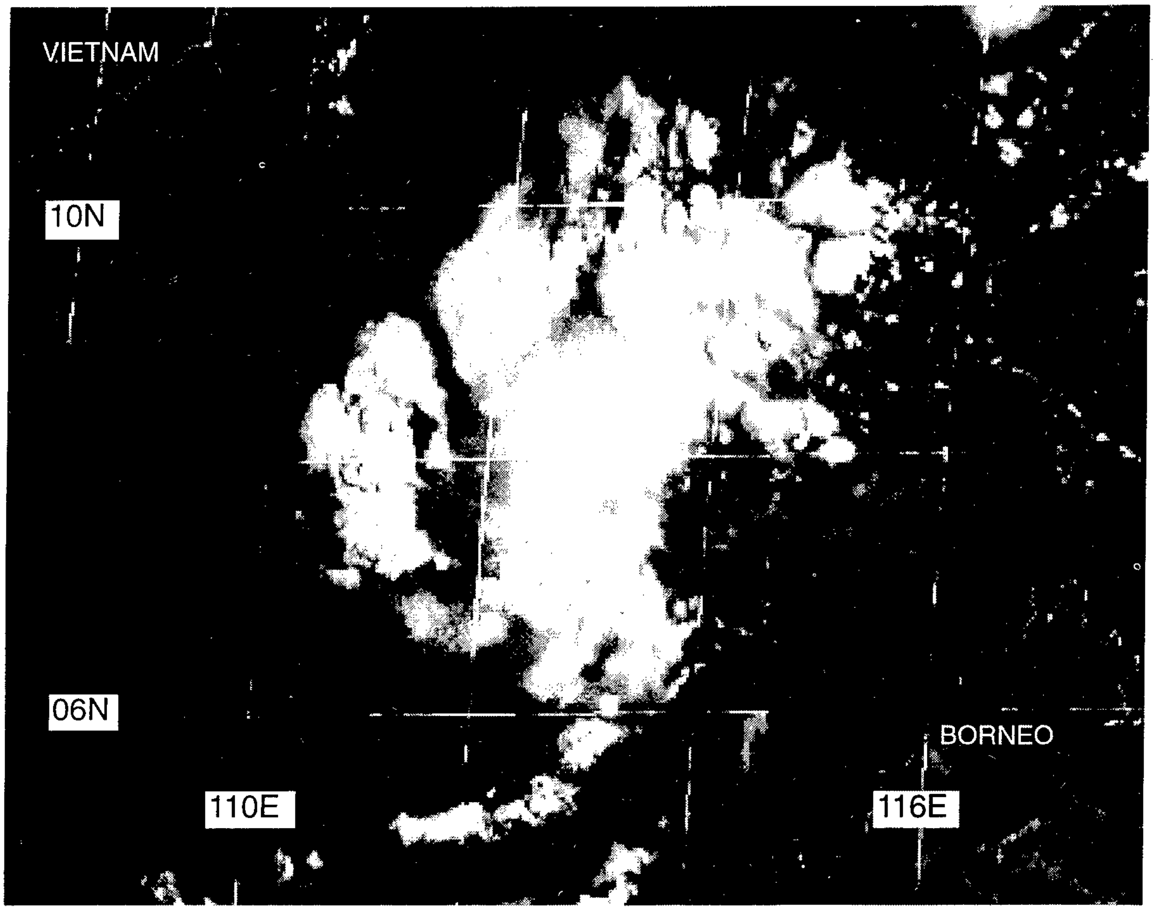

Figure 3-03-1 In the genesis stage of TD 03W, deep convection becomes loosely organized into a cyclonically curved band north and west of a partially exposed LLCC (250331Z April visible GMS imagery).

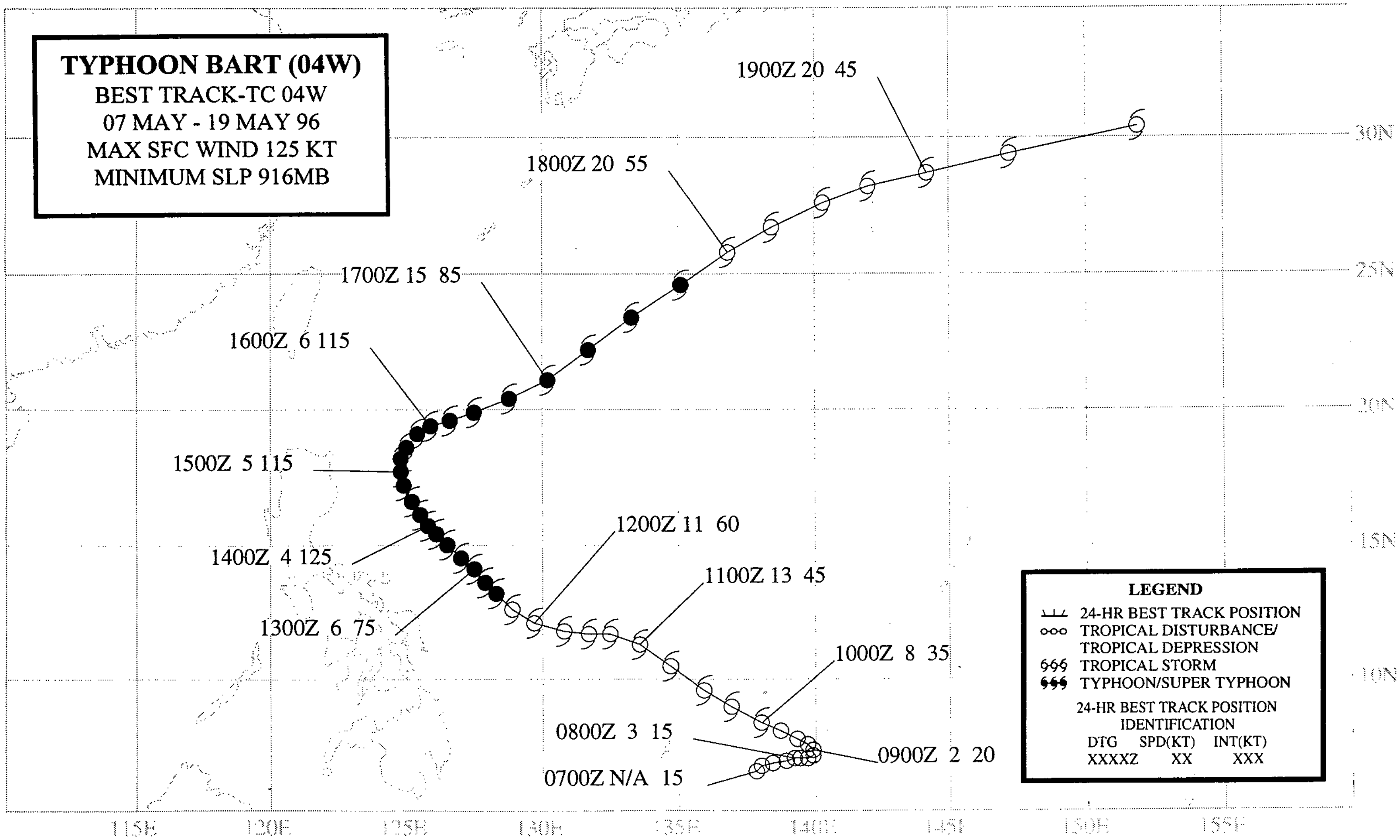
TYPHOON BART (04W)
BEST TRACK-TC 04W
07 MAY - 19 MAY 96
MAX SFC WIND 125 KT
MINIMUM SLP 916MB
1900Z 20 45
1800Z 20 55
1700Z 15 85
1600Z 6 115
1500Z 5 115
1400Z 4 125
1300Z 6 75
1200Z 11 60
1100Z 13 45
1000Z 8 35
0900Z 2 20
0800Z 3 15
0700Z N/A 15
LEGEND
24-HR BEST TRACK POSITION
TROPICAL DISTURBANCE/
TROPICAL DEPRESSION
TROPICAL STORM
TYPHOON/SUPER TYPHOON
24-HR BEST TRACK POSITION
IDENTIFICATION
DTG SPD(KT) INT(KT)
XXXXZ XX XXX
30N
25N
20N
15N
10N
115E
120E
125E
130E
135E
140E
145E
150E
155E

TYPHOON BART (04W)

I. HIGHLIGHTS

Bart was the first western North Pacific (WNP) TC of 1996 to reach typhoon intensity. It became a very intense typhoon, peaking at 125 kt (64 m/sec). Initially moving toward the Philippines, it turned to the north and remained at sea. Pronounced diurnal variations in Bart's central deep convection were noted.

II. TRACK AND INTENSITY

During the first week of May, the tropics of the WNP were dominated by low-level easterly wind flow accompanied by westerly wind flow aloft. A zonally-oriented band of convection stretched east-west across Micronesia south of 10°N. This convection was highly sheared from the west, and possessed a structure more characteristic of the convergence-zone cloud band that normally dominates the central North Pacific; that is, a linear band of disorganized mesoscale convective systems located along the confluence line of the northeast and southeast trades. This synoptic regime slowly changed, and by 05 May, monsoonal low-level westerly winds had penetrated into the WNP eastward to 140°E and south of 5°N. Accompanying the arrival of the monsoonal westerlies, amounts of deep convection increased in the southern portion of the Philippine Sea, and the cirrus outflow from this region became organized into a pattern indicative of an anticyclone aloft.

As amounts of deep convection began to increase in this area, the region of persistent deep convection that became Bart was first noted on the Significant Tropical Weather Advisory valid at 050600Z May. Remarks on the advisory included:

"Convective activity (near 4°N 136°E) has increased.... Visible satellite imagery and synoptic data indicate the presence of a weak circulation beneath diffluent upper-level winds. Surface and gradient level (3000 ft) analysis indicate 10-knot westerly winds along the equator enhancing surface convergence. . . . Minimum sea level pressure is estimated to be 1007 mb. . . ."

For the next four days, this disturbance — which now possessed the characteristics of a monsoon depression (see definitions section) — was slow to gain organization (e.g., well-defined low-level cloud lines, and persistent central convection). Based upon satellite imagery showing the system had acquired a small area of persistent central deep convection associated with well-defined low-level cloud lines, a Tropical Cyclone Formation Alert (TCFA) was issued valid at 090300Z May. Shortly after the TCFA was issue, cloud-top temperatures of the area of central deep convection became colder on infrared satellite imagery, and the first warning on Tropical Depression (TD) 04W was issued valid at 090600Z. Based upon indication of some shearing from the east, and implications of the structure of the system (i.e., a monsoon depression), a slower than normal rate of intensification was forecast.

Eighteen hours later (100000Z), TD 04W was upgraded to Tropical Storm Bart, based upon an improved satellite signature (an increase in the areal extent of very cold central convection), and upon the indication of 35-kt (18-m/sec) surface wind speeds from microwave imagery. A gradual turn from a westward motion to a more northward track was indicated on this warning — a track that would now spare the Philippines a landfall. With relatively low environmental shear, Bart was now forecast to intensify at a normal rate and become a typhoon in 48 hours (i.e., at 120000Z).

Evolving a classic banding-type eye (Dvorak, 1984) (see definitions section), Bart was upgraded to a typhoon at 121200Z. After becoming a typhoon, Bart began to intensify more rapidly, and reached its peak intensity of 125 kt (64 m/sec) at 140000Z (Figure 3-04-1). The estimated fall

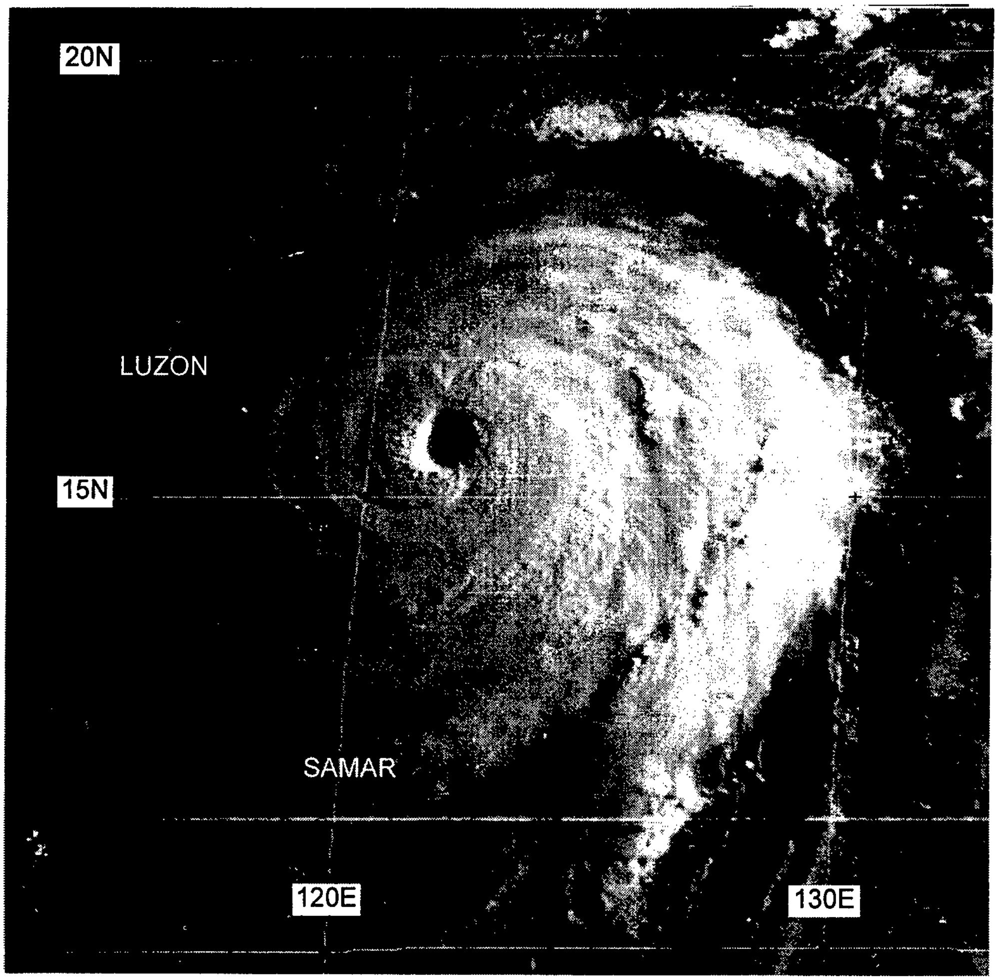

Figure 3-04-1 Bart reaches its peak intensity (132131Z May GMS visible imagery).

of central pressure of 52 mb during the 24-hour period, 130000Z to 140000Z, was sufficient to be classified as rapid intensification (Holliday and Thompson, 1979) (see definitions section).

Twenty-four hours after reaching peak intensity (i.e., at 150000Z), Bart reached its point of recurvature at 18°N, which is the climatological mean latitude of recurvature during May (Shanghai Typhoon Institute, 1990). Following recurvature at 150000Z, Bart did not begin to significantly accelerate until after 170000Z. Also during this period of slow east-northeast motion, its intensity fell only gradually. As Bart began to accelerate on 17 May, its intensity began to decrease — falling below typhoon intensity after 171800Z. On 18 May, its speed of forward motion increased to 20 kt (37 km/hr), and Bart began to shear while undergoing extratropical transition. The final warning was issued valid at 181800Z as Bart lost all its central deep convection and completed its extratropical transition.

III. DISCUSSION

Use of digital Dvorak (DD) numbers

One of the utilities installed in the MIDDAS satellite image processing equipment is an automated routine for computing Dvorak "T" numbers for TCs that possess eyes. The routine, developed by Zehr (personal communication) and programmed by Schaeffer (personal communication), adapts the rules of the Dvorak technique as subjectively applied to enhanced-infrared imagery (Dvorak, 1984) in order to arrive at an objective T number, or "digital Dvorak" T number (hereafter

referred to as DD numbers). Infrared imagery is available hourly from the GMS satellite, and hourly DD numbers were calculated for all of the typhoons of 1996.

The DD numbers presented herein are experimental, and methods for incorporating them into operational practice are being explored. In some cases, the DD numbers differ substantially from the warning intensity and also from the subjectively determined T numbers obtained from application of Dvorak's technique. The output of the DD algorithm, when performed hourly, often undergoes rapid and large fluctuations. The fluctuations of the DD numbers may lay the ground work for future modifications to the current methods of estimating tropical cyclone intensity from satellite imagery. The discussion of the behavior of the time series of the DD numbers for Bart, and for some of the other typhoons of 1996, is intended to highlight certain aspects of the DD time series that may prove to have important research and/or warning implications.

In Dvorak's 1975 and 1984 papers, he advises that the intensity estimation from satellite imagery be made at 24-hour intervals in order to remove any possible diurnal cycles that the TC might be undergoing. Dvorak further claims that the intensity of a TC is not influenced by diurnal changes in the central convection. Diurnal variations of convection reported to occur in TCs are similar to those reported to occur over the marine tropics in general: a peak in the amount of very cold cloud tops during the early morning hours with warmer cloud-top temperatures during the afternoon (Dvorak, 1985; Zehr, 1992). Observations by Black and collaborators (e.g., Black, 1983; Black et al., 1986; Black and Marks, 1987) show that major cold convective eruptions in TCs tend to be initiated in the early morning.

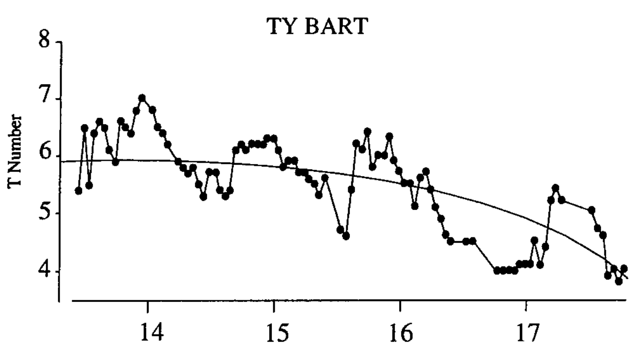

Figure 3-04-2 Bart's DD time series for the period 131030Z May through 171530Z May.

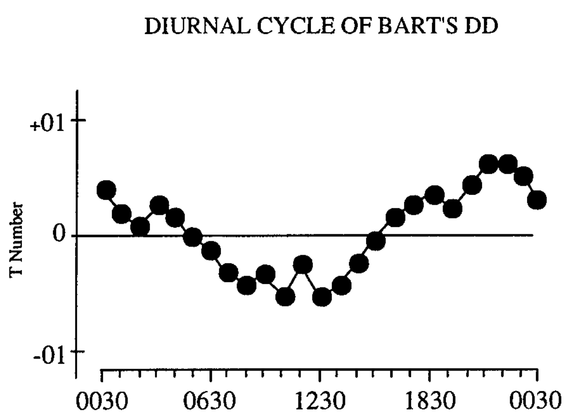

Figure 3-04-3 The diurnal cycle of Bart's DD time series as obtained by averaging the DD numbers at each hour during the period 131030Z May through 160930Z.

Bart is one of only a few cases during the past two years in which a strong diurnal cycle can be found in the time series of its DD numbers (Figure 3-04-2). Although the DD number is based upon both the cloud-top temperature of the eye-wall cloud and the temperature within the eye, the strong diurnal cycle in Bart's DD time series (Figure 3-04-3) is certainly linked to a diurnal cycle of the eye-wall cloud-top temperatures. The DD time series of Bart has an unusually strong diurnal cycle when compared with those of other typhoons of 1996 and with those typhoons of 1995 for which the DD time series was compiled (see the 1995 ATCR). Consistent with Dvorak's rules, Bart's warning and best track intensities do not contain the large diurnal fluctuations that appear in its DD time series.

IV. IMPACT

No reports of significant damage or injuries were received at the JTWC.

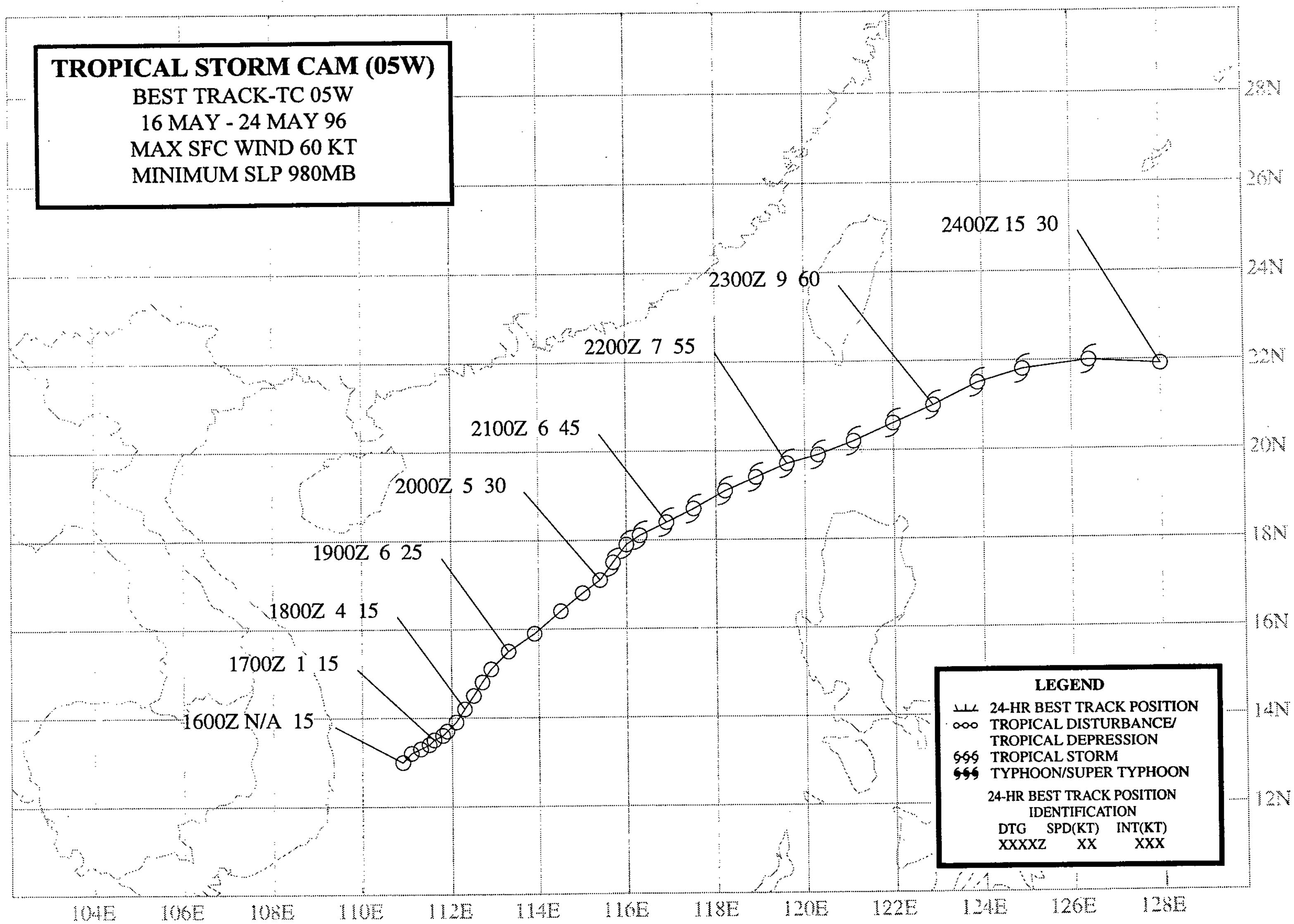

TROPICAL STORM CAM (05W)
BEST TRACK-TC 05W
16 MAY - 24 MAY 96
MAX SFC WIND 60 KT
MINIMUM SLP 980MB
1600Z N/A 15
1700Z 1 15
1800Z 4 15
1900Z 6 25
2000Z 5 30
2100Z 6 45
2200Z 7 55
2300Z 9 60
2400Z 15 30
LEGEND
24-HR BEST TRACK POSITION
TROPICAL DISTURBANCE/
TROPICAL DEPRESSION
TROPICAL STORM
TYPHOON/SUPER TYPHOON
24-HR BEST TRACK POSITION
IDENTIFICATION
DTG SPD(KT) INT(KT)
XXXXZ XX XXX
28N
26N
24N
22N
20N
18N
16N
14N
12N
104E
106E
108E
110E
112E
114E
116E
118E
120E
122E
124E
126E
128E

TROPICAL STORM CAM (05W)

I. HIGHLIGHTS

Originating from a monsoon depression in the South China Sea (SCS), Cam moved toward the east-northeast for its entire life. While at peak intensity, it passed through the Luzon Strait and then slowly weakened as it drifted eastward into the Philippine Sea and dissipated.

II. TRACK AND INTENSITY

As Typhoon Bart (04W) was moving eastward while located south of Japan, cloudiness began to increase in the southwesterly monsoon flow across the SCS and extended east-northeastward toward Bart. Most of the deep convection associated with this monsoon flow was located within the SCS in the form of a large ensemble of mesoscale convective systems (MCS). The ensemble of MCSs showed some signs of low-level organization around a weak low-level cyclonic circulation, and extensive cirrus outflow indicative of anticyclonic outflow aloft. These structural attributes are typical of a monsoon depression (see Appendix A and the Discussion). The system was first mentioned on the Significant Tropical Weather Advisory valid at 170600Z May. Remarks on this advisory included:

" . . . An area of convection is located [in the South China Sea]. . . . Satellite imagery and synoptic data indicate an area of strong convergence being driven by monsoon flow in a sharp trough. . . ."

The organization of the deep convection within this monsoon depression slowly improved, and a Tropical Cyclone Formation Alert was issued valid at 181630Z. The broad circulation center of this system, as defined by low-level cloud lines and by the center of symmetry of the extensive cirrus outflow, appeared to be drifting very slowly toward the northeast.

Further improvements in the low-level organization coupled with a consolidation of persistent convection closer to the low-level circulation center (Figure 3-05-1) prompted the JTWC to upgrade the system to Tropical Depression (TD) 05W on the warning valid at 181800Z. Slow northeastward motion was occurring (and was forecast to continue), as deep southwesterly monsoonal flow dominated the steering.

During the daylight hours of 20 May, the convection near the center of TD 05W increased and deepened (i.e., expanded and became colder on infrared satellite imagery). The primary and peripheral cloud bands became more tightly curved and better organized around the low-level circulation center (LLCC) (Figure 3-05-2). Given these improvements in the satellite signature, TD 05W was upgraded to Tropical Storm Cam on the warning valid at 200600Z. Motion continued toward the northeast under the influence of southwesterly steering that was dominated by strong monsoon southwest winds to the south of the system.

Continuing on a relatively slow east-northeast track, Cam intensified. The peak intensity of 60 kt (31 m/sec) occurred as Cam moved through the Luzon Strait on the morning of 23 May. At this time, infrared satellite imagery (Figure 3-05-03a) indicated a tightly wound primary cloud band, and visible satellite imagery (Figure 3-05-03b) indicated the presence of a ragged eye.

After passing through the Luzon Strait, Cam accelerated eastward within deep westerly flow in the subtropics. It also weakened under the influence of westerly shear. The final warning was issued valid at 240000Z as the remnants of Cam entered the mei-yu front (which stretched eastward from Taiwan) and dissipated.

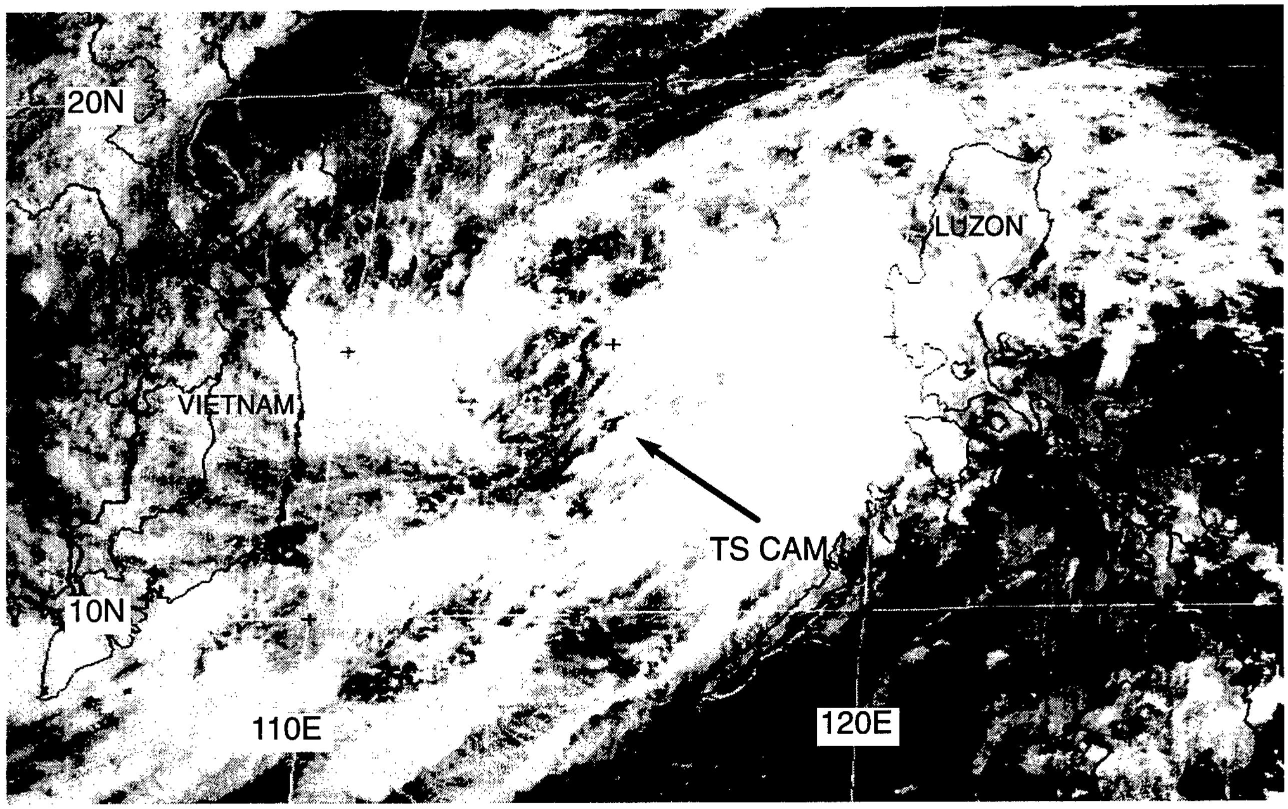

Figure 3-05-1 Near the time of the first warning, the disturbance that became Cam is organized as a monsoon depression (182331Z May visible GMS imagery).

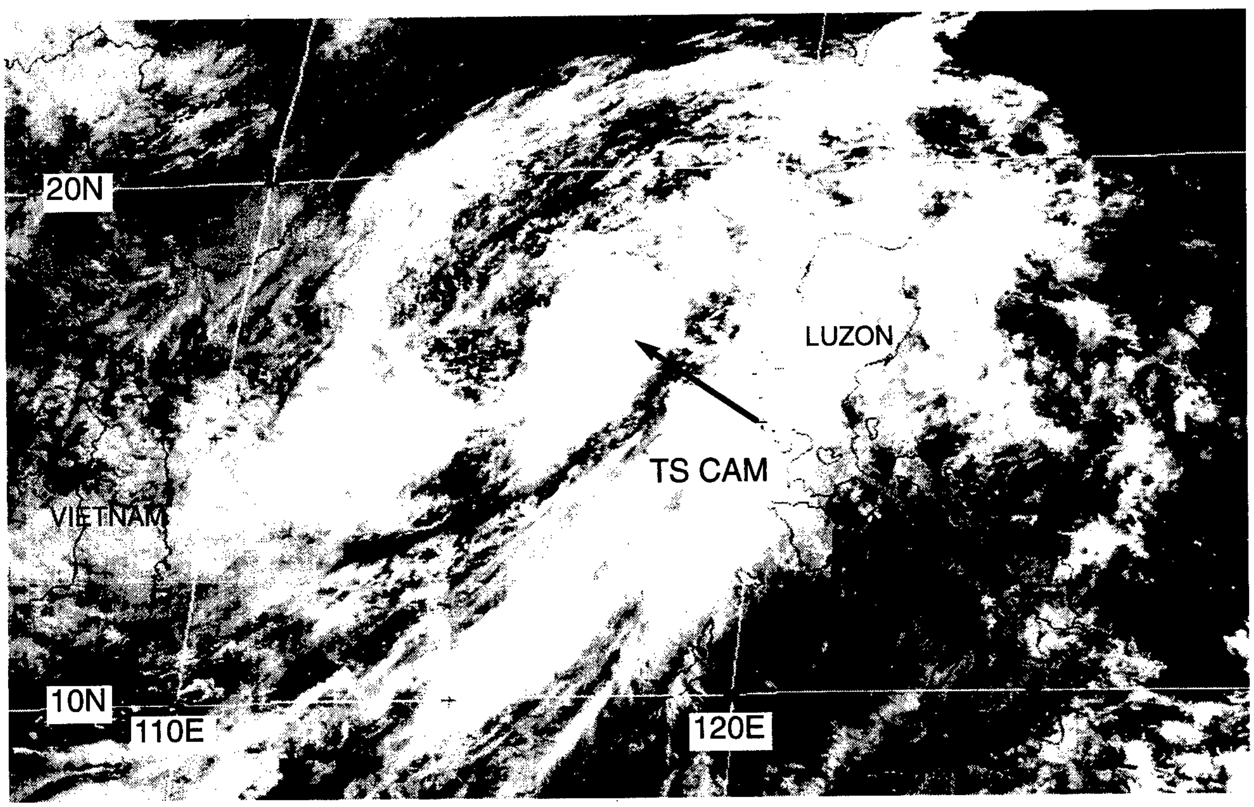

Figure 3-05-2 Deep convection has consolidated near the low-level circulation center marking the transition of the pre-Cam monsoon depression into a tropical storm (192331Z May visible GMS imagery).

III. DISCUSSION

a. The Monsoon Depression

Dvorak (1975, 1984) developed techniques for estimating the intensity of TCs from satellite imagery. His techniques are now used worldwide. The TC pattern types identified by Dvorak will be referred to as conventional TCs. In the Dvorak classification scheme, persistent deep convection must be located near the LLCC in order to initiate classification. The intensity of the TC is determined by several properties of the deep convection (e.g., the proximity of the low-level circulation center to the deep convection, the size of the central dense overcast, the cloud-top temperatures and

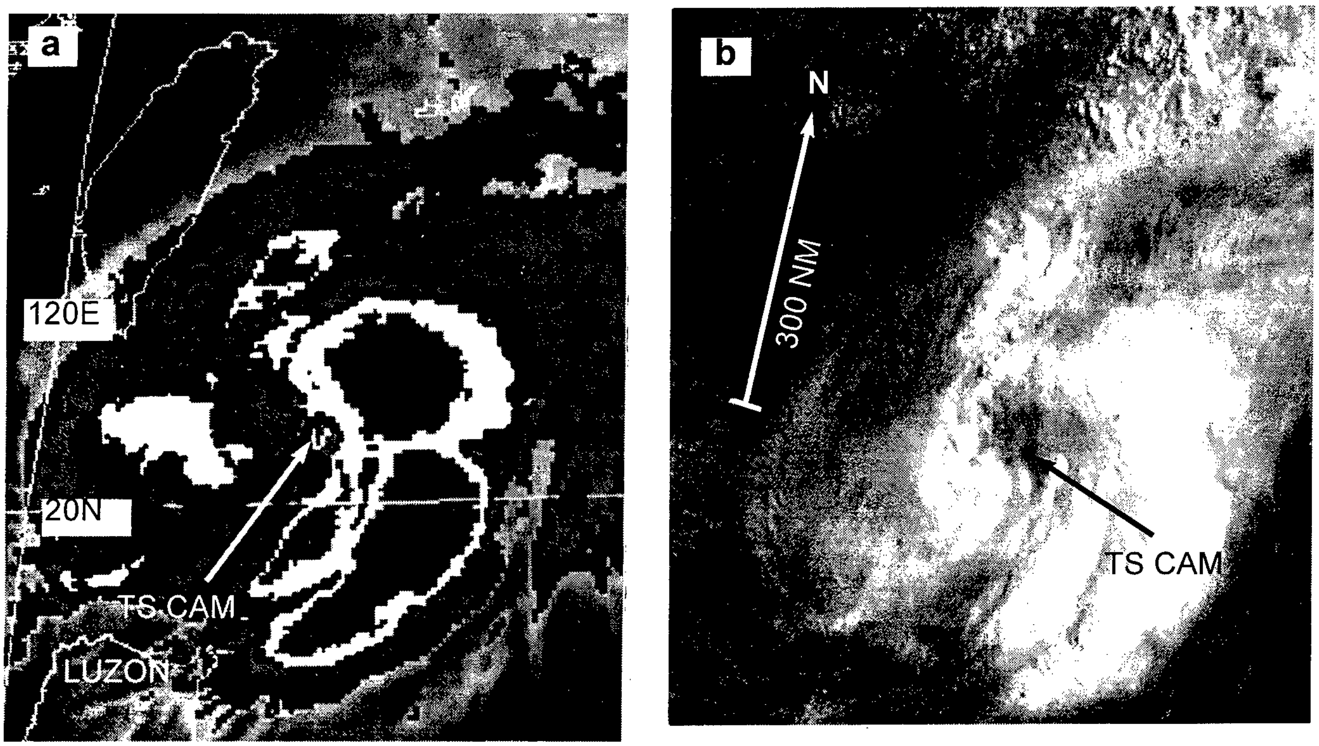

Figure 3-05-3 Cam at peak intensity: (a) 222331Z May enhanced infrared GMS imagery, and (b) 222331Z May visible GMS imagery.

horizontal width of the eye wall cloud, the width and extent of peripheral banding features). The basic TC data types identified by Dvorak are:

1) the "curved band" pattern (Figure 3-05-4a, b);
2) the "shear" pattern (Figure 3-05-4c, d);
3) the "central dense overcast" pattern (Figure 3-05-4e, f); and,
4) the "eye" pattern (Figure 3-04-4g, h).

This set of basic TC data types comprise the suite of conventional TCs.

Some conventional TCs that form in the WNP start out as monsoon depressions. The monsoon depression is a type of cyclone in the tropics that differs in several ways from the conventional types of TCs as described in Dvorak's work. The canonical monsoon depression forms over the northern Bay of Bengal in summer, and tracks west-northwestward across northeastern India (Ramage, 1971). These monsoon depressions have been studied for decades (e.g., Ramanathan and Ramakrishnan, 1932; Desai and Koteswaram, 1951; and Ramaswamy, 1969). Later, it was realized that monsoon depressions with structures similar to those of the Indian monsoon depressions occur in the Australian tropical region (Davidson and Holland, 1987), in the tropics of the western North

Pacific (JTWC, 1993), and over the deep tropics of Africa. The monsoon depression differs from conventional TCs in some respects:

1) very large size (the outer-most closedisobar may have a diameter on the order of 1000 km);

2) a lack of persistent deep convection near the LLCC (most of the deep convection in monsoon depressions is loosely organized in clusters or bands displaced from a few to several hundred kilometers from the low-level circulation center); and,

3) a low-level wind distribution that features a 200-km diameter light-wind core which may be partially surrounded by areas of gales or even storm force winds.

Because of the structure of monsoon depressions (e.g., their lack of persistent central deep convection), the use of Dvorak's techniques to estimate their intensity may be a misapplication. When applied to monsoon depressions, Dvorak's techniques yield intensities which are below the maximum winds that are usually present in areas displaced a few hundred kilometers from the LLCC. The intensity estimates yielded by Dvorak's techniques for monsoon depressions may, however, be representative of the lighter winds near their LLCCs.

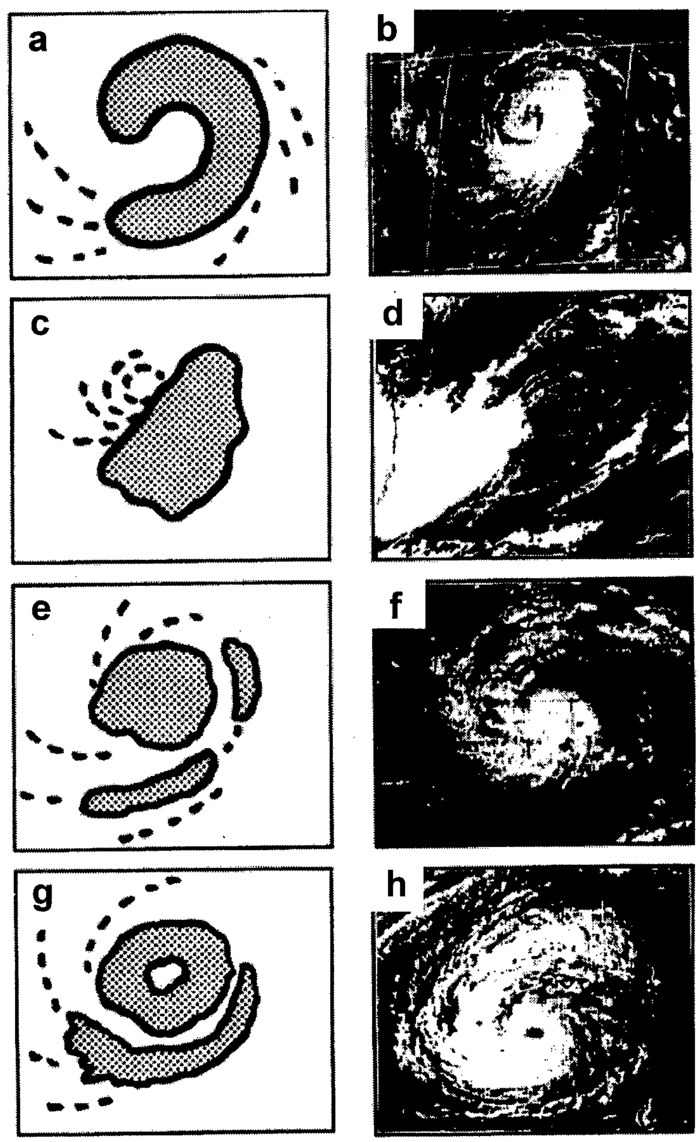

Figure 3-05-4 Schematic illustration (left column) and representative satellite imagery (right column) of Dvorak's (1975) basic tropical cyclone data types: (a,b) the "curved band" pattern; (c,d) the "shear" pattern; (e,f) the "central dense overcast" pattern; and, (g,h) the "eye" pattern.

Monsoon depressions can evolve into conventional TCs. As they slowly intensify, many monsoon depressions observed over the WNP eventually acquire persistent central deep convection and become conventional TCs. An unresolved question remains concerning the transition of a monsoon depression into a conventional TC: does the monsoon depression become the conventional TC, or does a conventional TC form within the circulation of the monsoon depression?

Cam began as a monsoon depression in the South China Sea. Initially it was a large ensemble of mesoscale convective systems embedded within a region of lowered sea-level pressure. It lacked persistent central deep convection, and the maximum winds in the system were displaced outward from the low-level circulation center, particularly to the south where monsoonal flow was strong. Eventually, as the system moved toward the northeast, circulation intensified and persistent central deep convection became established, marking its transition to a conventional TC.

b. *Unusual motion*

Persistent eastward motion of a TC at low latitude is unusual. Cam moved eastward for its entire track: forming near 13°N in the South China Sea it moved slowly toward the east-northeast for its entire track and eventually dissipated in the subtropics at 22°N. Most cases of eastward motion of a TC at low latitude in the WNP can be attributed to the influence of the monsoon circulation on the steering flow. In Cam's case, the deep southwesterly monsoon flow to its south was, for much of its track, the dominant flow asymmetry responsible for its northeastward motion. Monsoonal influences on TC motion form an important part of Carr and Elsberry's "Systematic and Integrated Approach" to TC forecasting (see Chapter 1).

IV. IMPACT

No reports of significant damage or injuries were received at the JTWC.

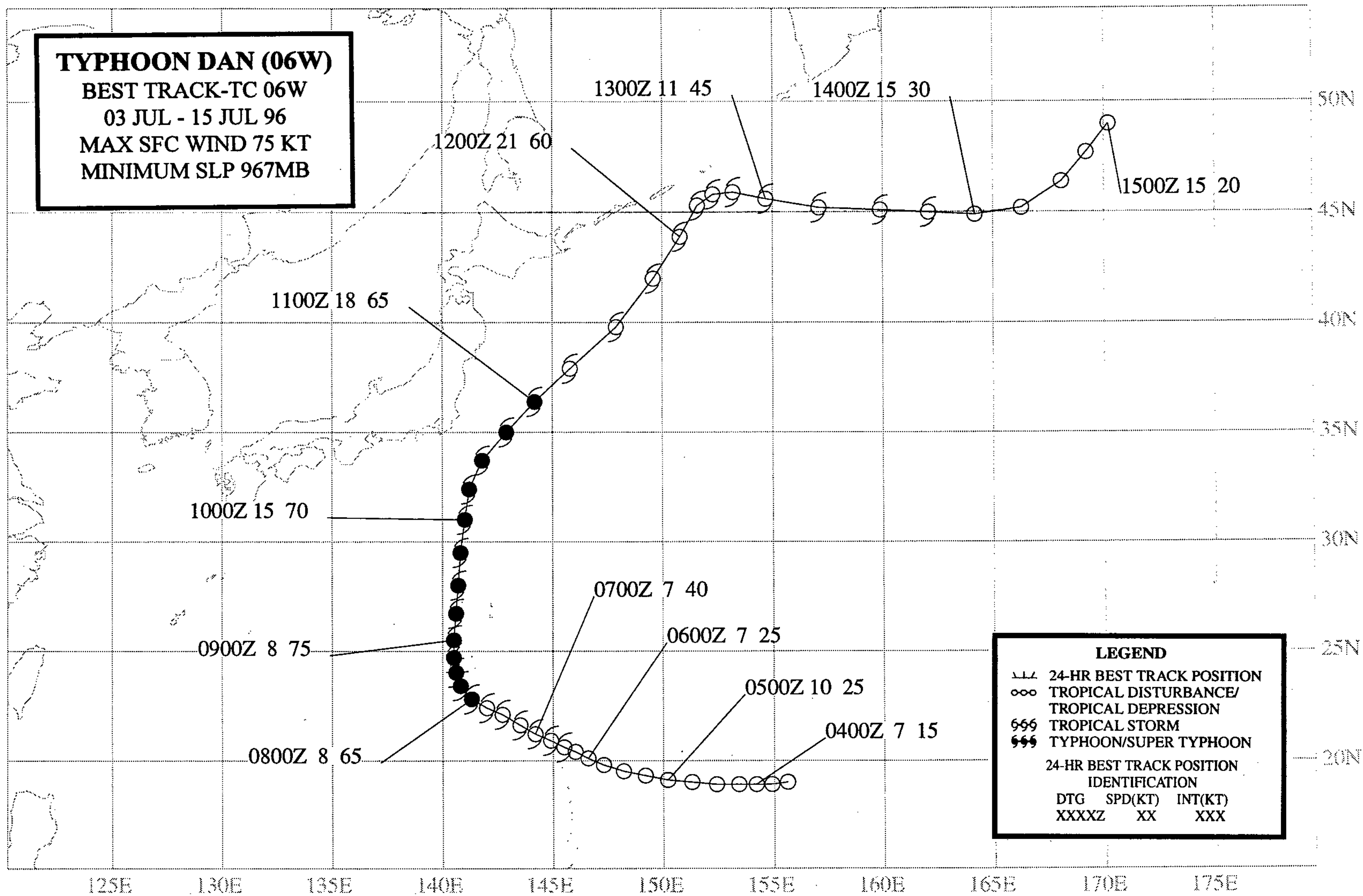

TYPHOON DAN (06W)
BEST TRACK-TC 06W
03 JUL - 15 JUL 96
MAX SFC WIND 75 KT
MINIMUM SLP 967MB
1300Z 11 45
1400Z 15 30
1500Z 15 20
1200Z 21 60
1100Z 18 65
1000Z 15 70
0900Z 8 75
0800Z 8 65
0700Z 7 40
0600Z 7 25
0500Z 10 25
0400Z 7 15
LEGEND
24-HR BEST TRACK POSITION
TROPICAL DISTURBANCE/
TROPICAL DEPRESSION
TROPICAL STORM
TYPHOON/SUPER TYPHOON
24-HR BEST TRACK POSITION
IDENTIFICATION
DTG SPD(KT) INT(KT)
XXXXZ XX XXX
50N
45N
40N
35N
30N
25N
20N
125E
130E
135E
140E
145E
150E
155E
160E
165E
170E
175E

TYPHOON DAN 06W

I. HIGHLIGHTS

After Cam (05W) dissipated in the mei-yu front during the last week of May, there were no significant TCs in the WNP until early July when Dan formed. The tropical disturbance which became Dan was associated with the tropical upper-tropospheric trough (TUTT) and with cyclonic circulations (TUTT cells) within it. Scatterometer data received on 07 July resulted in JTWC doubling the radius of gales on the warning, and ship reports of 60 kt (31 m/sec) provided crucial ground truth for the intensity after Dan recurved and was becoming extratropical.

II. TRACK AND INTENSITY

During June, the WNP tropics were inactive. There were no significant TCs, amounts of deep convection were below normal, low-level winds were anomalously easterly and upper-level winds were anomalously westerly (Climate Prediction Center (CPC), 1996). In early July, the Southwest Monsoon remained inactive in the WNP with large-scale climatic wind anomalies similar to those of June. The tropical disturbance which became Dan was associated with the TUTT (see the discussion section), and first appeared as an inverted trough in the low-level easterly flow (Figure 3-06-1a, b). This disturbance was first mentioned on the 031700Z July Significant Tropical Weather Advisory. This advisory included the comments:

". . . An area of convection is located near 21N 155E. Satellite imagery and synoptic data indicate a closed circulation exists within a . . . TUTT. Animated infrared satellite imagery indicates the circulation of this TUTT cell has likely built down to the mid-levels of the atmosphere. Convection near the center of the TUTT cell has improved over the past 6 to 12 hours. . . ."

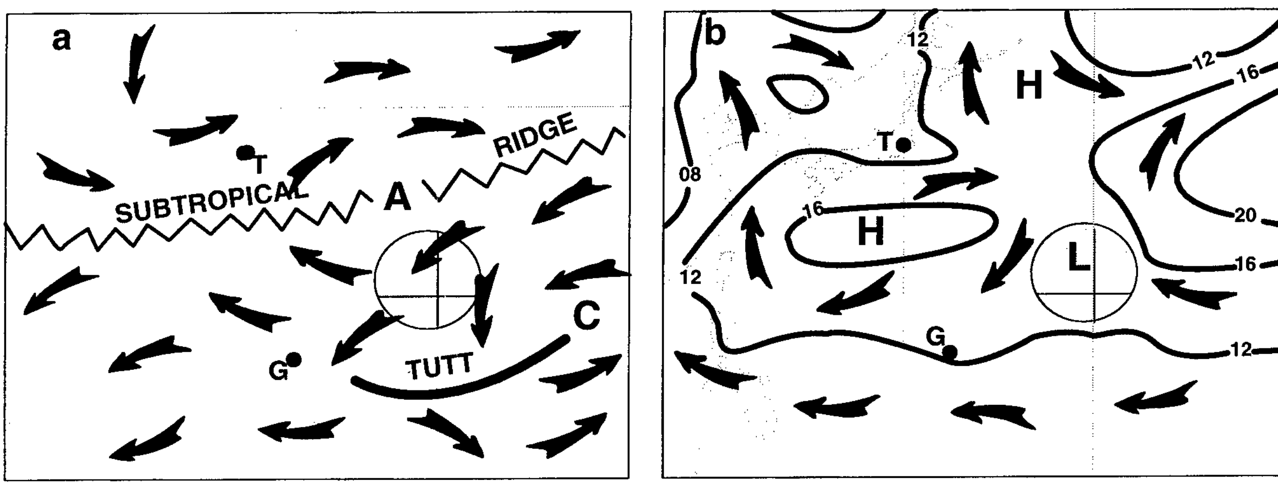

Figure 3-06-1 (a) An area of deep convection (shaded circle) forms in the diffluent northeasterly flow between the axis of the TUTT and the subtropical ridge at 200 mb. (b) At the surface, the area of deep convection (shaded circle) is associated with an inverted trough in the easterly flow southwest of a subtropical high. Arrows depict wind direction, A = anticyclone, C = TUTT cell, L = low pressure, G = Guam, and T = Tokyo. Analyses are adapted from the 021200Z July NOGAPS 200-mb and SLP products.

When synoptic data showed that a low-level cyclonic circulation was located beneath an area of organized deep convection, the JTWC issued a Tropical Cyclone Formation Alert, valid at 041951Z. At this time, the LLCC and most of the deep convection were located to the northeast of

a TUTT cell. The first warning on Tropical Depression (TD) 06W was issued, valid at 050000Z, based upon satellite intensity estimates of 25 kt (13 m/sec).

Dan intensified to a tropical storm at 061200Z, and at 080000Z became a typhoon (Figure 3-06-2). A scatterometer pass over the cyclone at 071304Z (Figure 3-06-3) resulted in a large increase in the radius of gales reported on the warning valid at 071800Z (see the discussion). After becoming a typhoon, Dan turned toward the north and reached its peak intensity of 75 kt (39 m/sec). Moving on a poleward-oriented track, Dan's intensity changed very little for three days following the peak: at 100000Z the intensity was 70 kt (36 m/sec), at 110000Z it was 65 kt (33 m/sec), and at 120600Z it was still at 60 kt (31 m/sec) despite reaching 45°N.

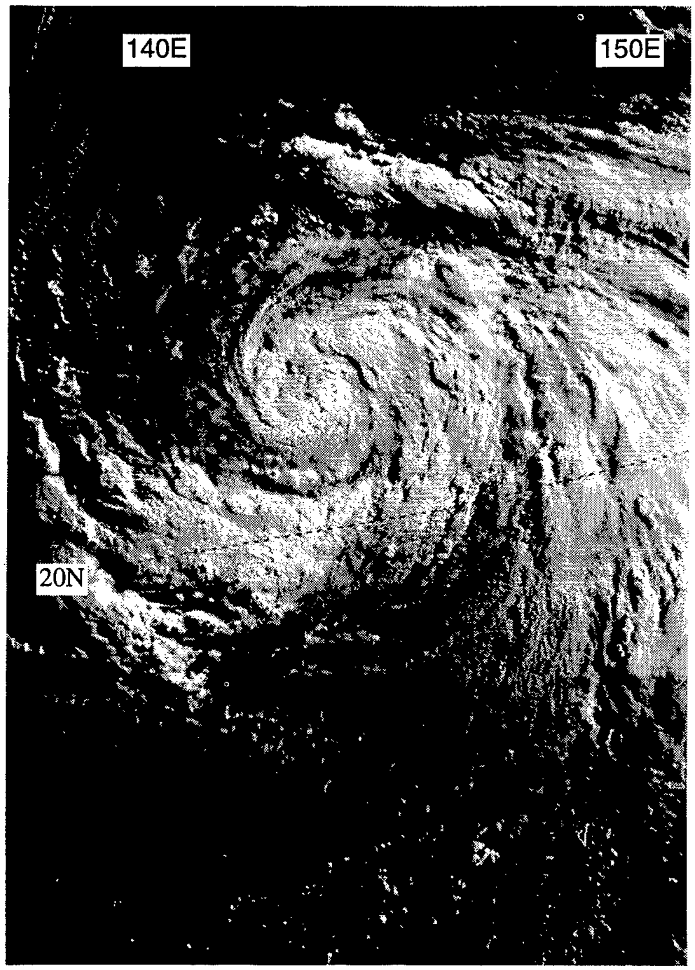

Figure 3-06-2 Dan becomes a typhoon (072040Z July visible DMSP imagery).

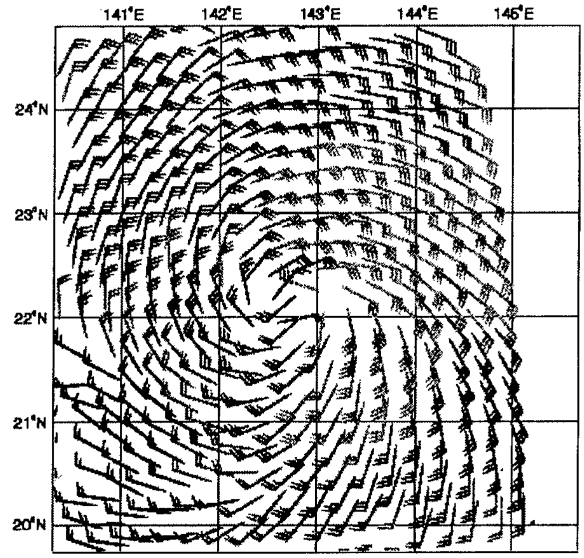

Figure 3-06-3 Scatterometer-derived wind speeds in a swath that passed over Dan (071304Z July ERS-2 scatterometer-derived marine surface wind speeds). This product was used in real time to expand the area of gales on the TC warning.

After 111200Z, satellite intensity estimates began to fall. Based on synoptic data, intensity estimates of Dan after 111200Z were kept significantly higher than satellite intensity estimates (Table 3-06-1). The problem of dropping the satellite intensity estimates far too low as a TC becomes extratropical is long-standing. During 1996, JTWC satellite analysts developed and implemented a new technique for estimating the intensity of TCs which are undergoing extratropical transition (Miller and Lander, 1996) (see the discussion).

The JTWC issued the final warning on Dan, valid at 120600Z, as the system moved eastward and completed its extratropical transition.

III. DISCUSSION

a. *TUTT-related genesis*

Dan (06W) originated and developed in association with a TUTT cell. Typical of TCs which develop in association with TUTT cells, Dan formed at a relatively high latitude (20°N), and as Figure 3-06-1 indicates, the system developed in the low-level easterly flow on the southwest flank of a subtropical high. For a more complete discussion of TUTT-related TC genesis, see Carlo's (33W) summary. In Carlo's (33W) case, and also in the case of Joy (12W), water-vapor imagery very clearly depicted the process of TC genesis associated with a TUTT cell. The formation of Dan (and also of Eve (07W)) in association with TUTT cells was more complicated than that of Carlo (33W) or Joy (12W), and its description is beyond the scope of this summary.

b. *Scatterometer aids diagnosis of wind distribution*

On the warning valid at 071800Z, the radius of 35-kt (18-m/sec) wind was nearly doubled from its value on the warning valid at 071200Z. This large change in the wind radius was based upon scatterometer data from the European Remote Sensing Satellite-2 (ERS-2) (Figure 3-06-3). Comments on the 071800Z warning included:

". . . The most significant change in this warning compared to the previous warning is the sudden change of wind radii, which is based on satellite scatterometry data from an overhead pass of the European ERS-2 polar orbiter . . ."

The JTWC has access to scatterometer wind data, and has used it to help determine the position, intensity and wind distribution of TCs. Some drawbacks of the scatterometer data are its small swath width, 180° directional ambiguity, relatively coarse resolution, an upper limit on the wind speeds that it can accurately detect, and a low-speed bias. For a more detailed discussion of scatterometer data, see Rick's (22W) summary.

c. *On the intensity of TCs undergoing extratropical transition: the "XT" technique*

For many years, the JTWC has had a problem diagnosing the intensity of TCs as they undergo extratropical transition. In general, the application of Dvorak's techniques to these systems has resulted in intensity estimates that are significantly lower than what is reported by ships or land stations. An extreme example of this problem occurred during the approach of Seth (1994) to Korea which is highlighted in Seth's summary in the 1994 ATCR. Dan provided another good example of this problem: as it was becoming extratropical (Figure 3-06-4), the satellite intensity estimates fell to values that were later proven to be far too low when compared to ship reports (Table 3-06-1). Attempts to apply Hebert and Poteat's (1975) techniques for estimating the intensity of subtropical cyclones to these systems were not successful.

In order to address the problem of underestimating the intensity of TCs undergoing extratropical transition, satellite analysts at the JTWC in conjunction with ONR-supported researchers at the University of Guam devised a technique (Miller and Lander, 1996) for estimating the intensity of TCs undergoing extratropical transition. This technique yields XT (for extratropical transition) numbers that equate to wind speeds identical to Dvorak's T numbers of the same magnitude. The technique also defines the completion of extratropical transition. On the few independent cases for which it was applied during 1996 the technique appears to have worked well. Though operational, the technique may be refined as more cases are examined. Specific details are beyond the scope of this summary, and those interested are invited to request a copy of the Miller and Lander (1996) technique.

IV. IMPACT

Skirting east of Japan, Dan drenched the Tokyo metropolitan area with over 5 inches of rain, and over twice that much in the adjoining Chiba prefecture. High water stalled trains and flooded streets. In Chiba prefecture, 29 houses were evacuated and at least 200 were reported damaged by flooding.

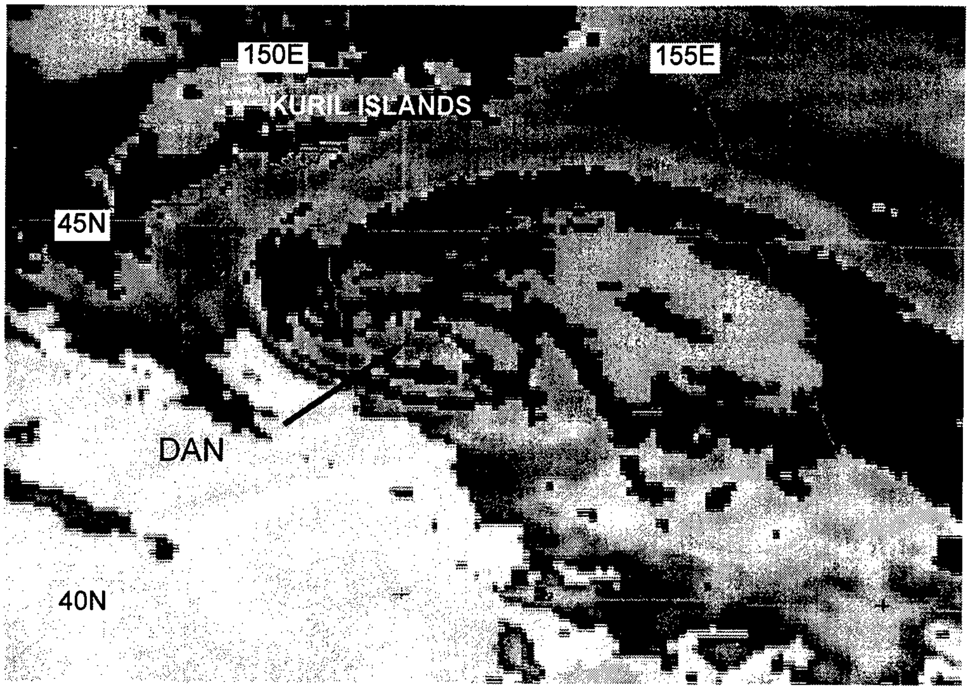

Figure 3-06-4 Dan begins its extratropical transition. Satellite intensity estimates as low as 35 kt (18 m/sec) at this time were far lower than ship reports of 60 kt (31 m/sec) used to support the best-track intensity (112031Z July enhanced infrared GMS imagery).

Table 3-06-1 Intensity estimates derived from satellite imagery during Dan's extratropical transition. In the code, T = Dvorak tropical numbers, ST = Hebert and Poteat subtropical numbers, and the number that follows the "/" is the current intensity which is always held higher when the TC is weakening over water.

Time (Z)	Code	Intensity (kt)	Best Track Intensity (kt)
101430	T 2.5/3.5	55	65
101432	T 2.5/3.5	55	65
101730	T 2.5/3.0	45	65
102014	T 2.5/3.0	45	65
102032	T 2.0/3.0	45	65
102330	T 2.5/3.5	55	65
110230	T 2.0/3.0	45	65
110407	T 2.5/3.0	45	60
110530	T 2.5/3.5	55	60
110717	T 2.5/3.0	45	60
110830	T 2.5/3.5	55	60
110832	T 1.5/2.5	35	60
111130	T 2.5/3.0	45	60
111432	T 2.0/2.5	35	60
112030	T 2.0/2.5	35	60
112002	ST 2.5/2.5	35	60
112032	T 2.0/2.0	30	60
112330	ST 3.0/3.0	45	60
120530	ST 3.0/3.0	45	60
120703	T 0.5/1.0	25	60
120830	ST 3.0/3.0	45	60

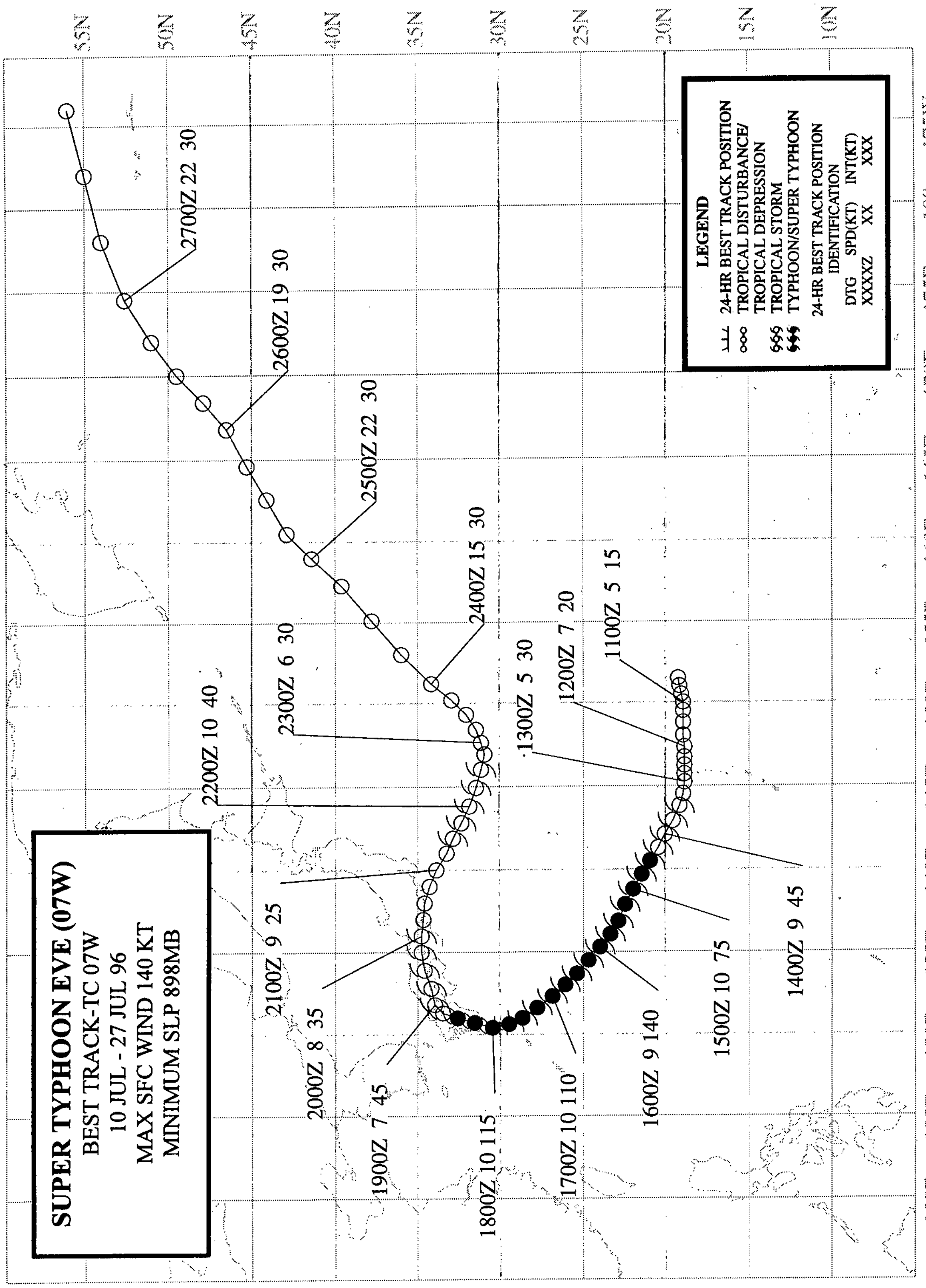
SUPER TYPHOON EVE (07W)
BEST TRACK-TC 07W
10 JUL - 27 JUL 96
MAX SFC WIND 140 KT
MINIMUM SLP 898MB
LEGEND
24-HR BEST TRACK POSITION
TROPICAL DISTURBANCE/
TROPICAL DEPRESSION
TROPICAL STORM
TYPHOON/SUPER TYPHOON
24-HR BEST TRACK POSITION
IDENTIFICATION
DTG SPD(KT) INT(KT)
XXXXZ XX XXX
1100Z 5 15
1200Z 7 20
1300Z 5 30
1400Z 9 45
1500Z 10 75
1600Z 9 140
1700Z 10 110
1800Z 10 115
1900Z 7 45
2000Z 8 35
2100Z 9 25
2200Z 10 40
2300Z 6 30
2400Z 15 30
2500Z 22 30
2600Z 19 30
2700Z 22 30
55N
50N
45N
40N
35N
30N
25N
20N
15N
10N
120E
125E
130E
135E
140E
145E
150E
155E
160E
165E
170E
175E
180
175W

SUPER TYPHOON EVE (07W)

I. HIGHLIGHTS

Eve, like Dan (06W) which preceded it, originated in association with a TUTT cell. After undergoing explosive deepening, Eve became the first WNP super typhoon of 1996. The typhoon passed through the northern Ryukyu Islands and made landfall in southern Japan. Moving eastward over Japan, the system weakened before intensifying to tropical storm intensity after moving offshore.

II. TRACK AND INTENSITY

As Dan was recurving to the east of Japan, a TUTT cell formed to its southeast. A band of deep convection formed a "U" shape to the south of this TUTT cell (Figure 3-07-1). Although not mentioned until 120600Z July on the Significant Tropical Weather Advisory, the disturbance which became Eve was tracked in post analysis back to the place where, at 100600Z, it consolidated in the TUTT-related area of deep convection. On 13 July, an area of persistent deep convection located about 300 nm (550 km) to the north of Guam, began to show signs of increasing organization. Synoptic data indicated that a low-level cyclonic circulation was located within this area of deep convection, and the JTWC issued a Tropical Cyclone Formation Alert valid at 130800Z July. During the night of 13 July, the persistent area of deep convection became well-organized, and satellite intensity estimates of 25 kt (13 m/sec) (later adjusted to 35 kt (18 m/sec) in post analysis) prompted the JTWC to issue the first warning on Tropical Depression (TD) 07W, valid at 131200Z.

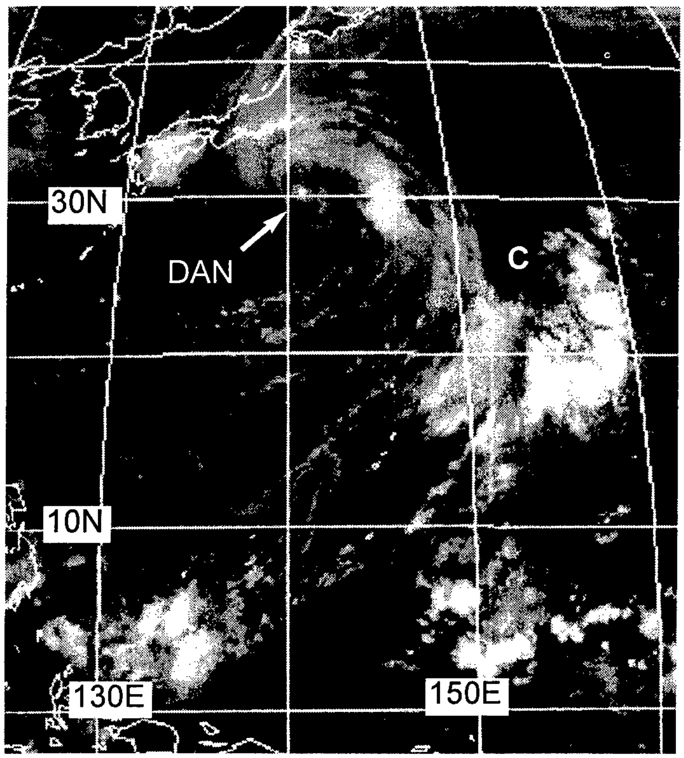

Figure 3-07-1 The tropical disturbance that became Eve originated from an area of deep convection to the south of a TUTT cell (C). This TUTT cell was, in turn, located to the southeast of the recurving Dan (06W) (091831Z July infrared GMS imagery).

When Eve formed a beautiful banding eye on the morning of 15 July (Figure 3-07-2), it was upgraded to a typhoon on the warning valid at 150000Z. From 150000Z to 160000Z, Eve underwent a period of explosive deepening (see the discussion section). At 151800Z, it became a super typhoon, and at 160000Z it reached its peak intensity of 140 kt (72 m/sec) (Figure 3-07-3). Forming concentric wall clouds (Figure 3-07-4), the intensity decreased to 100 kt (51 m/sec) by 170600Z. Just prior to making landfalling at Kyushu, Japan, on 18 July, the eye once again became small and well defined, and the intensity increased to 115 kt (59 m/sec). The system made landfall at approximately 180300Z and began to weaken over the mountainous terrain of Kyushu. The system was downgraded to a tropical storm at 191200Z, and the final warning was issued, valid at 200000Z, as the system moved eastward over the main Japanese island of Honshu and weakened.

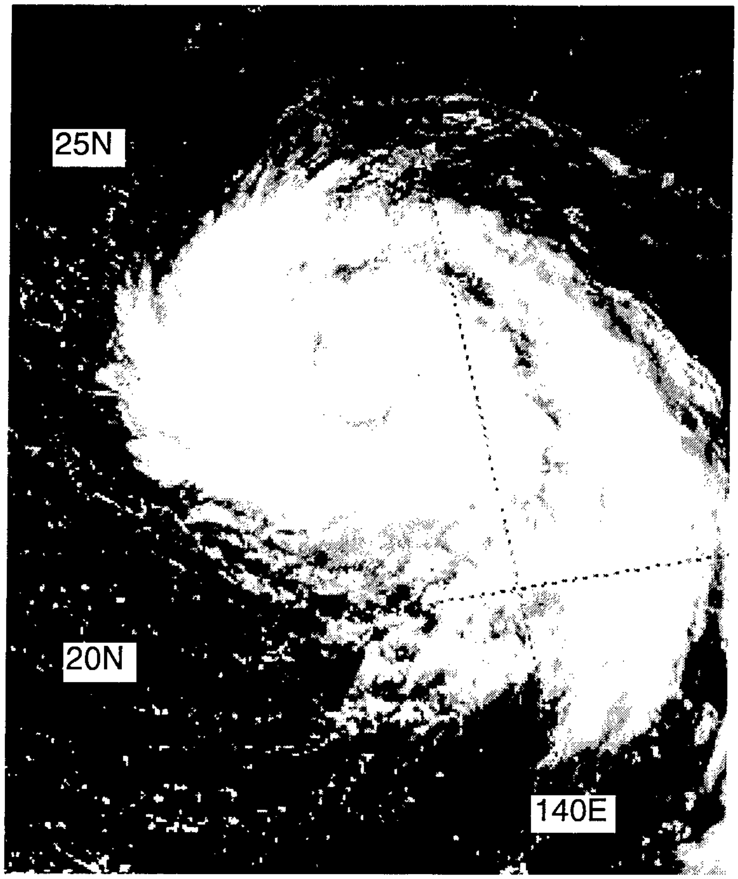

Figure 3-07-2 Eve forms a text-book quality banding eye pattern (150019Z July visible DMSP imagery).

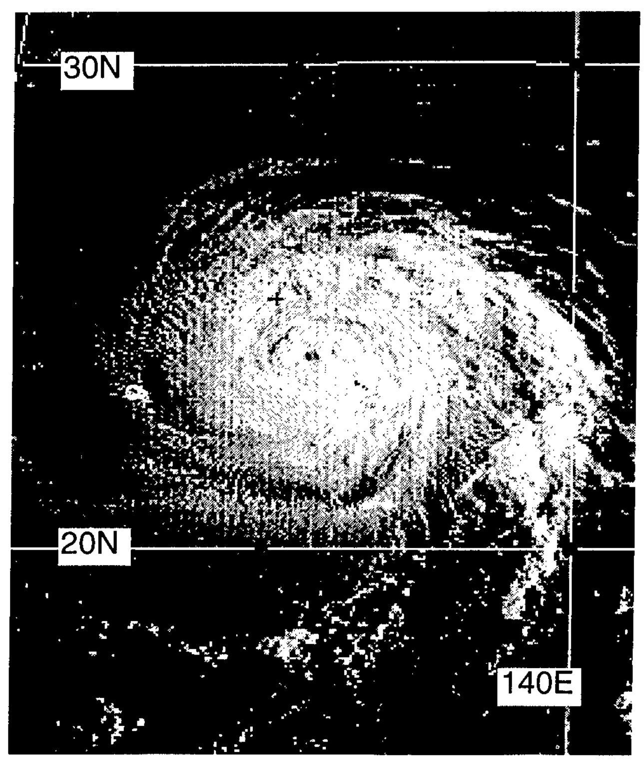

Figure 3-07-3 Eve at its peak intensity 140 kt (72 m/sec) (152131Z July visible GMS imagery).

When the system moved over water to the east of Japan, it regenerated. A post analysis of synoptic data, and a reanalysis of satellite imagery (e.g., Figure 3-07-5), supported a regeneration to tropical-storm intensity for the 24-hour period 211200Z to 221200Z, with a maximum intensity of 40 kt (21 m/sec) at 211800Z. After 251200Z, all deep convection was sheared away from the LLCC, marking the completion of extratropical transition. The system was identifiable on satellite imagery as it tracked all the way to the Aleutian Island chain where hourly data from Shemya (WMO 70414) indicated a small pressure fall and a wind shift attributable to the remnants of Eve passing to the southeast on 27 July.

III. DISCUSSION

a. *TUTT-related genesis*

Eve, like Dan (06W) which preceded it by a week, originated in association with a TUTT cell. Typical of TCs which develop in association with TUTT cells, Eve formed at a relatively high latitude (20°N), and it formed in the cloud-minimum region north of the cloudiness associated with the monsoon trough. For a more complete discussion of TUTT-related TC genesis, see Carlo's (33W) summary. In Carlo's (33W) case, and also in the case of Joy (12W), water-vapor imagery very clearly depicted the process of TC genesis from a TUTT cell.

b. *Explosive deepening*

Between 150000Z and 160000Z July, Eve's intensity increased from 75 kt (39 m/sec) to 140 kt (72 m/sec). The equivalent 24-hour pressure fall (using Atkinson and Holliday's (1977) wind-pressure relationship) was 70 mb, resulting in an average decrease of 2.92 mb/hr. This rate of pressure fall easily qualifies as a case of explosive deepening which is described by Dunnavan (1981) as a decrease in the minimum sea-level pressure of a TC of 2.5 mb/hr for at least 12 hours or 5 mb/hr for at least six hours. If one honors the digital Dvorak (DD) time series at this time (Figure 3-07-6), the rate of intensity increase is even more remarkable: the DD numbers at 150000Z were on the order of T 4.5, and then rose to their peak of approximately T 7.5 at 151800Z. The equivalent pressure fall using the DD

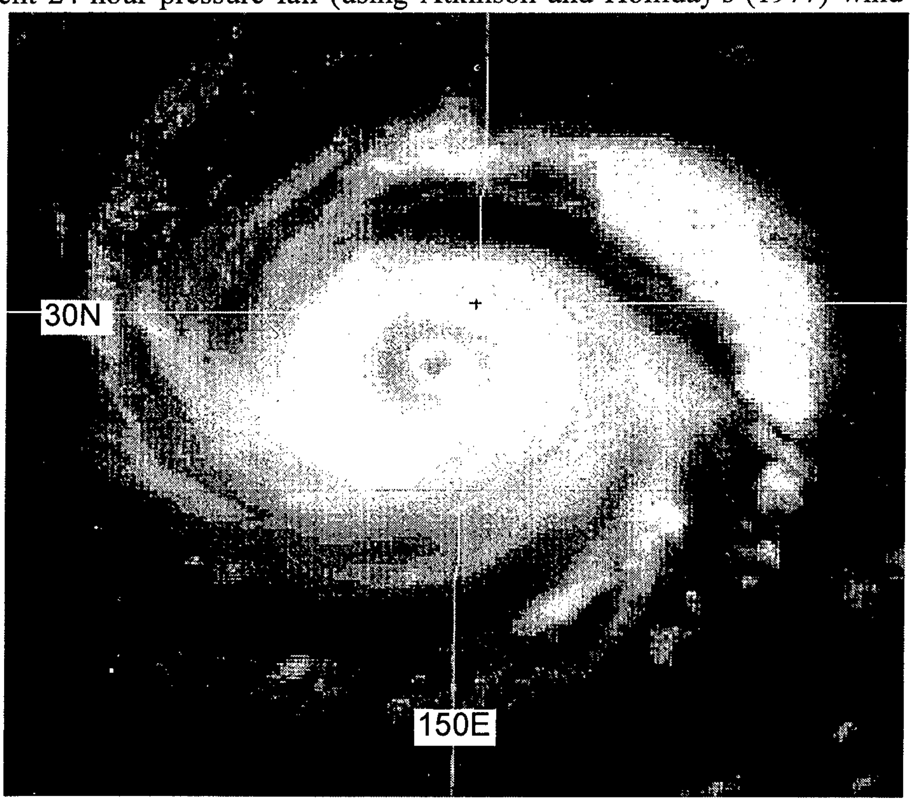

Figure 3-07-4 Shortly after reaching its peak intensity, Eve formed concentric eye walls. The relatively cloud-free moat between the eye walls resulted in a substantial drop in the default values of the DD number (160331Z July visible GMS imagery).

intensity estimates was 87 mb in 18 hours, resulting in an average decrease of 4.8 mb/hr. The explosive deepening was not anticipated, and 24-hour and 48-hour forecasts of Eve's intensity fell short by as much as 70 kt (36 m/sec) and 90 kt (46 m/sec) respectively during the two days prior to the event.

c. *A discussion of Eve's DD time series*

Infrared imagery is available hourly from the GMS satellite, and hourly DD numbers were calculated for all of the typhoons of 1996 (see Bart's (04W) summary for a detailed description of the DD algorithm installed on the JTWC's satellite image processing equipment). The discussion of the behavior of the time series of the DD numbers for Eve, and for some of the other typhoons of 1996, is intended to highlight certain aspects of the DD time series that may prove to have important research and/or warning implications.

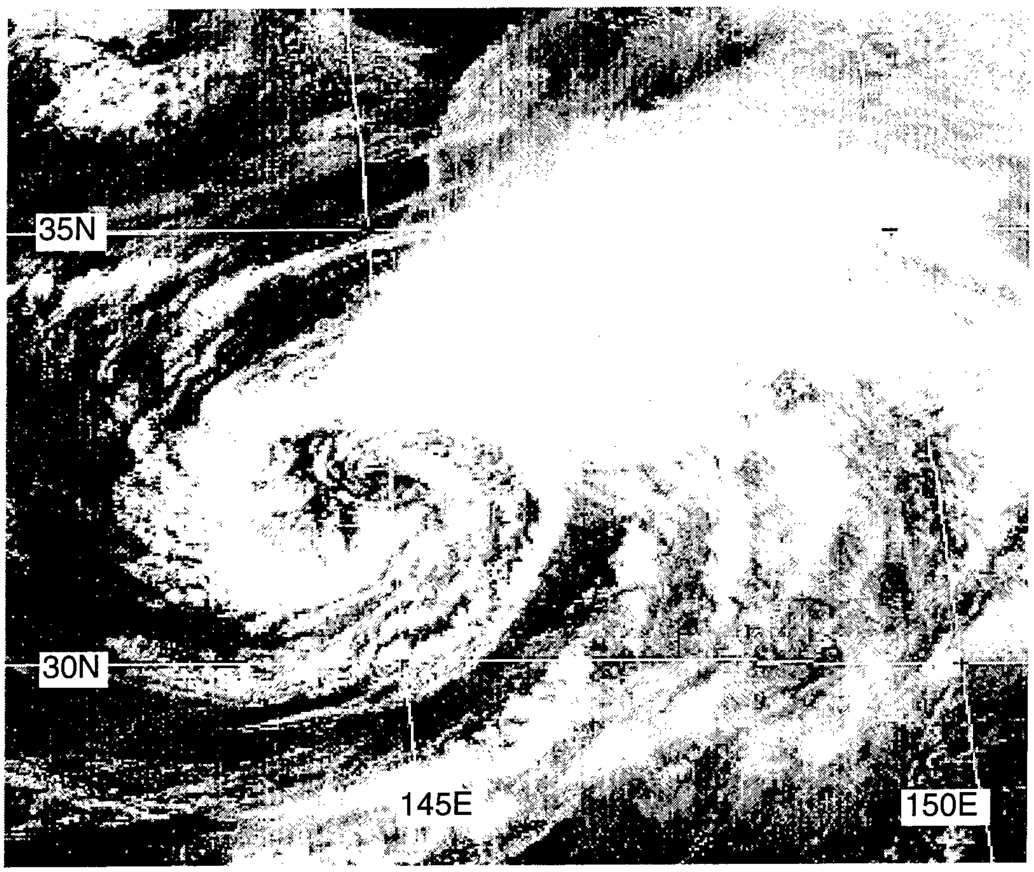

Figure 3-07-5 Exhibiting a Dvorak "shear" pattern type, Eve has regenerated and reached tropical-storm intensity after moving back over water to the east of Japan (220231Z July visible GMS imagery).

Eve is one of only a few cases during the past two years in which a strong diurnal cycle can be found in the time series of its DD numbers (Figure 3-04-6): higher DD numbers occur in the early morning hours (around 1800Z), and lower DD numbers occur in the late afternoon (around 0600Z). Although the DD number is based upon both the cloud-top temperature of the eye-wall cloud and the temperature within the eye, the apparently cyclical fluctuations in Eve's DD time series are linked more to major structural changes of the TC rather than fluctuations in the cloud-top temperatures of an otherwise stable cloud pattern. During the rise to the first DD peak during 15 July, Eve's eye evolved from a banding eye to a well-defined small eye. The fall of the DD numbers on 16 July is predominantly a manifestation of the formation of concentric eye walls. The default radius used to define the eye wall cloud-top temperature in the DD algorithm is 30 nm. When Eve

possessed concentric eye walls, this radius fell in the relatively cloud-free moat between the inner and outer wall clouds, and resulted in the period of low DD values after the first peak. The radius used to define the eye-wall cloud-top temperature is an adjustable parameter on the MIDDAS system, and when set to 10 nm it was able to measure Eve's intensity based on the cloud-top temperature of the inner eye wall. This resulted in DD numbers approximately one T number higher than those computed using the default radius when Eve possessed concentric eye walls.

Thus, while diurnal fluctuations of the intensity estimate of a TC may be the result of the general observation that cloud-top temperatures of deep convection in the tropics tend to be coldest in the early morning, the diurnal fluctuations of Eve's DD time series can be linked to major structural changes of the eye which may have only coincidentally occurred at the diurnal time scale. A similar sharp rise of the DD time series to a peak of over T 7.0 followed by a drop to near T 5.0 (due to the formation of concentric wall clouds) occurred with Dale (36W). In the case of Dale (36W), the timing of the rise and fall of the DD time series was 180° out of phase with that of Eve and with the generally observed diurnal cycle of tropical cloud-top temperatures.

Figure 3-07-6 The time series of Eve's hourly DD numbers (small black dots connected by thin solid line). For comparison, the final best track intensity at six-hour intervals (converted to a T number) is superimposed (open circles connected by thin solid line).

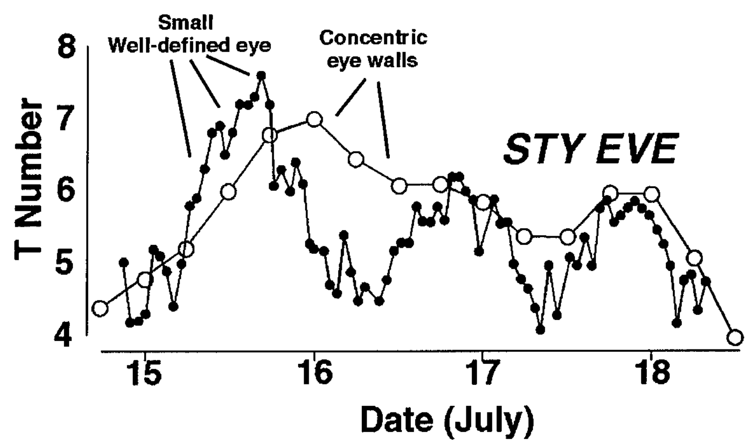

IV. IMPACT

Strong winds and heavy rains affected the Japanese island of Kyushu, disrupting sea and air transport. Nine people were reported injured. The eye of Eve passed directly over the island of Yaku Jima (WMO 47836) in the northern Ryukyus where reports of wind gusts to 83 kt (43 m/sec) were received at the JTWC.

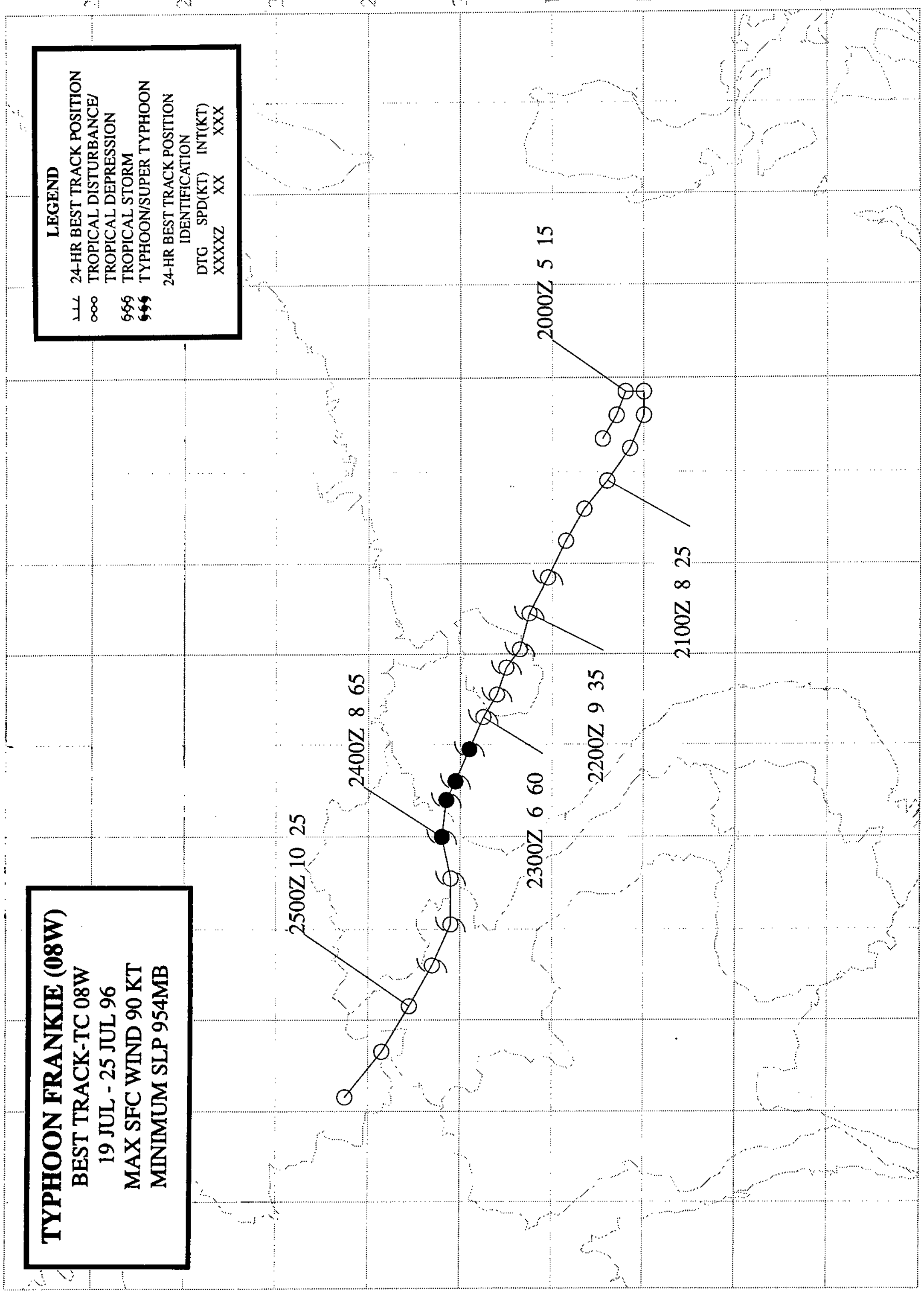
TYPHOON FRANKIE (08W)
BEST TRACK-TC 08W
19 JUL - 25 JUL 96
MAX SFC WIND 90 KT
MINIMUM SLP 954MB
LEGEND
24-HR BEST TRACK POSITION
TROPICAL DISTURBANCE/
TROPICAL DEPRESSION
TROPICAL STORM
TYPHOON/SUPER TYPHOON
24-HR BEST TRACK POSITION
IDENTIFICATION
DTG SPD(KT) INT(KT)
XXXXZ XX XXX
2000Z 5 15
2100Z 8 25
2200Z 9 35
2300Z 6 60
2400Z 8 65
2500Z 10 25
28N
26N
24N
22N
20N
18N
16N
14N
12N
98E
100E
102E
104E
106E
108E
110E
112E
114E
116E
118E
120E
122E

TYPHOON FRANKIE (08W)

I. HIGHLIGHTS

During late July, the monsoon trough became established across the northern half of the South China Sea and extended east-southeastward into Micronesia. Three TCs formed in this trough — Frankie, Gloria (09W), and Herb (10W). The westernmost of these three, Frankie originated from a monsoon depression in the South China Sea tracked to the west-northwest, and made landfall in northern Vietnam.

II. TRACK AND INTENSITY

During June and the first half of July, the monsoon trough was either very weak or absent from the tropics of the WNP. Easterly winds prevailed, and TC formation occurred at relatively high latitude (20°N) in association with disturbances in the TUTT. During the latter half of July, the first major penetration of the monsoon trough into Micronesia occurred. Inevitably, the monsoon cloud band consolidated into discrete areas of deep convection (in this case, three of them). The westernmost of the three areas of deep convection along the monsoon trough became a monsoon depression in the South China Sea (see the discussion section). It was first mentioned on the 180600Z July Significant Tropical Weather Advisory. A small well-defined LLCC (Figure 3-08-1) embedded within this monsoon depression became Frankie. A Tropical Cyclone Formation Alert was issued valid at 201100Z when deep convection continued to consolidate around the LLCC shown in Figure 3-08-1. Rapid development of a CDO pattern type with well-defined peripheral low-level cloud lines (Figure 3-08-2) prompted the JTWC to issue the first warning on Tropical Depression (TD) 08W, valid at 210000Z. During the early morning of 22 July, TD 08W formed a large CCC (Figure 3-08-3) prompting its upgrade to Tropical Storm Frankie on the warning valid at 211800Z. After becoming a tropical storm, Frankie passed over the island of Hainan and continued to intensify. After clearing the west coast of Hainan, Frankie developed a ragged eye (Figure 3-08-4). Over the Gulf of Tonkin, the eye became better defined and Frankie was upgrade to a typhoon on the warning valid at 230600Z. The intensity peaked at 90 kt (46 m/sec) at 231200Z, and remained at that intensity until it crossed the coast of northern Vietnam at approximately 232200Z July. Thereafter, the system weakened, and the final warning was issued, valid at 240600Z.

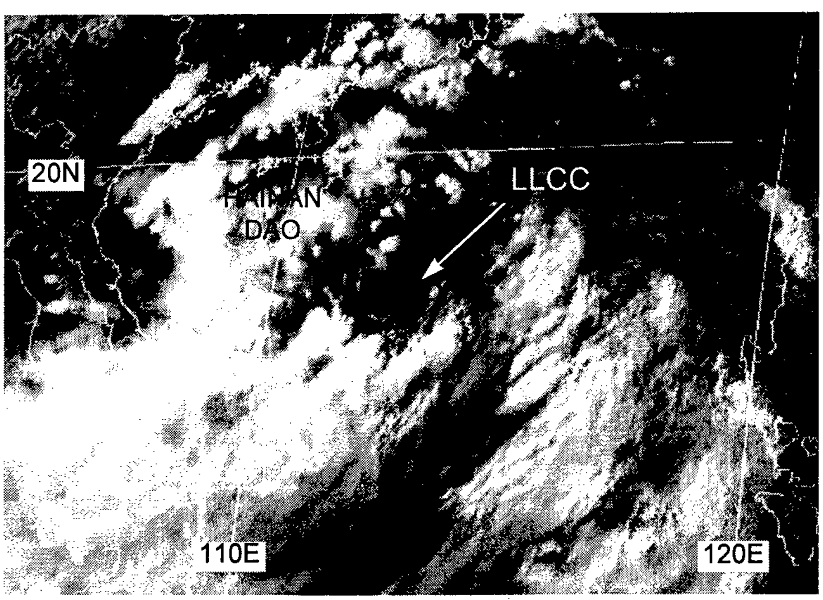

Figure 3-08-1 A small well-defined LLCC is present near the center of a monsoon depression. This LLCC became Frankie (210731Z July visible GMS imagery).

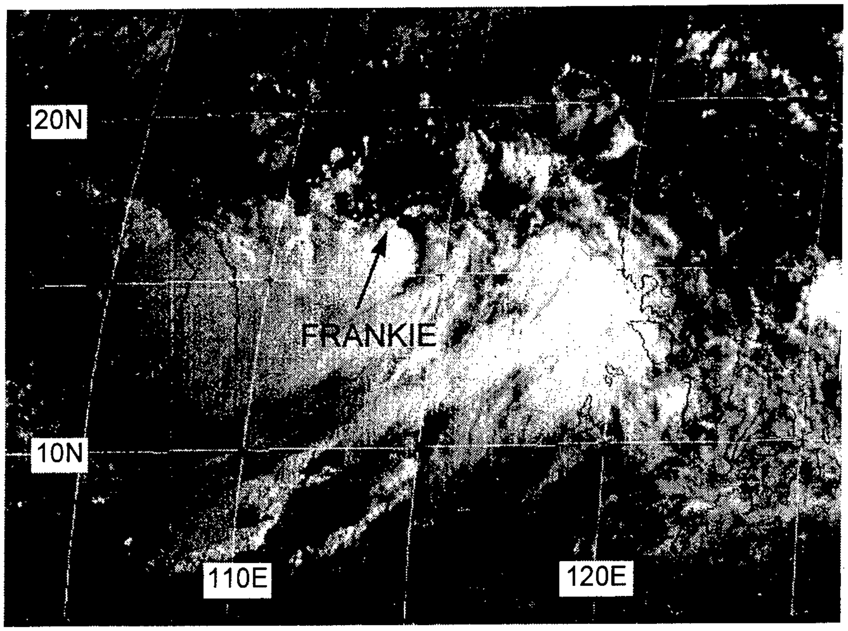

Figure 3-08-2 Deep convection becomes established over the LLCC shown in Figure 3-08-1 (202331Z July visible GMS imagery).

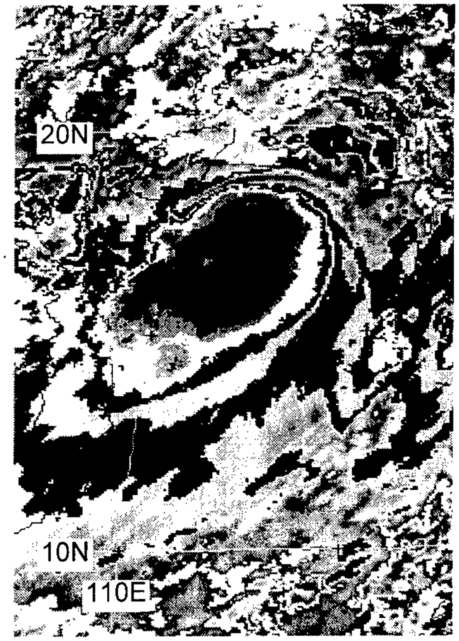

Figure 3-08-3 A large CCC erupts over the LLCC of Frankie. Coldest cloud-top temperature was -97°C (indicated by the arrow) (212224Z July enhanced infrared GMS imagery).

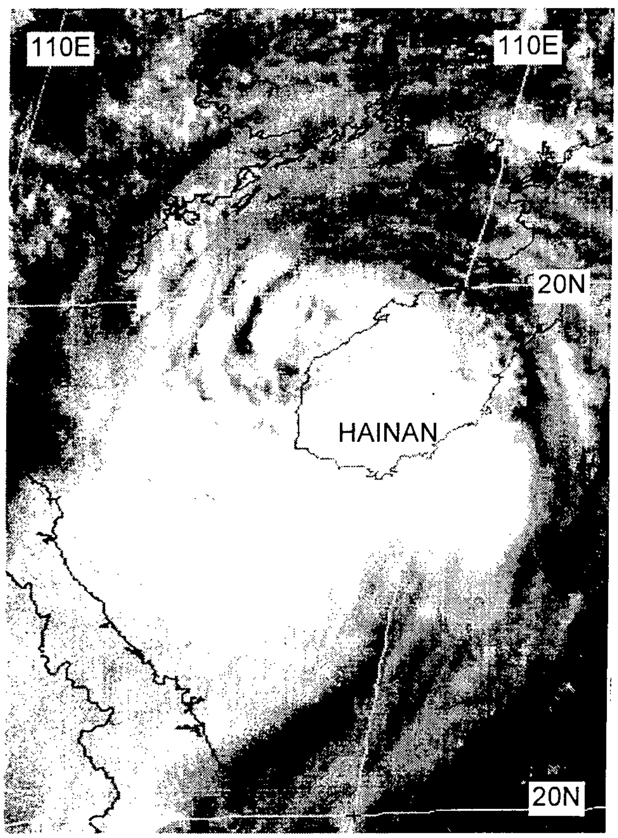

Figure 3-08-4 Frankie acquires a ragged eye as it clears the coast of Hainan island (230031Z July visible GMS imagery).

III. DISCUSSION

a. *The transformation of a monsoon depression into a typhoon*

Frankie originated from a monsoon depression — a common genesis pathway for TCs in the WNP (see Appendix A for a detailed description of monsoon depressions in the WNP). An unresolved question remains concerning the transition of a monsoon depression into a conventional TC: does the monsoon depression become the conventional TC, or does a conventional TC form within the circulation of the monsoon depression? In Frankie's case, it can be argued that the conventional TC (Frankie) formed within the preexisting circulation of the monsoon depression. The well-defined exposed LLCC (Figure 3-08-1) that became the focus of Frankie's deep convection was surrounded by an area of gales (Figure 3-08-5) before the core winds increased. When persistent deep convection appeared in the core of the monsoon depression, it quickly became a CDO-type conventional TC. Soon after the formation of Frankie's CDO, the peripheral cloudiness in the monsoon depression was suppressed and the areal extent and amount of

deep convection in the system became much smaller. TCs in the WNP that develop from monsoon depressions tend to be large, and Frankie's small size is somewhat unusual. Perhaps the geomorphology of the Gulf of Tonkin contributed to the evolution of this monsoon depression into a small TC. Many TCs which move into the Gulf of Tonkin become smaller.

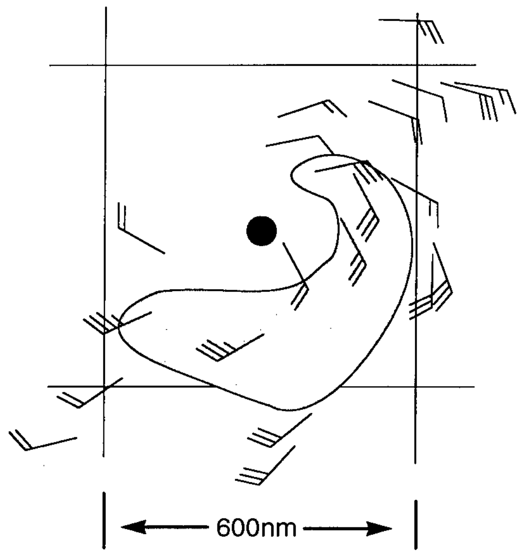

Figure 3-08-5 An area of gales existed in the monsoon depression before deep convection grew in its center (black dot) and the system became a conventional tropical cyclone. Wind reports are a center-relative composite of ship observations at 201200Z, 210000Z and 211200Z July.

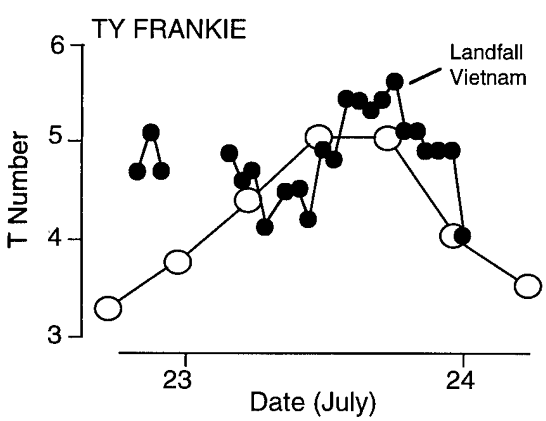

Figure 3-08-6 A time series of Frankie's intensity as it crossed the Gulf of Tonkin and made landfall in Vietnam. The hourly DD time series is indicated by black dots, and the six-hourly best-track intensity (converted to a T number) is indicated by the open circles.

b. *Frankie's intensity time series*

Upon entering the Gulf of Tonkin, Frankie acquired an eye and intensified from 50 kt (26 m/sec) to 90 kt (46 m/sec) in a period of 24 hours (Figure 3-08-6). The equivalent pressure drop of 33 mb in 24 hours was below the criteria for rapid deepening, defined as a decrease of 42 mb in 24 hours (Holliday and Thompson, 1979). The intensity increase did, however, qualify as "fast" in terms of its rise of more than 1.5 Dvorak T numbers in 24 hours. Dvorak classifies the rate of intensification of a TC as "slow", "normal", or "fast" if the 24-hour rise in its T-number estimate is 0.5, 1.0, and 1.5 respectively. Another aspect of Frankie's intensification over the Gulf of Tonkin concerns the timing of its peak. The best track indicates it reached its peak intensity approximately eight hours prior to landfall, while the DD numbers (Figure 3-08-6) continued to rise until the western eye-wall cloud made landfall. The discussion of the behavior of the time series of the DD numbers for Frankie, and for some of the other typhoons of 1996, is intended to highlight certain aspects of the DD time series that may prove to have important research and/or warning implications. Differences between the DD numbers and the best-track intensity are expected, and substantial disagreements are curiosities that lack ground-truth verification.

IV. IMPACT

Frankie caused extensive property damage and loss of life in the northern provinces of Vietnam. There were 104 people reported dead or missing, and 466 were reported injured. Total economic losses were estimated at over US $200 million.

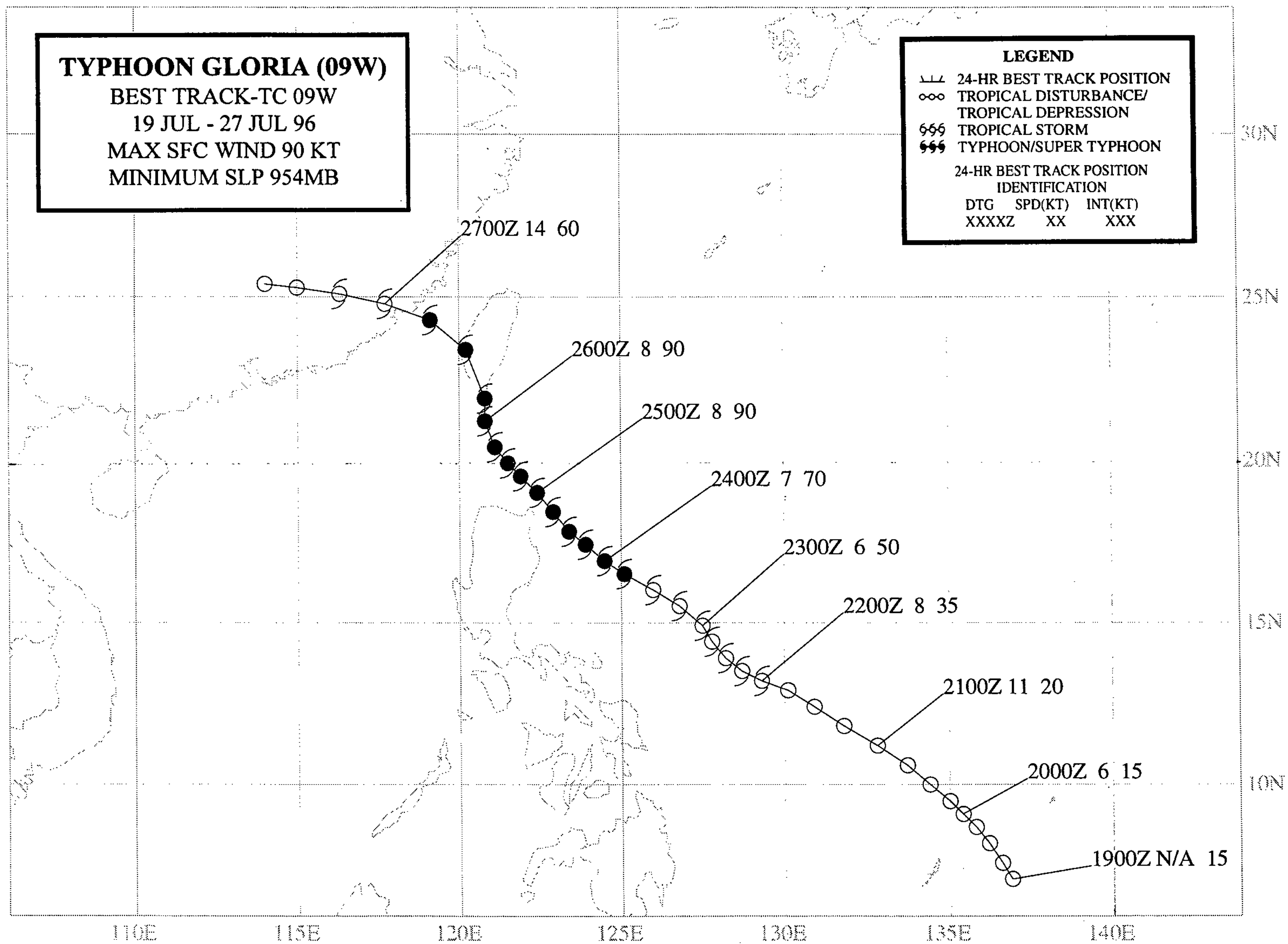
TYPHOON GLORIA (09W)
BEST TRACK-TC 09W
19 JUL - 27 JUL 96
MAX SFC WIND 90 KT
MINIMUM SLP 954MB
LEGEND
24-HR BEST TRACK POSITION
TROPICAL DISTURBANCE/
TROPICAL DEPRESSION
TROPICAL STORM
TYPHOON/SUPER TYPHOON
24-HR BEST TRACK POSITION
IDENTIFICATION
DTG SPD(KT) INT(KT)
XXXXZ XX XXX
2700Z 14 60
2600Z 8 90
2500Z 8 90
2400Z 7 70
2300Z 6 50
2200Z 8 35
2100Z 11 20
2000Z 6 15
1900Z N/A 15
30N
25N
20N
15N
10N
110E
115E
120E
125E
130E
135E
140E

TYPHOON GLORIA (09W)

I. HIGHLIGHTS

Developing from a monsoon depression in the Philippine Sea, Gloria moved northwestward, became a typhoon, and affected Luzon, Taiwan, and eastern China. During the early phases of its development, Gloria formed a very large Central Cold Cover (CCC) with a near-record cloud-top temperature of -100°C.

II. TRACK AND INTENSITY

During the latter half of July, extensive amounts of deep convection formed in an east-west band extending across the WNP from the coast of Southeast Asia to the Marshall Islands. By 21 July, this cloud band had consolidated into three distinct cloud clusters (see Figure 3-10-1 in Herb's (10W) summary), all of which became named tropical cyclones — from west to east: Frankie (08W), Gloria, and Herb (10W). The tropical disturbance which became Gloria was first mentioned on the 170600Z July Significant Tropical Weather Advisory when synoptic data from Koror (WMO 91408) indicated the presence of a weak cyclonic circulation associated with a region of enhanced deep convection along the monsoon trough. Over the course of the next few days this disturbance moved slowly westward without much sign of increased organization in the deep convection or the surface wind field.

Early on 21 July, convection in the pre-Gloria disturbance became more organized and the first of two Tropical Cyclone Formation Alerts (TCFA) was issued valid at 201830Z. The areal extent of deep convection in this disturbance increased markedly, and the system acquired the structure of a monsoon depression. Although the cloud system appeared to be well organized, synoptic data still indicated that the winds were weak, and most of the deep convection had not yet consolidated near the low-level circulation center (LLCC). Thus, a second TCFA was issued valid at 211830Z, containing a caution stating deep convection had begun to develop near the LLCC (Figure 3-09-1), and formation of a significant tropical cyclone was anticipated within 6 to 12 hours. Indeed, when synoptic reports were received which indicated the wind speed had reached 30 kt (15 m/sec) in the broad circulation, the first warning on Tropical Depression 09W was issued valid at 220000Z. Steering flow was dominated by a strong subtropical ridge to its north, and Gloria was forecast to move on a steady west-northwest track towards Luzon.

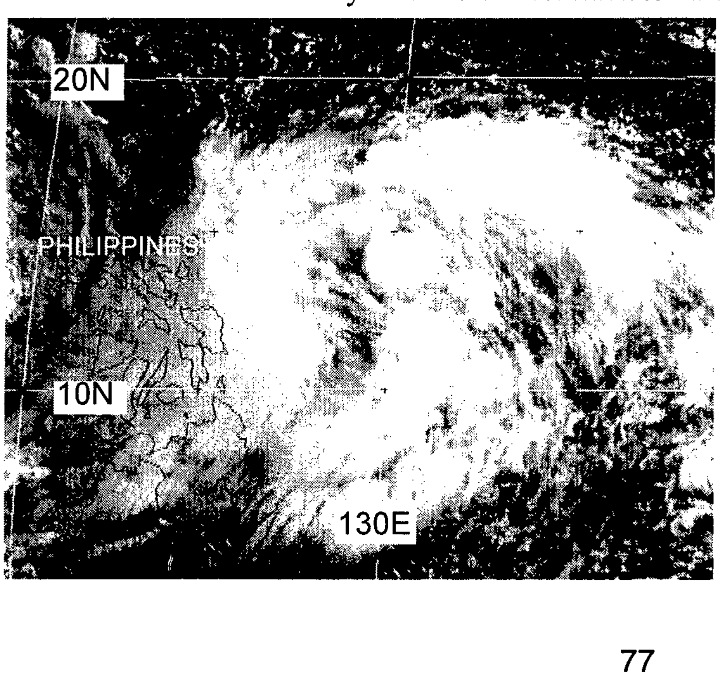

Figure 3-09-1 The mesoscale convective systems within the pre-Gloria monsoon depression show signs of increased organization and consolidation toward the LLCC, prompting the first warning (212224Z July visible GMS imagery).

Based upon synoptic reports of gales within the large circulation, TD 09W was upgraded to Tropical Storm Gloria on the warning valid at 221200Z. During the night, following its upgrade to tropical-storm intensity, and subsequent increase to 55 kt (28 m/sec), Gloria underwent a profound structural change: a very large Central Cold Cover (CCC) formed (see the discussion section). This CCC persisted from the late evening of 23 July to the morning of 24 July. As the CCC began to dissipate, Gloria became a typhoon. By the afternoon of 24 July, the cirrus debris of the CCC had largely cleared away revealing that Gloria had acquired a visible eye.

Tracking on a more northwestward course than forecast, Gloria brushed by Luzon and entered the Luzon Strait. It is here, during the afternoon of 26 August that Gloria made an abrupt jog to the north to make landfall on the southern tip of Taiwan. The typhoon then made a quick jump to the western coast of Taiwan, where it then turned to the west, crossed the Taiwan Strait and went inland in southeastern China. The peak intensity of 90 kt (46 m/sec) was maintained from 241200Z to 260600Z as Gloria moved across the Luzon Strait and made landfall in Taiwan. After landfall in Taiwan, its intensity dropped to the typhoon threshold, and having little time to recover during its passage across the Taiwan Strait, it entered mainland China as a minimal typhoon and quickly dissipated over land. The final warning was issued at 270600Z.

III. DISCUSSION

a. *An unusually large Central Cold Cover*

Dvorak (1984) noted that the use of enhanced IR imagery required the introduction of a new concept — the central cold cover (CCC) — in order to deal with the occurrence of a sudden spreading of cold clouds over the central features of a TC. When a CCC persists, it signals an interruption in the development of the TC. Specific details of the CCC pattern are found in Dvorak (1984):

"The CCC pattern is defined when a more or less round, cold overcast mass of clouds covers the storm center or comma head obscuring the expected signs of pattern evolution. The outer curved bands and lines usually weaken with the onset of CCC. When using VIS pictures, substitute the word 'dense' for 'cold'. It is only rarely that the CCC pattern is used with VIS pictures since the CDO [central dense overcast] or curved lines are usually visible through the thin cirrus clouds. When the CCC persists . . . , development has been arrested until signs of development or weakening once again appear in the cloud features. Care should be exercised under the following conditions:

"1) Do not confuse a CCC pattern with a very cold comma pattern. A very cold (usually white [i.e., a gray-shade enhancement on the BD curve that is indicative of temperatures between -70 to -75°C]) pattern is indicated by a very cold (very smooth texture) comma tail and head with some indication of a wedge in between. Curved cirrus lines or boundaries usually appear around the [very] cold [comma] pattern and not around the CCC pattern. The very cold [comma] pattern for T-numbers of T3 or less warrant an additional 1/2 number in intensity estimate and often indicates rapid growth.

"2) Do not assume weakening in a CCC pattern when the comma tail begins to decrease in size. It is common to observe the tail decreasing in size at the onset of the CCC. Also, the CCC often warms as the eye of the T4 pattern begins to be carved out by a warm incursion into the side of the cold overcast. This signals the resumption of pattern evolution (intensification) even though some warming is evident."

In the WNP, the CCC pattern is observed every year in the developmental process of several of the named TCs. One major difference between the CCC pattern observed in the WNP versus the North Atlantic (where Dvorak obtained most of the data for the development of his techniques) is that the cloud-top temperature of the CCC tends to be at least 10°C to 15°C colder in the WNP. Another difference between the CCC patterns observed in the WNP versus those observed in the Atlantic is the very large size of some of the CCC patterns observed in the WNP.

Prior to the formation of its CCC, Gloria had been developing as a monsoon depression. During the evening hours of 23 July, a cluster of small cold-topped MCSs began to grow near the estimated center position of Gloria. During a six-hour period, this cluster of MCSs mushroomed into an enormous CCC (Figure 3-09-2a-e). By local midnight, the average diameter of the area within which the cloud-top temperature was at or below -70°C was approximately 700 km (Figure 3-09-3). Roughly half of this area was colder than -90°C. The coldest IR pixel, with an equivalent black-body temperature of -100°C, was located near the geometric center of the CCC. This is an extremely cold cloud-top temperature which is rarely seen. It is only 2°C shy of the record cold cloud-top temperature of -102°C reported by Ebert and Holland (1992) in the deep convection associated with a TC near Australia.

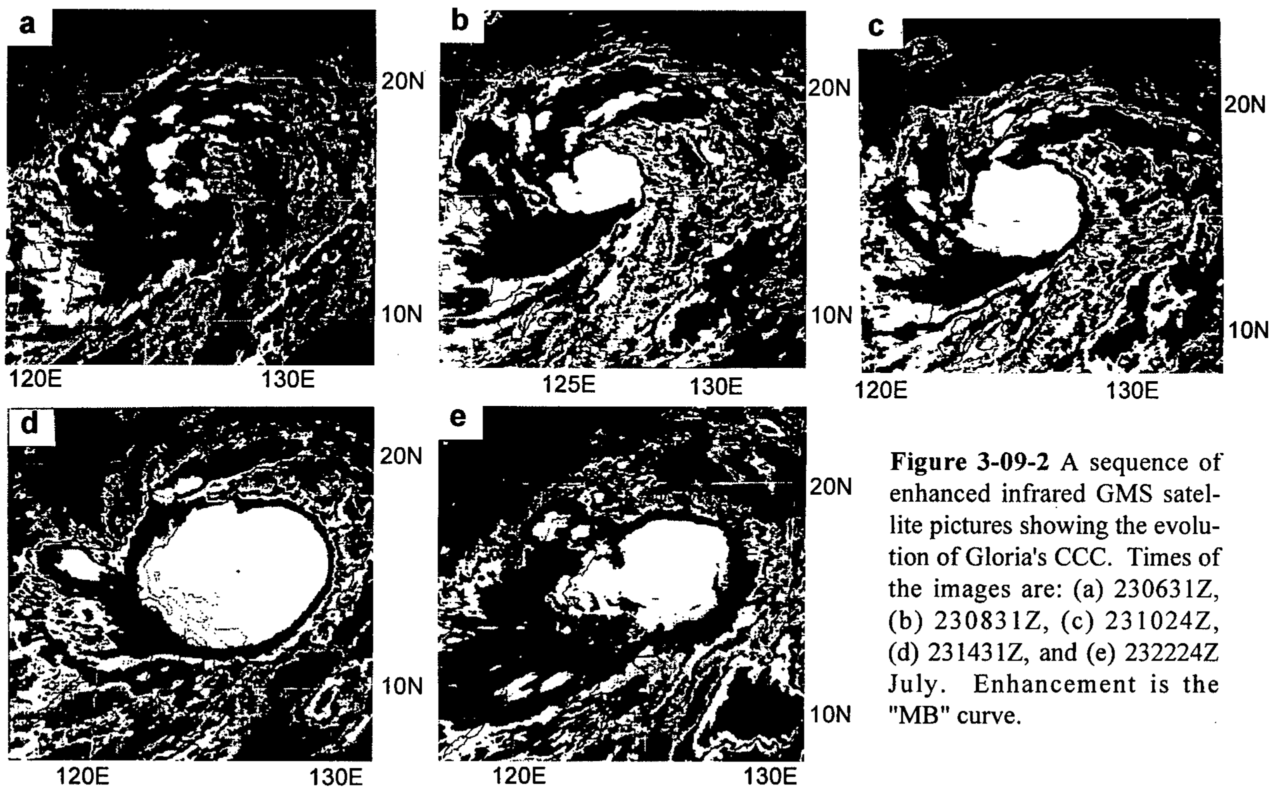

Figure 3-09-2 A sequence of enhanced infrared GMS satellite pictures showing the evolution of Gloria's CCC. Times of the images are: (a) 230631Z, (b) 230831Z, (c) 231024Z, (d) 231431Z, and (e) 232224Z July. Enhancement is the "MB" curve.

By the early daylight hours of 24 July, the periphery of the CCC began to warm on IR imagery, and a new smaller CCC mushroomed into the preexisting cold cirrus canopy (Figure 3-09-4). As the day progressed, the underlying structure of Gloria gradually emerged in VIS imagery as the supporting convection of the CCC ended, and the large cirrus canopy of the CCC thinned. By mid-afternoon, the cold cirrus of the CCC became nearly transparent, and the eye, wall cloud, and peripheral convective cloud bands of the intensifying Gloria were then plainly seen (Figure 3-09-5).

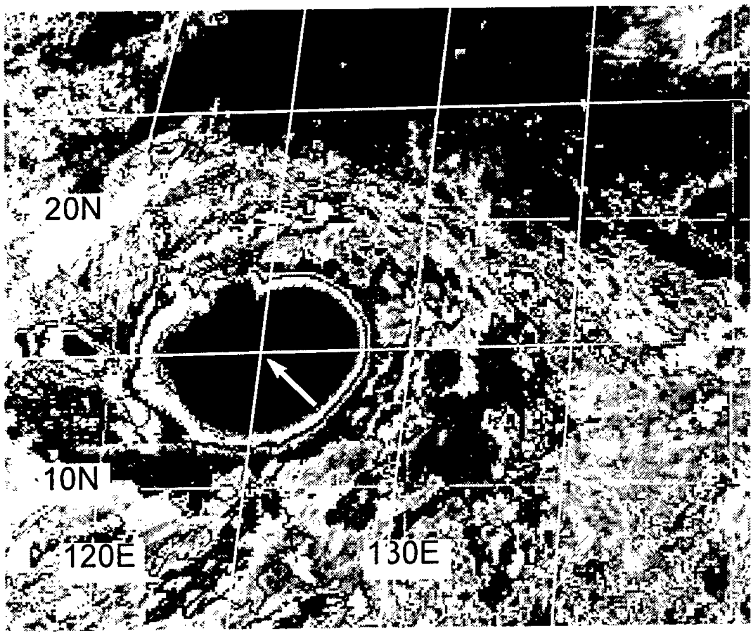

Figure 3-09-3 Gloria's CCC reaches its maximum areal extent, and registers its coldest temperatures. The location of the coldest temperature of -100°C is indicated by the arrow. Enhancement is the basic Dvorak, or "BD", curve applied to the 231431Z July infrared GMS imagery.

In the 24-hour period encompassing the full evolution of Gloria's CCC, the estimated intensity increased from 55 kt to 75 kt; hardly a remarkable change considering the extreme changes in the cloud pattern. This is consistent with Dvorak's findings that the appearance of a CCC signals arrested (or at least slowed) development which is renewed as the eye pattern of the T4 (minimal typhoon intensity) emerges beneath the thinning cirrus. Additional observations made during the occurrence of the CCC pattern in WNP TCs include the following:

1) the CCC usually begins to form at local sunset (this is at some variance with observations by Black and collaborators (e.g., Black, 1983; Black, et al., 1986; Black and Marks, 1987) who

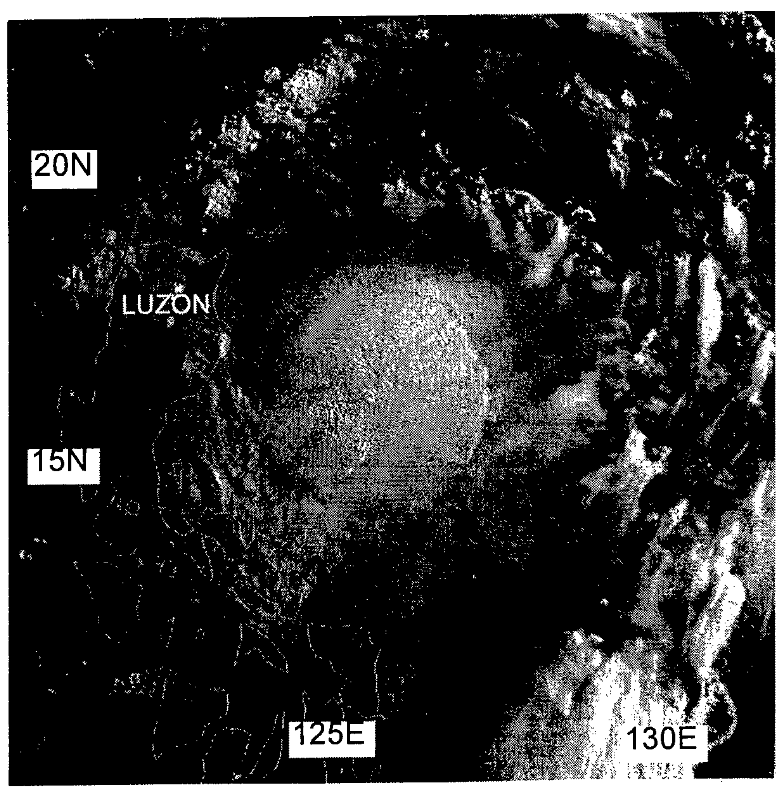

Figure 3-09-4 The appearance of Gloria's CCC by the early local daylight hours of 24 July: another pulse of dense cirrus is mushrooming into the thinning remains of earlier cold cirrus (232224Z July visible GMS imagery).

show that major cold convective eruptions in TCs tend to be initiated in the early morning);

2) the CCC reaches its greatest size and coldest temperature between local midnight and predawn; and,

3) the CCC pattern is most commonly observed to occur in weaker TCs that are at intensities of between T3 to T4 (45 - 65 kt) (this is consistent with observations of the aforementioned Black and collaborators; it is not consistent with guidance in Dvorak's 1984 report wherein it is stated that the CCC could occur at any stage of development of the TC and last for several hours to several days).

b. *The influence of Taiwan on the motion of tropical cyclones*

As Gloria was moving slowly to the northwest in the Luzon Strait, it made an abrupt turn to the north, and made landfall on the extreme southern tip of Taiwan. It then made an abrupt jump to the west coast of Taiwan before resuming a westward track toward mainland China. It is offered as a hypothesis that this abrupt meander in Gloria's track was induced by the island of Taiwan. Research by the Taiwan Central Weather Bureau (CWB) (1982) has demonstrated that the island of Taiwan can significantly alter the tracks of typhoons that approach it. The effects differ depending upon the angle of approach. The track changes noted during Gloria's approach to Taiwan are consistent with the track changes noted by the CWB which occur when a typhoon approaches Taiwan from the south or southeast.

IV. IMPACT

In the Philippines, Gloria was reported to have killed at least 20 people and caused nearly US $40 million in property damage. Hardest hit were the northeastern provinces of Luzon, where the eye of Gloria approached to within 60 nm (110 km) of the northeastern tip of the island. Gloria also passed to within 60 nm (110 km) of some of the smaller islands in the Luzon Strait where, although there were reports of typhoon force winds, the JTWC received no reports of any damage or injuries. On Taiwan, three people were reported killed: a child by a falling tree, an adult as he was blown from his motorcycle into a creek, and another adult as he fell from a roof. Rock slides disrupted traffic along Taiwan's east coast, and heavy rains flooded fields and caused several rivers to overflow their banks.

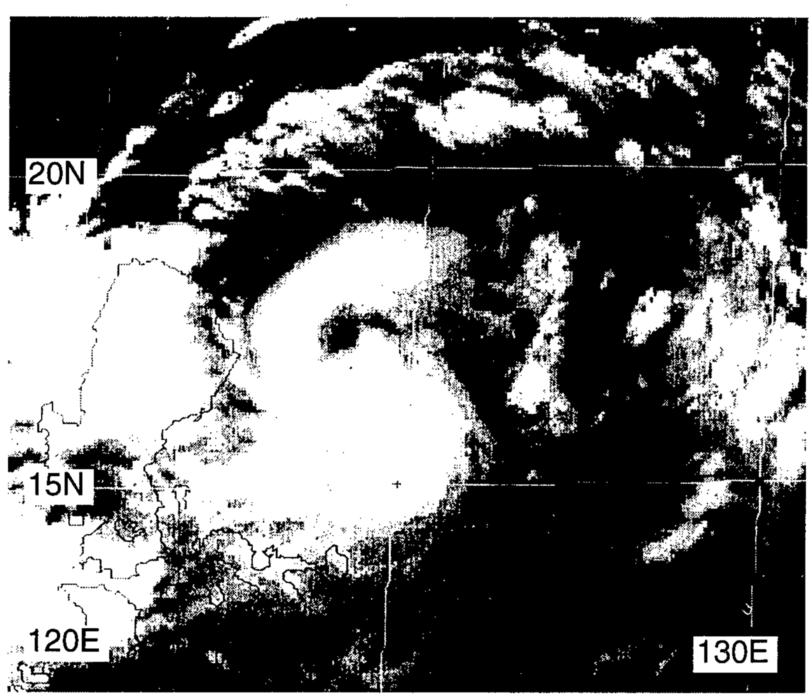

Figure 3-09-5 The eye, wall cloud, and peripheral rainbands of Gloria are plainly visible after the cirrus overcast of the CCC cleared away (240531Z visible GMS imagery).

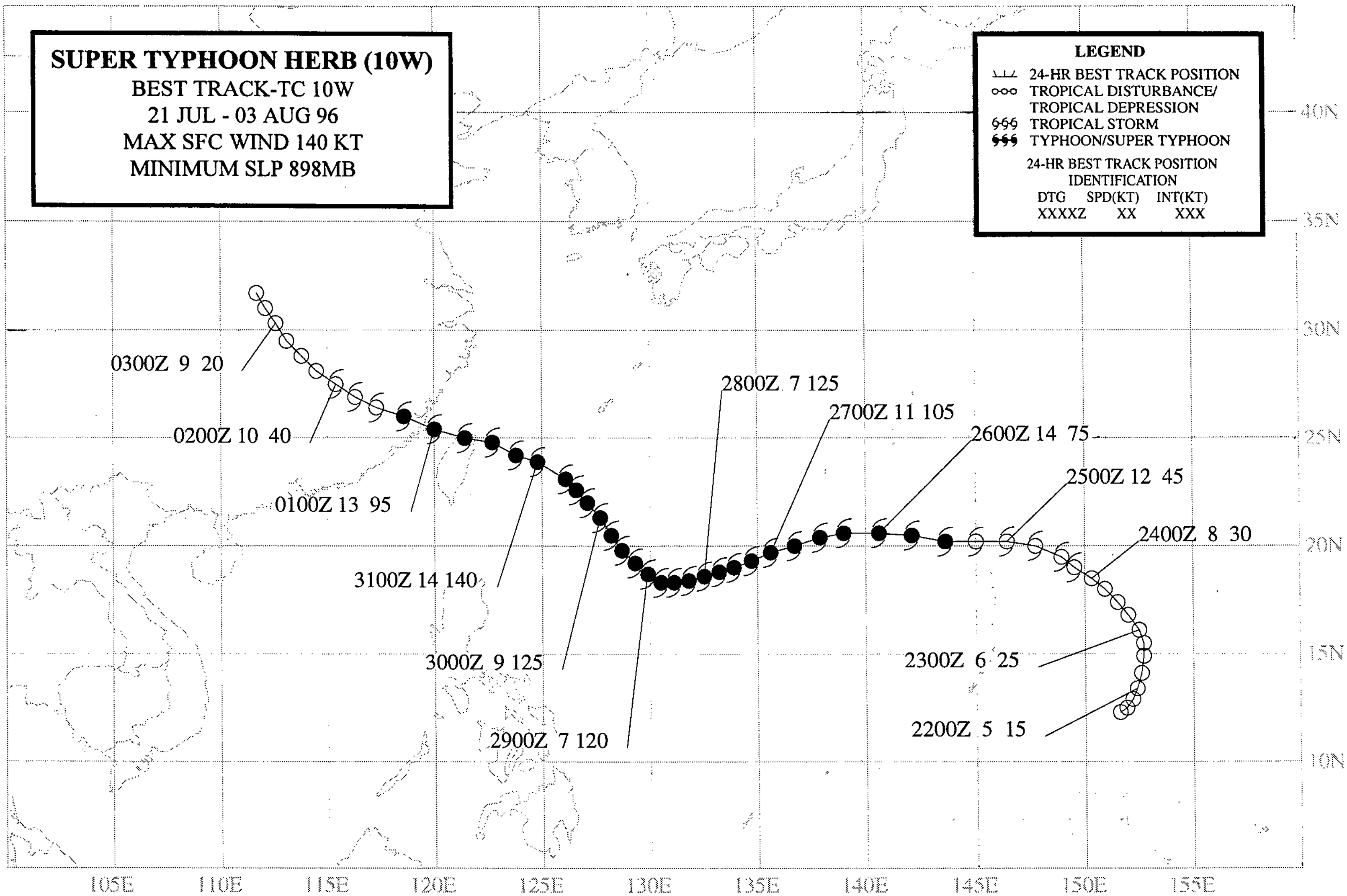
SUPER TYPHOON HERB (10W)
BEST TRACK-TC 10W
21 JUL - 03 AUG 96
MAX SFC WIND 140 KT
MINIMUM SLP 898MB
LEGEND
24-HR BEST TRACK POSITION
TROPICAL DISTURBANCE/
TROPICAL DEPRESSION
TROPICAL STORM
TYPHOON/SUPER TYPHOON
24-HR BEST TRACK POSITION
IDENTIFICATION
DTG SPD(KT) INT(KT)
XXXXZ XX XXX
0300Z 9 20
0200Z 10 40
0100Z 13 95
3100Z 14 140
3000Z 9 125
2900Z 7 120
2800Z 7 125
2700Z 11 105
2600Z 14 75
2500Z 12 45
2400Z 8 30
2300Z 6 25
2200Z 5 15
40N
35N
30N
25N
20N
15N
10N
105E
110E
115E
120E
125E
130E
135E
140E
145E
150E
155E

SUPER TYPHOON HERB (10W)

I. HIGHLIGHTS

When Herb formed, it became the easternmost of three tropical cyclones simultaneously active along the monsoon trough — the other two were Frankie (08W) and Gloria (09W). Herb's mode of formation was somewhat unusual: the cloud cluster from which it developed became organized into a "fishhook" cloud pattern. While moving generally westward toward China, Herb peaked twice in intensity. As the tropical cyclone neared its second peak intensity, it possessed a large eye. In addition, Herb was also a very large tropical cyclone; the largest tropical cyclone in terms of the mean Radius of Outermost Closed Isobar (ROCI) in the WNP during 1996. Herb made landfall in the southern Ryukyu Islands, Taiwan, and mainland China. Significant property damage and loss of life were attributed to Herb in these areas. On Taiwan, a new NEXRAD WSR 88D took a direct hit from Herb, and was severely damaged.

II. TRACK AND INTENSITY

During the latter half of July, extensive amounts of deep convection formed in an east-west band extending across the WNP from the coast of Southeast Asia to the Marshall Islands. By 21 July, this cloud band had consolidated into three distinct cloud clusters (Figure 3-10-1), all of which became named tropical cyclones — from west to east: Frankie (08W), Gloria (09W), and Herb. Based upon 24-hours of persistent deep convection, and synoptic data indicating the presence of an associated weak low-level cyclone beneath upper-level anticyclonic flow, the tropical disturbance that became Herb was first mentioned on the 210600Z July Significant Tropical Weather Advisory. Convection in this disturbance remained poorly organized until the morning of 23 July, when deep convection consolidated within a smaller area, and microwave imager data and visible satellite imagery indicated improved organization of the low-level circulation center (LLCC). This prompted the JTWC to issue a TCFA valid at 230000Z. Continued improvements in the organization of low-level cloud lines accompanying a persistent area of deep convection near the LLCC led to the first warning on Tropical Depression (TD) 10W valid at 230600Z.

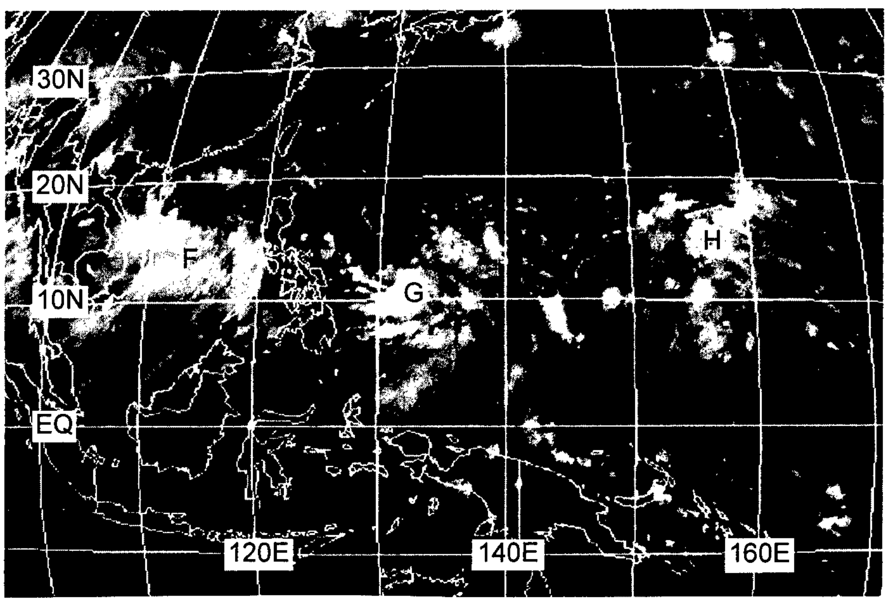

Figure 3-10-1 The cloudiness associated with the monsoon trough consolidates into three distinct cloud clusters that will soon become Frankie (08W), Gloria (09W), and Herb (201831Z July Infrared GMS imagery).

Based upon satellite intensity estimates, TD 10W was upgraded to Tropical Storm Herb on the warning valid at 240600Z. After becoming a tropical storm, Herb's central deep convection began to detach from the peripheral monsoon cloudiness to form a fishhook pattern (Figure 3-10-2).

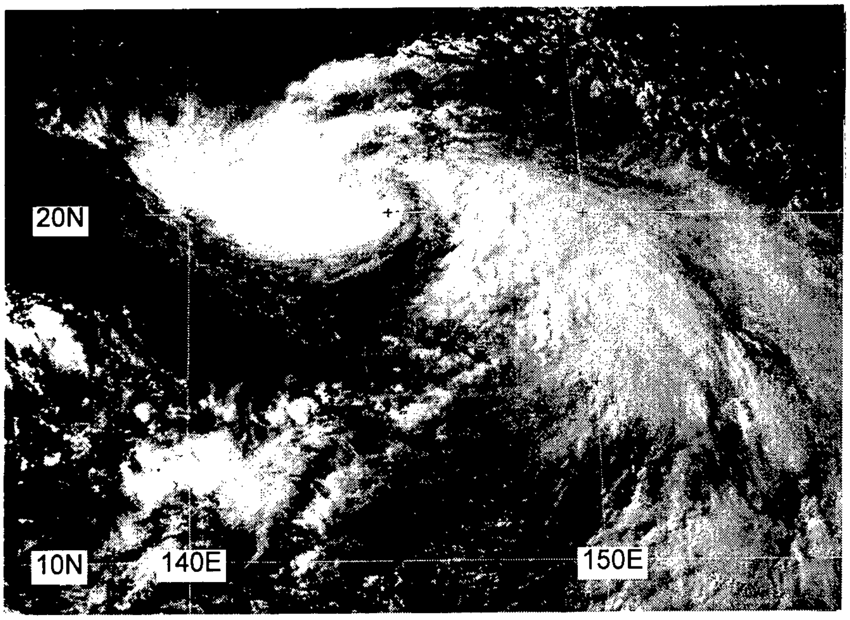

Figure 3-10-2 Herb's central deep convection begins to detach from the end of a fishhook shaped cloud pattern (250631Z July visible GMS imagery).

As the cloud system center moved to the head of the fishhook cloud pattern, Herb's motion became more westward. On a westward heading, Herb began to intensify and grow in size. Herb became a typhoon at 251200Z, and 48 hours later it reached 125 kt (64 m/sec) (Figure 3-10-3a,b); the first of two intensity maxima. At this time, Herb was moving in an unusual west-southwestward direction. This unusual motion may have been the result of an indirect interaction with Typhoon Gloria (09W) (the various types of direct and indirect interactions between two tropical cyclones are discussed in detail by Carr and Elsberry (1994)).

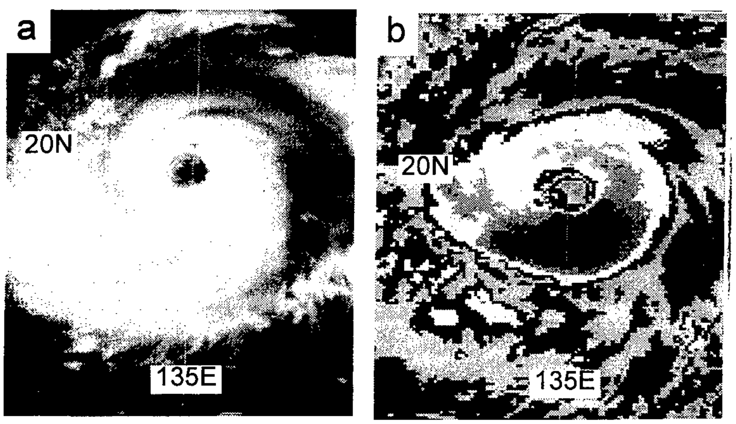

Figure 3-10-3 Herb nears its first of two intensity maxima: (a) 270331Z July visible GMS imagery and (b) 270331Z July enhanced infrared GMS imagery.

On 29 July, Herb began to weaken with its intensity falling to 115 kt (59 m/sec) at 290600Z. While the typhoon weakened, the system made a gradual track change from a west-southwestward heading during 28 July to a northwestward heading during 29 July. Although weakened slightly, Herb had become a very large tropical cyclone with a mean ROCI of approximately 8.5° of great-circle arc (Figure 3-10-4). Early on 30 July, Herb began to intensify once again, reaching a peak of 140 kt (72 m/sec) at 301800Z (Figure 3-10-5). After reaching its peak intensity, Herb took a more westward course which brought it ashore on the northeast tip of Taiwan at approximately 311600Z with a landfall intensity of 130 kt (67 m/sec). Passing over Taiwan, Herb lost its eye, but then regained a ragged eye during its short passage across the Taiwan Strait. It quickly lost its eye over land in China. The final warning was issued valid at 011200Z August as the system moved farther inland and dissipated.

III. DISCUSSION

a. *Unusual genesis*

While Herb was forming in the monsoon trough, it followed an unusual developmental pathway: the deep convection associated with Herb's LLCC moved on a backwards "C" shaped trajecto-

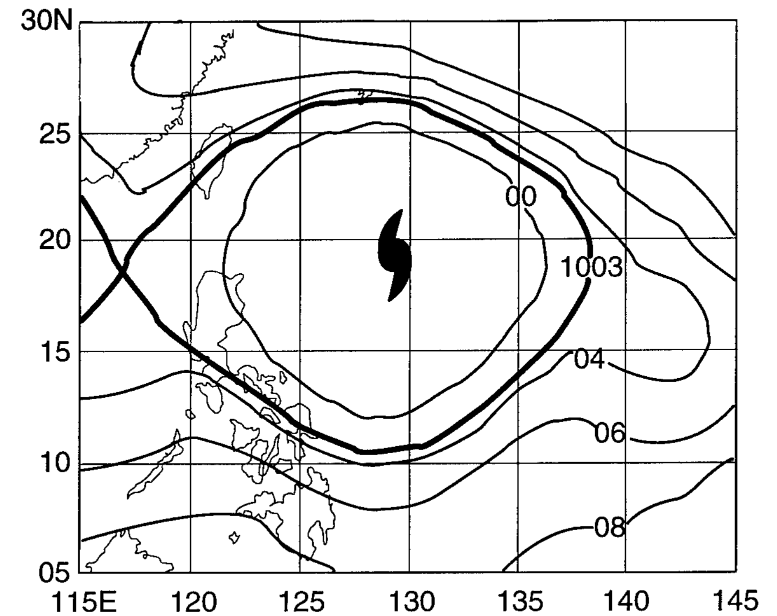

Figure 3-10-4 Herb became a very large tropical cyclone, the largest of 1996 in the WNP. As a measure of its size, the average radius of the outermost closed isobar is over 8.5° of great circle arc at 290000Z July. (290000Z July NOGAPS SLP analysis).

ry and gradually detached from the peripheral monsoon cloudiness to form a fishhook pattern (Figure 3-10-2). When the monsoon trough becomes organized as a monsoon gyre (Lander 1994) (see Appendix A), the large-scale monsoon cloud band often becomes organized into a large fishhook cloud pattern. One, or more, tropical cyclones may traverse the eastern periphery of the monsoon gyre (in a cyclonic orbit of the gyre) and emerge from the end of the fishhook. Although smaller in scale than the monsoon gyres cited by Lander (1994), the process of organization of the monsoon cloud pattern into a fishhook, and the backwards "C" motion of Herb as the fishhook evolved, are consistent with the cloud evolution and behavior of tropical cyclones associated with larger monsoon gyres.

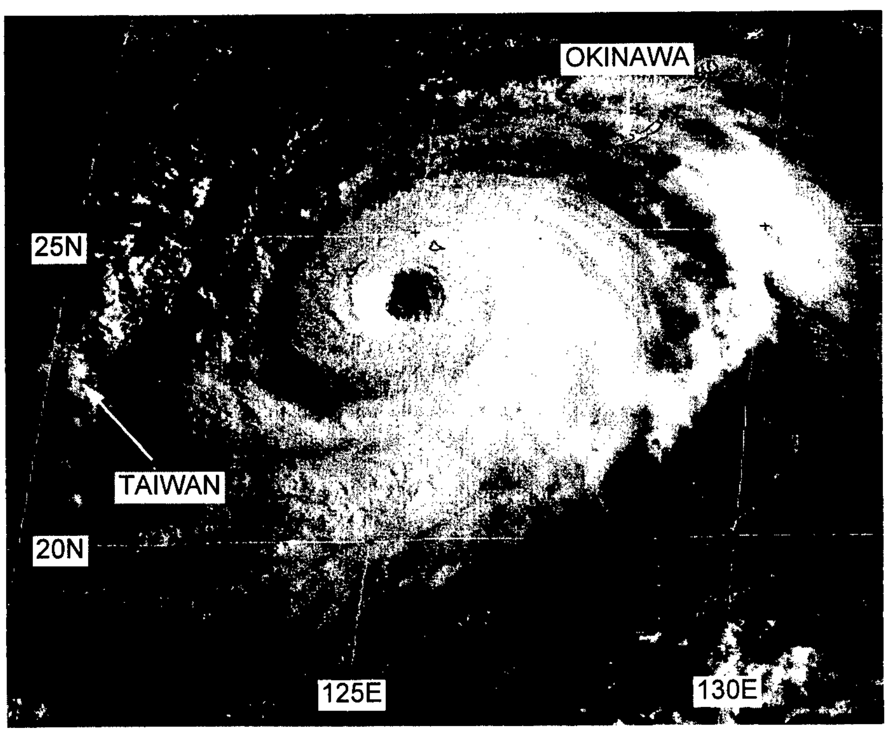

Figure 3-10-5 Herb at peak intensity of 140 kt (72 m/sec) (302224Z July visible GMS imagery).

b. *Three periods of intensification*

The time series of the DD numbers obtained for Herb (Figure 3-10-6) indicate three maxima: one maximum at approximately 270000Z, a second at approximately 281800Z, and a third sustained maximum during 30 July. The first maximum indicated by the DD algorithm occurred a little bit ahead of the first maximum in the final best track intensity. The best track intensity does not reflect the fall and rise of the DD time series to its second maximum. One reason for this, is that as the T-number falls, the Dvorak

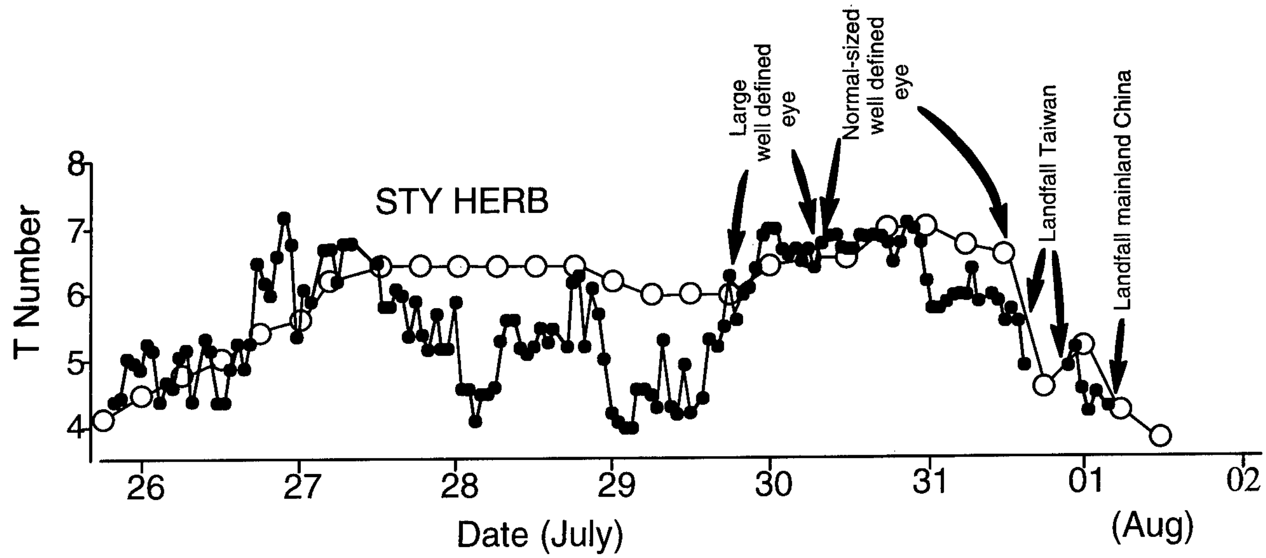

Figure 3-10-6 The time series of Herb's Digital Dvorak "DD" numbers (small dark circles) with the final best track intensity superimposed (large open circles).

technique requires that the current intensity be held one-half to one number higher than the T-number for at least 12 hours. For the most part, this is true of a comparison of Herb's DD time series with its final best track intensities (Figure 3-10-6). The second drop of intensity indicated on the DD time series was reflected by a slight drop in the warning and best track intensity before both rose once again to the peak that occurred on 30 July. Note that the DD time series contains some rather large fluctuations that do not appear in the final best track intensity time series. It is not known to what extent the fluctuations in the DD time series may represent actual short term changes in the intensity of tropical cyclones (see Bart's (04W) summary for a discussion of the DD algorithm).

c. *Largest tropical cyclone of 1996*

Super Typhoon Herb was the largest tropical cyclone of 1996. Using the mean ROCI as a measure of Herb's size, the system surpassed the threshold of the "very large" size category used by the JTWC (see Appendix A). At its largest, the mean ROCI of Herb was about 8.5° of great-circle arc (GCA) (Figure 3-10-4).

Tropical cyclone size is a very difficult parameter to objectively measure. Merrill (1984) classified a tropical cyclone as "small" if the mean ROCI was three degrees (180 nm, 335 km) GCA, or smaller; as "medium" if the mean ROCI was between three to five degrees GCA (180 nm (335 km) to 300 nm (555 km)), and as "large" if the mean ROCI was greater than five degrees GCA (greater than 300 nm). The Japan Meteorological Agency (JMA) recognizes two additional size categories — "very small" and "ultra large" — that mesh neatly with Merrill's scheme. The definitions of size used herein (see Appendix A) have been adapted by a mesh of the JMA size categories with those of Merrill.

d. *Eyewall mesocyclonic vortices as seen by Taiwan's NEXRAD*

Eyewall mesocyclonic vortices (EMs) were first detected and documented in airborne Doppler radar data by Marks and Houze (1984) and also with aircraft inertial navigation equipment as noted by Black and Marks (1991). Stewart and Lyons (1996) identified EMs with the Guam

NEXRAD in association with the passage of Super Typhoon Ed (1993). Until the implementation of the NEXRAD radar network in the United States during the early 1990s, only chance encounters with EMs have occurred during reconnaissance aircraft penetrations. However, now that Doppler velocity data are available, strong mesocyclones associated with TC outer convective bands and eyewall convection are frequently detected.

Stewart et al. (1997) used NEXRAD data to show that EMs in the wall clouds of TC eyes may be a mechanism for TC intensification and for extreme wind bursts in TCs as noted with Hurricane Andrew damage (Wakimoto and Black 1993). In three cases (including Herb), the TC underwent a period of rapid intensification during which time several vertically deep, EMs formed prior to the occurrence of rapid intensification and persisted for several hours while rapid deepening was occurring. Comments from Stewart et al. (1996) include:

"Approximately three hours prior to landfall in Taiwan, satellite imagery indicated Herb had weakened . . . In contrast, the [Taiwan NEXRAD] indicated that Herb was actually intensifying . . . As early as 310656Z July, [the NEXRAD] indicated intense EMs had begun to develop and this trend continued until the last available data at 311350Z [when the data record ended because of damage to the radar by high wind.] . . . . Although the [Taiwan NEXRAD] detected several EMs (as many as 6 EMs occurred simultaneously in the eyewall), one particular EM became quite intense and persisted for more than 1.5 hours just prior to Herb's landfall . . . This particular EM peaked at 311314Z with a rotational shear of 0.075/sec which is more than triple the [NEXRAD] criteria for a Tornadic Vortex Signature . . ."

Based on observations of EMs in TCs (including Herb), Stewart et al. (1997) conclude that the EMs appear to have a positive feedback on TC intensification.

IV. IMPACT

In addition to the destruction of Taiwan's NEXRAD, Herb caused extensive damage to property and agriculture in Taiwan and China. At least 51 lives were lost and 22 missing in Taiwan. Twenty-four of these lives were lost in the city of Nantou, 120 miles south of Taipei, due to rock-slides and flooding. Daily rain totals of nearly 40 inches (1000 mm) were reported over the central mountain range. An estimated US $5 billion dollars of damage to crops, roads and power equipment was reported in Taiwan. In China, rains from Herb contributed to flooding that killed upwards of 250 people. In Fujian Province, 950 miles south of Beijing, at least 233 people were reported killed and 284 missing when flooding destroyed 70,000 homes.

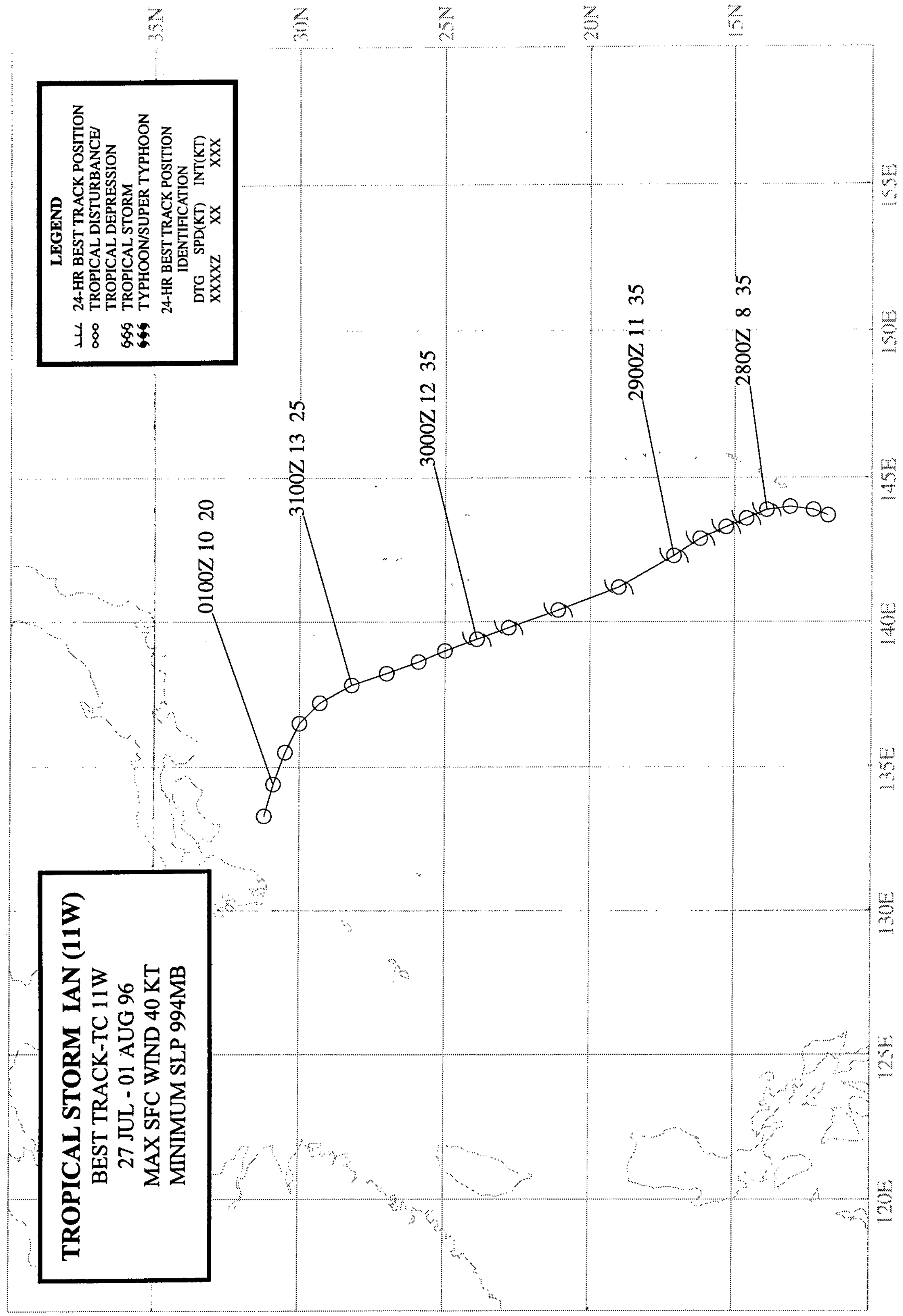
TROPICAL STORM IAN (11W)
BEST TRACK-TC 11W
27 JUL - 01 AUG 96
MAX SFC WIND 40 KT
MINIMUM SLP 994MB
LEGEND
24-HR BEST TRACK POSITION
TROPICAL DISTURBANCE/
TROPICAL DEPRESSION
TROPICAL STORM
TYPHOON/SUPER TYPHOON
24-HR BEST TRACK POSITION
IDENTIFICATION
DTG SPD(KT) INT(KT)
XXXXZ XX XXX
0100Z 10 20
3100Z 13 25
3000Z 12 35
2900Z 11 35
2800Z 8 35
35N
30N
25N
20N
15N
120E
125E
130E
135E
140E
145E
150E
155E

TROPICAL STORM IAN (11W)

I. HIGHLIGHTS

Ian formed at the end of the monsoon trough and then moved on a north-northwestward track while embedded within the peripheral southerly flow on the eastern side of the very large Super Typhoon Herb (10W). The initial warnings on Ian were based primarily on synoptic reports from the islands of Guam and Saipan because the circulation was poorly organized on satellite imagery.

II. TRACK AND INTENSITY

During the final week of July, Super Typhoon Herb (10W) grew in size and came to dominate much of the flow of the WNP. On 27 July, a large area of deep convection became established in the monsoon flow to the south and east of Herb (Figure 3-11-1). The possibility of tropical cyclogenesis occurring in association with this area of deep convection was first mentioned on the 271800Z Significant Tropical Weather Advisory. Comments on this advisory included:

". . . An area of convection is located [southeast of Guam] . . . within the monsoon trough. Sounding data from Guam indicates falling heights throughout the lower troposphere. Additionally, northerly winds at Guam suggest a circulation center southeast of the island. As Typhoon Herb moves westward, this region becomes an increasingly favorable genesis area . . ."

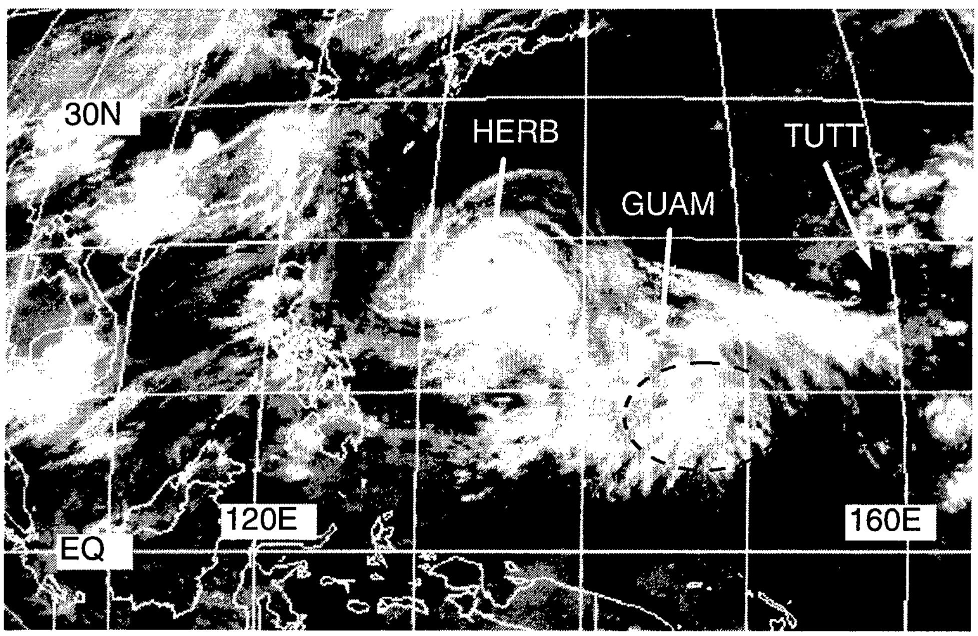

Figure 3-11-1 A large ensemble of mesoscale convective systems develops in monsoon flow to the southeast of Herb (dashed circular area) (271331Z July infrared GMS imagery).

Based upon reports of increasing winds and falling pressures on Guam and Saipan, a Tropical Cyclone Formation Alert was issued valid at 280430Z. The circulation center was then estimated to have been approximately 50 nm (90 km) to the west of Guam, and drifting slowly northward. Later that day, two ships moored at Saipan reported to the JTWC that they were experiencing gales and had to put to sea. Based upon these ship reports, and from high winds (20 to 30 kt) and low pressure (1003 mb) experienced on Guam and Saipan, the first warning on Tropical Depression (TD) 11W was released valid at 281200Z. When an area of persistent deep convection became established near the estimated center location, TD 11W was upgraded to Tropical Storm Ian on the warning valid at 290000Z. In post analysis, based upon data recorded in the logs of the

aforementioned ships which had to depart Saipan, and upon indications on microwave imagery (Figure 3-11-2) that the organization of the deep convection was better than indicated on conventional visible (Figure 3-11-3) and infrared satellite imagery, TD 11W was increased to a tropical storm at 280000Z.

On 29 July, a third TC — TD 12W formed within a TUTT cell to the northeast of Ian (see Joy's (12W) summary and figure 3-11-1) to create a reverse-oriented monsoon trough that stretched northeastward from Herb (10W). Embedded in this trough, and also embedded in the large circulation of Herb (10W), Ian moved northward, as anticipated. Strong upper-level northwesterly winds, which were part of Herb's extensive outflow, exerted shear on Ian, and the system failed to mature. Instead, the low-level circulation center (LLCC) became displaced to the north of Ian's deep convection, and the system was downgraded to a tropical depression on the warning valid at 300600Z. On 31 July, deep convection was completely sheared away from Ian's LLCC, and the final warning was issued valid at 310600Z as the exposed LLCC slowly dissipated over water to the south of Japan.

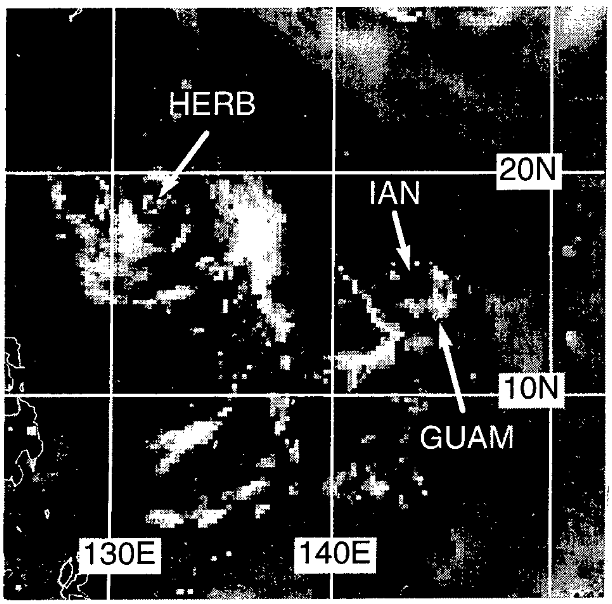

Figure 3-11-2 Deep convection associated with Ian is organized into cyclonically-curved bands (280914Z July 85 GHz microwave DMSP imagery).

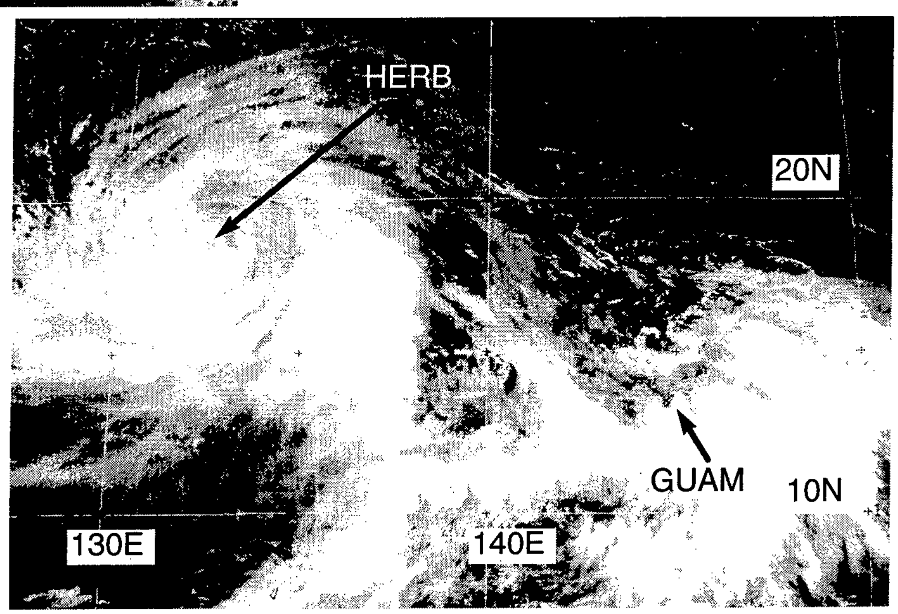

Figure 3-11-3 Although the deep convection appears to be poorly organized, a low pressure area associated with over-water gales has developed near Guam and Saipan. In post analysis, Ian became a tropical storm at this time (272331Z July visible GMS imagery).

III. DISCUSSION

a. *Unusual structure*

As Ian moved northward in a cyclonically-curved track around the eastern periphery of the larger circulation of Herb (10W), it was often difficult to establish whether it was an independent cyclonic circulation, vice a cusp or a wave. Synoptic data indicated for most of its life, Ian took the form of a cusp, with a region of gales on its eastern side and a zero velocity singularity at the center (or at most, a very small region of northerly winds on its western side) (Figure 3-11-4). When Ian passed Guam and Saipan, it was at first thought the high winds were associated with a surge (or squall line) in the monsoon. The drop of pressure to 1003 mb at its closest point of approach, the day-long duration of high wind, and a subsequent 24-hour pressure rise of 8 mb in 24 hours at Guam, however, were more consistent with the passage of a tropical cyclone.

b. *Ian as a "satellite" of Herb (10W)*

Occasionally, small TCs are observed to develop in the peripheral flow of very large TCs in the WNP. These small TCs tend to be weak, have short life spans, and are advected around the larger TC. These small TCs which form and orbit in the peripheral flow of very large TCs will herein be called "satellite" TCs, based upon the astronomical analogy of a small object (i.e., a satellite) in orbit of a much larger object. Very large TCs in recent years which have had smaller "satellite" TCs in their peripheral circulation include Abby (1983) which had two "satellites" (Ben and Carmen), and Hal (1988) which also had two "satellites" (Jeff and Irma). Ian was a "satellite" TC of the very large Herb (10W), and was closely analogous with respect to its cloud signature and relative position to Hal's "satellite", Irma (1988).

IV. IMPACT

Much of the northern half of Saipan lost power when high winds associated with Ian caused power lines to short out against tree branches. Some similar spot power outages occurred on Guam. Also on Saipan, some ships at anchor were forced to put to sea. No other reports of significant damage or injuries attributable to Ian were received by the JTWC.

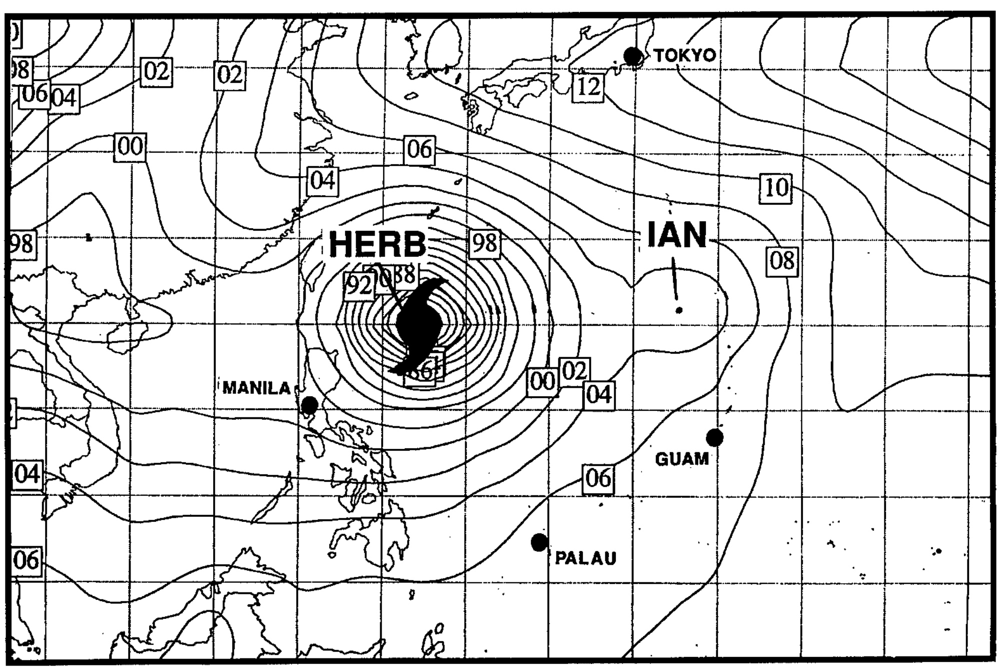

Figure 3-11-4 Ian, which is embedded within the strong southerly flow on the eastern side of Herb, is difficult to "close-off" (290000Z July NOGAPS sea-level pressure analysis).

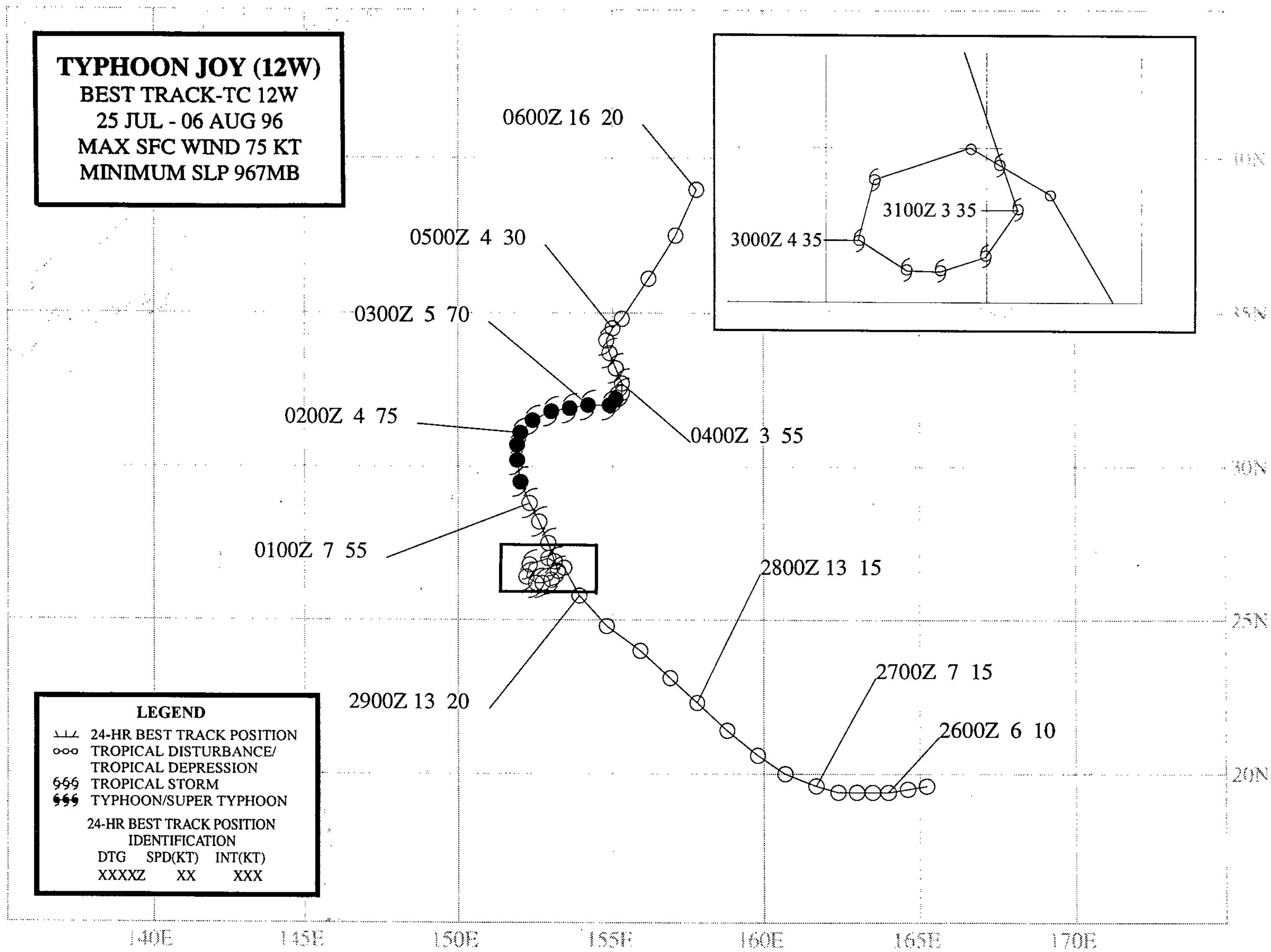
TYPHOON JOY (12W)
BEST TRACK-TC 12W
25 JUL - 06 AUG 96
MAX SFC WIND 75 KT
MINIMUM SLP 967MB
0600Z 16 20
0500Z 4 30
0300Z 5 70
0200Z 4 75
0400Z 3 55
0100Z 7 55
2800Z 13 15
2900Z 13 20
2700Z 7 15
2600Z 6 10
3100Z 3 35
3000Z 4 35
LEGEND
24-HR BEST TRACK POSITION
TROPICAL DISTURBANCE/
TROPICAL DEPRESSION
TROPICAL STORM
TYPHOON/SUPER TYPHOON
24-HR BEST TRACK POSITION
IDENTIFICATION
DTG SPD(KT) INT(KT)
XXXXZ XX XXX
35N
30N
25N
20N
140E
145E
150E
155E
160E
165E
170E

TYPHOON JOY (12W)

I. HIGHLIGHTS

Joy formed at a relatively high latitude in direct association with a TUTT cell, and did not become a typhoon until it had moved to nearly 30°N. Prevented from recurving by a blocking high, the system moved slowly on a meandering north-oriented track.

II. TRACK AND INTENSITY

During the final week of July, a monsoon trough became established across the WNP, and three tropical cyclones formed simultaneously in this trough — Frankie (08W), Gloria (09W), and Herb (10W). Several days later, Ian (11W) and Kirk (13W) also formed at the eastern end of this monsoon trough. During the time this activity was occurring in the monsoon trough, a TUTT cell (that was first detected near the international date line), was moving slowly westward along 20°N. The tropical disturbance which became Joy originated directly from deep convection associated with this TUTT cell (see the discussion section for more details). On 27 July, deep convection associated with this TUTT cell increased, cirrus outflow became organized into a well-defined anticyclonic pattern, and visible satellite imagery indicated that a low-level circulation had formed, which led to its inclusion on the 270600Z July Significant Tropical Weather Advisory. Comments on this advisory included:

". . . An area of convection is located near 21N 160E. Visible satellite imagery indicates the presence of a low-level cyclonic circulation beneath well-defined anticyclonic flow aloft. Water vapor imagery also indicates that a [TUTT] cell is located to the south of the disturbance. . . ."

The TUTT cell continued its westward motion for the next two days, and the convection located to its north remained poorly organized until 29 July when a small area of deep convection persisted near the estimated low-level circulation center. The first warning on Tropical Depression (TD) 12W was issued valid at 290600Z based on a satellite intensity estimate of 25 kt (13 m/sec). Upgrade of TD 12W to Tropical Storm Joy occurred on the warning valid at 300000Z, based upon a satellite intensity estimate of 35 kt (18 m/sec).

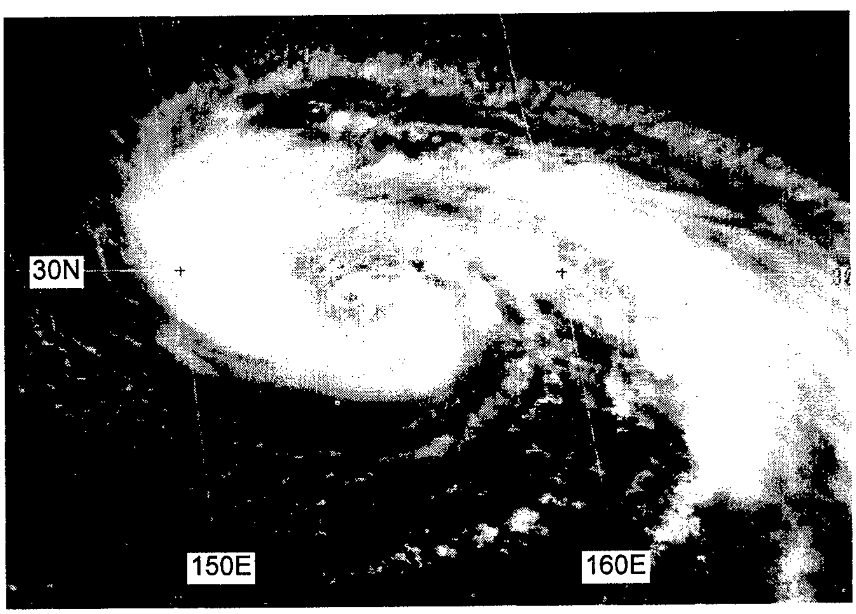

Figure 3-12-1 Joy's primary band of deep convection coils into a banding-type eye (010331Z August visible GMS imagery).

Between 29 and 30 July, Joy remained nearly stationary in weak steering before intensifying as it began moving slowly toward the north-northwest on 31 July. During the daylight hours of 01 August, Joy became well-organized, and its primary band of deep convection became tightly coiled to form a banding-type eye (Figure 3-12-1). This prompted the JTWC to upgrade Joy to a typhoon on the warning valid at 010600Z September.

Meandering slowly northward, Joy reached its peak intensity of 75 kt (39 m/sec) at 011800Z (Figure 3-12-2).

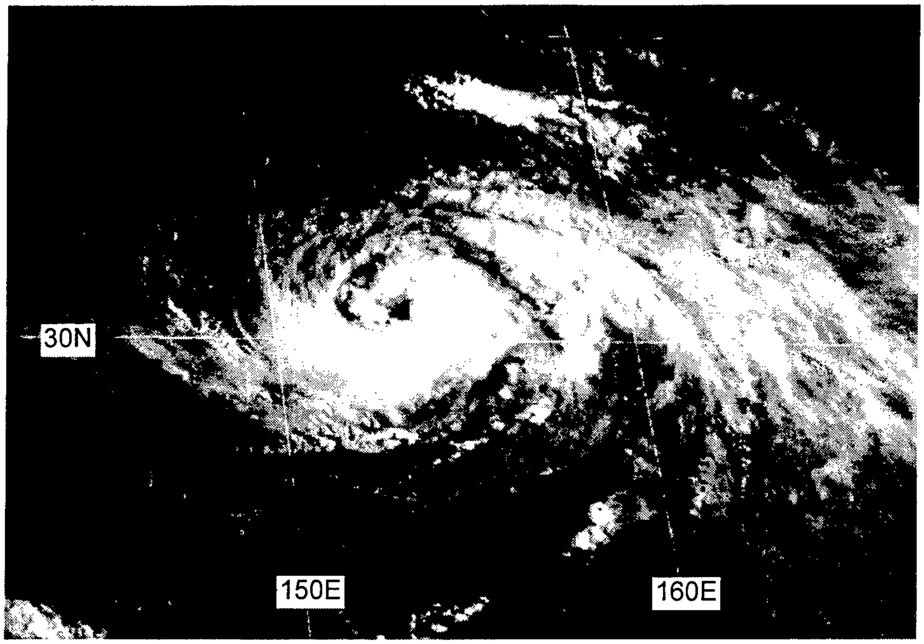

Figure 3-12-2 Joy at its peak intensity of 75 kt (39 m/sec) (012131Z August visible GMS imagery).

Continuing its slow northward drift, Joy began to shear on 04 August. On 05 August, Joy still had some deep convection located to the east of its exposed LLCC, but it had begun to accelerate toward the north-northeast as it interacted with a slow moving north-south oriented frontal cloud band. Expecting Joy to merge with the frontal cloud band and become extratropical, the JTWC issued the final warning valid at 050600Z.

III. DISCUSSION

Tropical cyclogenesis induced by a TUTT cell

A persistent feature of the upper-tropospheric flow over the tropics of the WNP and North Atlantic oceans during the summer is the tropical upper-tropospheric trough (TUTT) (Sadler, 1975). In the mean, the axis of the TUTT overlies low-level easterly trade wind flow approximately midway between the axis of the subtropical ridge and the axis of the monsoon trough.

In synoptic analyses, the TUTT is commonly observed to consist of a chain of westward moving synoptic-scale cyclonic vortices called "TUTT cells" in the WNP ("upper cold lows" in the Atlantic). The typical distribution of clouds associated with a TUTT cell features a relatively small region of isolated cumulonimbi (CB) or small mesoscale convective systems (MCS) within (or very near) its core. Sometimes extensive multi-layered clouds with embedded CB and MCSs are found to its south and east. The cloudiness to the south and east of a TUTT cell in the WNP is often associated with the monsoon trough, and the TUTT cell (or a chain of TUTT cells) acts to modulate the distribution of cloudiness along the axis of the trough, and also acts to produce an accentuated sinusoidal pattern to the outflow cirrus on the northern side of the monsoon cloud band.

Sadler (1967) proposed that the TUTT (with its embedded TUTT cells) was the primary source for disturbances (e.g., inverted troughs, isolated clusters of CB, etc.) in the trade wind flow. Sadler (1967) also credits TUTT cells with the capacity to induce TC genesis. TUTT-induced TC genesis was envisioned by Sadler to be the result of the distal penetration of the TUTT cell cyclonic circulation to the lower levels, thereby initiating deep convection which, through the release of latent heat, gradually converted the TUTT cell into a warm-core low (i.e., a TC). In two later papers (Sadler 1976, 1978), the role of the TUTT (and of TUTT cells within it) is relegated to one of contributing to the development of a TC by providing a region of persistent upper-level divergence to

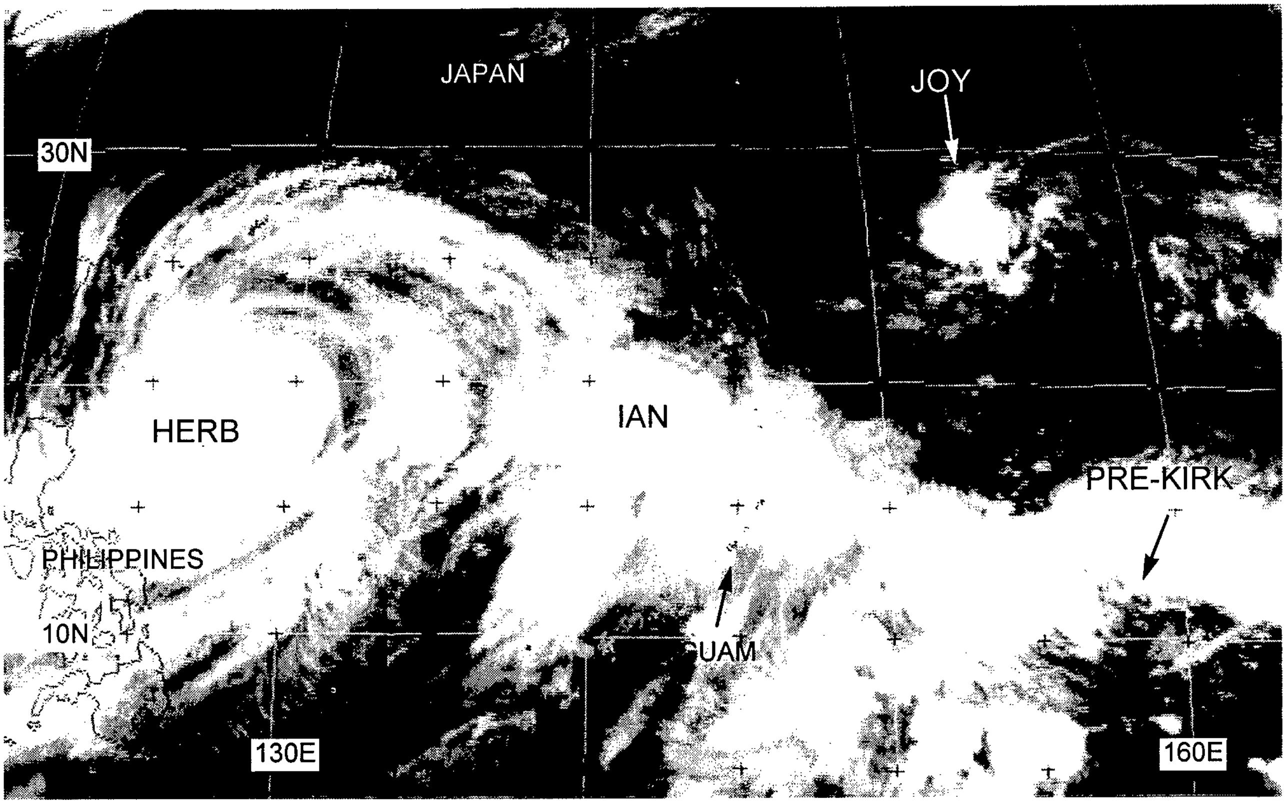

Figure 3-12-3 A characteristic typical of TUTT-induced tropical cyclones, Joy is isolated in the relatively cloud-free region of easterly low-level wind flow to the north of the monsoon cloud band (291331Z July infrared GMS imagery).

initiate and maintain deep convection. The TUTT cell also creates an efficient outflow channel for the incipient TC. In this scenario, the TC is usually located to the south or southeast of the TUTT, or a TUTT cell that propagates in tandem with it.

In our investigations of the role of the TUTT — and in particular, TUTT cells — in TC formation in the WNP, we have observed a process whereby a TC forms (sometimes rapidly) near the core of a TUTT cell. This process is similar to Sadler's (1967) distal mechanism of TUTT-cell induced TC formation. Careful observation has shown that the isolated convective cloud cluster (i.e., a mesoscale convective system) that forms a TC near the TUTT cell, does so not directly in the core of the TUTT cell, but usually within 200 to 400 km to the east through north of the upper-level circulation center of the TUTT cell where the upper-level flow is diffluent and anticyclonically curved. Also, it is here, on the northern side of the TUTT cell, that both the upper-level and lower-level flow is easterly resulting in a region of low vertical wind shear. Another typical characteristic of these TUTT-induced tropical cyclones is their isolation in the cloud minimum region of easterly wind flow to the north of the monsoon cloud band (e.g., Figure 3-12-3). The origin of Joy from a TUTT cell is well illustrated by water-vapor imagery (Figure 3-12-4a-g).

IV. IMPACT

No reports of injuries or damage were received at the JTWC.

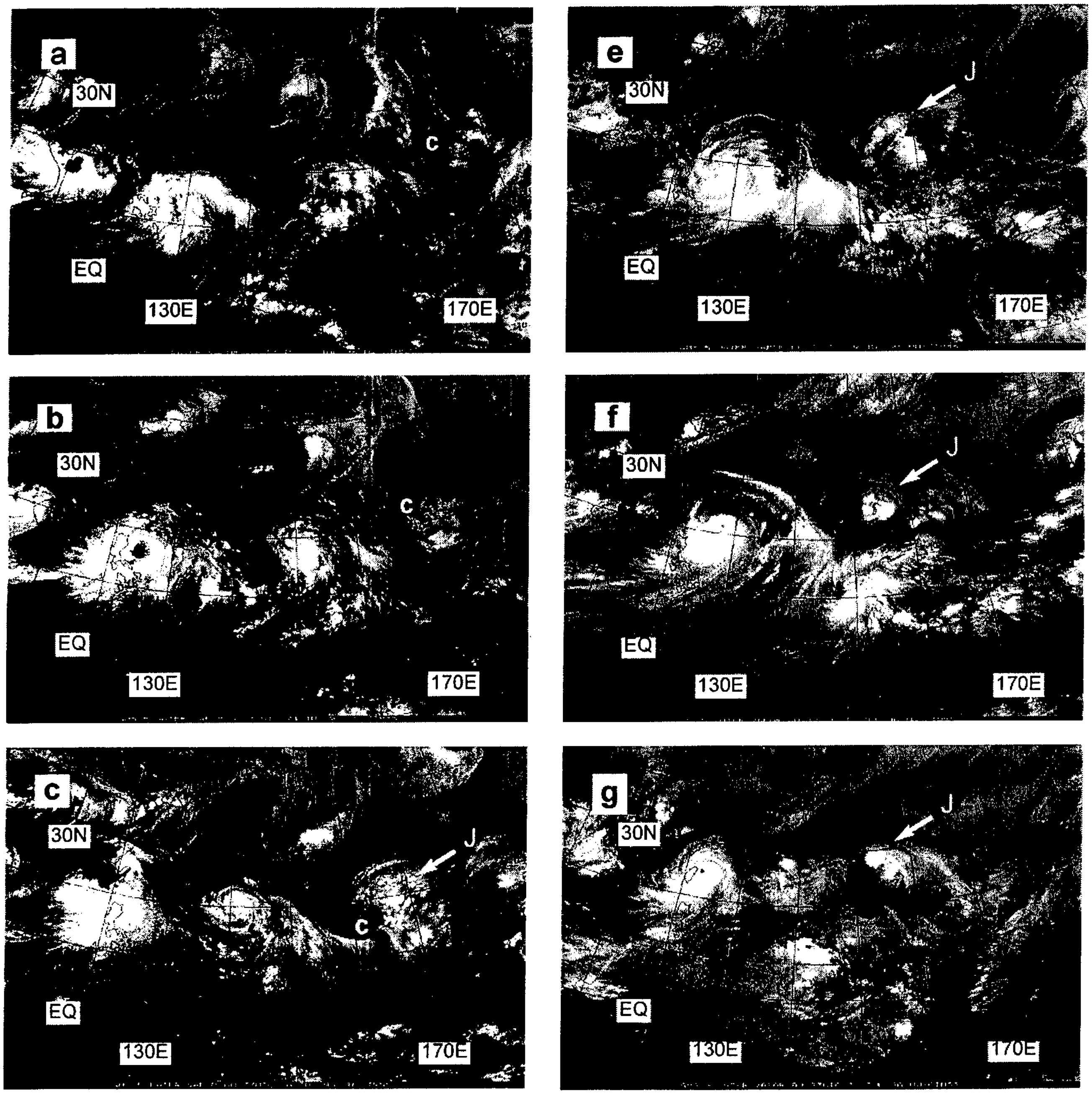

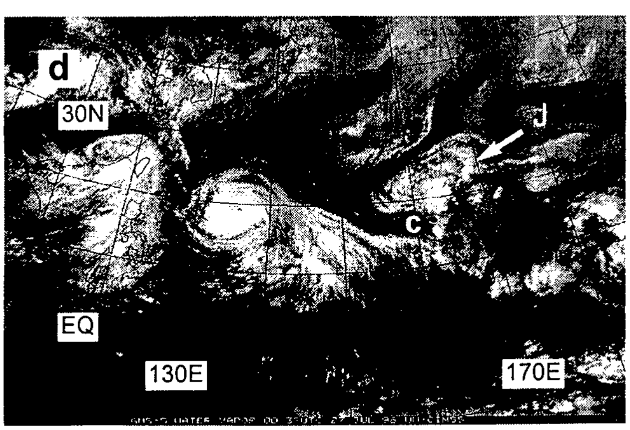

Figure 3-12-4 A TUTT cell (C) moves westward along 20°N in the WNP and induces the formation of Joy (J): (a) 212331Z July, (b) 240031Z, (c) 260031Z. (d)270031Z, (e) 290031Z, (f) 300031Z, and (g) 310931Z July water-vapor GMS imagery.

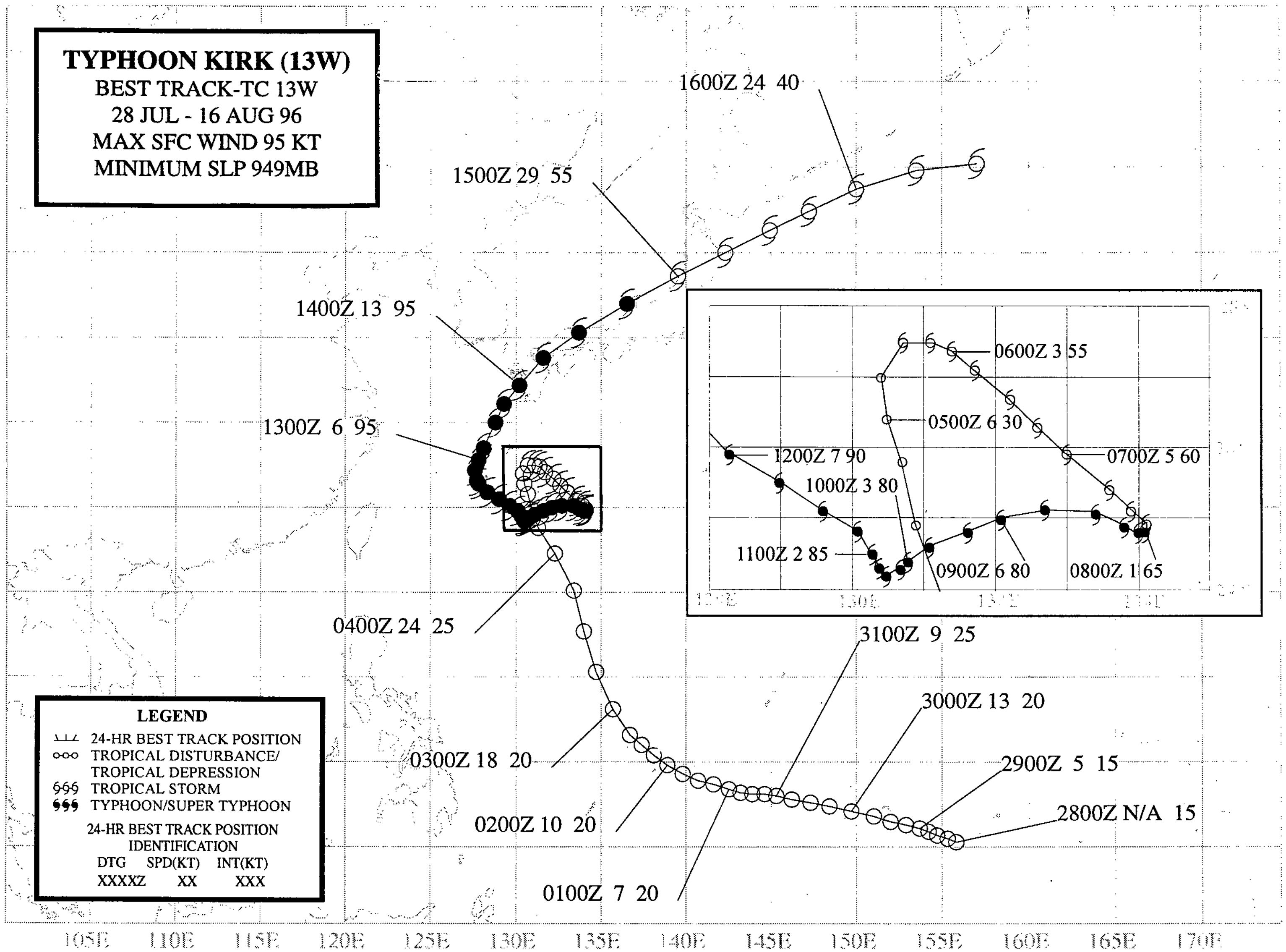
TYPHOON KIRK (13W)
BEST TRACK-TC 13W
28 JUL - 16 AUG 96
MAX SFC WIND 95 KT
MINIMUM SLP 949MB
LEGEND
24-HR BEST TRACK POSITION
TROPICAL DISTURBANCE/
TROPICAL DEPRESSION
TROPICAL STORM
TYPHOON/SUPER TYPHOON
24-HR BEST TRACK POSITION
IDENTIFICATION
DTG SPD(KT) INT(KT)
XXXXZ XX XXX
1600Z 24 40
1500Z 29 55
1400Z 13 95
1300Z 6 95
0400Z 24 25
0300Z 18 20
0200Z 10 20
0100Z 7 20
3100Z 9 25
3000Z 13 20
2900Z 5 15
2800Z N/A 15
0600Z 3 55
0500Z 6 30
1200Z 7 90
0700Z 5 60
1000Z 3 80
1100Z 2 85
0900Z 6 80
0800Z 1 65
50N
45N
40N
35N
30N
25N
20N
15N
10N
5N
105E
110E
115E
120E
125E
130E
135E
140E
145E
150E
155E
160E
165E
170E

TYPHOON KIRK (13W)

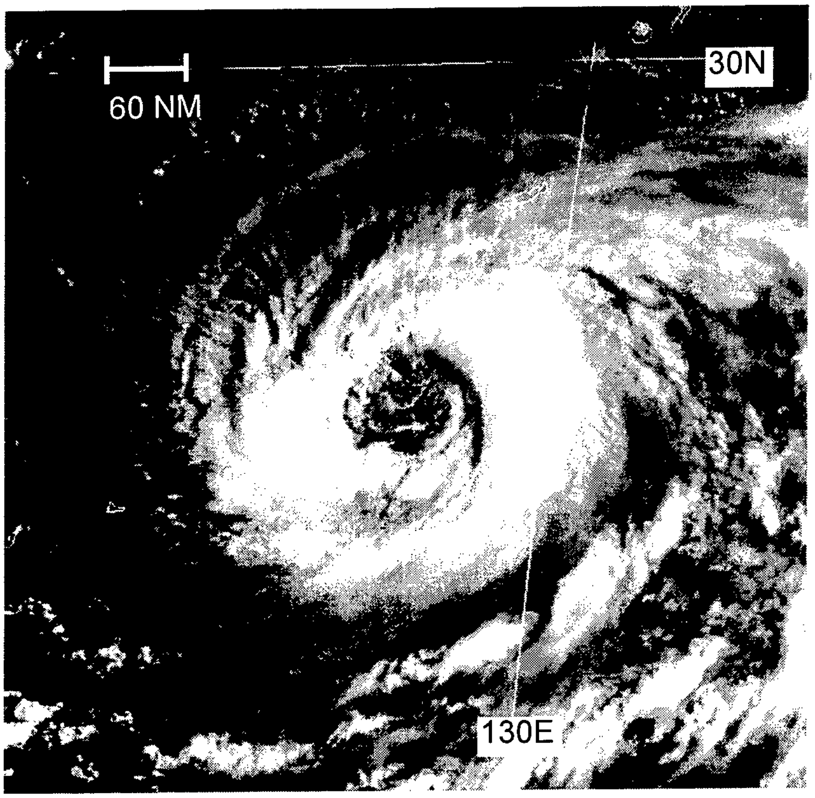

Figure 3-13-1 Kirk exhibits a very large eye as it approaches Okinawa (112331Z August visible GMS imagery).

I. HIGHLIGHTS

Forming from a monsoon depression in the Philippine Sea, Kirk moved on a complex north-oriented track which saw it undergo an unusual anticyclonic loop before passing directly over Okinawa. Kirk was the first of three TCs during 1996 to acquire a very large eye (Figure 3-13-1) — it took a full 12 hours for Kirk's 70-nm (130-km) diameter eye to pass over Okinawa. The NEXRAD Doppler radar at Kadena AB afforded a rare chance to investigate a typhoon with a ground-based radar from within the eye. After passing over Okinawa, Kirk moved north and passed over southern Japan where extensive property damage and loss of life were reported.

II. TRACK AND INTENSITY

During the final days of July, the tropical disturbance which became Kirk formed at the end of the monsoon trough to the southeast of Guam while both Herb (10W) and Joy (12W) were still active. During the first few days of August, Herb moved into China, Joy moved into the midlatitudes, and the pre-Kirk tropical disturbance was subsumed by a larger monsoon depression that formed in the Philippine Sea (Figure 3-13-2). Slow to consolidate (and undergoing a major structural change), the pre-Kirk disturbance received a total of five Tropical Cyclone Formation Alerts (TCFA) prior to the issuance of the first warning.

The tropical disturbance which became Kirk was first mentioned on the Significant Tropical Weather Advisory valid at 290600Z July, when synoptic data showed that a weak low-level circulation accompanied an area of convection near Chuuk. The first TCFA was issued valid at 292100Z when amounts of deep convection increased near the persistent low-level circulation center (LLCC). The second TCFA was issued valid at 300730Z to reposition the alert box for the continued west-northwestward motion of the pre-Kirk disturbance. This disturbance was undergoing large fluctuations in the amounts and organization of its deep convection which consisted of an ensemble of mesoscale convective systems (MCS), a hallmark characteristic of a monsoon depression. At 310300Z, the second TCFA was canceled when convection became more poorly organized. On 01 August, extensive amounts of deep convection formed in the Philippine Sea — disorganized bands and small clusters of MCSs occupied an area within a box bounded by 5°N to 25°N and 130°E to 150°E. On 02 August, this large area of deep convection became organized as a large monsoon depression (Figure 3-13-2) comprised of an enormous ensemble of MCSs associated with a large, but weak, cyclonic circulation and extensive cirrus outflow organized into an anticyclonic pattern. A third TCFA was issued valid at 020030Z August when scatterometer data indicated the presence of an LLCC with monsoon gales located to its southeast. Remarks on this TCFA include:

". . . A disturbance resembling a monsoon depression is located within the monsoon trough. Scatterometer data [from an earlier pass of the ERS-1 satellite] supports the presence of a closed low-level circulation center, with gale force winds located 180 nm to the southeast of the circulation. These winds are associated with a surge in the monsoon. . . ."

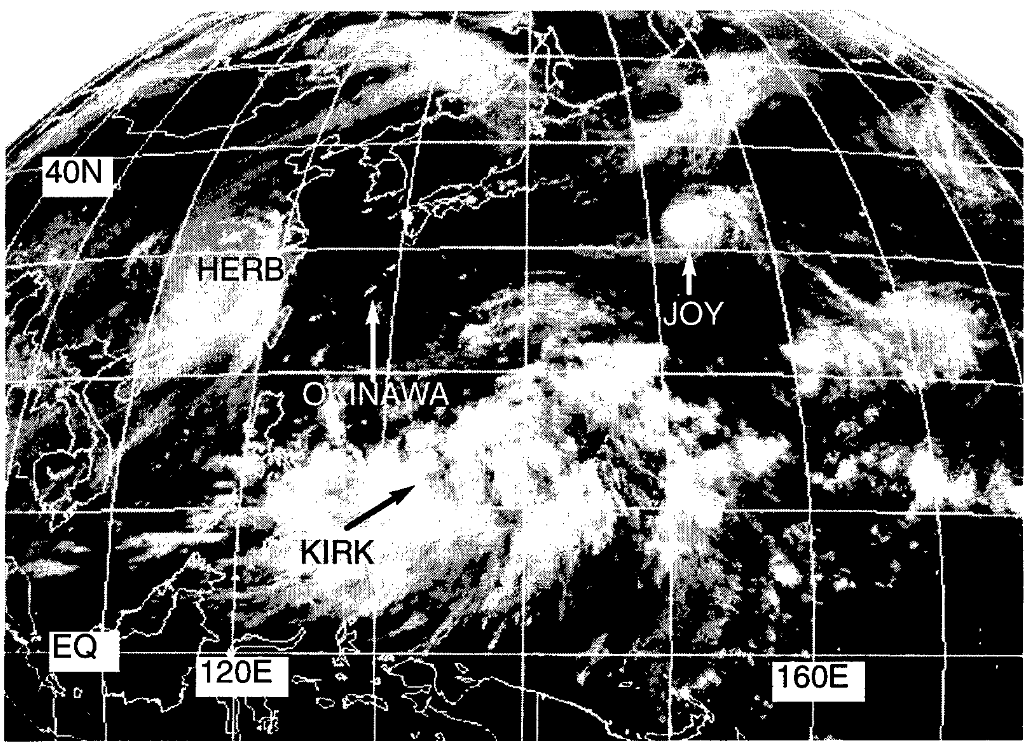

Figure 3-13-2 The monsoon depression in the Philippine Sea from which Kirk developed (020631Z August infrared GMS imagery).

As is often the case with TCs originating from a monsoon depression, the extensive ensemble of MCSs associated with the monsoon depression fluctuated greatly, and were slow to consolidate near a well-defined LLCC. Thus a fourth TCFA was issued valid at 030030Z when satellite

imagery could not confirm the presence of a well-defined LLCC, and deep convection was still widely distributed and not showing signs of consolidation. The fifth, and last, TCFA was issued valid at 031100Z in order to reposition the alert box to encompass an area of deep convection that was becoming organized outside the alert box specified by the fourth TCFA. This area of deep convection increased in organization near the LLCC, and the first warning on Tropical Depression (TD) 13W was issued valid at 031800Z.

Moving on a north-oriented track within a monsoon trough which had become reverse oriented (see Appendix A), TD 13W gradually slowed its forward speed, and on 06 August, it turned toward the southeast as it began an anticyclonic loop in its track. On the warning valid at 060000Z, TD 13W was upgraded to Tropical Storm Kirk.

While executing its anticyclonic loop, Kirk intensified and became a typhoon at 080000Z. At this time, it began to move on a generally westward heading toward Okinawa. Before reaching Okinawa on 12 August, Kirk's eye became extremely large (see Discussion section). Radar and satellite measurements of its eye diameter exceeded 60 and 70 nm respectively during most of 12 August (Table 3-13-1).

After passing over Okinawa, Kirk turned toward the north, its eye diameter decreased, and the system reached its peak intensity of 95 kt (49 m/sec) (Figure 3-13-3) while accelerating along a recurving track that brought it across southern Japan and into the Sea-of - Japan. Kirk dropped below typhoon intensity as it skirted northeastward along the coast line on the Sea of Japan side of Honshu. On 15 August, Kirk crossed the northern end of Honshu from west to east and entered the Pacific. The system then accelerated within the midlatitude westerlies, became extratropical, and the final warning was issued valid at 160600Z August.

Table 3-13-1 EYE DIAMETER OF KIRK FROM NEXRAD AND SATELLITE DURING PASSAGE OVER OKINAWA.

DTG (Z)	NEXRAD eye diameter (nm)	Satellite eye diameter (nm)
120501	—	76
120530	—	70
120630	—	70
120640	70	—
120830	—	67
120930	61	71
120942	—	70
121030	63	74
121130	—	77
121151	63	—
121230	55	70
121240	—	65
121330	53	70
121430	51	68
121530	60	68
121630	66	67
121730	53	70
121815	58	—

III. DISCUSSION

a) *Unusual motion: a synoptic-scale anticyclonic loop*

It is well known that TCs tend to meander or oscillate about a mean path. These oscillations cover a wide range of scales and can take on several forms, including small-amplitude and short-period trochoidal oscillations around an otherwise smooth track, larger-scale and longer-period meanders, more erratic and nonperiodic meanders (occasionally including stalling, or small loops), or highly-erratic wandering with no well-defined track. A wide range of scales are involved as the meanders vary in period from a few days to less than an hour and have amplitudes up to a few hundred kilometers.

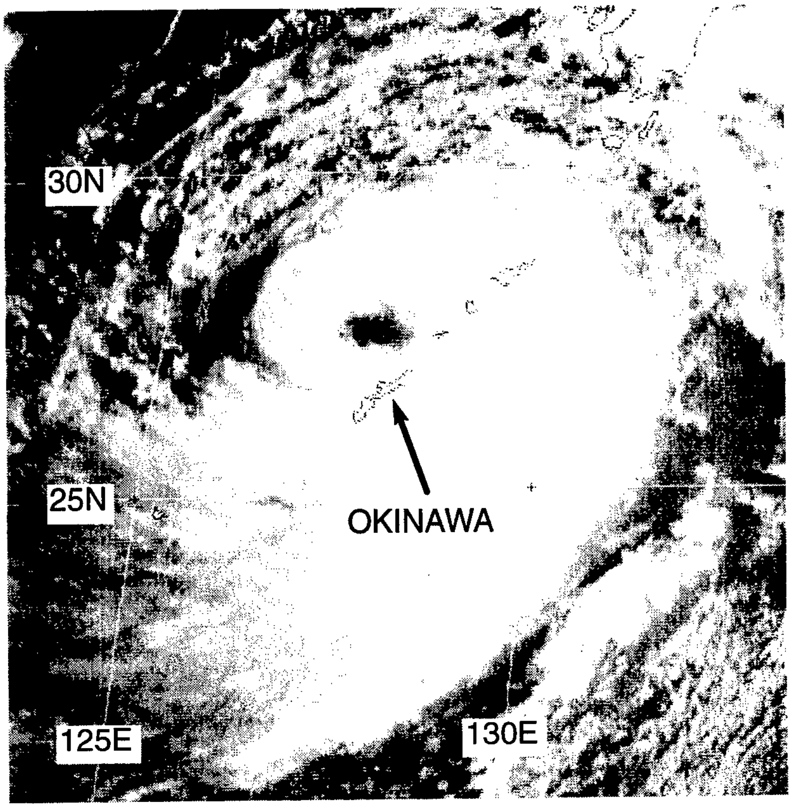

Figure 3-13-3 Kirk reaches its peak intensity of 95 kt (49 m/sec) (122131Z August visible GMS imagery).

During the two days prior to passing over the island of Okinawa, Kirk executed an anticyclonic loop with a diameter of approximately 300 nm (550 km). Well-defined looping of a TC, whereby the looping motion results in the TC recrossing its track, is unusual. According to Holland and Lander (1993), medium-scale meanders with period greater than one day and amplitude of several tens to hundreds of kilometers tend to have an equal distribution of cyclonic and anticyclonic rotation. There is a strong tendency toward exclusively cyclonic rotation at shorter periods as confirmed by an examination of 17 radar tracks of TCs provided by Meighen (1987): seven of these had no clearly discernible oscillation, and the remainder contained 23 small-scale meanders, all of which were cyclonic.

Potential mechanisms for the larger meanders include interactions with surrounding weather systems such as other TCs, TUTT cells, and synoptic-scale troughs and ridges in the subtropics or midlatitudes. During the period of its anticyclonic meander, Kirk probably interacted with other circulations in the monsoon trough and with a high-pressure system to its north. While Kirk was executing its anticyclonic loop, the monsoon trough had lifted to a very high latitude (Figure 3-13-4) and had become reverse-oriented along the portion of it that contained Kirk. Reverse orientation of the monsoon trough is often associated with north-oriented motion of its associated TCs (Lander, 1996). While this may be a satisfactory explanation for Kirk's overall northward drift, it does not offer much insight on the slow anticyclonic loop Kirk made during the period 050000Z through 120000Z. Possible explanations for this loop include an interaction of Kirk with other low-pressure systems along the reverse-oriented monsoon trough, and the affects of a midlevel anticyclone which passed slowly to Kirk's north during this time period. Once the midlevel high moved eastward into the Pacific, Kirk recurved and entered the midlatitude westerlies.

b) *Extremely large eye*

In Dvorak's analysis techniques (Dvorak 1975, 1984), the eye of a TC is considered to be small if its satellite-observed diameter is less than 30 nm (55 km), average if between 30 nm and 45 nm (55 km and 85 km), and large if greater than 45 nm (85 km). Kirk's satellite-observed eye diameter was in excess of 70 nm (150 km) during much of 12 August (the day it passed over Okinawa). This very large eye required 12 full hours to pass directly across Okinawa. Kirk was one of three TCs during 1996 — the others were Orson (19W) and Violet (26W) — which possessed, at some time during their evolution, an eye with an exceptionally large diameter (on the order of 75 nm).

Eye diameters on the order of 75 nm, or greater, are not common. None were observed during 1995. One of the TCM-90 TCs — Abe — possessed an eye with an exceptionally large diameter of about 80 nm. The unusual form of these TCs on satellite imagery led to their being called "truck tires" by JTWC satellite analysts and forecasters.

In a survey of past ATCRs, the largest eye diameter ever reported was that of Typhoon Carmen (1960). By strange coincidence, Carmen, like Kirk, passed directly over Okinawa. Carmen's eye diameter, as measured by the weather radar at Kadena was 200 statute miles (175 nm ; 325 km). Comments in the 1960 Annual Typhoon Report include:

" . . . Another feature quite unusual about this typhoon was the diameter of its eye. Reconnaissance aircraft frequently reported eye diameters of 100 mi, using as the basis of measurement, surface winds and pressure gradient. However, with respect to wall clouds surrounding the eye, radar photographs taken from the CPS-9 at Kadena AB show quite clearly that on 20 August, the eye had a diameter of approximately 200 mi . . . The eye diameter of Carmen was probably one of the largest ever reported . . ."

Kirk, like Carmen, was also viewed by a radar at Kadena: this time a new NEXRAD.

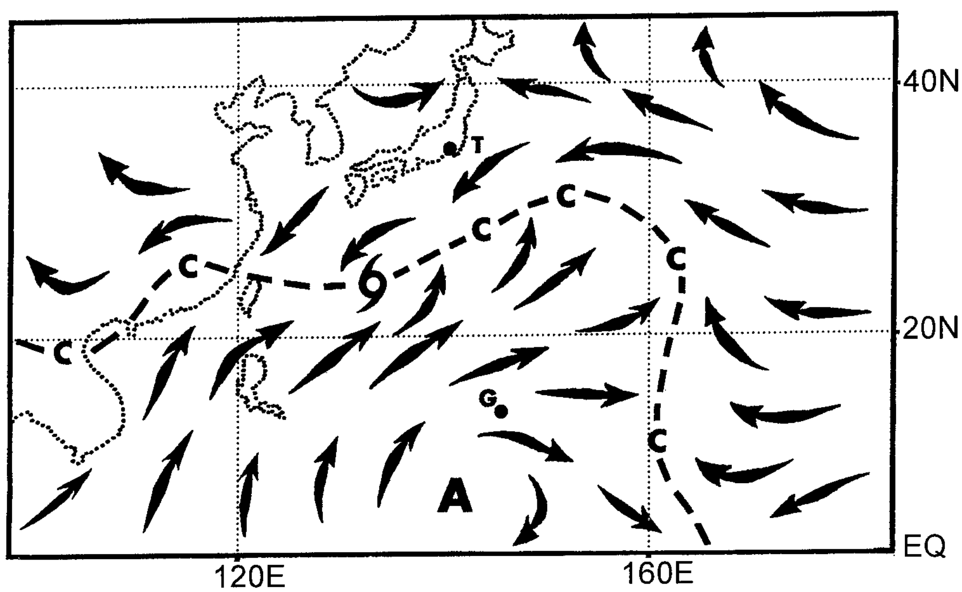

Figure 3-13-4 Schematic illustration of the monsoon circulation which became organized in an unusual pattern as Kirk underwent its anticyclonic loop along its north-oriented track (illustration based on 090000Z August JTWC surface analysis).

c) *Kirk's passage over Kadena's NEXRAD*

One of only four NEXRAD radar units to be installed in the WNP (the others are on Guam and in Korea), the NEXRAD installed on Okinawa affords an excellent opportunity to gather data on the TCs which frequently pass near or over this island. When Kirk passed directly over Okinawa, it was continuously under surveillance by NEXRAD. The NEXRAD support provided to the JTWC by Kadena base weather personnel was superb. They provided timely, thorough information on center positions, wind distribution and intensity. The most striking aspect of Kirk's radar signature was its large eye. During 12 August, as Kirk passed over the radar site from east to west the eye diameter was reported to have been consistently on the order of 60 nm (110 km) (Figure 3-13-5). This is about 10 to 15 nm less than the eye diameters as derived from satellite imagery during this time (Table 3-13-1). It is common for the eye diameter as observed from satellite to be larger than the radar-observed eye diameter due to the general outward sloping with height of the eyewall cloud.

Another fascinating aspect of the radar coverage occurred when the radar was exactly in the center of the eye: the Doppler velocity product indicated almost zero velocity along all radials. This is certainly what might be expected, but it may be the first time it has actually been observed. Another feature of the velocity product at this time was a slight asymmetry in the radial velocity which were mostly light inbound to the east-southeast and light outbound toward the west-northwest (i.e., indicative of the motion of the typhoon at that time).

d) *Fog in the eye, and other ground observations*

In recent years, there has been much debate concerning the possible effects of warmer sea-surface temperatures (SST) on the annual numbers and the potential peak intensities of TCs under conditions of a warmer climate. Emanuel (1988) set the theoretical ground work for this problem when he introduced his method for calculating the potential peak intensity of TCs. The potential peak intensity of a TC, in his framework, is largely a function of the difference between the warm SST and the colder temperatures of the upper-level outflow layer. Observationally, there is a relationship between the SST and the upper bound of TC intensity.

Granting for sake of argument that the climate will soon become warmer, and that the SST may become on the order of 1°C higher, a question arose as to the affects of this on TC distribution and intensity. This question was addressed in a special symposium at the third International Workshop on Tropical Cyclones (held in Huatulco, Mexico in 1993). The findings of this symposium (published in Lighthill, et al., 1994) were that any effects of a warmer world would likely be masked by the natural variability in TC distribution and intensity and the natural large-scale factors that govern TC formation and development.

A crucial part of this argument hinges on the physical processes which limit the intensity of a TC. As the intensity of a TC increases, frictional drag and evaporative cooling of sea spray have been suggested as brakes on the continued intensification of the TC. Other limiting factors on intensity may be the efficiency of the deep convection in the eye wall to evacuate the mass of the low-level inflow.

The thermodynamics of the TC are not fully understood. The relative contributions to the energy available to the TC by latent heat release and sensible heat fluxes from the ocean are not fully known. The cooling effects of sea spray which is produced at higher wind speeds has been introduced as an important factor in the energetics of the TC (Kepert and Fairall, 1993).

A tangential sidelight which may have important implications on the debate on the role of sea-surface fluxes on the energetics of TCs is the frequent observation of fog within the eye of TCs. During all TCs which have passed over Guam during recent years, ground fog has been reported in the eye. Observations from Kadena indicate fog was present in the eye of Kirk for the first three hours within the eye. Ramage (1974) discusses the occurrence of fog reported at sea by a ship in the eye of a typhoon (this was under the special condition of the SST having been significantly cooled by the recent passage over the same location by another typhoon). Simpson (personal communication, 1996) indicates ground fog was often reported in the eye of landfalling hurricanes in the United States. The suggested mechanism was sensible cooling of the air within the eye as it passes over land chilled by the rain and wind of the eye wall. Fog in the eye at ground or sea level could have relevance to the thermodynamic arguments concerning TC intensity (e.g., rates of sea-spray evaporation in the inflow layer, and extent of subsidence of warm dry air within the eye).

IV. IMPACT

Kirk's impact on Okinawa was largely superficial with many trees blown down, street signs broken, decorative wooden fences knocked over, and street light fixtures twisted or damaged. Some local flooding was reported. Some economic losses were incurred due to the cancellation of normal air service, the closing of shops, and a halting of an oil refinery.

Damage was more extensive, and loss of life was reported, as Kirk moved into southern Japan. There, at least two people were reported killed (a Japanese woman and a U.S. Navy serviceman were swept out to sea by high surf) and 15 injured. Over 100,000 homes were left without electricity.

At the Navy base at Sasebo, superficial damage was reported on some ships, while several other ships dragged anchor. Numerous trees were reported down on the main base, as well as a brief loss of power. At Misawa AB, some aircraft were evacuated and some others secured in hangars, but the effects of Kirk there were minimal, and no damage was reported.

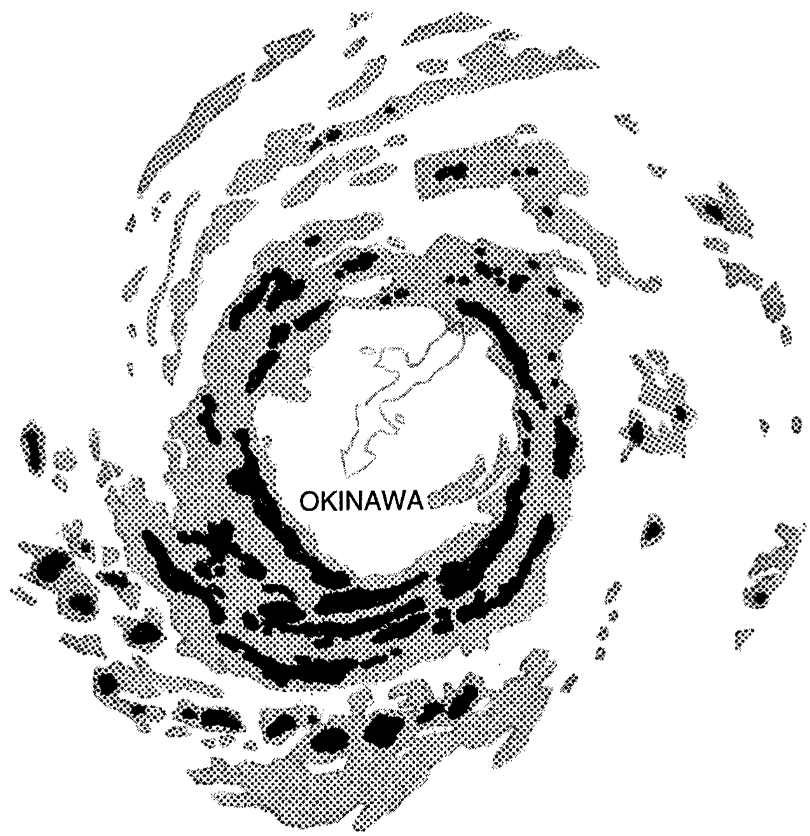

Figure 3-13-5 A radar depiction of Kirk while it was centered over Kadena. Shaded regions indicate reflectivity values of at least 30 dBZ, and the black regions indicate reflectivity values of at least 40 dBZ. (Depiction based upon the 120611Z NEXRAD composite reflectivity product).

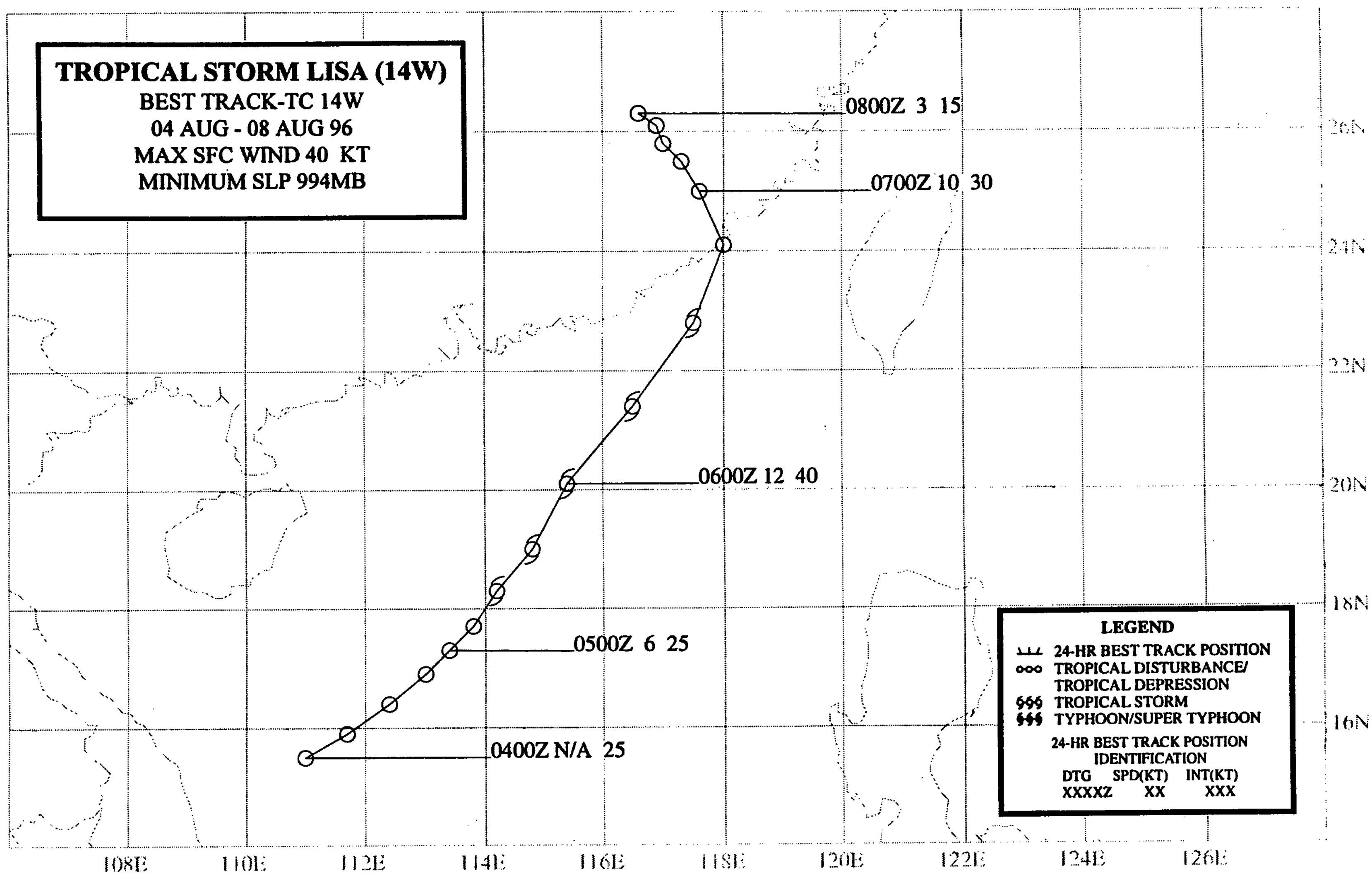
TROPICAL STORM LISA (14W)
BEST TRACK-TC 14W
04 AUG - 08 AUG 96
MAX SFC WIND 40 KT
MINIMUM SLP 994MB
0800Z 3 15
0700Z 10 30
0600Z 12 40
0500Z 6 25
0400Z N/A 25
LEGEND
24-HR BEST TRACK POSITION
TROPICAL DISTURBANCE/
TROPICAL DEPRESSION
TROPICAL STORM
TYPHOON/SUPER TYPHOON
24-HR BEST TRACK POSITION
IDENTIFICATION
DTG SPD(KT) INT(KT)
XXXXZ XX XXX
26N
24N
22N
20N
18N
16N
108E
110E
112E
114E
116E
118E
120E
122E
124E
126E

TROPICAL STORM LISA (14W)

In early August, as Herb (10W) moved into China, and Joy (12W) recurved into the midlatitudes, deep convection began to increase in the monsoon trough which stretched across the Philippines into the Philippine Sea. On 02 August, deep convection consolidated within two regions, one (which became Kirk (13W)) in the Philippine Sea, and the other (which became Lisa) over the Philippines. The area of deep convection in the Philippine Sea became a monsoon depression and moved north, while the area of convection over the Philippines moved westward and became a monsoon depression in the South China Sea (SCS). Indications of organization of the deep convection over the SCS were first mentioned on the 040600Z Significant Tropical Weather Advisory. When satellite imagery and synoptic data indicated the presence of a low-level cyclonic circulation within an area of persistent deep convection (Figure 3-14-1a), the JTWC issued a Tropical Cyclone Formation Alert, valid at 050430Z. The first warning on Tropical Depression (TD) 14W soon followed (valid time 050600Z) based on satellite intensity estimates of 25 kt (13 m/sec). With Kirk (13W) east of Okinawa, the axis of the monsoon trough became reverse oriented, and TD 14W moved northeastward toward Taiwan. The upgrade of TD 14W to Tropical Storm Lisa at 060000Z was based upon synoptic reports of gales near the LLCC at a time when the satellite signature was not well-organized. Late in the day on 06 August, the persistent deep convection associated with Lisa moved over land in southeastern China. Microwave imagery (Figure 3-14-1b), however, indicated that the LLCC was sheared to the east of this convection and remained offshore through the night. On the morning of 07 August, synoptic data indicated the LLCC of Lisa had moved ashore in China, and the final warning was issued valid at 070000Z.

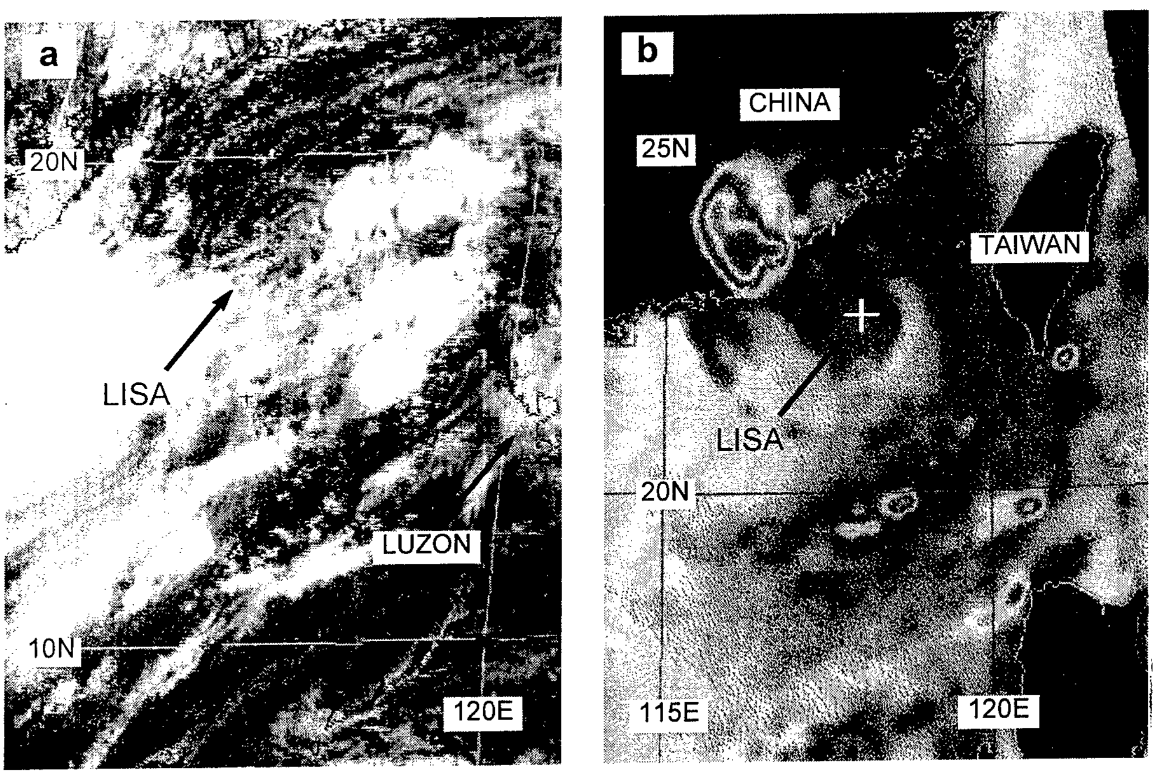

Figure 3-14-1 (a) A well defined LLCC is exposed amidst the ensemble of MSCs associated with a monsoon depression in the SCS (050031Z August visible GMS imagery). (b) Lisa's LLCC is clearly located over water to the southeast of the deep convection in microwave imagery (061415Z August 85 GHz horizontally-polarized microwave DMSP imagery).

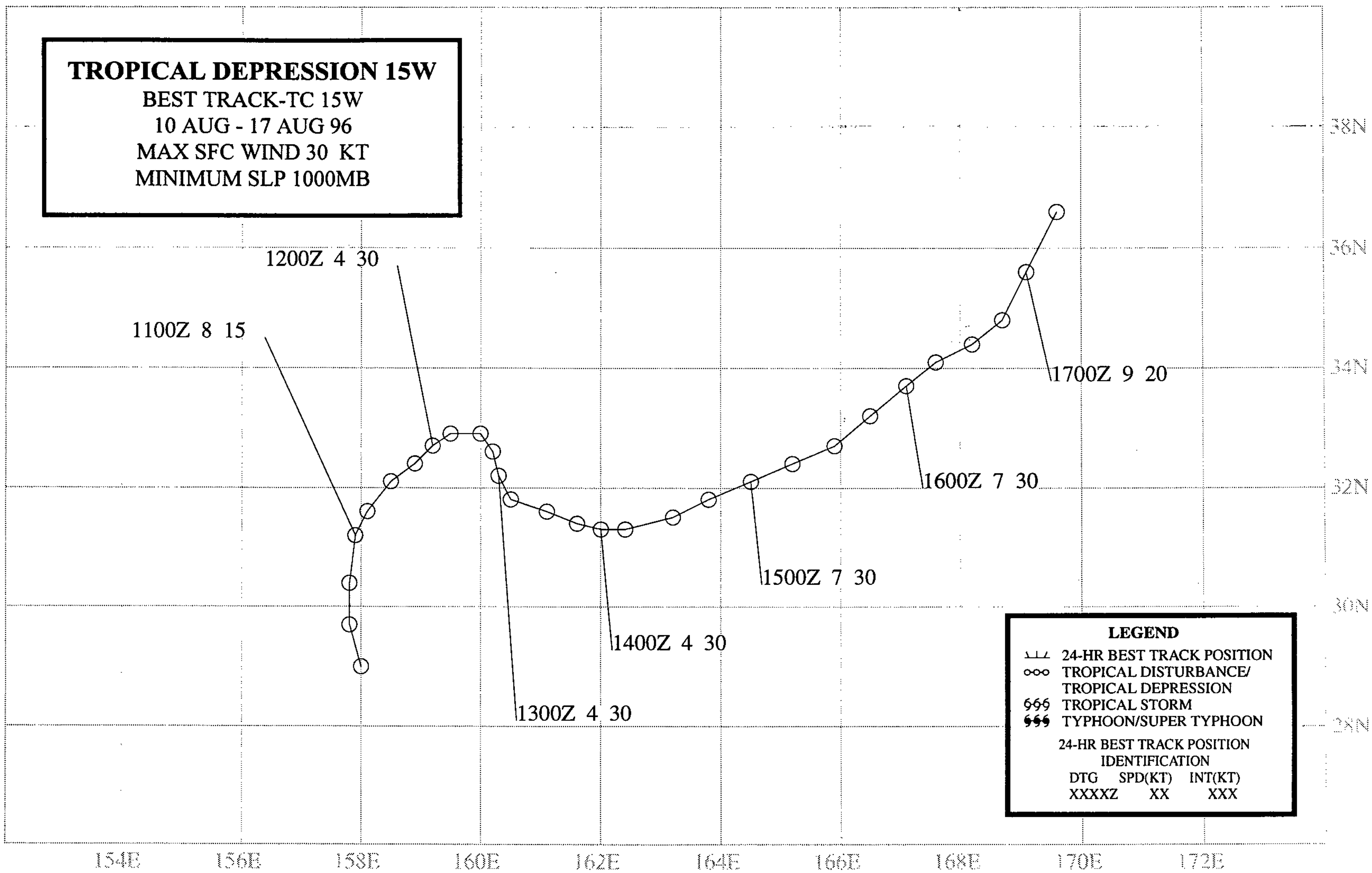
TROPICAL DEPRESSION 15W
BEST TRACK-TC 15W
10 AUG - 17 AUG 96
MAX SFC WIND 30 KT
MINIMUM SLP 1000MB
1100Z 8 15
1200Z 4 30
1300Z 4 30
1400Z 4 30
1500Z 7 30
1600Z 7 30
1700Z 9 20
LEGEND
24-HR BEST TRACK POSITION
TROPICAL DISTURBANCE/
TROPICAL DEPRESSION
TROPICAL STORM
TYPHOON/SUPER TYPHOON
24-HR BEST TRACK POSITION
IDENTIFICATION
DTG SPD(KT) INT(KT)
XXXXZ XX XXX
38N
36N
34N
32N
30N
28N
154E
156E
158E
160E
162E
164E
166E
168E
170E
172E

TROPICAL DEPRESSION 15W

Tropical Depression (TD) 15W originated in the subtropics at a time when the monsoon trough was displaced far to the north of normal (see Figure 3-13-4 in Kirk's summary for a graphic depiction of this unusual low-level flow pattern). TD 15W had an unusual structure comprised of an extensive region of low-level cloud lines surrounding a small area of deep convection (Figure 3-15-1a). First identified on the 100600Z August Significant Tropical Weather Advisory, the system drifted slowly northward and became better organized. Based on satellite intensity estimates of 25 kt (13 m/sec), the first warning was issued, valid at 120600Z. Moving generally toward the east-northeast, the system maintained its unusual cloud pattern. The peak intensity of 30 kt (15 m/sec) — as estimated from satellite imagery, and confirmed by a scatterometer pass (Figure 3-15-1b) — was maintained for several days. When the system lost its deep convection, and the extent and organization of the low-level cloud lines decreased, the final warning was issued valid at 160600Z.

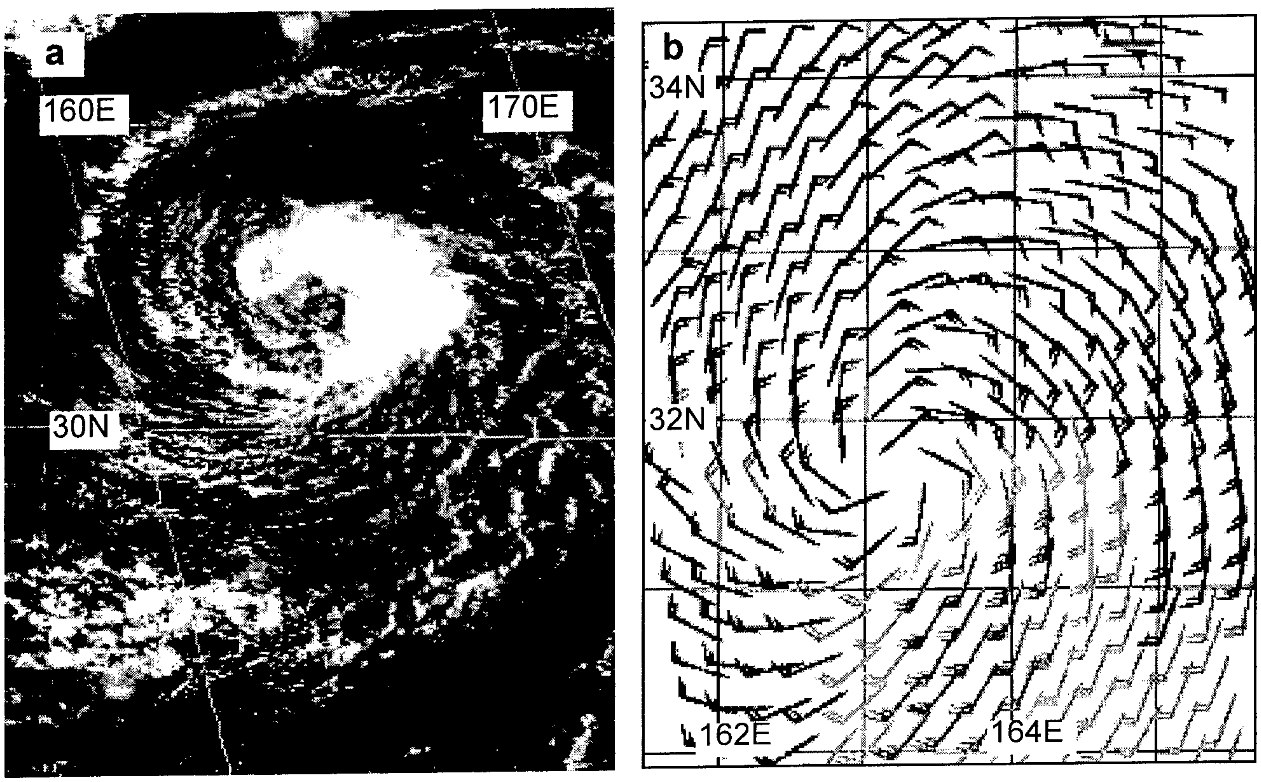

Figure 3-15-1 (a) Well-defined low-level cloud lines coil tightly around a poorly organized area of deep convection (132331Z August visible GMS imagery). (b) A region of 25- to 30-kt (13- to 15-m/sec) winds was detected by scatterometry in the southeastern quadrant of TD 15W (141132Z August ERS-2 scatterometer-derived marine surface winds).

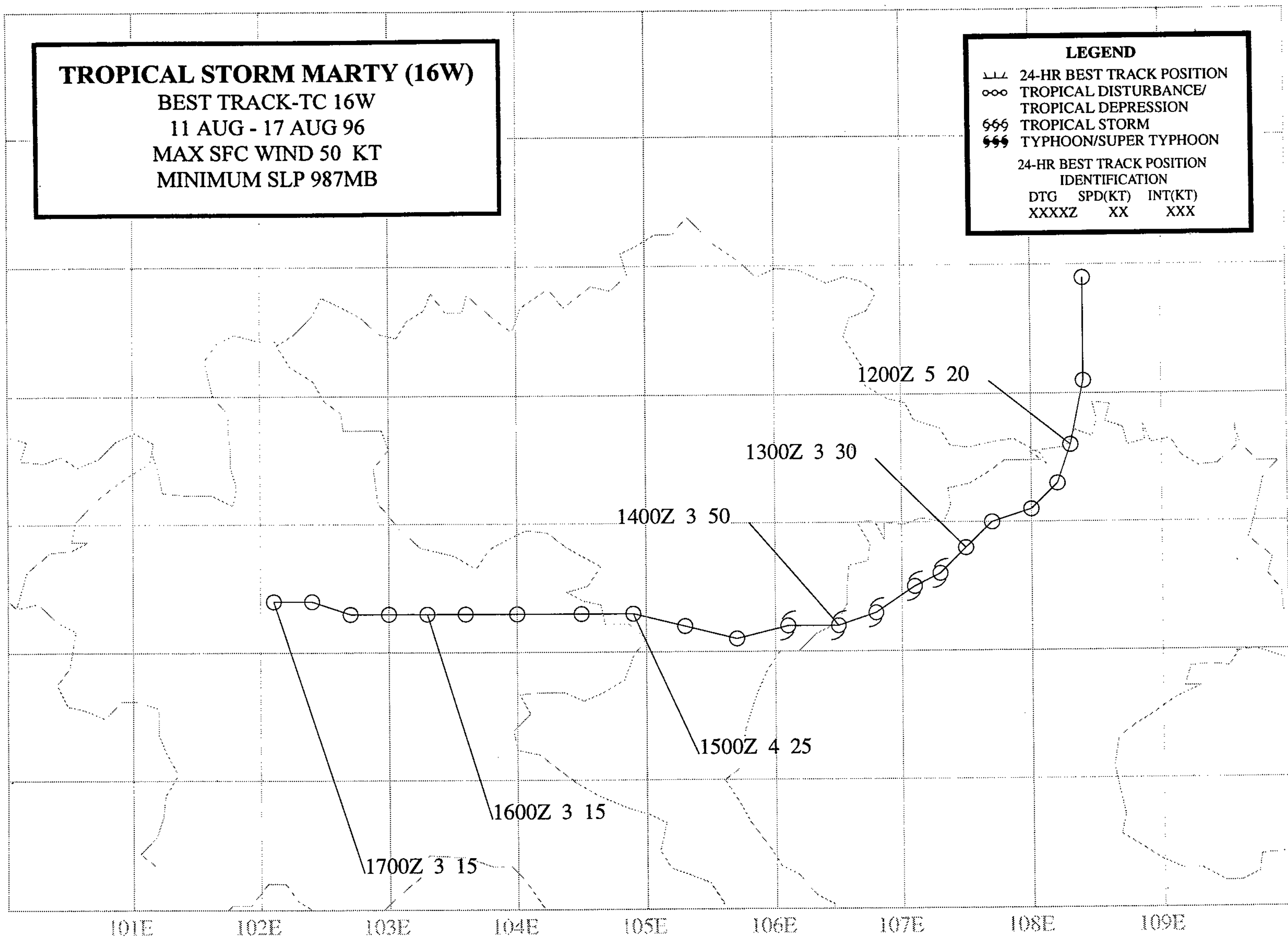
TROPICAL STORM MARTY (16W)
BEST TRACK-TC 16W
11 AUG - 17 AUG 96
MAX SFC WIND 50 KT
MINIMUM SLP 987MB
LEGEND
24-HR BEST TRACK POSITION
TROPICAL DISTURBANCE/
TROPICAL DEPRESSION
TROPICAL STORM
TYPHOON/SUPER TYPHOON
24-HR BEST TRACK POSITION
IDENTIFICATION
DTG SPD(KT) INT(KT)
XXXXZ XX XXX
1200Z 5 20
1300Z 3 30
1400Z 3 50
1500Z 4 25
1600Z 3 15
1700Z 3 15
24N
23N
22N
21N
20N
19N
101E
102E
103E
104E
105E
106E
107E
108E
109E

TROPICAL STORM MARTY (16W)

I. HIGHLIGHTS

Developing in the Gulf of Tonkin, Marty was a very small tropical cyclone. In real time, satellite intensity analyses did not agree with synoptic data and with news reports of the devastation of Vietnamese fishing boats in the Gulf of Tonkin where 125 people were reported killed and another 107 missing. Marty was upgraded to a tropical storm after it had crossed the coast because synoptic data indicated that gales were present along the coast and over waters to the east. The final best track increases Marty to a tropical storm while it was over the Gulf of Tonkin and raises its peak intensity from 35 to 50 kt.

II. TRACK AND INTENSITY

Marty originated in the monsoon trough over land in southwestern China. Though first mentioned on the 130600Z August Significant Tropical Weather Advisory, the area of deep convection that became Marty could be identified (in post analysis) as early as 11 August (Figure 3-16-1). The pre-Marty disturbance moved southward into the Gulf of Tonkin and intensified. Based on indications from satellite and synoptic data that the system had moved over water, the first warning (valid at 130600Z August) was issued on Tropical Depression (TD) 16W. The TD then turned more to the west, and shortly after 140000Z (after a short path over water) it made landfall about 60 nm (110 km) south of Hanoi. Although over land at 140600Z, TD 16W was upgraded to Tropical Storm Marty when synoptic data indicated that gales were occurring along the coast and over water to the east. The upgrade to a tropical storm after the system made landfall is unusual, but it was realized the intensity of Marty had been underestimated. Ironically, the warning that upgraded Marty to a tropical storm was also the final warning, since the system was then weakening over land.

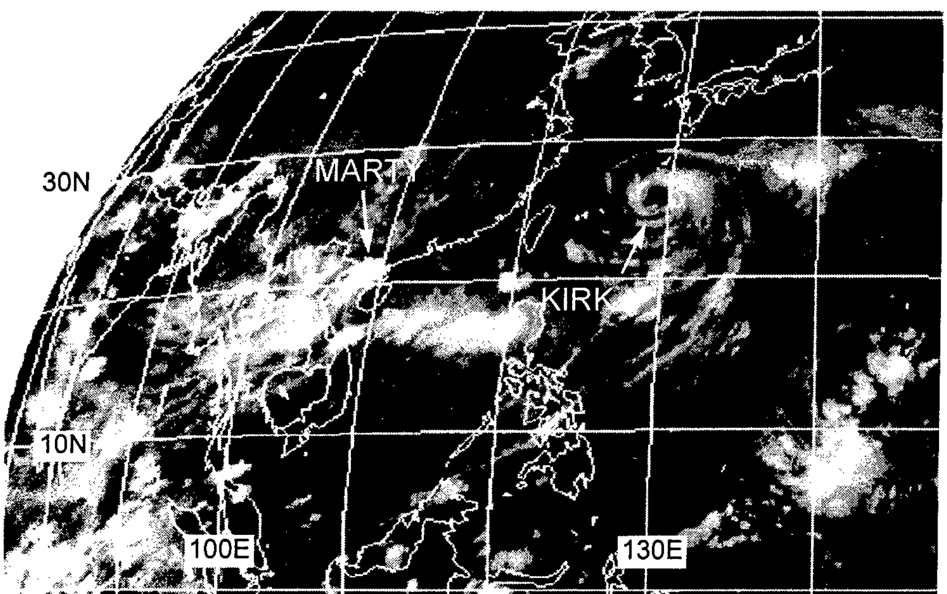

Figure 3-16-1 The disturbance that became Marty formed in southwestern China along the axis of the monsoon trough (111831Z August infrared GMS imagery).

III. DISCUSSION

The importance of post analysis

A comprehensive post analysis provides insight into the behavior of a TC in a specific situation. The goal of such an analysis is to produce a more exact, definitive product from the usually vague, imprecise, and often incomplete real-time data input. In the case of Marty, there was very lit-

tle synoptic data available in the region. When the TC made landfall in Vietnam, crucial synoptic data (including a scatterometer pass) became available which indicated Marty was more intense than thought. Also hindering an accurate assessment of Marty's intensity was its small size (Figure 3-16-2) which biased the satellite intensity estimates on the low side. A careful review of Marty was conducted and it included a reassessment of intensity estimates from satellite imagery (Table 3-16-1). Concerning Marty's intensity, the following was noted by the reassessment team:

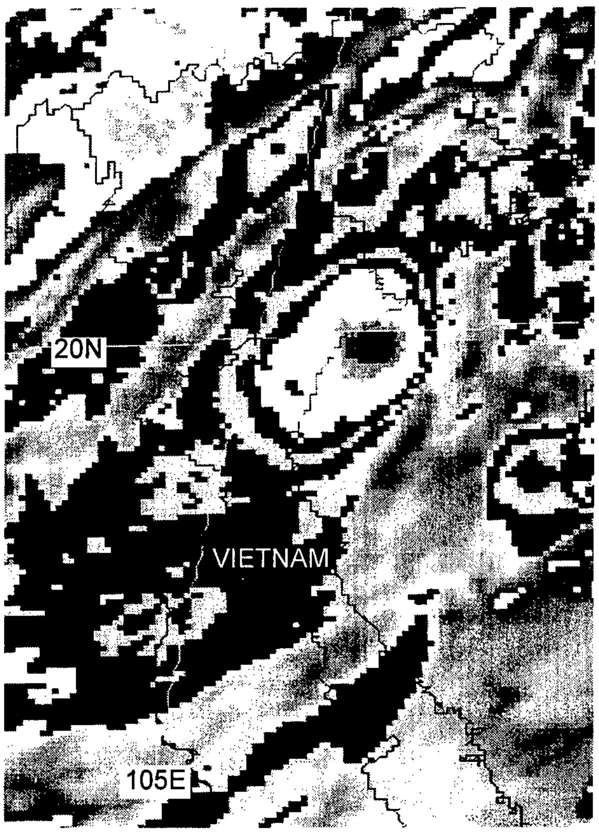

Figure 3-16-2 Exhibiting a CDO pattern, the very small Marty attains its peak intensity of 50 kt (26 m/sec) while over the Gulf of Tonkin (132131Z August enhanced infrared GMS imagery).

"TS Marty was close to a midget in size. Dvorak [satellite intensity estimates] did not appear to coincide with synoptic data and news reports of 'whirlwind destroying numerous fishing boats with the loss of from 125 to 232 people'. All T number [intensity estimates] . . . were 0.0 [less than 25 kt] except for a T2.0 . . . at 13/1730Z just before it went on shore in Vietnam. Pressures were below 997 mb within 60 nm of the circulation center — lots of room for greater intensity of the cyclone if it was 'truly' a midget".

Figure 3-16-3 is satellite imagery on 13 August originally thought to indicate wind speeds less than 25 kt (13 m/sec), but in post analysis was considered to be indicative of 30 kt (15 m/sec). Figure 3-16-2 (and later visible imagery — not shown) was reassessed to be indicative of an intensity of 50 kt (26 m/sec).

IV. IMPACT

News out of Vietnam claimed that a "whirlwind" capsized fishing boats along the northern Vietnamese coast, killing at least 125 people with another 107 missing and feared dead.

Table 3-16-1 Reanalysis of satellite intensity estimates used to support Marty's best track.

DTG	New T Number	Intensity (kt)	Old T Number	Intensity (kt)
12/03Z	1.0	25	0.0	<25
13/03Z	2.0	30	0.0	<25
13/09Z	2.5	35	0.0	<25
13/21Z	3.5	55	2.0	30

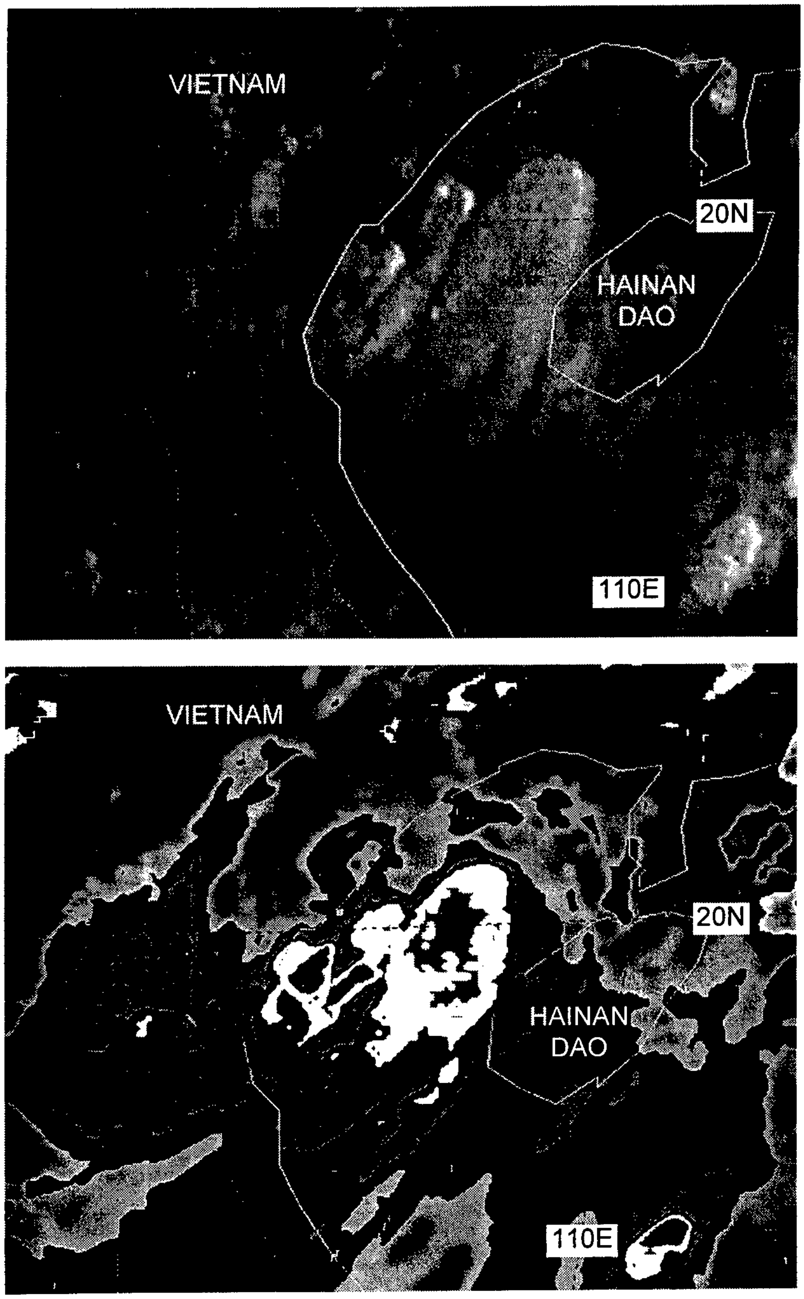

Figure 3-16-3 This satellite imagery of the tropical disturbance that became Marty was reassessed to be indicative of 30 kt (15 m/sec) intensity instead of the original diagnosis of less than 25 kt (13 m/sec) ((a) 130031Z August visible GMS imagery, and (b)130031Z enhanced infrared GMS imagery).

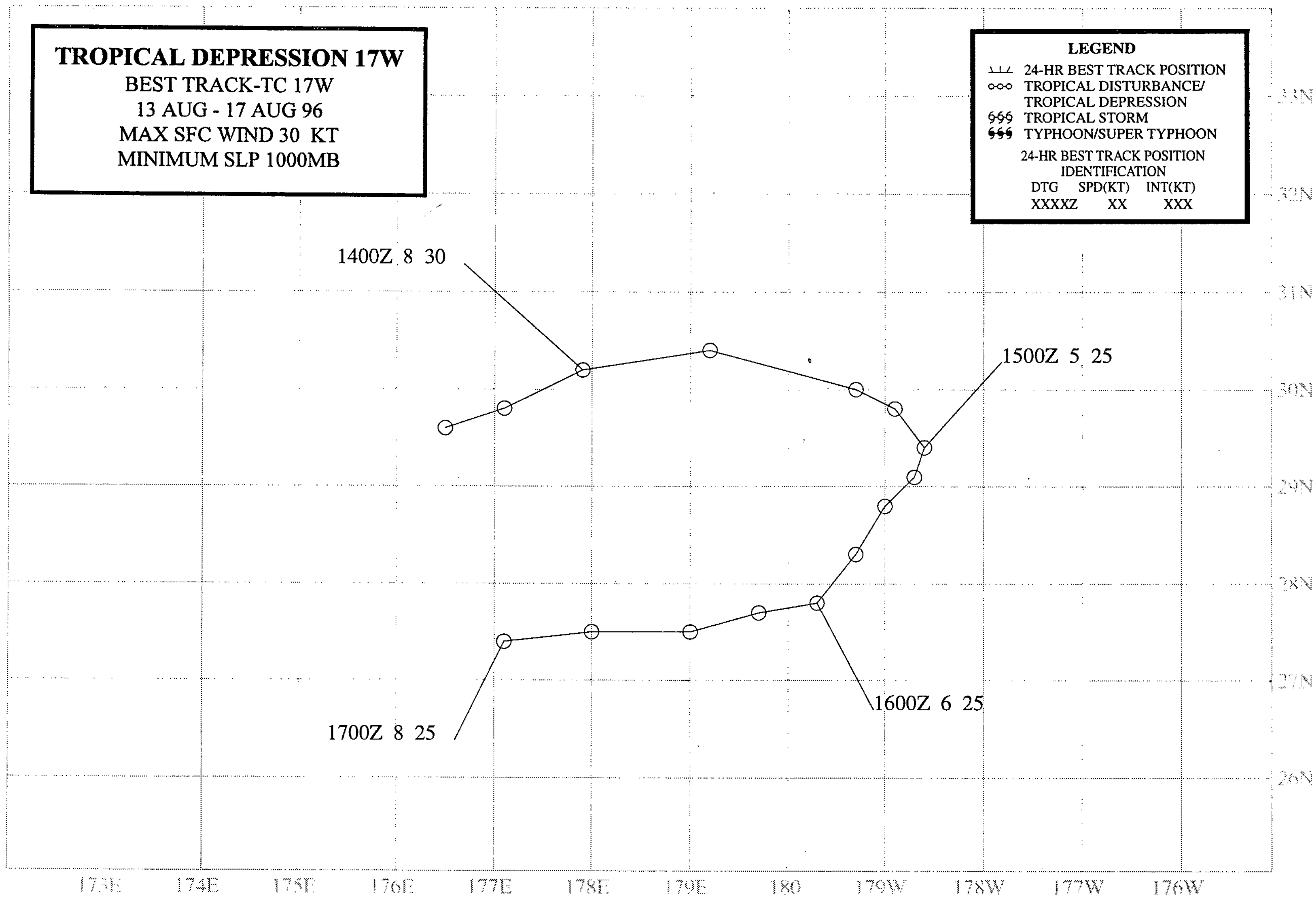

TROPICAL DEPRESSION 17W
BEST TRACK-TC 17W
13 AUG - 17 AUG 96
MAX SFC WIND 30 KT
MINIMUM SLP 1000MB
LEGEND
24-HR BEST TRACK POSITION
TROPICAL DISTURBANCE/
TROPICAL DEPRESSION
TROPICAL STORM
TYPHOON/SUPER TYPHOON
24-HR BEST TRACK POSITION
IDENTIFICATION
DTG SPD(KT) INT(KT)
XXXXZ XX XXX
1400Z 8 30
1500Z 5 25
1600Z 6 25
1700Z 8 25
33N
32N
31N
30N
29N
28N
27N
26N
173E
174E
175E
176E
177E
178E
179E
180
179W
178W
177W
176W

TROPICAL DEPRESSION 17W

Tropical Depression (TD) 17W originated in the subtropics at a time when the monsoon trough was displaced far to the north of normal (see Figure 3-13-4 in Kirk's summary for a graphic depiction of this unusual low-level flow pattern). TD 17W and Tropical Depression 15W formed and developed in this trough simultaneously (Figure 3-17-1). First identified on the 110600Z August Significant Tropical Weather Advisory, the area of deep convection which became TD 17W drifted slowly eastward and became better organized. The first warning was issued, valid at 140000Z when visible satellite imagery revealed a well-defined LLCC to the north of an area of persistent deep convection on the morning of 14 August (Figure 3-17-1). Whereas TD 15W drifted east-northeastward into higher latitudes, TD 17W executed an anticyclonic oval-shaped loop (centered at 29°N 179°E) with an average diameter of approximately 200 nm (370 km). After 141200Z, TD 17W moved across the international date line, and the JTWC passed warning responsibility to the Central Pacific Hurricane Center (CPHC). The depression continued east and came within 90 nm (170 km) of Midway Island (WMO 91066) (Figure 3-17-2) and began to weaken. The CPHC issued the final warning valid at 150000Z. At Midway, gusty winds and showers persisted for several days: the automatic remote collector there recorded a peak gust of 35 kt (18 m/sec) and approximately 2.5 inches (64 mm) of rain. TD 17W turned back to the west, recrossing the international date line on 16 August, and dissipated on 17 August.

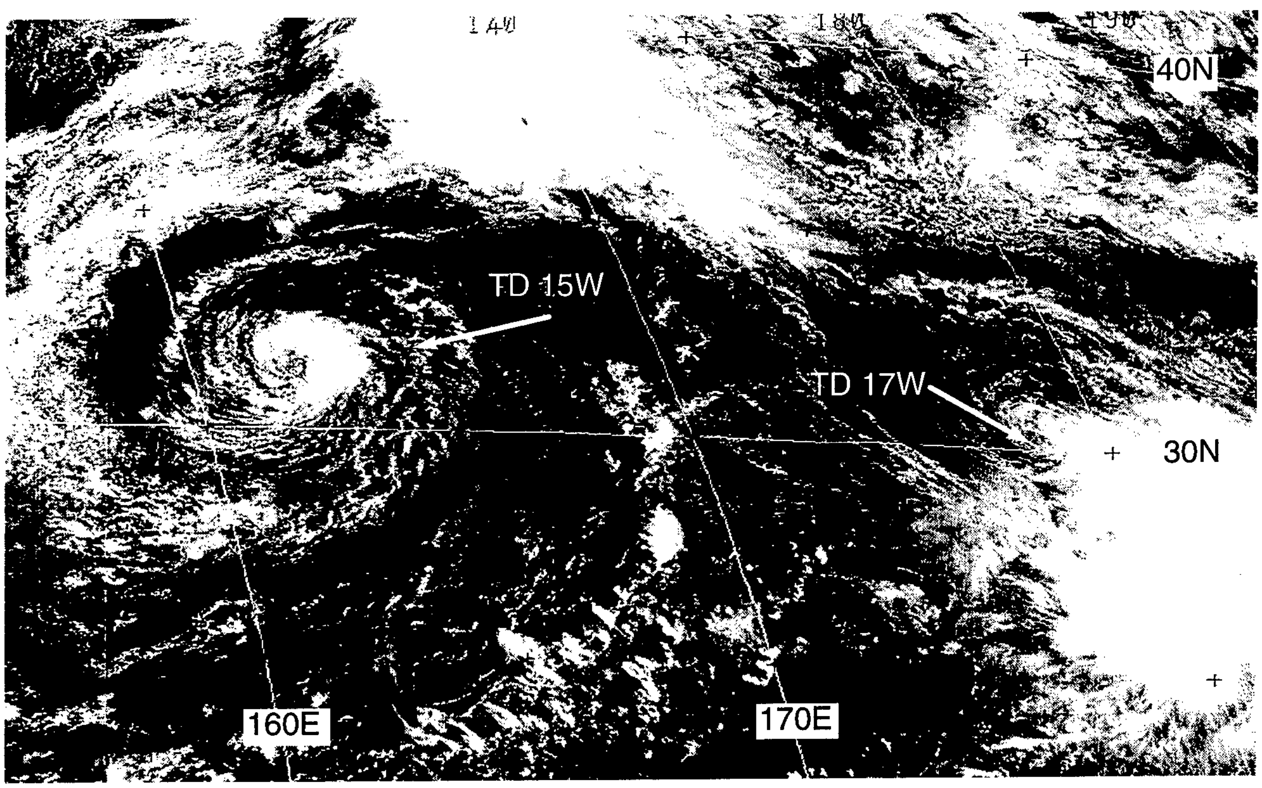

Figure 3-17-1 TD 17W and TD 15W both formed in subtropical latitudes within a monsoon trough which had moved far to the north and east of normal (132331Z August visible GMS imagery).

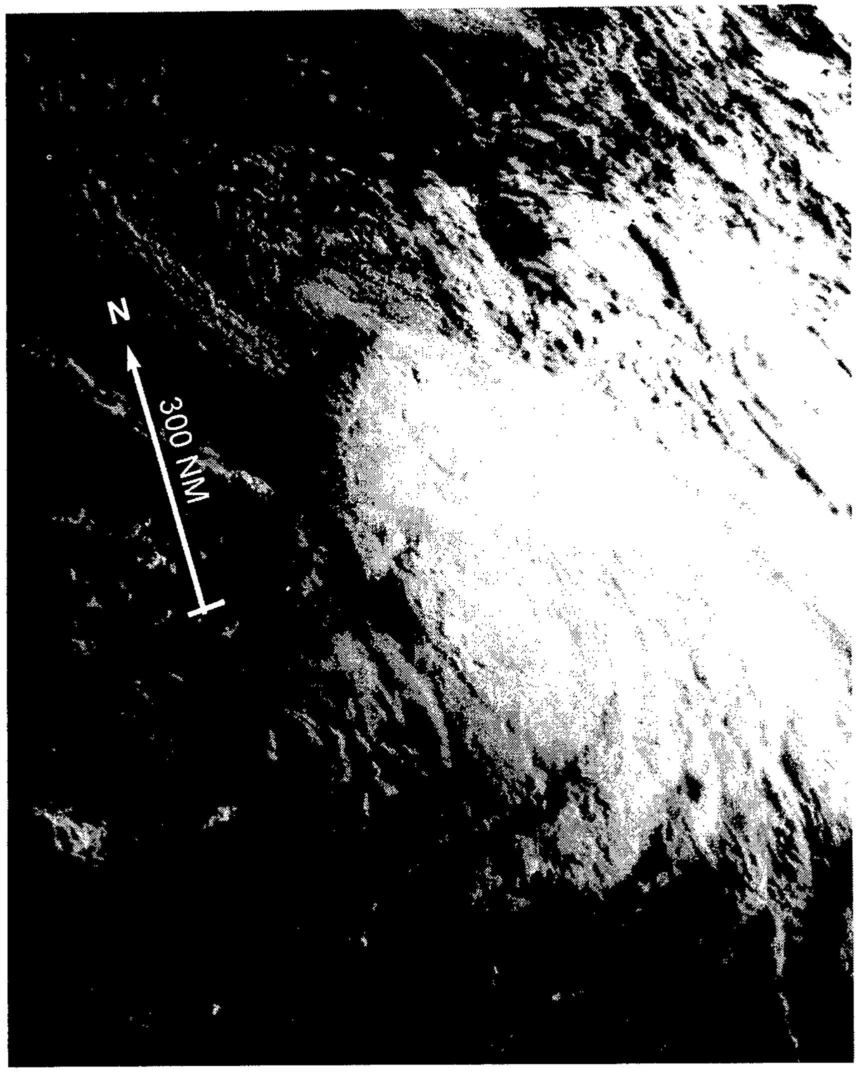

Figure 3-17-2 TD 17W exhibits a classical Dvorak "shear" type cloud pattern after crossing to the east side of the international date line (141830Z August visible GMS imagery).

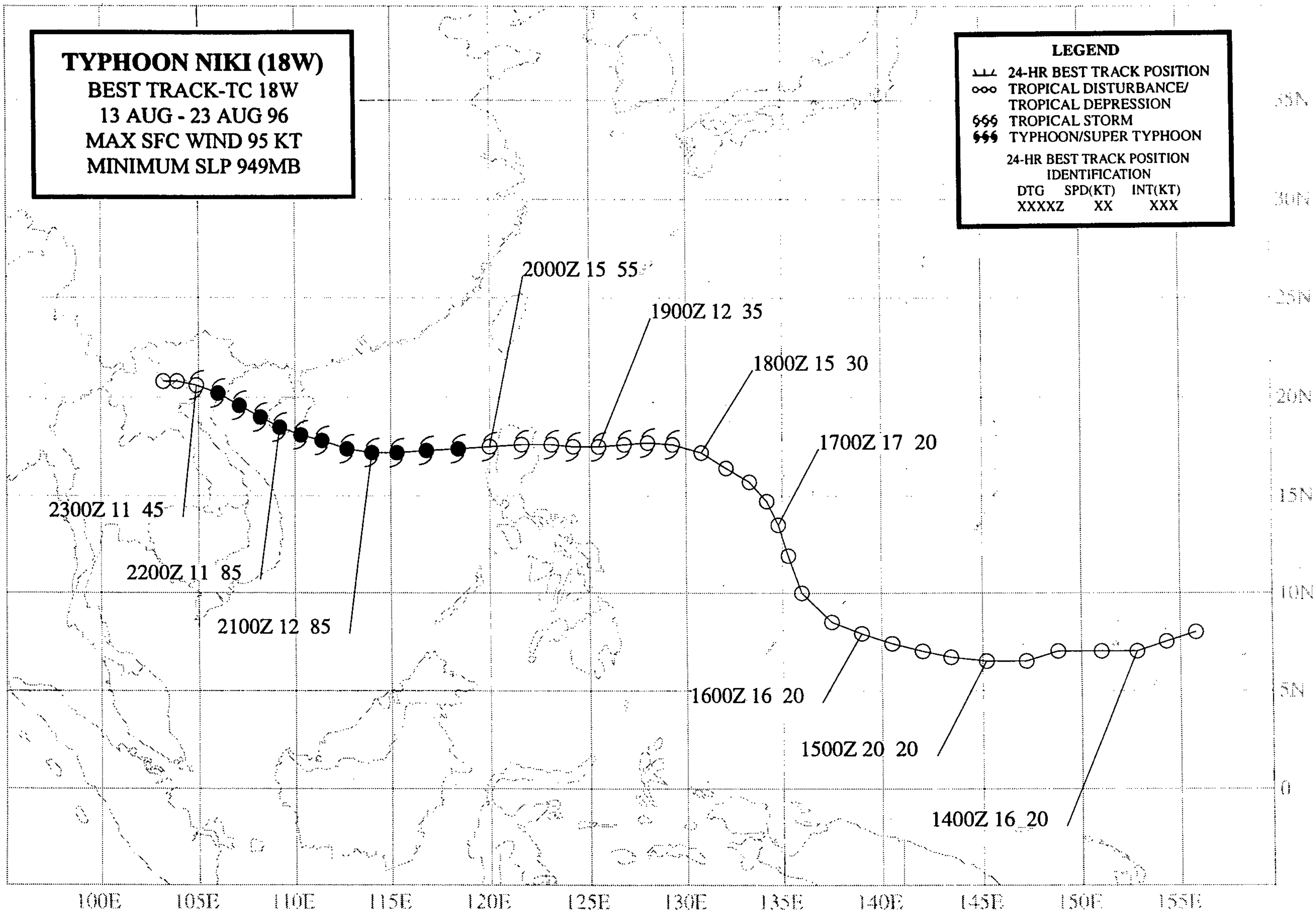
TYPHOON NIKI (18W)
BEST TRACK-TC 18W
13 AUG - 23 AUG 96
MAX SFC WIND 95 KT
MINIMUM SLP 949MB
LEGEND
24-HR BEST TRACK POSITION
TROPICAL DISTURBANCE/
TROPICAL DEPRESSION
TROPICAL STORM
TYPHOON/SUPER TYPHOON
24-HR BEST TRACK POSITION
IDENTIFICATION
DTG SPD(KT) INT(KT)
XXXXZ XX XXX
2000Z 15 55
1900Z 12 35
1800Z 15 30
1700Z 17 20
1600Z 16 20
1500Z 20 20
1400Z 16 20
2300Z 11 45
2200Z 11 85
2100Z 12 85
100E
105E
110E
115E
120E
125E
130E
135E
140E
145E
150E
155E
35N
30N
25N
20N
15N
10N
5N
0

TYPHOON NIKI (18W)

I. HIGHLIGHTS

Niki persisted as a weak tropical disturbance for several days as it moved toward the west at low latitude in Micronesia. It did not intensify until it reached the Philippine Sea east of Luzon. Crossing Luzon, it became a typhoon in the South China Sea (SCS) where it crossed the southern tip of Hainan island, and later made landfall in Vietnam south of Haiphong. Early in its life, satellite fixes were consistently north of the synoptic fixes. In the Philippine Sea, a circular exhaust cloud formed near Niki's center.

II. TRACK AND INTENSITY

During the middle of August, the monsoon trough moved to a very high latitude, and a ridge of high pressure to its south produced easterly low-level winds across the deep tropics of the WNP. Within these low-latitude easterly winds, several tropical disturbances formed. The tropical disturbance that became Niki can be traced to a small ensemble of MCSs which appeared in the eastern Caroline Islands on 13 August. This disturbance moved westward (south of 10°N) and, though first mentioned on the 130600Z August Significant Tropical Weather Advisory, there was no definitive evidence that it possessed a LLCC until 15 August when the system had moved due south of Guam. The JTWC issued a Tropical Cyclone Formation Alert (TCFA) at 170600Z August when, according to remarks on the alert:

"Convection surrounding a low-level circulation center has become better organized over the past 6 hours. Water vapor winds courtesy of the University of Wisconsin and synoptic data indicate the presence of an upper-level anticyclone over the LLCC which is enhancing the convective signature. . . ."

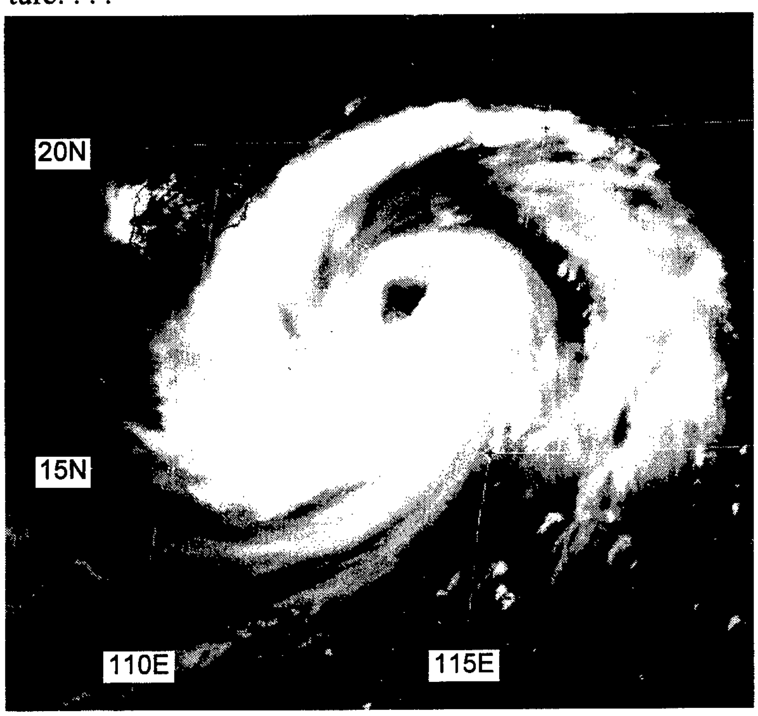

Figure 3-18-1 Typhoon Niki intensifies to 90 kt (46 m/sec) in its track across the South China Sea toward Hainan Island (210424Z August visible GMS imagery).

A second TCFA was issued at 172330Z August (primarily to reposition the TCFA box). The first warning on Tropical Depression (TD) 18W soon followed (valid at 180000Z) based on satellite intensity estimates of 30 kt (15 m/sec). TD 18W was upgraded to Tropical Storm Niki on the warning valid at 190000Z (post analysis pushed this back to 180600Z). Moving nearly due west, Niki passed across the northern end of Luzon during the six-hour period 191600Z to 192200Z. Northern Luzon had very little effect upon Niki's intensity, and as soon as it moved into the SCS, an eye began to form and Niki became a typhoon at 200600Z. The typhoon continued to intensify as it moved across the SCS (Figure 3-18-1), and reached a peak intensity of 95 kt (49 m/sec) at 211800Z just as the sys-

tem made landfall on the southern end of Hainan Island. Niki's eye became large and ragged as it passed from Hainan into the Gulf of Tonkin. Intensity estimates slowly fell, and the system (at minimal typhoon intensity) made landfall approximately 50 nm (95 km) south of Haiphong on the coast of Vietnam at 221800Z. The final warning was issued valid at 23000Z as the system weakened over land.

III. DISCUSSION

a. *Common fix errors for low-latitude tropical depressions*

When TCs form at low latitude (i.e., between 5° and 10°N) it is common that the satellite fixes tend to be located to the north of the synoptic fixes (Figure 3-18-2), especially when the TC is very weak and poorly defined. At such times, the satellite fix is often based upon the point of symmetry of anticyclonic cirrus outflow, and the curvature of poorly defined and transient bands of deep convection. A careful post analysis of the synoptic data indicated that the satellite fixes were too far north during the period 13 to 17 August.

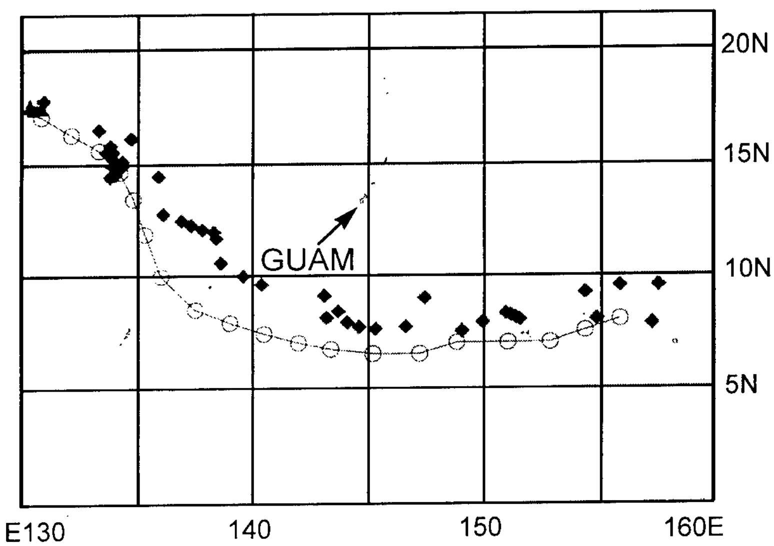

Figure 3-18-2 Based on a reanalysis of synoptic data, Niki's best track (small circles connected by thin line) was moved approximately 100 nm (185 km) to the south of the satellite fixes (black diamonds) during the period 13 to 17 August.

b. *The circular exhaust cloud*

In the early days of satellite reconnaissance, a peculiar structural feature was sometimes observed during the intensification phase of some TCs: the circular exhaust cloud. The term (coined by Fujita) was used to describe the emergence — in a developing TC — of an extremely tall, nearly circular, and sharply delineated cirrus canopy possessing an overshooting top surrounded by overlapping concentric rings and radial spokes (in visible imagery) which are the manifestation of gravity waves. On the morning of 19 August, a circular exhaust cloud formed near the center of Niki (Figure 3-18-3). Originally thought to represent the center of the TC (in the context of a small CDO), it was later revealed by aircraft reconnaissance (Black, personal communication ; Black, et al., 1986), that the circular exhaust cloud was a "hurricane supercell" with its roots in the primary rainband (or developing wall cloud). Thus, its centroid did not lie over the TC center (Figure 3-18-4). In his work with infrared imagery, Dvorak (1984) noted that the use of IR imagery required the introduction of a new concept — the central cold cover (CCC) — in order to deal with the occurrence of a sudden spreading of cold clouds over the central features of a TC. The circular exhaust cloud may be a particular form of the general phenomenon of the CCC, however, the term "circular exhaust cloud" has fallen into disuse. See Gloria's (09W) summary for a more complete description of the concept of the CCC.

IV. IMPACT

When Niki made landfall in Vietnam, a total of 61 people were reported dead or missing with another 161 injured. Total economic losses were reported to be US $66 million.

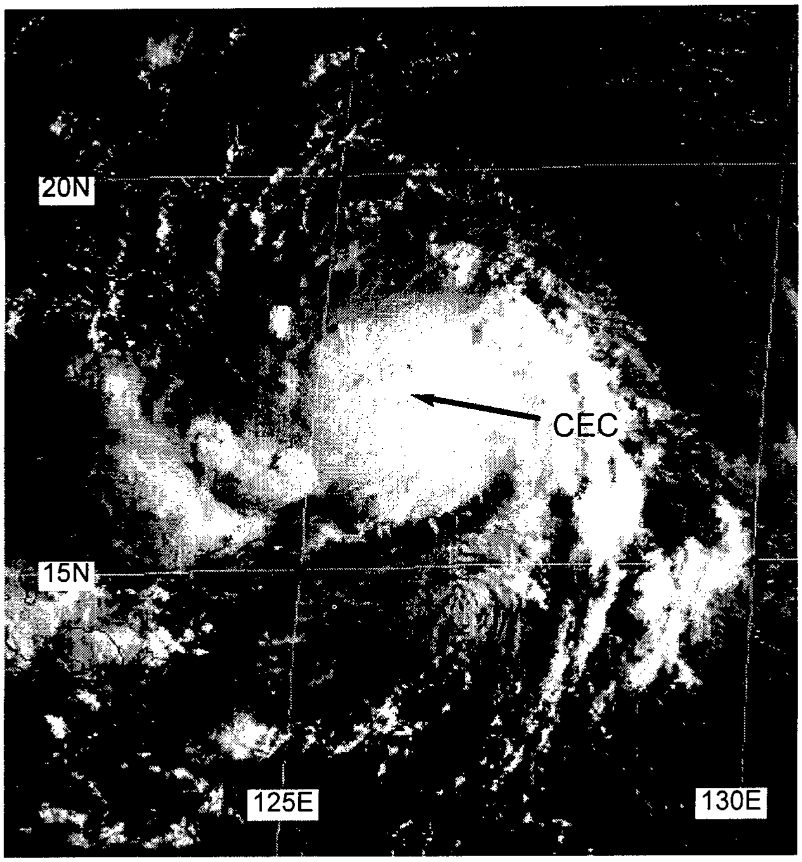

Figure 3-18-3 A circular exhaust cloud (CEC) appears within Niki's CDO (182224Z visible GMS imagery).

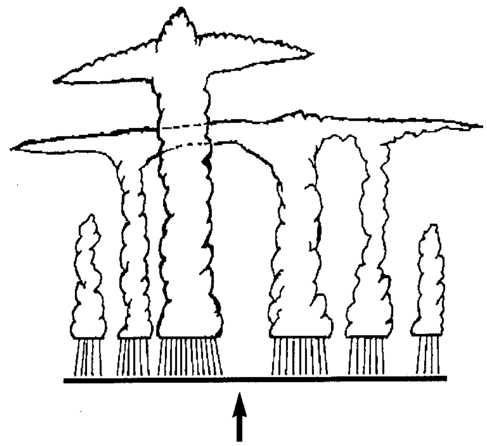

Figure 3-18-4 A schematic illustration of the vertical structure of the circular exhaust cloud.

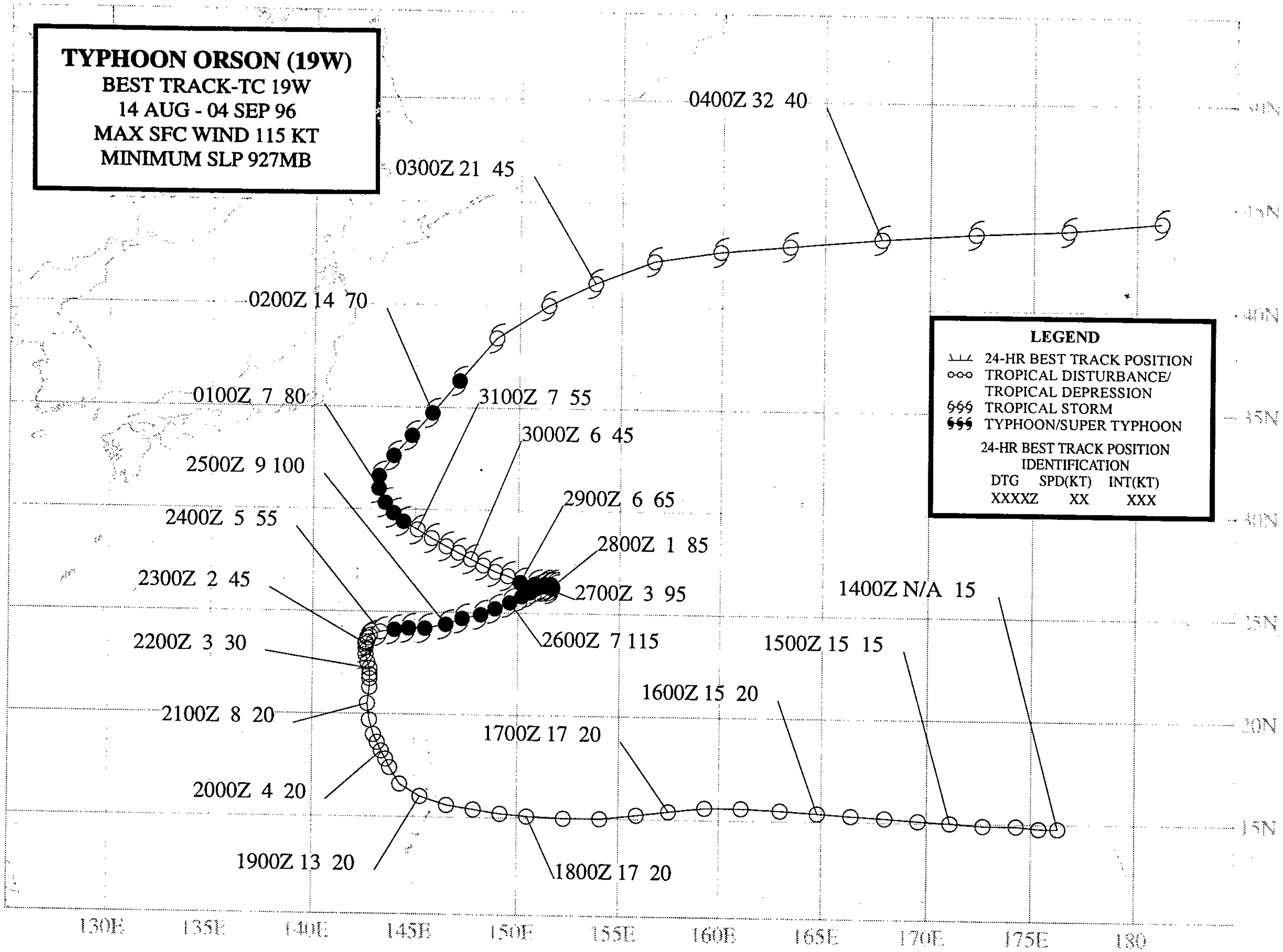
TYPHOON ORSON (19W)
BEST TRACK-TC 19W
14 AUG - 04 SEP 96
MAX SFC WIND 115 KT
MINIMUM SLP 927MB
LEGEND
24-HR BEST TRACK POSITION
TROPICAL DISTURBANCE/
TROPICAL DEPRESSION
TROPICAL STORM
TYPHOON/SUPER TYPHOON
24-HR BEST TRACK POSITION
IDENTIFICATION
DTG SPD(KT) INT(KT)
XXXXZ XX XXX
0400Z 32 40
0300Z 21 45
0200Z 14 70
0100Z 7 80
3100Z 7 55
3000Z 6 45
2500Z 9 100
2400Z 5 55
2900Z 6 65
2800Z 1 85
2700Z 3 95
2600Z 7 115
2300Z 2 45
2200Z 3 30
2100Z 8 20
2000Z 4 20
1900Z 13 20
1800Z 17 20
1700Z 17 20
1600Z 15 20
1500Z 15 15
1400Z N/A 15
130E
135E
140E
145E
150E
155E
160E
165E
170E
175E
180
15N
20N
25N
30N
35N
40N
45N
50N

TYPHOON ORSON (19W)

I. HIGHLIGHTS

Tracing its origins to a mesoscale convective system (MCS) which formed on the northeastern side of a TUTT cell, Orson had a complex developmental history including two periods of intensification, the formation of an enormous eye, and a highly erratic track.

II. TRACK AND INTENSITY

The tropical disturbance that became Orson was first noted on the 150600Z Significant Tropical Weather Advisory near 15°N 170°E within a very complex circulation pattern that can best be described as the early stages of the breakdown of the very high latitude monsoon trough within which Kirk (13W), TD 15W, and TD 17W were located. When the Pre-Orson tropical disturbance formed on 15 August, Kirk (13W) was moving eastward over northern Honshu (and becoming extratropical), and TDs 15W and 17W were dissipating at high latitude (30°N) and east of 160°E. After Kirk became an extratropical low, a ridge of high pressure became established along 27°N. To the south of this ridge the pre-Orson tropical disturbance moved westward, accompanied by a westward moving TUTT cell aloft and to its southwest (Figure 3-19-1). As this disturbance neared the Mariana Island chain, its organization improved and the first of three Tropical Cyclone Formation Alerts (TCFA) was issued at 172230Z August. The second TCFA was issued at 180930Z primarily to move the alert box westward to accommodate the rapid (20 kt) westward translation of the disturbance. At 190330Z, the second TCFA was canceled when much of the deep convection associated with the system collapsed and became disorganized. During the night of 19 August a large area of deep convection developed over Guam (Figure 3-19-2). This area of convection collapsed, and on the morning of 21 August, a smaller MCS was located north of the collapse region (Figure 3-19-3). Synoptic data indicated the presence of a low-level cyclonic circulation center beneath this MCS, so a TCFA was issued at 202300Z August. Drifting slowly northward, the deep convection persisted,

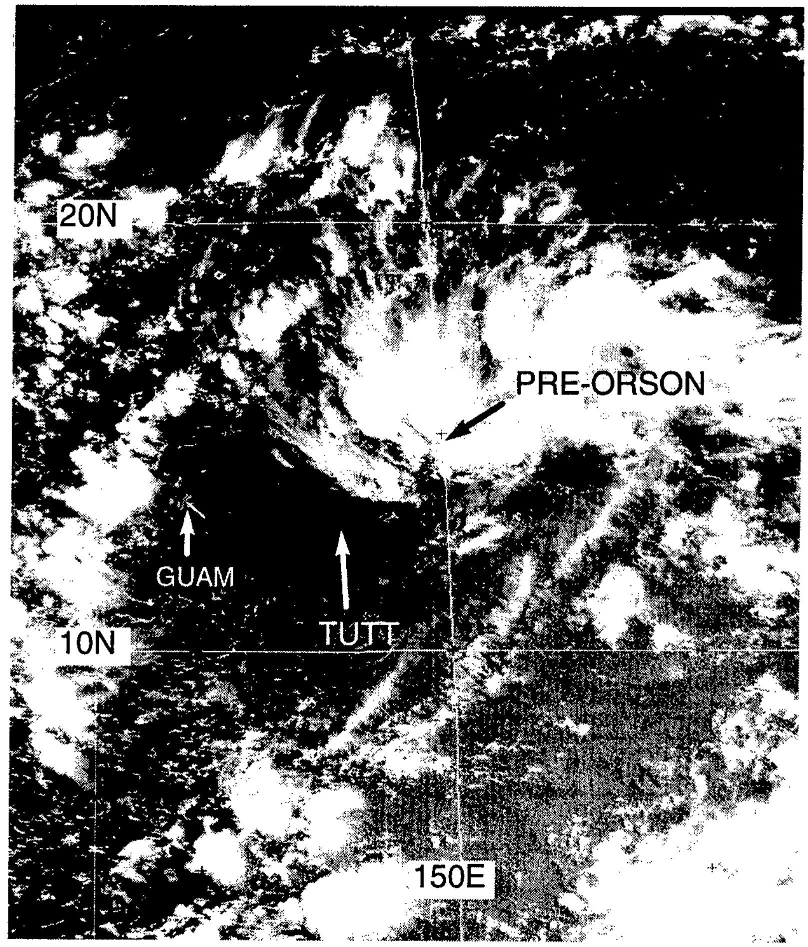

Figure 3-19-1 The tropical disturbance that became Orson was accompanied by a TUTT cell (180031Z August visible GMS imagery).

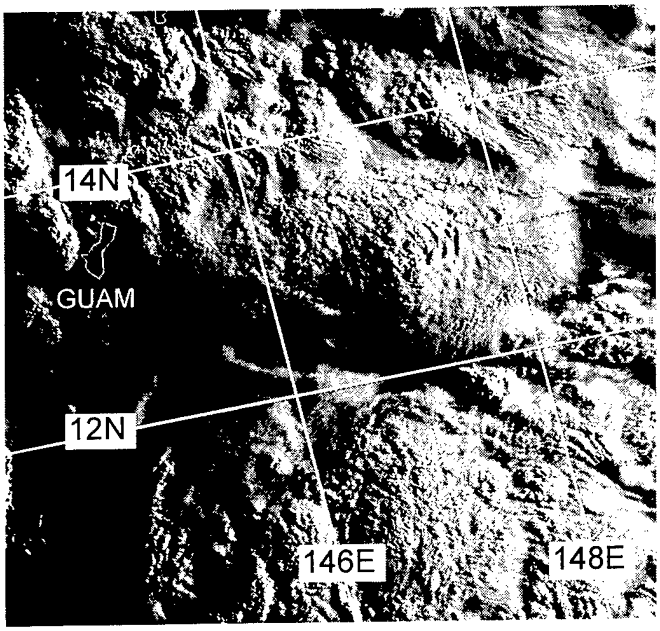

Figure 3-19-2 A very high-resolution image of the cloud-top topography of deep convection that developed near Guam as the pre-Orson tropical disturbance passed to the north (192026Z August high resolution visible DMSP imagery).

and on the night of 21 August, based upon a satellite intensity estimate of 25 kt (13 m/sec), the first warning on Tropical Depression (TD) 19W was issued valid at 211800Z. As TD 19W drifted very slowly to the north it slowly intensified and was upgraded to Tropical Storm Orson at 221200Z. At this time another TC — Piper (20W) — was developing northeast of Orson. With the development of Piper (20W), the monsoon trough became reverse oriented (Figure 3-19-4), and Orson began to move slowly toward the east-northeast along the axis of this trough. Orson intensified while moving east-northeast; becoming a typhoon at 240600Z and reaching a peak intensity of 115 kt (59 m/sec) at 250600Z (Figure 3-19-5). Thereafter, the system weakened as concentric (but ragged) eye walls formed, and the forward motion slowed as high pressure built to the north and east of the typhoon. On the morning of 29 August, the system lost its eye, and it was downgraded to a tropical storm on the warning valid at 290600Z. Under the influence of a ridge to its north, Orson began to track toward the northwest. While on this leg of its erratic track, the system underwent a remarkable structural evolution: several distinct MCSs began to orbit a large (100 nm diameter) central cloud-minimum area (Figure 3-19-6a, b). Its intensity estimate had bottomed out at 45 kt (23 m/sec) at this time. As the MCSs consolidated into a more contiguous cloud band around the very large ragged eye (Figure 3-19-7), the system once again rose to typhoon intensity, and reached a second relative intensity maximum of 80 kt (41 m/sec) at 311800Z. After reaching its second peak of intensity, Orson recurved and entered the accelerating westerly steering flow north of the subtropical ridge. The final warning was issued valid at 030600Z September as the system transitioned into an extratropical low.

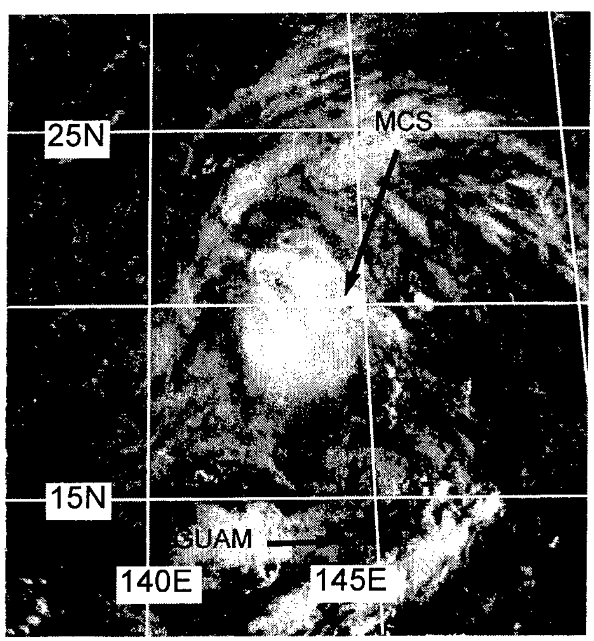

Figure 3-19-3 After the area of deep convection near Guam collapsed, a new MCS (accompanied by a LLCC) developed further to the north (202131Z August visible GMS imagery).

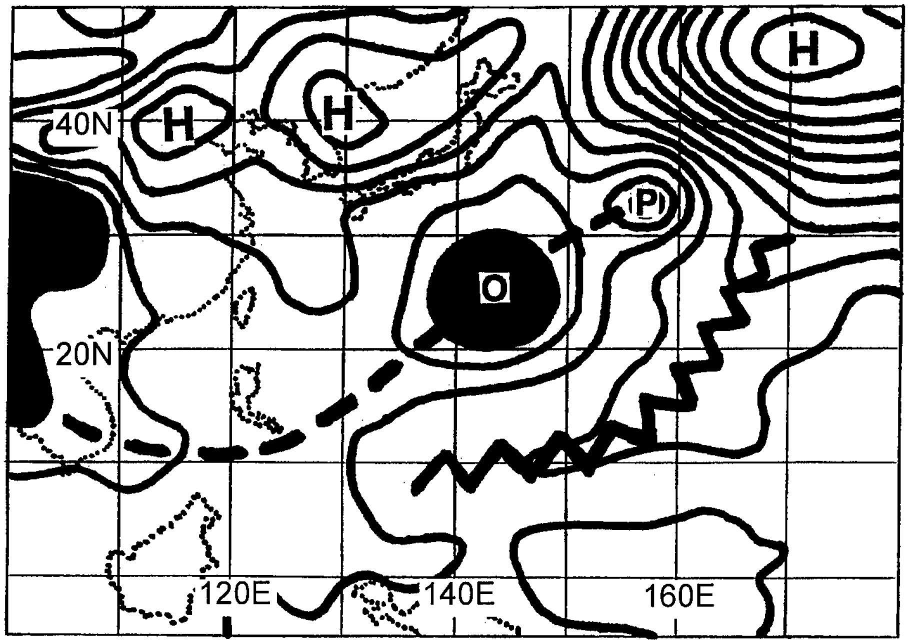

Figure 3-19-4 With the formation of Piper (20W) (P), it was clear that the monsoon trough (thick dashed line) had become reverse oriented. Influenced by the southwest monsoon flow between the trough axis and a ridge (bold zigzag line) which had become established in low latitude, Orson began to move to the east-northeast on the first leg of its "S" track (isobars at 2 mb intervals adapted from the 241200Z August NOGAPS SLP analysis).

III. DISCUSSION

a. *Unusual motion*

Orson's erratic motion can be described as a special variant of the north-oriented track type: the "S" track. The north-oriented track was first recognized by the Japan Meteorological Agency (JMA) (1976). Carr and Elsberry (1996) renamed this track type as "poleward oriented" to make the term appropriate for both the Northern and Southern hemispheres. Lander (1996) further elaborated on the characteristics of north-oriented tracks, with a special emphasis on "S"-shaped tracks. "S" motion is poleward-oriented motion of a Northern Hemisphere TC that features eastward motion at low latitude, a later bend to the north or northwest, and then eventually northeastward motion as the TC enters the mid-latitude westerlies. Most cases of "S" motion (including that of Orson) occur when a TC is located along the axis of a reverse-oriented monsoon trough. Surprisingly, the Navy's dynamic models often handle "S" motion (and poleward-oriented motion in general) quite well (Carr, personal communication). Indeed, NOGAPS and GFDN did a good job in predicting the erratic motion of Orson.

b. *Very large eye*

Orson was one of three TCs during that acquired very large eyes during 1996 — the other two were Kirk (13W) and Violet (26W). Once the large ragged clearing within the ring of MCSs was interpreted as an eye, its diameter on satellite imagery ranged from 70 nm (130 km) to 102 nm (190 km) (Table 3-19-1).

IV. IMPACT

No reports of damage or injuries were received.

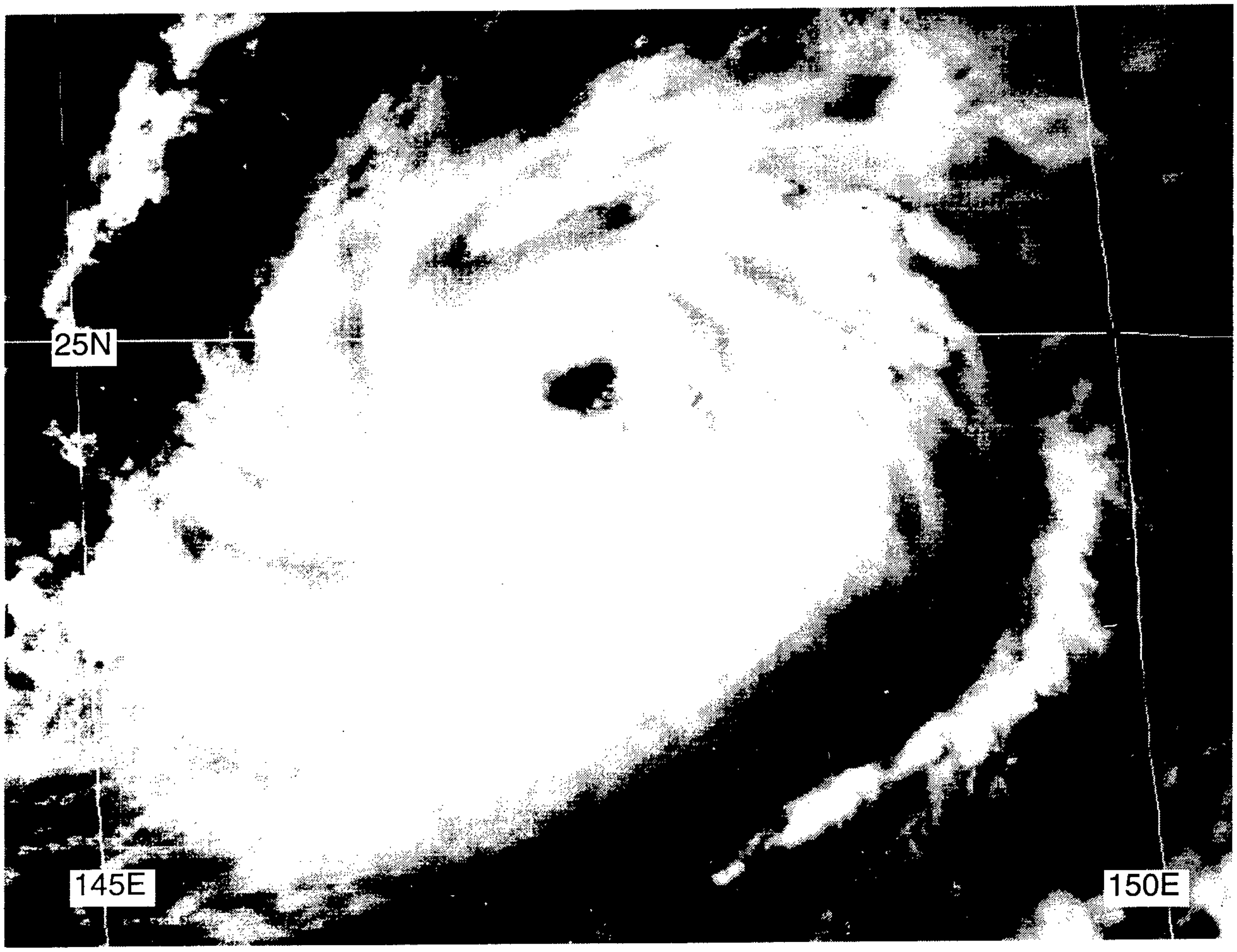

Figure 3-19-5 Orson at its peak of 115 kt (59 m/sec) (250531Z August visible GMS imagery).

Table 3-19-1 EYE DIAMETER OF ORSON FROM SATELLITE DURING ITS SECOND PERIOD OF INTENSIFICATION.

DTG (Z)	T Number	Satellite eye diameter (nm)
301042	3.5	98
301130	3.5	84
301610	3.5	81
301730	3.5	75
310530	4.0	75
310830	---	74
311130	4.0	84
311559	4.0	70
312030	---	77
312330	4.5	90
010230	---	102
010530	4.0	94
010830	---	98

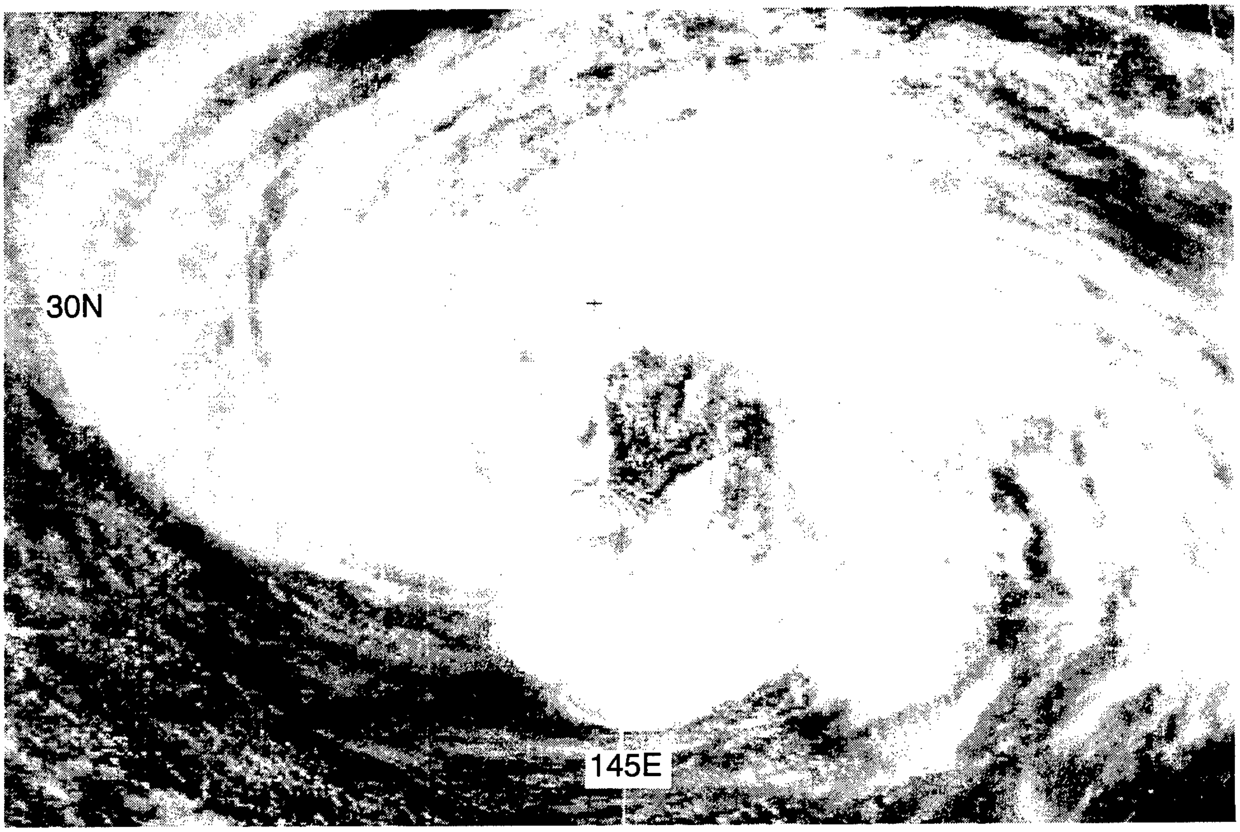

Figure 3-19-6 A ring of MCSs orbit a central clear region as a precursor to the formation of Orson's very large eye. (a) 302131Z August visible GMS imagery. (b) 302131Z August enhanced infrared GMS imagery.

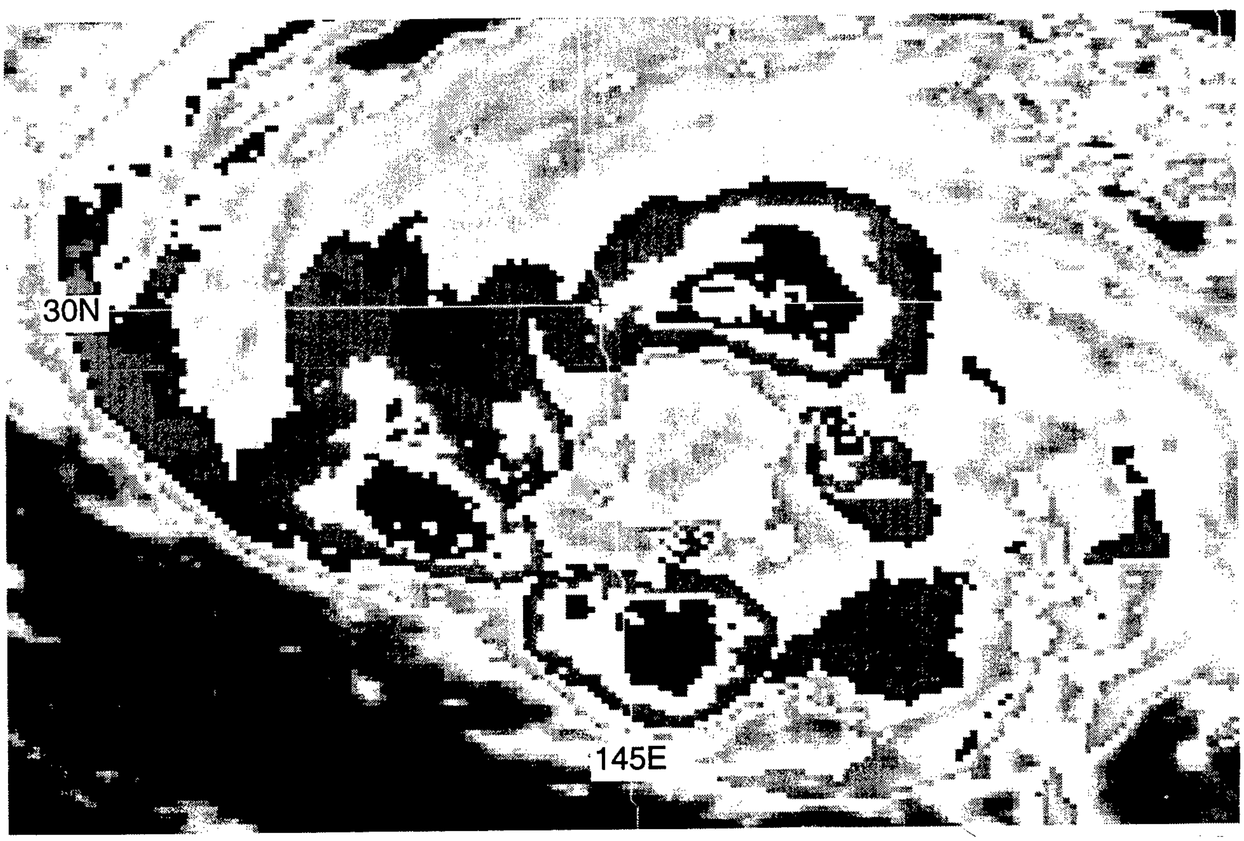

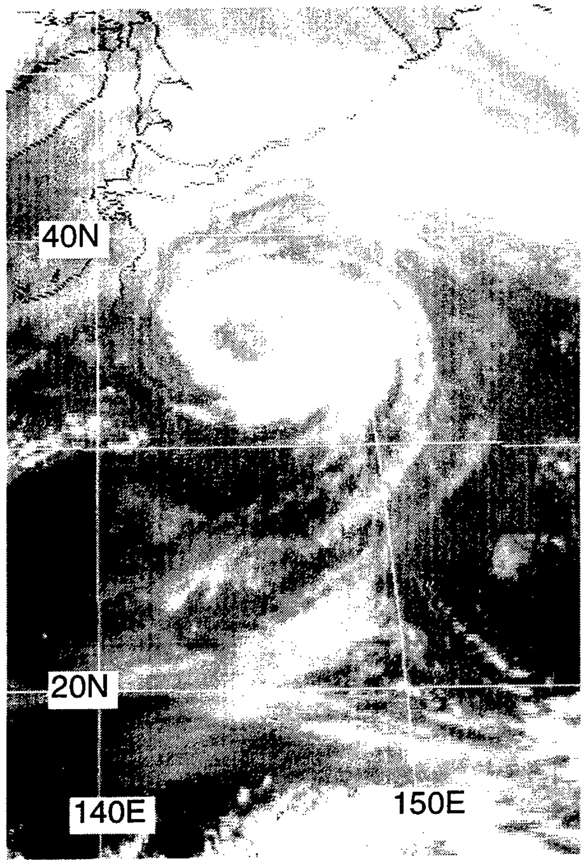

Figure 3-19-7 Orson's very large eye evokes the analogy of a "truck tire" rolling across the ocean (012231Z September infrared GMS imagery).

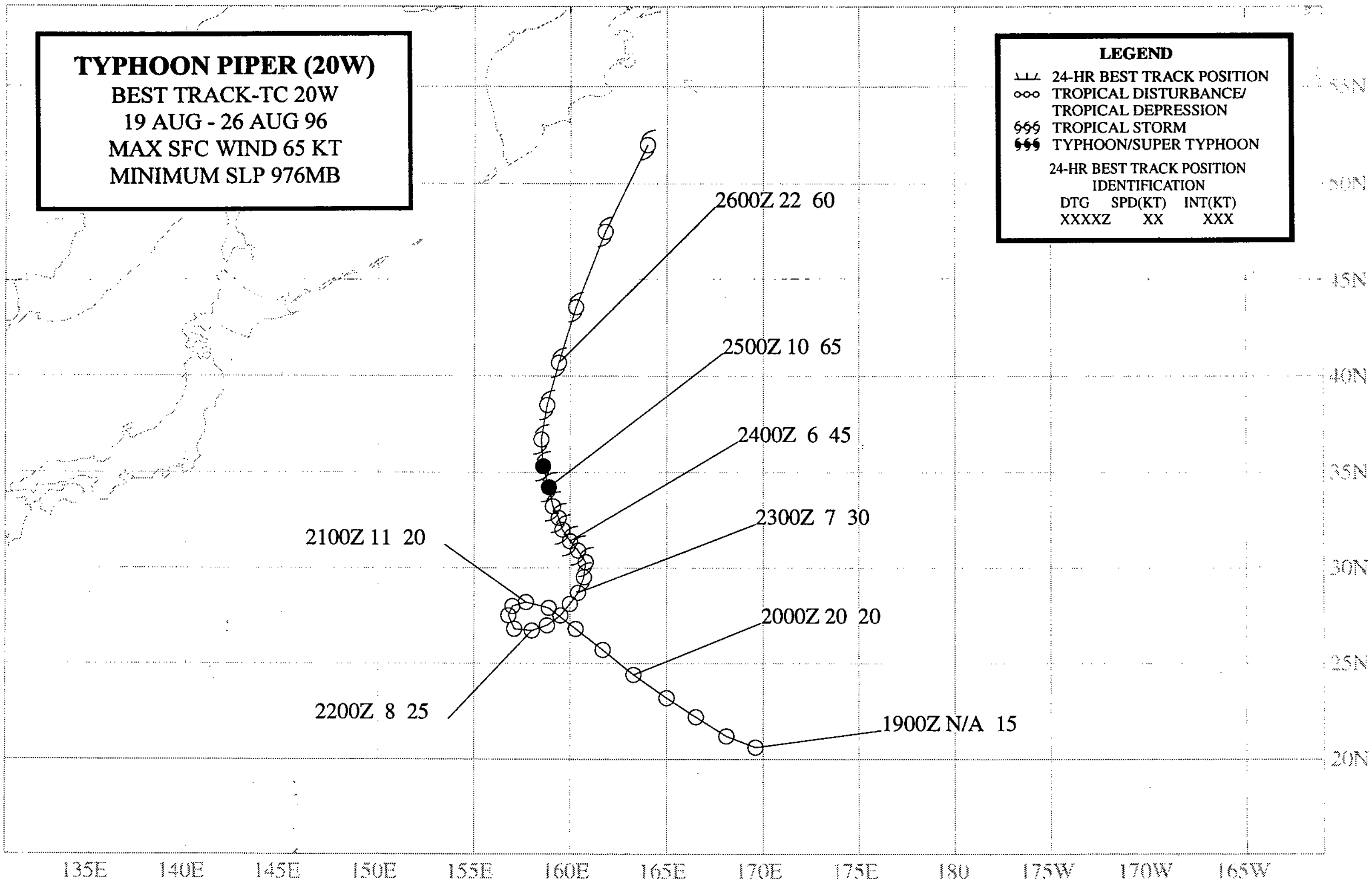

TYPHOON PIPER (20W)
BEST TRACK-TC 20W
19 AUG - 26 AUG 96
MAX SFC WIND 65 KT
MINIMUM SLP 976MB
LEGEND
24-HR BEST TRACK POSITION
TROPICAL DISTURBANCE/
TROPICAL DEPRESSION
TROPICAL STORM
TYPHOON/SUPER TYPHOON
24-HR BEST TRACK POSITION
IDENTIFICATION
DTG SPD(KT) INT(KT)
XXXXZ XX XXX
2600Z 22 60
2500Z 10 65
2400Z 6 45
2300Z 7 30
2000Z 20 20
1900Z N/A 15
2100Z 11 20
2200Z 8 25
55N
50N
45N
40N
35N
30N
25N
20N
135E
140E
145E
150E
155E
160E
165E
170E
175E
180
175W
170W
165W

TYPHOON PIPER (20W)

I. HIGHLIGHTS

Piper was another of the TCs of 1996 which originated directly from a TUTT cell. It was a very small TC — the smallest in the WNP during 1996. Developing at a relatively high latitude to the east of Orson (19W), Piper was located at the eastern end of a reverse-oriented monsoon trough (RMT). Typical of TCs associated with a RMT, Piper's motion was north oriented.

II. TRACK AND INTENSITY

During 19 August, a well-defined TUTT cell was moving westward along 25°N and had crossed 165°E. Mesoscale convective systems populated the eastern through northern segment of a curved moisture band that wrapped into this TUTT cell (Figure 3-20-1a). Synoptic data at 190000Z indicated that a weak low-level cyclonic circulation was located west of this cloud band and close to the estimated center of the TUTT cell, prompting its inclusion on the 190600Z August Significant Tropical Weather Advisory. During the next two days, the low-level cyclonic circulation became associated with an area of deep convection. On 22 August, the deep convection consolidated under the anticyclonically curved flow on the eastern side of the TUTT cell, and scatterometry indicated the wind speeds had increased to 20 kt (10 m/sec) on the north side of the accompanying low-level circulation center (LLCC). This prompted JTWC to issue a Tropical Cyclone Formation Alert valid at 221500Z.

On 23 August, persistent deep convection in the eastern quadrant of the TUTT cell became coupled with well-defined anticyclonic flow aloft. The persistence of deep convection and its increased organization prompted the first warning on Tropical Depression (TD) 20W valid at

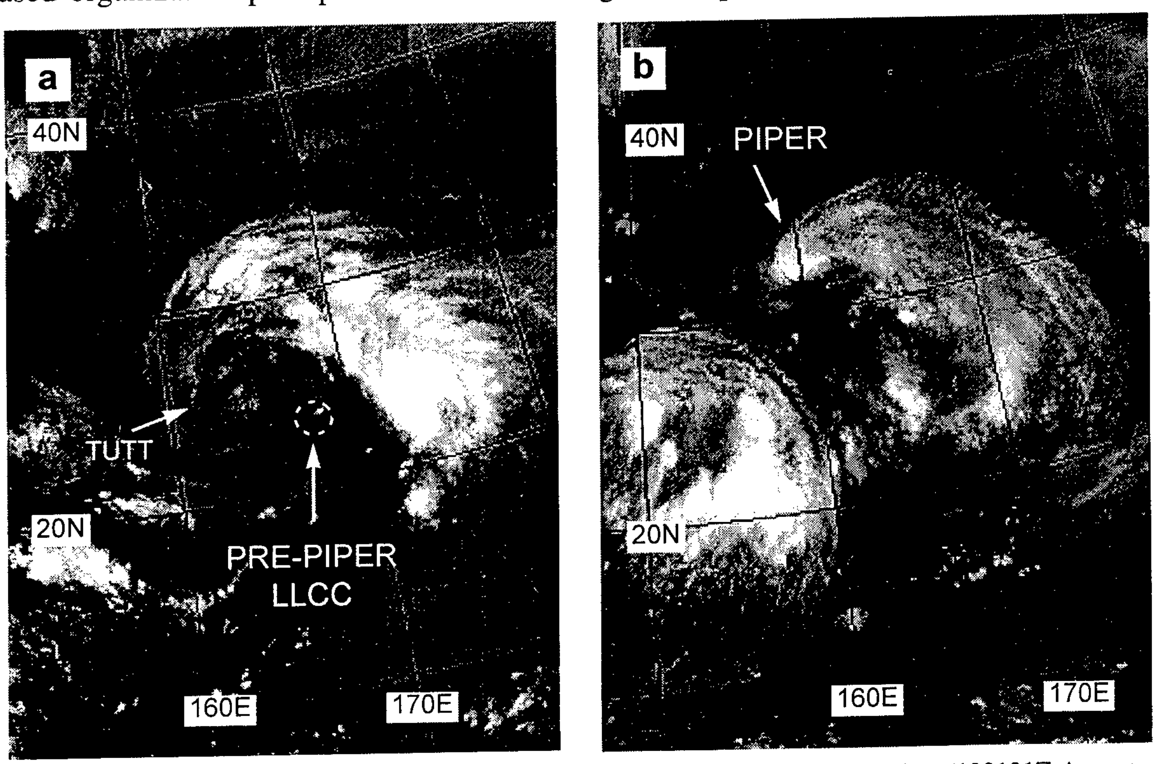

Figure 3-20-1 A westward moving TUTT cell (a) induces the formation of Piper (b). (192131Z August water-vapor GMS imagery and 240031Z August water-vapor GMS imagery respectively).

230000Z. Synoptic data at this time showed the monsoon westerlies had extended to the LLCC of TD 20W, creating a reverse-oriented monsoon trough which included the larger Orson (19W) to the west. Based on a satellite intensity estimate of 35 kt (18 m/sec), TD 20W was upgraded to Tropical Storm Piper on the warning valid at 230600Z. With a ridge located to its southeast, and a blocking high to its northeast, Piper moved on a north-oriented track.

Late on 24 August, Piper's small CDO moved north, became detached from the monsoon cloud band, and intensified. At 250000Z, Piper acquired a visible eye, and reached its peak intensity of 65 kt (33 m/sec) (Figure 3-20-2). Piper retained its small 7-nm (13-km) eye for about 12 hours (Figure 3-20-3a, b). During 26 August, Piper's central convection became a small well-defined CDO (Figure 3-20-4), as it accelerated to the north-northeast and slowly weakened. Late on 26 August, Piper's forward motion increased to more than 40 kt (75 km/hr) as it merged with a frontal cloud band which stretched southward from a low over the Kamchatka peninsula. The final warning was issued valid at 260600Z when Piper's CDO became associated with the frontal cloud band. Post analysis indicated Piper's CDO could be followed for an additional 12 hours as it sped northward within the frontal cloud band, and therefore, the final best track continues until 261800Z.

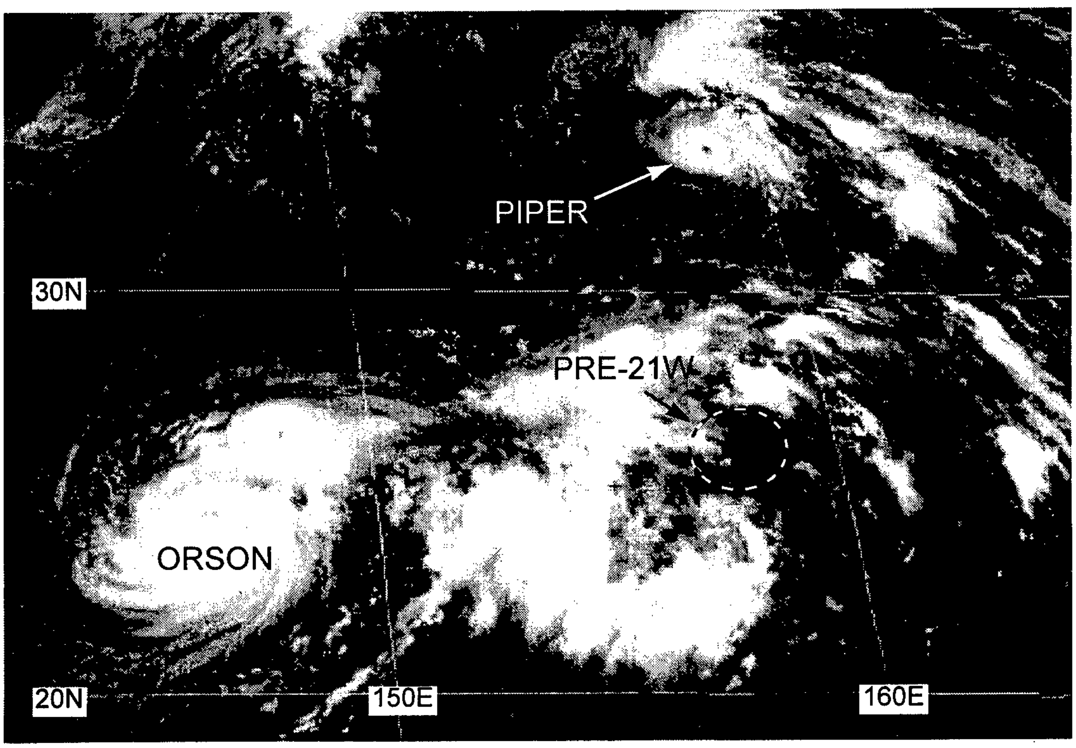

Figure 3-20-2 Piper at its peak intensity of 65 kt (33 m/sec) (242331Z August visible GMS imagery).

III. DISCUSSION

a. *Tropical cyclogenesis induced by a TUTT cell*

Piper originated directly from a TUTT cell (see Joy's (12W) summary for a more complete description of tropical cyclogenesis induced directly by a TUTT cell). This is well illustrated by water-vapor imagery (Figure 3-20-1a, b). Water-vapor imagery has only been available since the GMS-5 satellite became operational during June of 1995. It has allowed a greatly improved presentation of TUTT cells, and their movement and evolution can now be studied as never before. Water-vapor imagery should open new opportunities for research on the effects of the TUTT and its associated TUTT cells on TC genesis and TC development.

b. *Small size*

Like most TCs that form at high latitude in association with TUTT cells, Piper was a very small TC — the smallest of 1996. The diameter of its dense cirrus cloud shield was less than 100 nm (185 km) (Figure 3-20-3a, b), and it encompassed a very small eye whose diameter was 7 nm (13 km) on satellite imagery. As with many very small TCs, the intensity forecasts erred on the low side: on the first eight warnings (issued at six-hour intervals from 230000Z August to 241800Z August), the 24-hour intensity was under-forecast by anywhere from 5 to 25 kt; the 48-hour intensity was under-forecast by as much as 30 kt (15 m/sec).

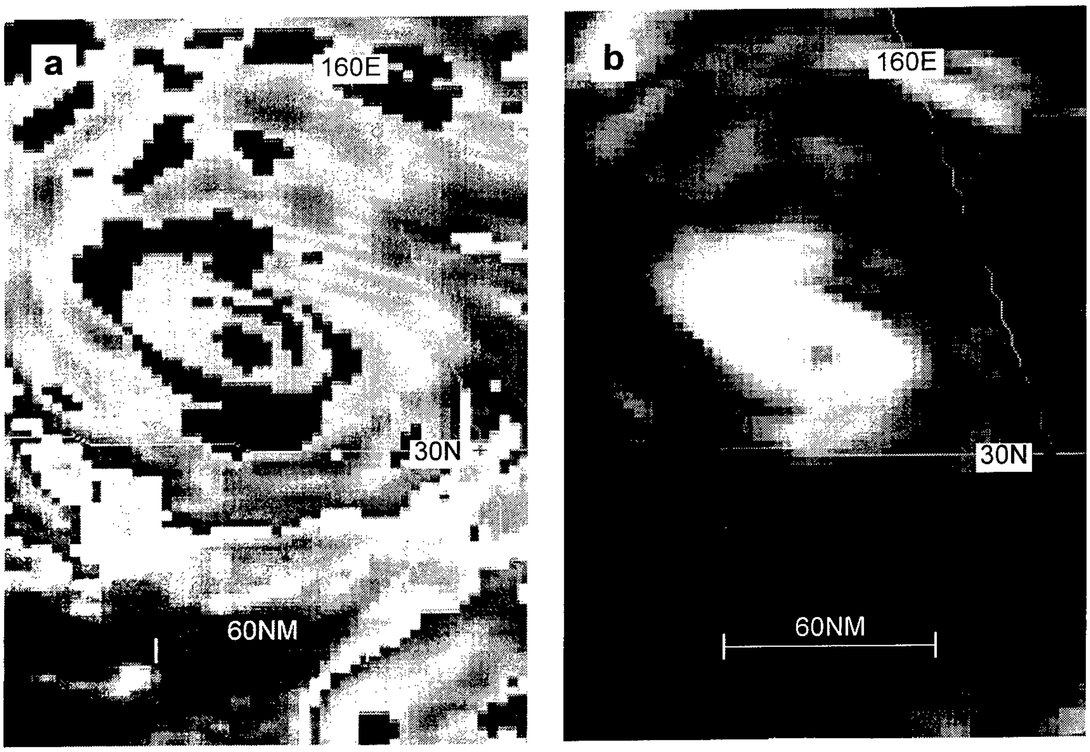

Figure 3-20-3a, b Piper was a very small TC — the smallest of 1996. Its eye was only 7 nm (13 km) in diameter, and its dense cold cirrus shield had a diameter of less than 100 nm (185 km). (a) 250931Z August enhanced infrared GMS imagery, and (b) 250931Z August high-contrast infrared GMS imagery.

c. *Development over cool SST*

Relatively few TCs in the WNP first attain typhoon intensity poleward of 30°N — during the 25-year period 1970 to 1994 only thirty-one of 729 TCs (4%) which formed in the WNP first attained 65-kt (33-m/sec) intensity at, or north, of 25°N; only twelve at, or north, of 30°N; and only one north of 35° N. Piper first attained 65-kt (33-m/sec) intensity at 34°N. It remained a typhoon for approximately nine hours, and fell below typhoon intensity after crossing 35°N. The sea-surface temperature (SST) at the point where Piper's intensity peaked was approximately 25°C (Figure 3-14-5). Piper remained a well-defined TC with an intensity of 60 kt (31 m/sec) near 40°N, (Figure 3-20-4), even though SSTs were only 20°C.

IV. IMPACT

No reports of damage or injury were received at the JTWC.

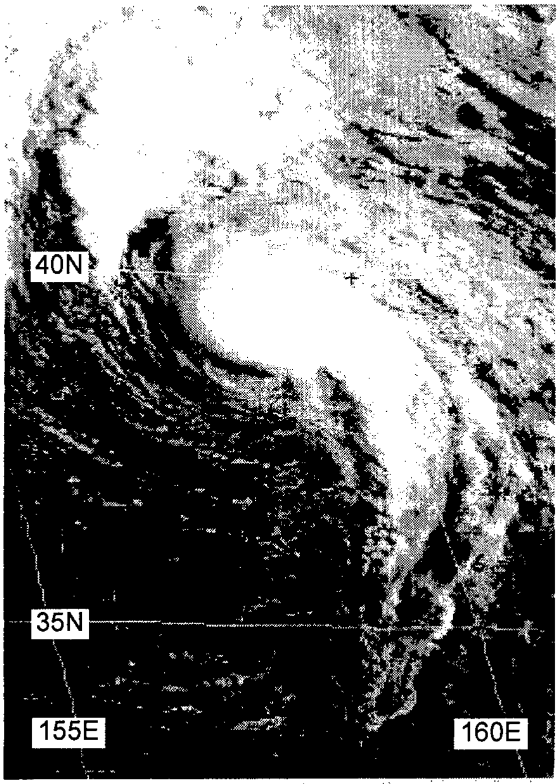

Figure 3-20-4 Piper's small well-defined CDO begins its northward acceleration over cooler SST and toward a frontal cloud band (252131Z August visible GMS imagery).

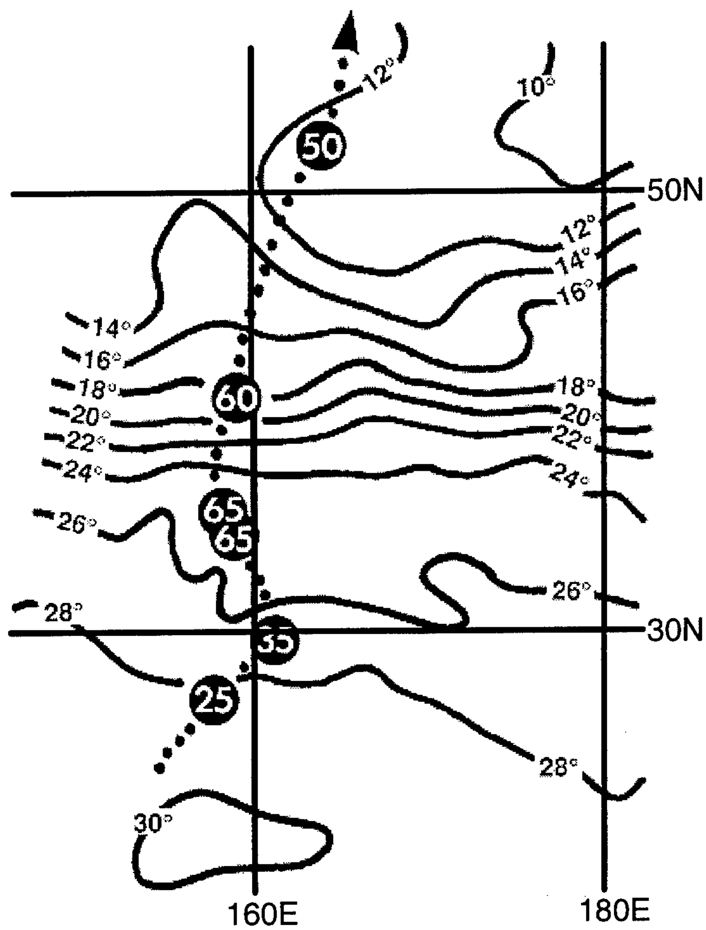

Figure 3-20-5 Piper reaches typhoon intensity at an unusually high latitude, and over relatively cool SST. (SST contours are based upon 220000Z August FNMOC analysis).

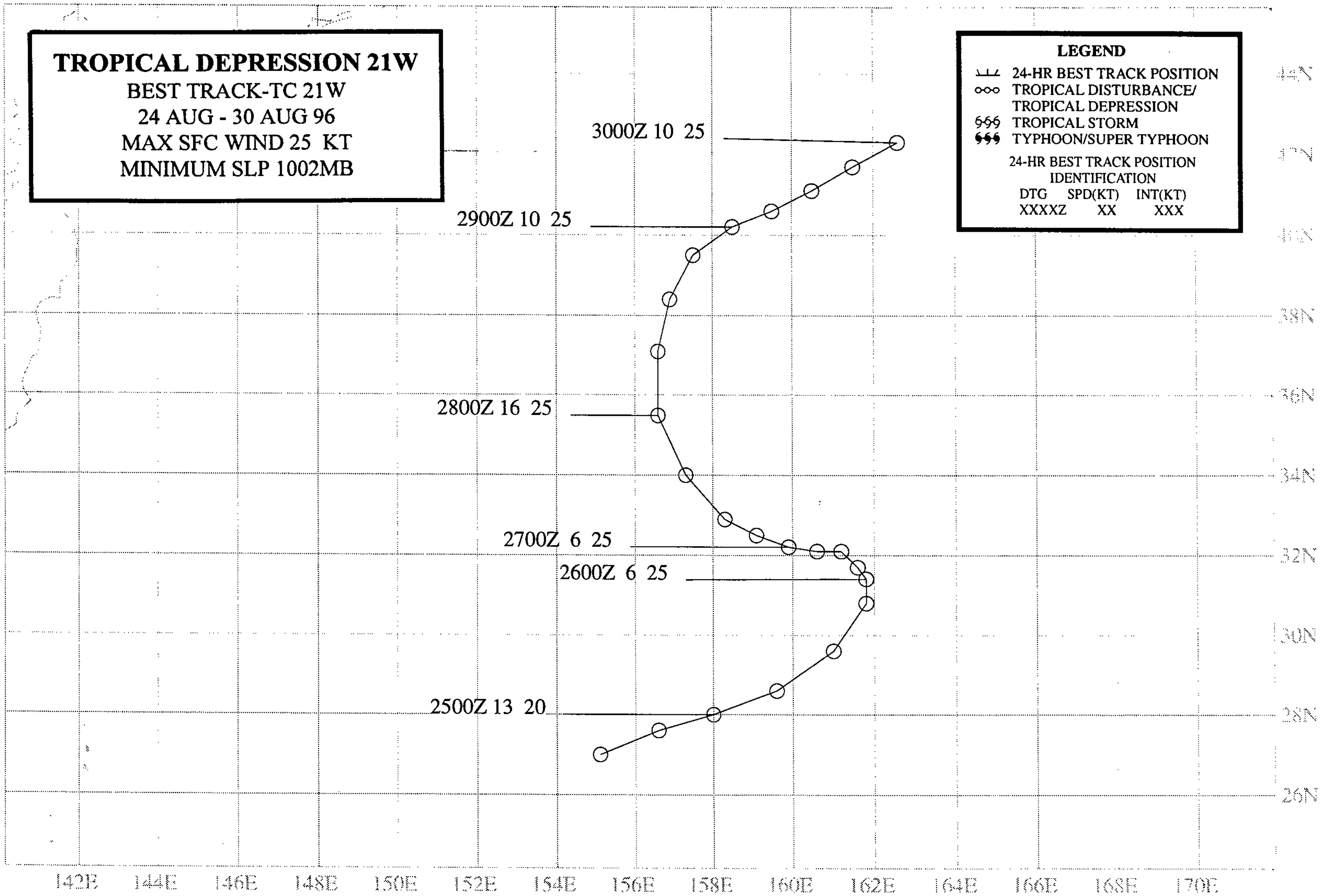
TROPICAL DEPRESSION 21W
BEST TRACK-TC 21W
24 AUG - 30 AUG 96
MAX SFC WIND 25 KT
MINIMUM SLP 1002MB
LEGEND
24-HR BEST TRACK POSITION
TROPICAL DISTURBANCE/
TROPICAL DEPRESSION
TROPICAL STORM
TYPHOON/SUPER TYPHOON
24-HR BEST TRACK POSITION
IDENTIFICATION
DTG SPD(KT) INT(KT)
XXXXZ XX XXX
3000Z 10 25
2900Z 10 25
2800Z 16 25
2700Z 6 25
2600Z 6 25
2500Z 13 20
142E
144E
146E
148E
150E
152E
154E
156E
158E
160E
162E
164E
166E
168E
170E
38N
36N
34N
32N
30N
28N
26N

TROPICAL DEPRESSION 21W

Forming at the end of a northward-displaced monsoon trough, Tropical Depression 21W followed an "S"-shaped poleward-oriented track close on the heels of Typhoon Piper (20W) (Figure 3-21-1). Emerging rather quickly from the end of the monsoon trough, the tropical disturbance that became TD 21W was never mentioned on the Significant Tropical Weather Advisory, but rather, a Tropical Cyclone Formation Alert (TCFA) was issued at 252330Z August followed immediately by a warning valid at 260000Z. Remarks on the TCFA included:

"A tropical disturbance has developed within the monsoon trough, between Tropical Storm Piper (20W) and Typhoon Orson (19W). Upper-level data favors continued development. At this time, the system is expected to follow Piper (20W) up the midlatitude trough axis. A warning message is forthcoming."

Soon after the first warning, TD 21W lost most of its central deep convection and it failed to mature (although a well-defined LLCC persisted). The final warning was issued valid at 271200Z, when it was thought that the LLCC of TD 21W was going to dissipate over water. The LLCC did not dissipate, however, and in post analysis it was carried as a 25 kt (13 m/sec) tropical depression for another 60 hours as it recurved on the final leg of its "S"-shaped track.

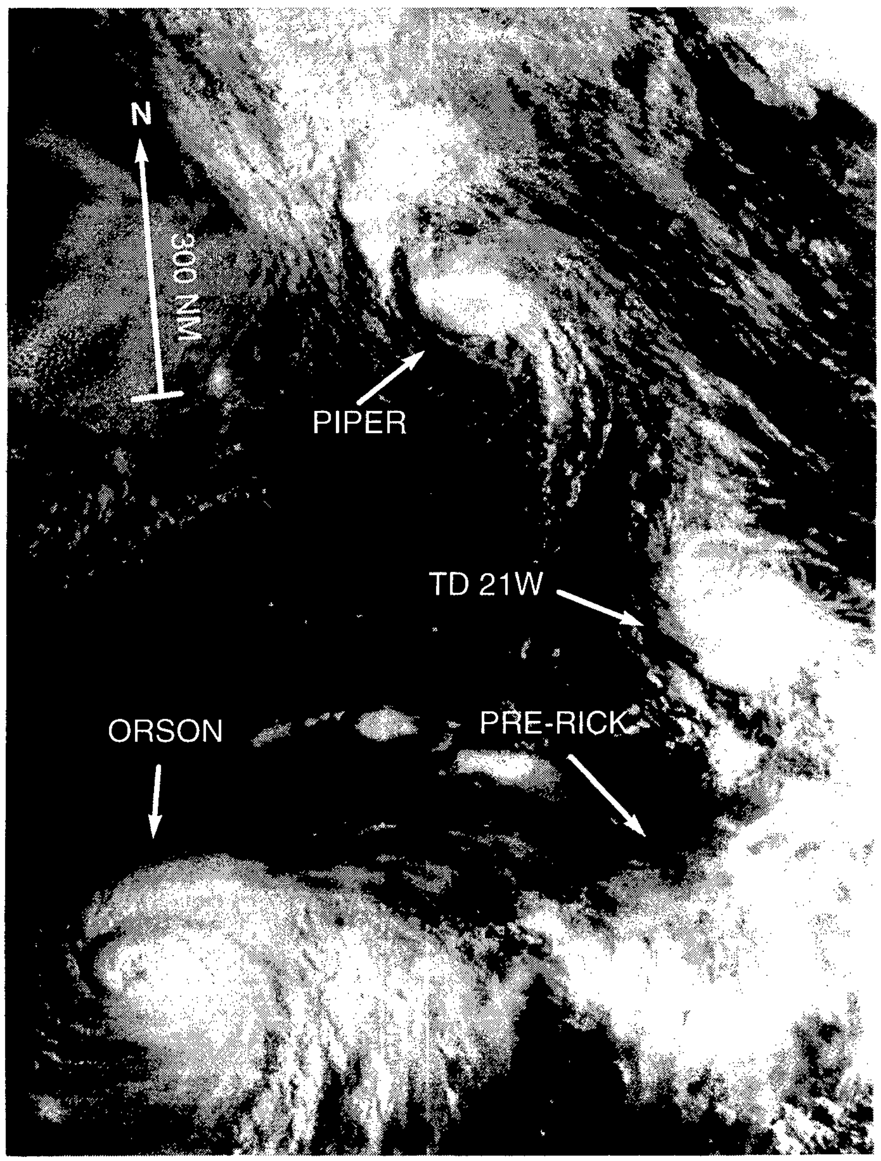

Figure 3-21-1 Tropical Depression 21W is forming at the end of the monsoon trough. With Piper (20W) to its north, and Orson (19W) to its southwest, TD 21W is set to move north and leave a vacancy at the end of the trough to be filled by yet another TC, Rick (22W) (252224Z August visible GMS imagery).

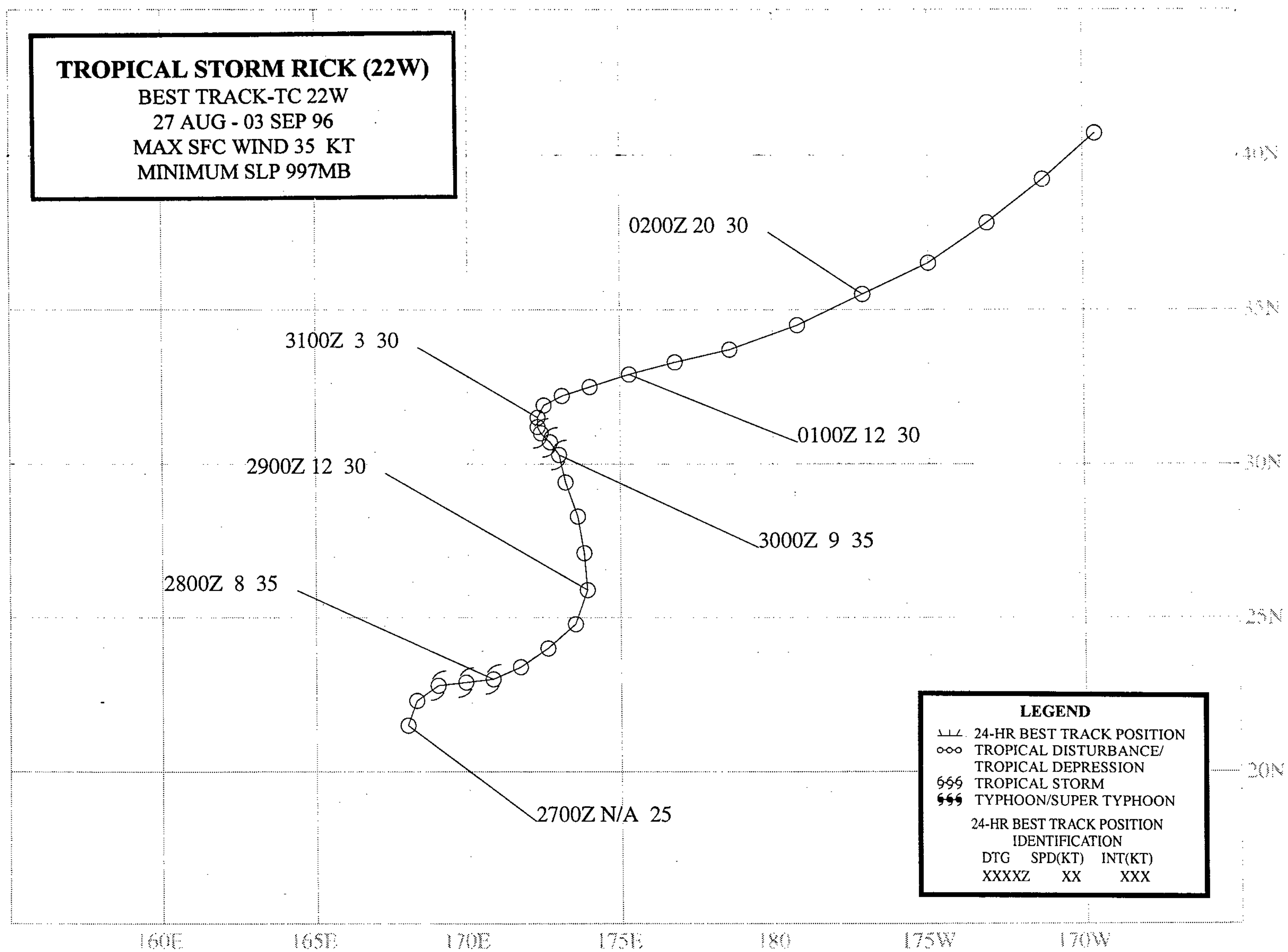

TROPICAL STORM RICK (22W)
BEST TRACK-TC 22W
27 AUG - 03 SEP 96
MAX SFC WIND 35 KT
MINIMUM SLP 997MB
0200Z 20 30
3100Z 3 30
0100Z 12 30
2900Z 12 30
3000Z 9 35
2800Z 8 35
2700Z N/A 25
40N
35N
30N
25N
20N
160E
165E
170E
175E
180
175W
170W
LEGEND
24-HR BEST TRACK POSITION
TROPICAL DISTURBANCE/
TROPICAL DEPRESSION
TROPICAL STORM
TYPHOON/SUPER TYPHOON
24-HR BEST TRACK POSITION
IDENTIFICATION
DTG SPD(KT) INT(KT)
XXXXZ XX XXX

TROPICAL STORM RICK (22W)

I. HIGHLIGHTS

Rick formed at a high latitude at the end of a northward-displaced monsoon trough. The first warning was issued without a prior Tropical Cyclone Formation Alert when scatterometer data indicated the well-defined low-level circulation possessed winds of at least 30 kt (15 m/sec).

II. TRACK AND INTENSITY

During the last week of August, the axis of the monsoon trough was displaced well to the north of its normal location. Anchored at 25°N by the slow-moving Orson (19W), the axis of the monsoon trough extended east-northeastward toward the international date line. Prior to Rick's formation, two other TCs — Typhoon Piper (20W) and Tropical Depression 21W — formed at the end of this monsoon trough and moved on poleward-oriented "S"-shaped tracks.

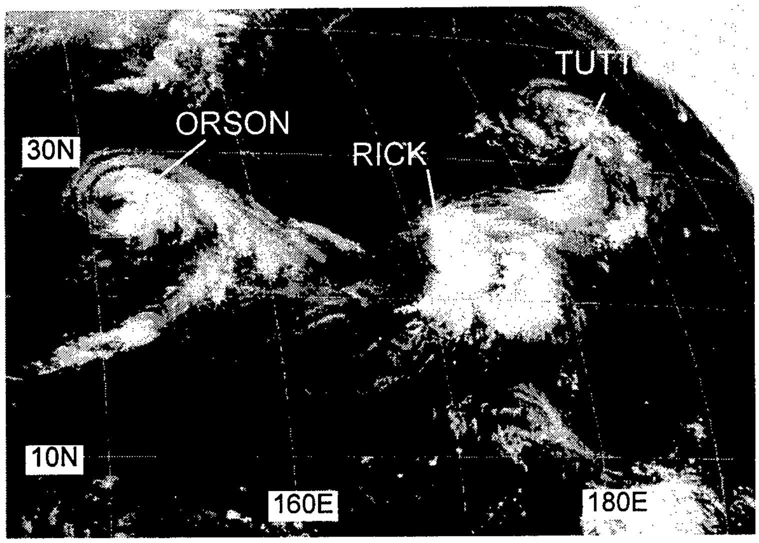

Figure 3-22-1 The tropical disturbance that became Rick is located between Orson (19W) and a TUTT cell. Scatterometer data at this time showed that it was already at tropical-storm intensity, and the final best track was adjusted accordingly (272130Z August infrared GMS imagery).

The tropical disturbance which became Rick was located between Orson (19W) and a well-defined TUTT cell (Figure 3-22-1). This disturbance was first mentioned on the 260600Z August Significant Tropical Weather Advisory when synoptic data indicated that it was accompanied by a weak LLCC. When a scatterometer pass at 271121Z (Figure 3-22-2) revealed that a well-defined LLCC (with maximum winds of 30 kt) accompanied the poorly-organized cloud system shown in Figure 3-22-1, the JTWC issued the first warning (valid at 280000Z) on Tropical Depression (TD) 22W. In post analysis, the scatterometer pass was used to upgrade TD 22W to tropical-storm intensity at an earlier time than upgraded while in warning status.

Initially moving northeastward along the axis of the monsoon trough, TD 22W turned to the north when it approached a blocking high. After crossing 30°N, TD 22W slowed and its cloud pattern became better defined (Figure 3-22-3, see also Figure 3-21-1 in the summary of TD 21W). Better cloud organization and satellite-based microwave data (SSM/I) indicating 35 kt (18 m/sec)

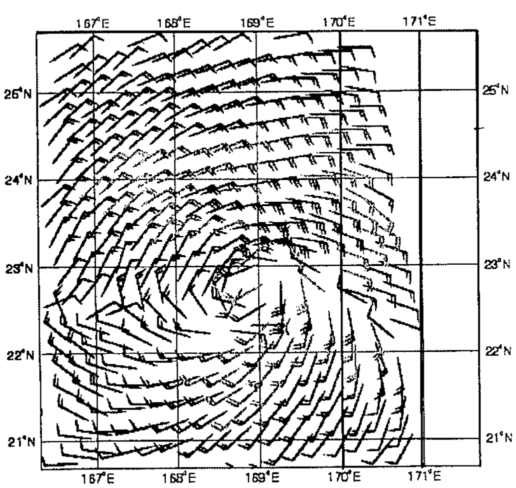

Figure 3-22-2 A well-defined LLCC with maximum winds of 30 kt accompanies "Rick's" cloud system at the time of the image in figure 3-22-1 (272110Z August ERS-2 scatterometer-derived winds).

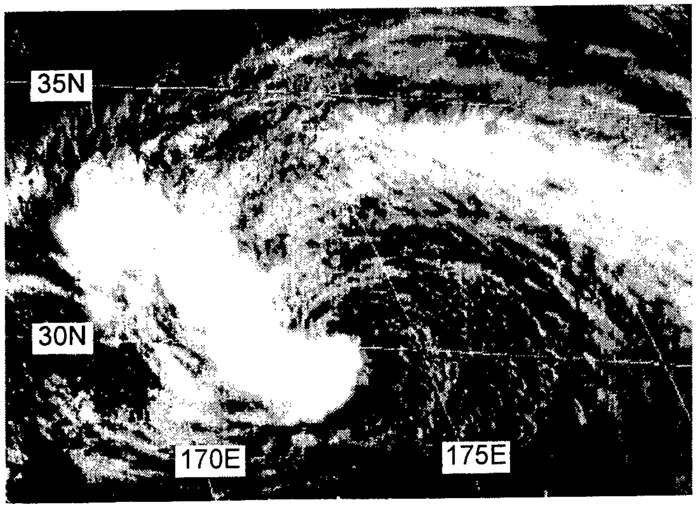

Figure 3-22-3 The primary band of deep convection coils around the western side of Rick's partially exposed LLCC (292131Z August visible GMS imagery).

prompted the JTWC to upgrade TD 22W to Tropical Storm Rick on the warning valid at 300000Z. On the warning valid at 301200Z, the system was downgraded to a tropical depression when the amount of its central deep convection decreased.

On 31 August, the system entered the accelerating westerlies regime north of the subtropical ridge. While Rick was moving east-northeastward at the base of an advancing frontal cloud band, its final warning was issued valid at 311200Z. The remnants of Rick continued to sweep northeastward within the frontal cloud band. The final best track carries the system across the international date line and north of 40°N.

III. DISCUSSION

a. *High latitude of formation*

Tropical cyclogenesis (TC genesis) is relatively rare east of 160°E and north of 20°N in the WNP. There are two synoptic conditions that lead to most of the TC genesis there: (1) TUTT-induced TC genesis, and (2) TC genesis that occurs when the monsoon trough has penetrated unusually far to the north and east. In Rick's case, the monsoon trough had migrated to an unusually high latitude, and the disturbance that became Rick formed at the eastern end of this trough. There was also a large well-defined TUTT cell northeast of this disturbance (Figure 3-22-1), but its role (if any) in Rick's development is not clear.

b. *Scatterometer data*

The first warning on Rick was based upon scatterometer data from the European Remote Sensing Satellite-2 (ERS-2) (Figure 3-22-2). The JTWC has access to scatterometer wind data, and has used it to help determine the position, intensity and wind distribution of TCs for nearly one and a half years. Some drawbacks of the scatterometer data are its small swath width, 180° directional ambiguity, relatively coarse resolution, limitations on the wind speeds it can accurately detect, and a low-speed bias.

The scatterometer pass which prompted the first warning on TD 22W (Figure 3-22-2) contains many 25-kt (13-m/sec) wind reports, with a maximum report of 30 kt (15 m/sec) just east of the system center. In real time, this was used to support a warning intensity of 30 kt, but, in post analysis was used to upgrade TD 22W to tropical-storm intensity at an earlier time. When compared with buoys and ship reports, the scatterometer winds generally have a low-speed bias (Quilfen, 1992; Laing, 1994; and Laing and Brenstrum, 1996). Laing and Brenstrum (1996) showed that the ERS-1 winds had a mean low-speed bias of about 4 kt (2 m/sec) when compared with the winds recorded on a New Zealand research ship (Figure 3-22-4). The magnitude of this bias increases with increasing wind speed. The low-speed bias increases to near 6 kt (3 m/sec) at wind speeds of 30 kt (15 m/sec). In operational practice, the JTWC treats a 30-kt scatterometer wind as representative of a 35-kt one-minute average 10-m wind. Hence, the 30-kt maximum scatterometer wind in Figure 3-22-2 was used in post analysis as grounds for upgrading the intensity of TD 22W from 30 kt to 35 kt (i.e., from a tropical depression to a tropical storm).

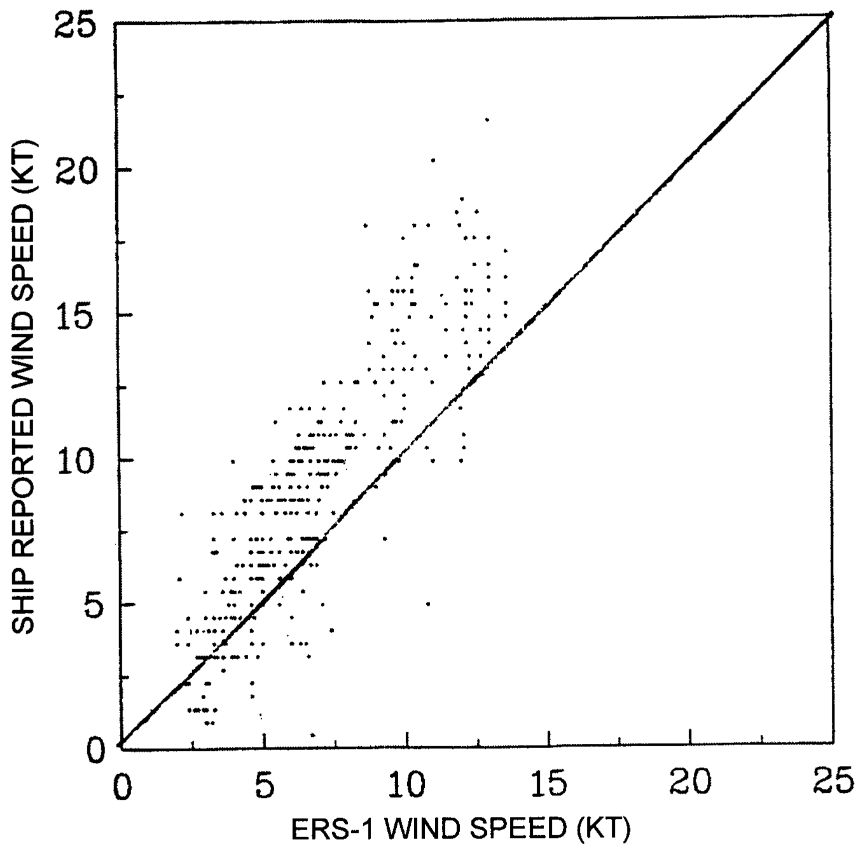

Figure 3-22-4 A comparison of the wind speeds recorded by the New Zealand research ship Tangaroa with wind speeds obtained from the ERS-1 scatterometer. That most of the points are above the 45° line indicate that the ship wind speeds are generally higher than those estimated by the scatterometer. (Figure adapted from Figure 2 of Laing and Brenstrum (1996).)

IV. IMPACT

No reports of damage or injury were received at the JTWC.

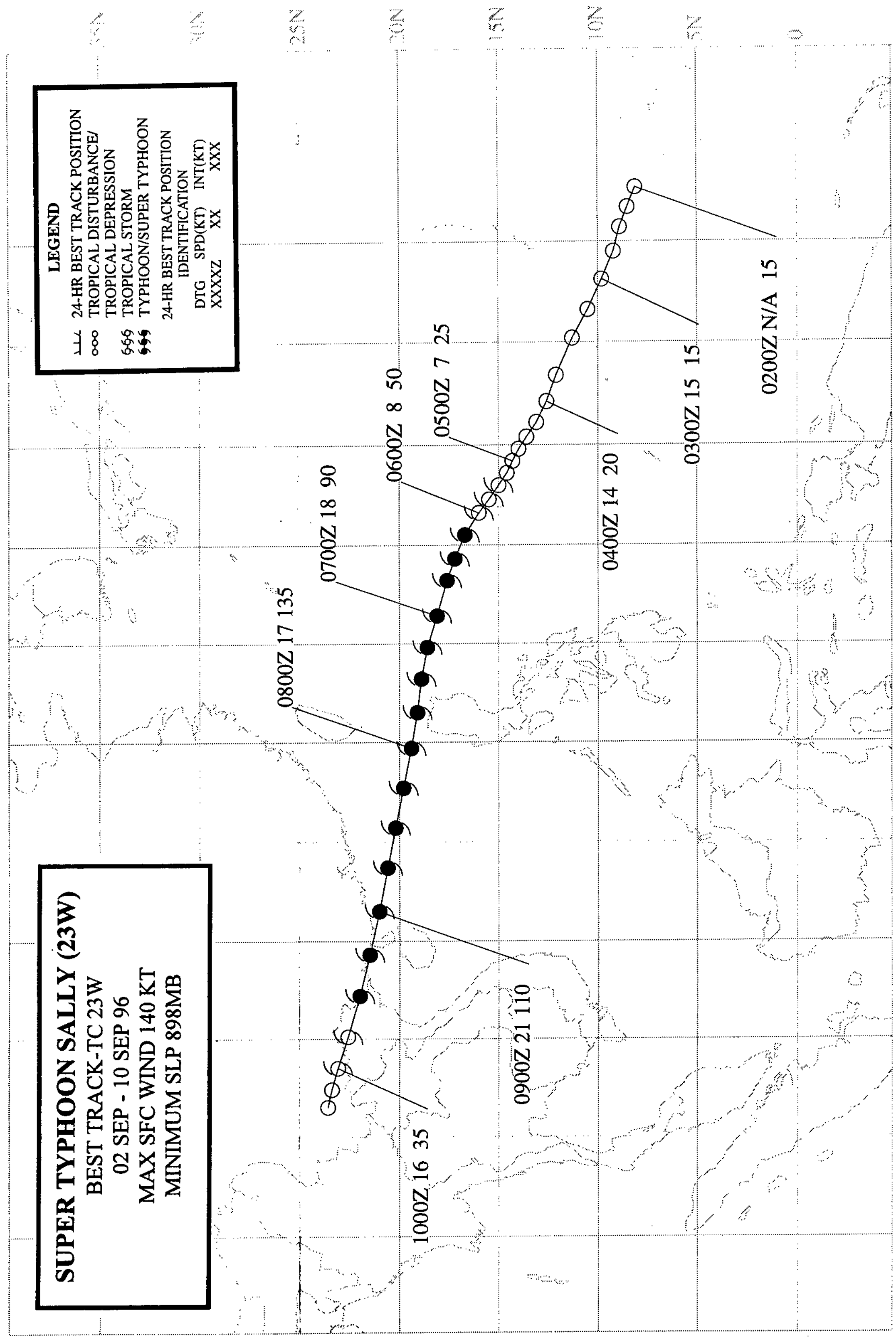
SUPER TYPHOON SALLY (23W)
BEST TRACK-TC 23W
02 SEP - 10 SEP 96
MAX SFC WIND 140 KT
MINIMUM SLP 898MB
LEGEND
24-HR BEST TRACK POSITION
TROPICAL DISTURBANCE/
TROPICAL DEPRESSION
TROPICAL STORM
TYPHOON/SUPER TYPHOON
24-HR BEST TRACK POSITION
IDENTIFICATION
DTG SPD(KT) INT(KT)
XXXXZ XX XXX
1000Z 16 35
0900Z 21 110
0800Z 17 135
0700Z 18 90
0600Z 8 50
0500Z 7 25
0400Z 14 20
0300Z 15 15
0200Z N/A 15
25N
20N
15N
10N
5N
0
95E
100E
105E
110E
115E
120E
125E
130E
135E
140E
145E
150E

SUPER TYPHOON SALLY (23W)

I. HIGHLIGHTS

As the long-lived Orson (19W) recurved at the beginning of September, the unusual monsoon flow pattern of August (See figure 3-13-4 in Kirk's summary) gave way to a pattern more in line with climatology: the maximum cloud zone and the axis of the monsoon trough became established from the Philippines east-southeastward into Micronesia. Sally was the first of five significant TCs to develop in this new monsoon flow pattern. Forming to the southwest of Guam, Sally moved on a relatively steady west-northwest straight-moving track. It became a super typhoon while moving through the Luzon Strait, and later, though weaker, it made landfall in southwestern China where it caused extensive damage and considerable loss of life.

II. TRACK AND INTENSITY

On the first day of September, Typhoon Orson (19W) was recurving to the east of Japan, and the deep tropics of the WNP were abnormally free of deep convection. Over the next two days, as Orson (19W) recurved into the midlatitudes, amounts of deep convection in the low latitudes of the WNP began to rapidly increase as a new monsoon trough was becoming established there. On 02 September, when amounts of deep convection in the low latitudes of the WNP began to increase, a tropical disturbance quickly consolidated near the island of Guam. It was first mentioned on the 020600Z Significant Tropical Weather Advisory, which described it as follows:

"An area of convection is located near 11N 145E. Satellite imagery and synoptic data indicate a broad area of convection surrounding an inverted trough in the trade wind flow. . . ."

Early on 04 September, synoptic data showed that a low-level cyclonic circulation had formed in the monsoon trough in association with this disturbance. Cirrus outflow was well organized into an anticyclonic pattern with a center of symmetry over the LLCC. This prompted the JTWC to issue a Tropical Cyclone Formation Alert (TCFA) at 032300Z September. The MCSs comprising this disturbance were growing and collapsing at the typical 06- to 12-hour MCS time scale, creating some difficulty for the satellite analysts to accurately locate the LLCC. The uncertain knowledge of the location of the LLCC led to a second TCFA at 042300Z in order to carry the alert beyond the expiration of the first, and to give JTWC forecasters some time to gather information for the first warning (which was in preparation when the first TCFA was about to expire). As expected, the second TCFA was quickly followed by the first warning on Tropical Depression (TD) 23W, valid at 050000Z, when morning visible satellite imagery allowed for a more accurate determination of the position of the LLCC and indicated an intensity of 25 kt (13 m/sec). From this time onward (until peak), intensification proceeded at a faster than normal rate (i.e., 1.5 T numbers per day versus the normal 1 T number per day). TD 23W was upgraded to Tropical Storm Sally on the warning valid at 051800Z. The system became a typhoon at 060600Z, and a super typhoon at approximately 071600Z. The peak intensity of 140 kt (72 m/sec) occurred at 071800Z (Figure 3-23-1) as the cyclone moved through the Luzon Strait. Moving west-northwestward at nearly 20 kt (37 km/hr), the typhoon crossed the northern reaches of the South China Sea (SCS) under the steering influence of a dominant subtropical ridge. The system weakened as it moved across the SCS, but it was still potent with an intensity of approximately 100 kt (51 m/sec) when it made landfall on the Luichow peninsula in southwestern China. The typhoon crossed the Luichow peninsula and then moved along the Chinese Gulf-of-Tonkin coastline. The system went inland for good just north of China's border with Vietnam. The final warning was issued, valid at 091200Z, as the weakening TC continued its trek inland across the far north of Vietnam and southwestern China.

III. DISCUSSION

Sally's digital Dvorak (DD) numbers: a pattern begins to emerge

During 1996, the hourly time series of the DD numbers was computed and archived for all typhoons (during 1995, hourly DD numbers were computed for some selected TCs, Ward, for example). The hourly time series of Sally's DD numbers (Figure 3-23-2) shows a characteristic pattern that appears to be typical of some of the other very intense typhoons of 1996 and 1995:

1) the DD time series rises more rapidly than the best-track intensity (which is based primarily upon the manual application of Dvorak's techniques);

2) the DD time series peaks earlier than the best-track intensity;

3) the peak of the DD time series is approximately one-half of a T number higher that the best-track peak; and,

4) within 24 hours of the DD peak, there is a dramatic drop of the DD values of 2 or more T numbers, and then a recovery. Some or all of these behaviors are seen in the DD time series of Eve (07W), Dale (36W) and to a lesser extent Herb (10W) and Violet (26W).

These specific characteristic behaviors of the DD time series are closely tied to the evolution of the character of the eye. As TCs approach their peak intensity, their eyes are usually small and well defined. Why the DD numbers rise more quickly and peak earlier and higher than the best track has not been determined. The dramatic fall of the DD time series following the peak can usually be linked to the formation of concentric wall clouds. The DD numbers recover from the dramatic fall after the inner wall cloud collapses and a new larger eye is established.

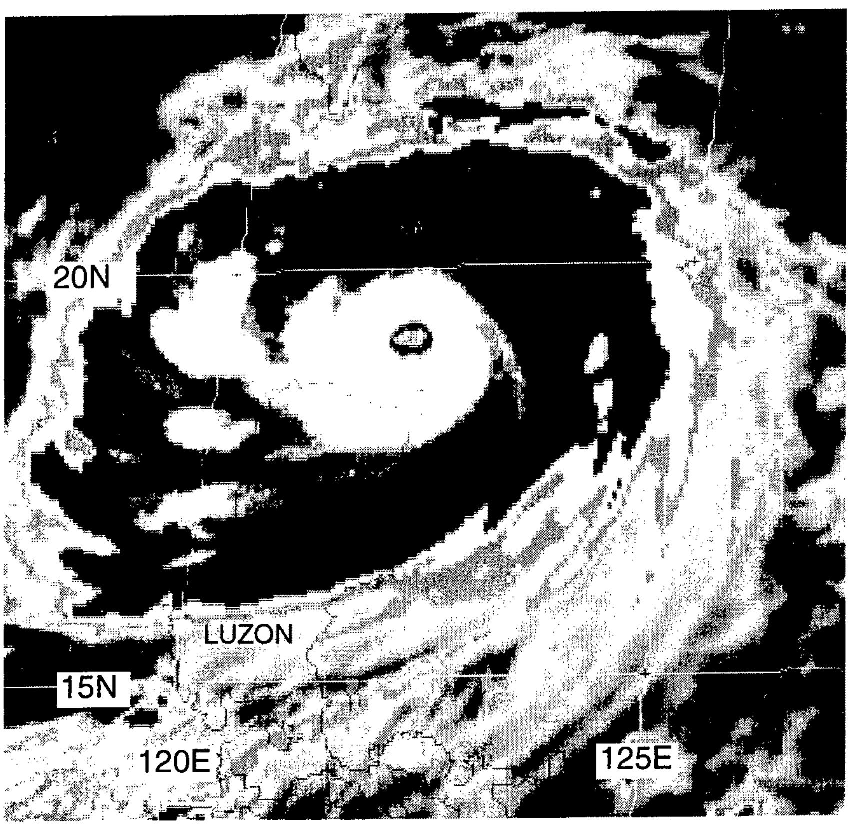

Figure 3-23-1 Sally shortly before reaching its peak intensity of 140 kt (72 m/sec) (071631Z September enhanced infrared GMS imagery). Enhancement curve is "MB".

IV. IMPACT

Sally was catastrophic in southern China. At least 114 people were reported killed with another 110 missing. The city of Zhanjiang on the east coast of the Luichow peninsula was one of the hardest hit. Here, 79 people were reported killed. Almost all trees in this city and its suburbs were reported to have been uprooted by high winds. Economic losses were described as the worst since 1954. Combined losses in the cities of Zhanjiang and Maoming were estimated at US $1.5 billion.

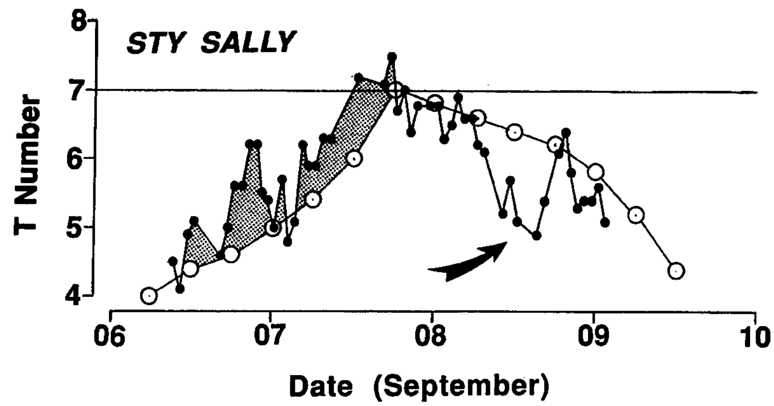

Figure 3-23-2 The time series of Sally's hourly DD numbers (small black dots connected by thin solid line). For comparison, the final best track intensity at six-hour intervals (converted to a T number) is superimposed (open circles connected by thin solid line). Shaded regions indicate that the DD number is higher than the best-track intensity. The arrow points to the relative minimum in the DD time series which occurred approximately 24 hours after the peak in the DD numbers.

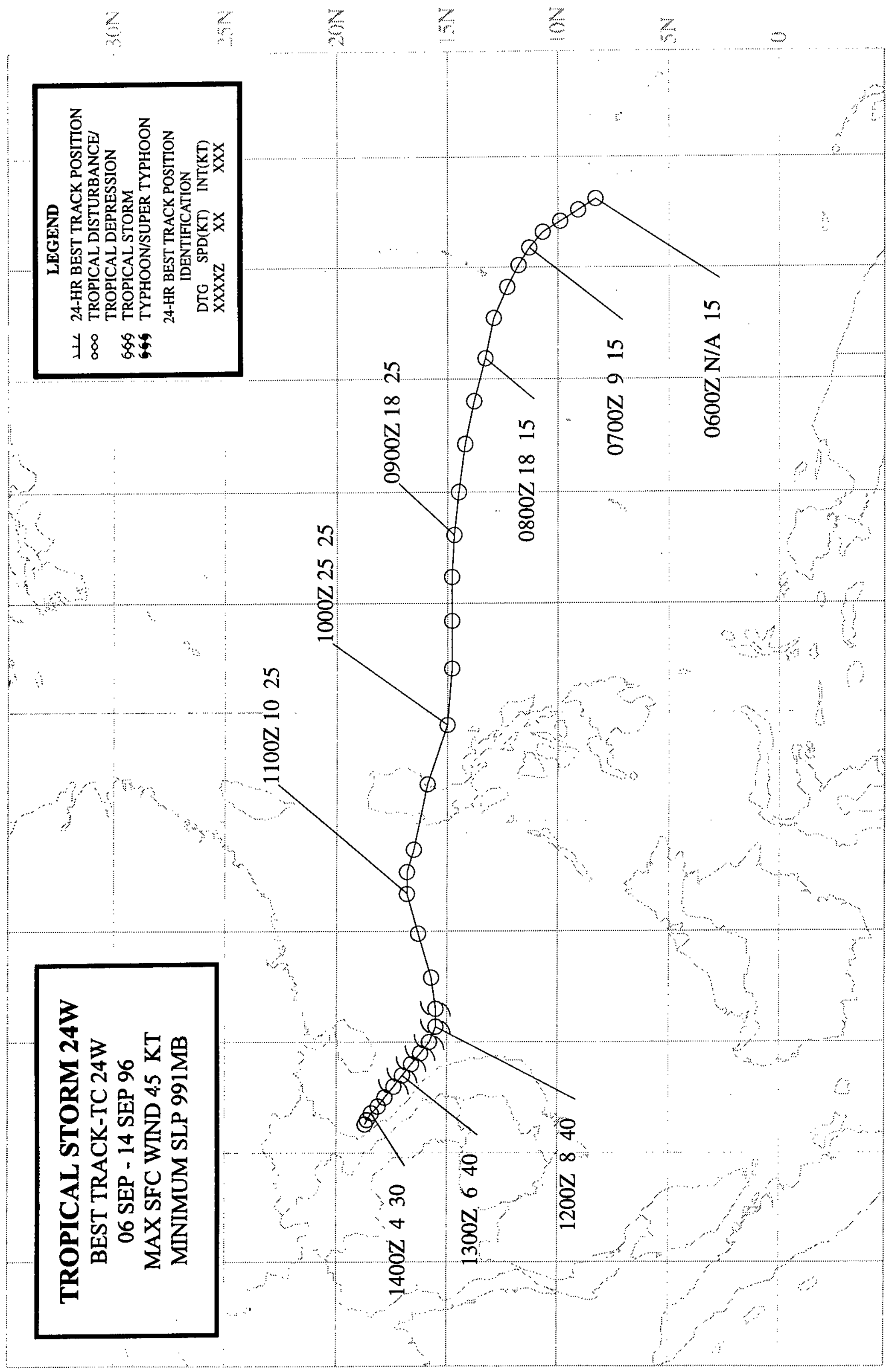

TROPICAL STORM 24W
BEST TRACK-TC 24W
06 SEP - 14 SEP 96
MAX SFC WIND 45 KT
MINIMUM SLP 991MB
LEGEND
24-HR BEST TRACK POSITION
TROPICAL DISTURBANCE/
TROPICAL DEPRESSION
TROPICAL STORM
TYPHOON/SUPER TYPHOON
24-HR BEST TRACK POSITION
IDENTIFICATION
DTG SPD(KT) INT(KT)
XXXXZ XX XXX
0600Z N/A 15
0700Z 9 15
0800Z 18 15
0900Z 18 25
1000Z 25 25
1100Z 10 25
1200Z 8 40
1300Z 6 40
1400Z 4 30
30N
25N
20N
15N
10N
5N
0
100E
105E
110E
115E
120E
125E
130E
135E
140E
145E
150E

TROPICAL STORM 24W

As the long-lived Orson (19W) recurved at the beginning of September, the unusual monsoon flow pattern of August (see figure 3-13-4 in Kirk's summary) gave way to a pattern more in line with climatology: the maximum cloud zone and the axis of the monsoon trough extended from the Philippines east-southeastward into Micronesia. Tropical Storm 24W was the second of five significant TCs to form in this trough.

On 07 September, an area of deep convection began to consolidate into a discrete tropical disturbance located near Guam. First mentioned on the 071600Z September Significant Tropical Weather Advisory, this disturbance became a large monsoon depression in the Philippine Sea by the morning of 09 September (Figure 3-24-1). Although the definition of a monsoon depression includes large size, the disturbance which became Tropical Storm 24W was exceptionally large with its loosely organized ensemble of MCSs stretching nearly 25° (1500 nm; 2800 km) from the Philippines to Guam. Based upon consolidation of deep convection into a smaller area, the JTWC issued a Tropical Cyclone Formation Alert valid at 090500Z. Remarks on this alert included:

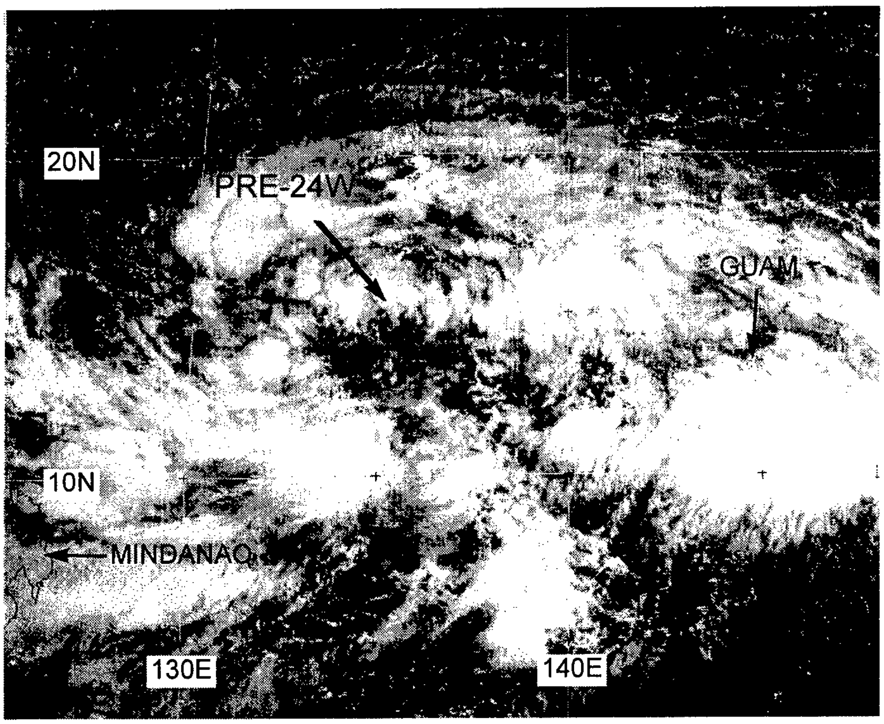

Figure 3-24-1 The cyclonic circulation center which became Tropical Storm 24W consolidated within a large monsoon depression. Another area of deep convection near Guam later detached from the monsoon depression and became Violet (26W) (082224Z September visible GMS imagery).

"Synoptic data and visible satellite imagery reveal the presence of a broad monsoon depression with the dominant circulation center [located near 15°N; 133°E]. Convection associated with this disturbance is limited to a broad ring approximately 600 nm in diameter. Maximum sustained winds are limited to the convective regions on the periphery of this system. . . ."

The first warning on Tropical Depression (TD) 24W was issued valid an hour later at 090600Z based upon ship reports of 20 to 25 kt (10-13 m/sec) in the convective regions approximately 120 nm (220 km) to the north and southwest of the LLCC.

The monsoon depression which became TD 24W had a complex evolution. Not only did it lead to the formation of TD 24W, but another cyclonic circulation associated with it became Violet (26W). This complexity is described in remarks on the 100600Z Significant Tropical Weather Advisory:

"An area of convection [pre-Violet] is located near 13N 140E. Satellite imagery and synoptic data indicate this is a convective region formerly associated with Tropical Depression 24W that has separated from TD 24W and remained quasi-stationary as TD 24W moves west. . . ."

On 10 September, TD 24W crossed Luzon and entered the South China Sea. During the following three days it traversed the SCS, moved into the Gulf of Tonkin on 14 September, and weakened. The final warning, valid at 141200Z, was issued when the system dissipated near the coast of northern Vietnam.

TD 24W was upgraded to a tropical storm in postanalysis based on synoptic data which indicated sustained winds in the system reached a peak of 45 kt (23 m/sec) at 120600Z.

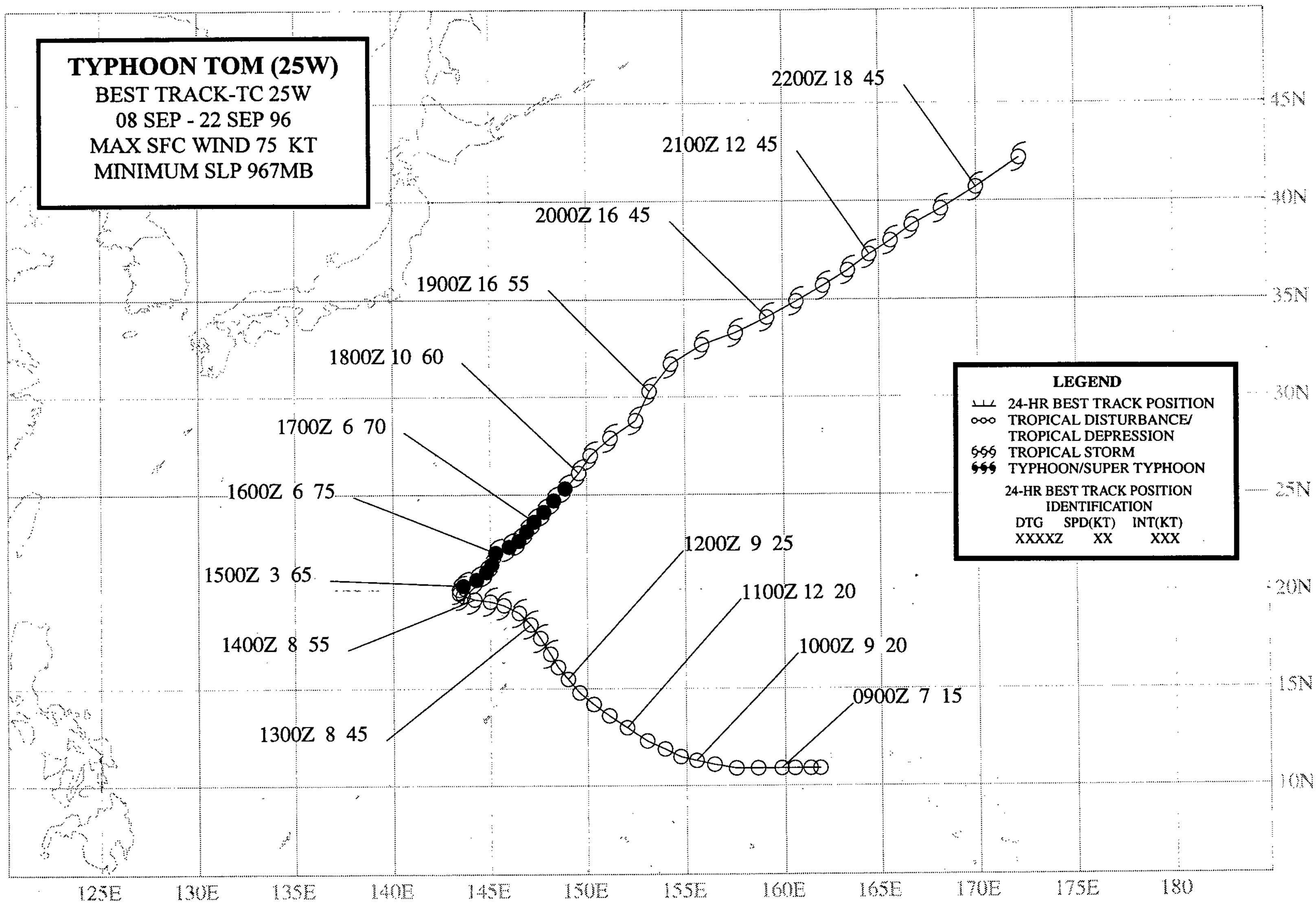
TYPHOON TOM (25W)
BEST TRACK-TC 25W
08 SEP - 22 SEP 96
MAX SFC WIND 75 KT
MINIMUM SLP 967MB
LEGEND
24-HR BEST TRACK POSITION
TROPICAL DISTURBANCE/
TROPICAL DEPRESSION
TROPICAL STORM
TYPHOON/SUPER TYPHOON
24-HR BEST TRACK POSITION
IDENTIFICATION
DTG SPD(KT) INT(KT)
XXXXZ XX XXX
2200Z 18 45
2100Z 12 45
2000Z 16 45
1900Z 16 55
1800Z 10 60
1700Z 6 70
1600Z 6 75
1500Z 3 65
1400Z 8 55
1300Z 8 45
1200Z 9 25
1100Z 12 20
1000Z 9 20
0900Z 7 15
45N
40N
35N
30N
25N
20N
15N
10N
125E
130E
135E
140E
145E
150E
155E
160E
165E
170E
175E
180

TYPHOON TOM (25W)

I. HIGHLIGHTS

Tom was the third of five significant TCs to form in the monsoon trough. At one point, Tom, Violet (26W), Willie (27W) and a subtropical (ST) low existed simultaneously along the trough axis (Figure 3-25-1a, b). Due to the relative motions of these TCs (and the ST low), the trough axis became reverse oriented. Both Tom and Violet (26W) were large TCs. Tom also had an unusual structure featuring a "pin-hole" eye in a small central cloud mass surrounded by extensive peripheral rain bands within a large outer wind field. Tom is a good case for the argument that the core of a TC is largely independent of its outer structure.

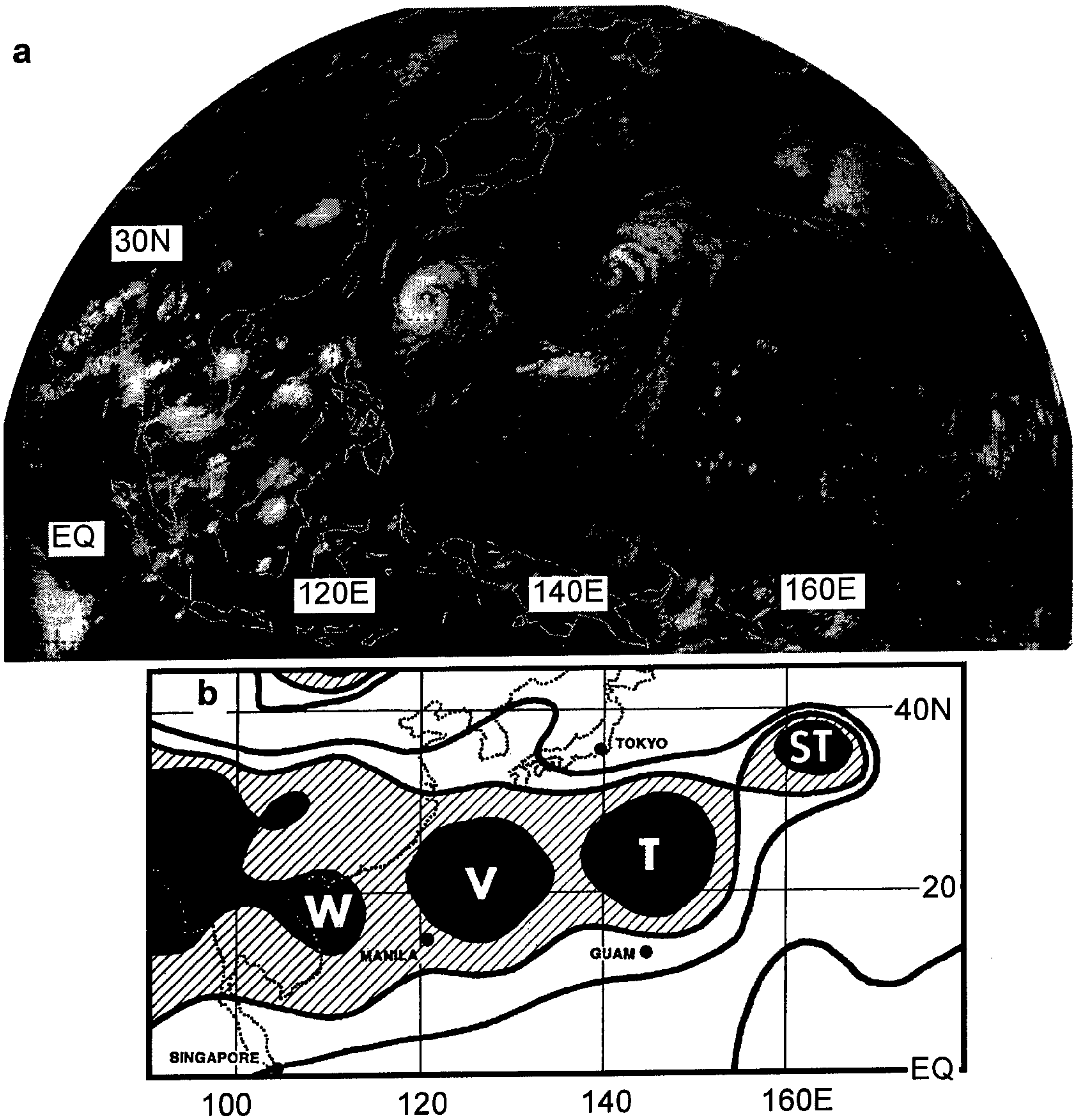

Figure 3-25-1 From west-to-east, TCs Willie (27W), Violet (26W), Tom (25W), and a subtropical low lie along the axis of a reverse-oriented monsoon trough. (a) 171231Z September infrared GMS imagery. (b) Sea-level pressure analysis (outer contour is 1010 mb, cross-hatched areas are between 1004 and 1008 mb, and black regions are less than 1004 mb) (Illustration based upon NOGAPS 170000Z September SLP analysis).

II. TRACK AND INTENSITY

During the second week of September, the cloudiness associated with the monsoon trough began to consolidate into discrete areas of persistent convection. A low-level cyclonic circulation located to the southwest of the easternmost of these areas became Tom, and was first mentioned on the 080600Z September Significant Tropical Weather Advisory. Embedded in an ensemble of poorly organized MCSs, the weak surface low drifted westward for two days with little development. Then, early on 11 September, the convection associated with the surface circulation became better organized, prompting the JTWC to issue a Tropical Cyclone Formation Alert valid at 102030Z. Moving toward the northwest, the deep convection associated with the system began to consolidate. Based on satellite intensity estimates of 25 kt (13 m/sec) and synoptic conditions deemed favorable for further development (e.g., good outflow in all quadrants as revealed by water-vapor derived winds), the first warning on Tropical Depression (TD) 25W was issued valid at 111800Z. Moving slowly toward the northwest, TD 25W became Tropical Storm Tom on the warning valid at 121200Z. Tom became a typhoon at 150000Z. Also at 150000Z, Tom began to move slowly toward the northeast, almost at the same time as Typhoon Violet (26W) (located approximately 1100 nm (2050 km) to Tom's west-southwest) did likewise. The turn to the northeast of Tom and Violet (26W) was associated with the monsoon trough acquiring a reverse orientation (as mentioned in the 150000Z Prognostic Reasoning for Typhoon Tom).

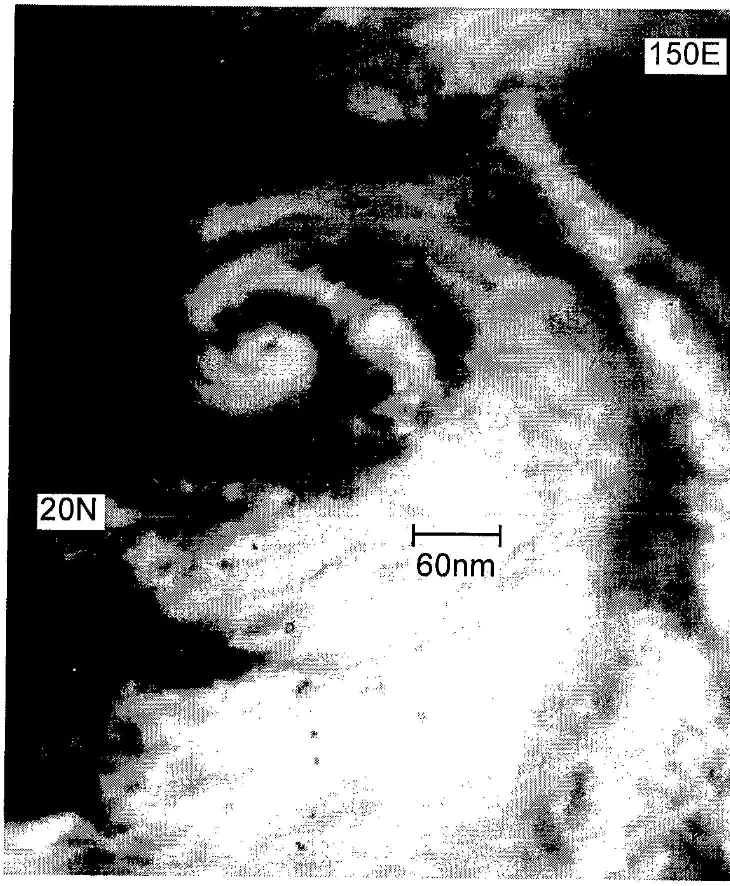

Figure 3-25-2 Tom reaches its peak intensity of 75 kt (39 m/sec). Note the small size of the eye and core cloud features with respect to the peripheral cloud features (160131Z September visible GMS imagery).

A common behavior of typhoons moving northeastward in a reverse-oriented monsoon trough, Tom continued to intensify while moving northeastward at 6 kt (11 km/hr), reached its peak of 75 kt (39 m/sec) at 151800Z (Figure 3-25-2), and maintained that intensity until after 161800Z. Slowly gaining forward speed, Tom gradually weakened as it moved toward the northeast. It eventually became a large extratropical low, but not before undergoing a lengthy period of extratropical transition for which the JTWC satellite forecasters instituted a new intensity estimation technique developed by Miller and Lander (1996) (see the discussion). Deemed to have nearly completed its extratropical transition, the final warning was issued valid at 200600Z.

III. DISCUSSION

a. *Tom's behavior in a reverse-oriented monsoon trough*

When the monsoon trough acquires a reverse orientation, a ridge of high pressure often builds to its south creating steering flow which causes TCs associated with the reverse-oriented monsoon trough (RMT) to move on north-oriented tracks. Premature eastward motion at low latitude is a common behavior of TCs located along the axis of an RMT. Such eastward turns at low-latitude are not considered "classic recurvature" because the TC is being steered by dominating monsoonal flow rather than by entry into the midlatitude westerlies. Often, the subtropical ridge is still in-place to the north of the RMT, and the TC is seen to undergo "S" motion (i.e., making a turn back to the northwest while moving through the subtropical ridge and entering the midlatitude westerlies). Another characteristic behavior of TCs while embedded in an RMT is intensification of the TC while moving on a track with an eastward component of motion (such was the case with Tom). The monsoon trough within which Tom was embedded, became reverse oriented by virtue of the relative motion of Tom and Violet (26W) (Figure 3-25-3). Both of these TCs moved on similarly shaped tracks, however, there was a gradual cyclonic rotation of the two about their centroid so that Tom, once east-southeast of Violet, moved to the east-northeast of Violet. For further information regarding the behavior of TCs associated with an RMT see Lander (1996) and the discussion of reverse-trough formation and poleward-oriented motion in Carr and Elsberry (1994).

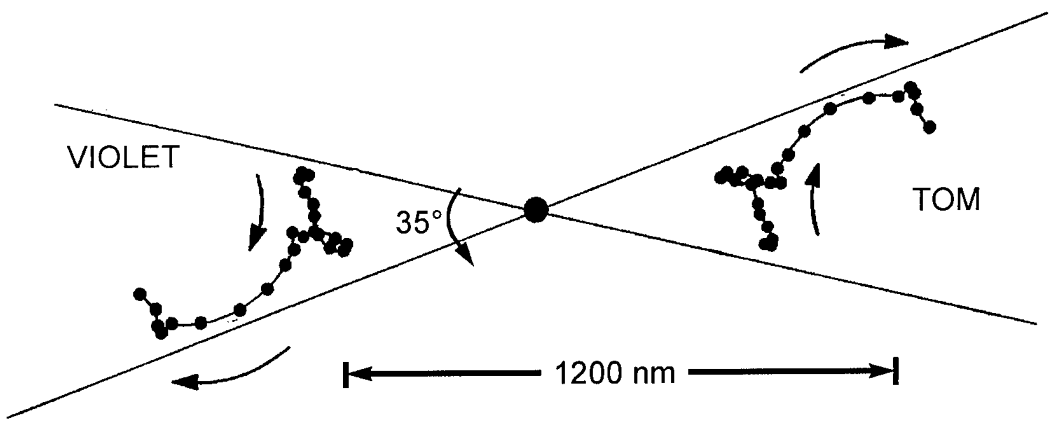

Figure 3-25-3 Centroid relative motion of Tom and Violet (26W). Dots are at 12-hour intervals beginning at 100000Z and ending at 220000Z.

b. *Unusual cloud signature*

When Tom reached its peak intensity of 75 kt (39 m/sec), it had an unusual structure featuring a "pin-hole" eye in a small central cloud mass surrounded by extensive peripheral rain bands within a large outer wind field (Figure 3-25-2). Tom is a good case for the argument that the core of a TC is largely independent of its outer structure. Take away the peripheral rain bands and the deep convection extending southwestward within the monsoon flow and Tom's small core is indistinguishable from a small TC with a small eye. By contrast, Typhoon Violet (26W) (located to the west of Tom) had a size similar to Tom, and yet the structure of its core was quite different: Violet's eye began small, but then expanded to a diameter on the order of 75 nm (140 km). The distinction between the TC core and its outer structure also has relevance to the evolution of monsoon depressions to conventional TCs (i.e., one of Dvorak's four data types). It is not clear by what pathway monsoon depressions become conventional TCs.

c. *On the use of scatterometry to assess the wind distribution of large TCs*

One of the limitations of the ERS-2 scatterometer data is its narrow swath width (approximately 7 degrees of great circle arc). When available, JTWC uses scatterometer data to evaluate the outer wind distribution of TCs (i.e., the radial extent of gales). For small TCs, the scatterometer often misses the TC for several passes, and even misses the peripheral gale area. For larger TCs like Tom, almost every scatterometer pass in the region of the TC samples a portion of its gale area, and thus, by piecing together the several hits on portions of the gale area, a picture of the wind distribution emerges —the problem of narrow swath width has less impact.

d. *First use of the "XT" technique*

A review of the 1994 and 1995 WNP TC data revealed the intensity estimates of a significant number of TCs that recurved and moved out of the tropics were underestimated by the TC satellite reconnaissance network which used Dvorak's techniques to determine intensity. Intensity estimates for Dan (06W) as it was recurving illustrate the problem (see Dan's (06W) summary). In order to address the problem of underestimating the intensity of TCs undergoing extratropical transition, satellite forecasters at the JTWC in conjunction with ONR-supported researchers at the University of Guam devised a technique (Miller and Lander, 1996) for estimating the intensity of TCs undergoing extratropical transition (see Dan's summary for more details on the technique). This technique yields XT (for extratropical transition) numbers that equate to wind speeds identical to Dvorak's T numbers of the same magnitude. The first application of the technique was on Tom as it was becoming extratropical. The JTWC satellite fix at 192330Z represented the first assignment ever of an XT number to a TC. The XT number determined for Tom at this time was XT 3.0. Other agencies using Dvorak's T numbers, or Hebert and Poteat's ST numbers were up to two T numbers lower than the JTWC intensity estimate. Scatterometer data and other synoptic data at the time supported the JTWC intensity estimate of XT 3.0 (i.e., 45 kt (23 m/sec)).

IV. IMPACT

No reports of damage or injury were received at the JTWC.

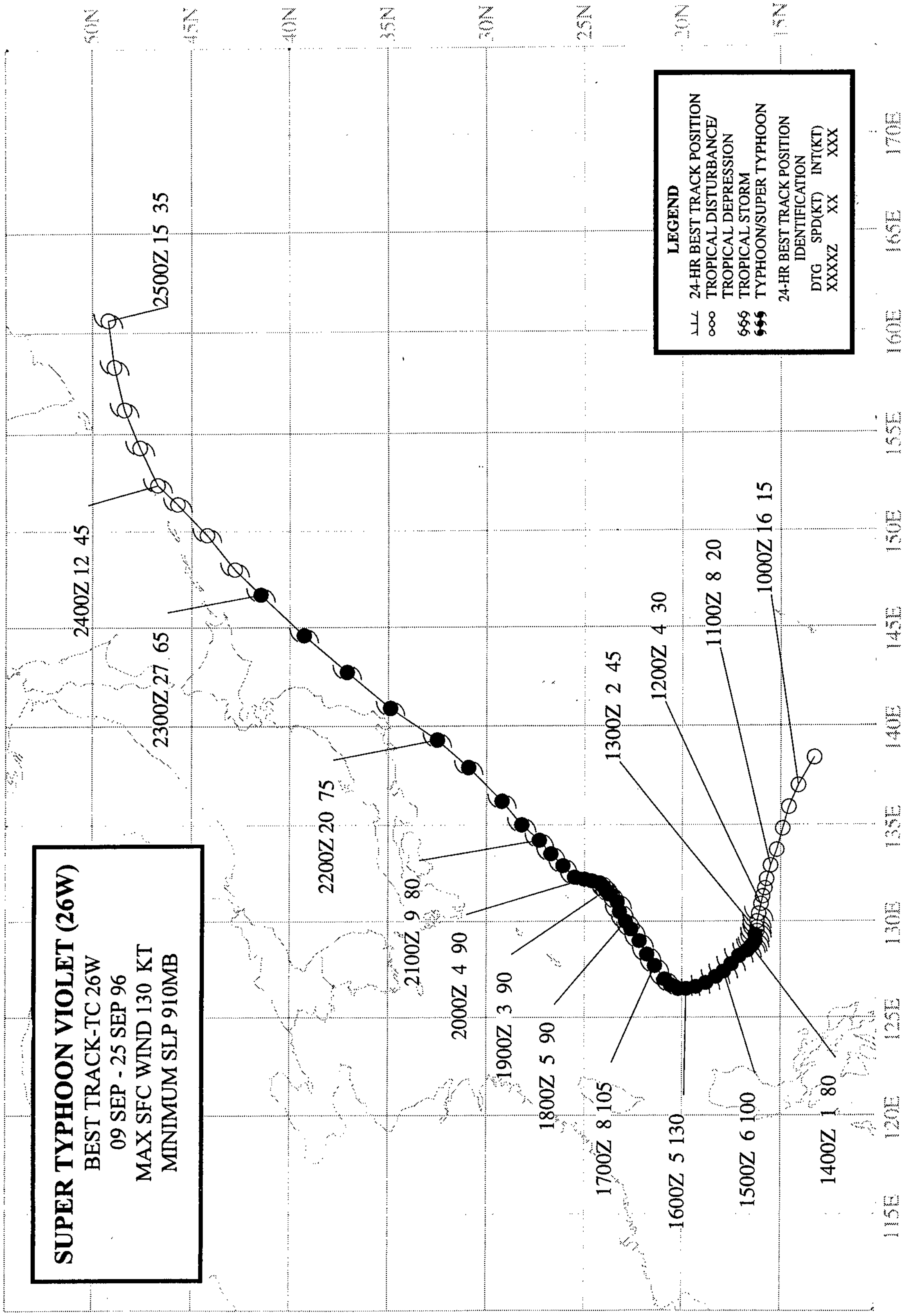
SUPER TYPHOON VIOLET (26W)
BEST TRACK-TC 26W
09 SEP - 25 SEP 96
MAX SFC WIND 130 KT
MINIMUM SLP 910MB
LEGEND
24-HR BEST TRACK POSITION
TROPICAL DISTURBANCE/
TROPICAL DEPRESSION
TROPICAL STORM
TYPHOON/SUPER TYPHOON
24-HR BEST TRACK POSITION
IDENTIFICATION
DTG SPD(KT) INT(KT)
XXXXZ XX XXX
2500Z 15 35
2400Z 12 45
2300Z 27 65
2200Z 20 75
2100Z 9 80
2000Z 4 90
1900Z 3 90
1800Z 5 90
1700Z 8 105
1600Z 5 130
1500Z 6 100
1400Z 1 80
1300Z 2 45
1200Z 4 30
1100Z 8 20
1000Z 16 15
50N
45N
40N
35N
30N
25N
20N
15N
115E
120E
125E
130E
135E
140E
145E
150E
155E
160E
165E
170E

SUPER TYPHOON VIOLET (26W)

I. HIGHLIGHTS

As the long-lived Orson (19W) recurved at the beginning of September, the unusual monsoon flow pattern of August (See Figure 3-13-4 in Kirk's summary) gave way to a pattern more in line with climatology: the maximum cloud zone and the axis of the monsoon trough extended from the Philippines east-southeastward into Micronesia. Violet was the fourth of five significant TCs to form in this trough. At one point, Tom (25W), Violet, Willie (27W) and a subtropical (ST) low existed simultaneously along the trough axis (see Figure 3-25-1a, b in Tom's (25W) summary). Due to the relative motions of these TCs (and the ST low), the trough axis became reverse oriented. Violet was one of three TCs during 1996 which acquired a very large eye — the other two were Kirk (13W) and Orson (19W). Passing just off the southeastern tip of the Japanese main island of Honshu, Violet was responsible for extensive damage and loss of life.

II. TRACK AND INTENSITY

On 10 September, an area of deep convection began to consolidate into a discrete tropical disturbance located between the Philippines and Guam. The early stages of this tropical disturbance were somewhat complicated as noted in the remarks on the 100600Z Significant Tropical Weather Advisory: "An area of convection is located near 13N 140E. Satellite imagery and synoptic data indicate this is a convective region formerly associated with Tropical Depression 24W that has separated from TD 24W and remained quasi-stationary as TD 24W moves west. . . ." On 11 September, the disturbance became better organized, and remarks on the 110600Z Significant Tropical Weather Advisory included:

"The area of convection previously located near 13N 140E [has moved west]. . . . Synoptic data indicate this convective region lies near a broad cyclonic circulation along the monsoon trough. . . ."

Further consolidation of the deep convection and rapid improvements in the organization of the convection and of its outflow cirrus prompted JTWC to issue a Tropical Cyclone Formation Alert at 111100Z September, followed by the first warning on Tropical Depression (TD) 26W, valid at 111800Z. This is the same valid time for the first warning on the tropical depression that became Tom (25W) — a TC located approximately 1000 nm (1900 km) to the east-southeast of TD 26W. At the time of the first warning on TD 26W, NOGAPS was indicating TD 25W (Tom) would become the dominant system and engulf the smaller circulation of TD 26W. The official forecast reflected the dynamic guidance and dissipated TD 26W as a significant tropical cyclone in 36 hours. The dynamic guidance was in error, and TD 26W intensified and eventually became a large intense TC with a size comparable to that of Tom (25W) (see Figure 3-25-1b in Tom's summary). TD 26W was upgraded to Tropical Storm Violet on the warning valid at 121800Z. The system became a typhoon at 130600Z and reached its peak intensity of 130 kt (67 m/sec) at 160000Z (Figure 3-26-1).

After becoming a typhoon, Violet turned and began to move very slowly toward the northwest. When the typhoon reached its peak intensity at 160000Z, it began to track slowly toward the northeast in tandem with Tom (25W) (located approximately 1100 nm (2050 km) to Violet's east-northeast). The turn to the northeast of Violet and of Tom (25W) was associated with the monsoon trough acquiring a reverse orientation. Whereas Tom continued to intensify while moving northeastward, Violet began to weaken. As it weakened, its eye became very large (Figure 3-26-2) (see the discussion). Slowly gaining forward speed, Violet continued to weaken as it moved toward the

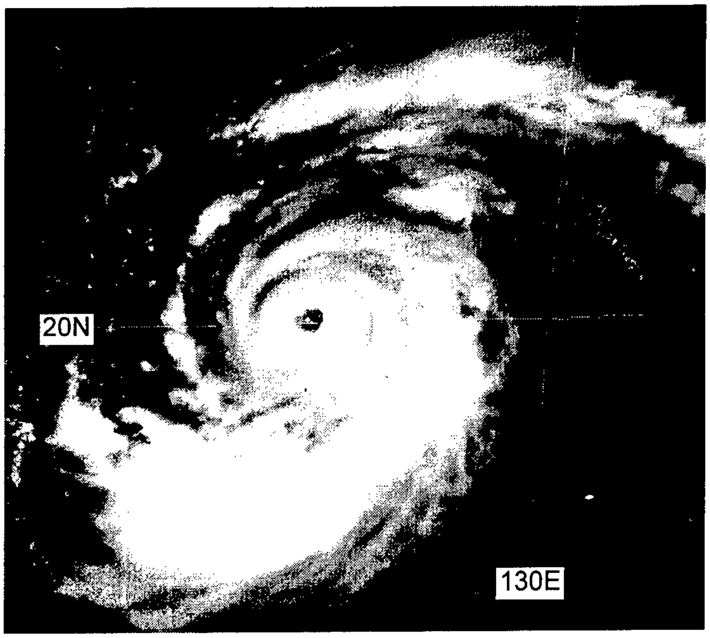

Figure 3-26-1 Violet at its peak intensity of 130 kt (67 m/sec) (160131Z September visible GMS imagery).

northeast. Its large eye passed just offshore to the east of the Tokyo area. High winds and heavy rains caused damage and loss of life in southeastern Japan (see the Impact section). The final warning was issued valid at 230000Z as the typhoon continued on a northeastward track toward the eastern end of the Kuril Island chain where it became an extratropical low.

III. DISCUSSION

a. *Violet's behavior in a reverse-oriented monsoon trough*

The monsoon trough within which Violet was embedded, became reverse oriented by virtue of the relative motion of Tom (25W) and Violet (see Figure 3-25-3 in Tom's summary). Both of these TCs moved on similarly shaped tracks, however, there was a gradual cyclonic rotation of the two about their centroid so that Tom, once east-southeast of Violet, moved so as to be located to the east-northeast of Violet. For more details on the characteristics of TC motion in a reverse-oriented monsoon trough see Tom's (25W) summary.

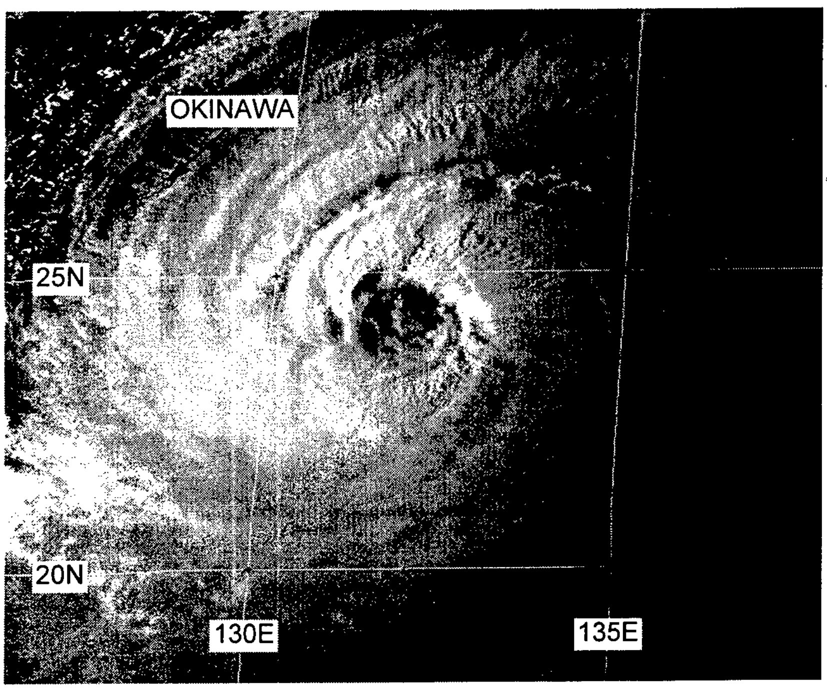

Figure 3-26-2 Violet was one of three WNP TCs during 1996 which acquired a very large eye with a maximum satellite-observed diameter greater than 75 nm (140 km) (190831Z September visible GMS imagery).

b. *Very large eye*

Violet was one of three TCs during 1996 — the other two were Kirk (13W) and Orson (19W) — that acquired very large eyes. Violet's eye evolved greatly during its life: it was at times a banding eye, a large ragged eye, an eye with concentric wall clouds, a small well-defined eye, and a very large eye. The changes in the character of Violet's eye were reflected in fluctuations of Violet's digital Dvorak (DD) numbers (Figure 3-26-3). From 172330Z to 201130Z Violet's satellite-observed eye diameter exceeded 45 nm (85 km) (Figure 3-26-4). From 190450Z to 192030Z the eye diameter ranged from 62 to 79 nm (115 to 145 km) (Table 3-26-1).

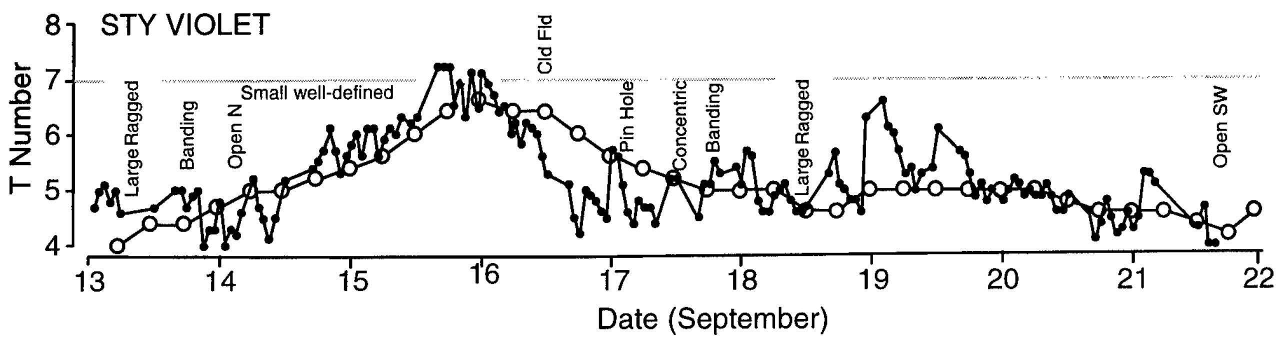

Figure 3-26-3 Violet's DD time series for the period 130130Z September through 211830Z September. Small black dots are the hourly DD values, open circles are the best track intensity (converted to a T number). Comments on the structure of the eye are included.

Table 3-26-1 Eye diameter of Violet from satellite during its period of very large eye size.

DTG (Z)	T Number	Satellite-derived eye diameter (nm)
172330	4.0	52
180230	---	45
180330	---	65
180430	---	42
180501*	4.0	58
180511*	4.0	64
182030	---	46
182111	4.5	55
182330	5.0	63
190230	---	59
190450	4.5	76
190530	5.0	62
190828	4.5	72
190830	---	78
191130	5.0	75
191630	---	79
191730	5.0	78
192030	---	71
192330	4.5	59
200230	---	49
200430	4.5	51
200830	---	64
201130	4.0	72

* These fixes are from different agencies using the same NOAA-14 pass.

c. *Gravity waves*

When Violet passed through the eastern part of the Kuril Island chain on 24 September, the rugged high islands produced a spectacular display of gravity waves in the low and middle cloud field (Figure 3-26-5). Such displays of terrain-induced gravity waves are commonly observed in the flow of typhoons which are becoming extratropical. Stabilization of the lower atmosphere by ocean chilling sets up conditions favorable for these gravity waves. In the deep tropics (e.g., over the islands of the Philippines), terrain-induced gravity waves in the circulation of a TC are far less common.

IV. IMPACT

Violet was responsible for killing seven people and injuring 44 others in southeastern Japan. Based on radar and satellite data, the center of Violet's large ragged eye passed approximately 80 nm (150 km) to the east-southeast of the Tokyo metropolitan area, and about 30 nm (55 km) east of the coastal cities of Tateyama and Choshi in Chiba prefecture. The western wall cloud passed over Tokyo and nearby areas, dumping 10.4 inches (265 mm) of rain in 24 hours on Tokyo's main business district (the third-largest 24-hour rainfall recorded there since 1876), and producing wind gusts to near 100 kt (51 m/sec) in exposed coastal areas. Tateyama (on the southern tip of Chiba prefecture) recorded a peak gust to 106 kt (55 m/sec) and a minimum SLP of 969 mb. No significant damage occurred at Fleet Activities Yokosuka, although numerous trees were uprooted or blown down and fencing along a sea wall was torn down due to wave action.

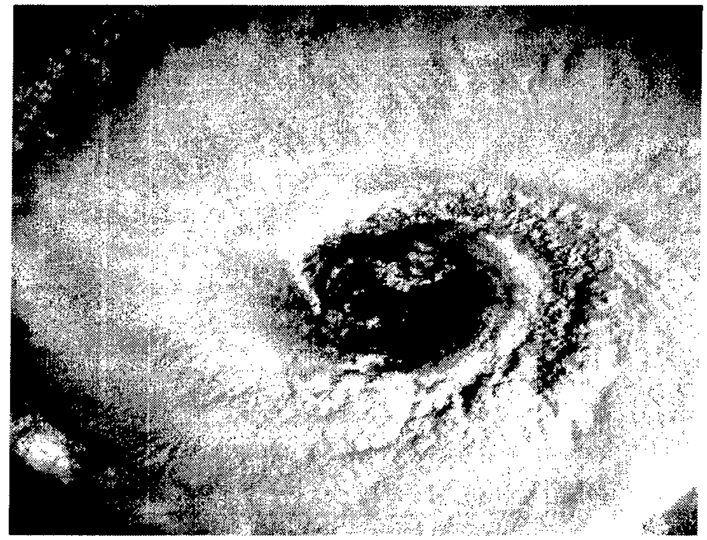

Figure 3-26-4 A close-up view of Violet's very large eye. The relatively clear region in the eye has a diameter of approximately 60 nm in this image (190038Z September visible DMSP imagery).

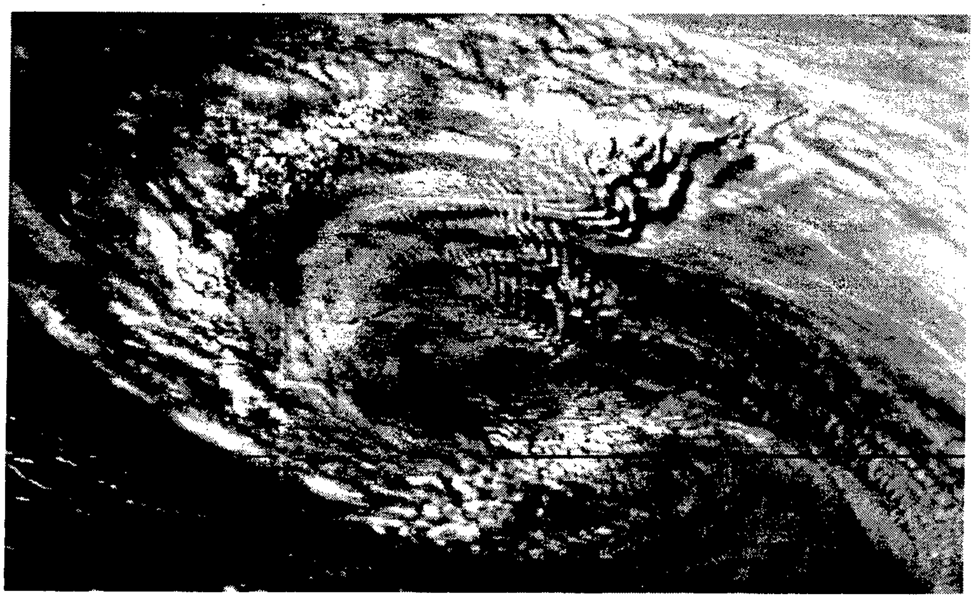

Figure 3-26-5 A multitude of gravity waves is apparent in the low and middle clouds of Violet as the system moves northeastward over the Kuril Islands (240332Z September visible GMS imagery).

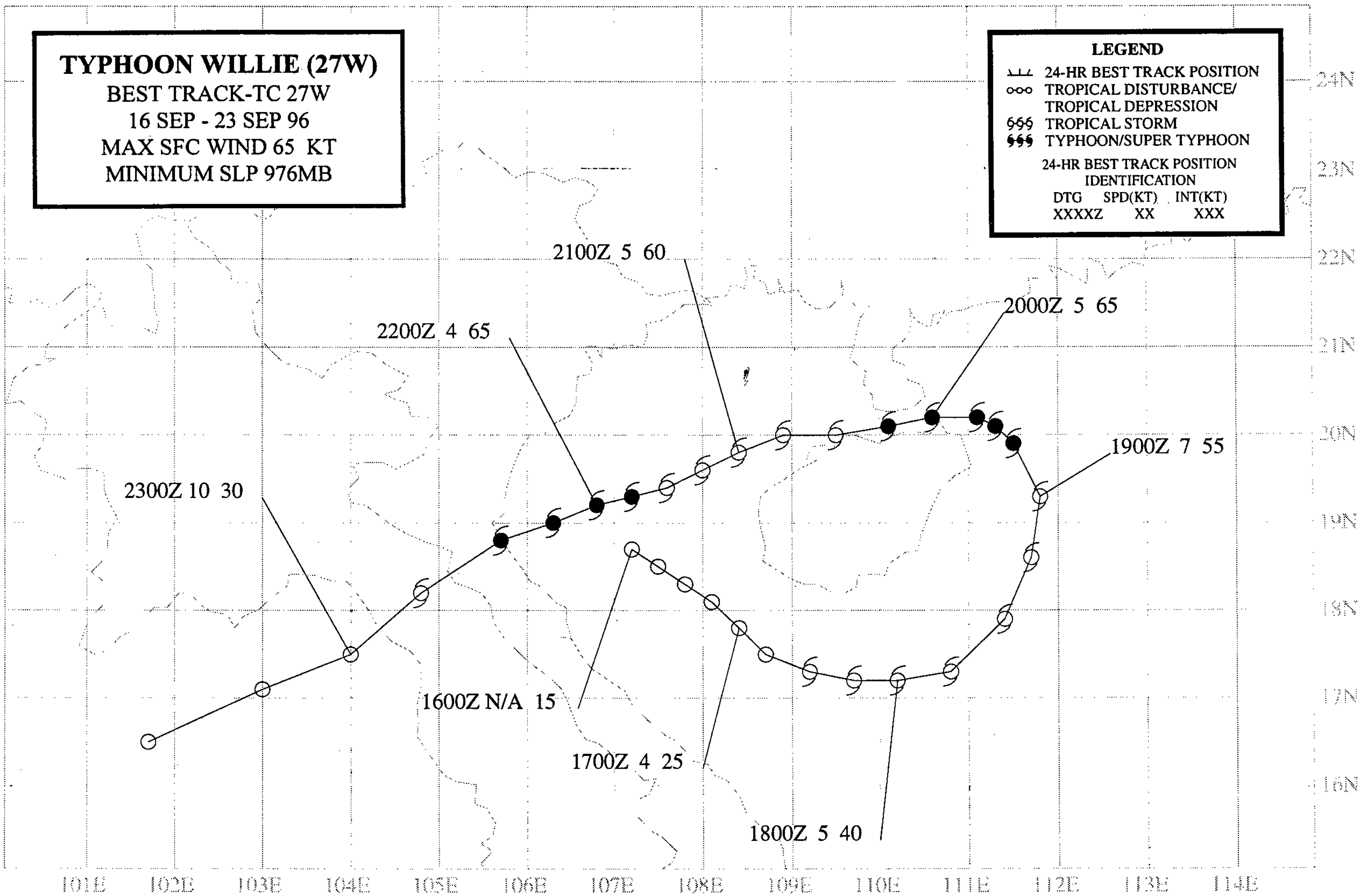

TYPHOON WILLIE (27W)
BEST TRACK-TC 27W
16 SEP - 23 SEP 96
MAX SFC WIND 65 KT
MINIMUM SLP 976MB
LEGEND
24-HR BEST TRACK POSITION
TROPICAL DISTURBANCE/
TROPICAL DEPRESSION
TROPICAL STORM
TYPHOON/SUPER TYPHOON
24-HR BEST TRACK POSITION
IDENTIFICATION
DTG SPD(KT) INT(KT)
XXXXZ XX XXX
2100Z 5 60
2000Z 5 65
2200Z 4 65
1900Z 7 55
2300Z 10 30
1600Z N/A 15
1700Z 4 25
1800Z 5 40
24N
23N
22N
21N
20N
19N
18N
17N
16N
101E
102E
103E
104E
105E
106E
107E
108E
109E
110E
111E
112E
113E
114E

TYPHOON WILLIE (27W)

I. HIGHLIGHTS

Never more than 90 nm (170 km) from shore, Willie circumnavigated Hainan Island while undergoing a counter-clockwise loop. Willie was a small TC, and was part of a three-TC outbreak along the monsoon trough, with the larger TCs Tom (25W) and Violet (26W) to its northeast.

II. TRACK AND INTENSITY

On 17 August, the axis of the monsoon trough stretched from Bangladesh to the Gulf of Tonkin, and from there into the WNP where the large typhoons Tom (25W) and Violet (26W) and a subtropical low had formed along it (see Figure 3-25-1a, b in Tom's (25W) summary). The small area of deep convection that became Willie was first mentioned on the 170600Z September Significant Tropical Weather Advisory based on its persistence near a low-level cyclonic circulation located to the southwest of Hainan Island. The area of deep convection moved to the east-southeast and became better organized, prompting the JTWC to issue a TCFA at 171130Z followed by the first warning, valid at 171800Z, on Tropical Depression (TD) 27W. Six hours later, TD 27W was upgraded to Tropical Storm Willie based on several data sources:

1) a 171000Z report (received later at the JTWC) of 35 kt (18m/sec) sustained wind from the M/V GECO Emerald (a ship servicing the oil rigs south of Hainan);

2) a scatterometer pass at 171521Z supporting 35 kt one-minute sustained wind near the LLCC; and,

3) a significant improvement in convective organization.

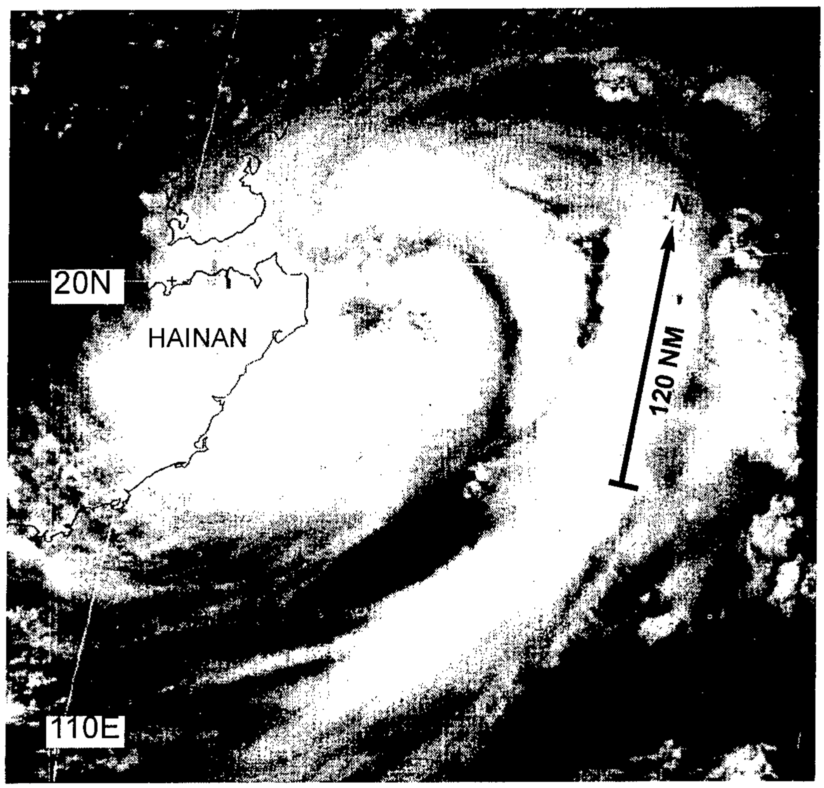

Figure 3-27-1 Willie becomes a typhoon (190531Z September visible GMS imagery).

During the afternoon of 19 August Willie acquired a ragged eye and became a typhoon (Figure 3-27-1). Willie maintained a peak intensity of 65 kt (33 m/sec) for 24 hours as it rounded the northeastern end of Hainan. The system weakened slightly after passing through the narrow Hainan Strait, but became a minimal typhoon once again as it crossed the Gulf of Tonkin on a west-southwest track. As a minimal typhoon, Willie made landfall at approximately 221200Z in northern Vietnam near Vinh. Continuing on a southwestward track it crossed Laos into Thailand. The final warning, valid at 230000Z, was issued as the weakening system moved into northeastern Thailand and dissipated.

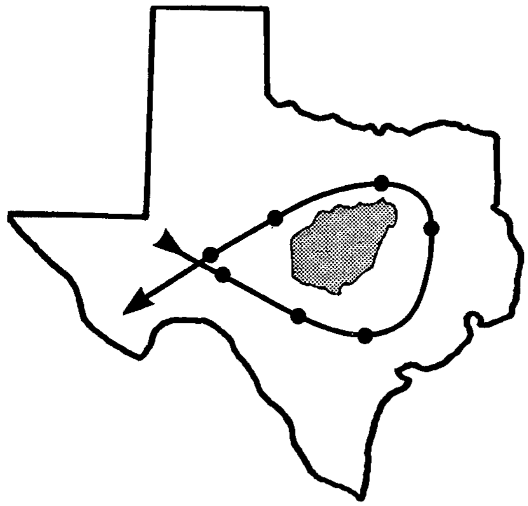

Figure 3-27-2 Willie's counter-clockwise loop fits comfortably within the boundaries of the State of Texas. Hainan Island (shaded) is superimposed. Dots show Willie's position at 24-hour intervals.

III. DISCUSSION

Unusual motion

Willie circumnavigated Hainan Island while undergoing a counter-clockwise loop. The dimensions of the oval-shaped loop were 300 nm by 180 nm (550 km by 330 km) which would fit comfortably within the boundaries of the State of Texas (Figure 3-27-2). The eastward motion of Willie during the first portion of its track is consistent with its position at the southwestern end of a reverse-oriented monsoon trough with typhoons Tom (25W) and Violet (26W) located further to the east-northeast along the trough axis. Initially steered eastward by deep monsoon flow along the trough axis, Willie turned toward the north and then toward the west, as Tom (25W) and Violet (26W) exited the tropics and a ridge gradually built to the north and east of Willie.

IV. IMPACT

At least 38 people were reported killed, dozens injured and 96 missing on Hainan Island. Willie smashed homes, washed away fishing boats and dumped up to 16 inches (400 mm) of rain on areas of this island province. Most of the deaths were attributed to flooding. No reports of damage or injuries in Vietnam were received at the JTWC.

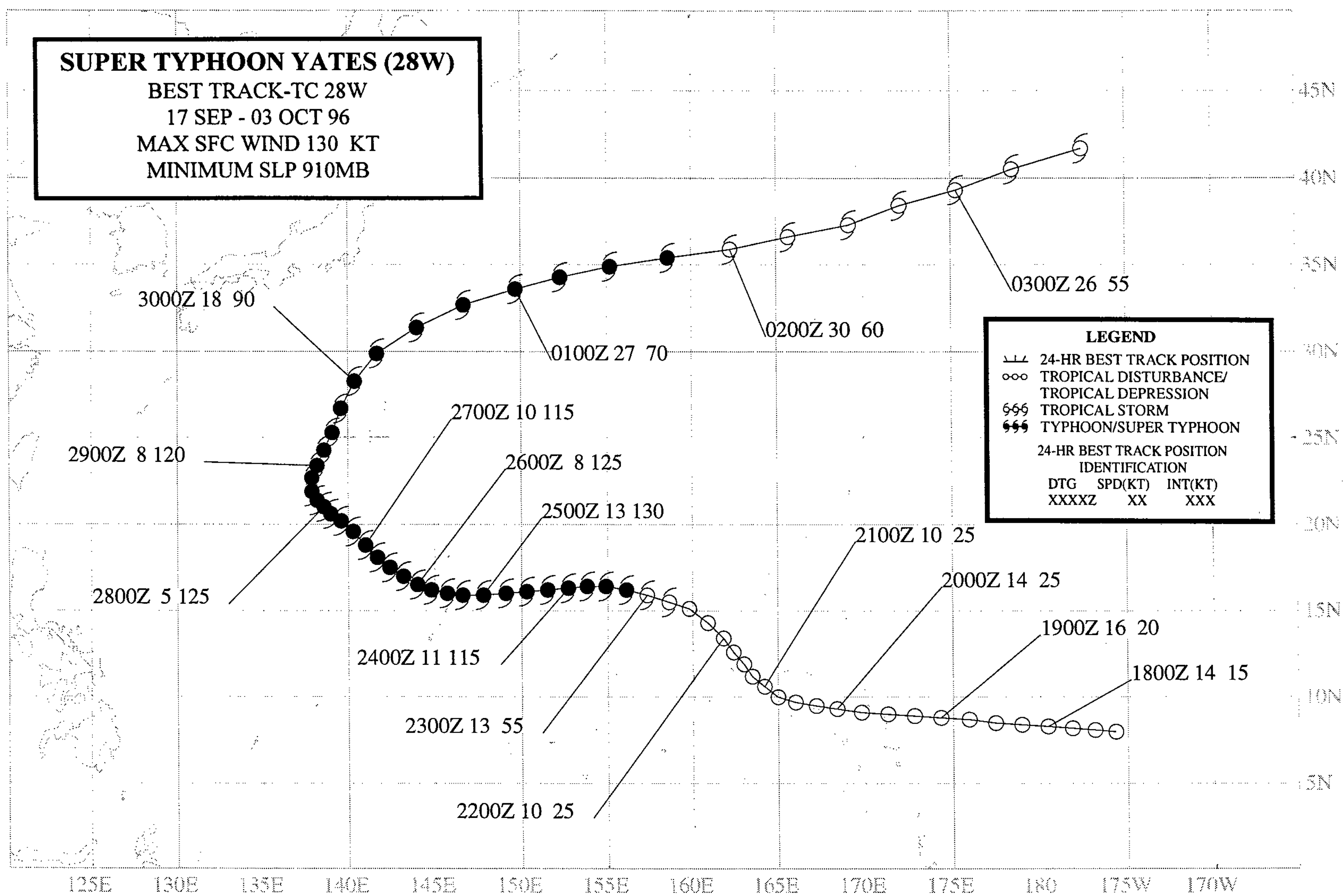
SUPER TYPHOON YATES (28W)
BEST TRACK-TC 28W
17 SEP - 03 OCT 96
MAX SFC WIND 130 KT
MINIMUM SLP 910MB
LEGEND
24-HR BEST TRACK POSITION
TROPICAL DISTURBANCE/
TROPICAL DEPRESSION
TROPICAL STORM
TYPHOON/SUPER TYPHOON
24-HR BEST TRACK POSITION
IDENTIFICATION
DTG SPD(KT) INT(KT)
XXXXZ XX XXX
1800Z 14 15
1900Z 16 20
2000Z 14 25
2100Z 10 25
2200Z 10 25
2300Z 13 55
2400Z 11 115
2500Z 13 130
2600Z 8 125
2700Z 10 115
2800Z 5 125
2900Z 8 120
3000Z 18 90
0100Z 27 70
0200Z 30 60
0300Z 26 55
45N
40N
35N
30N
25N
20N
15N
10N
5N
125E
130E
135E
140E
145E
150E
155E
160E
165E
170E
175E
180
175W
170W

SUPER TYPHOON YATES (28W)

I. HIGHLIGHTS

While passing between Saipan and Anatahan (two islands in the Northern Marianas), Yates was observed with Guam's NEXRAD. Although Yates became a super typhoon, its surface wind field was relatively compact, and it possessed a very small satellite-observed eye for much of its life. Yates and Zane (29W) developed in the same monsoon trough, at approximately the same time, and recurved simultaneously along similarly shaped and spatially-proximate tracks.

II. TRACK AND INTENSITY

During early September, five TCs — Sally (23W), TS 24W, Tom (25W), Violet (26W), and Willie (27W) — formed in the monsoon trough. This very active monsoon trough moved northward, became reverse oriented, and by the final week of September had migrated to a relatively high latitude. As this monsoon trough exited the tropics, a new monsoon trough formed at low latitudes, and was the site of development for the next two TCs in the WNP: Yates and Zane (29W).

The tropical disturbance which became Yates was mentioned on the Significant Tropical Weather Advisory as early as 170600Z September, when a persistent area of deep convection was observed at low latitude just east of the international date line. At this time the WNP was still dominated by the reverse-oriented monsoon trough which contained Tom (25W), Violet (26W) and Willie (27W). The low latitudes of the WNP were dominated by high pressure and low-level easterly flow, and the pre-Yates tropical disturbance was the only significant area of deep convection which was deemed to have any chance of becoming a TC. During the next three days, this disturbance traveled westward into the Marshall Islands. Amounts of deep convection associated with this disturbance began to increase, along with a gradual increase in the amount and extent of deep convection throughout the rest of Micronesia. On 21 September, a small area of persistent deep convection consolidated northwest of Kwajalein. Visible and water-vapor satellite imagery indicated good upper-level anticyclonic outflow over this disturbance, prompting the JTWC to issue a TCFA at 210100Z. Over the next 24 hours, the small system showed no signs of development, but maintained its organization. Thus, a second TCFA was issued at 220100Z. During the night of 22 September, the pre-Yates tropical disturbance rapidly acquired well-organized cyclonically-curved convective cloud bands surrounding a small area of persistent deep convection over the LLCC. Based upon this improvement in convective organization, the first warning on Tropical Depression (TD) 28W was issued valid at 221800Z. Within three hours after its issuance, the first warning was amended to indicate that TD 28W was a tropical storm. The amended warning stated:

"Tropical Storm Yates (28W) is moving west-northwestward at 14 knots. Justification [for amendment]: this warning has been amended based on intensity. Satellite analysis indicates that this system is [of] tropical storm intensity. Due to its small size and diffluent [divergent] winds aloft, rapid intensification is expected. . . ."

Yates did indeed intensify rapidly. During the period 221800Z to 231200Z it increased from a minimal tropical storm to a typhoon with an intensity of 115 kt (59 m/sec). The equivalent pressure fall of 57 mb during this 18-hour time period (or 3.2 mb/hr) met the criterion for explosive deepening (i.e., a decrease in the minimum sea-level pressure of a TC of 2.5 mb/hr for at least 12 hours) as defined by Dunnavan (1981). At 250000Z, Yates reached its peak intensity of 130 kt (67 m/sec) (Figure 3-28-1). Yates was a minimal super typhoon for only six hours, and then its intensity fell slightly to 125 kt (64 m/sec) as it passed between the islands of Saipan and Anatahan. During

the four-day period 250000Z to 290000Z, Yates remained a powerful typhoon as its intensity fluctuated slightly between 115 and 125 kt (59 to 64 m/sec) and maintained a very small eye which was, at times, cloud filled.

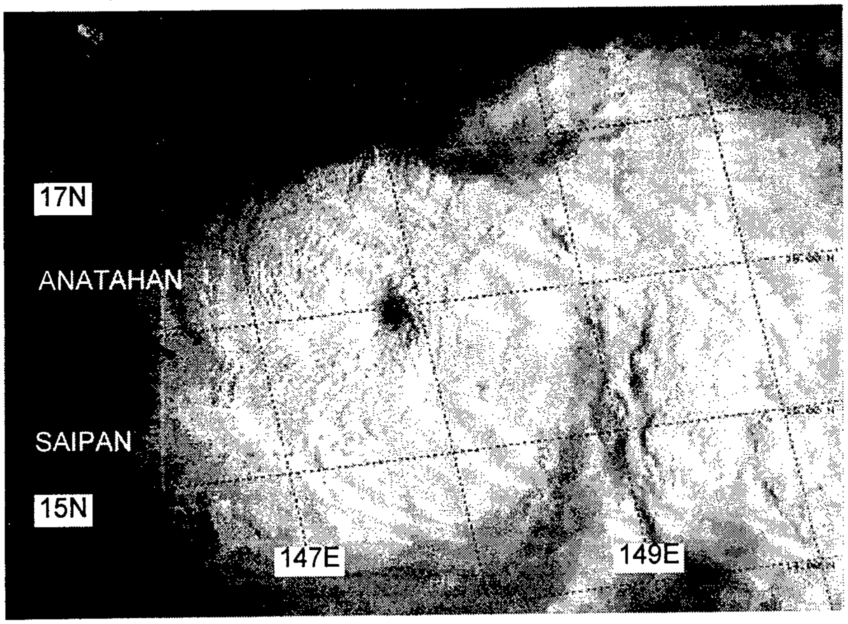

Figure 3-28-1 Yates at peak intensity of 130 kt (67 m/sec) (242319Z September visible DMSP imagery).

Late on 28 September, Yates began to recurve. It moved slowly toward the north-northeast on 29 September, and then on 30 September, it entered the deep-layer westerly air flow of the midlatitudes, turned more toward the east and accelerated. The final warning was issued valid at 011800Z October as the system neared the completion of its extratropical transition. Yates became a powerful extratropical low in the North Pacific after it crossed the international date line (Figure 3-28-2).

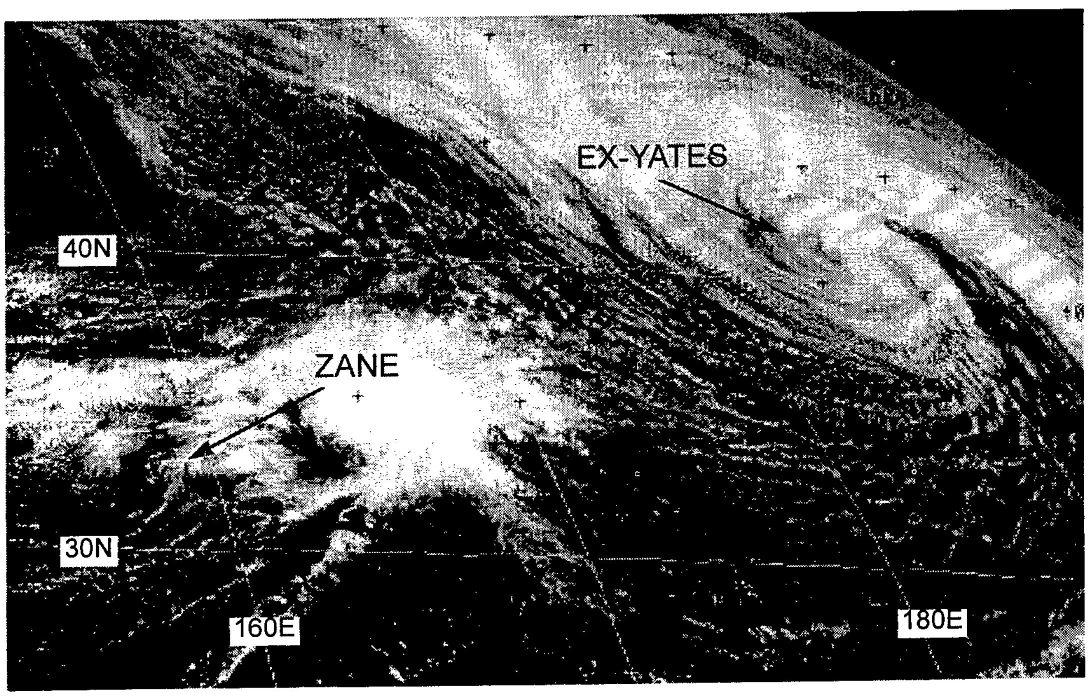

Figure 3-28-2 After recurvature, Yates became an intense extratropical low in the central North Pacific, while Zane (29W) slowed and dissipated (032331Z October visible GMS imagery).

III. DISCUSSION

a. *Persistent pin-hole eye*

Visible and infrared satellite imagery indicated that Yates possessed a very small, or "pin-hole", eye (i.e., a diameter of 10 nm or less) throughout most of its life. Many typhoons which acquire a pin-hole eye usually evolve to possess a larger eye (see the summaries of Super Typhoon Dale (36W) and Super Typhoon Ward (1995)). The evolution from pin-hole eye to larger eye typically begins with the formation of concentric wall clouds. Having formed concentric wall clouds, the outer wall cloud contracts as the small eye and inner wall cloud collapse. Eye wall replacement processes are described more fully by Willoughby (1982, 1990). Yates was somewhat unusual in that it retained a pin-hole eye for four days.

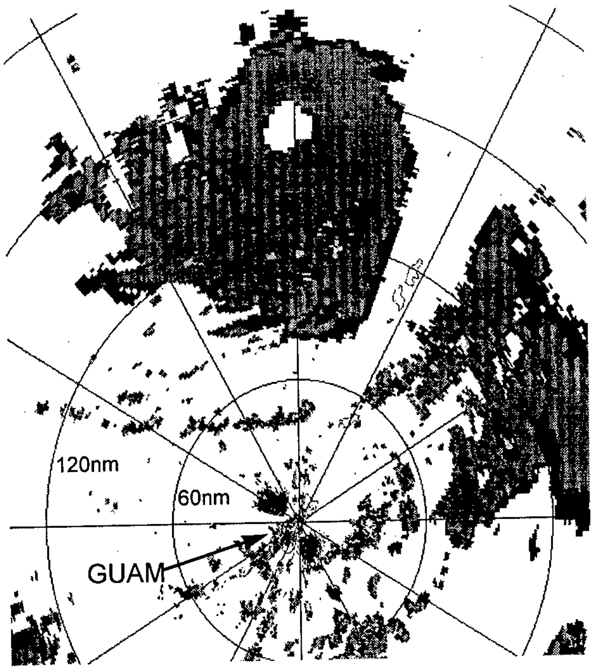

Figure 3-28-3 Yates maintained a well-defined 18 nm (33 km) diameter eye on NEXRAD as it passed to the north of Guam (251844Z September base reflectivity NEXRAD product).

b. *Passage though Guam's NEXRAD coverage*

On 25 September, Yates passed between the islands of Saipan and Anatahan. Its small eye passed approximately 50 nm (100 km) to the north of Saipan, 20 nm (40 km) to the south of Anatahan, and 155 nm (290 km) to the north of Guam. Yates was close enough to Guam to be scanned with Guam's NEXRAD (Figure 3-28-3). The following comments were received in an after-action report by the Andersen AFB NEXRAD operators:

"Yates' well-defined circular eye became visible on radar [at] 25/0131Z shortly after being upgraded to STY intensity and continued to track west at 14 kt average. [Its] symmetrical eye, with an average diameter of 18 nm [33 km], was well surrounded with up to ninety percent high reflectivity wall cloud. . . . [it] went out of range on 26/0834Z. . . Yates never came within [the] 124 nm (230 km) velocity range. . . Reflectivity products were sufficient to fix its eye and movement with a high degree of accuracy. . . ."

It is interesting to note that in Yates' case, the radar-observed eye was larger than the satellite-observed eye. On satellite, the eye diameter was approximately 10 nm (18 km) when not cloud filled. That the pin-hole eye of Figure 3-28-1 had a larger diameter on radar than that which was seen on the satellite imagery implies that cirrus of the wall cloud was obscuring the eye somewhat.

c. *Segregation of TCs into families based upon monsoon trough evolution*

The tendency of the monsoon trough of the WNP to form and then migrate northward lends itself to a natural segregation of TCs into "families" with the commonality among the TCs within each "family" being that they were associated with the same monsoon trough. The five-TC sequence of early September — Sally (23W), TS 24W, Tom (25W), Violet (26W), and Willie (27W) — all had in common an origin within the same monsoon trough. By late September, this monsoon trough moved northward, became reverse oriented, and migrated to higher latitude as TCs Tom (25W) and Violet (26W) carried it with them out of the tropics. As this trough exited the tropics, a new monsoon trough formed at low latitudes, and was the site of development for the next two

TCs in the WNP: Yates and Zane (29W). Yates and Zane therefore comprise another "family" by virtue of their development within the same monsoon trough.

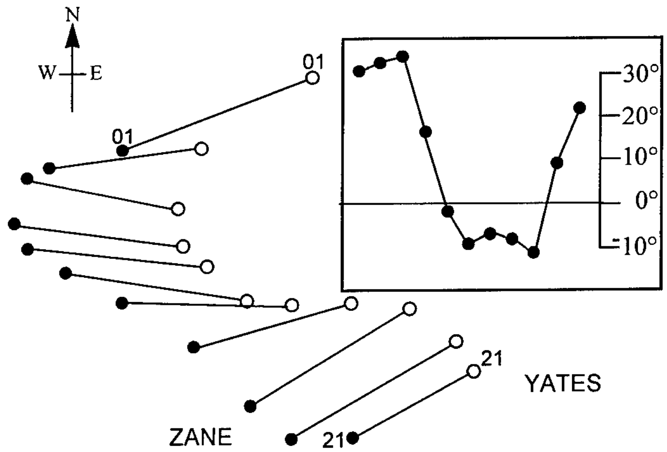

Figure 3-28-4 A schematic illustration of the similarly shaped and spatially proximate recurving tracks of both Yates and Zane (29W). Thin lines connect the TCs at 24 hour intervals beginning at 210000Z September and ending at 010000Z October. The inset shows the bearing of Yates from Zane at 24-hour intervals during the same time period. Positive values indicate Yates north of Zane.

d. *Direct, semi-direct, and indirect TC interaction*

Like Tom (25W) and Violet (26W) before them, Yates and Zane moved on nearly identical spatially-proximate recurving tracks (Figure 3-28-4). The inset of Figure 3-28-4 shows the bearing of Yates from Zane. Note the initial cyclonic change of bearing, followed by a period of anticyclonic change of bearing, then as Yates recurved, the change of bearing was once again cyclonic. Although these two TCs approached to within 780 nm (1450 km), there is little evidence that the TCs were mutually advecting each other (i.e., the Fujiwhara effect) during any of the periods of relative cyclonic orbit. In the Systematic and Integrated Approach, there are three basic kinds of TC interactions: direct (a mutual cyclonic orbit resulting from the TCs being advected by each other's outer winds), semi-direct (a mutual cyclonic orbit resulting from the alteration by one TC of the steering flow between the other TC and the subtropical ridge), and indirect (i.e., a mutual anticyclonic orbit resulting from the establishment of a ridge between the two TCs). Yates and Zane (29W) had motion characteristics suggestive of semi-direct and indirect TC interaction. The mutual anticyclonic orbit of Yates and Zane during the period 23 to 26 September (manifested in a south-of-west track for Yates) are typical of indirect TC interaction. The periods of mutual cyclonic orbit at the beginning and at the end of the tracks is consistent with semi-direct TC interaction. It is often difficult to differentiate between semi-direct and direct TC interaction, but one clue is often the separation distance. True direct interaction of two TCs usually occurs when the TCs are within 780 nm (1450 km) of each other. Yates and Zane were at this threshold, and it is possible that they may have interacted directly, especially at the end of their tracks when the cyclonic orbit increased rapidly.

TC interaction often results in complicated forecast scenarios. When Yates and Zane came abreast of one another at the same latitude, it was unclear which of the two would recurve first. Zane (29W) had been gaining latitude faster than Yates, and once south of Yates, it moved so as to be at a higher latitude. When Zane slowed near Okinawa, Yates turned to the north, accelerated, and moved to a higher latitude relative to Zane. Yates then recurved ahead of Zane.

IV. IMPACT

Because of Yates' small size, there was only minor damage on Saipan and Anatahan. On Saipan, Yates felled several trees and caused minor flooding. On Anatahan, where estimated winds of 80 kt (41 m/sec) were reported, tin roofs were blown off houses and the entire taro crop was destroyed. Only a handful of people live on the island and they were reported safe and in possession of plenty of food after the cyclone's passage.

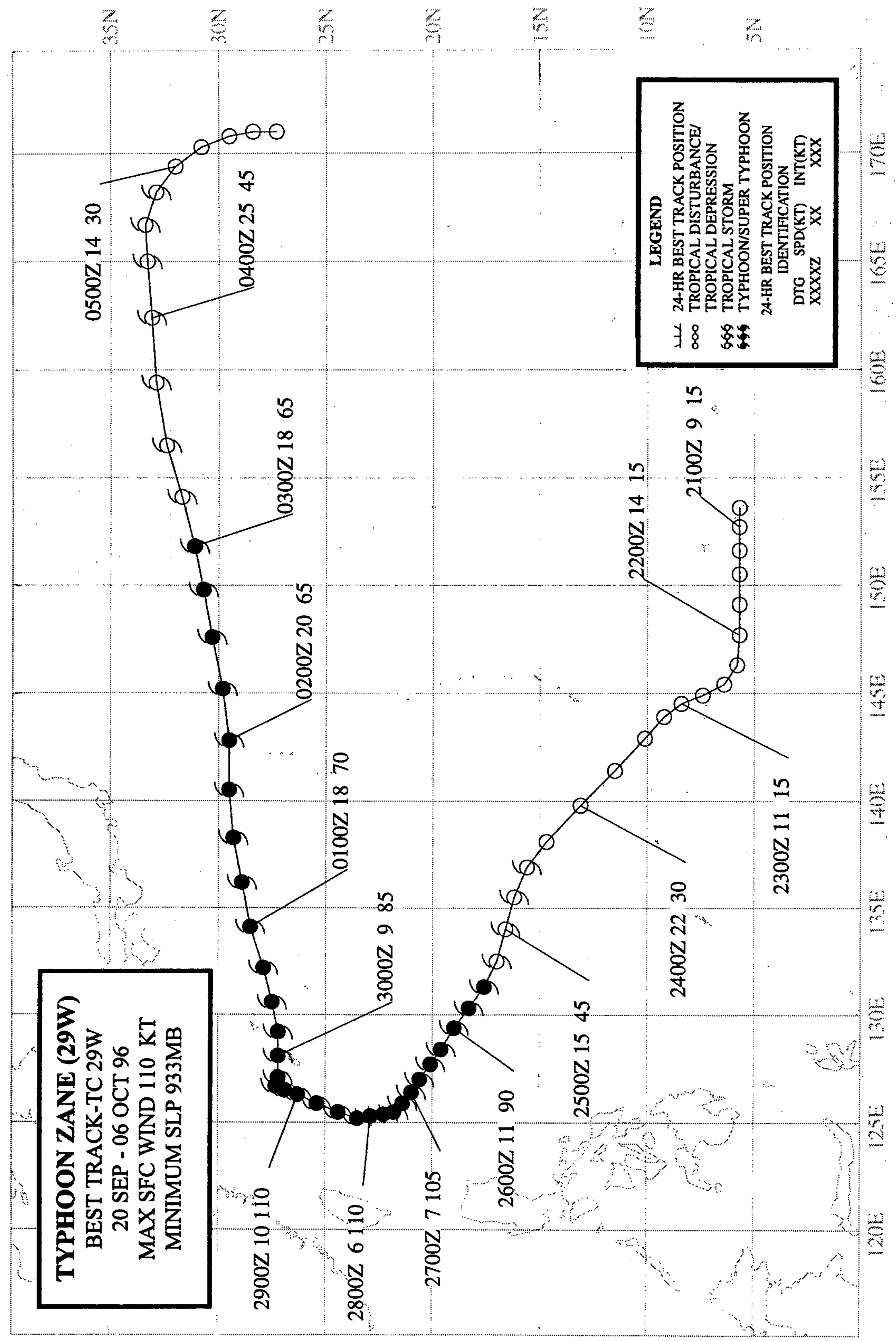
TYPHOON ZANE (29W)
BEST TRACK-TC 29W
20 SEP - 06 OCT 96
MAX SFC WIND 110 KT
MINIMUM SLP 933MB
LEGEND
24-HR BEST TRACK POSITION
TROPICAL DISTURBANCE/
TROPICAL DEPRESSION
TROPICAL STORM
TYPHOON/SUPER TYPHOON
24-HR BEST TRACK POSITION
IDENTIFICATION
DTG SPD(KT) INT(KT)
XXXXZ XX XXX
2100Z 9 15
2200Z 14 15
2300Z 11 15
2400Z 22 30
2500Z 15 45
2600Z 11 90
2700Z 7 105
2800Z 6 110
2900Z 10 110
3000Z 9 85
0100Z 18 70
0200Z 20 65
0300Z 18 65
0400Z 25 45
0500Z 14 30
35N
30N
25N
20N
15N
10N
5N
120E
125E
130E
135E
140E
145E
150E
155E
160E
165E
170E

TYPHOON ZANE (29W)

I. HIGHLIGHTS

Zane and Yates (28W) developed in the same monsoon trough, at approximately the same time, and recurved simultaneously along similarly-shaped and spatially-proximate tracks. The typhoon affected both Taiwan and Okinawa. Passing Okinawa, Zane came within range of Kadena's NEXRAD. After recurvature, Zane maintained its central deep convection despite being embedded in deep-layer westerly flow to the north of the subtropical ridge.

II. TRACK AND INTENSITY

During early September, five TCs — Sally (23W), TS 24W, Tom (25W), Violet (26W), and Willie (27W) — formed in the monsoon trough. This very active monsoon trough moved northward, and became reverse oriented. By the final week of September, it had migrated to a relatively high latitude as TCs Tom (25W) and Violet (26W) carried the trough with them out of the tropics. As this monsoon trough exited the tropics, a new monsoon trough formed at low latitudes, and was the site of development for the next two TCs in the WNP — Yates (28W) and Zane.

While the WNP was still dominated by the reverse-oriented monsoon trough which contained Tom (25W), Violet (26W) and Willie (27W), the low latitudes of the WNP were dominated by high pressure and low-level easterly flow. As Tom (25W) and Violet (26W) recurved, a new monsoon trough formed in Micronesia. Deep convection associated with this monsoon trough consolidated within two areas. The eastern area became Yates (28W) and the western area became Zane. The large area of deep convection which became Zane was larger than the one which became Yates (28W) and is a good example of a monsoon depression (Figure 3-29-1). It was first mentioned on the 201900Z Significant Tropical Weather Advisory. This monsoon depression moved westward and, typical of monsoon depressions, it was several days before deep convection persisted near the low-level circulation center. When the deep convection persisted near the LLCC, a TCFA was issued at 230600Z. A second TCFA was issued at 232030Z in order to reposition the alert box. Based on satellite intensity estimates of 25 kt (13 m/sec), the first warning on Tropical Depression (TD) 29W was issued, valid at 240000Z September. Remarks on this warning included:

"... Tropical Depression 29W is located in the monsoon trough equatorward of the subtropical ridge. TD 29W is located approximately 800 nm west of Typhoon Yates (28W). Satellite imagery indicates the presence of weak ridging to the southeast of 29W. The rapid north-northwestward movement of TD 29W is associated with the enhanced southerly steering component associated with the weak ridging between TD 29W and Typhoon Yates (28W). . . ."

The rationale for the motion of TD 29W in this remark is a good description of what is known as "indirect TC interaction" in the "Systematic and Integrated Approach". Yates' (28W) summary contains a more complete description of the interaction between Zane and Yates.

During the night of 24 September, deep convection rapidly consolidated over the LLCC of TD 29W and, on the warning valid at 241200Z, TD 29W was upgraded to Tropical Storm Zane. Soon after the formation of Zane's CDO, the peripheral cloudiness in the monsoon depression was suppressed and the areal extent and amount of deep convection became smaller. Moving northwestward, Zane intensified and became a typhoon at 251200Z. The peak intensity of 110 kt (57 m/sec) was reached at 280000Z, which was maintained until 291200Z. During this time, the typhoon moved on a slow northward track and passed approximately 90 nm (170 km) to the west of Okinawa. On 29 September, Zane slowed and made a sharp turn to the east, passing approximately

20 nm (40 km) to the north of the northern end of Okinawa (Figure 3-29-2) and, despite being embedded in westerly flow north of the subtropical ridge maintained typhoon intensity. On 02 October, Zane (still a typhoon) possessed a very unusual cirrus outflow pattern: cirrus debris streamed eastward on both the north and south sides of the system, evoking the analogy of debris being stripped from a comet by the solar wind (Figure 3-29-3a) (see the discussion). On 03 October, westerly shear finally began to have an effect, and the LLCC of Zane became partially exposed on the west side of the deep convection. At 031200Z, the final warning was issued, as Zane began its extratropical transition. After the final warning, the system moved east and then south as it encountered the vigorous outer circulation of the large intense extratropical low which was once Yates (28W) (see Figure 3-28-2 in Yates' (28W) summary).

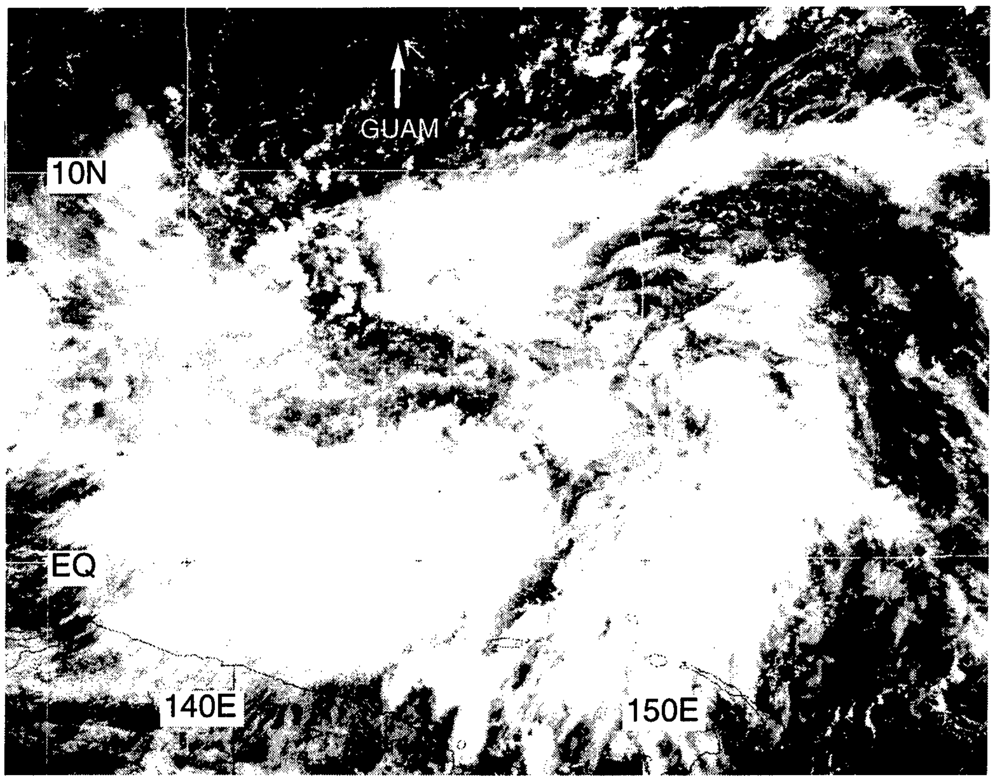

Figure 3-29-1 Zane originated from this monsoon depression located to the south of Guam (212224Z September visible GMS imagery).

III. DISCUSSION

a. *Origin as a monsoon depression south of Guam*

Zane began as a monsoon depression near Guam. Initially it was a large ensemble of mesoscale convective systems embedded within a region of lowered sea-level pressure. It lacked persistent central deep convection, and the maximum winds in the system were displaced outward from the low-level circulation center. Eventually as the system moved toward the northwest, the circulation intensified, and persistent central deep convection became established marking its transition to a conventional TC. Cam's (05W) summary contains a detailed discussion of the structure and evolution of monsoon depressions in the WNP.

b. *Passage within range of Guam's and Kadena's NEXRADs*

When forming near Guam, some of the rainbands (that were part of the monsoon depression which became Zane) came within the range of Guam's NEXRAD. One of the most interesting features of these rainbands was the presence of mesoscale vortices associated with convective cells in these rainbands. These mesovortices were detected by the meso-alert algorithm of the NEXRAD. Mesoscale vortices are often associated with tornadic activity over land, however, tornadic activity (e.g., tornadic waterspouts) have yet to be associated with NEXRAD-observed mesoscale vortices near Guam. They frequently are seen when tornadic activity is occurring in TC rainbands over land in the US mainland.

When Zane passed close to Okinawa, it came within range of the NEXRAD's velocity detection capability. Nothing unusual was noted as the well-defined radar eye of Zane passed. The base velocity product showed maximum inbound and outbound velocities on the order of 115 kt (59 m/sec) at altitudes of approximately 5,000 ft.

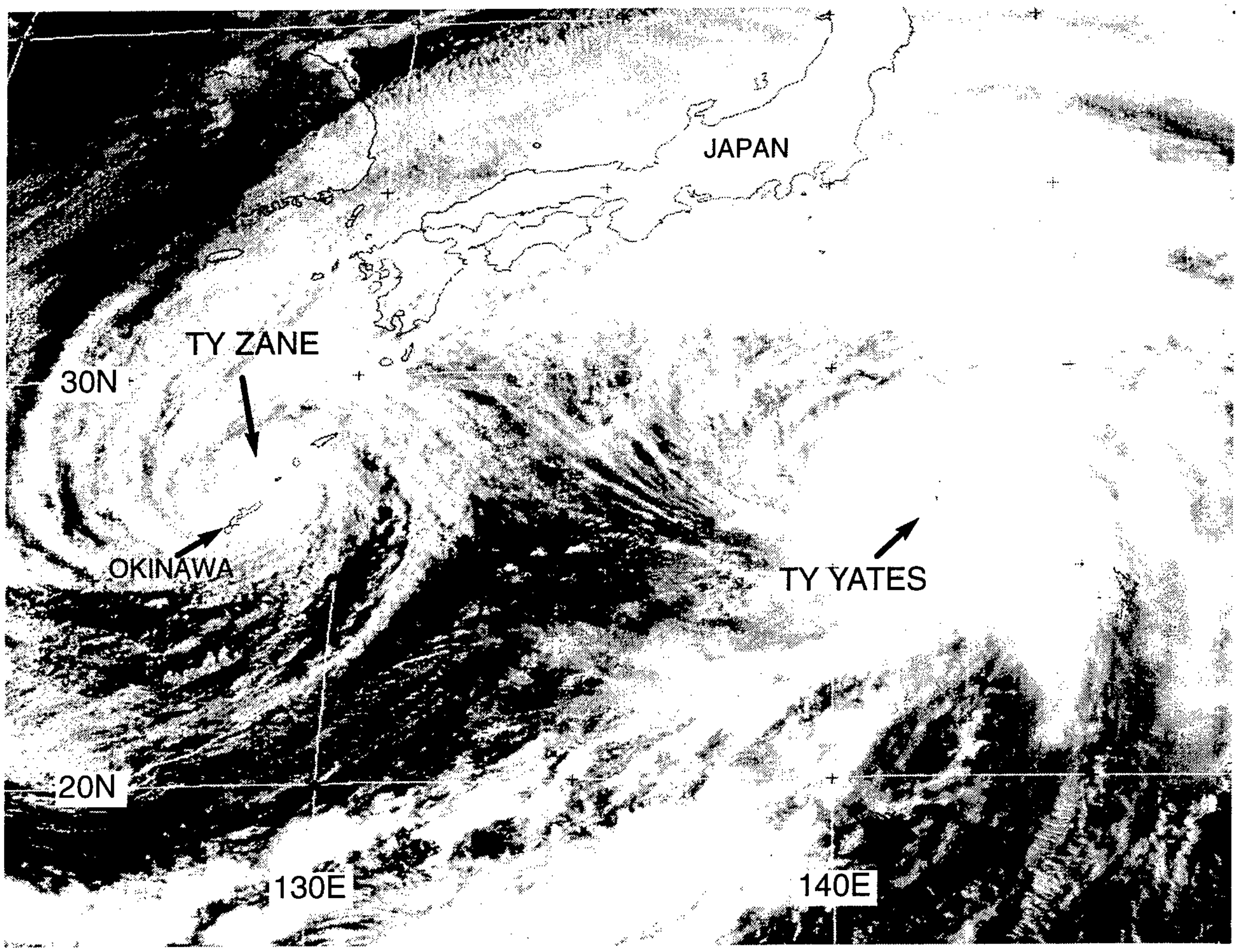

Figure 3-29-2 The rainbands of Zane sweep across Okinawa while at its closest point of approach to that island. Typhoon Yates (28W) is seen approximately 900 nm (1700 km) to the east of Zane (292224Z September visible GMS imagery).

c. *Unusual persistence as a tropical cyclone while embedded in midlatitude westerlies*

On 02 October, Zane (still a typhoon) possessed a very unusual cirrus outflow pattern: cirrus debris streamed eastward on both the north and south sides of the system, evoking the analogy of debris being stripped from a comet by the solar wind (Figure 3-29-3a). Water-vapor derived winds clearly show the upper-level winds to the north and south of Zane were from the west (Figure 3-29-3b). Zane was moving approximately 20 kt (37 km/hr) to the east-northeast at this time, while the azimuthally averaged 200-mb wind (at a radius of 300 nm) around the TC was from the west at approximately 50 kt. One might expect that a TC in such an environment would shear apart. This did not happen to Zane. The maintenance of Zane's CDO under apparent shearing conditions, and the near symmetry of the cirrus outflow within strong westerly winds aloft are unusual phenomena that raise questions about the relationship between the structure of a TC and the vertical shear of the horizontal wind.

IV. IMPACT

No reports of serious damage or injuries in Okinawa were received at the JTWC. About US $50 thousand in damage was reported by US military installations on Okinawa —mostly downed trees and power lines. Another US $118 thousand in damage was reported on the island, mostly to crops. Highest wind gusts reported on Okinawa were 79 kt (41 m/sec) at Kadena AB and 64 kt (33 m/sec) at Naha. Up to 12 inches (307 mm) of rain soaked the island. In Taiwan, heavy rains from Zane triggered mudslides that killed two people.

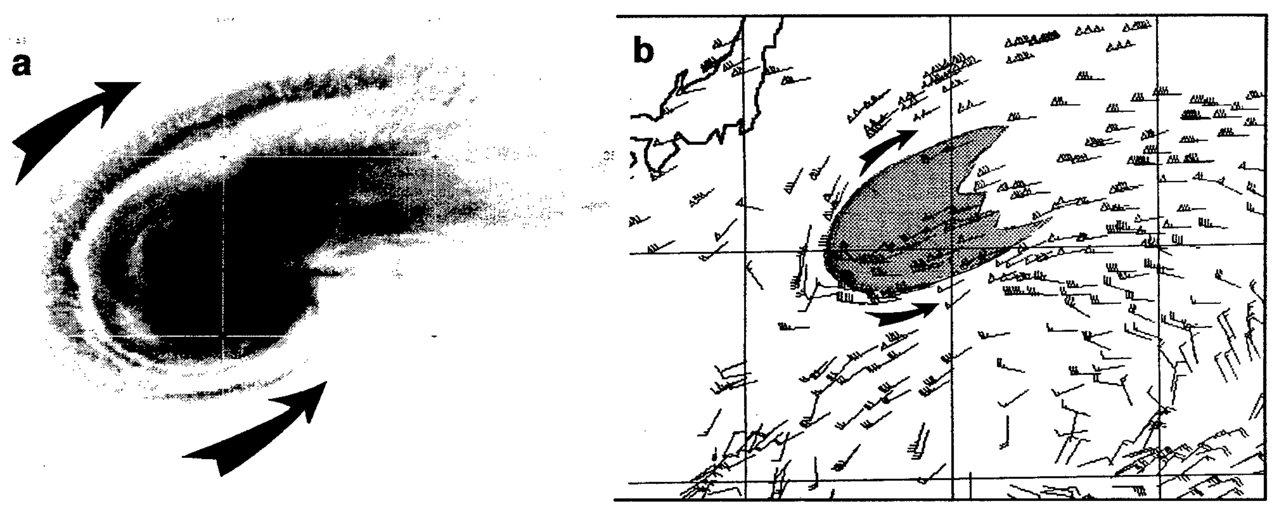

Figure 3-29-3 (a) Cirrus outflow is carried off to the east by strong upper-level westerly winds on both the north and south sides of Zane (021624Z October infrared GMS imagery, inverted-IR enhancement). (b) Water-vapor derived upper-tropospheric winds show Zane (the shaded region) was completely embedded in a westerly airstream. The divergence from the typhoon's convection caused the winds to split and go around the TC (021200Z October water-vapor derived upper-tropospheric winds).

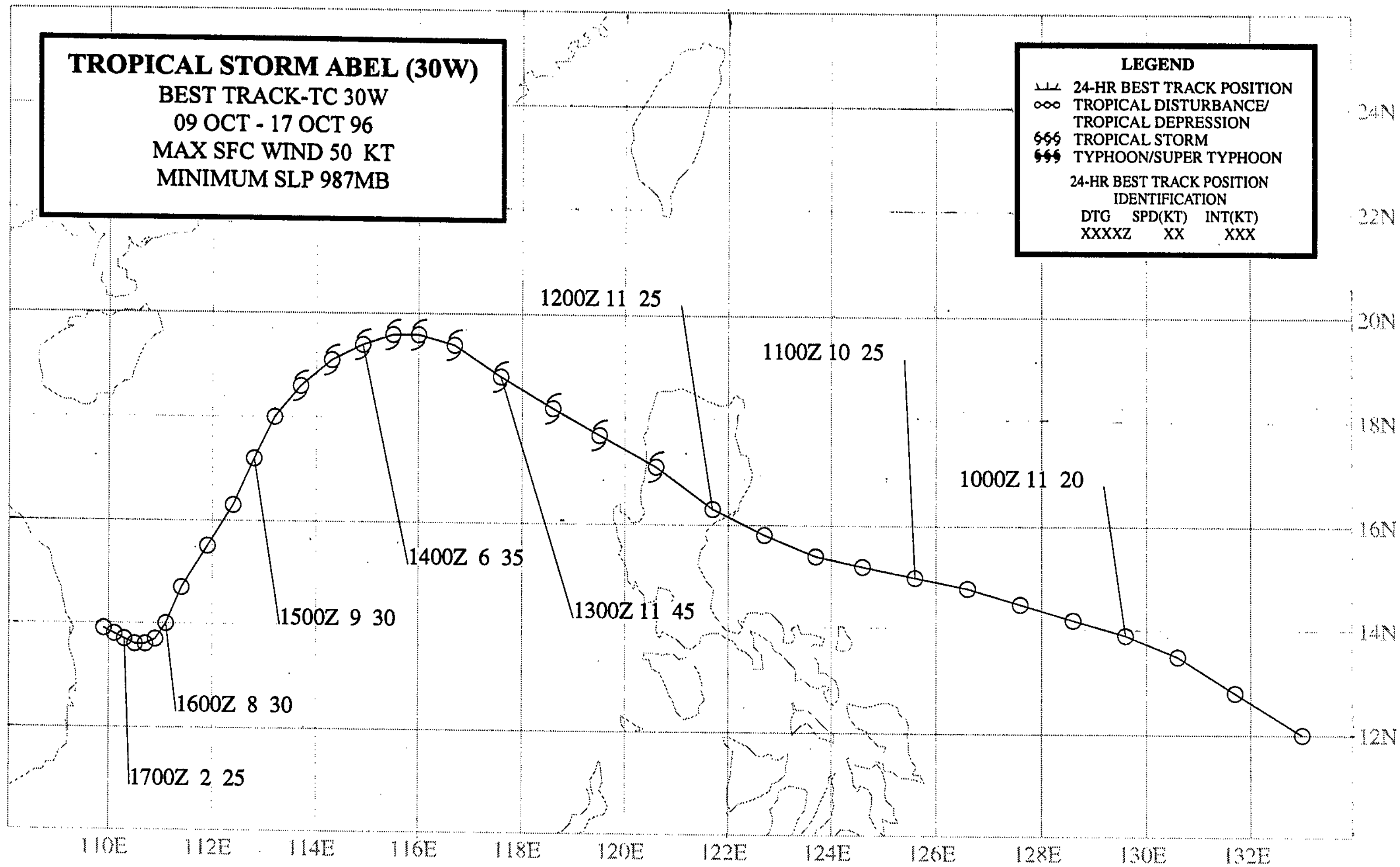
TROPICAL STORM ABEL (30W)
BEST TRACK-TC 30W
09 OCT - 17 OCT 96
MAX SFC WIND 50 KT
MINIMUM SLP 987MB
LEGEND
24-HR BEST TRACK POSITION
TROPICAL DISTURBANCE/
TROPICAL DEPRESSION
TROPICAL STORM
TYPHOON/SUPER TYPHOON
24-HR BEST TRACK POSITION
IDENTIFICATION
DTG SPD(KT) INT(KT)
XXXXZ XX XXX
1200Z 11 25
1100Z 10 25
1000Z 11 20
1400Z 6 35
1300Z 11 45
1500Z 9 30
1600Z 8 30
1700Z 2 25
24N
22N
20N
18N
16N
14N
12N
110E
112E
114E
116E
118E
120E
122E
124E
126E
128E
130E
132E

TROPICAL STORM ABEL (30W)

I. HIGHLIGHTS

Abel originated from a monsoon depression in the Philippine Sea, crossed Luzon, and became a tropical storm in the South China Sea. Forced to move southwestward by the northeast monsoon, it dissipated over water while approaching the coast of southern Vietnam.

II. TRACK AND INTENSITY

At the beginning of October, Yates (28W) and Zane (29W) recurved and moved into the midlatitudes. After this, for about one week, the low latitudes of the WNP became relatively free of deep convection, and there was a break in TC activity. By the end of the first week of October, amounts of deep convection began to increase in the low latitudes of the WNP, and became concentrated within two large areas: one near Guam and the other north of the Marshall Islands. The area of deep convection located near Guam moved westward and became a monsoon depression in the Philippine Sea. With the help of animated high-resolution visible satellite imagery, a LLCC was detected south of a band of persistent deep convection, embedded in the large cyclonic circulation of the monsoon depression. This LLCC was mentioned on the 100600Z October Significant Tropical Weather Advisory. Shortly thereafter, at 100730Z, the JTWC issued a TCFA when conditions appeared to favor the formation of a TC. Remarks on the TCFA included:

". . . Latest animated visual satellite imagery indicates a well defined low-level circulation has developed [east of the Philippines]. Newly developed convection is primarily to the north of the circulation center but is showing signs of improved organization. . . ."

The first warning on Tropical Depression (TD) 30W was issued valid at 110000Z. Remarks on the first warning included:

"A tropical depression has formed in the Philippine Sea approximately 80 nm east-northeast of Catanduenas Island in the Philippines. Animated visual satellite imagery . . . and data from several ships . . . indicates that a partially exposed 1003 mb low-level circulation exists within a larger monsoonal circulation that stretches almost 400 nm to the northeast of the [LLCC]. . . ."

On 12 October, the system crossed the island of Luzon and entered the South China Sea. Perhaps as a result of lee-side effects, northerly gale-force winds were reported over water as soon as the low-pressure center reached the northwestern tip of Luzon. In real time, satellite intensity estimates below 35 kt (18 m/sec) were favored over the gale-force ship reports, and TD 30W was upgraded to Tropical Storm Abel on the warning valid at 131200Z. In post analysis, however, the satellite imagery was reevaluated, the ship reports of gale force winds were given a higher weight, and TD 30W became a tropical storm at 120600Z. Abel reached its peak intensity of 50 kt (26 m/sec) at 121200Z.

On 14 October, Abel began to move toward the southwest under the influence of high pressure over southern China, which contributed to strong low-level northeasterly flow to Abel's west and north. While moving toward the southwest, Abel began to weaken. The deep convection accompanying the well defined LLCC on 16 October (Figure 3-30-1) decayed, and the final warning was issued, valid at 170600Z, as the system dissipated over water while approaching the coast of southern Vietnam.

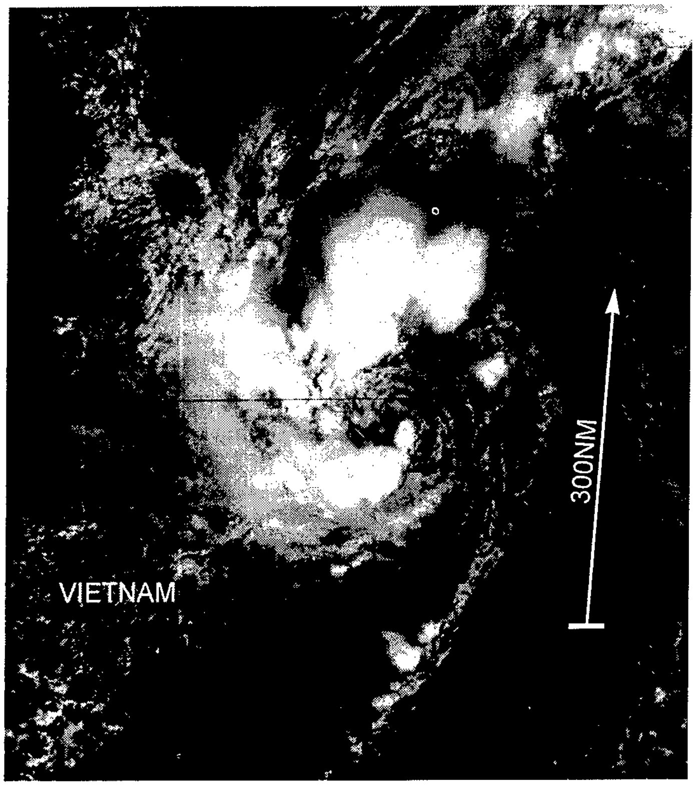

Figure 3-30-1 Abel moves slowly toward the coast of southern Vietnam, its well-defined LLCC is surrounded by cells of deep convection (160331Z October visible GMS

III. DISCUSSION

Unusual structure revealed by animated visible satellite imagery

When Abel was forming east of the Philippines, animation of visible satellite imagery indicated that the LLCC was displaced well to the south of the deep convection and also well to the south of the center of symmetry of the cirrus outflow (Figure 3-30-2). It is common for satellite fixes to be too far north in the monsoon depression stage of TC development, but in the case of Abel, the LLCC was unusually distant from the deep convection and the center of symmetry of the upper-level anticyclonic pattern of the cirrus. Synoptic data, and scatterometer data also supported this large displacement.

IV. IMPACT

As the weakening Abel approached Vietnam, rough seas overturned 146 boats and two fishermen were lost. At least 11 other people were reported missing.

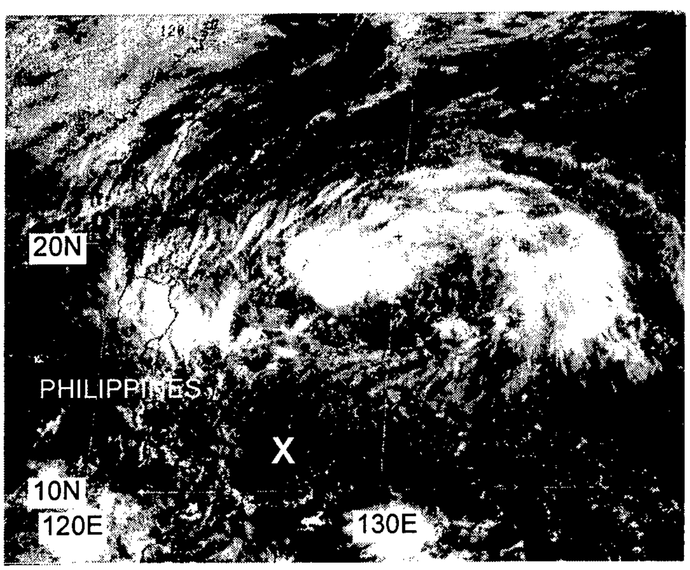

Figure 3-30-2 Animation showed that the LLCC (labeled, X) of the pre-Abel monsoon depression was displaced unusually far from its deep convection and from the center of symmetry of its upper-level cirrus outflow (102331Z October visible GMS imagery).

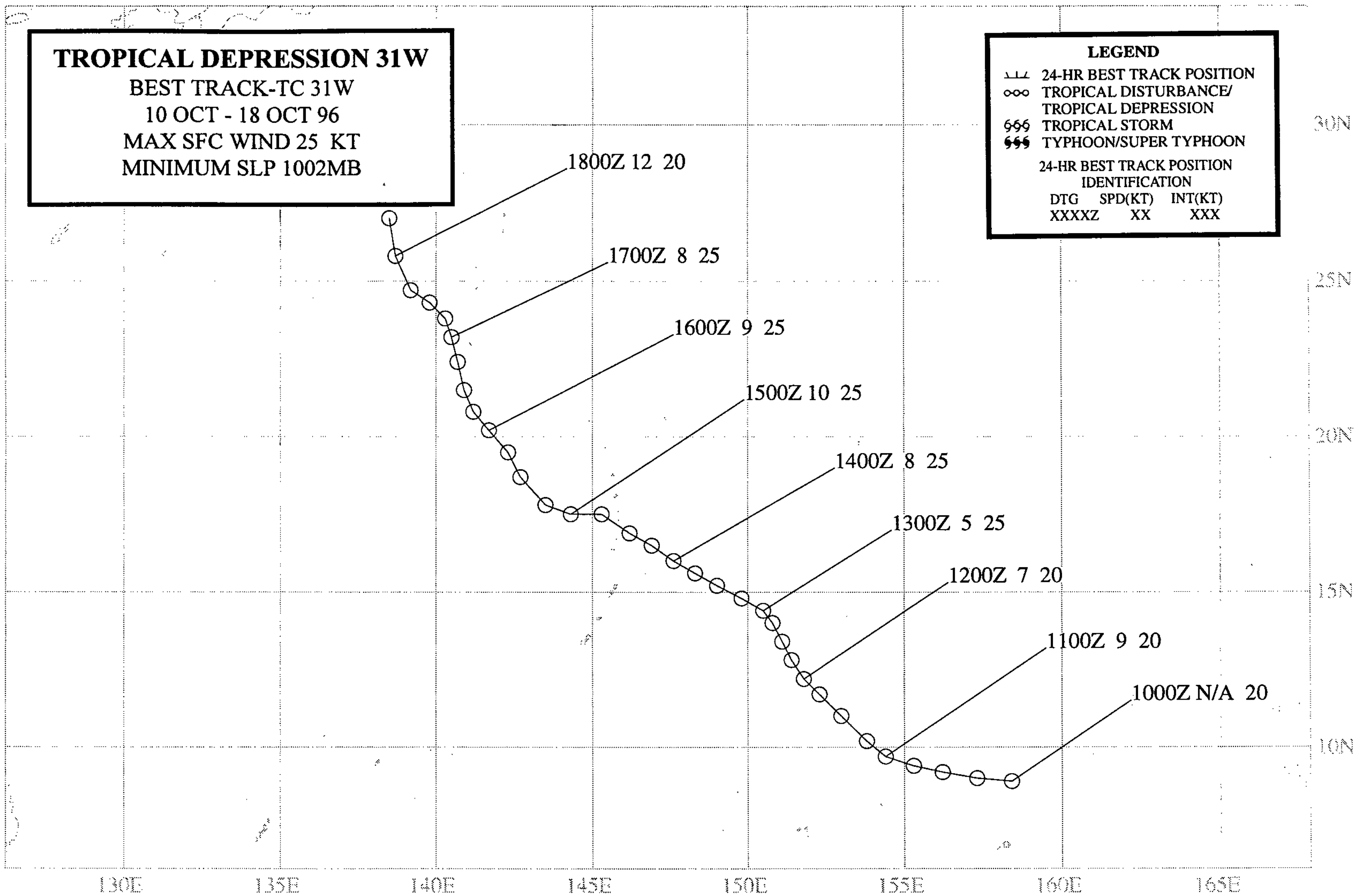
TROPICAL DEPRESSION 31W
BEST TRACK-TC 31W
10 OCT - 18 OCT 96
MAX SFC WIND 25 KT
MINIMUM SLP 1002MB
LEGEND
24-HR BEST TRACK POSITION
TROPICAL DISTURBANCE/
TROPICAL DEPRESSION
TROPICAL STORM
TYPHOON/SUPER TYPHOON
24-HR BEST TRACK POSITION
IDENTIFICATION
DTG SPD(KT) INT(KT)
XXXXZ XX XXX
1800Z 12 20
1700Z 8 25
1600Z 9 25
1500Z 10 25
1400Z 8 25
1300Z 5 25
1200Z 7 20
1100Z 9 20
1000Z N/A 20
30N
25N
20N
15N
10N
130E
135E
140E
145E
150E
155E
160E
165E

TROPICAL DEPRESSION 31W

For much of October, winds throughout most of Micronesia were light and variable in association with a weak monsoon trough. Deep convection (loosely organized into discrete ensembles of MCSs) was located in an east-west zone across the low latitudes of the WNP. Several of the tropical disturbances in this maximum cloud zone became significant TCs. The first TC of October, Abel (30W), originated from a monsoon depression in this cloud band. The next two TCs following Abel — Tropical Depression (TD) 31W and Typhoon Beth (32W) — developed simultaneously during the middle of the month (Figure 3-31-1). The tropical disturbance which became TD 31W originated southeast of Guam, and was located approximately 600 nm (1100 km) southeast of the tropical disturbance which became Beth (32W). This tropical disturbance was first mentioned on the 100600Z October Significant Tropical Weather Advisory. On 13 October, the pre-TD 31W disturbance acquired a clearly defined LLCC on satellite imagery, prompting the JTWC to issue a Tropical Cyclone Formation Alert at 130330Z October. The first warning on TD 31W, valid at 130600Z, soon followed when satellite intensity estimates indicated 25 kt (13 m/sec).

Moving toward the northwest, TD 31W exhibited a shear-type cloud pattern (Figure 3-31-2) for all of its life. Satellite intensity estimates and the best-track intensities remained at 25 kt (13 m/sec) for several days. During the night of 17 October, the deep convection associated with TD 31W decreased in amount and became sheared well to the east of the LLCC. The final warning on TD 31W was issued, valid at 171200Z, as the system dissipated over water.

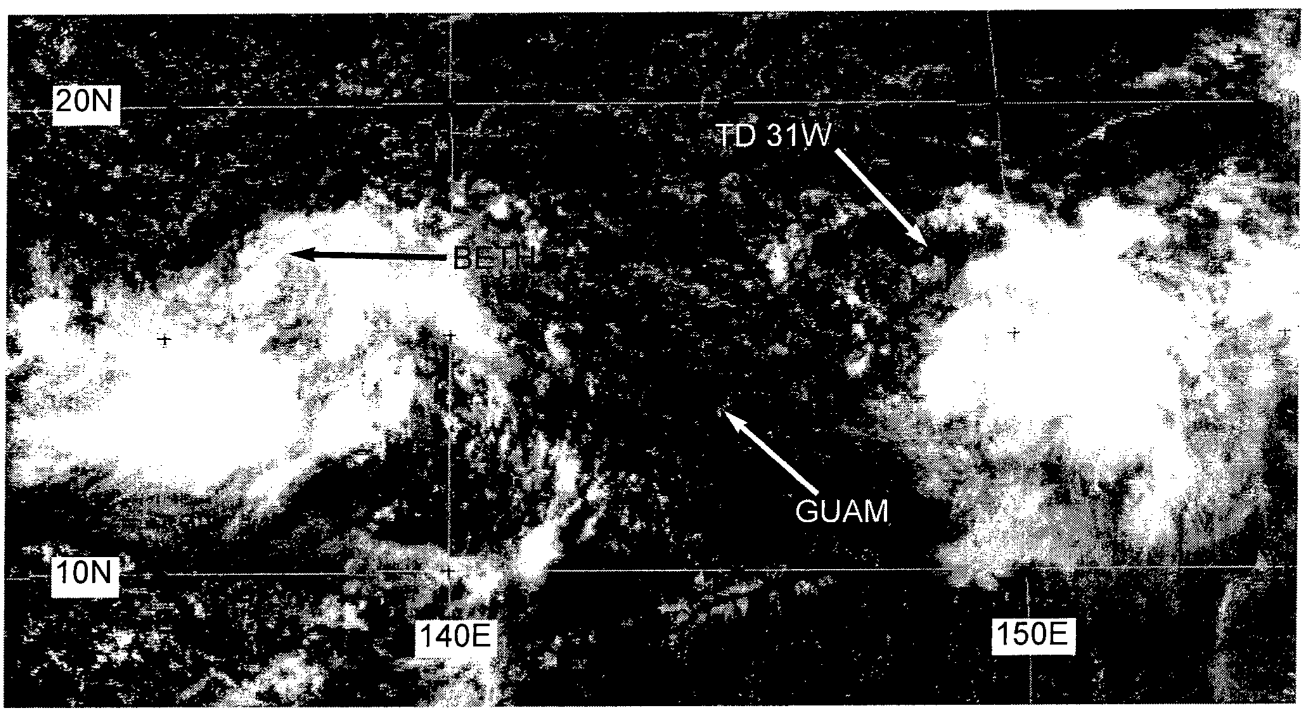

Figure 3-31-1 Typhoon Beth (32W) and TD 31W developed simultaneously. Beth became a typhoon, but TD 31W failed to become a mature TC (122331Z October visible GMS imagery).

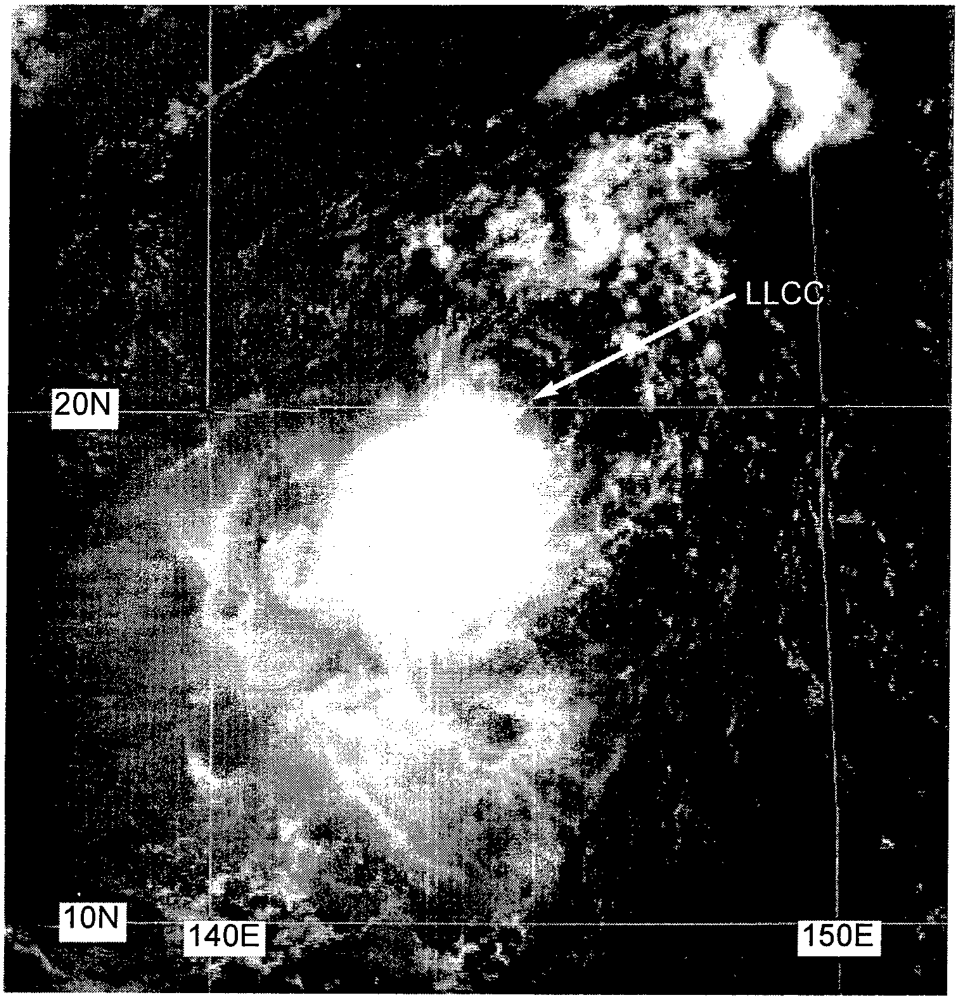

Figure 3-31-2 For all its life, TD 31W exhibited a shear-type cloud pattern. The LLCC is located to the north of the deep convection in this image (152224Z October visible GMS imagery).

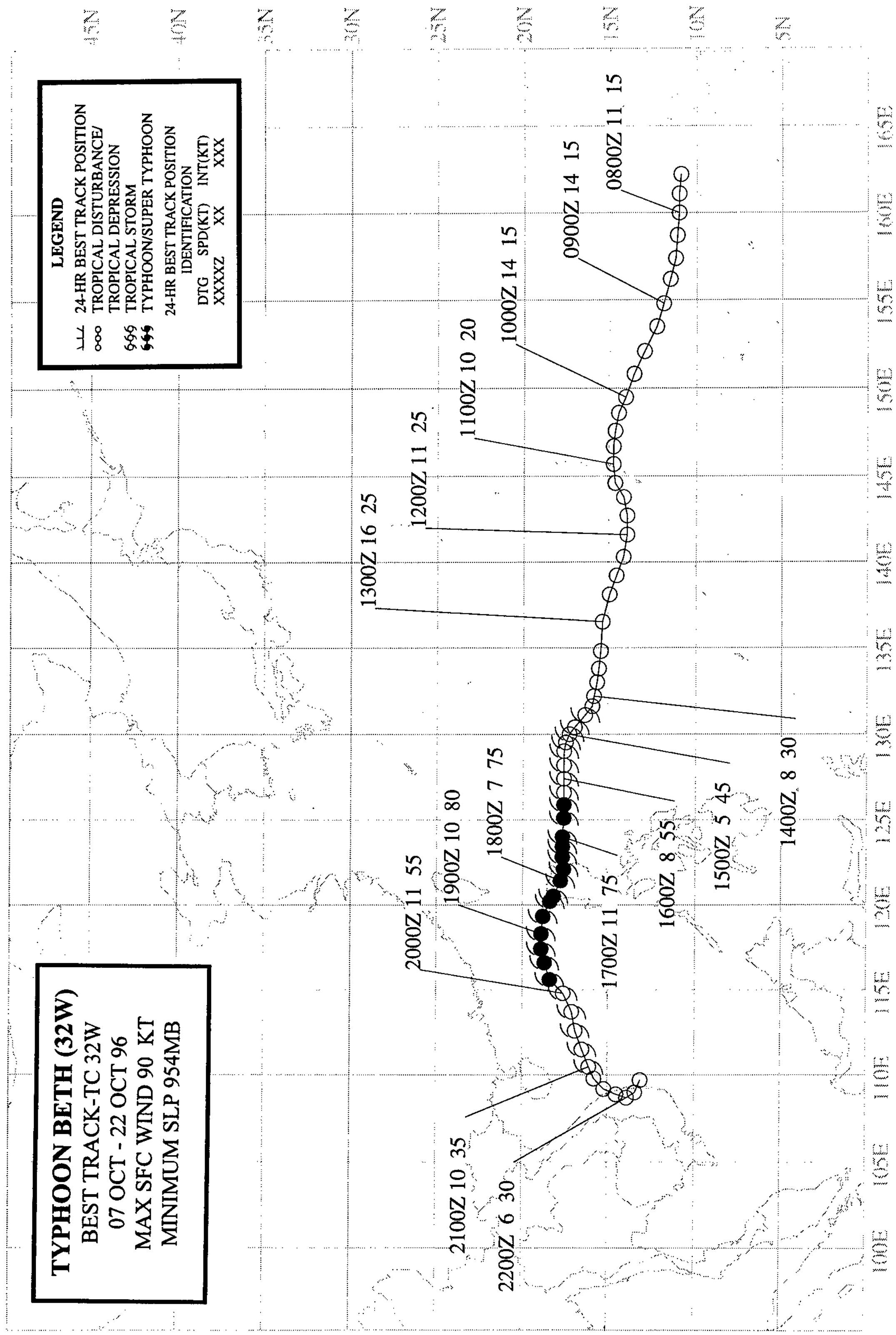
TYPHOON BETH (32W)
BEST TRACK-TC 32W
07 OCT - 22 OCT 96
MAX SFC WIND 90 KT
MINIMUM SLP 954MB
LEGEND
24-HR BEST TRACK POSITION
TROPICAL DISTURBANCE/
TROPICAL DEPRESSION
TROPICAL STORM
TYPHOON/SUPER TYPHOON
24-HR BEST TRACK POSITION
IDENTIFICATION
DTG SPD(KT) INT(KT)
XXXXZ XX XXX
0800Z 11 15
0900Z 14 15
1000Z 14 15
1100Z 10 20
1200Z 11 25
1300Z 16 25
1400Z 8 30
1500Z 5 45
1600Z 8 55
1700Z 11 75
1800Z 7 75
1900Z 10 80
2000Z 11 55
2100Z 10 35
2200Z 6 30
45N
40N
35N
30N
25N
20N
15N
10N
5N
100E
105E
110E
115E
120E
125E
130E
135E
140E
145E
150E
155E
160E
165E

TYPHOON BETH (32W)

I. HIGHLIGHTS

The tropical disturbance which became Beth was first detected in the eastern Caroline Islands. It developed very slowly, and four Tropical Cyclone Formation Alerts were issued on the system prior to the first warning. Passing over Guam, it produced a thunderstorm with a spectacular display of cloud-to-ground lightning (unusual in the maritime tropics). Beth became a typhoon in the Philippine Sea and passed over Luzon where loss of life was reported. Encountering the northeast monsoon in the South China Sea, it turned to the southwest, weakened, and made landfall in central Vietnam.

II. TRACK AND INTENSITY

For much of October, winds throughout most of Micronesia were light and variable in association with a weak monsoon trough. Deep convection (loosely organized into discrete ensembles of MCSs) was located in an east-west zone across the low latitudes of the WNP. Several of the tropical disturbances in this maximum cloud zone became significant TCs. The first TC of October, Abel (30W), originated from a monsoon depression in this cloud band. The next two TCs — Tropical Depression (TD) 31W and Beth (32W) — developed simultaneously during the middle of the month (Figure 3-32-1). The tropical disturbance which became Beth originated in the eastern Caroline Islands. It was first mentioned on the 071800Z Significant Tropical Weather Advisory. The system moved westward, and in the late afternoon of 11 October, synoptic data from Guam and Saipan, visible satellite imagery, and NEXRAD products indicated that a weak LLCC was associated with an area of increasing deep convection near Guam and Saipan. This prompted the JTWC to issue the first TCFA at 110730Z. At 111200Z, a second TCFA was issued in order to reposition the alert box to account for indications on NEXRAD data that a second LLCC had formed to the east of Guam. At 120130Z October, a third TCFA was issued to move the alert box further to the west to incorporate indications on visible satellite imagery that the primary LLCC had moved to a position 260 nm (480 km) west of Guam. The pre-Beth tropical disturbance moved west and did not intensify, although conditions still appeared favorable for further development, and a fourth TCFA was issued at 130000Z. During the night of 13 October, the deep convection in the pre-Beth tropical disturbance consolidated near the LLCC and became organized into a well-defined curved band. The first warning, valid at 131200Z, was issued on Tropical Depression (TD) 32W. The cloud pattern of TD 32W evolved into a sheared pattern type with the LLCC exposed on the eastern side (Figure 3-32-2). When satellite imagery indicated an intensity of 35 kt (18 m/sec), TD 32W was

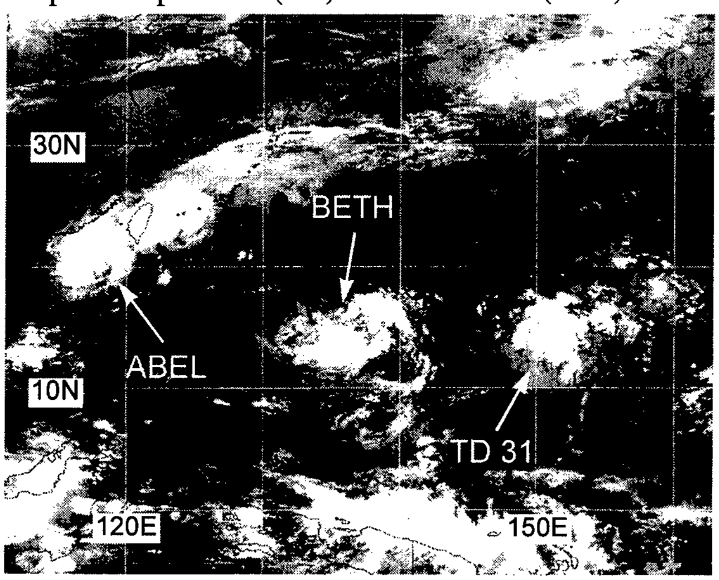

Figure 3-32-1 The tropical disturbances which became Beth and TD 31W developed simultaneously while Abel (30W) moved across the South China Sea (122331Z October infrared GMS imagery).

upgraded to Tropical Storm Beth on the warning valid at 150000Z. Beth became a typhoon at 161200Z and reached its peak intensity of 90 kt (46 m/sec) at 171200Z just prior to landfall on the east coast of northern Luzon (Figure 3-32-3). While crossing northern Luzon, Beth weakened only slightly to 75 kt (39 m/sec), and then reintensified to 80 kt (41 m/sec) at 181200Z when it entered the South China Sea. The period of reintensification was short-lived and by the morning of 20 October, the deep convection became sheared to the east of Beth's LLCC as the system weakened steadily over water. As Beth began to weaken, it began to move toward the west-southwest in response to high pressure over southern China and a strengthening of low-level northeasterly flow to its west and north. The final warning was issued, valid at 211800Z, as the poorly defined LLCC reached the coast of central Vietnam and dissipated.

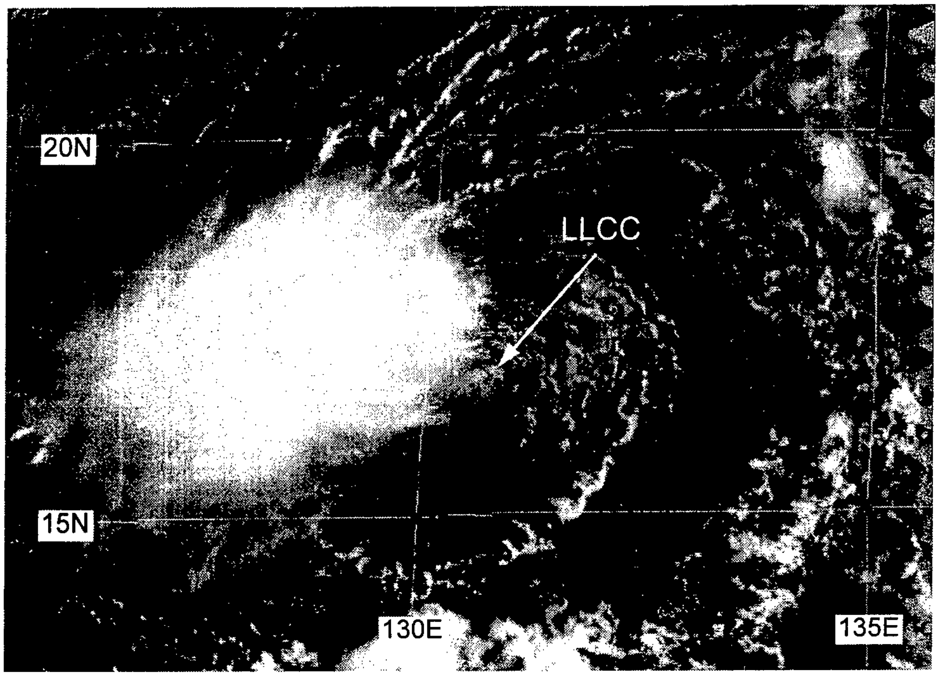

Figure 3-32-2 Beth's LLCC is partially exposed to the east of the deep convection, indicating the presence of easterly vertical wind shear (142224Z October visible GMS imagery).

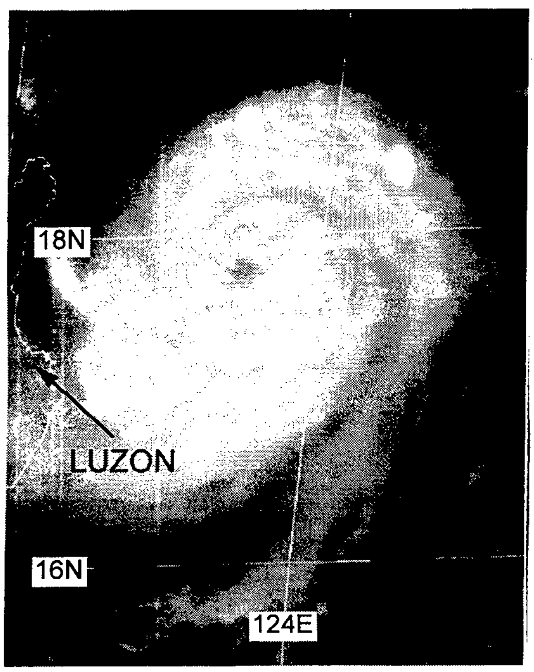

Figure 3-32-3 Beth acquires a small visible eye shortly before reaching peak intensity (170424Z October visible GMS imagery).

III. DISCUSSION

a. *Lightning in the maritime tropics*

On the night of 11 October, a thunderstorm associated with the pre-Beth tropical disturbance produced a spectacular display of cloud-to-ground (CG) lightning on Guam. Frequent CG lightning is rare on Guam, even in large cumulonimbus clouds with tops exceeding 50,000 ft. Indeed, lightning frequencies are low in general over the maritime regions when compared with lightning frequencies within thunderstorms over large land areas (Orville and Henderson 1986). The cause of reduced lightning frequencies in maritime cumulonimbus clouds has been narrowed to two primary mechanisms:

1) reduced vertical velocities in maritime thunderstorms; and,

2) differences between the continental versus maritime aerosols which comprise the cloud condensation nuclei.

A more detailed discussion of the mechanisms of cloud electrification are beyond the scope of this summary.

In the case of the relatively frequent CG lightning discharges in the 11 October Guam thunderstorm, only one other unusual factor was noted: reflectivity values as high as 60 dBZ on the NEXRAD composite reflectivity product persisted in the core of the thunderstorm as it moved southwestward across Guam.

b. *Intensification of a sheared TC*

One of the factors known to influence genesis and development of a TC is vertical shear of the horizontal wind: too much shear, and the TC is torn apart. Zehr (1992) found that an 850-200 mb wind shear of 15 kt (8 m/sec) or greater was unfavorable for TC genesis and development. On the morning of 15 October, Beth possessed a shear-type cloud pattern (Figure 3-32-2), and the LLCC was partially exposed on the east side of the deep convection. Shear is often detrimental to the further development of a TC. In Beth's case, however, the system intensified despite the shear and by 17 October, Beth was a typhoon with a visible eye and a symmetrical pattern of cirrus outflow (Figure 3-32-3). It is a difficult forecast problem to determine whether vertical shear is going to inhibit development, or whether the TC will continue to develop despite a shearing environment. Fundamental questions remain in the case of intensification in a sheared environment: does the TC outflow manage to overcome the shear? Does the shear decrease? Do changes occur in its vertical profile?

IV. IMPACT

At least three people were reported dead after Beth moved across the northern Philippines. The TC tore away roofs, smashed windows, and triggered floods. In the hardest-hit province of Cagayan, Beth damaged municipal buildings and crops, and eroded roads.

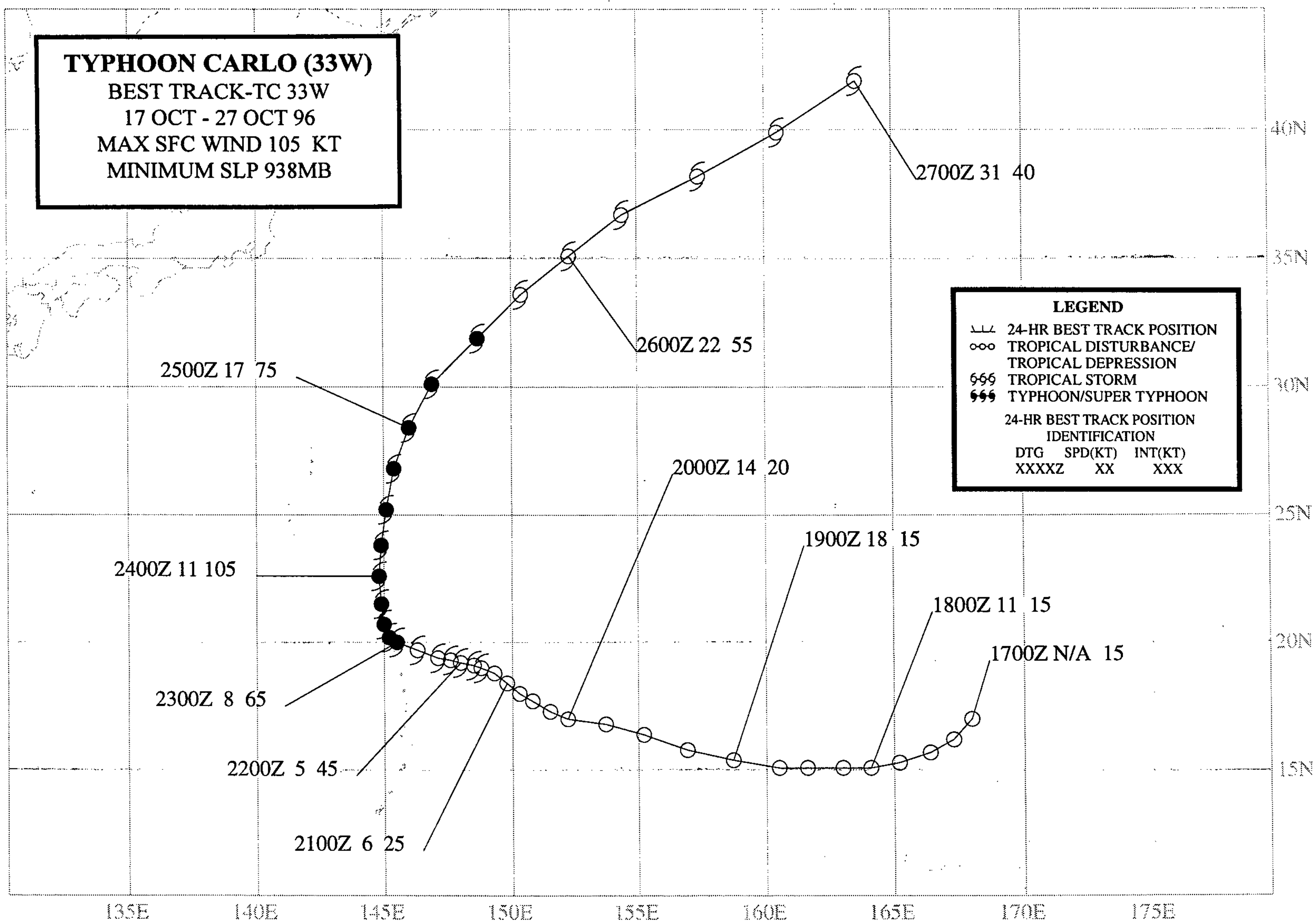
TYPHOON CARLO (33W)
BEST TRACK-TC 33W
17 OCT - 27 OCT 96
MAX SFC WIND 105 KT
MINIMUM SLP 938MB
LEGEND
24-HR BEST TRACK POSITION
TROPICAL DISTURBANCE/
TROPICAL DEPRESSION
TROPICAL STORM
TYPHOON/SUPER TYPHOON
24-HR BEST TRACK POSITION
IDENTIFICATION
DTG SPD(KT) INT(KT)
XXXXZ XX XXX
2700Z 31 40
2600Z 22 55
2500Z 17 75
2400Z 11 105
2300Z 8 65
2200Z 5 45
2100Z 6 25
2000Z 14 20
1900Z 18 15
1800Z 11 15
1700Z N/A 15
40N
35N
30N
25N
20N
15N
135E
140E
145E
150E
155E
160E
165E
170E
175E

TYPHOON CARLO (33W)

I. HIGHLIGHTS

Carlo's TUTT-cell-induced formation is one of the best examples of this process witnessed during 1996. Water-vapor imagery provided detailed information on the evolution of upper-level winds, clouds, and moisture for this event. Carlo reached its peak intensity after its apparent "point of recurvature" — unusual behavior of TCs which recurve. Accelerating to a speed of 30 kt (55 km/hr), Carlo was absorbed into the frontal cloud band of an intense extratropical low.

II. TRACK AND INTENSITY

On 17 October, three TCs were active in the western part of the WNP: Abel (30W) (in the South China Sea), TD 31W (halfway between Guam and Japan), and Beth (32W) (near the coast of Luzon). Elsewhere in the tropics of the WNP, amounts of deep convection were below normal and the low-level winds were predominantly from the east. The only area of deep convection considered to have potential for TC formation was associated with a TUTT cell, and was centered near 17°N 168°E. It was first mentioned on the 170600Z October Significant Tropical Weather Advisory. Moving westward on the northern side of the TUTT cell (Figure 3-33-1), this tropical disturbance (which became Carlo) gradually became more organized. At 200230Z October, the JTWC issued a TCFA when persistent deep convection (located in a region of divergent upper-level flow) consolidated near the LLCC. Based on satellite intensity estimates of 25 kt (13 m/sec), the first warning on Tropical Depression (TD) 33W was issued valid at 210000Z.

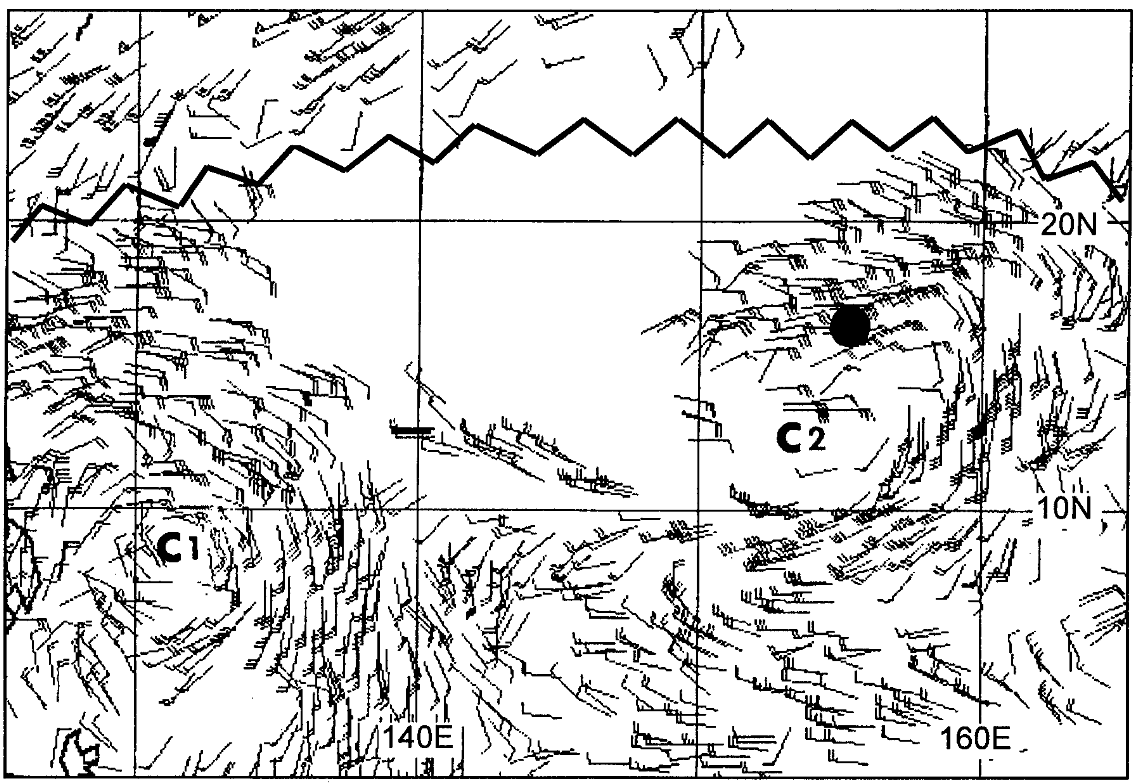

Figure 3-33-1 The location of the LLCC of the pre-Carlo tropical disturbance (shown by the black dot) is under the easterly upper-level flow to the north of a TUTT cell (labeled, C2). Another TUTT cell (labeled, C1) is located further to the west. The zig-zag line indicates the upper-level subtropical ridge axis (191025Z October GMS water-vapor winds).

Developing a CDO, TD 33W was upgraded to Tropical Storm Carlo on the warning valid at 211200Z. Carlo became a typhoon at 230000Z as a small ragged eye formed within its CDO (Figure 3-33-2). After becoming a typhoon, Carlo turned northward and further intensified, reaching a peak intensity of 105 kt (54 m/sec) at 240000Z. Late on 24 October, Carlo began a gradual turn toward the northeast accompanied by an increase in it speed of translation. Westerly shear began to affect Carlo and by 250000Z the typhoon weakened to 80 kt (41 m/sec); at 251800Z the intensity dropped to 60 kt (31 m/sec). The system continued to weaken as it accelerated to the northeast. The final warning was issued, valid at 261800Z, as the system moved northeastward at 29 kt (54 km/hr), lost its deep convection, and began to merge with a frontal cloud band.

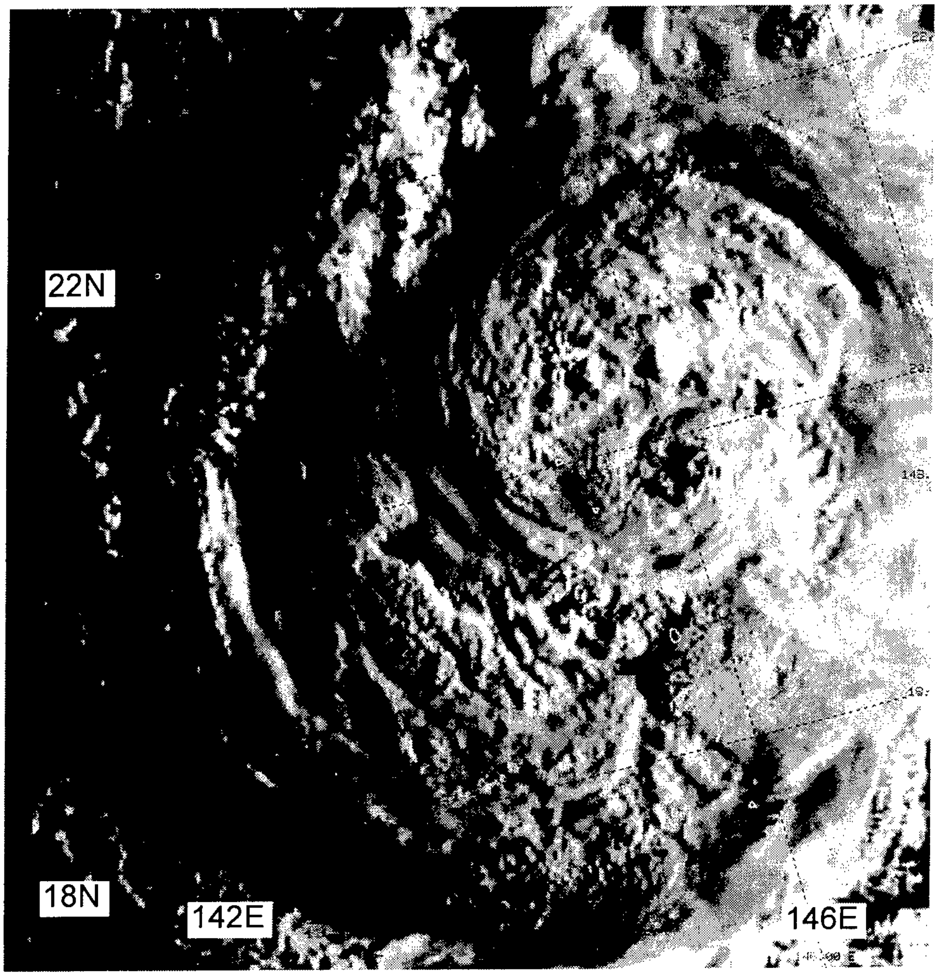

Figure 3-33-2 An overshooting cloud top casts a shadow over Carlo's incipient eye (222101Z October visible DMSP imagery).

III. DISCUSSION

a. *Tropical cyclogenesis induced by a TUTT cell*

Water vapor imagery (Figure 3-33-3) showed that Carlo formed in an area of upper-level moisture (with embedded deep convection) on the north side of a TUTT cell. Typical of TCs which form in association with TUTT cells, Carlo formed north of 15°N latitude, was embedded in low-level easterly flow, and was isolated in a cloud-minimum region south of the subtropical ridge. See Joy (12W) for a more detailed discussion of TUTT-related TC genesis.

b. *Peak intensity after making a sharp turn toward the north*

Most typhoons that undergo classic recurvature (i.e., a roughly "<"-shaped track which features initial steady west-northwestward motion, then a northward turn while slowing, followed by an acceleration toward the northeast) reach peak intensity at, or before, the point of recurvature; where the point of recurvature is identified as that point where the typhoon reaches its westernmost longitude (JTWC, 1994). Many TCs do not undergo classic recurvature. Some never recurve, while others move on a track type designated by the Japan Meteorological Agency (JMA) (1976) as north-

oriented. North-oriented TC tracks have been renamed poleward-oriented tracks in Carr and Elsberry (1996) to make the concept applicable to both the Northern and Southern Hemispheres. TCs that move on north-oriented tracks move generally on long, northward paths from their genesis location and may feature large meanders and abrupt turns to the left or right (Lander 1996). North-oriented tracks occur predominantly during July through October. Carr and Elsberry found that a TC may undergo north-oriented motion for only a portion of its track — even if some, or most, of the track was of some other type (e.g., straight moving). A characteristic behavior of some TCs undergoing north-oriented motion is reaching peak intensity after acquiring a persistent eastward component of motion, but before the TC begins to significantly increase its speed of translation within the "accelerating westerlies" regime north of the subtropical ridge. Synoptic regimes associated with specific TC behavior, such as "poleward oriented" and "accelerating westerlies", are described in Carr and Elsberry (1996), and briefly at the beginning of this chapter.

Carlo reached peak intensity while moving north-northeastward on the north-oriented leg of its track. It weakened as it entered the "accelerating-westerly" regime north of the subtropical ridge.

IV. IMPACT

No reports of damage or injuries were received at JTWC.

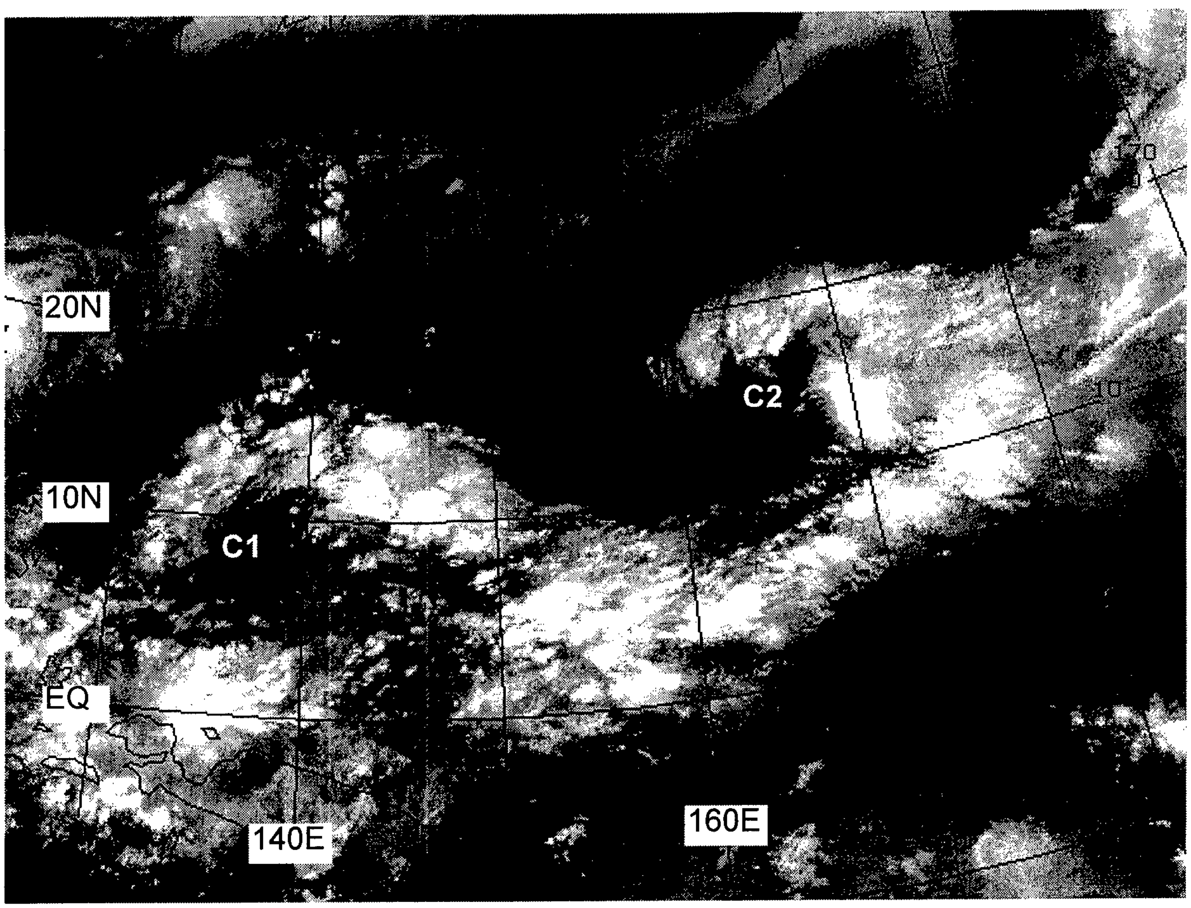

Figure 3-33-3 Two TUTT cells (C1 and C2) show prominently in water vapor imagery. Carlo formed under the moist tongue on the north side of TUTT cell C2 (180033Z October water vapor GMS imagery).

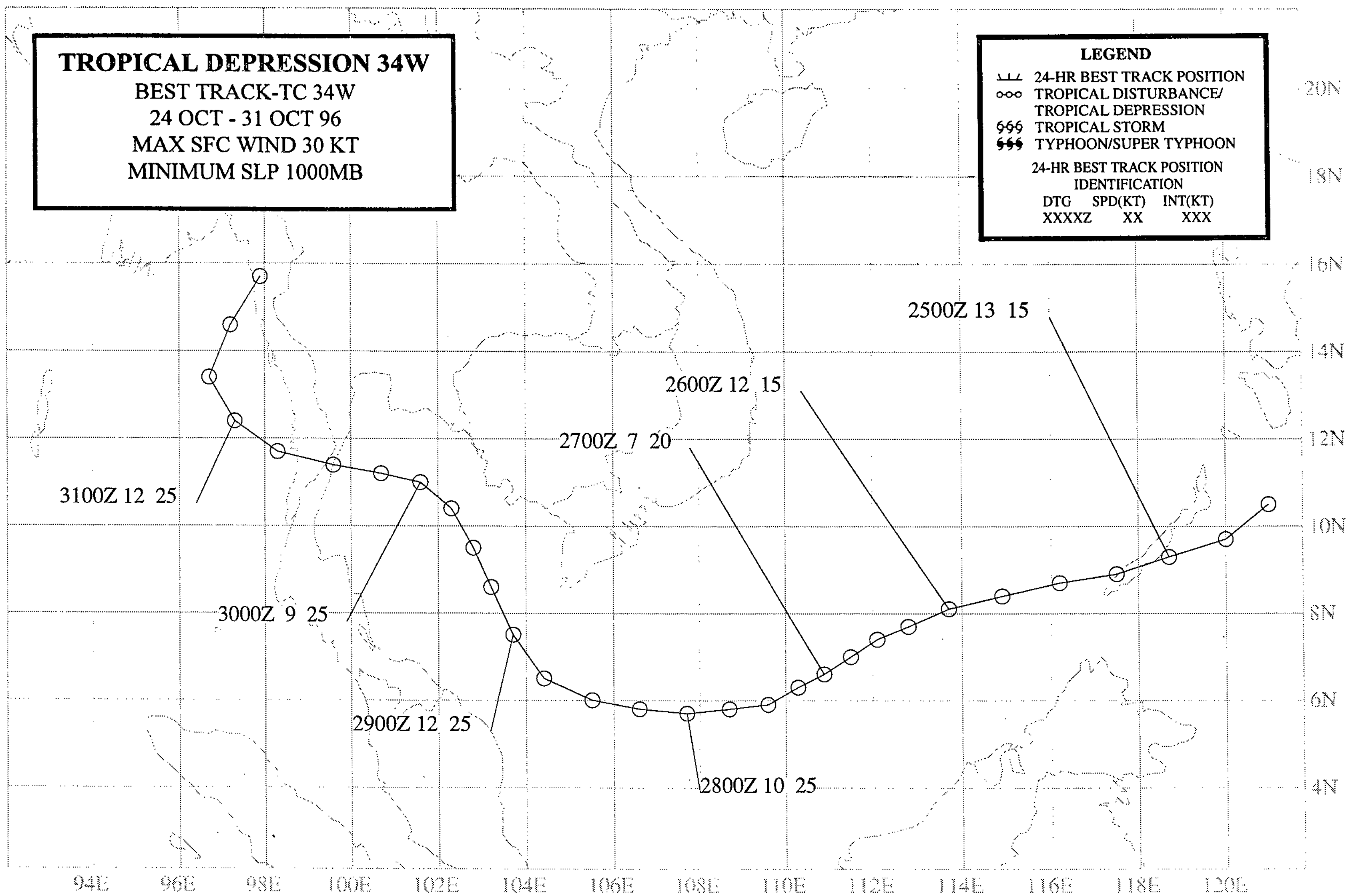
TROPICAL DEPRESSION 34W
BEST TRACK-TC 34W
24 OCT - 31 OCT 96
MAX SFC WIND 30 KT
MINIMUM SLP 1000MB
LEGEND
24-HR BEST TRACK POSITION
TROPICAL DISTURBANCE/
TROPICAL DEPRESSION
TROPICAL STORM
TYPHOON/SUPER TYPHOON
24-HR BEST TRACK POSITION
IDENTIFICATION
DTG SPD(KT) INT(KT)
XXXXZ XX XXX
2500Z 13 15
2600Z 12 15
2700Z 7 20
2800Z 10 25
2900Z 12 25
3000Z 9 25
3100Z 12 25
20N
18N
16N
14N
12N
10N
8N
6N
4N
94E
96E
98E
100E
102E
104E
106E
108E
110E
112E
114E
116E
118E
120E

TROPICAL DEPRESSION 34W

The tropical disturbance which became Tropical Depression (TD) 34W originated from an area of persistent deep convection over the central Philippines. As the deep convection drifted west-southwestward across the South China Sea, a weak LLCC persisted to the eastern edge of the convection. The tropical disturbance was first mentioned on the 270600Z October Significant Tropical Weather Advisory when water vapor satellite imagery indicated that an upper-level anticyclone was forming over the deep convection. Although the cloud system remained poorly organized (Figure 3-34-1), JTWC anticipated further development and issued the first TCFA at 272030Z. A scatterometer pass over the system at 280251Z indicated a well-defined LLCC with wind speeds of 15 to 25 kt (8 to 13 m/sec) on its north side and equatorial westerlies to the south. A second TCFA followed at 282030Z. Based upon ship reports and satellite intensity estimates of 25 kt (13 m/sec), JTWC issued the first warning on TD 34W valid at 290600Z. TD 34W tracked northwestward across the Gulf of Thailand, crossed the Isthmus of Kra and became completely disorganized after moving into the Bay of Bengal. The final warning was issued valid at 301800Z. On 31 October, the remnants of TD 34W turned northward and dissipated over southern Myanmar. In postanalysis, a ship report near the LLCC of 30-kt winds and 1004 mb pressure at 271200Z was used to upgrade the maximum intensity of the best track to 30 kt.

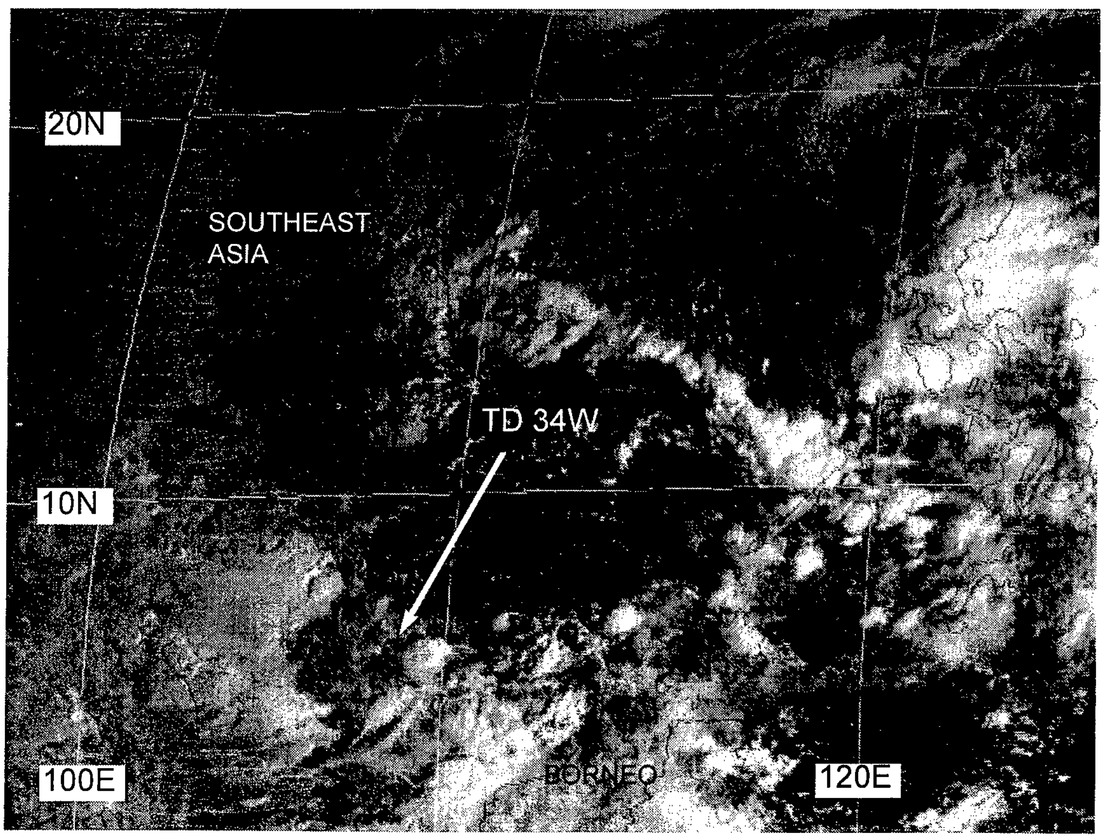

Figure 3-34-1 TD 34W moves west-southwestward in the South China Sea. Most of the deep convection lies to the west of the LLCC (272331Z October visible GMS imagery).

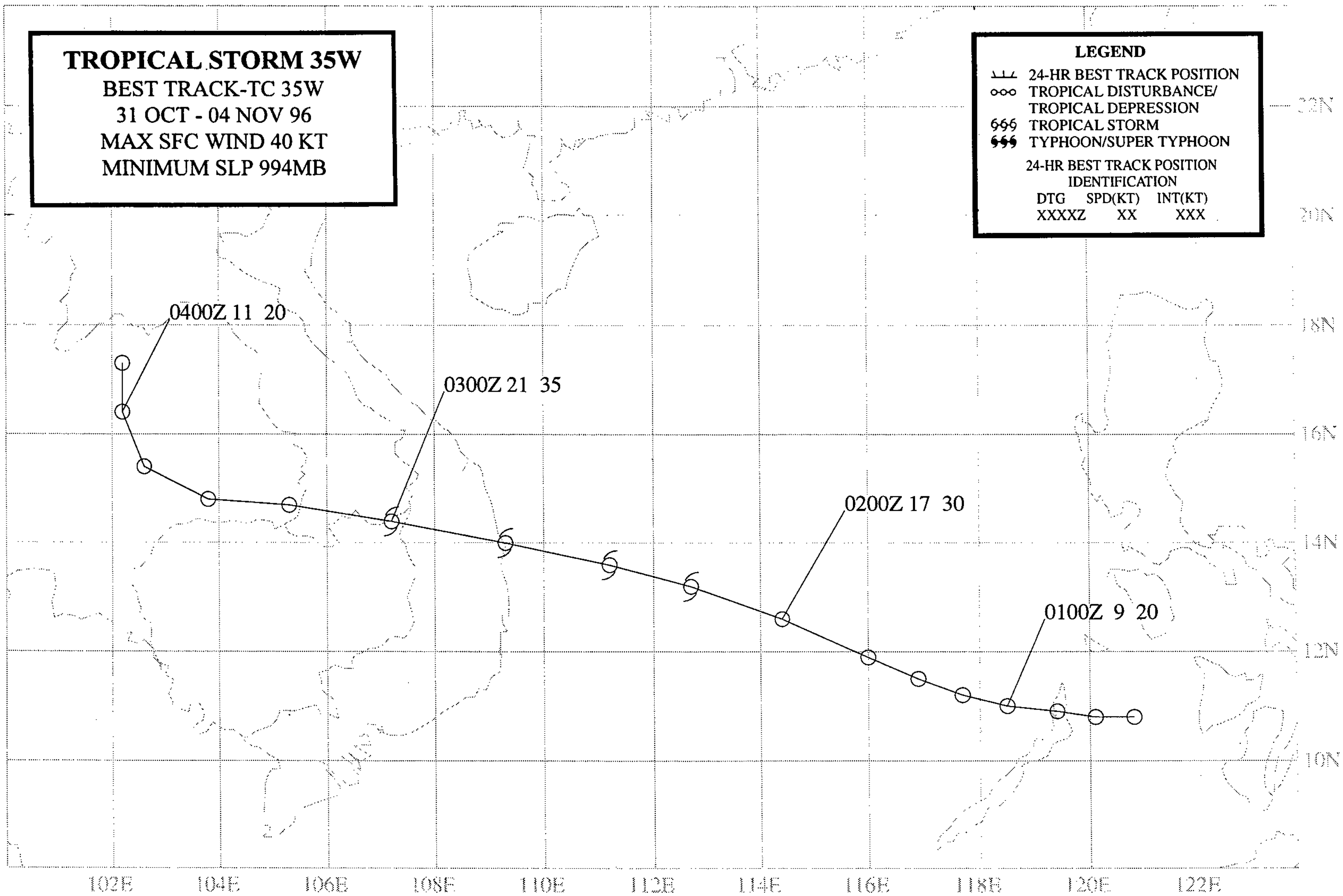
TROPICAL STORM 35W
BEST TRACK-TC 35W
31 OCT - 04 NOV 96
MAX SFC WIND 40 KT
MINIMUM SLP 994MB
LEGEND
24-HR BEST TRACK POSITION
TROPICAL DISTURBANCE/
TROPICAL DEPRESSION
TROPICAL STORM
TYPHOON/SUPER TYPHOON
24-HR BEST TRACK POSITION
IDENTIFICATION
DTG SPD(KT) INT(KT)
XXXXZ XX XXX
0400Z 11 20
0300Z 21 35
0200Z 17 30
0100Z 9 20
22N
20N
18N
16N
14N
12N
10N
102E
104E
106E
108E
110E
112E
114E
116E
118E
120E
122E

TROPICAL STORM 35W

On the last day of October, the tropical disturbance that became Tropical Storm (TS) 35W formed over the Philippines at nearly the same location as Tropical Depression (TD) 34W had formed a week earlier. The tropical disturbance was first mentioned on the 010600Z November Significant Tropical Weather Advisory when a persistent area of deep convection was observed over the South China Sea to the west of a weak LLCC in the Sulu Sea. The convection persisted and JTWC issued a TCFA at 011430Z. Falling pressures (3 mb in 24 hours), 25-kt synoptic reports and satellite intensity estimates led to the issuance of the first warning valid at 020000Z. The TC moved westward and acquired the structure of a monsoon depression (Figure 3-35-1) as it approached Vietnam. A final warning was issued, valid at 030600Z, as the remnants of the cyclone dissipated over Southeast Asia.

In postanalysis, synoptic reports and satellite imagery indicate that this TC most probably reached tropical storm intensity at 020600Z, and peaked at 40 kt six hours later. Thus, TD 35W was redesignated as TS 35W.

It is interesting to note that TS 35W was accompanied in the Southern Hemisphere by TC Melanie/Bellamine (05S)(Figure 3-35-2), as the TC activity in the Southern Hemisphere got off to a prolific start during the latter half of 1996.

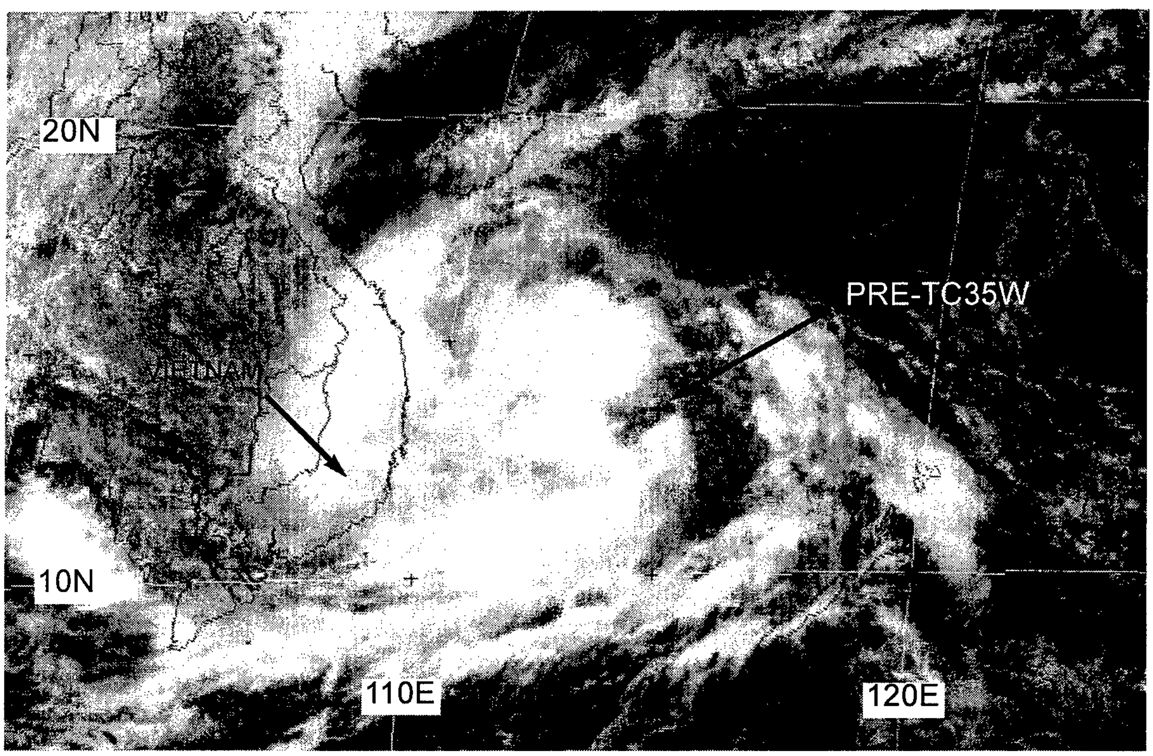

Figure 3-35-1 The monsoon depression just to the east of central Vietnam is approaching tropical storm intensity (020424Z November visible GMS imagery).

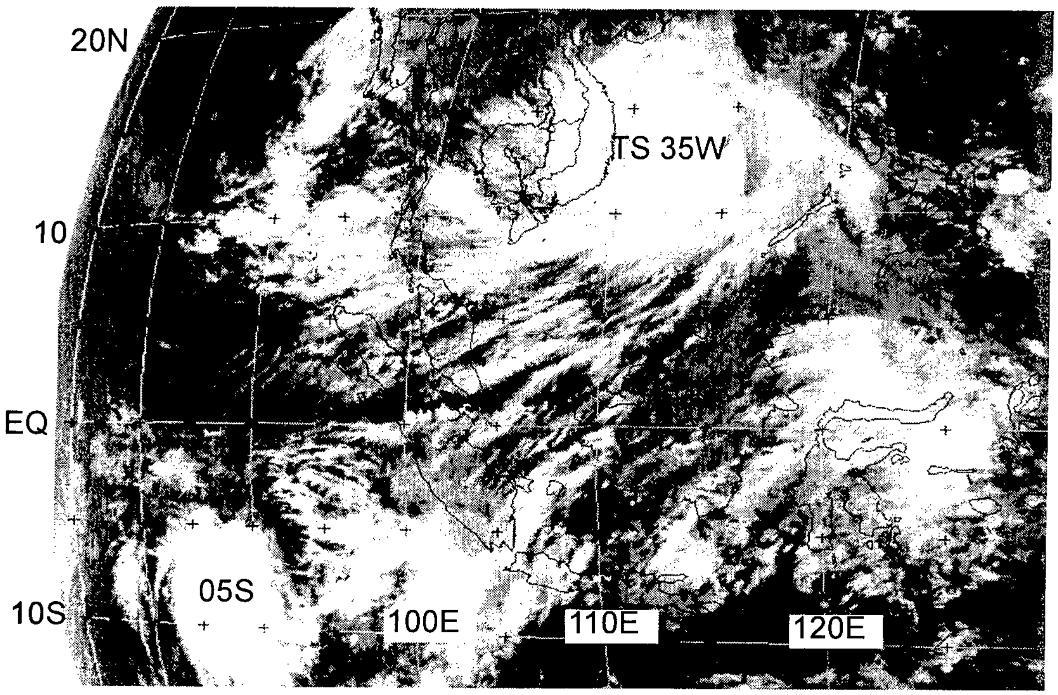

Figure 3-35-2 TS 35W is accompanied by TC Melanie/Bellamine (05S) in the Southern Hemisphere (020424Z November infrared GMS imagery).

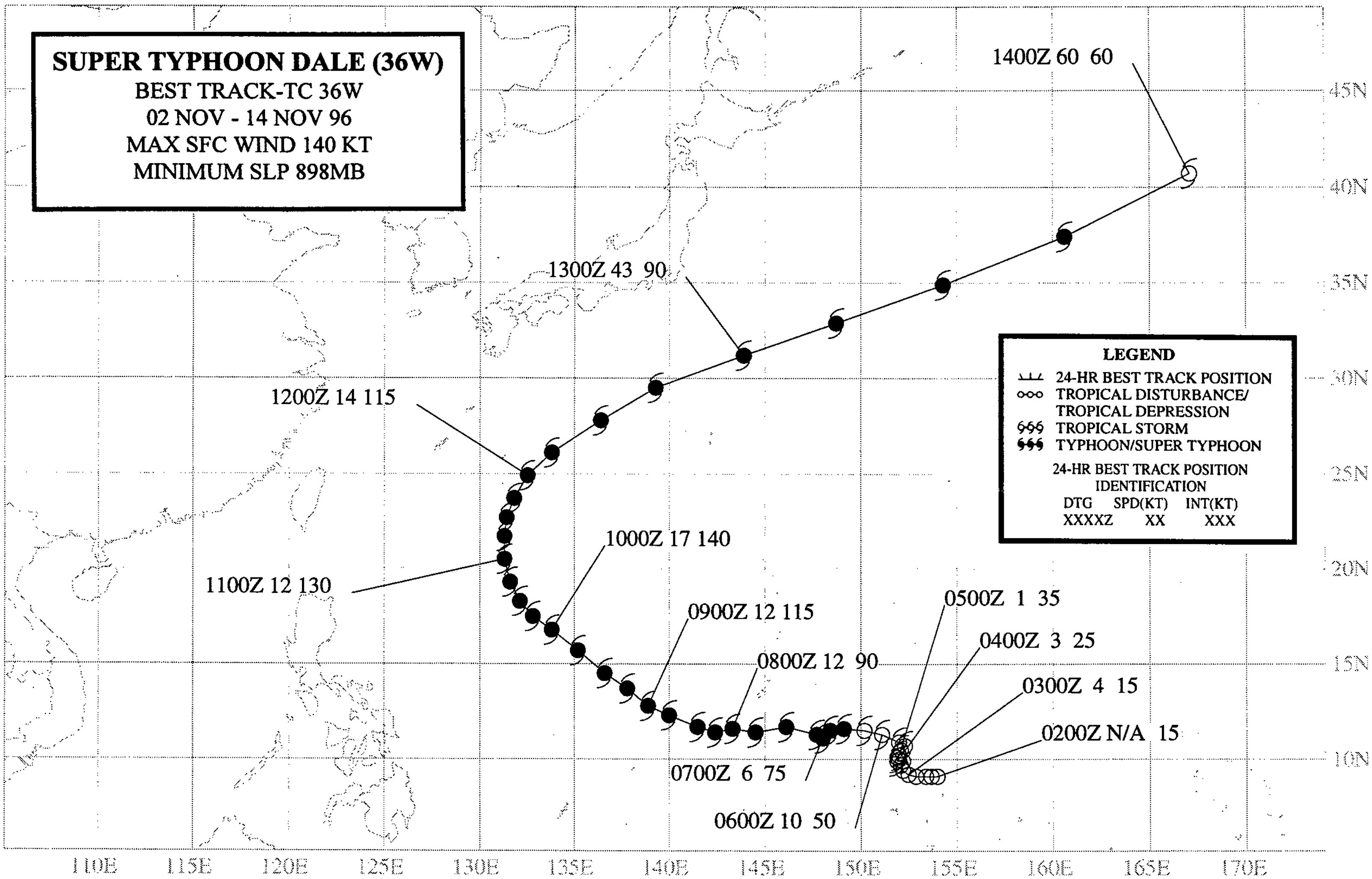
SUPER TYPHOON DALE (36W)
BEST TRACK-TC 36W
02 NOV - 14 NOV 96
MAX SFC WIND 140 KT
MINIMUM SLP 898MB
LEGEND
24-HR BEST TRACK POSITION
TROPICAL DISTURBANCE/
TROPICAL DEPRESSION
TROPICAL STORM
TYPHOON/SUPER TYPHOON
24-HR BEST TRACK POSITION
IDENTIFICATION
DTG SPD(KT) INT(KT)
XXXXZ XX XXX
1400Z 60 60
1300Z 43 90
1200Z 14 115
1100Z 12 130
1000Z 17 140
0900Z 12 115
0800Z 12 90
0700Z 6 75
0600Z 10 50
0500Z 1 35
0400Z 3 25
0300Z 4 15
0200Z N/A 15
45N
40N
35N
30N
25N
20N
15N
10N
110E
115E
120E
125E
130E
135E
140E
145E
150E
155E
160E
165E
170E

SUPER TYPHOON DALE (36W)

I. HIGHLIGHTS

Dale was a large and very intense typhoon that formed at the eastern end of the near-equatorial trough. Its passage resulted in phenomenal seas and surf on Guam's western shore. The equatorial westerly wind burst that preceded Dale's formation was accompanied by very low sea-level pressure reports along the equator. Passing 110 nm to the south of Guam, Dale was observed by Guam's NEXRAD. Dale caused an estimated $3.5 million worth of damage on Guam.

II. TRACK AND INTENSITY

From late October through the first day of November, the tropics of the WNP were dominated by easterly low-level wind and upper-level westerly wind; and, with the exception of the South China Sea, deep convection was disorganized and widely scattered. Beginning on 02 November, the amount of deep convection in the low latitudes of the WNP began to increase in association with lowering pressure throughout Micronesia accompanied by the onset of a near-equatorial trough along 5°N. On 03 November, the deep convection consolidated into two distinct clusters: one centered near 7°N 138°E (which became Ernie (37W)), and the other centered near 8°N 150°E (which became Dale). The pre-Dale cluster of deep convection was first mentioned on the 030600Z November Significant Tropical Weather Advisory when satellite imagery and synoptic data indicated the presence of a cyclonic circulation accompanied by a relatively low central pressure (1002 mb) and extensive divergence aloft (as indicated by animated water-vapor GMS imagery). With a continued fall of the central pressure, and improvements to the satellite cloud signature, a Tropical Cyclone Formation Alert was issued at 031800Z, followed by the first warning on Tropical Depression (TD) 36W, valid at 040600Z.

With an extensive surge in the southwesterly flow to its south and equally strong easterly winds to its north, TD 36W remained nearly stationary for approximately 24 hours while it slowly gained intensity. On the warning valid at 151200Z, TD 36W was upgraded to Tropical Storm Dale based upon satellite intensity estimates of 35 kt (18 m/sec) and a buoy report indicating that the central pressure had fallen below 996 mb (indicative of winds of at least 37 kt on the Atkinson and Holliday (1977) wind-pressure relationship). After becoming a tropical storm, Dale began to move westward, intensified, and became a typhoon at 061800Z. At approximately 071400Z Dale (moving west along 11.5°N) passed 110 nm (205 km) to the south of Guam where peak gusts reached 74 kt (38 m/sec) and high waves inundated some coastal roads and overtopped 100-ft (30-m) sea cliffs (see the Discussion and the Impact sections). Dale came within range of Guam's NEXRAD, which detected winds in excess of 100 kt (51 m/sec) in the lower troposphere (see the Discussion section).

On 09 November, while to the west of Guam in the Philippine Sea, Dale became a super typhoon with a peak intensity of 140 kt (72 m/sec) (Figure 3-36-1). On 10 November, Dale slowed and began a turn toward the north, and on 11 November reached its point of recurvature (i.e., the westernmost longitude). After recurvature, Dale accelerated rapidly to the east-northeast reaching translation speeds in excess of 60 kt (110 km/hr) after 140000Z. The final warning was issued, valid at 131800Z, when completion of extratropical transition was expected within six hours.

III. DISCUSSION

a. *Extremely low equatorial sea-level pressure associated with Dale's formation*

The sea-level pressure (SLP) along the equator has spatial and temporal variations of small

magnitude when compared with the magnitude of the SLP variations at higher latitudes. In the mean, the global equatorial SLP ranges from a maximum of approximately 1015.5 mb in the eastern Atlantic to a minimum of approximately 1008.5 mb in the WNP (Sadler et al. 1987). Lacking the Coriolis effect, and large inertial forces (e.g., centrifugal forces in atmospheric vortices such as typhoons), the pressure gradients on the equator must only be sufficient to drive the wind against friction. As such, a pressure gradient of 1 mb per 1000 km can support a sustained 10-m marine surface wind of 20 kt (10 m/sec). Even the vast easterly wind flow across the tropical Pacific is accompanied by an east-west pressure drop (along the equator) of only 4 mb from the eastern equatorial Pacific to the WNP. Given this background, it is now clear that the very low SLP readings of 1002 mb, and SLP changes of 10 mb along the equator in the WNP during the life of Dale are extraordinary.

While Dale and Ernie (37W) were forming at low-latitude in the WNP, the SLP throughout Micronesia was steadily falling. Even along the equator, to the south of the developing Dale, the SLP steadily fell to extraordinarily low values (Figures 3-36-2 and 3-36-3). On 04 November, several ships near the equator reported a SLP of 1002 mb or less. Values of SLP this low are rarely seen along the equator. Morrissey (1988) examined the SLP reports of ships within two degrees of the equator along a principal north-south shipping lane between 148°E to 152°E. The ship reports used by Morrissey were extracted from the Comprehensive Ocean-Atmosphere Data Set (COADS) for an 80-year (1900-1979) period. From his analysis (Figure 3-36-4), few, if any, SLP reports below 1004 mb are found along the equator in this region. Ironically, approximately 10 days after the very low SLP readings (and after Dale had exited the tropics), the equatorial SLP and the SLP throughout Micronesia rose to exceedingly high values. The SLP of 1013.5 mb on the equator on 14 November was, according to Figure 3-36-4, about as high as the SLP ever gets there.

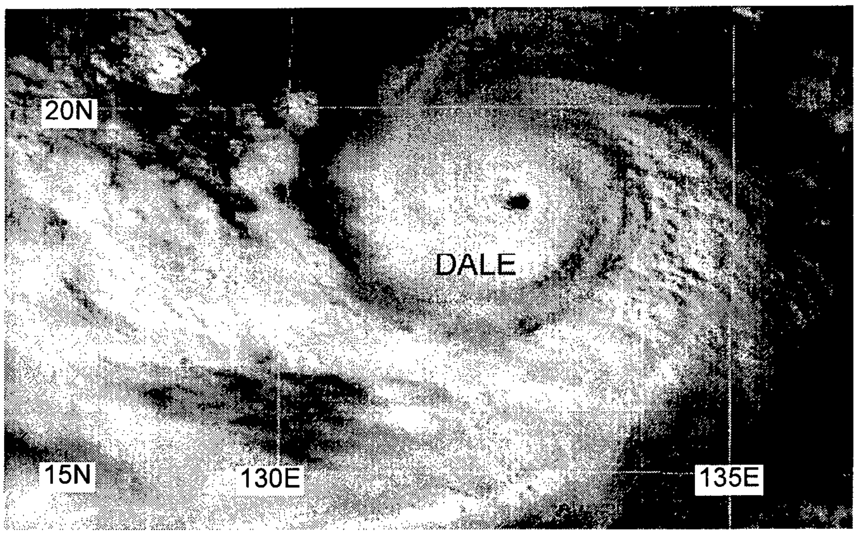

Figure 3-36-1 Dale nears its peak intensity of 140 kt (72 m/sec) (090530Z November visible GMS imagery).

b. Dale as seen by Guam's NEXRAD

On the night of 07 November, Dale passed 110 nm (205 km) to the south of Guam. Guam experienced the peripheral rain bands of Dale, but never entered the eye wall cloud (Figure 3-36-5). For much of the time during Dale's closest point of approach (CPA), Guam remained within a dry wedge between the outer rain bands and the eye wall cloud. The air was laden with salt spray, and some light rain which allowed the NEXRAD to obtain a deep vertical profile of the wind velocity (Figure 3-36-6). The highest winds of approximately 100 kt (51 m/sec), persisted in a layer between about 6,000 and 13,000 ft. At the gradient level (3,000 ft), the NEXRAD detected 75-kt (39-m/sec)

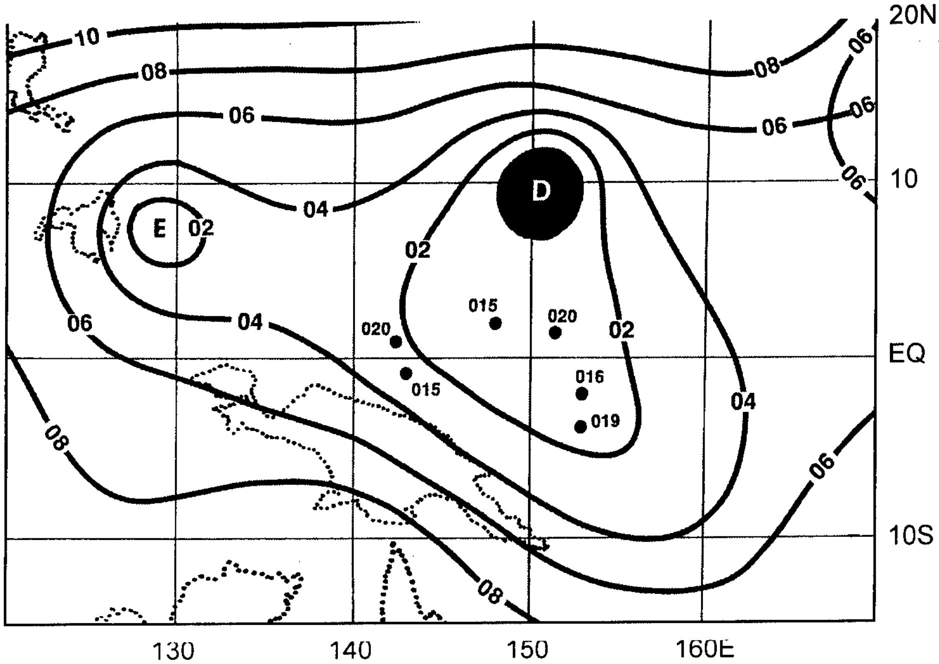

Figure 3-36-2 Sea-level pressure analysis based upon a composite of ship observations at 040600Z and 041800Z November. Individual ships near the equator with reports of 1002 mb or lower are indicated. D = Dale, E = Ernie, and SLP contours are drawn at 2 mb intervals.

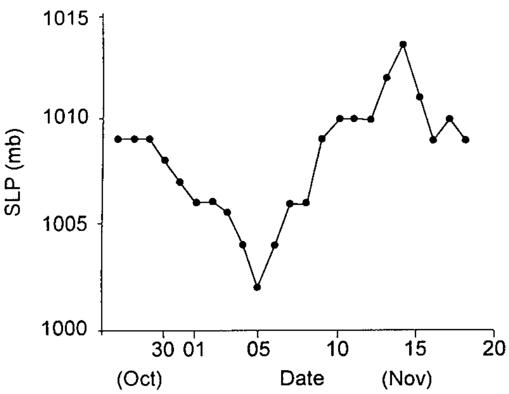

Figure 3-36-3 Time series of the equatorial SLP near 150°E based upon ship observations.

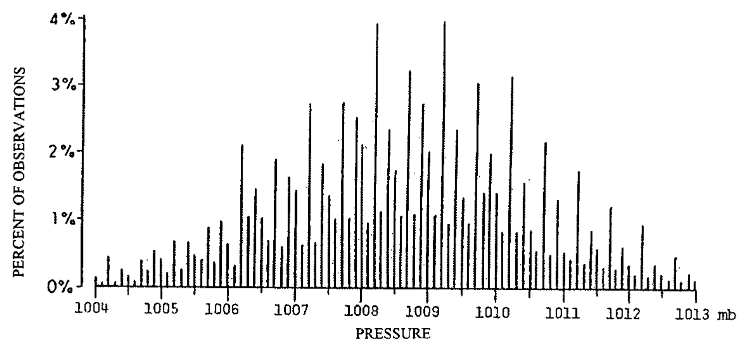

Figure 3-36-4 Histogram of ship SLP reports extracted from the COADS data set in the box bounded by 2°N and 2°S from 148°E to 152°E (adapted from Morrissey, 1988).

Figure 3-36-5 NEXRAD base reflectivity showing the eye, wall cloud and peripheral rain bands of Dale as it nears its CPA to Guam. Guam remained in the dry wedge between the outer rain bands and the eye-wall cloud for an extended period (071458Z NEXRAD base reflectivity product).

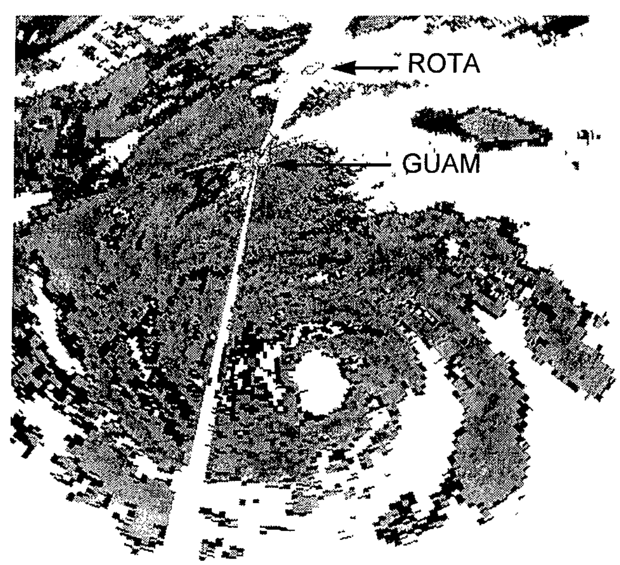

winds (not shown in Figure 3-36-6) which correlated well with the peak gusts observed on Guam (Figure 3-36-7). Although the maximum winds in a typical TC are expected to be at the gradient level, NEXRAD coverage of Dale showed they were considerably higher in altitude. Perhaps the lack of deep convection and associated torrential rain were factors in the relatively elevated level of the wind maximum during Dale's passage by Guam.

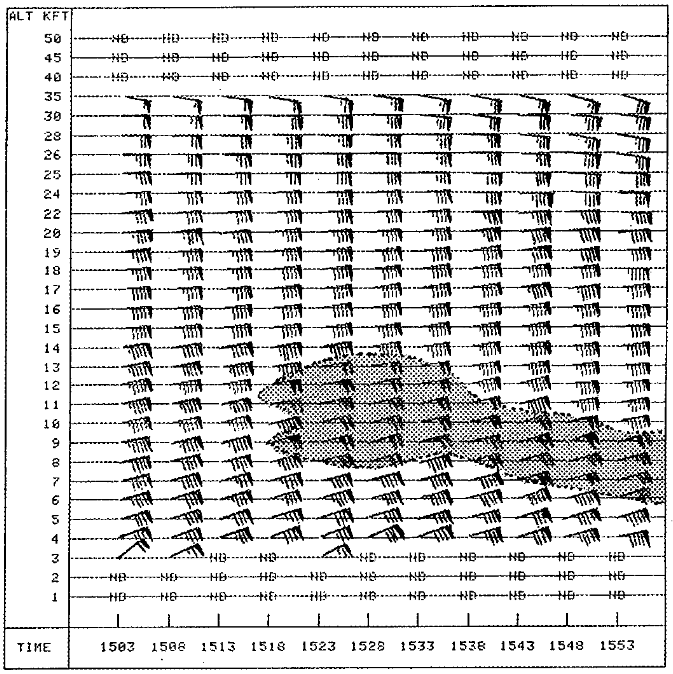

Figure 3-36-6 The NEXRAD velocity azimuth display (VAD) wind profile near the time of Dale's CPA to Guam showing winds of 100 kt (51 m/sec) or more between 6,000 and 12,000 ft (shaded region) (071553Z NEXRAD VAD wind profile product).

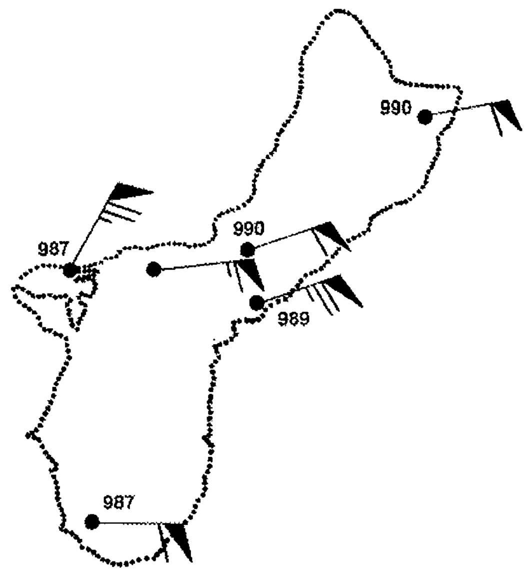

Figure 3-36-7 Peak gusts and minimum SLP recorded at several selected sites on Guam during Dale's passage.

c. *Dale's digital Dvorak (DD) numbers*

The time series of Dale's DD numbers (Figure 3-36-8) peaked at approximately 090600Z with values of approximately T 7.5. After this peak, the DD numbers fell sharply to below T 5.0 by 100000Z. The warning and best-track intensity lag the peak DD numbers by about six hours, and do not reflect the sharp drop in the DD numbers after the peak. As the DD numbers are considered experimental, and are not used operationally, it is not expected that the warning intensity would be strongly tied to them. The DD numbers do, however, often reflect prominent observable changes in the characteristics of the TC. In Dale's case, the rapid drop of the DD numbers after the peak occurred because concentric eye walls formed. At peak intensity, Dale had a well-defined small eye (Figure 3-36-1). When the DD numbers fell, it was because concentric eye walls formed (Figure 3-36-9a, b). The default radius used to define the eye-wall cloud-top temperature in the DD algorithm is 30 nm. This radius fell between the inner and outer eye walls, and resulted in the period of low DD values after the peak. The radius used to define the eye-wall cloud-top temperature is an adjustable parameter on the MIDDAS system, and when set to 10 nm, it was able to measure the inner eye wall. This resulted in DD numbers of about one T number higher than those computed

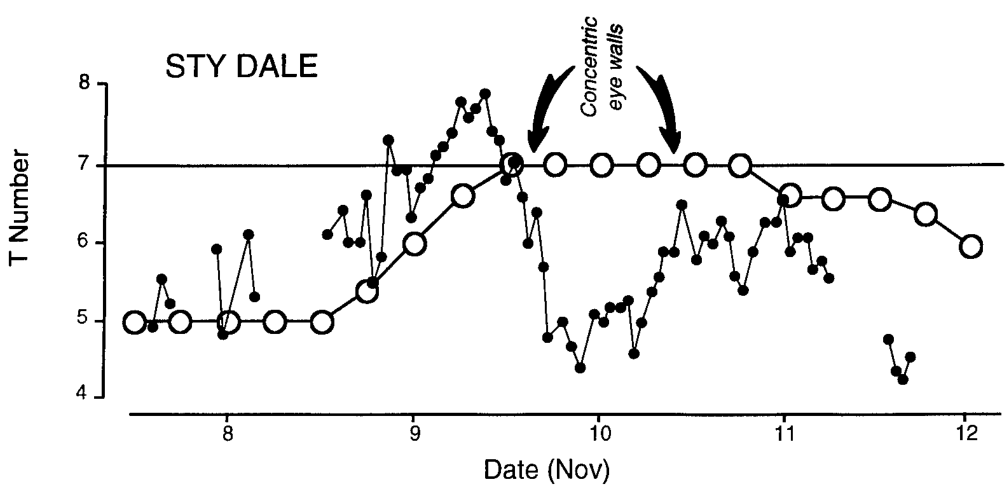

Figure 3-36-8 A time series of Dale's hourly DD numbers (small black dots) compared with the warning intensity converted to a T number (larger open circles at six-hour intervals). The large drop in the DD numbers after the peak was the result of the formation of concentric eye walls.

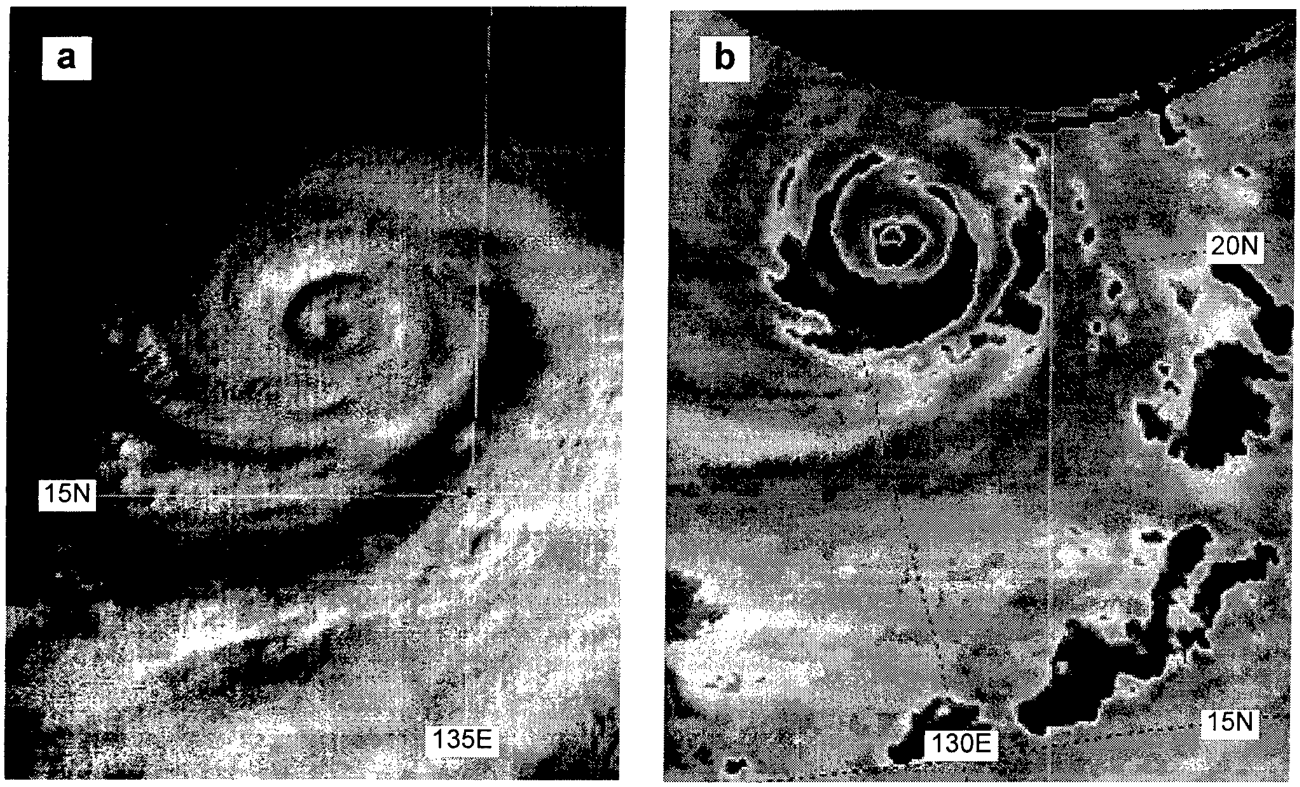

Figure 3-36-9 Dale's concentric eye walls as indicated by (a) visible satellite imagery (092331Z visible GMS imagery), and (b) microwave imagery (110117Z November 85 GHz SSM/I DMSP imagery).

using the default radius during the time when Dale possessed concentric eye walls. The structural changes of Dale show that, though automated, the DD algorithm still requires a satellite analyst to adjust its adaptable parameters and determine the quality of its output.

d. The generation of phenomenal seas in the periphery of a typhoon

While phenomenal surf is common on the eastern shores of Guam when typhoons pass to the south, it is rare that a typhoon produces phenomenal surf on the west side of Guam. Generally, on the north side of a westward moving typhoon, the seas are increased due to the increased wind on that side, but more importantly, due to the artificial fetch that is created as the moving typhoon

keeps up with its own wave train and allows the sea state to rise to its full potential. On the south side of westward-moving typhoons, there is a severe fetch restriction, and the seas can't reach their fully arisen state.

After Dale passed Guam, a very large swell of 20 to 30 feet pounded the western shores of Guam for two days. The wave run-up overtopped 100 ft (30 m) sea cliffs on Orote Point on the west side of Guam (Figure 3-36-10). Such extreme swell from the west is not common on Guam. Even the passage of the large Super Typhoon Yuri only 80-nm south of Guam during November 1991 and the direct eye passage over Guam of the 105-kt (54-m/sec) Omar (1992) did not result in very large westerly swell on Guam. Clearly, some special conditions are required for a typhoon to generate these conditions. Such swell is clearly not directly related to the intensity of the typhoon or even to its size (Yuri was both very intense and very large). It appears that in order for a typhoon to generate phenomenal westerly swell on Guam it must be accompanied by a large region of monsoonal gales extending to its south and west. This was true of Dale and also of the only other typhoon in recent history (Andy, 1989) that was known to have produced phenomenal surf on the west side of Guam. Another phenomenal surf event on the west side of Guam was not produced by a typhoon at all, but by a persistent monsoonal gale area that was associated with a monsoon gyre in the Philippine Sea in 1974.

IV. IMPACT

Dale affected the island of Guam and caused problems for ships at sea. Damage on Guam was mainly caused by high surf, first from the east and later from the west. High surf from the east washed out sections of the coastal road on the southeastern side of the island. Later, surf run-up from the west overtopped 100 ft sea cliffs and damaged Navy housing on Orote Point Naval Activities. Currents and surges inside the reef generated by the west swell also eroded and flooded the beach fronts. Damage estimates for Guam were approximately $3.5 million. Dale also caused damage in the Pulep Atoll, the Hall Islands and several islands of the Chuuk Atoll. The U.S. Coast Guard provided relief supplies to people on these islands. High seas contributed to the loss of the cattle ship, M/V Guernsey Express, enroute for Japan from Australia. Navy helicopters from Guam, USNS Zeus and Kilauea and U.S. Coast Guard search and rescue worked together to rescue the crew of 18 as the ship was sinking.

Figure 3-36-10 Sea water explodes 100 ft into the air as a wave reflecting off the Orote Point cliff line meets an oncoming breaker (Photo courtesy of Major R. Edson).

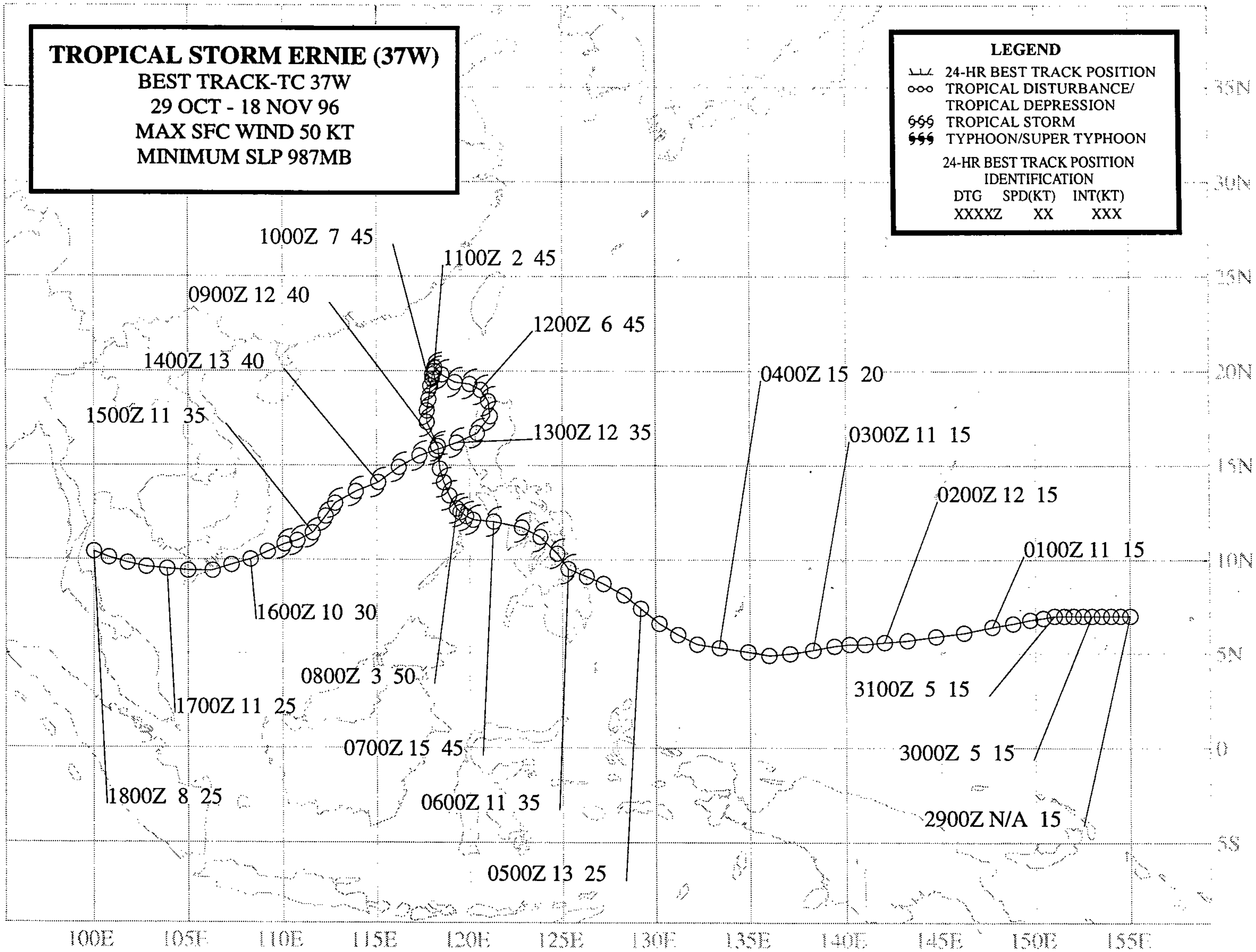

TROPICAL STORM ERNIE (37W)
BEST TRACK-TC 37W
29 OCT - 18 NOV 96
MAX SFC WIND 50 KT
MINIMUM SLP 987MB
LEGEND
24-HR BEST TRACK POSITION
TROPICAL DISTURBANCE/
TROPICAL DEPRESSION
TROPICAL STORM
TYPHOON/SUPER TYPHOON
24-HR BEST TRACK POSITION
IDENTIFICATION
DTG SPD(KT) INT(KT)
XXXXZ XX XXX
1000Z 7 45
1100Z 2 45
0900Z 12 40
1200Z 6 45
1400Z 13 40
1500Z 11 35
1300Z 12 35
0400Z 15 20
0300Z 11 15
0200Z 12 15
0100Z 11 15
1600Z 10 30
0800Z 3 50
1700Z 11 25
3100Z 5 15
0700Z 15 45
3000Z 5 15
1800Z 8 25
0600Z 11 35
2900Z N/A 15
0500Z 13 25
35N
30N
25N
20N
15N
10N
5N
0
5S
100E
105E
110E
115E
120E
125E
130E
135E
140E
145E
150E
155E

TROPICAL STORM ERNIE (37W)

I. HIGHLIGHTS

At the start of the second week of November, four TCs existed simultaneously in the WNP — Ernie, Dale (36W), Tropical Storm (TS) 38W, and Tropical Depression (TD) 39W. Ernie, Dale (36W) and TD 39W formed in the monsoon trough, while TS 38W developed in association with a TUTT cell. After entering the South China Sea, Ernie executed a clockwise loop as it merged with TD 39W. Earlier, while crossing the Philippines, Ernie was responsible for loss of life and extensive property damage.

II. TRACK AND INTENSITY

During the first week of November, a near-equatorial trough formed along approximately 5°N latitude in the WNP. Deep convection associated with this trough consolidated into two distinct systems: the easternmost became Dale (36W) and the westernmost became Ernie. The pre-Ernie tropical disturbance was first mentioned on the 290600Z October Significant Tropical Weather Advisory when satellite imagery and synoptic data indicated that a weak LLCC was associated with an area of persistent deep convection. Development of this disturbance was slow, perhaps hindered by persistent vertical wind shear from the east-northeast, and its transformation into a monsoon depression. Late on 03 November, a small area of deep convection near the core of the monsoon depression persisted; leading to the issuance, valid at 031800Z November, of a TCFA. The first warning on TD 37W followed, valid at 041200Z. Based on satellite intensity estimates, TD 37W was upgraded to Tropical Storm Ernie at 060600Z as the system moved into the central islands of the Philippine archipelago.

On 07 November, Ernie moved into the South China Sea, slowed, and intensified. Satellite imagery indicates that Ernie reached peak intensity of 50 kt (26 m/sec) at 070600Z. As the system reached peak intensity, it made an abrupt turn to the north, perhaps in response to strengthening southwesterly monsoonal flow into Dale (36W) (located to Ernie's east), and also the effects of a binary interaction with TD 39W (which had formed to Ernie's northeast). On 10 November, Ernie subsumed the weakening circulation of TD 39W (Figure 3-37-1) in a merger representing the final stage of a binary interaction (see the Discussion section). After the merger, Ernie executed a clockwise loop which saw the system make landfall in northwestern Luzon before moving back into the South China Sea. As Dale (36W) recurved, Ernie began to move toward the southwest in response to steering influences of a well-entrenched northeast monsoon over the northwestern portion of the South China Sea. In the time span of three and one-half days, Ernie traversed the South China Sea, slowly weakened, and made landfall on the southern tip of Vietnam. The final warning was issued, valid at 170000Z, as the weakened TC moved westward into the Gulf of Thailand and dissipated.

III. DISCUSSION

Merger of Ernie with TD 39W

Ernie and TD 39W underwent a binary interaction that ended in the merger of the two systems. The separation distance between the two systems was always within the 400 nm (740 km) separation threshold noted by Lander and Holland (1993) for TC merger. Though the centroid-relative motion of the two systems shows a clear cyclonic orbit (Figure 3-37-2), only the actual track of TD 39W shows clear signs of orbit. The merger of Ernie with TD 39W was asymmetric in that the smaller TD 39W was sheared and subsumed into the larger circulation of Ernie. Note that even in such cases, the centroid-relative motion of each TC will always be a mirror image of the other's.

IV. IMPACT

In the central Philippines, Ernie was reported to have killed 16 people and caused $US 4.1 million damage to property.

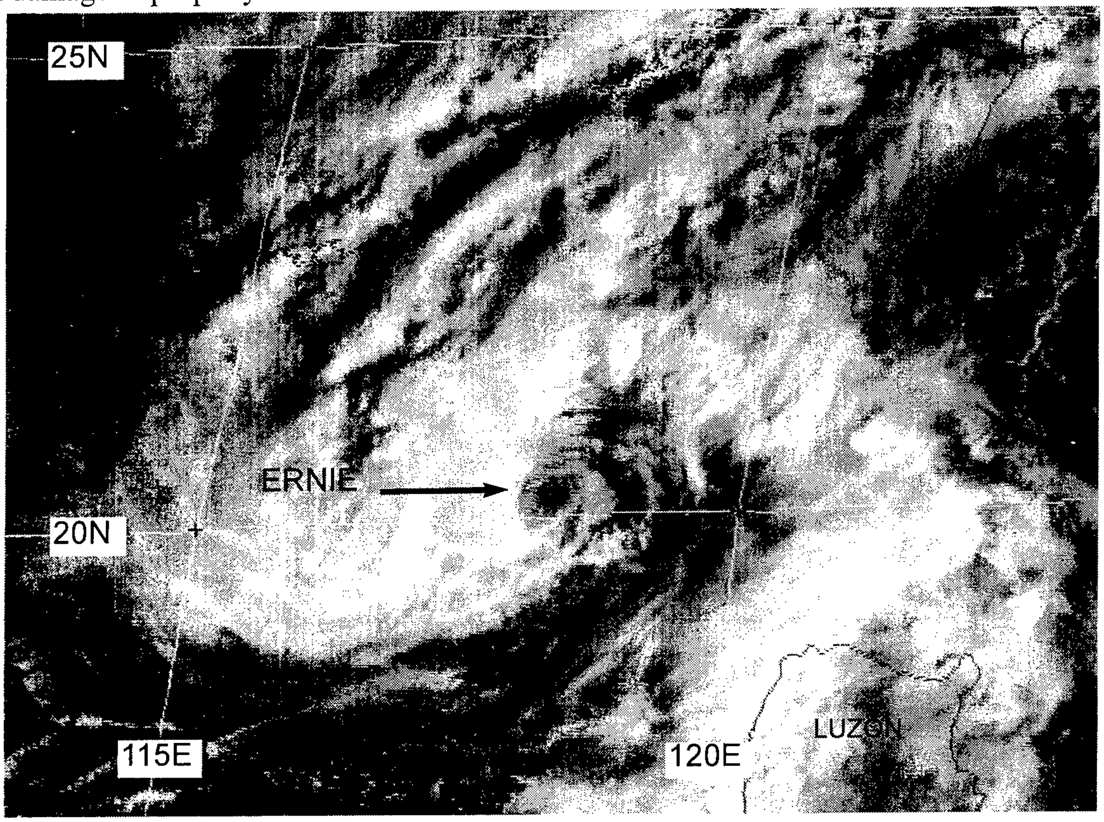

Figure 3-37-1 Tropical Storm Ernie (37W) shortly after its merger with TD 39W. An exposed low-level circulation center is visible (102331Z November visible GMS imagery).

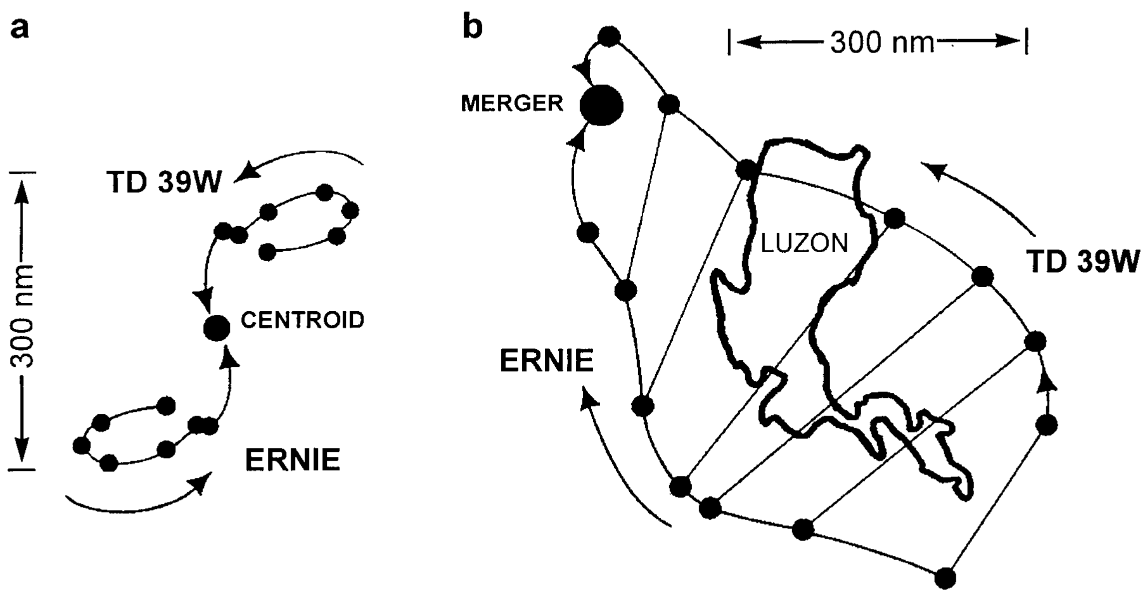

Figure 3-37-2 (a) The complex binary interaction of Ernie with TD 39W is revealed by a diagram of its centroid-relative motion which features a period of anticyclonic relative orbit prior to the period of cyclonic orbit leading to merger. (b) The tracks of these TCs do not as clearly exhibit the properties of the mutual interaction. Dots are at 12-hour intervals beginning at 061200Z November. Merger occurs at 100000Z.

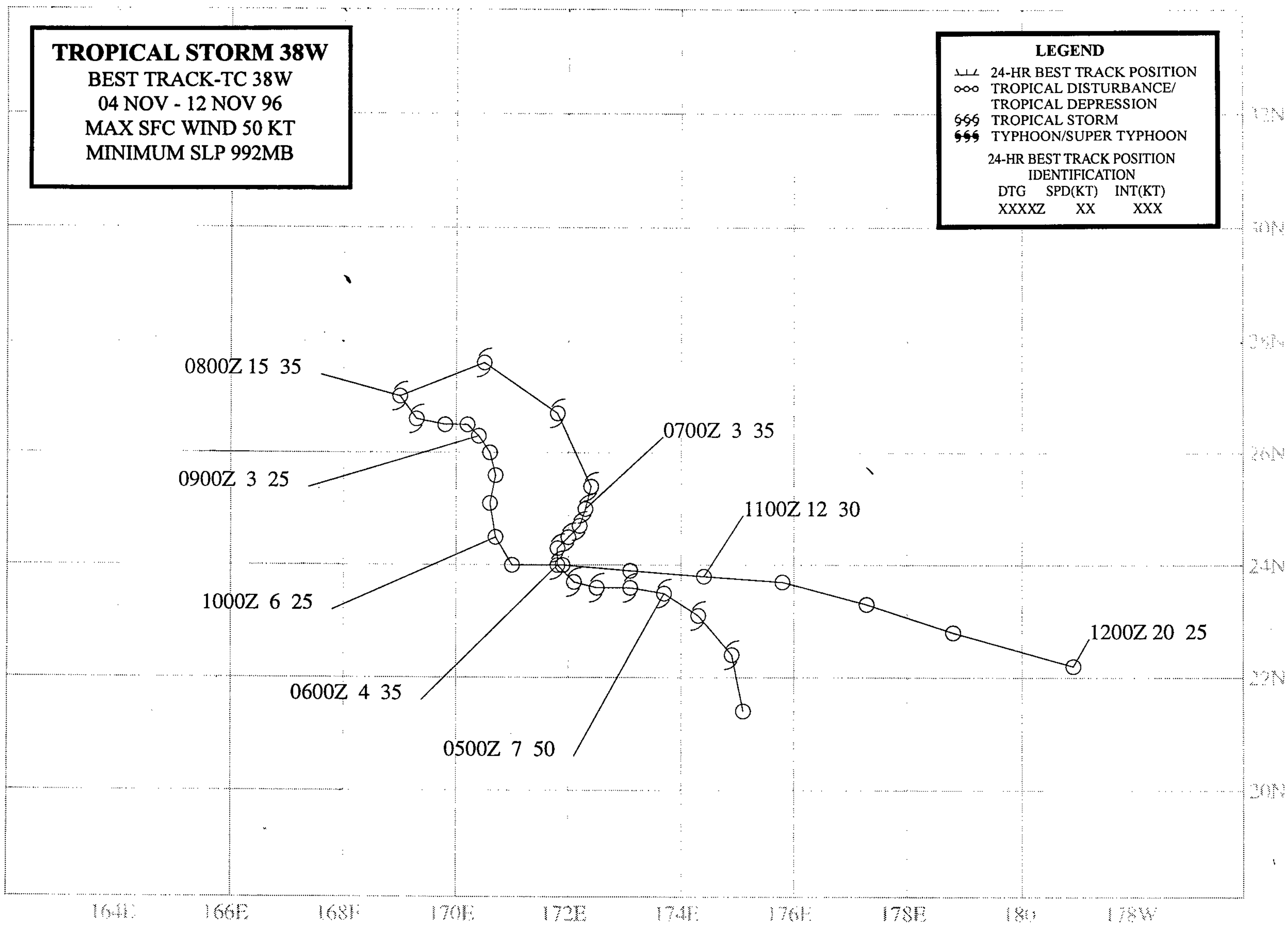
TROPICAL STORM 38W
BEST TRACK-TC 38W
04 NOV - 12 NOV 96
MAX SFC WIND 50 KT
MINIMUM SLP 992MB
LEGEND
24-HR BEST TRACK POSITION
TROPICAL DISTURBANCE/
TROPICAL DEPRESSION
TROPICAL STORM
TYPHOON/SUPER TYPHOON
24-HR BEST TRACK POSITION
IDENTIFICATION
DTG SPD(KT) INT(KT)
XXXXZ XX XXX
0800Z 15 35
0900Z 3 25
1000Z 6 25
0600Z 4 35
0500Z 7 50
0700Z 3 35
1100Z 12 30
1200Z 20 25
26N
24N
22N
20N
166E
168E
170E
172E
174E
176E
178E
180
178W

TROPICAL STORM 38W

I. HIGHLIGHTS

Tropical Storm (TS) 38W was the third unnamed WNP TC of 1996 which was considered in real time to have only been a tropical depression, but was determined in postanalysis to have reached tropical storm intensity. TS 38W was unusual in that it developed in association with a very late-in-the-year TUTT cell. During its 8-day life, TS 38W traced a highly erratic 1500 nm (2800 km) track, but it ultimately dissipated only 180 nm (335 km) from where it was first detected.

II. TRACK AND INTENSITY

While Dale (36W) and Ernie (37W) were developing east of the Philippines on 04 November, the tropical disturbance which became TS 38W was first detected as a circulation which formed in direct association with an unusually late-in-the-year TUTT cell. This disturbance was first mentioned on the 040600Z November Significant Tropical Weather Advisory. As cloud organization continued to improve, a TCFA was issued valid at 050600Z. The first warning on Tropical Depression 38W, valid at 060600Z, was prompted by the detection on the ERS-2 scatterometry data of 30-kt (15-m/sec) winds in association with a well-defined LLCC (Figure 3-38-1). In postanalysis, a reassessment of ship, microwave, scatterometer, and conventional visible and infrared satellite data revealed the need to upgrade the peak intensity of the tropical depression to an unnamed tropical storm (see the Discussion). The final warning was issued, valid at 080600Z, when all the deep convection sheared away to the northeast leaving the LLCC completely exposed.

Tropical Storm 38W exhibited a highly erratic track during its life over open water at relatively high latitude near the international date line. The erratic motion featured initial northwestward motion, followed by a counterclockwise loop, and finally (as the system dissipated) a two day period of eastward motion. The end result of the erratic motion was 1500 nm (2800 km) of total distance covered, but an end point only 180 nm (335 km) removed from the place of origin.

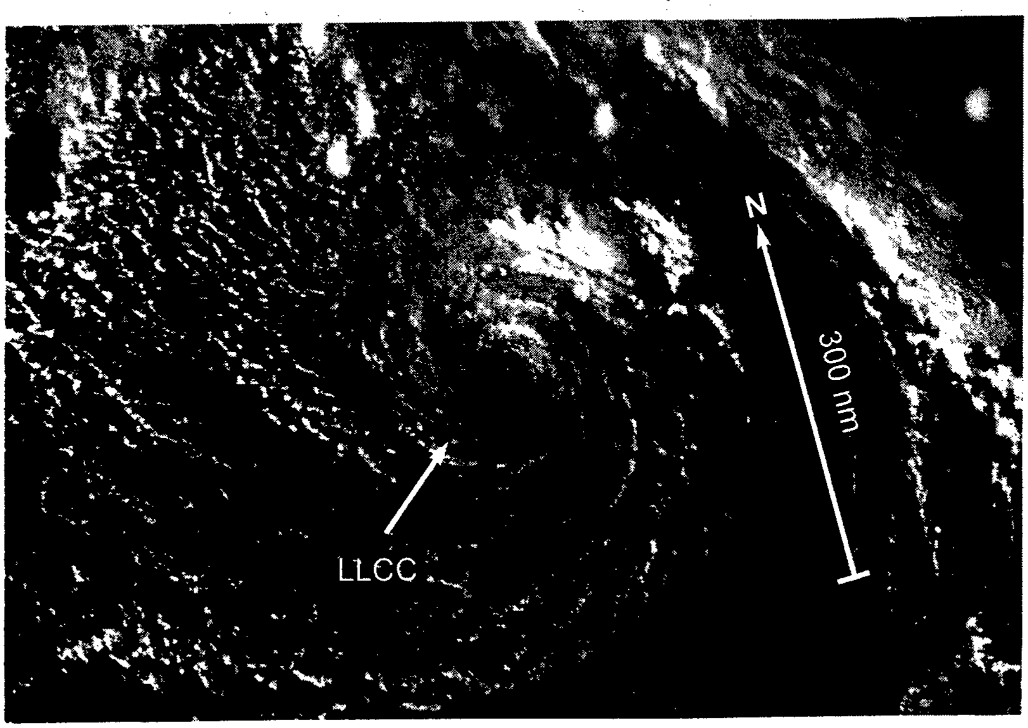

Figure 3-38-1 Tightly wound low-level cloud lines describe the well defined LLCC of TS 38W (060426Z November visible GMS imagery).

III. DISCUSSION

Postanalysis upgrade from tropical depression to tropical storm

Because of an unconventional structure for a TC (a large well-defined LLCC with most of the deep convection displaced a few hundred kilometers to the northeast — a structure common to many TUTT cell-related TCs, and also to subtropical cyclones) (Figure 3-38-1), the real-time satellite intensity estimates for TS 38W were only 25-30 kt (12-15 m/sec). A ship report at 050000Z with a pressure of 997 mb and a 50-kt (26-m/sec) north-northwesterly wind was considered suspect in real time. In postanalysis however, scatterometer data, microwave and visible satellite imagery were reassessed and judged to be supportive of an upgrade of TD 38W to a tropical storm. At 041200Z and 081200Z, ERS-2 scatterometer data showed a maximum wind speed of 35 kt (18 m/sec) near the LLCC of the system. The SSM/I at 050700Z (Figure 3-38-2) and visible satellite data at 060426Z (Figure 3-38-1) both confirmed that the TC possessed a very well organized and tightly wound LLCC that made plausible the 50-kt (26-m/sec) ship report. Additional features on the satellite imagery, including the "herringbone" pattern of the low-level cumulus extending outward from the LLCC on the northern semicircle indicated near-gale force winds in that area, also supported an increased intensity estimate. Hence TD 38W became TS 38W in postanalysis — the third such occurrence during 1996. Use of new satellite technologies (e.g., scatterometry and microwave imagery) and new understanding of TC structure have made such upgrades more common than in the past. The hope is to refine satellite applications to the point where more accurate assessments can be made in real time.

IV. IMPACT

No reports of damage or injuries were received at the JTWC.

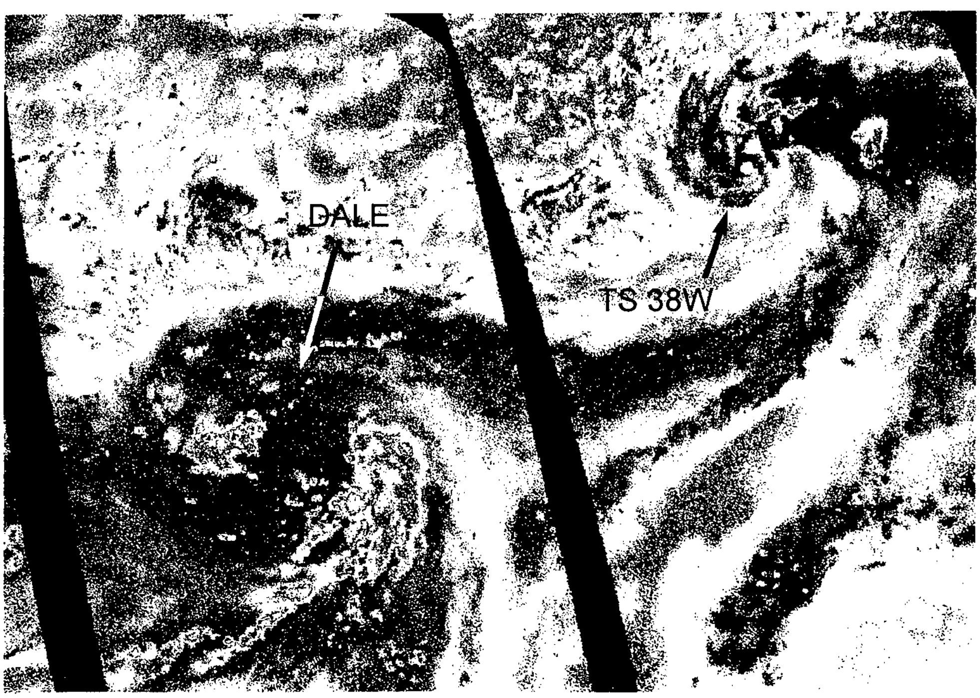

Figure 3-38-2 A mosaic of successive passes of 85-GHz horizontally polarized microwave imager data showing the circulations of Dale (36W) and TS 38W. Note the tight wrap of the low and middle cloud associated with TS 38W (Mosaics of 85-GHz horizontally polarized microwave DMSP imagery - the easternmost pass over TS 38W was dated 050715Z November).

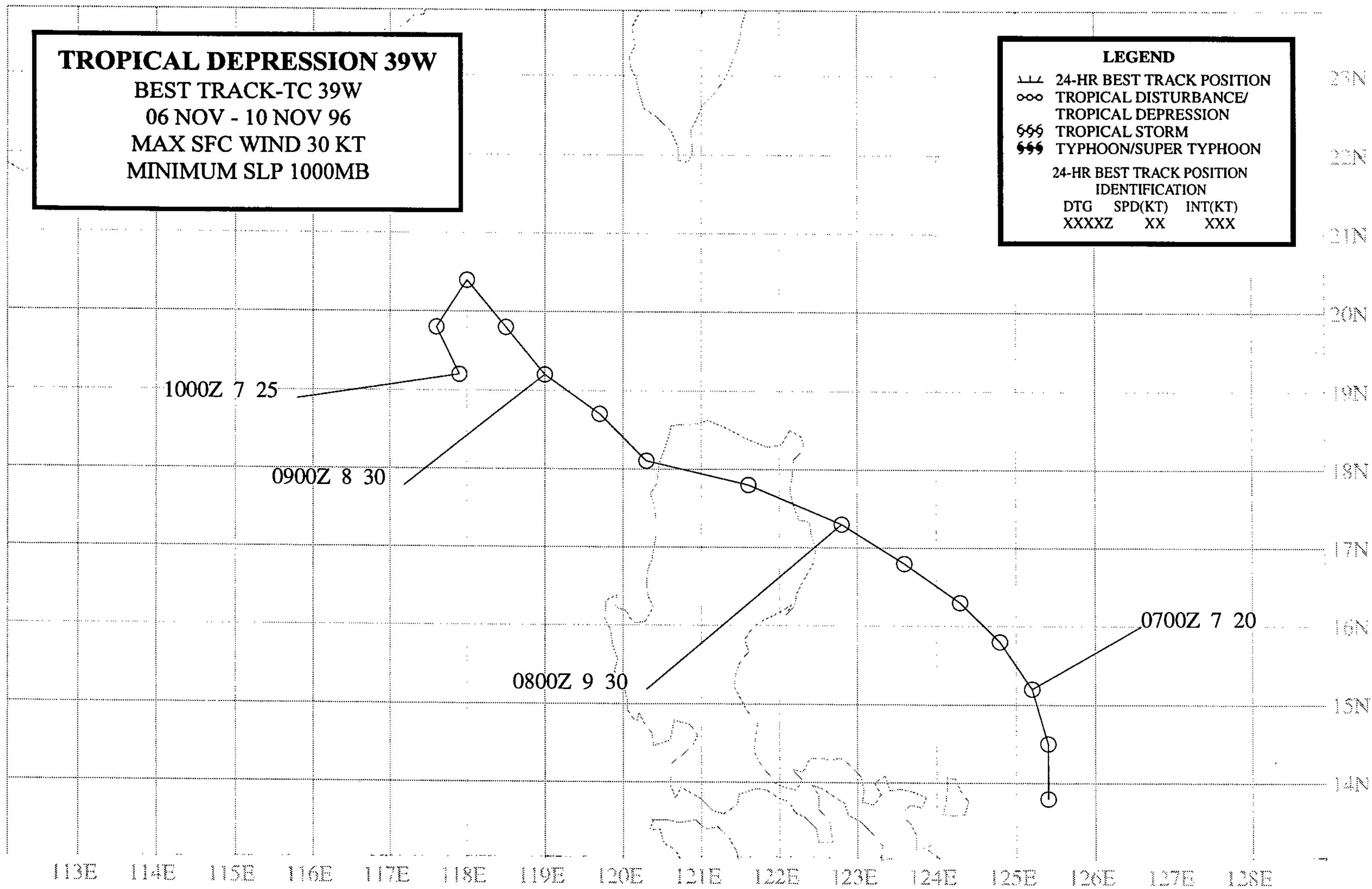

TROPICAL DEPRESSION 39W
BEST TRACK-TC 39W
06 NOV - 10 NOV 96
MAX SFC WIND 30 KT
MINIMUM SLP 1000MB
LEGEND
24-HR BEST TRACK POSITION
TROPICAL DISTURBANCE/
TROPICAL DEPRESSION
TROPICAL STORM
TYPHOON/SUPER TYPHOON
24-HR BEST TRACK POSITION
IDENTIFICATION
DTG SPD(KT) INT(KT)
XXXXZ XX XXX
1000Z 7 25
0900Z 8 30
0800Z 9 30
0700Z 7 20
23N
22N
21N
20N
19N
18N
17N
16N
15N
14N
113E
114E
115E
116E
117E
118E
119E
120E
121E
122E
123E
124E
125E
126E
127E
128E

TROPICAL DEPRESSION 39W

Tropical Depression (TD) 39W formed in the monsoon trough which extended eastward from Ernie (37W) across the central Philippines and into the Philippine Sea. When satellite imagery indicated that deep convection was becoming better organized east of Luzon, and satellite and ship reports indicated the presence of a LLCC associated with this area of deep convection, the tropical disturbance which became TD 39W was first mentioned on the 070600Z November Significant Tropical Weather Advisory. As the system tracked northwestward toward Luzon, a TCFA was issued at 080630Z. The TCFA was quickly superseded by the first warning, valid at 080600Z, and was based on ship wind reports of 25 kt (12 m/sec) and sea-level pressure reports near 1000 mb from land stations on the northeast coast of Luzon. The system tracked over the northern tip of Luzon and entered the South China Sea off the northwest tip of Luzon while retaining its peak intensity of 30 kt (15 m/sec). The final warning on TD 39W was issued, valid at 090600Z, as the system began to weaken while undergoing a binary interaction with Ernie (37W) (Figure 3-39-1; also see Figure 3-37-2 in Ernie's summary for a graphical depiction of the binary interaction of TD 39W with Ernie (37W)). On 10 November, the remnants of TD 39W were absorbed by the circulation of Ernie. No reports of damage or injuries were received at the JTWC.

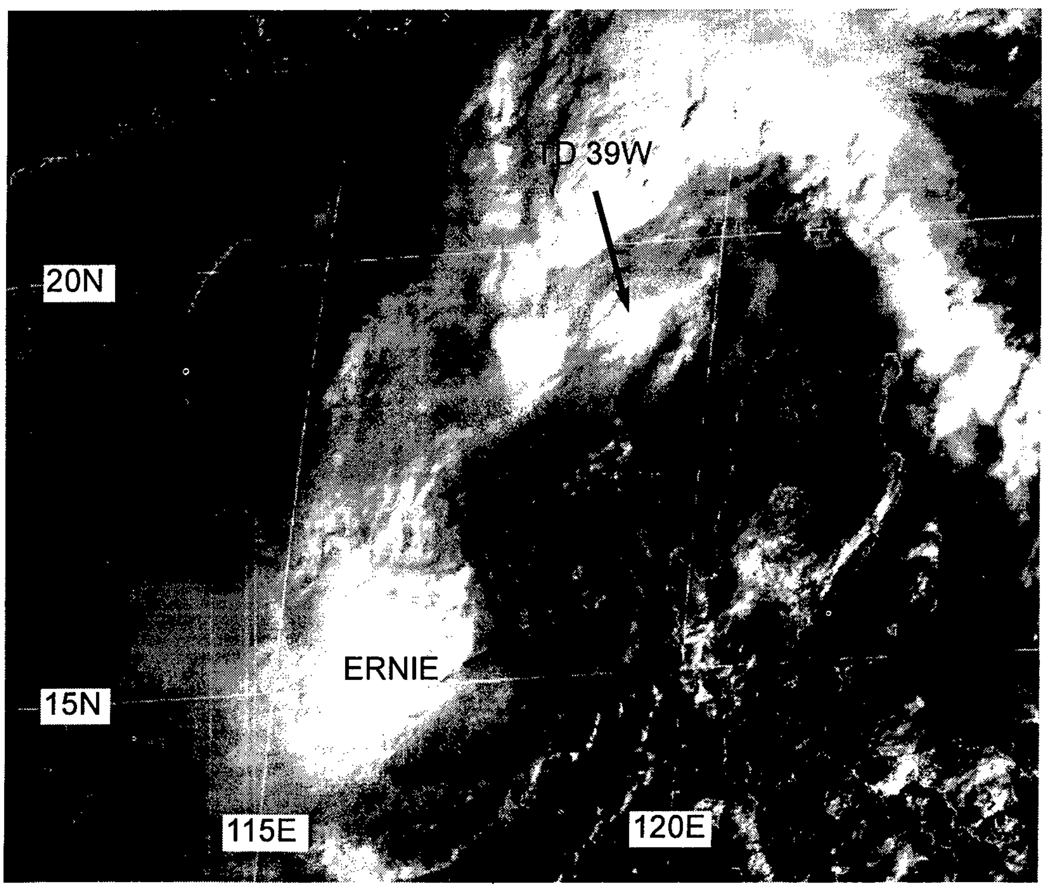

Figure 3-39-1 TD 39W and Ernie (37W) are approaching one another as they undergo a binary interaction (090033Z November visible GMS imagery).

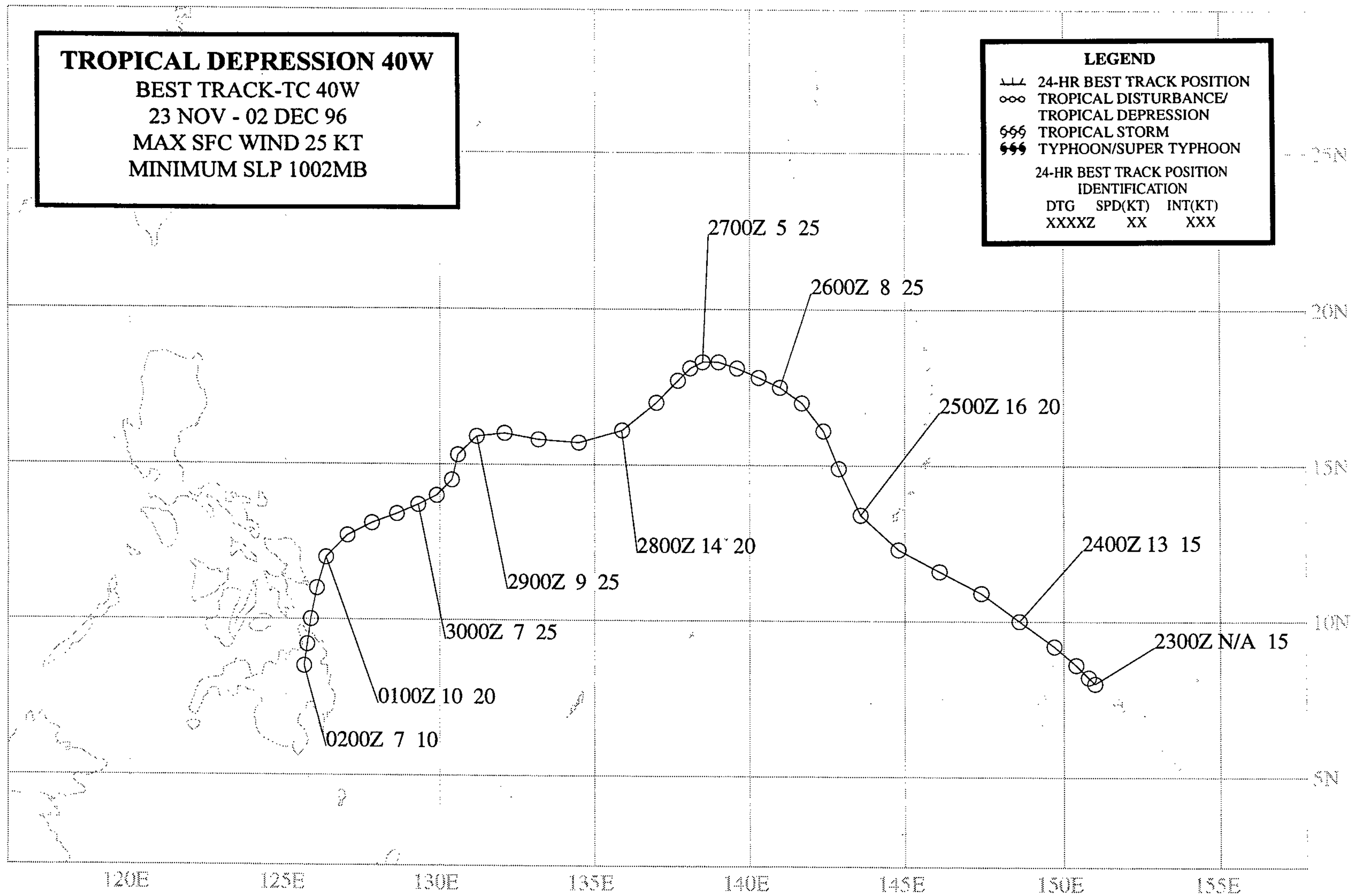
TROPICAL DEPRESSION 40W
BEST TRACK-TC 40W
23 NOV - 02 DEC 96
MAX SFC WIND 25 KT
MINIMUM SLP 1002MB
LEGEND
24-HR BEST TRACK POSITION
TROPICAL DISTURBANCE/
TROPICAL DEPRESSION
TROPICAL STORM
TYPHOON/SUPER TYPHOON
24-HR BEST TRACK POSITION
IDENTIFICATION
DTG SPD(KT) INT(KT)
XXXXZ XX XXX
2700Z 5 25
2600Z 8 25
2500Z 16 20
2800Z 14 20
2900Z 9 25
2400Z 13 15
3000Z 7 25
2300Z N/A 15
0100Z 10 20
0200Z 7 10
25N
20N
15N
10N
5N
120E
125E
130E
135E
140E
145E
150E
155E

TROPICAL DEPRESSION 40W

After Dale (36W) recurved, and Ernie (37W) moved into the South China Sea, the WNP experienced a break in TC activity. Overall sea-level pressures rose across the WNP tropics and light winds dominated the low latitudes. The break was short- lived, however, as increased convection soon spread across Micronesia and a large monsoon depression developed there. On 23 November, the monsoon depression was centered near Chuuk, and its growing size and increasing organization prompted its first mention on the 231800Z Significant Tropical Weather Advisory. The system drifted northwestward toward Guam, and continued consolidation and organization of the deep convection (Figure 3-40-1) prompted the JTWC to issue a TCFA at 241430Z. This was followed by the first warning on Tropical Depression (TD) 40W, valid at 250000Z. The northwestward motion of TD 40W continued until 27 November when the TC encountered a region of enhanced northeasterly low-level flow associated with an approaching shear line. Interaction with the shear line resulted in a track change to the southwest. As vertical wind shear increased, TD 40W weakened and a "final" warning was issued valid at 270000Z. Two days later, however, deep convection redeveloped within the LLCC and a "regenerated" warning followed, valid at 290000Z. The renewed deep convection did not last long — dissipation ensued and the final warning was issued valid at 010000Z December. On 02 December, the remnants of TD 40W dissipated over Mindanao, but not before unleashing torrential rains on Catanduenas province in the Philippines. Landslides resulting from this heavy precipitation were responsible for at least 14 deaths.

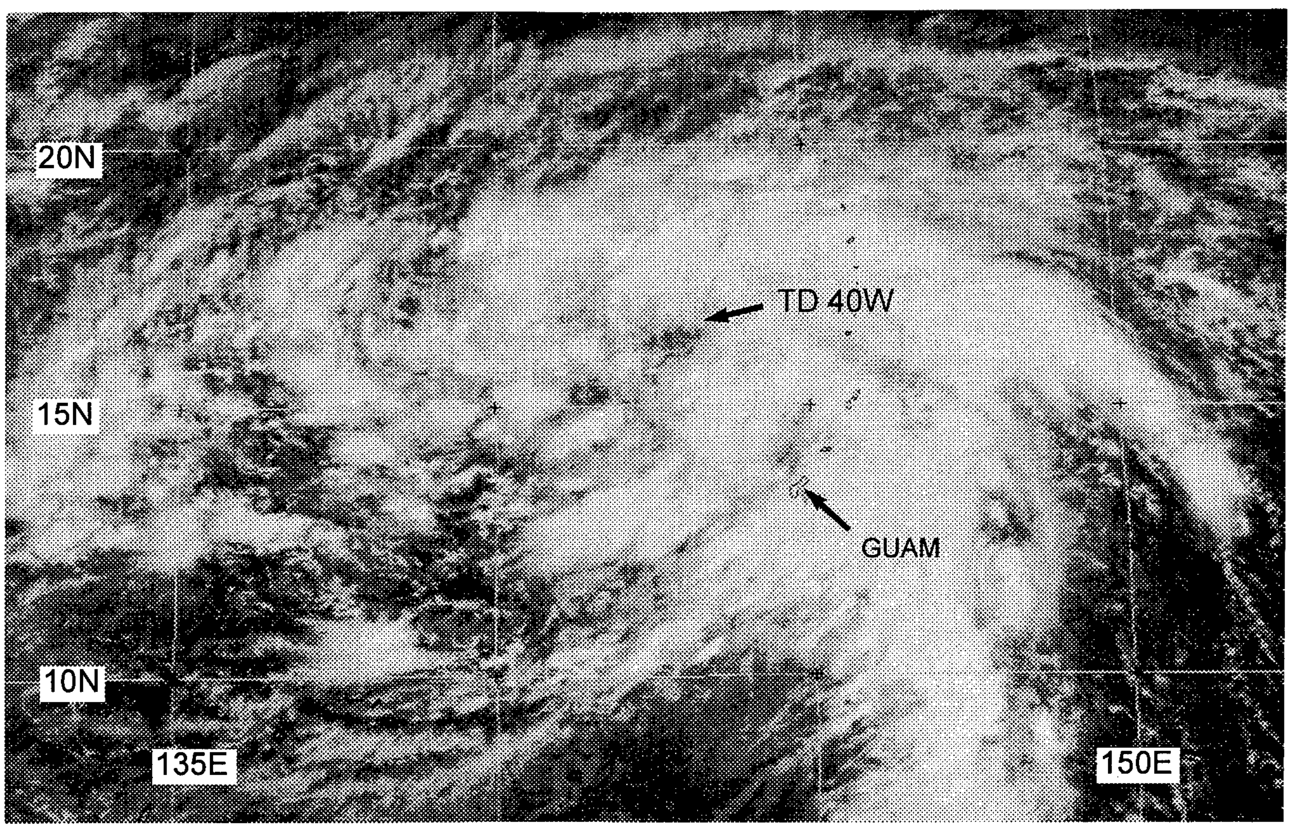

Figure 3-40-1 The monsoon depression which became TD 40W organizes its deep convection near Guam just prior to the first warning (242330Z November visible GMS imagery).

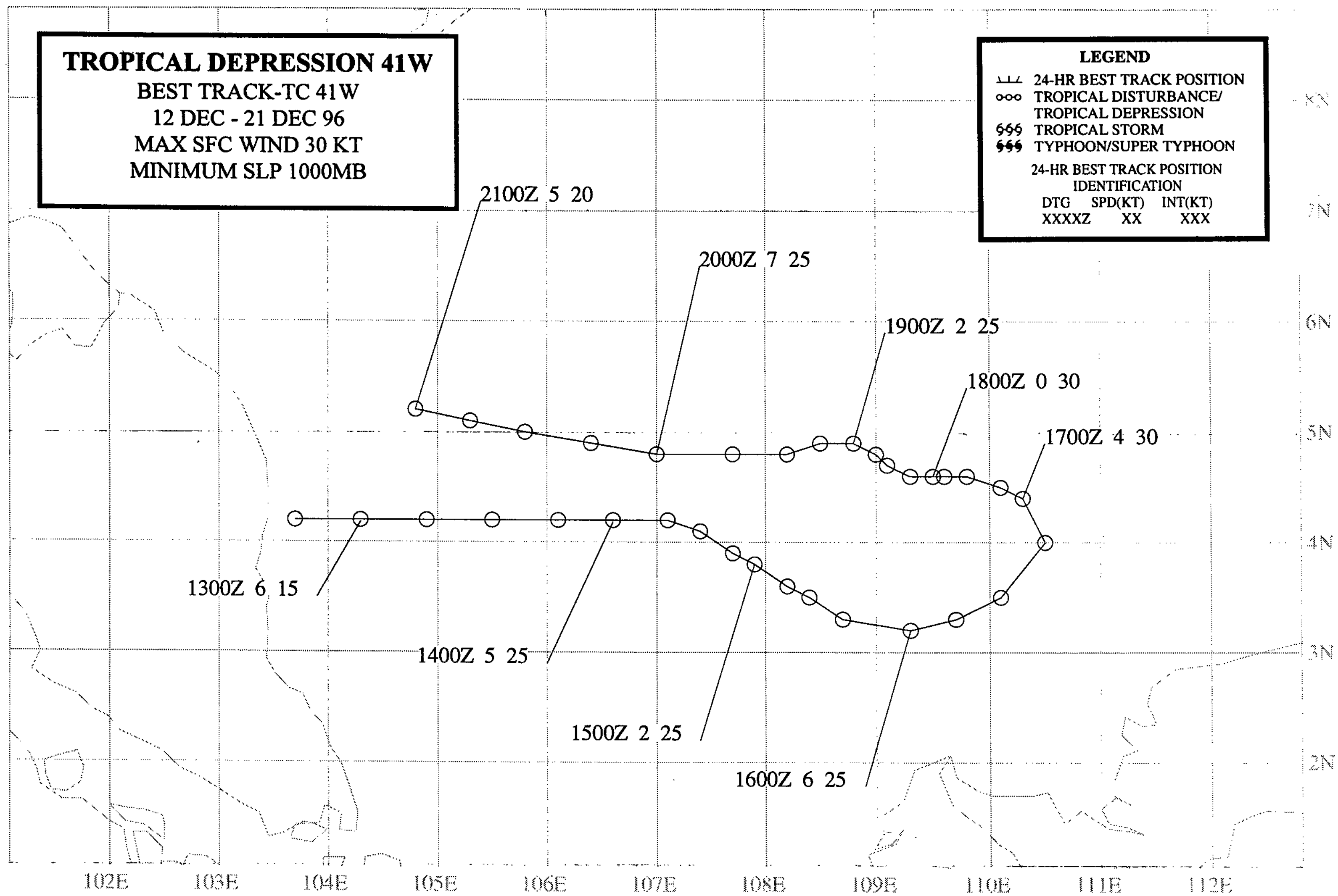

TROPICAL DEPRESSION 41W
BEST TRACK-TC 41W
12 DEC - 21 DEC 96
MAX SFC WIND 30 KT
MINIMUM SLP 1000MB
LEGEND
24-HR BEST TRACK POSITION
TROPICAL DISTURBANCE/
TROPICAL DEPRESSION
TROPICAL STORM
TYPHOON/SUPER TYPHOON
24-HR BEST TRACK POSITION
IDENTIFICATION
DTG SPD(KT) INT(KT)
XXXXZ XX XXX
2100Z 5 20
2000Z 7 25
1900Z 2 25
1800Z 0 30
1700Z 4 30
1300Z 6 15
1400Z 5 25
1500Z 2 25
1600Z 6 25
8N
7N
6N
5N
4N
3N
2N
102E
103E
104E
105E
106E
107E
108E
109E
110E
111E
112E

TROPICAL DEPRESSION 41W

After Tropical Depression 40W dissipated over the southern Philippines, there was a break in TC activity in the WNP until 10 December, when an area of deep convection became persistent in the South China Sea. On 13 December, synoptic data indicated a weak LLCC (located east of the Malay peninsula) was associated with this area of deep convection. The system moved eastward along the northern edge of a equatorial westerly wind burst (WWB) (Figure 3-41-1). Based upon synoptic data indicating a well-defined LLCC with maximum sustained wind speeds of 25 kt (13 m/sec), the first warning on Tropical Depression (TD) 41W was issued, valid at 140600Z December. Remarks on the first warning included:

" . . . The low-level circulation is in an area of convergence between the northeasterly monsoon and an equatorial westerly wind burst. Development is being aided by this strong WWB. . ." The strength and depth of the WWB to the south of TD 41W appeared to be the dominant steering mechanism, and TD 41W moved eastward until 16 December when the TC approached the northwest coast of Borneo. Here, the TC gradually turned northward and then westward as it came under the steering influence of the northeast monsoon. After doubling back toward the Malay peninsula, the TC continued westward and dissipated on 21 December when located near the location where it formed a week earlier. Strong upper-level easterlies persisted throughout the lifetime of TD 41W, and the resultant vertical wind shear likely limited the intensity of TD 41W to its peak of 30 kt (15 m/sec).

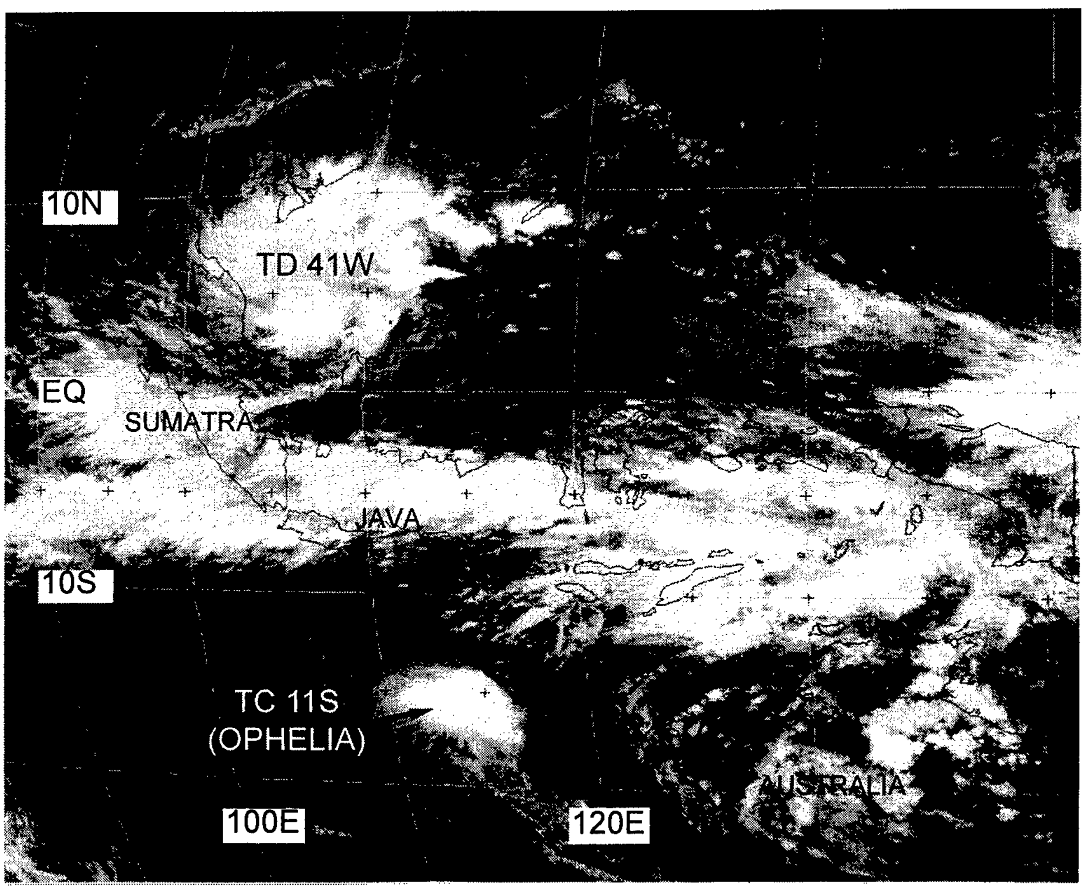

Figure 3-41-1 An extensive east-west cloud band associated with a equatorial WWB separates TD 41W (located in the South China Sea) and TC 11S (Ophelia) located in the Southern Hemisphere to the south of Java (170531Z December infrared GMS imagery).

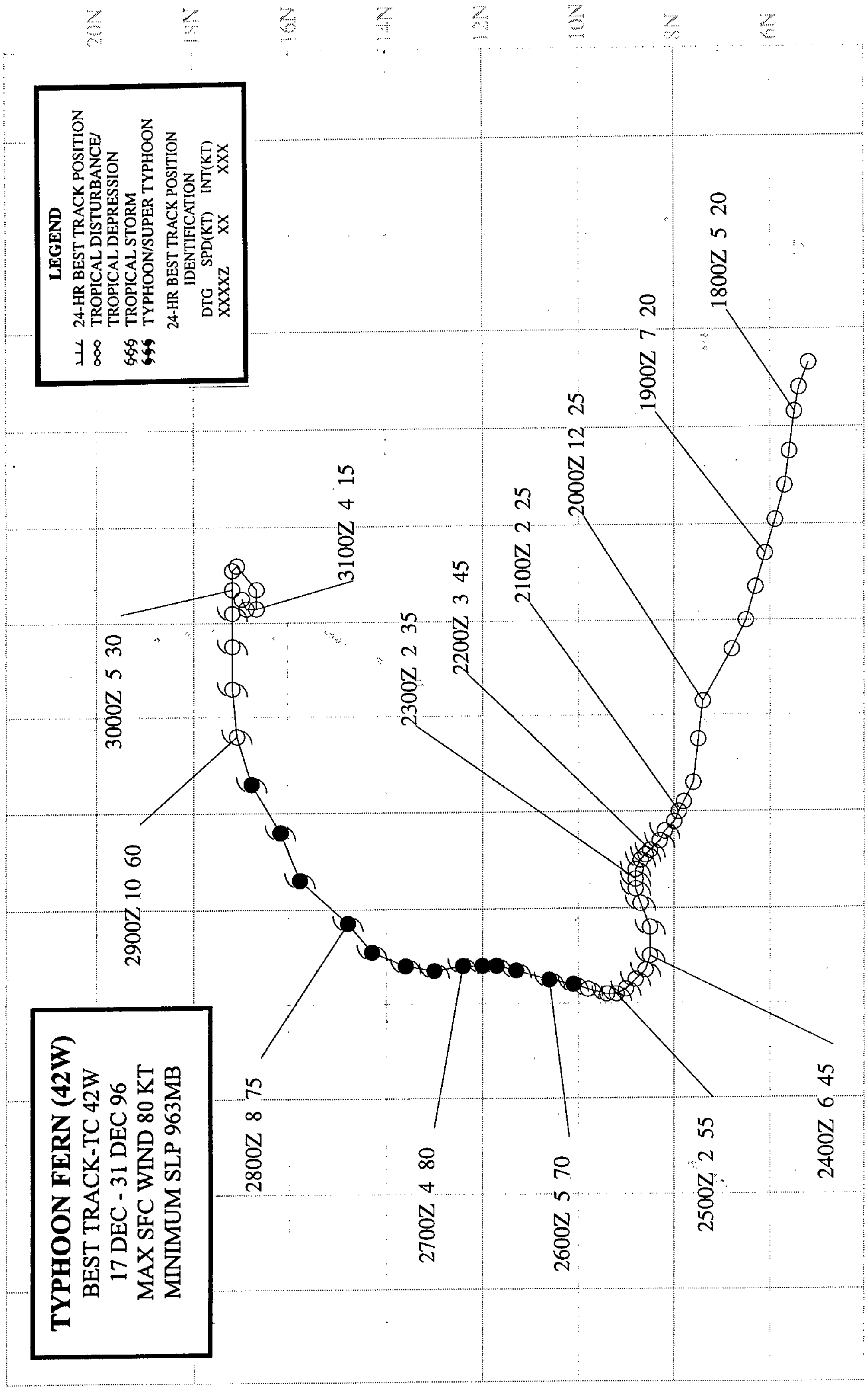
TYPHOON FERN (42W)
BEST TRACK-TC 42W
17 DEC - 31 DEC 96
MAX SFC WIND 80 KT
MINIMUM SLP 963MB
LEGEND
24-HR BEST TRACK POSITION
TROPICAL DISTURBANCE/
TROPICAL DEPRESSION
TROPICAL STORM
TYPHOON/SUPER TYPHOON
24-HR BEST TRACK POSITION
IDENTIFICATION
DTG SPD(KT) INT(KT)
XXXXZ XX XXX
1800Z 5 20
1900Z 7 20
2000Z 12 25
2100Z 2 25
2200Z 3 45
2300Z 2 35
2400Z 6 45
2500Z 2 55
2600Z 5 70
2700Z 4 80
2800Z 8 75
2900Z 10 60
3000Z 5 30
3100Z 4 15
20N
18N
16N
14N
12N
10N
8N
6N
132E
134E
136E
138E
140E
142E
144E
146E
148E
150E
152E
154E
156E

TYPHOON FERN (42W)

I. HIGHLIGHTS

The last typhoon of 1996, Fern formed at low latitude in association with a strong equatorial westerly wind burst (WWB). While passing over Yap, strong winds and torrential rains caused property damage and personal injury. Eight people were rescued at sea when high seas and winds crippled the cargo vessel, "Mister Bill", while it was enroute from Guam to Yap.

II. TRACK AND INTENSITY

During the second half of December, twin low-latitude monsoon troughs became established between approximately 100°E and 170°E. A band of low-level westerly winds persisted between the two trough axes. A total of five TCs — two in the Northern Hemisphere (Fern and Greg (43W)), and three in the Southern Hemisphere (Ophelia (11S), Phil (12P), and Fergus (13P)) — formed along the respective monsoon trough axis (see Figure 3-43-1 in Greg's (43W) summary).

On 14 December, deep convection began to increase along the equator between approximately 140°E and 160°E in association with an intensifying WWB. A poorly defined LLCC located south-southeast of Guam was noted on the 190600Z December Significant Tropical Weather Advisory. Moving slowly westward, this disturbance remained poorly defined until 21 December when an area of deep convection began to consolidate near a LLCC. Low sea-level pressure (SLP) of 1001 mb and evidence of upper-level divergence over the LLCC (on animated water vapor imagery) prompted the JTWC to issue a TCFA at 211500Z December. The first warning on Tropical Depression (TD) 42W, valid at 211800Z, soon followed based on synoptic data indicating falling SLP in the developing TC (998 mb at 211800Z). Six hours later, on the warning valid at 220000Z, TD 42W was upgraded to Tropical Storm (TS) Fern based on satellite and synoptic data. For the next two days, TS Fern moved slowly westward and remained near minimal TS intensity. On 24 December, the tropical storm turned northward and slowly approached Yap. On Christmas day, Fern passed over Yap (Figure 3-42-1a,b), where SLP fell to 983 mb and a peak wind gust of 63 kt (32 m/sec) was recorded at the Weather Service Office (WMO 91415) (Figure 3-42-2a,b). For several hours peak wind gusts in excess of 50 kt (26 m/sec) on Yap occurred in the westerly flow as Fern moved away to the north. Fern became a typhoon at 251800Z approximately 12 hours after passing over Yap. Continuing to move slowly north for the next three days on the north-oriented portion of its track, Fern reached its peak intensity of 80 kt (41 m/sec) at 261200Z. Reaching peak intensity after turning northward is a common behavior of TCs in north-oriented patterns (see the Discussion). On 28 December, Fern encountered a strong shear line in the low levels and, located within deep-layer westerly steering flow to the north of the subtropical ridge, it began to move toward the east-northeast and weaken. Fern gradually dissipated as it moved eastward along the shear line, and the final warning was issued valid at 300600Z December.

III. DISCUSSION

Peak intensity after recurvature

Most typhoons that undergo classical recurvature (i.e., a roughly "<"-shaped track which features initial steady west-northwestward motion, then a northward turn while slowing, followed by an acceleration toward the northeast) reach peak intensity at, or before, the point of recurvature; where the point of recurvature is identified as that point where the typhoon reaches its westernmost longitude (JTWC 1994). Many TCs do not undergo classical recurvature. Some never recurve, while others move on a track type designated by the Japan Meteorological Agency (JMA) (1976) as north-

oriented. North-oriented tracks occur predominantly during July through October. Carr and Elsberry (1996) found that a TC may undergo north-oriented motion for only a portion of its track — even if some, or most, of the track was of some other type (e.g., straight-moving). A behavior commonly exhibited by TCs undergoing north-oriented motion — and Fern provides a good example — is reaching peak intensity after turning northward or northeastward, but before the speed of translation of the TC significantly increases.

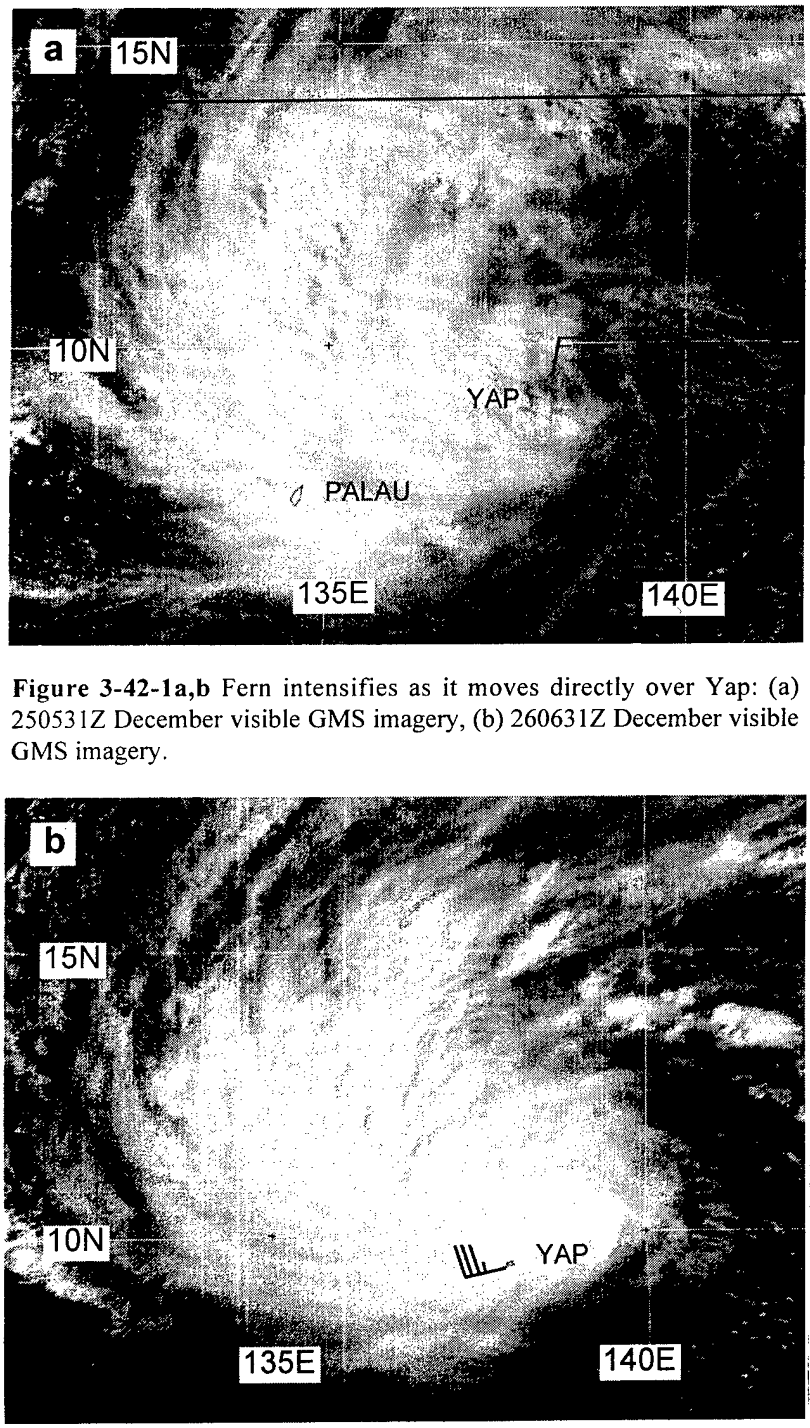

Figure 3-42-1a,b Fern intensifies as it moves directly over Yap: (a) 250531Z December visible GMS imagery, (b) 260631Z December visible GMS imagery.

Fern reached peak intensity while moving northward on the north-oriented leg of its track. It weakened when its speed of translation began to climb as it entered the "accelerating westerlies" regime north of the subtropical ridge. Synoptic regimes, such as "poleward oriented" and "accelerating westerlies", associated with specific TC behavior are described in Carr and Elsberry (1996). (See Carlo's (33W) summary for a discussion of a typhoon that underwent similar intensity changes as it moved on a north-oriented track).

IV. IMPACT

Fern passed directly over the island of Yap. High wind and heavy rain there caused an estimate of nearly US$ 3 million in damage and clean-up costs. Damage to roads and bridges of US $1.5 million was the highest single-item total. One person was reported injured. At sea, a Maltese tanker rescued eight people who abandoned a cargo ship, the "Mister Bill", after it was crippled by high seas while enroute from Guam to Yap. All (including a five-year-old girl) were unharmed. The eight people had entered a life raft which was spotted by a Navy search-and-rescue aircraft.

a

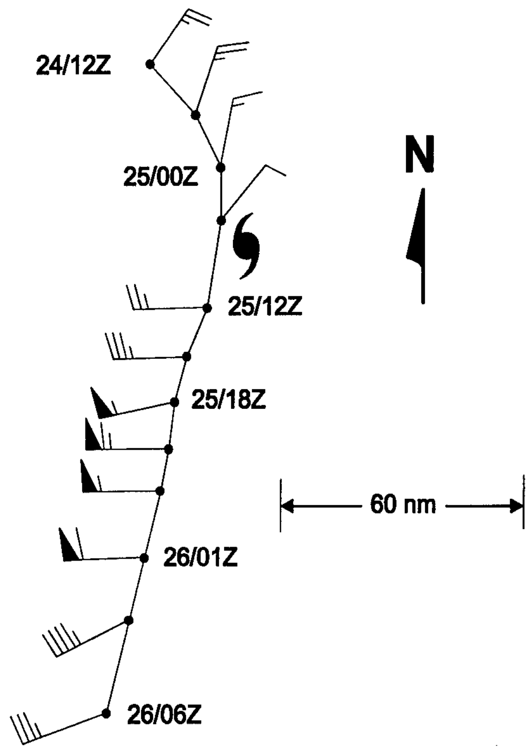

b

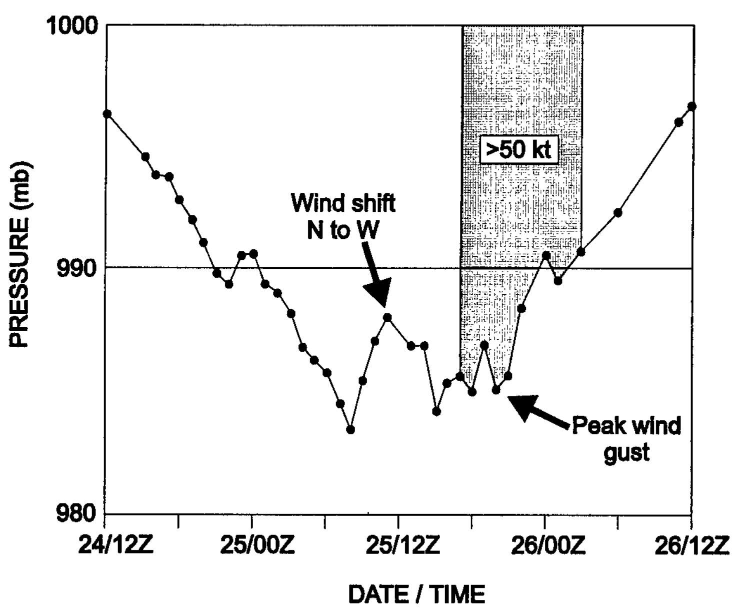

Figure 3-42-2a,b Schematic depiction of (a) peak gusts and (b) sea-level pressure (SLP) recorded at Yap (WMO 91415) during Fern's passage. The peak gust data are recorded with respect to Fern's center. The time series of SLP is based on hourly reports received at the JTWC. Shaded region on SLP diagram indicates wind speeds in excess of 50 kt.

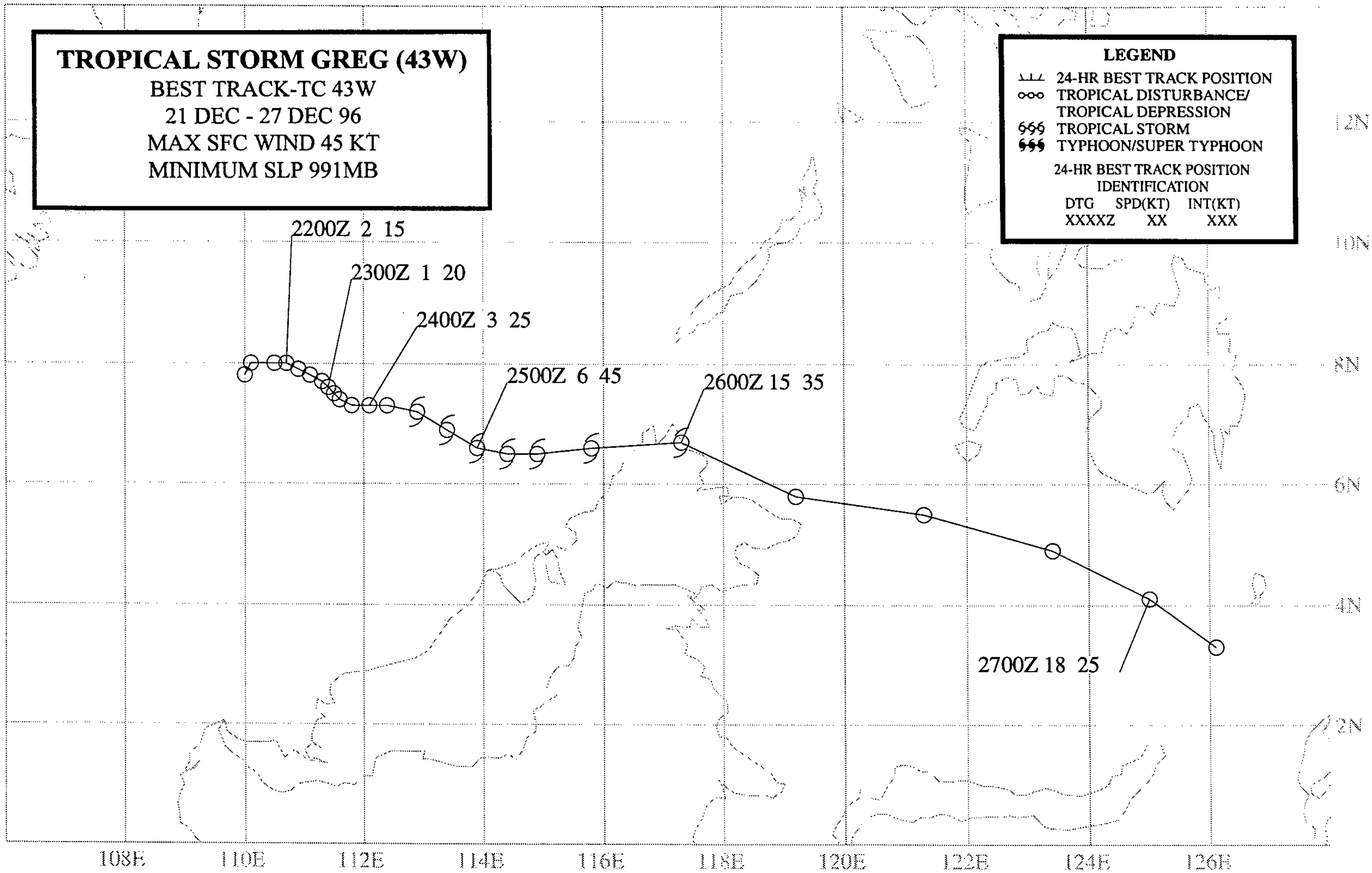
TROPICAL STORM GREG (43W)
BEST TRACK-TC 43W
21 DEC - 27 DEC 96
MAX SFC WIND 45 KT
MINIMUM SLP 991MB
LEGEND
24-HR BEST TRACK POSITION
TROPICAL DISTURBANCE/
TROPICAL DEPRESSION
TROPICAL STORM
TYPHOON/SUPER TYPHOON
24-HR BEST TRACK POSITION
IDENTIFICATION
DTG SPD(KT) INT(KT)
XXXXZ XX XXX
2200Z 2 15
2300Z 1 20
2400Z 3 25
2500Z 6 45
2600Z 15 35
2700Z 18 25
12N
10N
8N
6N
4N
2N
108E
110E
112E
114E
116E
118E
120E
122E
124E
126E

TROPICAL STORM GREG (43W)

I. HIGHLIGHTS

The last significant TC of 1996, Greg was one of the year's most unusual. It formed at low latitude in the South China Sea and moved toward the east-southeast. While passing over the northern tip of Borneo, Greg was responsible for the loss of many lives in the East Malaysian State of Sabah.

II. TRACK AND INTENSITY

During the second half of December, twin low-latitude monsoon troughs became established between approximately 100°E and 170°E. A band of strong low-level westerly winds persisted between the two trough axes. A total of five TCs — two in the Northern Hemisphere (Fern (42W) and Greg) and three in the Southern Hemisphere (Ophelia (11S), Phil (12P), and Fergus (13P)) — formed within these monsoon troughs (Figure 3-43-1).

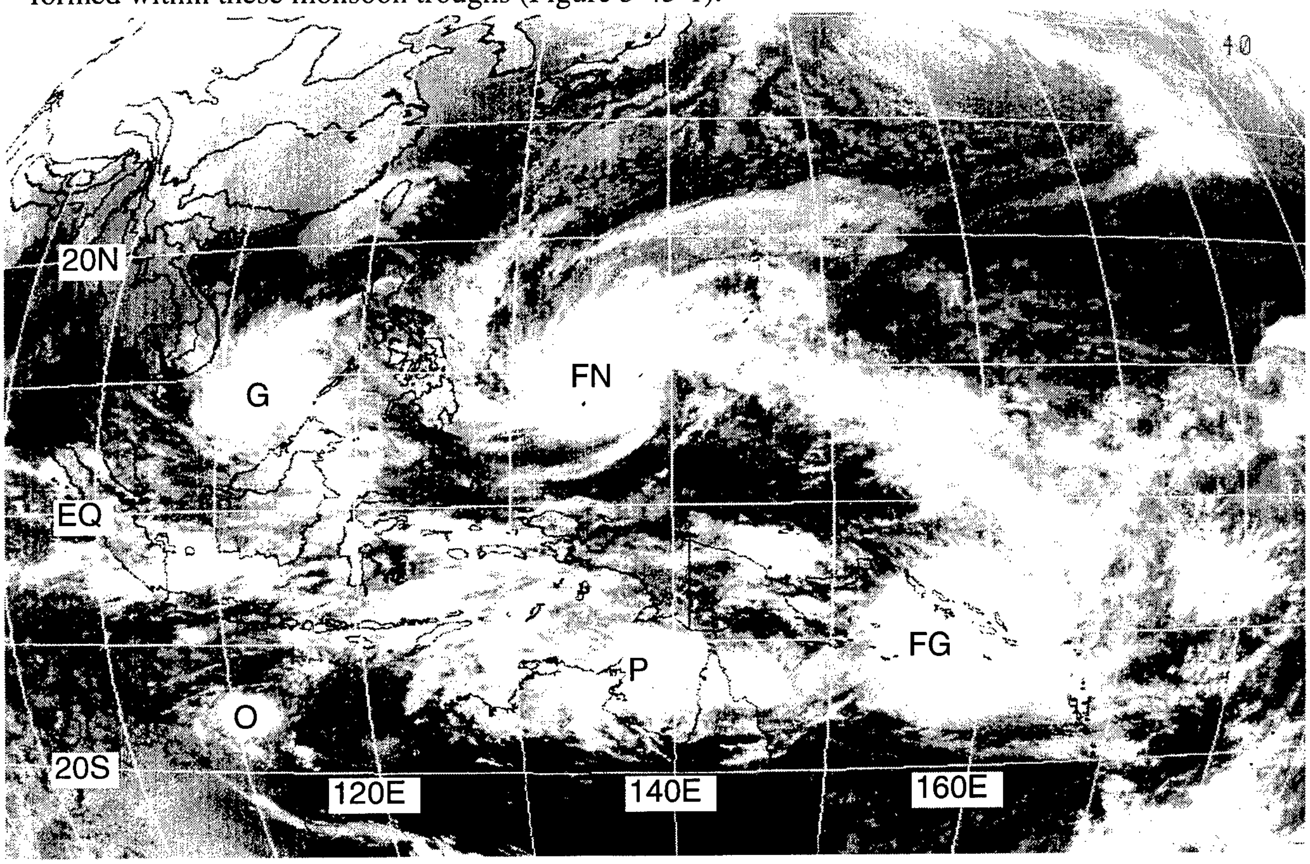

Figure 3-43-1 Five TCs — Greg (G), Fern (FN), Ophelia (O), Phil (P), and Fergus (FG) — lie within twin monsoon troughs (242330Z December infrared GMS imagery).

The tropical disturbance which became Greg was first mentioned on the 210600Z Significant Tropical Weather Advisory when an area of persistent deep convection was observed in the low latitudes of the South China Sea. On 23 December, this area of deep convection began to show signs of becoming better organized. Remarks on the 232100Z Significant Tropical Weather Advisory included:

"[An] area of convection . . . remains near 7N 112E. Animated infrared satellite imagery indicates that the convective organization associated with this system has improved over the past 12 hours in response to an equatorial westerly wind burst. Gradient-level [westerly and southwesterly] winds reported [by stations in East Malaysia are near 30 kt (15 m/sec).] . . ."

JTWC issued a TCFA at 240400Z as visible and microwave satellite imagery indicated that convective organization was improving, and water-vapor imagery supported upper-level divergence over the system. The first warning on Tropical Depression (TD) 43W soon followed, valid at 240600Z. TD 43W was upgraded to Tropical Storm Greg on the warning valid at 250000Z. In postanalysis, however, reanalysis of satellite data determined that Greg most probably became a tropical storm at 241200Z. Continuing to move on a very unusual east-southeastward track, Greg reached a peak intensity of 45 kt (23 m/sec) at 250000Z (Figure 3-43-2) and maintained this intensity until making landfall on the northern tip of Borneo. The final warning was issued, valid at 270600Z, when most of the deep convection associated with the system collapsed as Greg dissipated south of the Philippines.

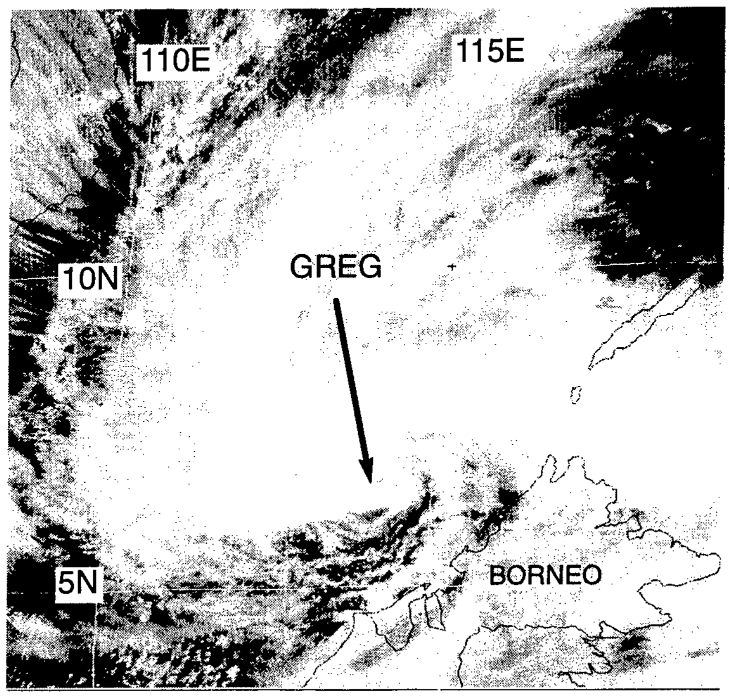

Figure 3-43-2 Greg at peak intensity of 45 kt (23 m/sec) bears down on the northwest coast of Borneo (250231Z December visible GMS imagery).

III. DISCUSSION

a. *On the importance of microwave imagery*

During the night of 24 December, as Greg (then TD 43W) was moving east-southeastward toward the northern tip of Borneo, a DMSP satellite passed over the system at 241452Z. Microwave imagery from this pass (Figure 3-43-3) indicated that a well-organized curved band of deep convection accompanied the LLCC. DMSP passes outside of the range of the Guam ground station are received several hours time-late at the JTWC via the MISTIC system. This imagery was used in postanalysis to upgrade Greg to a tropical storm earlier than indicated on the warnings. Though received late, the microwave imagery was nevertheless used to help support the real-time upgrade of Greg to a tropical storm at 250000Z.

b. *Greg's unusual east-southeastward motion*

Greg's east-southeastward motion from near 8°N 110°E to near 3°N 126°E was very unusual. TCs which form within (or move into) the South China Sea late in the year are often blocked from moving west by well-established northeasterly monsoon flow. Such TCs often remain quasi-stationary or move southwestward and dissipate. Greg formed in the SCS when an unusual large-scale wind pattern dominated the region: a belt of low-level westerly winds existed in equatorial latitudes between twin monsoon troughs (i.e., one north, the other south of the equator). With the Northeast Monsoon blocking its motion to the west, it is hypothesized that the strong westerly winds to the south of Greg provided the flow asymmetry responsible for its eastward motion. This factor, plus the existence of the large circulation of Fern (42W) to Greg's northeast were cited on prognostic reasoning messages as possible sources of the east-southeastward movement of Greg.

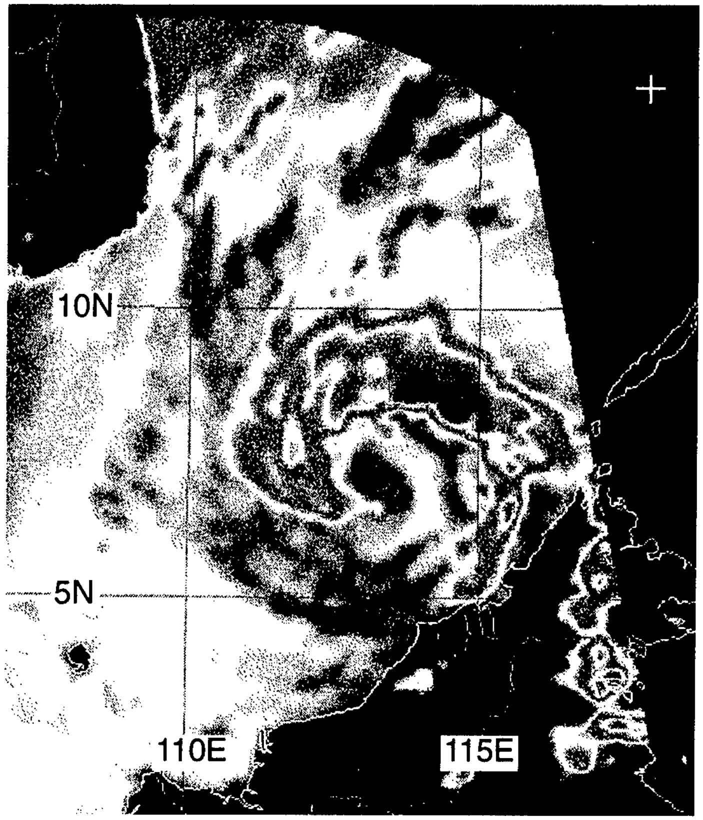

Figure 3-43-3 A well-defined spiral band of deep convection, wrapping almost one complete turn from tip to tail around Greg's LLCC, helped to support the postanalysis upgrade of the timing of tropical storm intensity (241452Z December horizontally polarized 85 GHz SSM/I DMSP imagery).

IV. IMPACT

Greg was responsible for loss of life and extensive damage to property in the East Malaysian State of Sabah (located on the northwest coast of Borneo). At least 124 lives were reported lost with another 100 reported missing primarily due to flooding from torrential rains. In Kota Kinabalu, the capital of the State of Sabah, high wind scattered billboards and other debris, and broke windows in the 30-story government building.

3.2 NORTH INDIAN OCEAN TROPICAL CYCLONES

In 1996, eight significant tropical cyclones occurred in the North Indian Ocean. Five of these were in the Bay of Bengal and three in the Arabian Sea (Table 3-5). Spring and fall in the North Indian Ocean are periods of transition between major climatic controls, and the most favorable seasons for tropical cyclone activity. This year was no exception (Table 3-6). The total number, eight, was three over than the 22-year average of five. Eight also tied with the total in 1987, however 1992 still holds the record, 13.

The best track composite is shown in Figure 3-9. There are four cyclones of typhoon intensity (a record) — the most intense being TC 07B. The track of TC 08B is unusual due to its length and large clockwise loop in the Bay of Bengal.

Table 3-5 NORTH INDIAN OCEAN SIGNIFICANT TROPICAL CYCLONES FOR 1996

TROPICAL CYCLONE	PERIOD OF WARNING	NUMBER OF WARNINGS ISSUED	MAXIMUM SURFACE WINDS-KT (M/SEC)	ESTIMATED MSLP (MB)
01B	07 MAY - 08 MAY	6	40 (21)	994
02A	11 JUN - 11 JUN	4	40 (21)	994
03B	02 JUN - 17 JUN	20	45 (23)	988*
04A	10 JUN - 19 JUN	8	65 (33)	972*
05A	22 OCT - 26 OCT	15	65 (33)	976
	28 OCT - 31 OCT	15		
06B	25 OCT - 29 OCT	16	45 (23)	991
07B	03 NOV - 07 NOV	16	115 (59)	927
08B	28 NOV - 06 DEC	35	75 (39)	967
	TOTAL	135		

*MSLP based on synoptic reports

The criteria used in Table 3-6 are as follows:

1. If a tropical cyclone was first warned on during the last two days of a particular month and continued into the next month for longer than two days, then that system was attributed to the second month.
2. If a tropical cyclone was warned on prior to the last two days of a month, it was attributed to the first month, regardless of how long the system lasted.
3. If a tropical cyclone began on the last day of the month and ended on the first day of the next month, that system was attributed to the first month. However, if a tropical cyclone began on the last day of the month and continued into the next month for only two days, then it was attributed to the second month.

Table 3-6 Legend

Total for the month/year → 8

Typhoons → 4 (first digit of "4 4 0")

Tropical Storms → 4 (second digit)

Tropical Depressions → 0 (third digit)

Table 3-6 DISTRIBUTION OF NORTH INDIAN OCEAN TROPICAL CYCLONES FOR 1975-1996

YEAR	JAN	FEB	MAR	APR	MAY	JUN	JUL	AUG	SEP	OCT	NOV	DEC	TOTALS
1975	1	0	0	0	2	0	0	0	0	1	2	0	6
	010	000	000	000	200	000	000	000	000	100	020	000	3 3 0
1976	0	0	0	1	0	1	0	0	1	1	0	1	5
	000	000	000	010	000	010	000	000	010	010	000	010	0 5 0
1977	0	0	0	0	1	1	0	0	0	1	0	2	5
	000	000	000	000	010	010	000	000	000	010	000	110	1 4 0
1978	0	0	0	0	1	0	0	0	0	1	2	0	4
	000	000	000	000	010	000	000	000	000	010	200	000	2 2 0
1979	0	0	0	0	1	1	0	0	2	1	2	0	7
	000	000	000	000	100	010	000	000	011	010	011	000	1 4 2
1980	0	0	0	0	0	0	0	0	0	0	1	1	2
	000	000	000	000	000	000	000	000	000	000	010	010	0 2 0
1981	0	0	0	0	0	0	0	0	1	0	1	1	3
	000	000	000	000	000	000	000	000	010	000	100	100	2 1 0
1982	0	0	0	0	1	1	0	0	0	2	1	0	5
	000	000	000	000	100	010	000	000	000	020	100	000	2 3 0
1983	0	0	0	0	0	0	0	1	0	1	1	0	3
	000	000	000	000	000	000	000	010	000	010	010	000	0 3 0
1984	0	0	0	0	1	0	0	0	0	1	2	0	4
	000	000	000	000	010	000	000	000	000	010	200	000	2 2 0
1985	0	0	0	0	2	0	0	0	0	2	1	1	6
	000	000	000	000	020	000	000	000	000	020	010	010	0 6 0
1986	1	0	0	0	0	0	0	0	0	0	2	0	3
	010	000	000	000	000	000	000	000	000	000	020	000	0 3 0
1987	0	1	0	0	0	2	0	0	0	2	1	2	8
	000	010	000	000	000	020	000	000	000	020	010	020	0 8 0
1988	0	0	0	0	0	1	0	0	0	1	2	1	5
	000	000	000	000	000	010	000	000	000	010	110	010	1 4 0
1989	0	0	0	0	1	1	0	0	0	0	1	0	3
	000	000	000	000	010	010	000	000	000	000	100	000	1 2 0
1990	0	0	0	1	1	0	0	0	0	0	1	1	4
	000	000	000	001	100	000	000	000	000	000	001	010	1 1 2
1991	1	0	0	1	0	1	0	0	0	0	1	0	4
	010	000	000	100	000	010	000	000	000	000	010	000	1 3 0
1992	0	0	0	0	1	2	1	0	1	3	3	2	13
	000	000	000	000	100	020	010	000	001	021	210	020	3 8 2
1993	0	0	0	0	0	0	0	0	0	0	2	0	2
	000	000	000	000	000	000	000	000	000	000	200	000	2 0 0
1994	0	0	1	1	0	1	0	0	0	1	1	0	5
	000	000	010	100	000	010	000	000	000	010	010	000	1 4 0
1995	0	0	0	0	0	0	0	0	1	1	2	0	4
	000	000	000	000	000	000	000	000	010	010	200	000	2 2 0
1996	0	0	0	0	1	3	0	0	0	2	2	0	8
	000	000	000	000	010	120	000	000	000	110	200	000	4 4 0
(1975-1995)													
MEAN	0.2	0.1	0.1	0.2	0.6	0.6	0.1	0.1	0.3	0.9	1.4	0.6	4.8
CASES	3	1	1	4	12	12	1	1	6	19	29	12	101

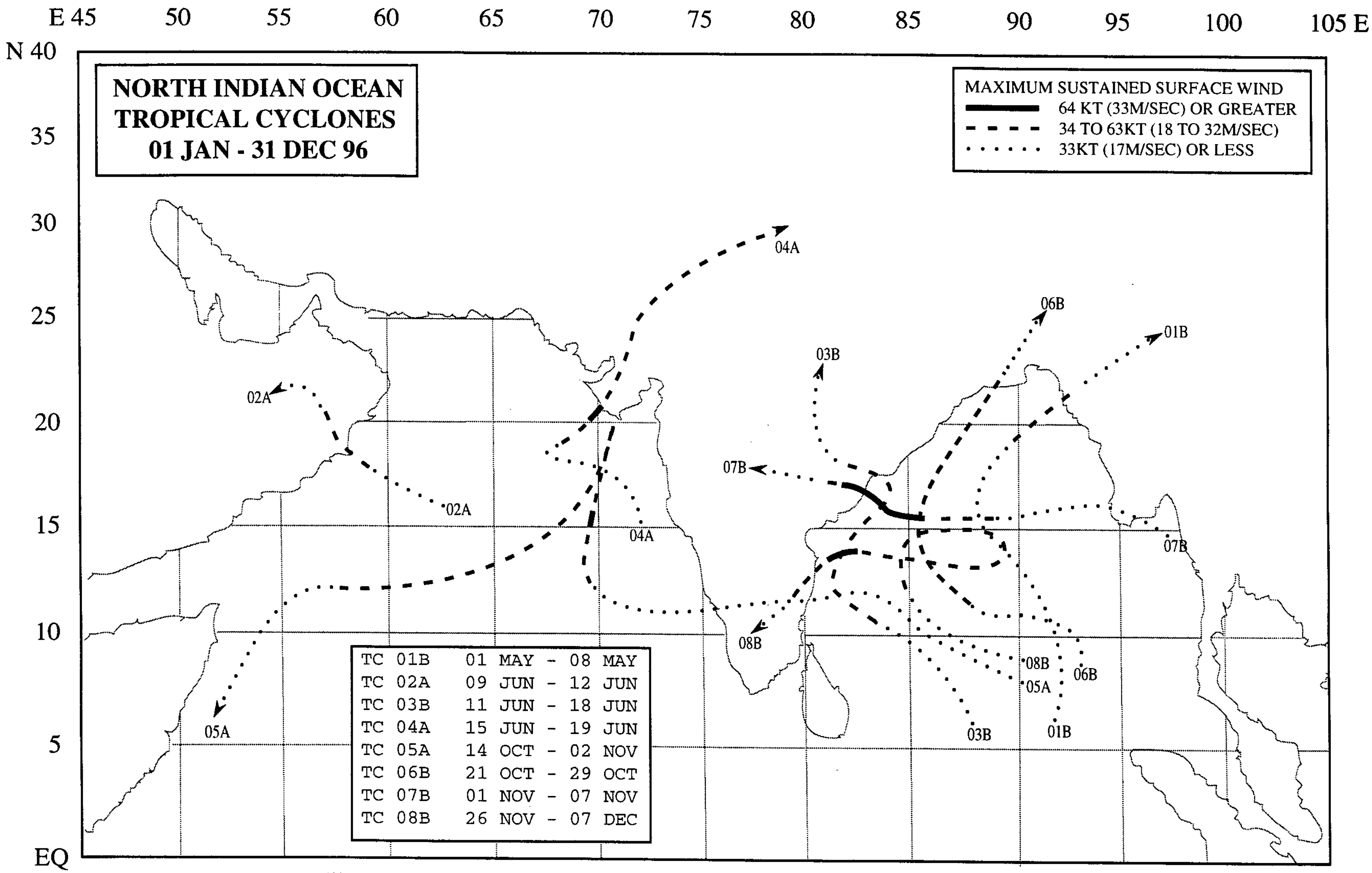

Figure 3-9 Composite of best tracks for North Indian Ocean tropical cyclones for 1996.

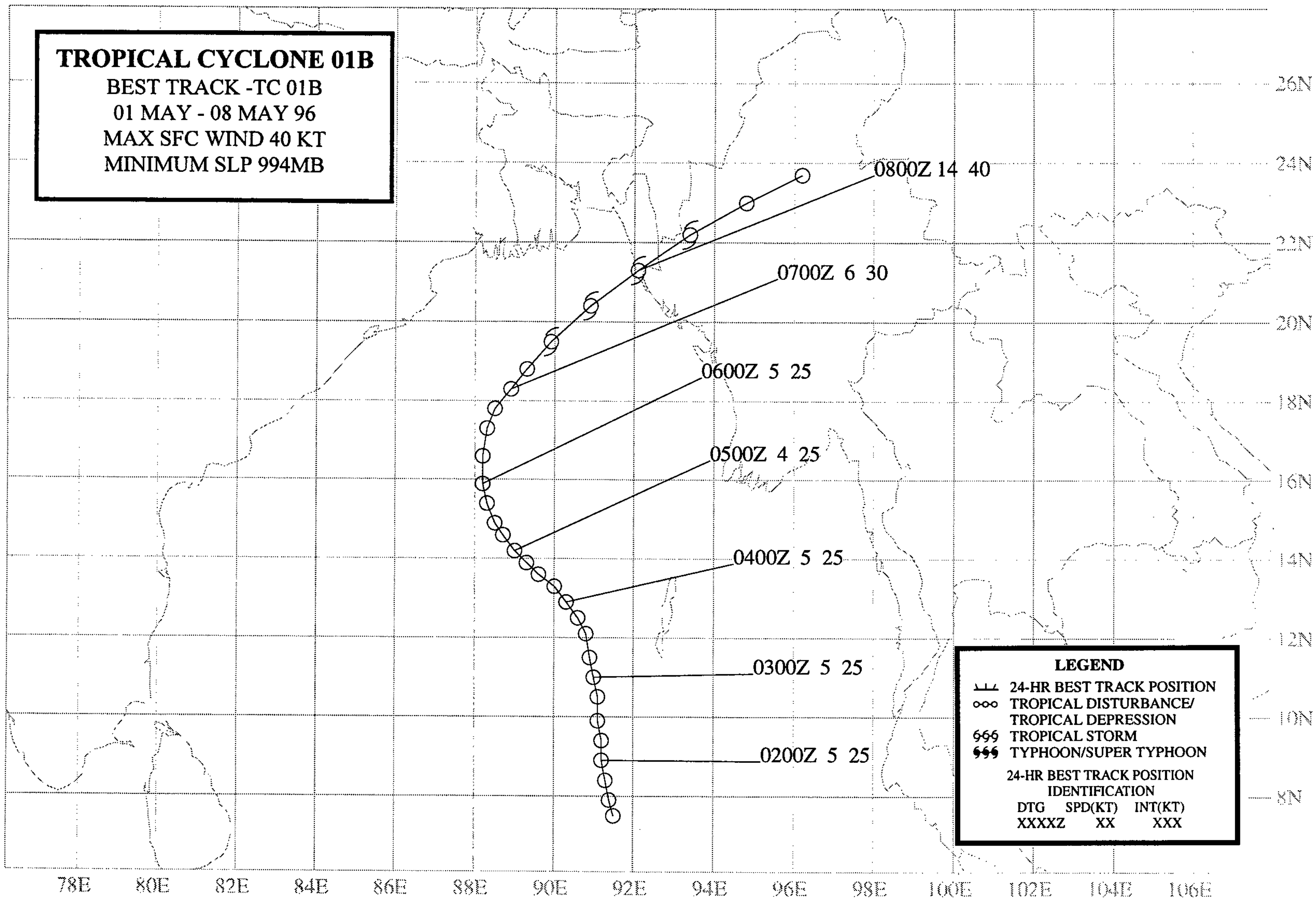
TROPICAL CYCLONE 01B
BEST TRACK -TC 01B
01 MAY - 08 MAY 96
MAX SFC WIND 40 KT
MINIMUM SLP 994MB
0800Z 14 40
0700Z 6 30
0600Z 5 25
0500Z 4 25
0400Z 5 25
0300Z 5 25
0200Z 5 25
LEGEND
24-HR BEST TRACK POSITION
TROPICAL DISTURBANCE/
TROPICAL DEPRESSION
TROPICAL STORM
TYPHOON/SUPER TYPHOON
24-HR BEST TRACK POSITION
IDENTIFICATION
DTG SPD(KT) INT(KT)
XXXXZ XX XXX
26N
24N
22N
20N
18N
16N
14N
12N
10N
8N
78E
80E
82E
84E
86E
88E
90E
92E
94E
96E
98E
100E
102E
104E
106E

TROPICAL CYCLONE 01B

On the first day of May, the tropical disturbance that was to become TC 01B was first observed as a broad area of deep convection in the monsoon trough, 240 nm (440 km) northwest of Sumatra. In the Southern Hemisphere, a "twin" cyclone, which would become Jenna (28S), was also developing (Figure 3-01B-1) in conjunction with the same equatorial westerly wind burst. At 020230Z, the Significant Tropical Weather Advisory was reissued to include both the persistent deep convection associated with pre-TC 01B and the first warning for TC 28S. As the pre-TC 01B disturbance tracked slowly northward, its cloud system organization finally improved to a point where JTWC issued the first TCFA at 051230Z. A second TCFA followed at 061230Z which stated: ". . . [Although] the [cloud] system organization has changed little from the previous alert ... [it] should improve in the low-shear environment . . [near] the ridge [axis].." Based on DMSP SSM/I and ERS-2 scatterometer data, indicating 30-kt (15-m/sec) winds near the LLCC, JTWC issued the first warning, valid at 070000Z. Intensification continued until TC 01B reached a peak of 40 kt (21 m/sec) at 071800Z — six hours prior to making landfall near Cox's Bazar. Cox's Bazar (WMO 41992) experienced a maximum sustained wind of 40 kt (21 m/sec) and a minimum sea-level pressure of 993 mb. The cyclone dissipated over the mountainous terrain of Myanmar less than a day later. The JTWC received no reports of death or significant damage.

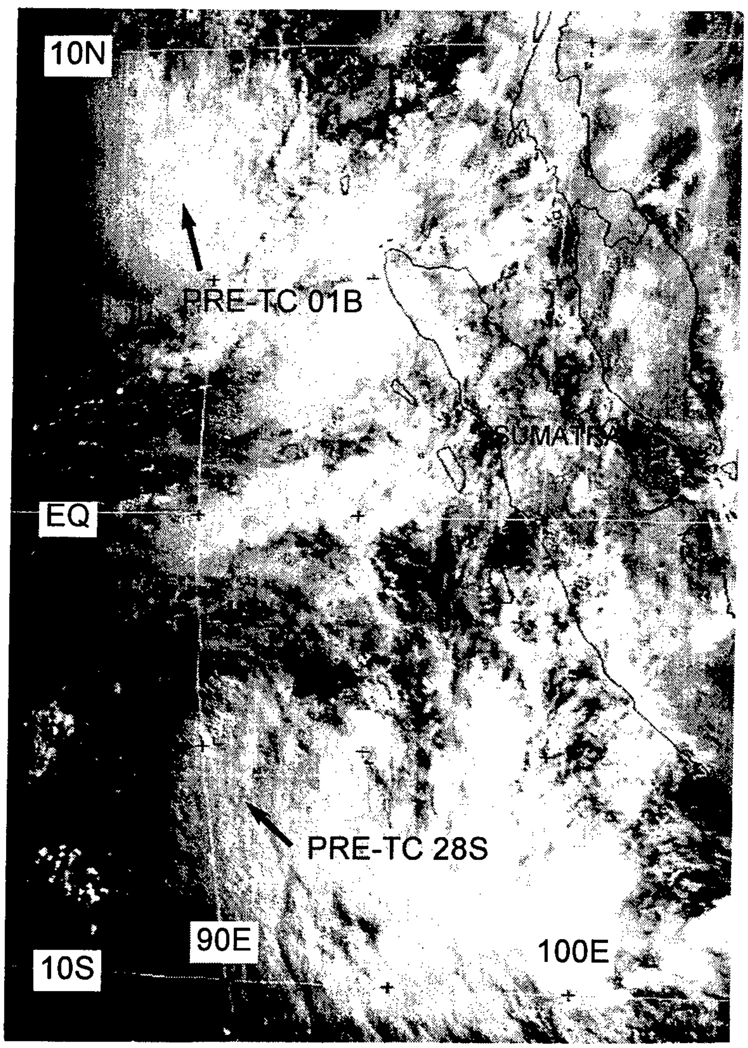

Figure 1-01B-1 The "twin" cyclones — pre-TC 01B and TC 28S — consolidate near the equator (020031Z May visible GMS imagery).

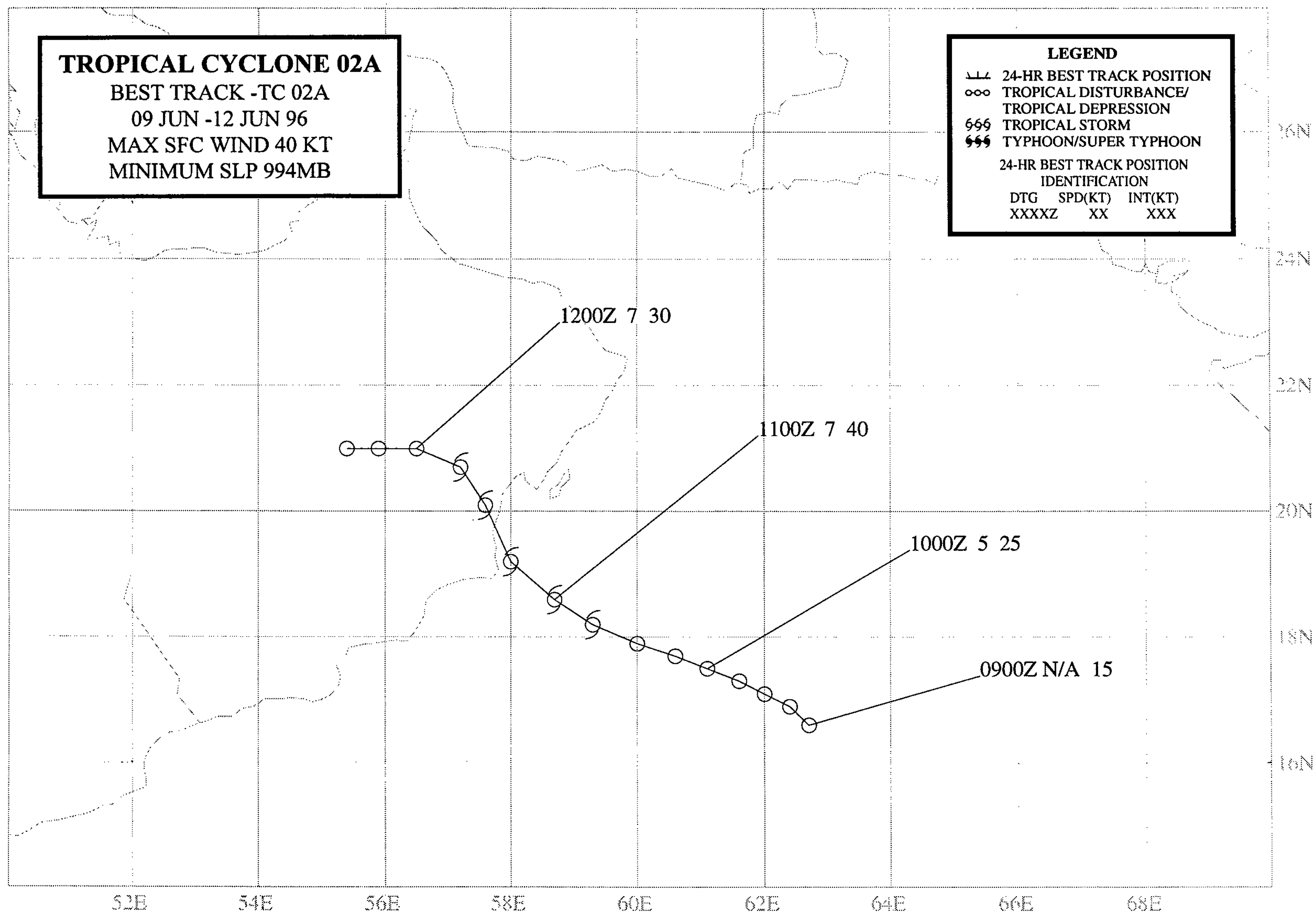
TROPICAL CYCLONE 02A
BEST TRACK -TC 02A
09 JUN -12 JUN 96
MAX SFC WIND 40 KT
MINIMUM SLP 994MB
LEGEND
24-HR BEST TRACK POSITION
TROPICAL DISTURBANCE/
TROPICAL DEPRESSION
TROPICAL STORM
TYPHOON/SUPER TYPHOON
24-HR BEST TRACK POSITION
IDENTIFICATION
DTG SPD(KT) INT(KT)
XXXXZ XX XXX
1200Z 7 30
1100Z 7 40
1000Z 5 25
0900Z N/A 15
26N
24N
22N
20N
18N
16N
52E
54E
56E
58E
60E
62E
64E
66E
68E

TROPICAL CYCLONE 02A

The second of eight 1996 North Indian Ocean cyclones, TC 02A was the first of three to occur in the Arabian Sea. The tropical disturbance which became TC 02A was initially observed as an area of poorly organized convection in the northwestern Arabian Sea 800 nm (1480 km) northeast of Somalia. Because the convection persisted, the Significant Tropical Weather Advisory was reissued at 092000Z June to include first mention of the disturbance. Based on a combination of infrared, microwave imager, and ERS-2 scatterometer data indicating sustained surface winds of 20-30 kt (10-15 m/sec), a TCFA was issued, valid at 102000Z. Moderate vertical wind shear was expected to slow intensification, however, intensification continued and the first warning was issued, valid at 110000Z. As TC 02A approached the coast, Fahad (WMO 41262), an inland air base on the Arabian Peninsula, recorded maximum sustained 10-minute mean northerly winds of 35 kt (17 m/sec) at 110300Z and Masirah (WMO 41268) recorded a minimum sea-level pressure of 994 mb at 110000Z. The system continued on a west-northwestward track at a peak of 40 kt (21 m/sec) until making landfall 70 nm (130 km) southwest of Al Masirah Island at 110900Z. Figure 3-02A-1 shows TC 02A a few hours before landfall. The final warning was issued, valid at 111800Z, as the remnants of the tropical cyclone dissipated over the desert. No reports of death or significant damage were received.

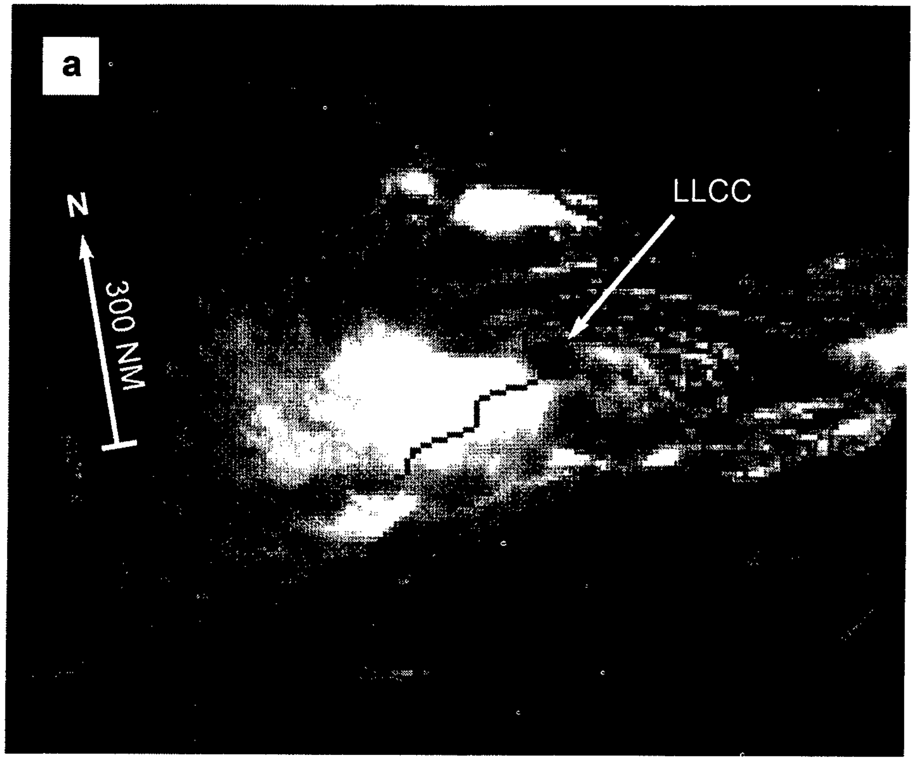

Figure 3-02A-1 TC 02A shortly before making landfall in Oman. Note the significant difference in the cloudiness as viewed in the visible (a) and infrared (b) images. The LLCC is apparent in the visible, but not in the infrared (DMSP imagery courtesy of the Space Physics Interactive Data Resource (SPIDR) Internet site maintained by the National Geophysical Data Center).

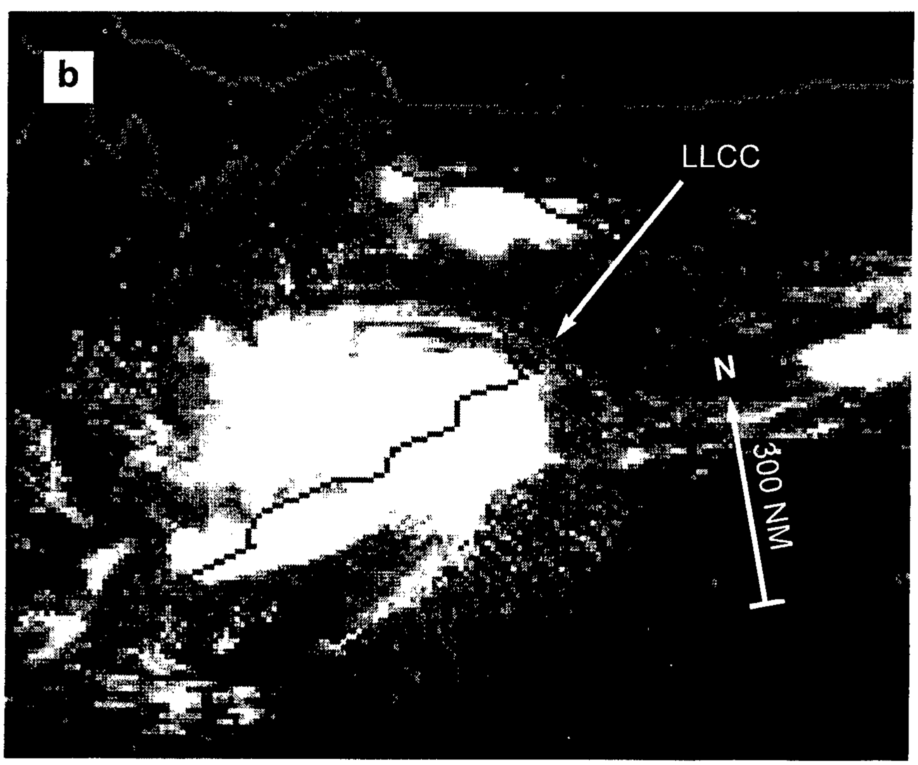

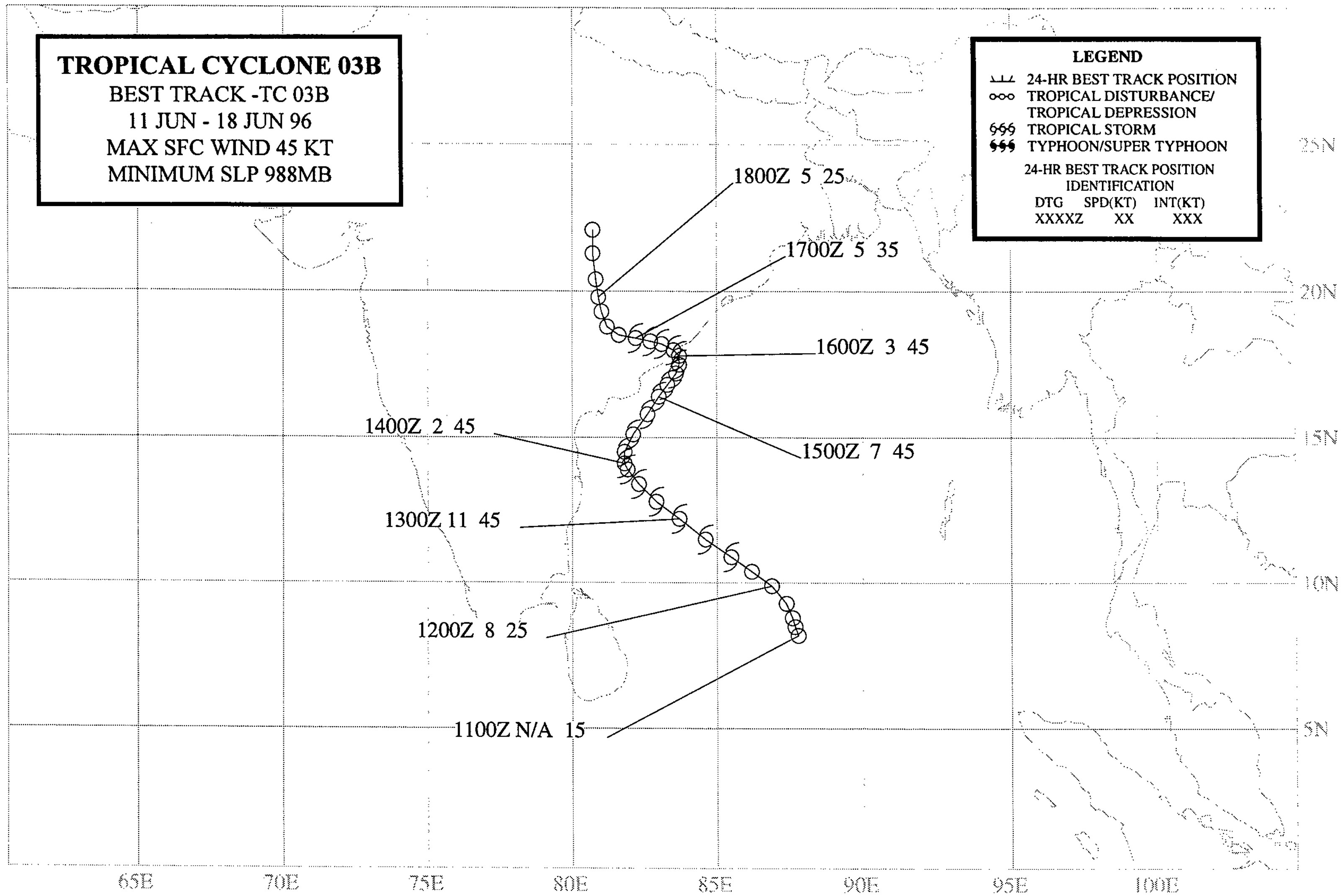
TROPICAL CYCLONE 03B
BEST TRACK -TC 03B
11 JUN - 18 JUN 96
MAX SFC WIND 45 KT
MINIMUM SLP 988MB
LEGEND
24-HR BEST TRACK POSITION
TROPICAL DISTURBANCE/
TROPICAL DEPRESSION
TROPICAL STORM
TYPHOON/SUPER TYPHOON
24-HR BEST TRACK POSITION
IDENTIFICATION
DTG SPD(KT) INT(KT)
XXXXZ XX XXX
1800Z 5 25
1700Z 5 35
1600Z 3 45
1500Z 7 45
1400Z 2 45
1300Z 11 45
1200Z 8 25
1100Z N/A 15
25N
20N
15N
10N
5N
65E
70E
75E
80E
85E
90E
95E
100E

TROPICAL CYCLONE 03B

The convection associated with the tropical disturbance that became Tropical Cyclone 03B (TC 03B) consolidated rapidly in the monsoon trough, prompting JTWC to issue a TCFA at 111930Z June. Based on animated satellite imagery, indicating increased convective organization, the first warning was issued, valid at 120600Z. Eighteen hours later, TC 03B reached its maximum intensity of 45 kt (23 m/sec), which it maintained for nearly four days (Figure 3-03B-1). As the cyclone began to weaken, its track changed to a northeastward motion. The cyclone changed to a west-northwest track at 160000Z and made landfall five hours later about 25 nm (46 km) northeast of Vishakhapatnam (WMO 43149) on the Andra Pradesh coast of India. Vishakhapatnam observed 30-kt (10-minute average) (15 m/sec) sustained winds and a minimal sea-level pressure of 987 mb at 160000Z. Waltair (43150) also reported 30 kt (15 m/sec) winds at that time. Once TC 03B was over land, JTWC issued a final warning valid at 170000Z.

Despite the relative weakness of the cyclone, torrential rains accompanied TC 03B inland (Figure 3-03B-2). Flooding from the heavy rains resulted in the loss of 175 lives, more than 3,000 families homeless, and extensive damage. News reports also indicated 270 people (mostly fishermen) were missing.

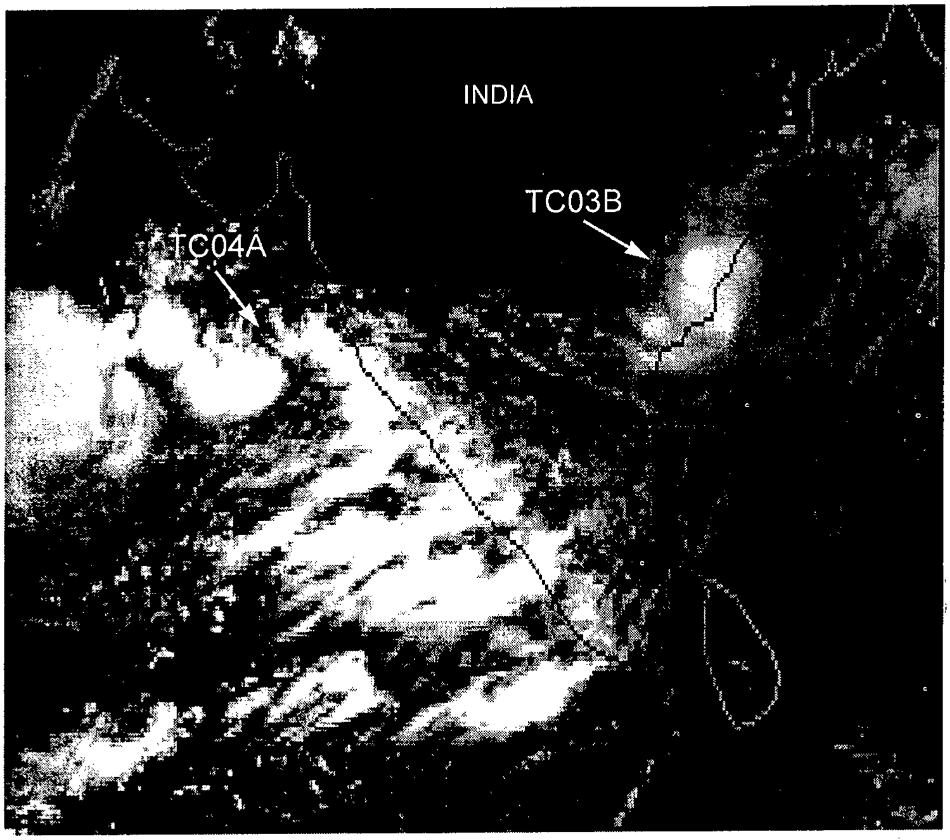

Figure 3-03B-1 As the LLCC of TC 03B nears the coast, deep convection builds inland (160350Z June visible DMSP imagery downloaded from the Space Physics Interactive Data Resource (SPIDR) Internet site maintained by National Geophysical Data Center (NGDC)).

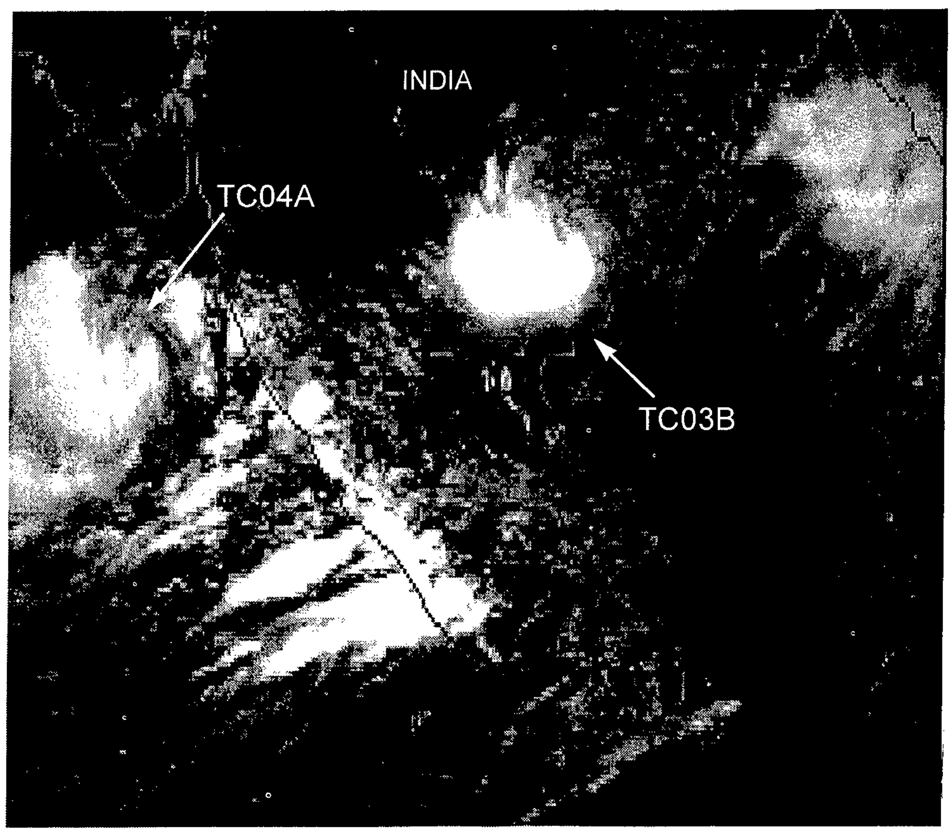

Figure 3-03B-2 In comparison with Figure 3-03B-1, approximately 24 hours later, the convection associated with TC 03B has increased dramatically and is producing widespread torrential rains (170337Z June visible DMSP imagery downloaded from SPIDR).

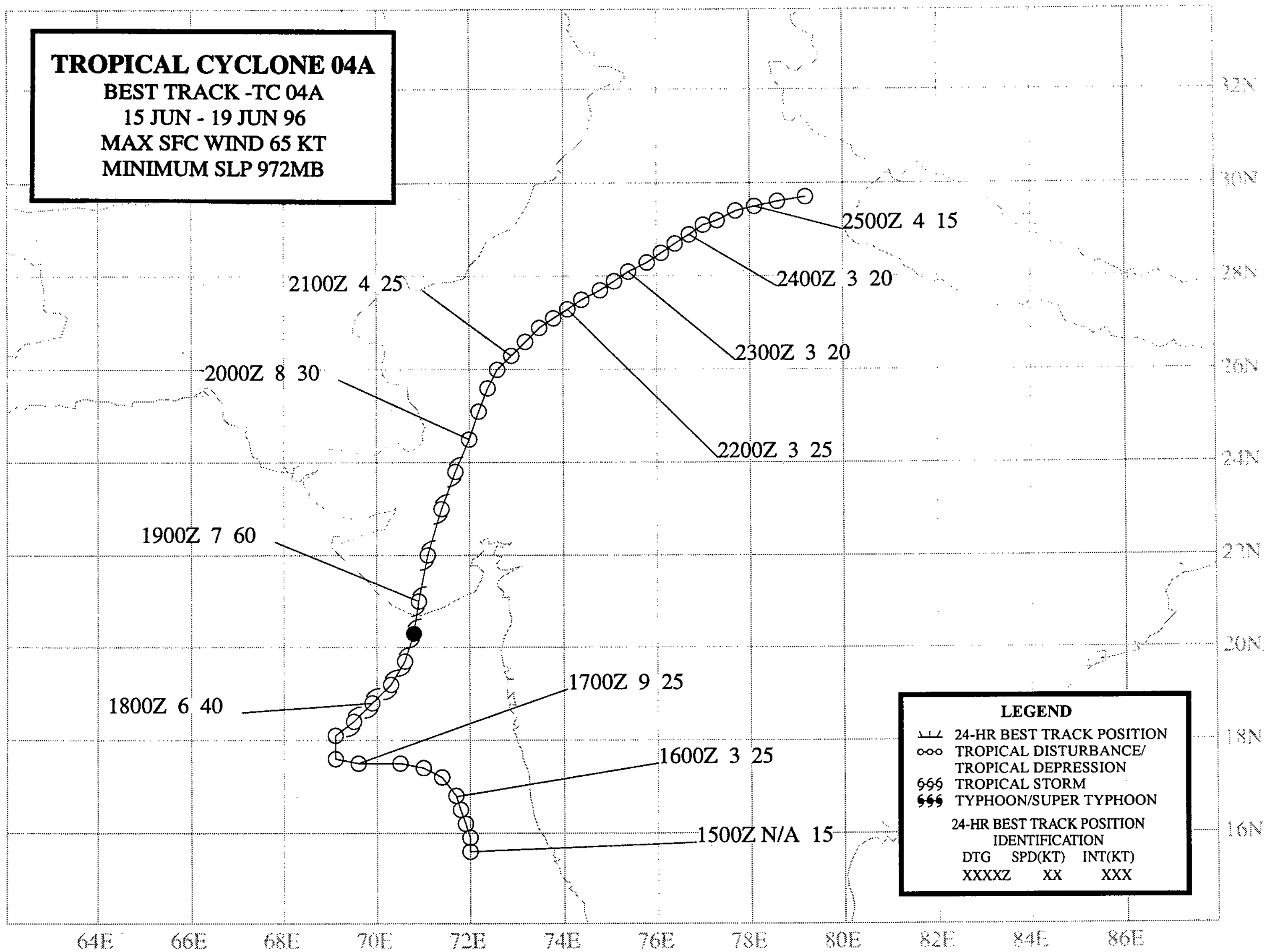
TROPICAL CYCLONE 04A
BEST TRACK -TC 04A
15 JUN - 19 JUN 96
MAX SFC WIND 65 KT
MINIMUM SLP 972MB
2500Z 4 15
2400Z 3 20
2300Z 3 20
2200Z 3 25
2100Z 4 25
2000Z 8 30
1900Z 7 60
1800Z 6 40
1700Z 9 25
1600Z 3 25
1500Z N/A 15
LEGEND
24-HR BEST TRACK POSITION
TROPICAL DISTURBANCE/
TROPICAL DEPRESSION
TROPICAL STORM
TYPHOON/SUPER TYPHOON
24-HR BEST TRACK POSITION
IDENTIFICATION
DTG SPD(KT) INT(KT)
XXXXZ XX XXX
64E
66E
68E
70E
72E
74E
76E
78E
80E
82E
84E
86E
30N
28N
26N
24N
20N
18N
16N

TROPICAL CYCLONE 04A

On 15 June, a day before TC 03B made landfall on the east coast of India, convection associated with the monsoon depression that became TC 04A was first detected on satellite imagery off the west coast of India 210 nm (390 km) south-southwest of Bombay. Although poorly organized, the convection persisted and was first mentioned on the Significant Tropical Weather Advisory at 170700Z. A TCFA was issued at 170730Z June after conventional and microwave satellite data indicated that the wind field had become better organized, and a first warning followed, valid at 171800Z. As TC 04A moved northward and intensified, available Dvorak intensity estimates peaked at 45 kt (23 m/sec). However, synoptic data supported a maximum of 65 kt (33 m/sec) as the cyclone approached the coast. TC 04A made landfall near Diu at 182300Z. Diu is located on the coast of India 330 nm (610 km) southeast of Karachi. Veraval (WMO 42909) reported a minimum sea-level pressure of 974 mb at 182300Z. Rajkot (WMO 42737), 75 nm (139 km) inland, reported a minimum sea-level pressure of 980 mb at 190600Z and 10-minute sustained wind of 46 kt (24 m/sec) at 191200Z. Figure 3-04A-1 shows the 3-hourly surface winds at Rajkot which reflect the passage of the cyclone. JTWC issued the final warning valid at 191200Z, as TC 04A dissipated inland. Figure 3-04A-2 shows convection associated with TC 04A as it moved northward into India.

The maximum storm surge on the southern coast was estimated to be 20 feet (6 meters). Indian government agencies reported 47 people were killed by the cyclone.

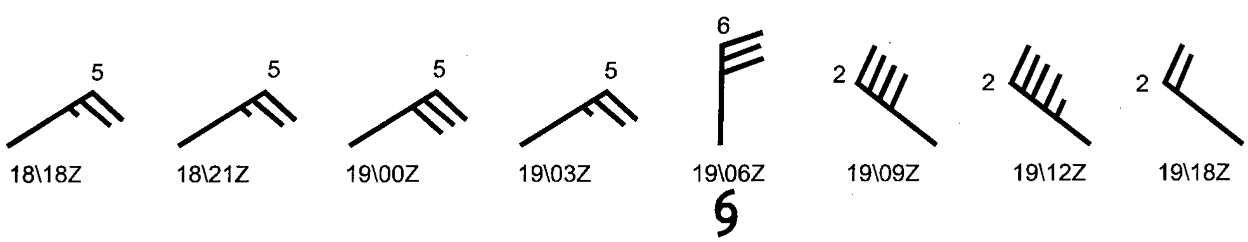

Figure 3-04A-1 Surface wind reports at Rajkot, India (WMO 42737) reflect the passage of TC 04A.

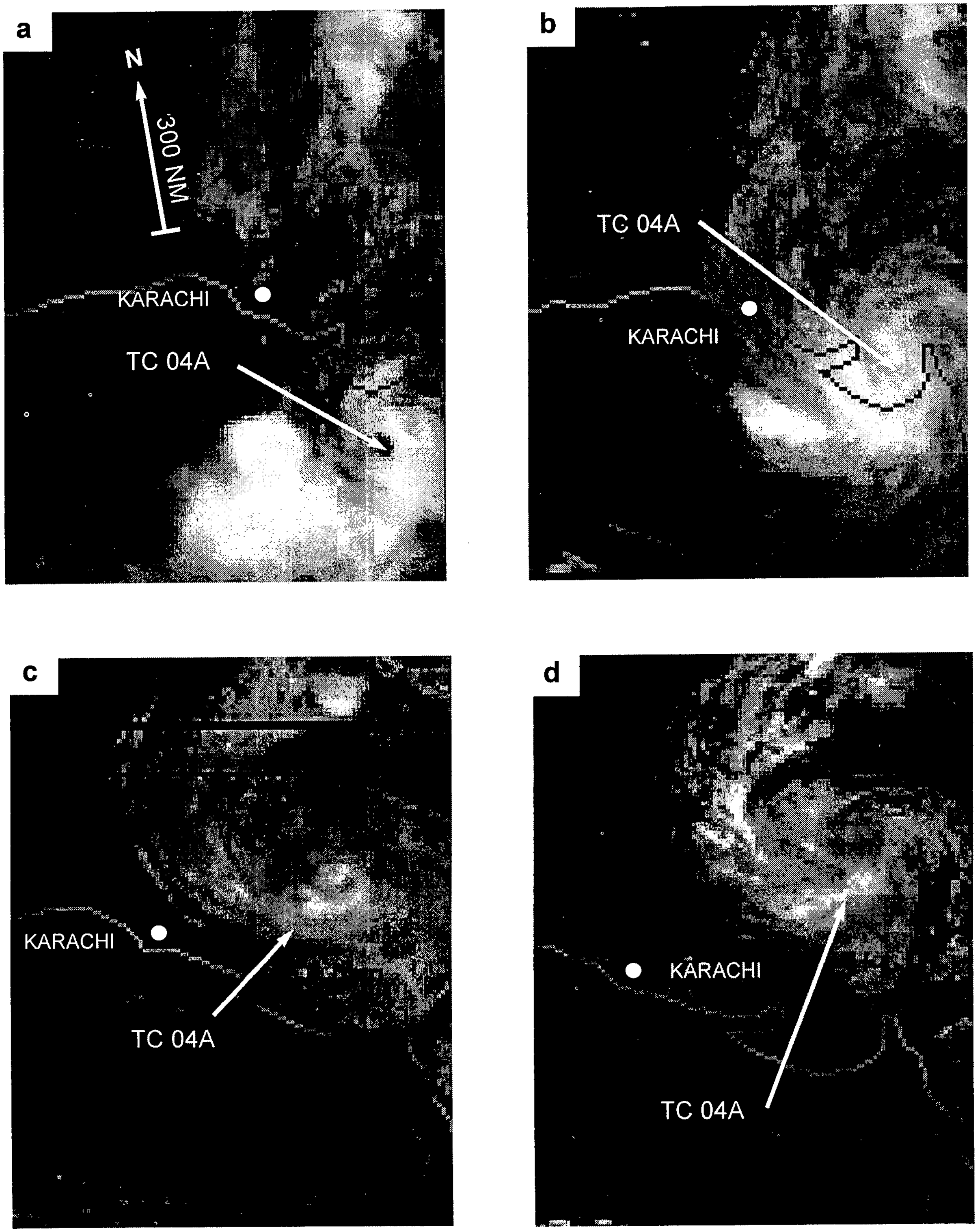

Figure 3-04A-2 Visible imagery — (a) 180507Z June; (b) 190455Z; (c) 200443Z; and (d) 210431Z — covering a 4-day period tracks TC 04A's passage from the Arabian Sea northward into India (Visible DMSP imagery downloaded from SPIDR).

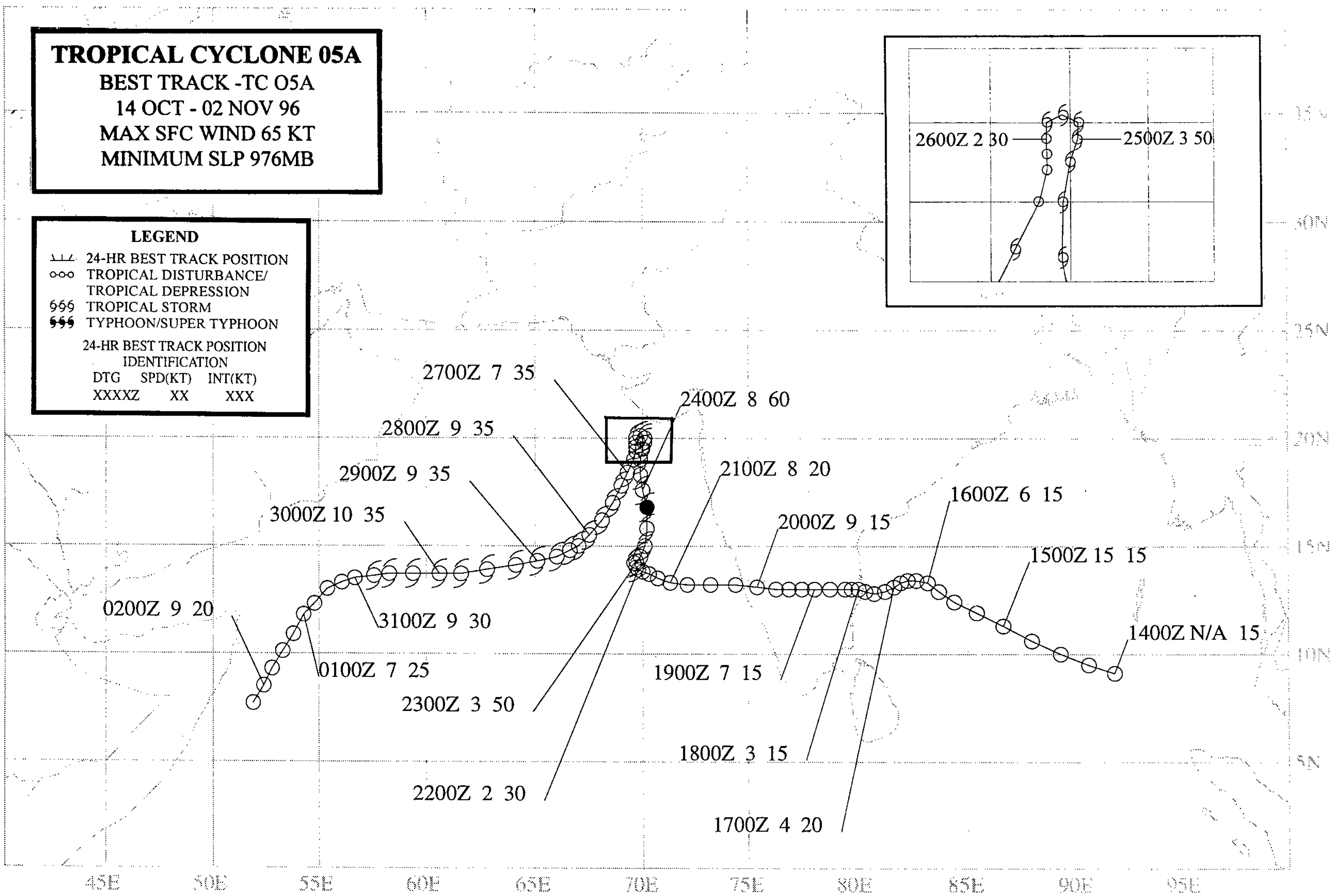

TROPICAL CYCLONE 05A
BEST TRACK -TC O5A
14 OCT - 02 NOV 96
MAX SFC WIND 65 KT
MINIMUM SLP 976MB
LEGEND
24-HR BEST TRACK POSITION
TROPICAL DISTURBANCE/
TROPICAL DEPRESSION
TROPICAL STORM
TYPHOON/SUPER TYPHOON
24-HR BEST TRACK POSITION
IDENTIFICATION
DTG SPD(KT) INT(KT)
XXXXZ XX XXX
2600Z 2 30
2500Z 3 50
2700Z 7 35
2400Z 8 60
2800Z 9 35
2900Z 9 35
2100Z 8 20
3000Z 10 35
1600Z 6 15
2000Z 9 15
1500Z 15 15
0200Z 9 20
3100Z 9 30
1400Z N/A 15
0100Z 7 25
1900Z 7 15
2300Z 3 50
1800Z 3 15
2200Z 2 30
1700Z 4 20
45E
50E
55E
60E
65E
70E
75E
80E
85E
90E
95E
30N
25N
20N
15N
10N
5N

TROPICAL CYCLONE 05A

I. HIGHLIGHTS

Tropical Cyclone 05A (TC 05A), the third Arabian Sea cyclone of 1996, initially started as a mid-October disturbance in the Bay of Bengal, and had one of the most unusual tracks in North Indian Ocean cyclone history. It moved across southern India into the Arabian Sea, stopped, turned north, and intensified. Near 20°N 70°E, the system turned to the southwest, and remained on that track for nine days before dissipating near the Somalia coast. TC-05A was one of the longest-lived cyclones ever in the North Indian Ocean. The Arabian Sea generally averages about one cyclone per year.

II. TRACK AND INTENSITY

TC 05A was first observed as a suspicious area of convection in the southwest Bay of Bengal, about 350 nm (648 km) east of Madras (WMO 43279) on 14 October. After crossing the southern part of the Indian Peninsula and entering the Arabian Sea at speeds ranging from 3-13 kt (5.5-24 km/hr), the disturbance began to organize, and a Tropical Cyclone Formation Alert was issued at 211600Z based on an observed increase in convective curvature and low-level cloud lines in satellite imagery. Shortly thereafter, the disturbance abruptly stopped, began to intensify, and turned to the north near 70°E. The first warning was valid at 221200Z based on a Dvorak T-number of T2.5 (35 kt; 18 m/sec) (Figure 3-05A-1). The system reached an intensity of 65 kt (34 m/sec) (Figure 3-05A-2) on its northward track, then suddenly stopped its northward movement about 50 nm (93 km) south of the southern coast of Gujarat State of northwestern India, after running into strong northeasterly shear. Six hours later, the system began to rapidly weaken from the shear, and took a south-southward track. The final warning was issued at 260000Z, but the system was monitored for regeneration. Figure 3-05A-3 shows the remnants of the cyclone on microwave imagery. These remnants of TC 05A drifted south, away from the region of strong vertical wind shear which had blown away the deep convection. A second Tropical Cyclone Formation Alert was generated at 271600Z when a ship indicated the remnants of TC 05A had a central pressure of 996 mb and 35-kt (18-m/sec) sustained winds. At 280000Z, warnings were resumed for the regenerated cyclone. The system remained, on a southwestward track at minimal tropical-storm intensity. TC 05A finally weakened about two days later, and the final warning was issued at 311200Z while the depression was 60 nm (111 km) northeast of Socotra Island (Figure 3-05A-4).

III. IMPACT

No reports of injuries or damage were received at the JTWC.

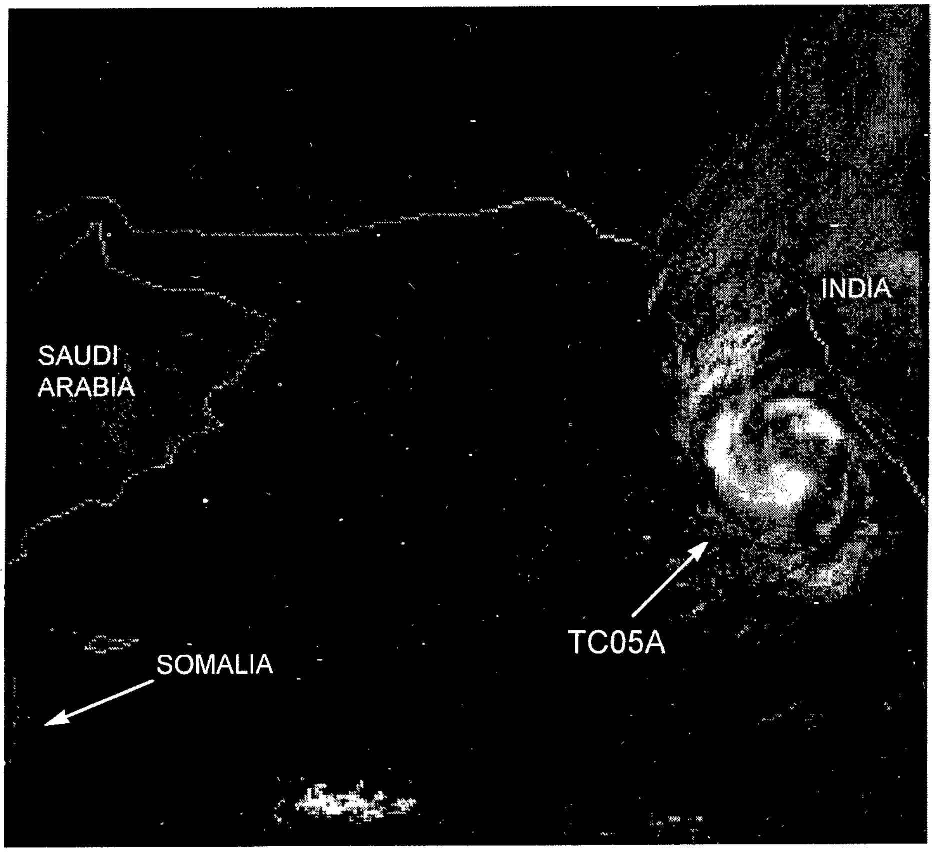

Figure 3-05A-1 TC-05A as deep convection begins to build over the LLCC. (230450Z October DMSP visible imagery). (Imagery downloaded from the Space Physics Interactive Data Resource (SPIDR) internet site maintained by NGDC).

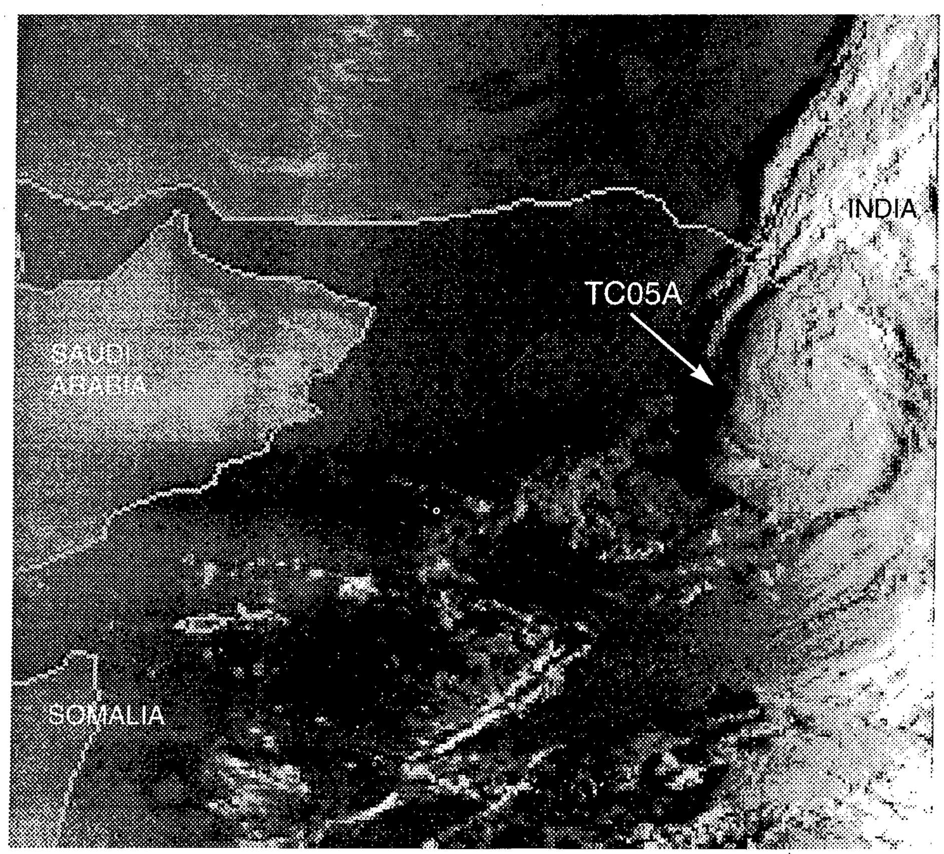

Figure 3-05A-2 TC-05A at a Dvorak T4.0 (240114Z October DMSP visible imagery). (Imagery downloaded from SPIDR).

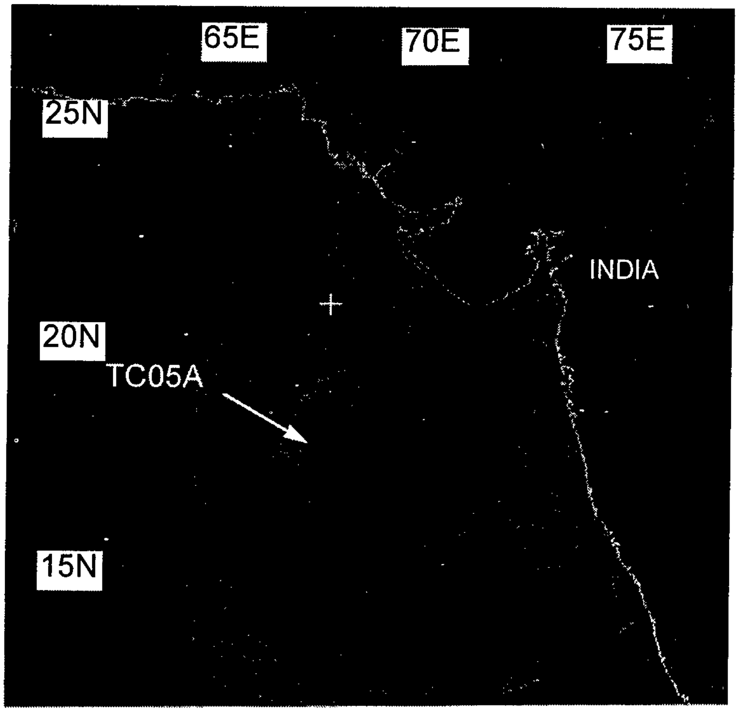

Figure 3-05A-3 The remnants of TC-05A after it had sheared from the convection. The dark circulation signifies low-and-middle-level clouds. (270127Z October DMSP microwave imagery).

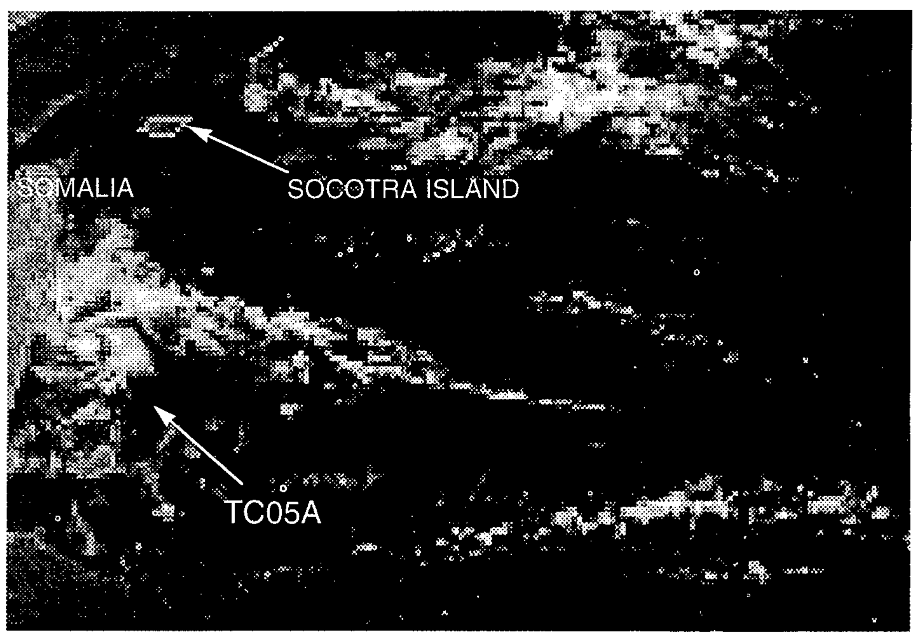

Figure 3-05A-4 The remnant LLCC of TC-05A as it approached the Somali coast (020430Z November DMSP visible imagery). (Imagery downloaded from SPIDR).

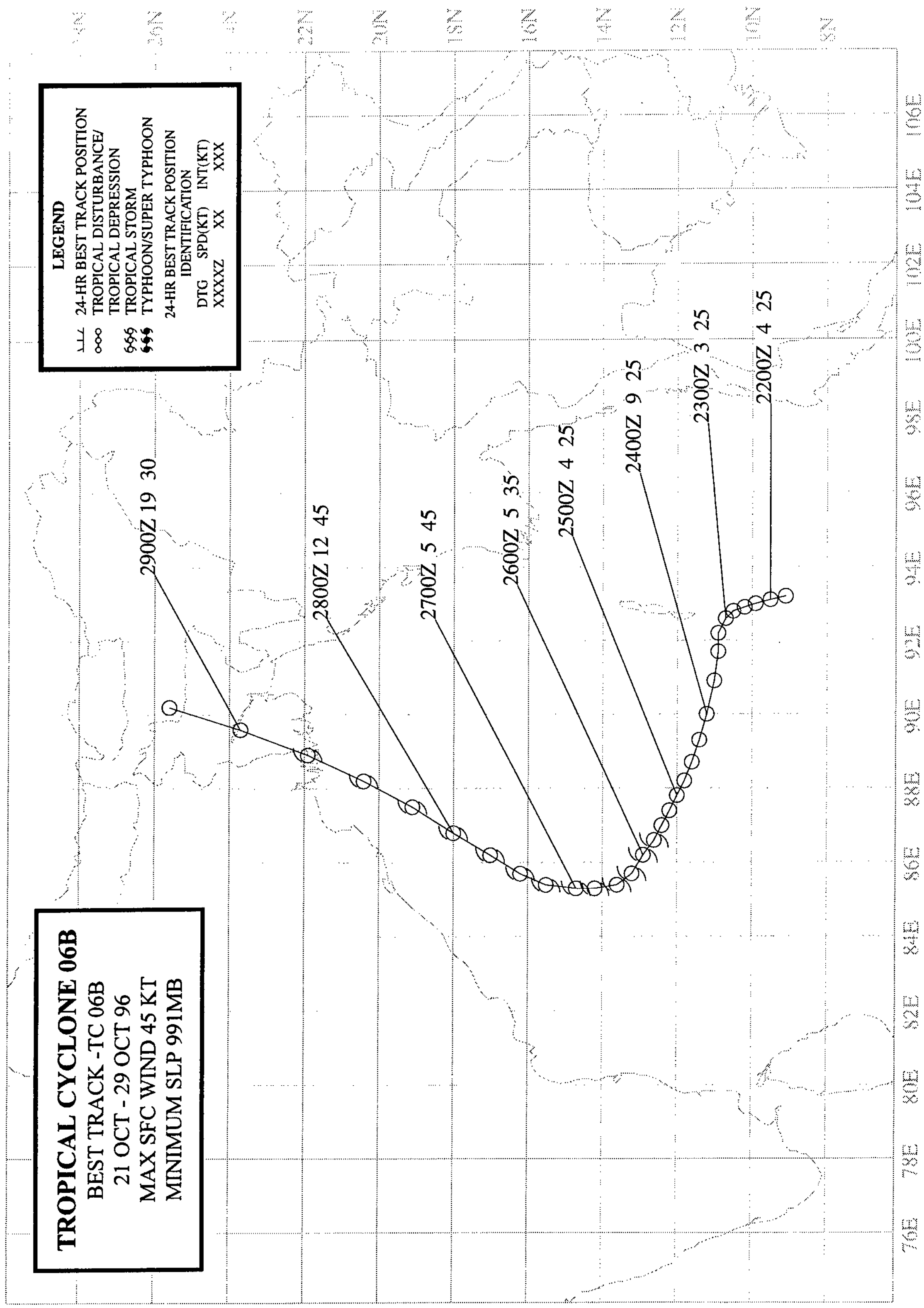
TROPICAL CYCLONE 06B
BEST TRACK -TC 06B
21 OCT - 29 OCT 96
MAX SFC WIND 45 KT
MINIMUM SLP 991MB
LEGEND
24-HR BEST TRACK POSITION
TROPICAL DISTURBANCE/
TROPICAL DEPRESSION
TROPICAL STORM
TYPHOON/SUPER TYPHOON
24-HR BEST TRACK POSITION
IDENTIFICATION
DTG SPD(KT) INT(KT)
XXXXZ XX XXX
2900Z 19 30
2800Z 12 45
2700Z 5 45
2600Z 5 35
2500Z 4 25
2400Z 9 25
2300Z 3 25
2200Z 4 25
22N
20N
18N
16N
14N
12N
10N
8N
76E
78E
80E
82E
84E
86E
88E
90E
92E
94E
96E
98E
100E
102E
104E
106E

TROPICAL CYCLONE 06B

The area of poorly organized convection that became Tropical Cyclone 06B (TC 06B) was detected south of the Andaman Islands and first mentioned on the 211800Z October Significant Tropical Weather Advisory. The tropical disturbance was under the influence of strong upper-level easterly wind shear, which resulted in the low-level circulation center being exposed to the east of the deep convection. JTWC issued the first of three TCFAs at 220930Z as the shear appeared to weaken. The anticipated development was delayed, however, and the TCFA was reissued at 230730Z, and again at 240600Z. The convection did finally become better organized and JTWC issued the first warning valid at 250600Z. After recurvature on 27 October, the cyclone accelerated to the northeast. TC 06B made landfall on the heavily populated delta region of West Bengal India near the Bangladesh border at 281800Z (See Figure 3-06B-1). The final warning was issued, valid at 290000Z, as the filling cyclone moved further inland. Heavy rains associated with TC 06B caused flooding, which immobilized much of metropolitan Calcutta. A 9-foot (3-m) storm surge inundated low lying coastal areas in Bangladesh where reports indicated that 14 people were killed, over 2000 people were injured, and 100 fishermen were missing.

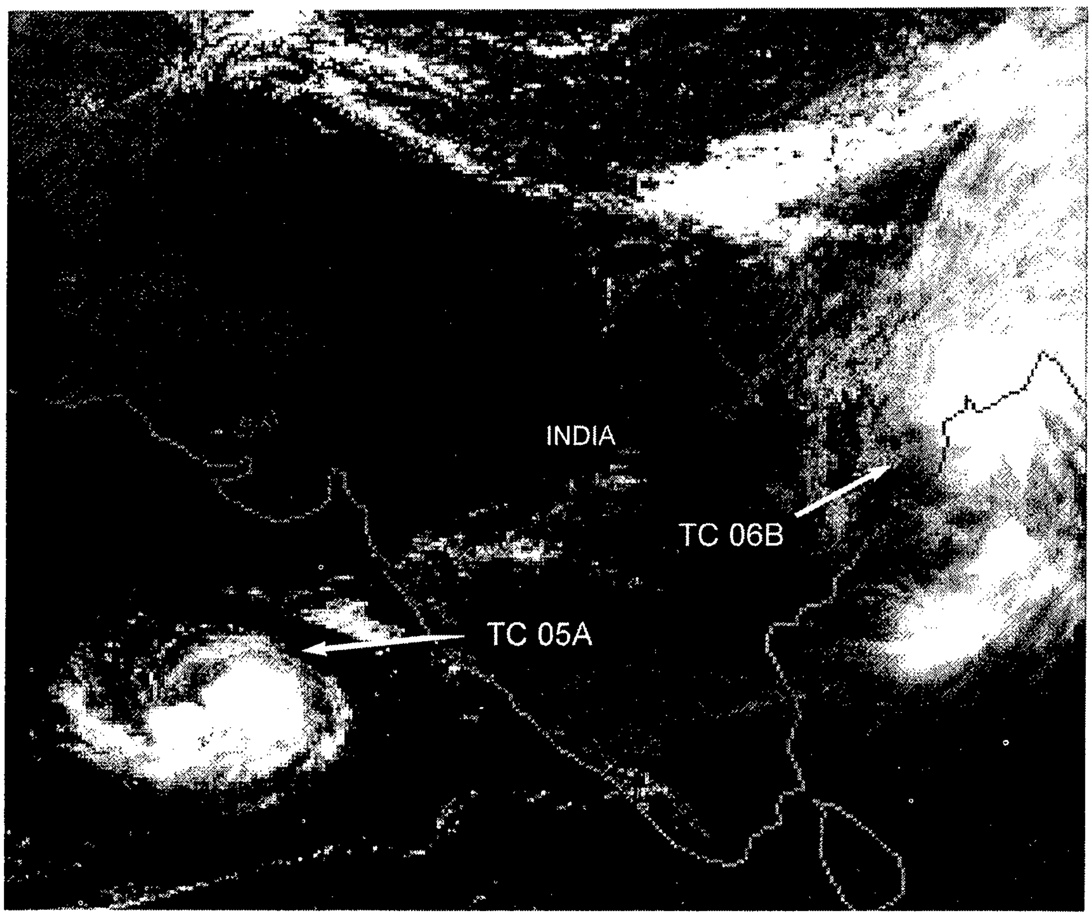

Figure 3-06B-1 TC 06B (upper right) just after making landfall. TC 05A is seen to the west of the India subcontinent (280350Z October visible DMSP imagery).

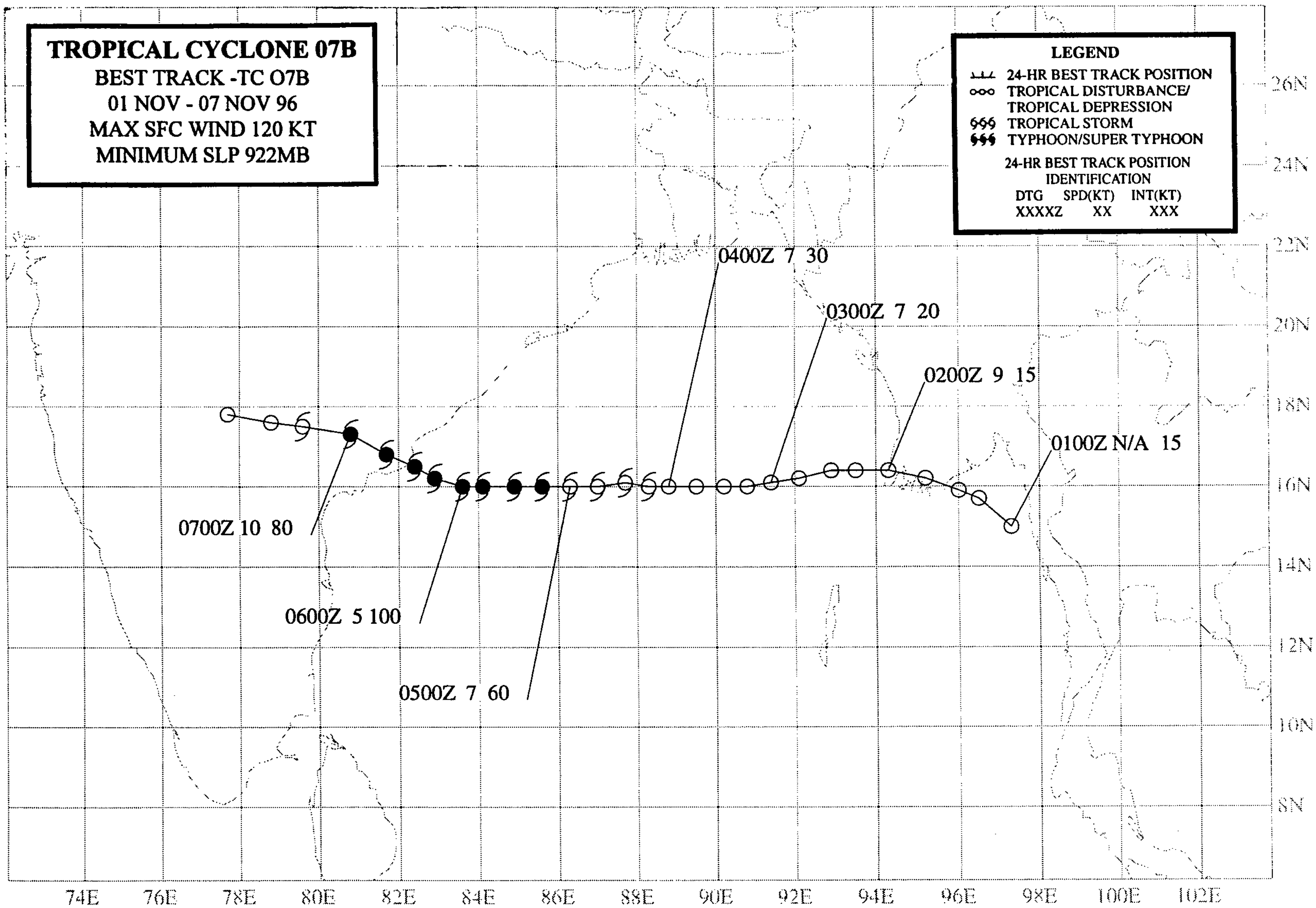
TROPICAL CYCLONE 07B
BEST TRACK -TC O7B
01 NOV - 07 NOV 96
MAX SFC WIND 120 KT
MINIMUM SLP 922MB
LEGEND
24-HR BEST TRACK POSITION
TROPICAL DISTURBANCE/
TROPICAL DEPRESSION
TROPICAL STORM
TYPHOON/SUPER TYPHOON
24-HR BEST TRACK POSITION
IDENTIFICATION
DTG SPD(KT) INT(KT)
XXXXZ XX XXX
0400Z 7 30
0300Z 7 20
0200Z 9 15
0100Z N/A 15
0700Z 10 80
0600Z 5 100
0500Z 7 60
26N
24N
22N
20N
18N
16N
14N
12N
10N
8N
74E
76E
78E
80E
82E
84E
86E
88E
90E
92E
94E
96E
98E
100E
102E

TROPICAL CYCLONE 07B

As the remnants of TD 43W dissipated over the rugged Malay peninsula, new convection was noted in the Andaman Sea and first mentioned on the 011800Z November Significant Tropical Weather Advisory. Improved convective organization led to the issuance of a TCFA at 030730Z, followed by the initial warning on TC 07B, valid at 031200Z. The system tracked steadily westward under the influence of deep easterly steering flow. Intensification was more rapid than the normal one-T-number per day, and continued until TC 07B peaked at 120 kt (62 m/sec) just before landfall (Figure 3-07B-1) at 061200Z. The development of the wind field associated with this cyclone was evident in the microwave imagery provided by FNMOC on the MISTIC system. After crossing the coast near Kakinada (240 nm (445 km) north-northeast of Madras) at 061300Z, TC 07B weakened as it continued inland. JTWC issued the final warning valid at 070600Z. The cyclone's impact in the coastal areas was significant, and more than 1,000 deaths were attributed to TC 07B. Of these fatalities, 42 passengers were lost when a ferry sank during the storm. More than 1,000 fisherman were reported missing at sea. TC 07B was also responsible for widespread flooding, the destruction of at least 10,000 homes, and the loss of hundreds of thousands of acres of rice crop. More than 250 villages were reported under water and many coastal communities were inundated by 12-foot-high waves. Worst hit was the coastal city of Kakinada where the cyclone dumped 8.8 inches (226 mm) of rain.

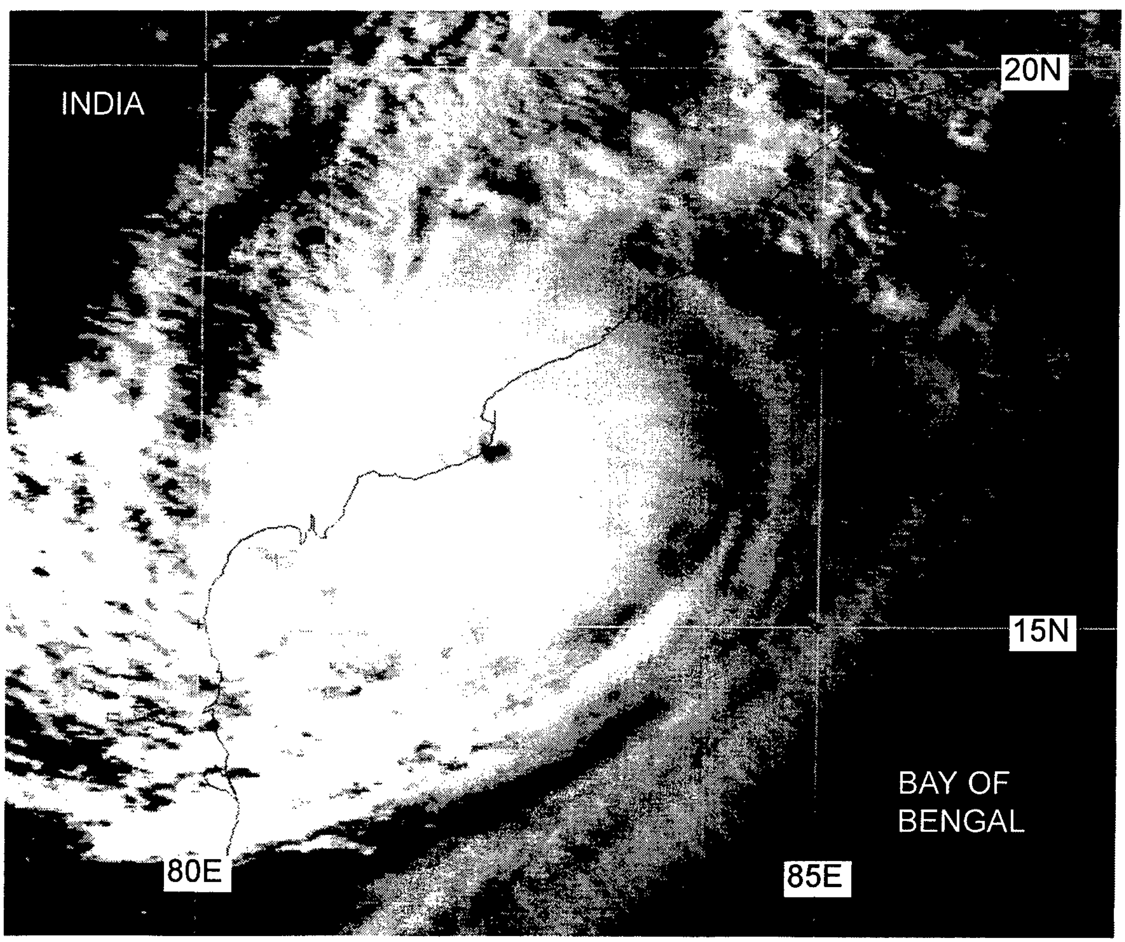

Figure 3-07B-1 TC 07B at peak intensity of 120 kt (62 m/sec)(061024Z November visible GMS imagery).

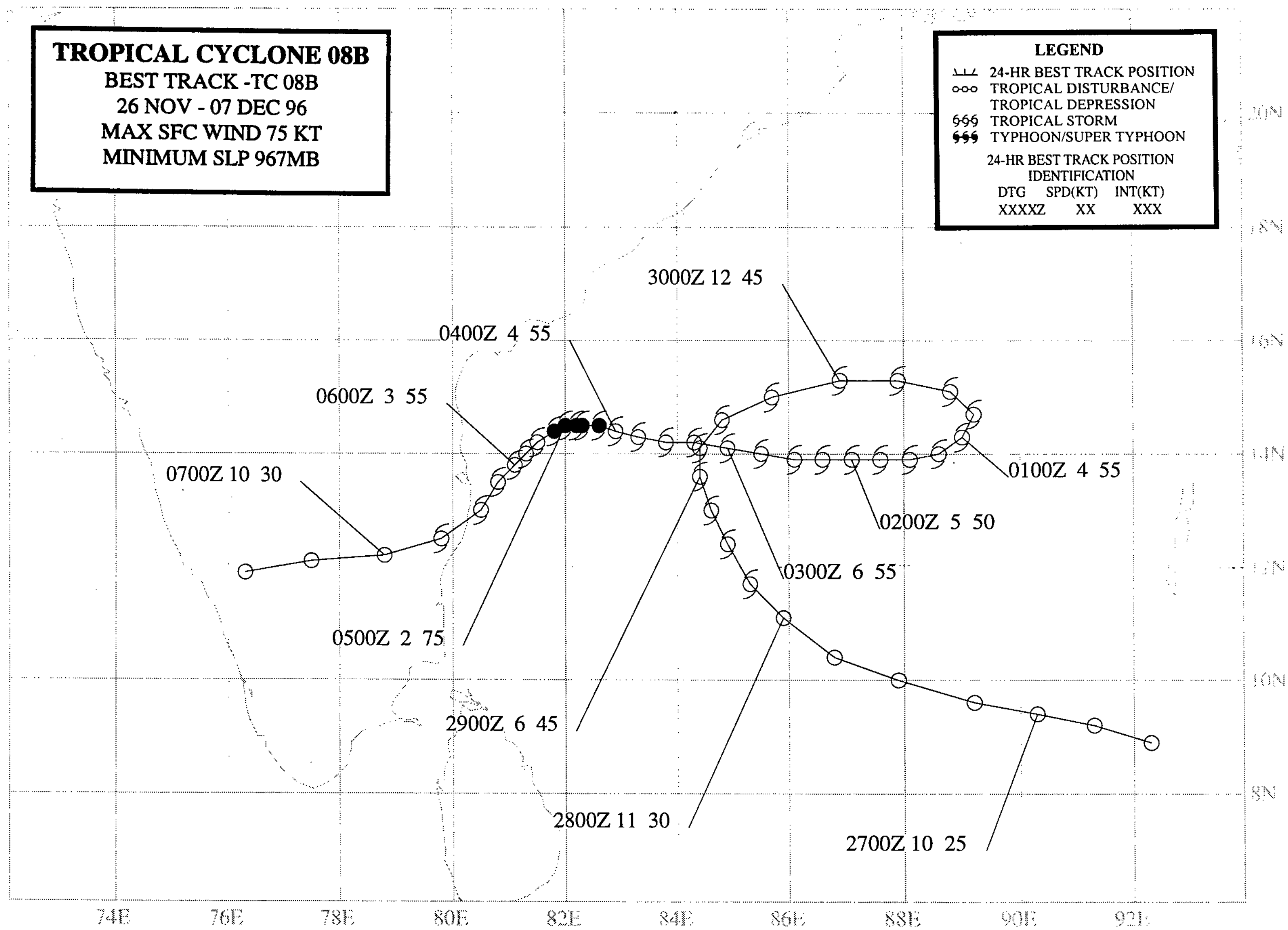
TROPICAL CYCLONE 08B
BEST TRACK -TC 08B
26 NOV - 07 DEC 96
MAX SFC WIND 75 KT
MINIMUM SLP 967MB
LEGEND
24-HR BEST TRACK POSITION
TROPICAL DISTURBANCE/
TROPICAL DEPRESSION
TROPICAL STORM
TYPHOON/SUPER TYPHOON
24-HR BEST TRACK POSITION
IDENTIFICATION
DTG SPD(KT) INT(KT)
XXXXZ XX XXX
3000Z 12 45
0400Z 4 55
0600Z 3 55
0700Z 10 30
0100Z 4 55
0200Z 5 50
0300Z 6 55
0500Z 2 75
2900Z 6 45
2800Z 11 30
2700Z 10 25
20N
18N
16N
14N
12N
10N
8N
74E
76E
78E
80E
82E
84E
86E
88E
90E
92E

TROPICAL CYCLONE 08B

I. HIGHLIGHTS

Tropical Cyclone 08B (TC 08B) was unusual for three reasons: 8 days in warning, a 4-day loop, and erratic southwestward movement along the coast of India. Hundreds of lives were probably spared because TC 08B weakened before making landfall.

II. TRACK AND INTENSITY

TC 08B formed in the monsoon trough just south of the Andaman Islands. The persistence of an area of poorly organized convection over a well developed low-level circulation resulted in JTWC's first mention of the tropical disturbance on the 261800Z November Significant Tropical Weather Advisory. As the system slowly developed, JTWC issued the first TCFA at 270130Z. However, a second TCFA was required at 272230Z to reposition the alert area to the west. An increase in overall organization and intensity prompted JTWC to issue the first warning valid at 280600Z. Although TC 08B's initial track was to the west-northwest, the cyclone started a large clockwise loop on 29 November that took four days to complete. Early on 04 December, the system slowed and peaked at 75 kt (39 m/sec). As the cyclone approached the eastern periphery of the blocking high in the low to middle levels over India, strong 50-kt (26 m/sec) upper-level southeasterly winds appeared (Figure 3-08B-1). These features resulted in a track change to the southwest, and increased vertical wind shear weakened the cyclone. By the end of 05 December, the upper and lower levels of the cyclone had become decoupled. The convection was displaced to the northwest and the LLCC moved to the southwest. At 061500Z, TC 08B moved ashore near Pondicherry, about 60 nm (110 KM) south of Madras. The final warning was issued, valid at 061800Z, as the system dissipated over southwestern India.

III. DISCUSSION

a. *Longevity*

An investigation of Bay of Bengal cyclones since 1972 indicates that no other looping tropical cyclone has taken four days to complete its looping motion. Also, the 8-day period of warning is considered very long, as the average period in warning for Bay of Bengal cyclones is less than four days. Longer warning periods have been noted for cyclones that form in the Bay and move westward in to the Arabian Sea before dissipating.

b. *NOGAPS performance*

With regard to TC 08B's change of track to the southwest near the coast of India, NOGAPS correctly anticipated the movement as early as 02 December — three days before it actually occurred.

IV. IMPACT

Because TC 08B weakened over water before making landfall, the death toll was very low, 7. There were no reports of significant damage.

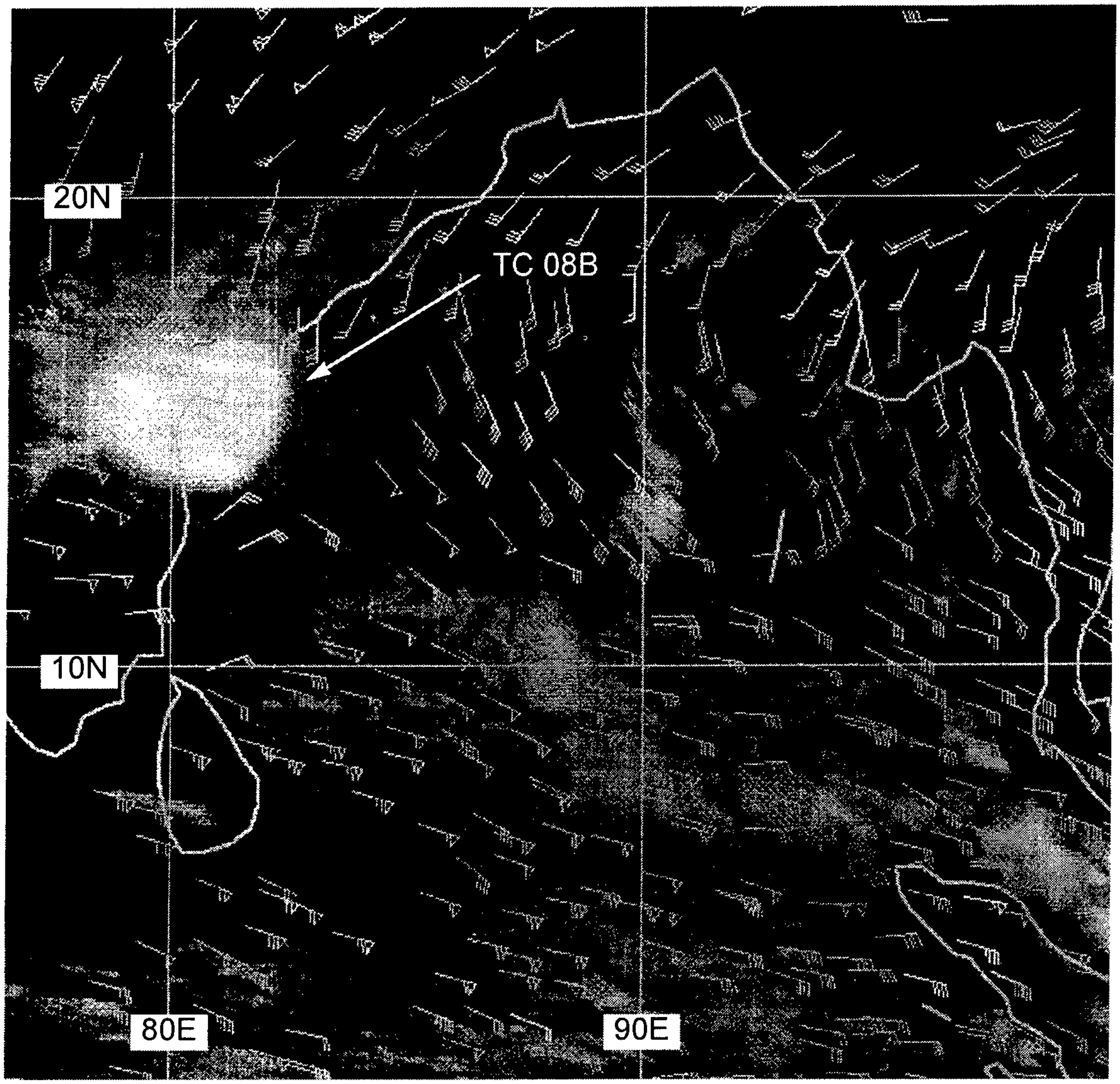

Figure 3-08B-1 Water vapor imagery and upper-level cloud-track winds reveal strong southeasterly winds impinging upon TC 08B (041132Z December water vapor GMS imagery).

4. SUMMARY OF SOUTH PACIFIC AND SOUTH INDIAN OCEAN TROPICAL CYCLONES

4.1 GENERAL

On 1 October 1980, JTWC's area of responsibility (AOR) was expanded to include the Southern Hemisphere from 180° longitude, westward to the coast of Africa. Details on Southern Hemisphere tropical cyclones and JTWC warnings from July 1980 through June 1982 are contained in Diercks et al. (1982), and from July 1982 through June 1984 in Wirfel and Sandgathe (1986). Information on Southern Hemisphere tropical cyclones after June 1984 can be found in the applicable Annual Tropical Cyclone Report.

The NAVPACMETOCCEN, Pearl Harbor, Hawaii issues warnings on tropical cyclones in the South Pacific which are east of 180° longitude. In accordance with CINCPACINST 3140.1W, Southern Hemisphere tropical cyclones are numbered sequentially from 1 July through 30 June. This convention is established to encompass the Southern Hemisphere tropical cyclone season, which primarily occurs from January through April. There are two Southern Hemisphere ocean basins for warning purposes - the South Indian Ocean (west of 135° East longitude) and the South Pacific (east of 135° East longitude) - which are identified by appending the suffixes "S" and "P," respectively, to the tropical cyclone number.

Intensity estimates for Southern Hemisphere tropical cyclones are derived from the interpretation of satellite imagery using the Dvorak (1984) technique and, when available, from surface observations and radar data. The Dvorak technique relates specific cloud signatures to maximum sustained one-minute average surface wind speeds. The conversion from maximum sustained winds to minimum sea-level pressure is obtained from Atkinson and Holliday (1977) (Table 4-1).

4.2 SOUTH PACIFIC AND SOUTH INDIAN OCEAN TROPICAL CYCLONES

The total number of significant tropical cyclones during the 1996 season (1 July 1995 - 30 June 1996; Table 4-2) was 28 which was slightly more than the overall climatological mean of 27 for the previous 16 years as shown in Table 4-3. Looking at the annual variation of Southern Hemisphere Tropical Cyclones by ocean basins (Table 4-4), it becomes apparent that tropical cyclone activity was slightly enhanced in the southern Indian Ocean and Australian regions, and slightly reduced in the South Pacific.

Table 4-1 MAXIMUM SUSTAINED 1-MINUTE MEAN SURFACE WINDS AND EQUIVALENT MINIMUM SEA-LEVEL PRESSURE RELATIONSHIP (ATKINSON AND HOLLIDAY, 1977)

WIND-KT	(M/SEC)	PRESSURE (MB)
30	(15)	1000
35	(18)	997
40	(21)	994
45	(23)	991
50	(26)	987
55	(28)	984
60	(31)	980
65	(33)	976
70	(36)	972
75	(39)	967
80	(41)	963
85	(44)	958
90	(46)	954
95	(49)	948
100	(51)	943
105	(54)	938
110	(57)	933
115	(59)	927
120	(62)	922
125	(64)	916
130	(67)	910
135	(69)	906
140	(72)	898
145	(75)	892
150	(77)	885
155	(80)	879
160	(82)	872
165	(85)	965
170	(87)	858
175	(90)	851
180	(93)	844

The JTWC warned on Southern Hemisphere tropical cyclones for 117 days of the 1996 season. This equates to roughly to 1 out of every 3 days of the 1996 Southern Hemisphere season having a tropical cyclone in active warning status. During 36 of the 117 days there were two or more Southern Hemisphere tropical cyclones in warning status at the same time. An additional 14 days of active warnings were covered by NAVPACMETOCCEN, Pearl Harbor, 3 days of which multiple tropical cyclones were in warning status.

A chronology of 1996 Southern Hemisphere tropical activity is provided in Figure 4-1. Composites of the tropical cyclone best tracks for the Southern Indian Ocean, the Australian Region, and the South Pacific Ocean, appear in Figures 4-2, 4-3, and 4-4 respectively.

Table 4-2 SOUTHERN HEMISPHERE TROPICAL CYCLONES FOR 1996

TROPICAL CYCLONE		PERIOD OF WARNING	NUMBER OF WARNINGS ISSUED	ESTIMATED MAX SURFACE WINDS KT (M/SEC)	ESTIMATED MSLP (MB)
01S	DARYL/AGNIELLE	17 NOV - 25 NOV	17	150 (77)	885
02S	EMMA*	04 DEC - 06 DEC	4	30 (15)	1000
	-	09 DEC - 12 DEC	7	40 (21)	994
	-	14 DEC - 15 DEC	3	30 (15)	1000
03S	FRANK	07 DEC - 13 DEC	24	115 (59)	927
04S	GERTIE	18 DEC - 21 DEC	14	75 (39)	967
05P	BARRY	04 JAN - 07 JAN	7	80 (41)	963
06S	BONITA	05 JAN - 15 JAN	20	135 (69)	904
07S	HUBERT/CORYNA	08 JAN - 12 JAN	9	75 (39)	967
08P	TASI♦	16 JAN - 19 JAN	0 (6)	45 (23)	991
09P	CELESTE	27 JAN - 30 JAN	7	65 (33)	976
10P	JACOB*	28 JAN - 29 JAN	4	50 (26)	987
	-	01 FEB - 07 FEB	19	90 (46)	954
11S	ISOBEL	28 JAN - 31 JAN	12	45 (23)	991
12S	-	07 FEB - 09 FEB	5	35 (18)	997
13P	DENNIS	13 FEB - 18 FEB	11	45 (23)	991
14S	DOLORESSE	15 FEB - 19 FEB	9	75 (39)	967
15S	-	16 FEB - 17 FEB	3	35 (18)	997
16S	EDWIGE*♦	22 FEB - 24 FEB	0 (6)	45 (23)	991
	-	25 FEB - 29 FEB	0(10)	95 (49)	949
17S	FLOSSY	27 FEB - 04 MAR	13	115 (59)	927
18S	KIRSTY	09 MAR - 12 MAR	13	100 (51)	943
19P	ETHEL	09 MAR - 13 MAR	10	45 (23)	991
20P	ZAKA	10 MAR - 11 MAR	3	40 (21)	994
21P	ATU	10 MAR - 13 MAR	10	55 (28)	984
22S	GUYLIANNE	20 MAR - 23 MAR	8	35 (18)	997
23P	BETI	21 MAR - 29 MAR	17	105 (54)	938
24S	HANSELLA	03 APR - 10 APR	15	95 (49)	949
25S	OLIVIA	05 APR - 11 APR	19	125 (64)	916
26S	ITELLE	08 APR - 17 APR	19	140 (72)	898
27S	-	16 APR - 19 APR	8	30 (15)	1000
28S	JENNA	01 MAY - 06 MAY	11	60 (31)	980
Grand total			321		
♦ Warnings issued by NAVPACMETOCCEN (NPMOC)			(22)		
JTWC total			343		

* Regenerated

Table 4-3 MONTHLY DISTRIBUTION OF SOUTH PACIFIC AND SOUTH INDIAN OCEAN TROPICAL CYCLONES

YEAR	JUL	AUG	SEP	OCT	NOV	DEC	JAN	FEB	MAR	APR	MAY	JUN	TOTAL
(1958-1977) AVERAGE*	-	-	-	0.4	1.5	3.6	6.1	5.8	4.7	2.1	0.5	-	24.7
1981	0	0	0	1	3	2	6	5	3	3	1	0	24
1982	1	0	0	1	1	3	9	4	2	3	1	0	25
1983	1	0	0	1	1	3	5	6	3	5	0	0	25
1984	1	0	0	1	2	5	5	10	4	2	0	0	30
1985	0	0	0	0	1	7	9	9	6	3	0	0	35
1986	0	0	1	0	1	1	9	9	6	4	2	0	33
1987	0	1	0	0	1	3	6	8	3	4	1	1	28
1988	0	0	0	0	2	3	5	5	3	1	2	0	21
1989	0	0	0	0	2	1	5	8	6	4	2	0	28
1990	2	0	1	1	2	2	4	4	10	2	1	0	29
1991	0	0	1	1	1	3	2	5	5	2	1	1	22
1992	0	0	1	1	2	5	4	11	3	2	1	0	30
1993	0	0	1	1	0	5	7	7	2	2	2	0	27
1994	0	0	0	0	2	4	8	4	9	3	0	0	30
1995	0	0	0	0	2	2	5	4	5	4	0	0	22
1996	0	0	0	0	1	3	7	6	6	4	1	0	28
TOTAL	5	1	5	8	24	52	96	105	76	48	15	2	437
AVERAGE (1981-1995)	0.3	0.1	0.3	0.5	1.5	3.3	5.9	6.6	4.7	2.9	0.9	0.1	27.3

* (Gray, 1978)

Table 4-4 ANNUAL VARIATION OF SOUTHERN HEMISPHERE TROPICAL CYCLONES BY OCEAN BASINS

YEAR	SOUTH INDIAN (WEST OF 105°E)	AUSTRALIAN (105°E - 165°E)	SOUTH PACIFIC (EAST OF 165°E)	TOTAL
(1958-1977) AVERAGE*	8.4	10.3	5.9	24.6
1981	13	8	3	24
1982	12	11	2	25
1983	7	6	12	25
1984	14	14	2	30
1985	14	15	6	35
1986	14	16	3	33
1987	9	8	11	28
1988	14	2	5	21
1989	12	9	7	28
1990	18	8	3	29
1991	11	10	1	22
1992	11	6	13	30
1993	10	16	1	27
1994	16	10	4	30
1995	11	7	4	22
1996	13	11	4	28
TOTAL	199	157	81	437
AVERAGE (1981-1995)	12.4	9.7	5.1	27.3

* (Gray,1978)

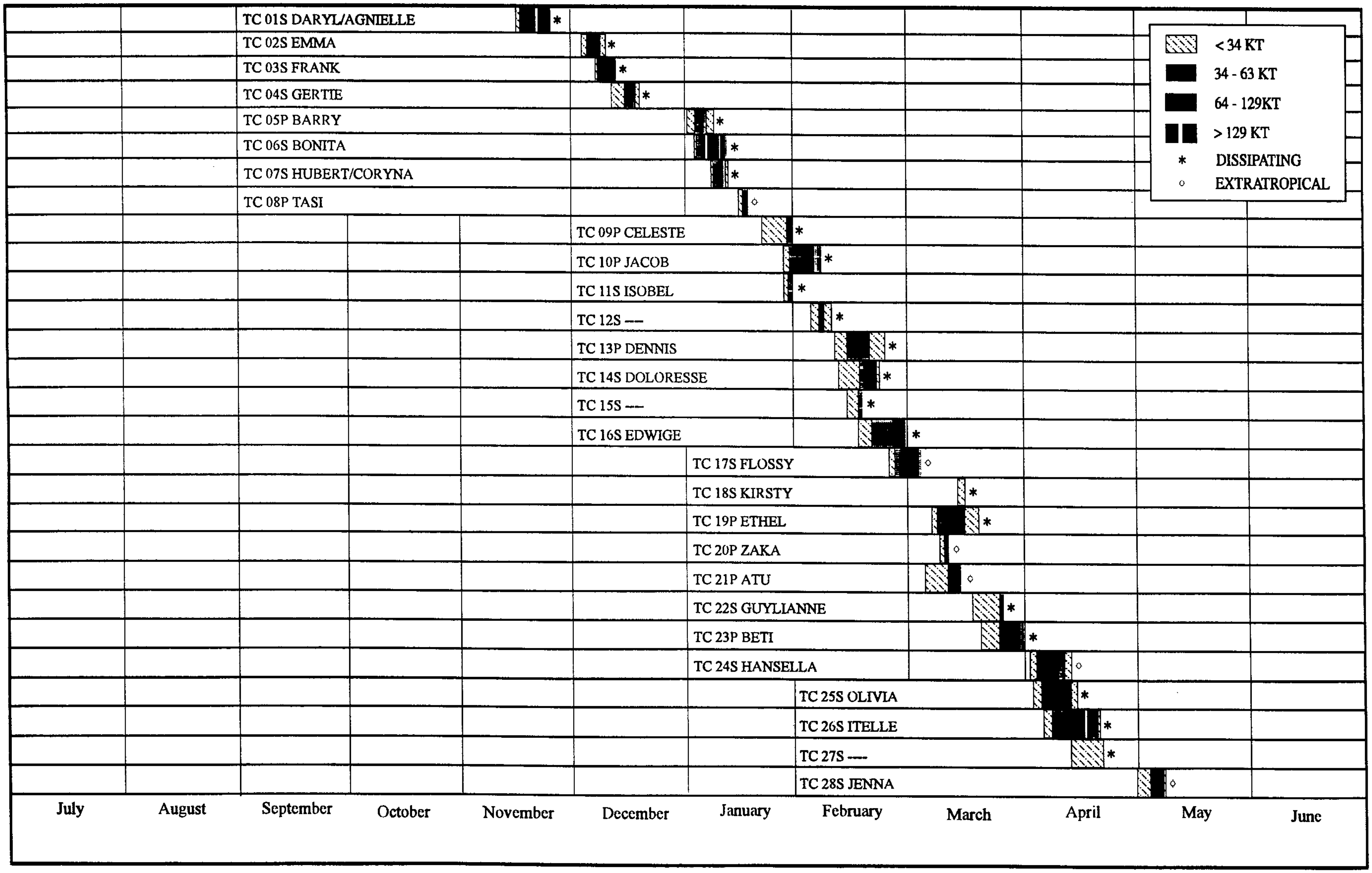

Figure 4-1 Chronology of South Pacific and South Indian Ocean tropical cyclones for 1996 (01 July 1995 - 30 June 1996).

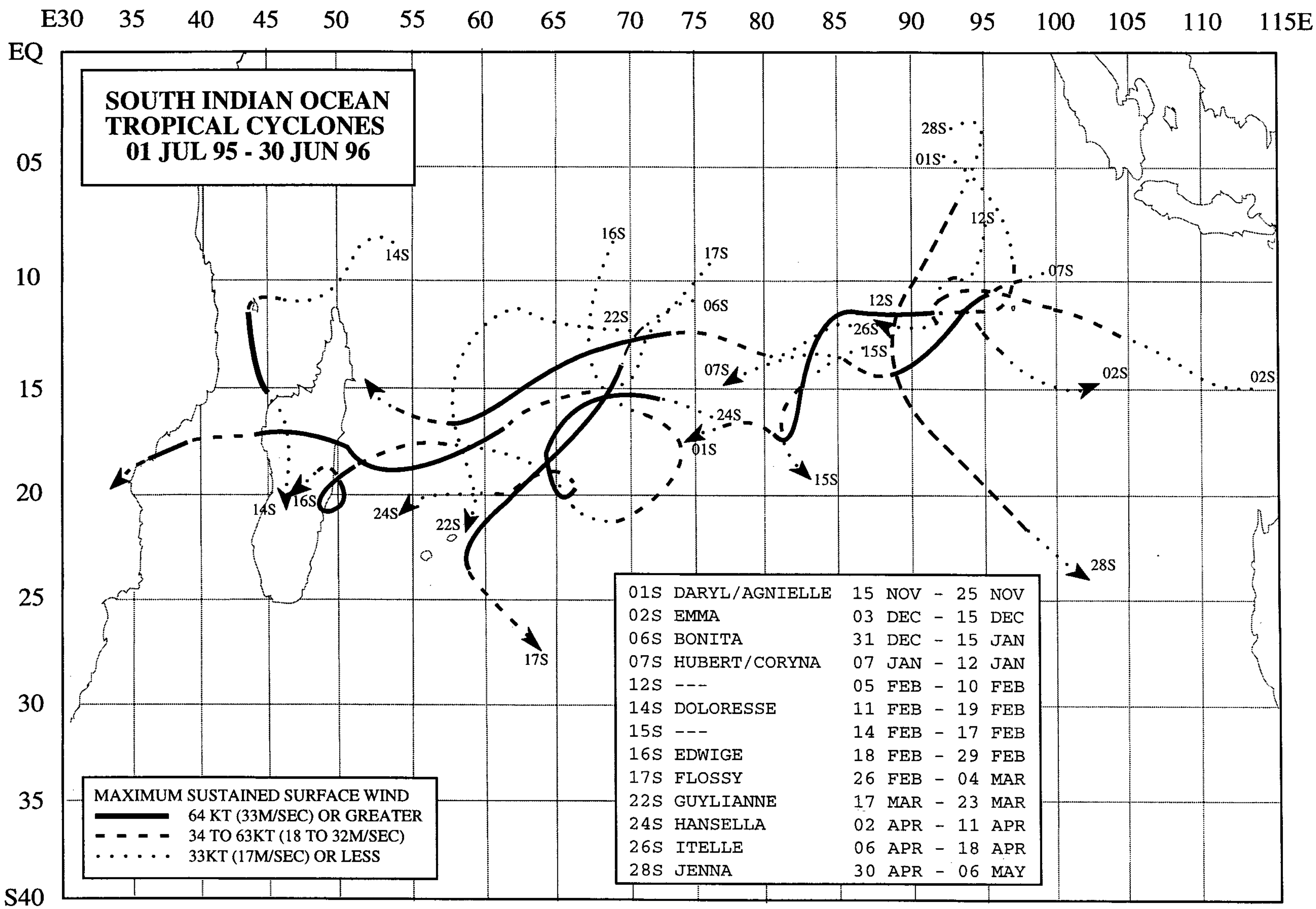

Figure 4-2 Tropical Cyclone best tracks for the South Indian Ocean

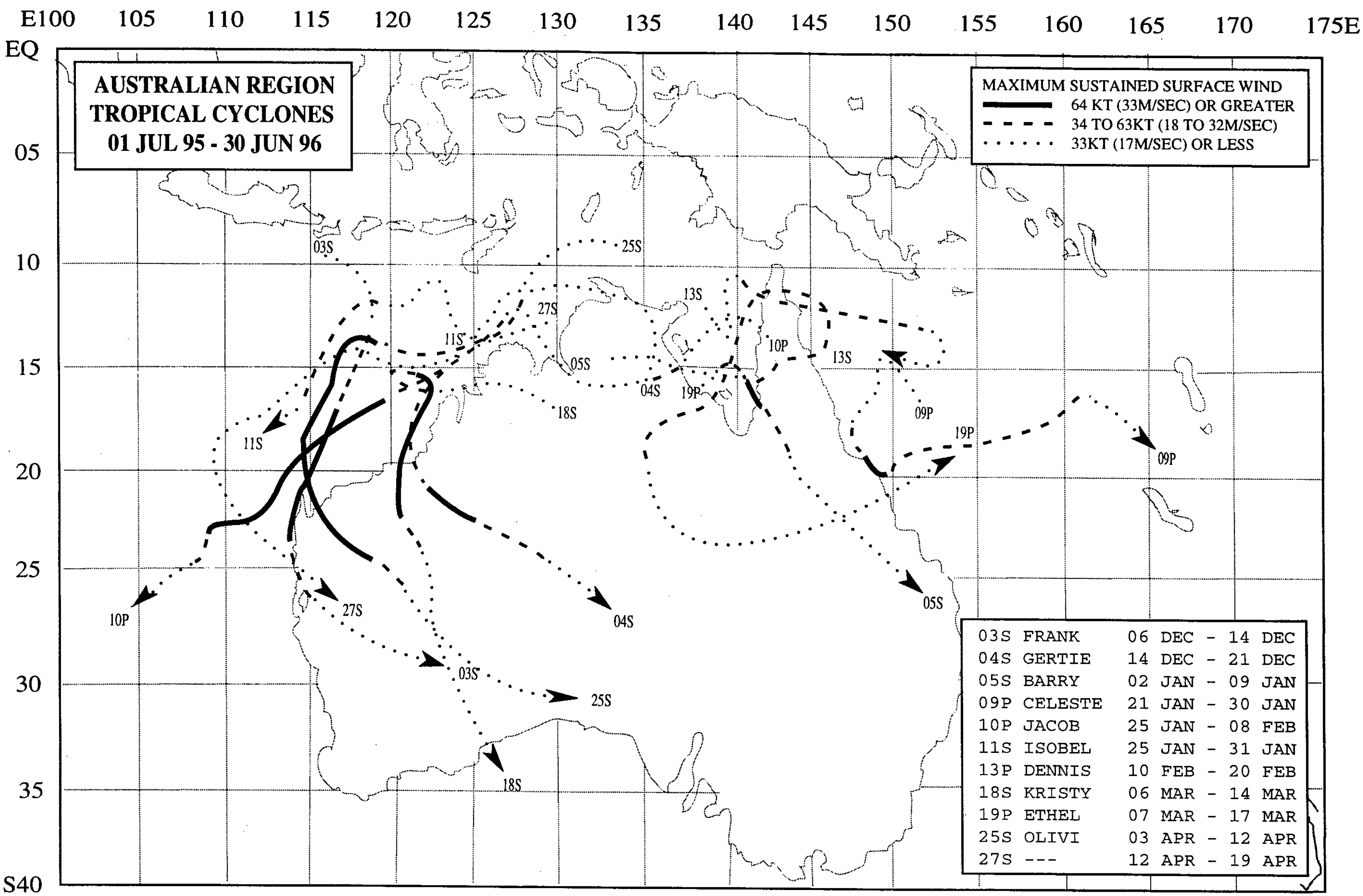

Figure 4-3 Tropical Cyclone Best Tracks for the Australian Region

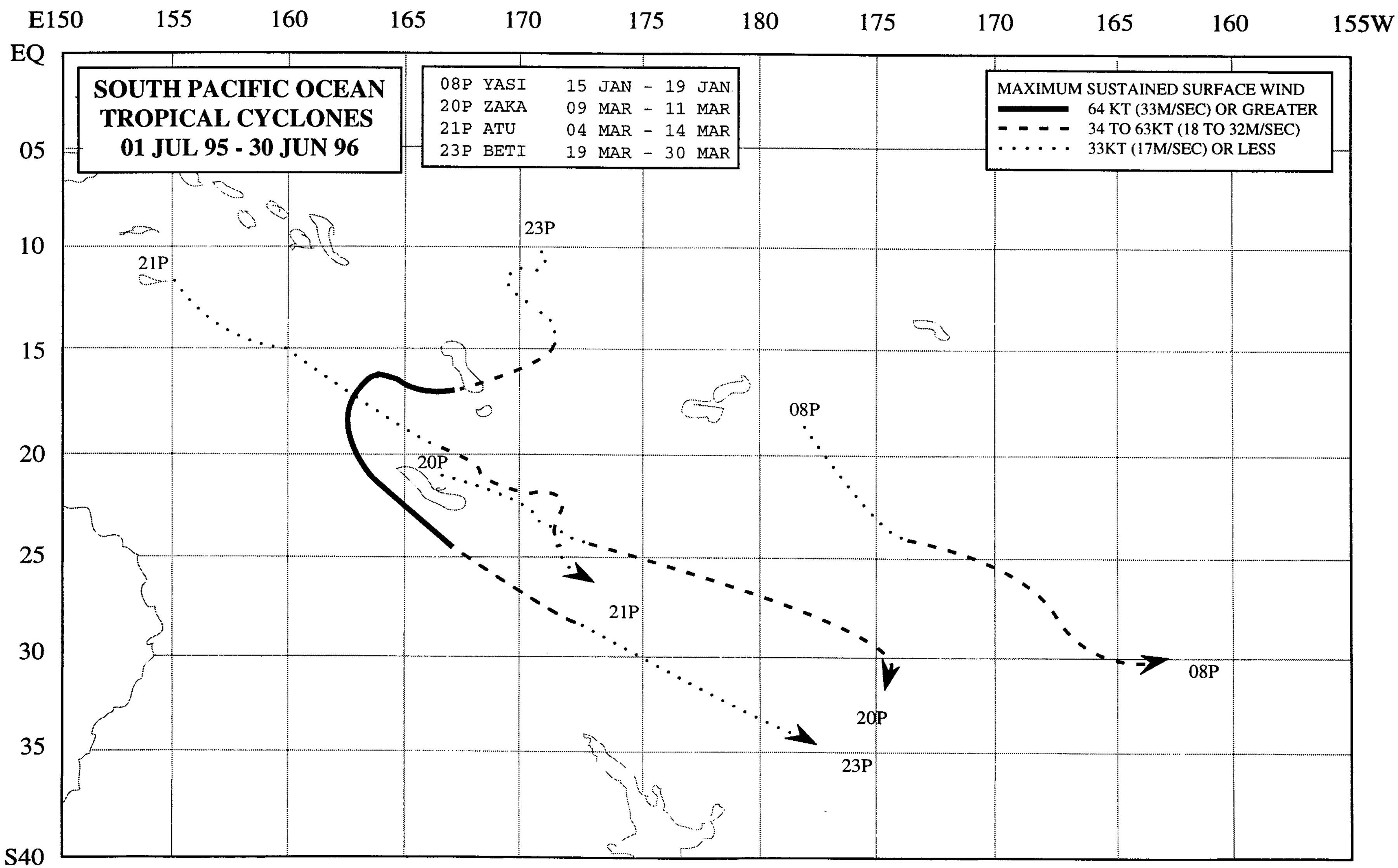

Figure 4-4 Tropical Cyclone Best Tracks for the South Pacific Ocean

Intentionally Left Blank

5. SUMMARY OF FORECAST VERIFICATION

5.1 ANNUAL FORECAST VERIFICATION

Verification of warning positions and intensities at initial, 24-, 48- and 72-hour forecast periods was made against the final best track. The (scalar) track forecast, along-track and cross-track errors (illustrated in Figure 5-1) were calculated for each verifying JTWC forecast. These data, in addition to a detailed summary for each tropical cyclone, are included as Chapter 6. This section summarizes verification data for 1996 and contrasts it with annual verification statistics from previous years.

5.1.1 NORTHWEST PACIFIC OCEAN — The frequency distributions of errors for initial warning positions and 12-, 24-, 36-, 48- and 72-hour forecasts are presented in Figures 5-2a through 5-2f. Table 5-1 includes mean track, along-track and cross-track errors for 1981-1996. Figure 5-3 shows mean track errors and a 5-year running mean of track errors at 24-, 48- and 72-hours for the past 20 years. Table 5-2 lists annual mean track errors from 1959, when the JTWC was founded, until the present.

5.1.2 NORTH INDIAN OCEAN — The frequency distributions of errors for warning positions and 12-, 24-, 36-, 48- and 72-hour forecasts are presented in Figures 5-4a through 5-4f, respectively. Table 5-3 includes mean track, along-track and cross-track errors for 1981-1996. Figure 5-5 shows mean track errors and a 5-year running mean of track errors at 24-, 48- and 72-hours for the past 20 years.

5.1.3 SOUTH PACIFIC AND SOUTH INDIAN OCEANS — The frequency distributions of errors for warning positions and 12-, 24-, 36-, 48- and 72-hour forecasts are presented in Figures 5-6a through 5-6f, respectively. Table 5-4 includes mean track, along-track and cross-track errors for 1981-1996. Figure 5-7 shows mean track errors and a 5-year running mean of track errors at 24-, 48-, and 72-hours for the 16 years that the JTWC has issued warnings in the region.

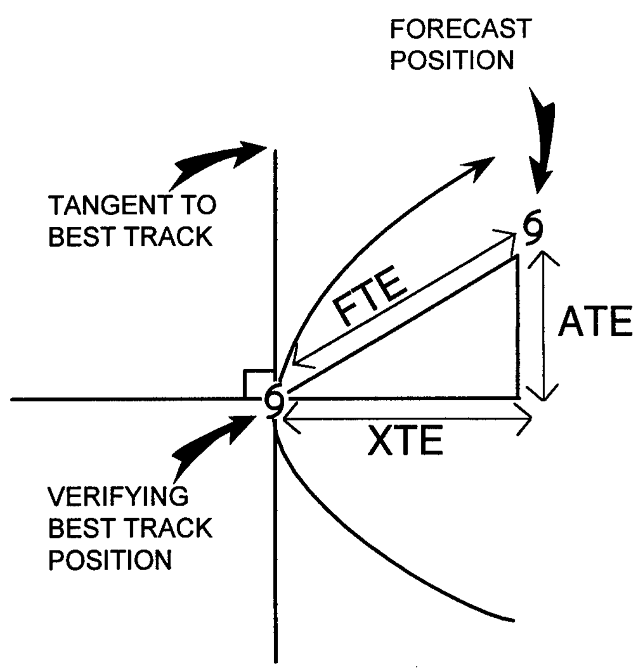

Figure 5-1 Definition of cross-track error (XTE), along-track error (ATE) and forecast track error (FTE). In this example, the forecast position is ahead of and to the right of the verifying best track position. Therefore, the XTE is positive (to the right of the best track) and the ATE is positive (ahead or faster than the best track). Adapted from Tsui and Miller, 1988.

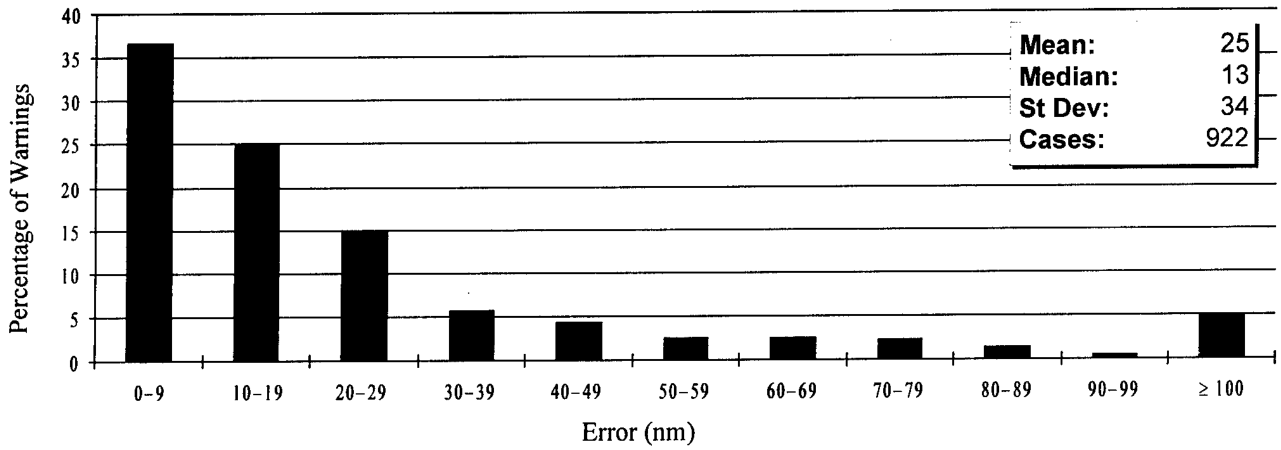

Figure 5-2a Frequency distribution of initial warning position errors (10-nm increments) for western North Pacific Ocean tropical cyclones in 1996. The largest error, 234 nm, occured on Tropical Depression 40W.

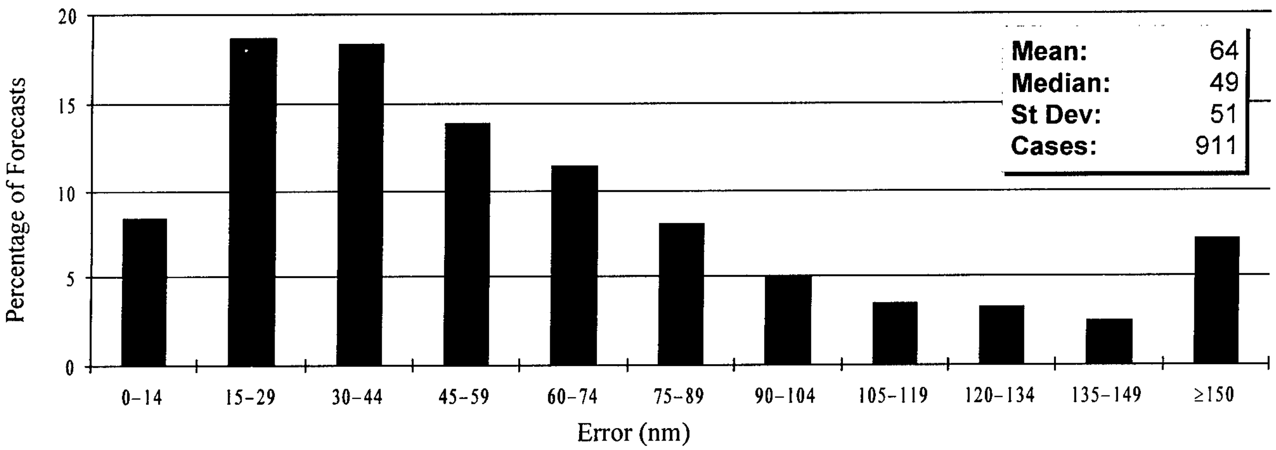

Figure 5-2b Frequency distribution of 12-hour track forecast errors (15-nm increments) for western North Pacific Ocean tropical cyclones in 1996. The largest error, 322 nm, occurred on Tropical Depression 40W.

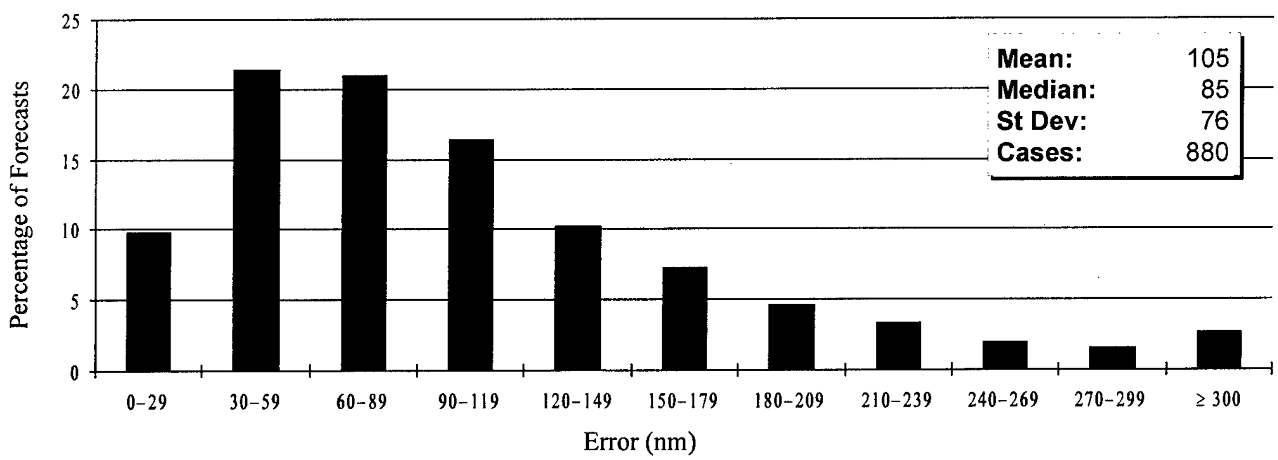

Figure 5-2c Frequency distribution of 24-hour track forecast errors (30-nm increments) for western North Pacific Ocean tropical cyclones in 1996. The largest error, 584 nm, occurred on Typhoon Piper (20W).

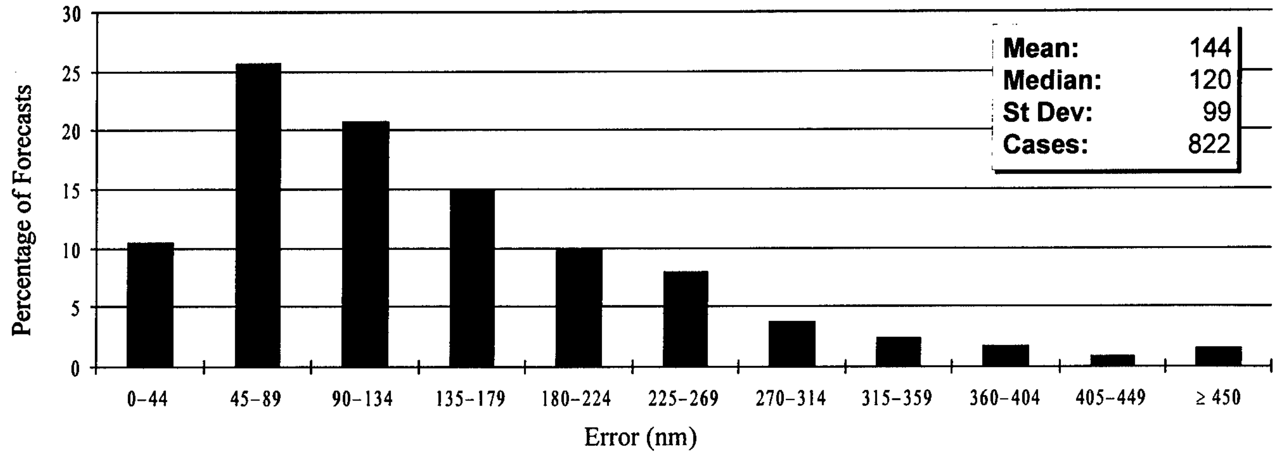

Figure 5-2d Frequency distribution of 36-hour track forecast errors (45-nm increments) for western North Pacific Ocean tropical cyclones in 1996. The largest error, 597 nm, occurred on Typhoon Piper (20W).

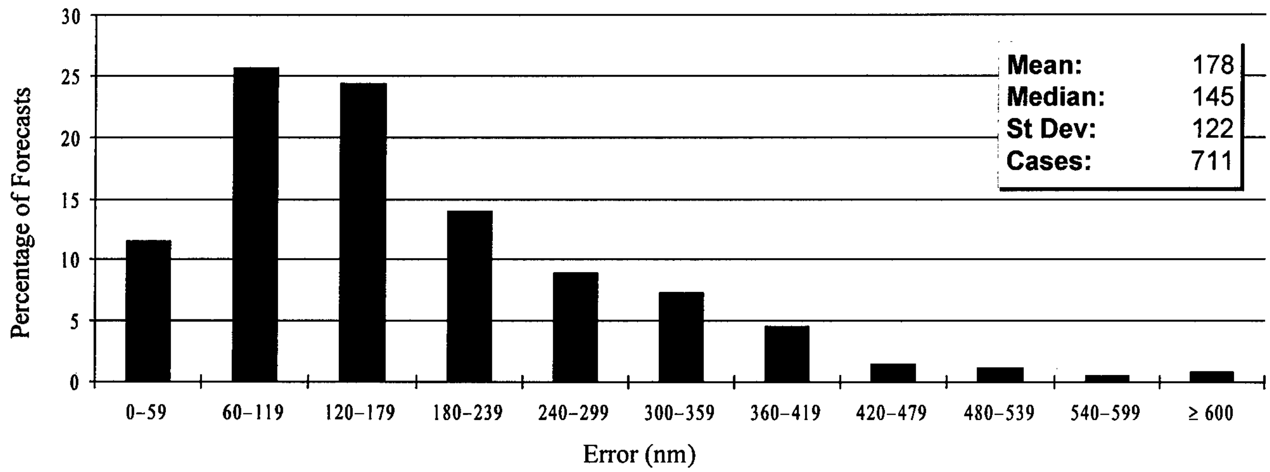

Figure 5-2e Frequency distribution of 48-hour track forecast errors (60-nm increments) for western North Pacific Ocean tropical cyclones in 1996. The largest error, 893 nm, occurred on Typhoon Piper (20W).

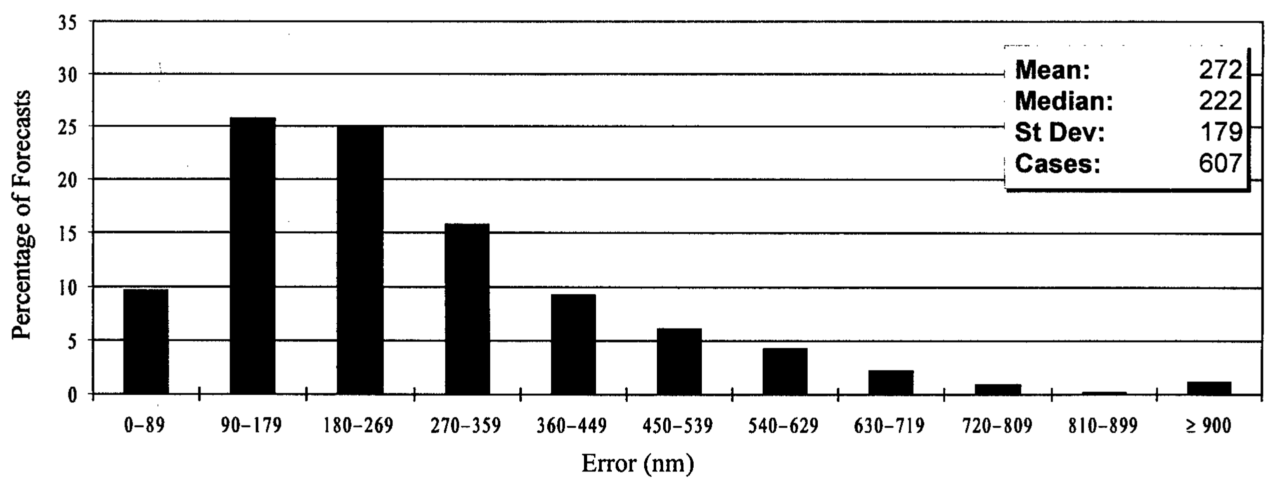

Figure 5-2f Frequency distribution of 72-hour track forecast errors (90-nm increments) for western North Pacific Ocean tropical cyclones in 1996. The largest error, 1129 nm, occurred on Super Typhoon Dale (36W).

Table 5-1 INITIAL POSITION AND FORECAST POSITION ERRORS (NM) FOR THE WESTERN NORTH PACIFIC FOR 1981 - 1996

			24-HOUR				48-HOUR				72-HOUR			
YEAR	NUMBER OF WARNINGS	INITIAL POSITION	NUMBER OF FORECASTS	TRACK	ALONG	CROSS	NUMBER OF FORECASTS	TRACK	ALONG	CROSS	NUMBER OF FORECASTS	TRACK	ALONG	CROSS
1981	584	25	466	124	80	77	348	221	146	131	246	334	206	219
1982	786	19	666	113	74	70	532	238	162	142	425	342	223	211
1983	445	16	342	117	76	73	253	260	169	164	184	407	259	263
1984	611	22	492	117	84	64	378	232	163	131	286	363	238	216
1985	592	18	477	117	80	68	336	231	153	138	241	367	230	227
1986	743	21	645	126	85	70	535	261	183	151	412	394	276	227
1987	657	18	563	107	71	64	465	204	134	127	389	303	198	186
1988	465	23	373	114	85	58	262	216	170	103	183	315	244	159
1989	710	20	625	120	83	69	481	231	162	127	363	350	265	177
1990	794	21	658	103	72	60	525	203	148	110	432	310	225	168
1991	835	22	733	96	69	53	599	185	137	97	484	287	229	146
1992	941	25	841	107	77	59	687	205	143	116	568	305	210	172
1993	853	26	725	112	79	63	570	212	151	117	437	321	226	173
1994*	1058	24	938	105	76	56	776	186	131	105	631	258	176	152
1995	599	29	539	123	89	67	421	215	159	117	319	325	240	167
1996	922	25	880	105	76	56	711	178	134	89	607	272	203	137
15-YEAR AVERAGE														
1981-1995	712	22	606	113	79	65	478	220	154	125	373	332	230	191

Note: Cross-track and along -track errors were adopted by the JTWC in 1986. Right-angle errors (used prior to 1986) were recomputed as cross-track and along-track errors after-the-fact to extend the data. See Figure 5-1 for the definitions of cross-track and along-track errors.
*Statistics were recalculated to resolve earlier along- and cross-track discrepancies.

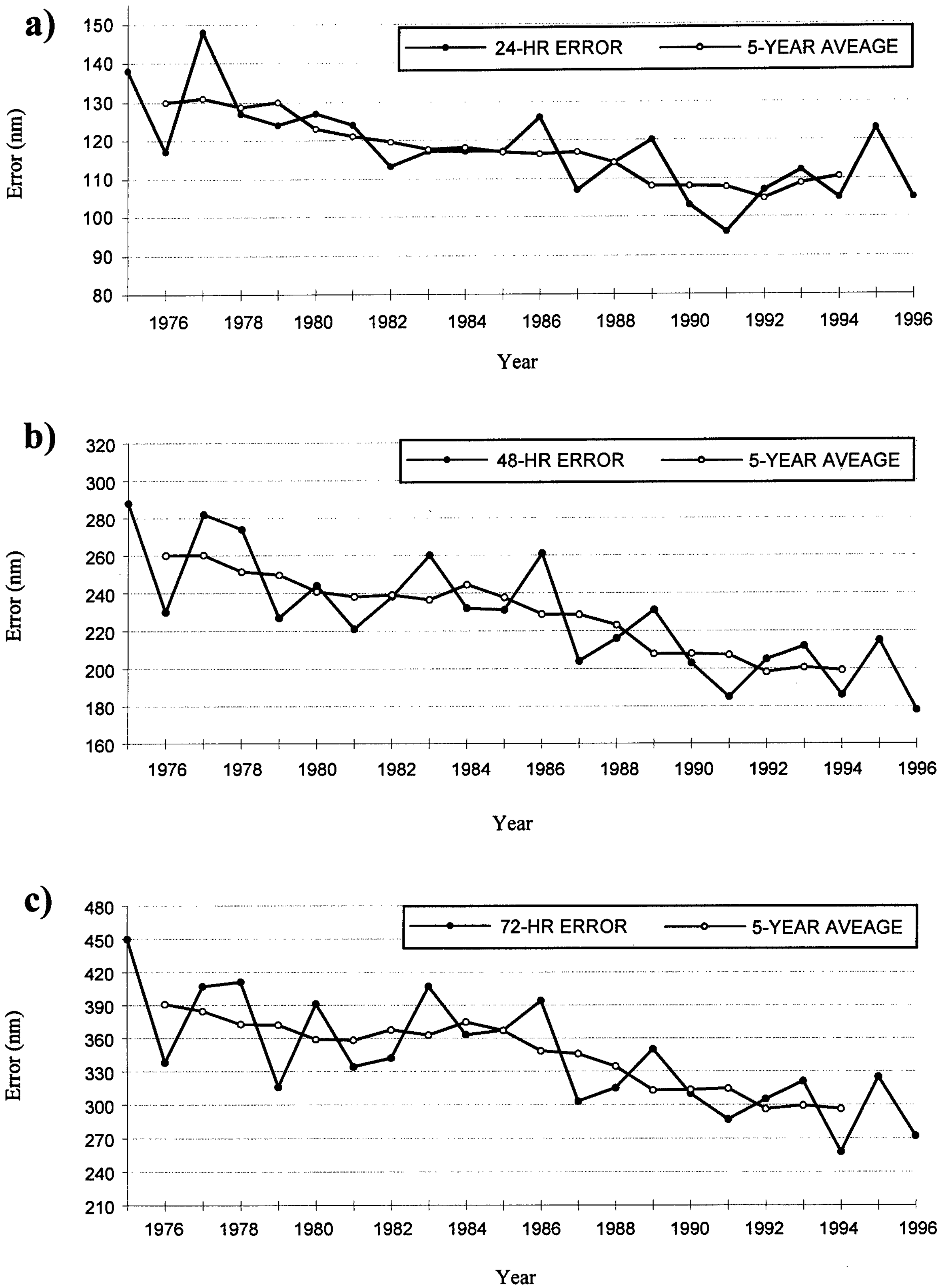

Figure 5-3 Mean track forecast error (nm) and 5-year running mean for a) 24 hours, b) 48 hours and c) 72 hours for the western North Pacific Ocean tropical cyclones for the period 1976 to 1996.

Table 5-2 MEAN FORECAST TRACK ERRORS (NM) FOR WESTERN NORTH PACIFIC TROPICAL CYCLONES FOR 1959-1996

	24-HOUR				48-HOUR				72-HOUR			
YEAR	TY[1]	TC	CROSS TRACK[2]	ALONG TRACK[2]	TY[1]	TC	CROSS TRACK[2]	ALONG TRACK[2]	TY[1]	TC	CROSS TRACK[2]	ALONG TRACK[2]
1959	117*				267*							
1960	177*				354*							
1961	136				274							
1962	144				287				476			
1963	127				246				374			
1964	133				284				429			
1965	151				303				418			
1966	136				280				432			
1967	125				276				414			
1968	105				229				337			
1969	111				237				349			
1970	98	104			181	190			272	279		
1971	99	111	64		203	212	118		308	317	177	
1972	116	117	72		245	245	146		382	381	210	
1973	102	108	74		193	197	134		245	253	162	
1974	114	120	78		218	226	157		357	348	245	
1975	129	138	84		279	288	181		442	450	290	
1976	117	117	71		232	230	132		336	338	202	
1977	140	148	83		266	283	157		390	407	228	
1978	120	127	71	87	241	271	151	194	459	410	218	296
1979	113	124	76	81	219	226	138	146	319	316	182	214
1980	116	126	76	86	221	243	147	165	362	389	230	266
1981	117	123	77	80	215	220	131	146	342	334	219	206
1982	114	113	70	74	229	237	142	162	337	341	211	223
1983	110	117	73	76	247	259	164	169	384	405	263	259
1984	110	117	64	84	228	233	131	163	361	363	216	238
1985	112	117	68	80	228	231	138	153	355	367	227	230
1986	117	121	70	85	261	261	151	183	403	394	227	276
1987	101	107	64	71	211	204	127	134	318	303	186	198
1988	107	114	58	85	222	216	103	170	327	315	159	244
1989	107	120	69	83	214	231	127	162	325	350	177	265
1990	98	103	70	81	191	203	138	162	299	310	211	242
1991	93	96	53	69	187	185	97	137	298	286	146	229
1992	97	107	59	77	194	205	116	143	295	305	172	210
1993	102	112	63	79	205	212	117	151	320	321	173	226
1994+	96	105	56	76	172	186	105	131	244	258	152	176
1995	105	123	89	67	200	215	159	117	311	325	240	167
1996	85	105	56	76	157	178	89	134	252	272	137	203

1. Forecasts were verified for typhoons when intensities were at least 35kt (18m/sec).
2. Cross-track and along-track errors were adopted by the JTWC in 1986. Right angle errors (used prior to 1986) were recomputed as cross-track errors after-the-fact to extend the data base. See Figure 5-1 for the definitions of cross-track and along-track.
* Forecast positions north of 35^0 north latitude were not verified.
+Statistics were recalculated to resolve earlier along- and cross-track discrepancies.

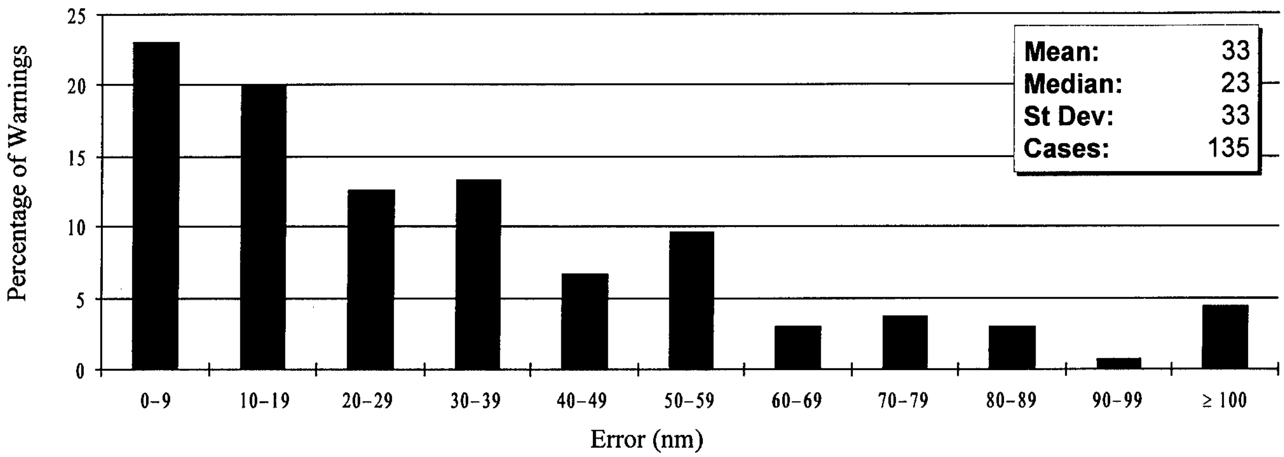

Figure 5-4a Frequency distribution of initial warning position errors (10-nm increments) for North Indian Ocean tropical cyclones in 1996. The largest error, 175 nm, was on Tropical Cyclone 06B.

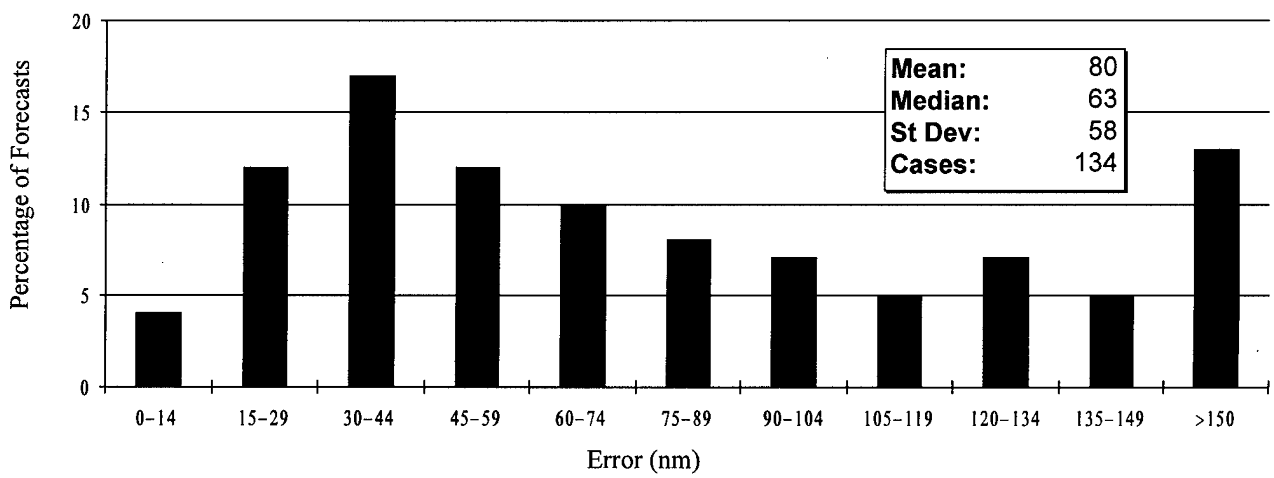

Figure 5-4b Frequency distribution of 12-hour track forecast errors (15-nm increments) for North Indian Ocean tropical cyclones in 1996. The largest error, 290 nm, was on Tropical Cyclone 06B.

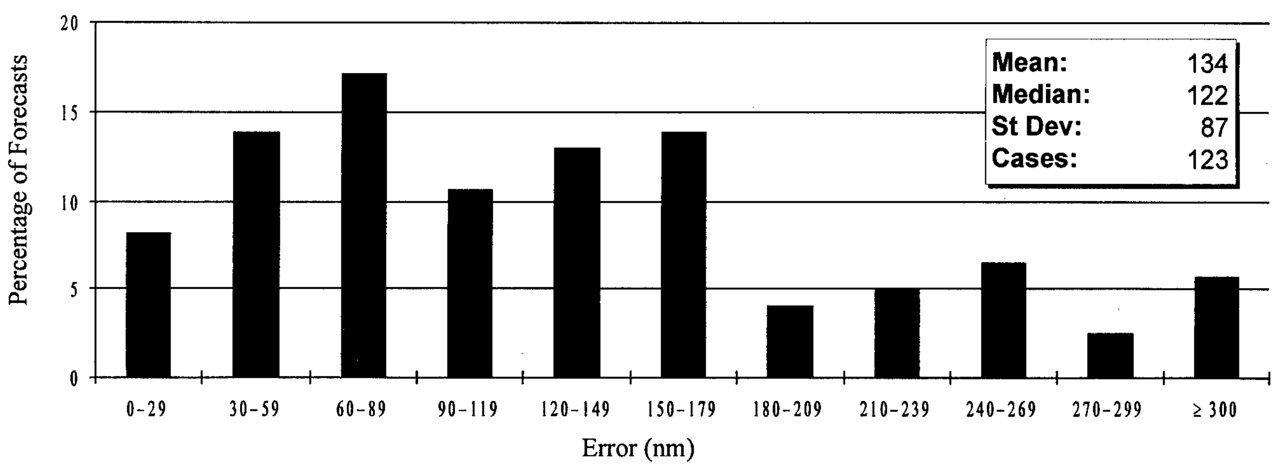

Figure 5-4c Frequency distribution of 24-hour track forecast errors (30-nm increments) for North Indian Ocean tropical cyclones in 1996. The largest error, 397 nm, was on Tropical Cyclone 08B.

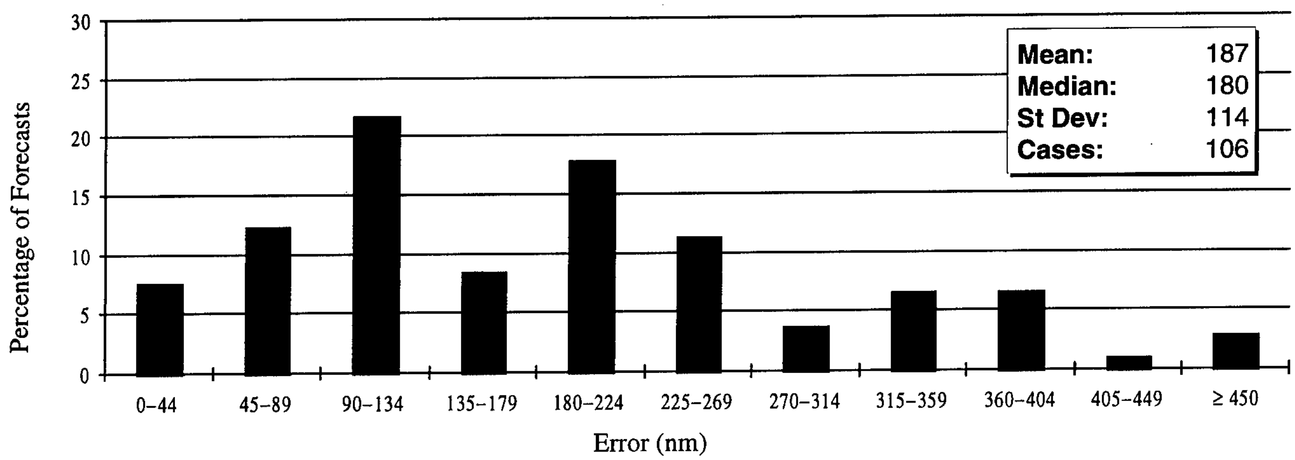

Figure 5-4d Frequency distribution of 36-hour track forecast errors (45-nm increments) for North Indian Ocean tropical-cyclones in 1996. The largest error, 483 nm, was on Tropical Cyclone 06B.

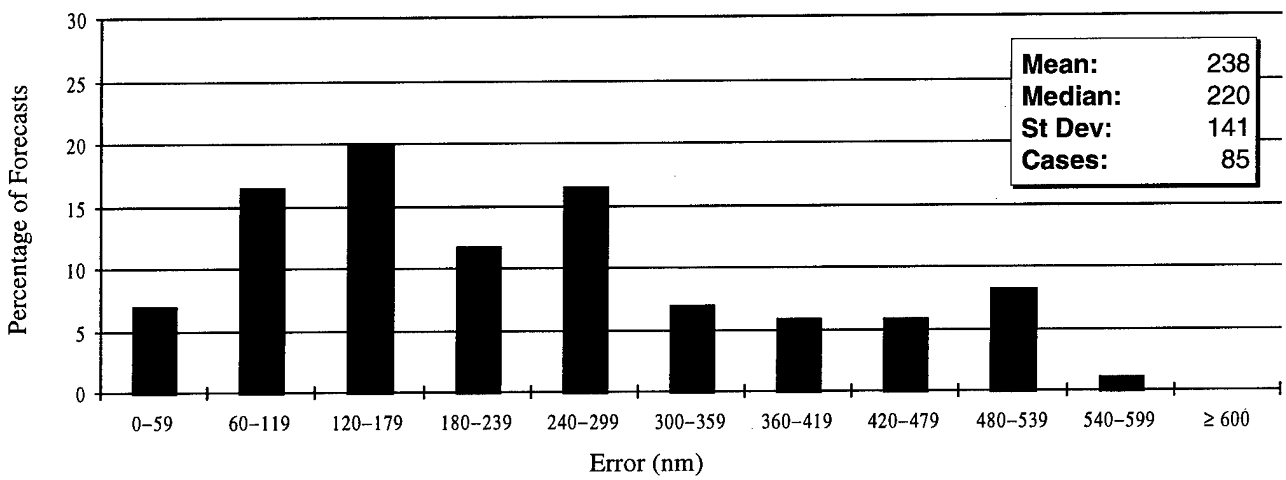

Figure 5-4e Frequency distribution of 48-hour track forecast errors (60-nm increments) for North Indian Ocean tropical cyclones in 1996. The largest error, 578 nm, was on Tropical Cyclone 08B.

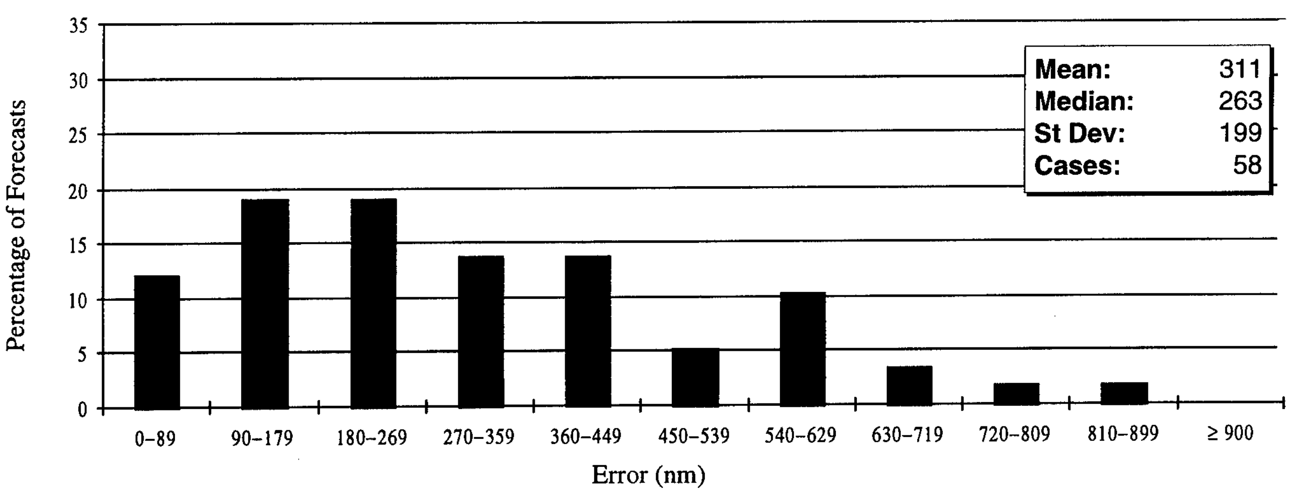

Figure 5-4f Frequency distribution of 72-hour track forecast errors (90-nm increments) for North Indian Ocean tropical cyclones in 1996. The largest error, 875 nm, was on Tropical Cyclone 08B.

Table 5-3 INITIAL POSITION AND FORECAST POSITION ERRORS (NM) FOR THE NORTH INDIAN OCEAN FOR 1981 - 1996

			24-HOUR				48-HOUR				72-HOUR			
YEAR	NUMBER OF WARNINGS	INITIAL POSITION	NUMBER OF FORECASTS	TRACK	ALONG	CROSS	NUMBER OF FORECASTS	TRACK	ALONG	CROSS	NUMBER OF FORECASTS	TRACK	ALONG	CROSS
1981	41	28	29	109	76	63	2	176	120	109	5	197	150	111
1982	55	35	37	138	110	68	17	368	292	209	7	762	653	332
1983	18	38	7	117	90	50	18	153	137	53	0			
1984	67	33	42	154	124	67	20	274	217	139	16	388	339	121
1985	53	31	30	122	102	53	8	242	119	194	0			
1986	28	52	16	134	118	53	7	168	131	80	5	269	189	180
1987	83	42	54	144	97	100	25	205	125	140	21	305	219	188
1988	44	34	30	120	89	63	18	219	112	176	12	409	227	303
1989	44	19	33	88	62	50	17	146	94	86	12	216	164	111
1990	46	31	36	101	85	43	24	146	117	67	17	185	130	104
1991	56	38	43	129	107	54	27	235	200	89	14	450	356	178
1992	191	35	149	128	73	86	100	244	141	166	62	398	276	218
1993	36	27	28	125	87	79	20	198	171	74	12	231	176	116
1994	60	25	44	97	80	44	28	153	124	63	13	213	177	92
1995	54	30	47	138	119	58	32	262	247	77	20	342	304	109
1996	135	33	123	134	94	80	85	238	181	127	58	311	172	237
15-YEAR AVERAGE														
1981-1995	58	33	42	123	95	62	24	213	156	115	14	291	224	144

Cross-track and along-track errors were adopted by the JTWC in 1986. Right angle errors (used prior to 1986) were recomputed as cross-track and along-track errors after-the-fact to extend the data base. See Figure 5-1 for the definitions of cross-track and along-track errrors.

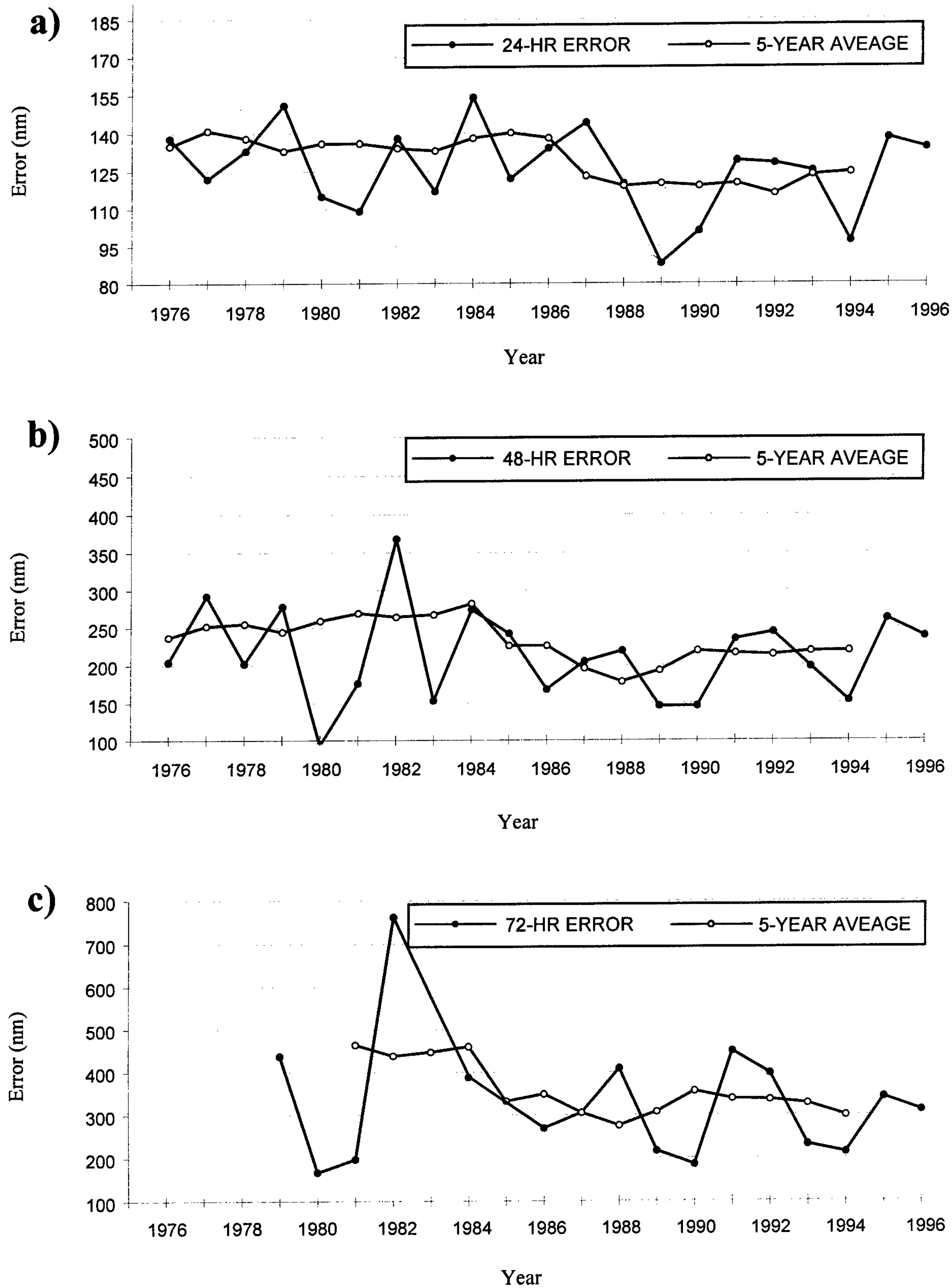

Figure 5-5 Mean track forecast error (nm) and 5-year running mean for a) 24 hours, b) 48 hours and c) 72 hours for the North Indian Ocean tropical cyclones for the period 1976 to 1996.

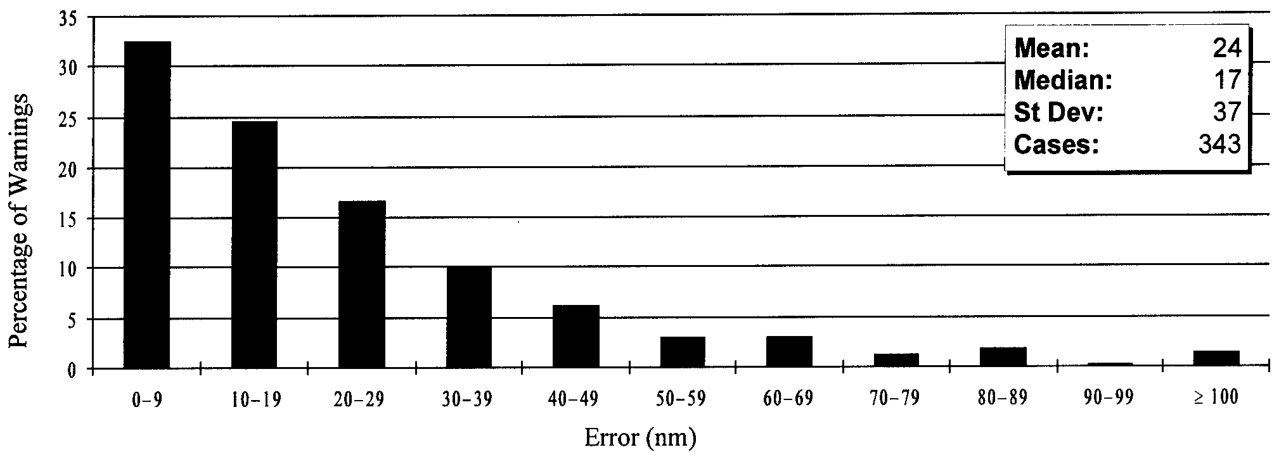

Figure 5-6a Frequency distribution of initial warning position errors (10-nm increments) for South Pacific and South Indian Ocean tropical cyclones in 1996. The largest error, 583 nm, occurred on Tropical Cyclone 20P (Zaka).

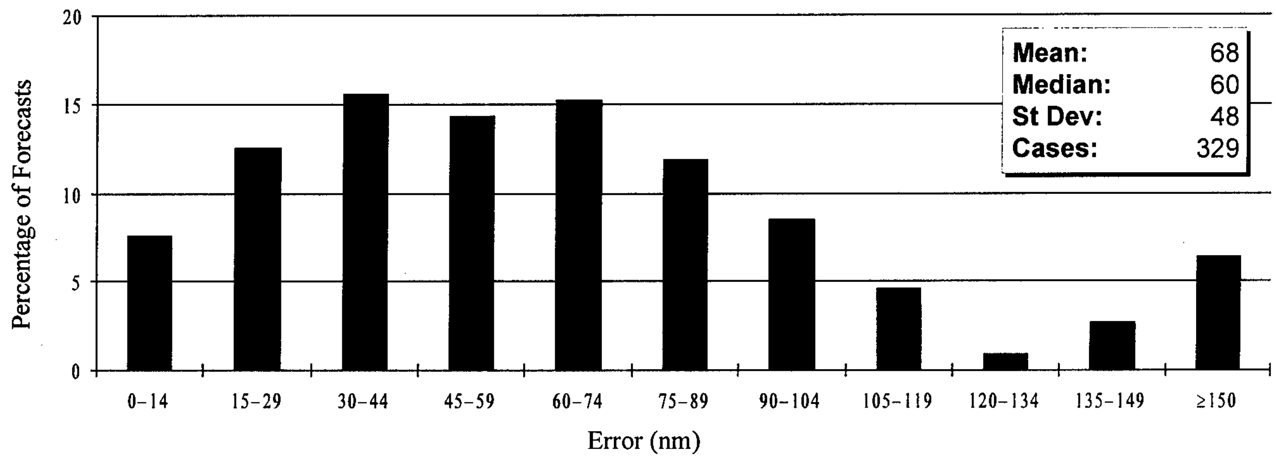

Figure 5-6b Frequency distribution of 12-hour track forecast errors (15-nm increments) for South Pacific and South Indian Ocean tropical cyclones in 1996. The largest error, 315 nm, occurred on Tropical Cyclone 24S (Hansella).

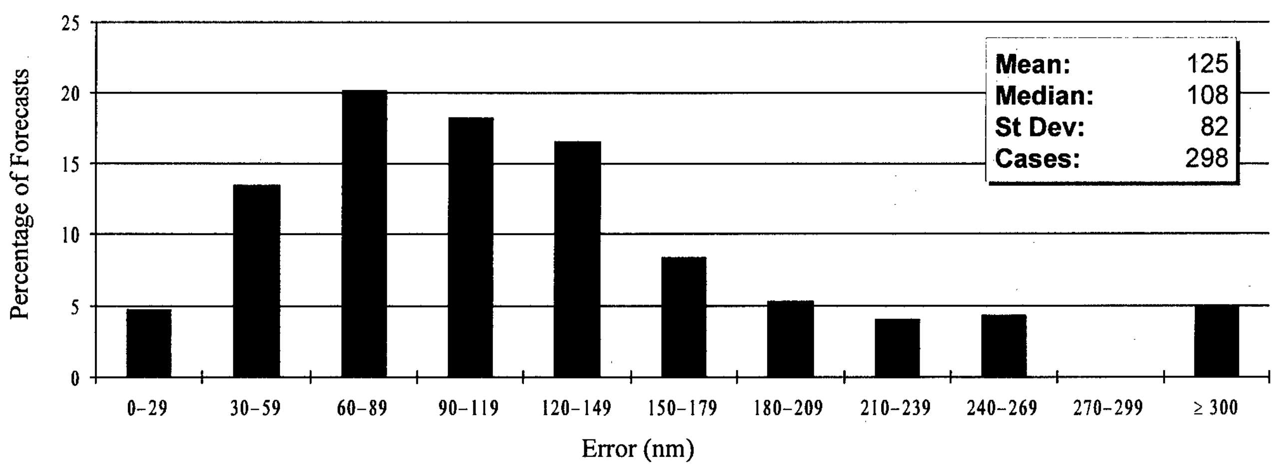

Figure 5-6c Frequency distribution of 24-hour track forecast errors (30-nm increments) for South Pacific and South Indian Ocean tropical cyclones in 1996. The largest error, 501 nm, occurred on Tropical Cyclone 27S.

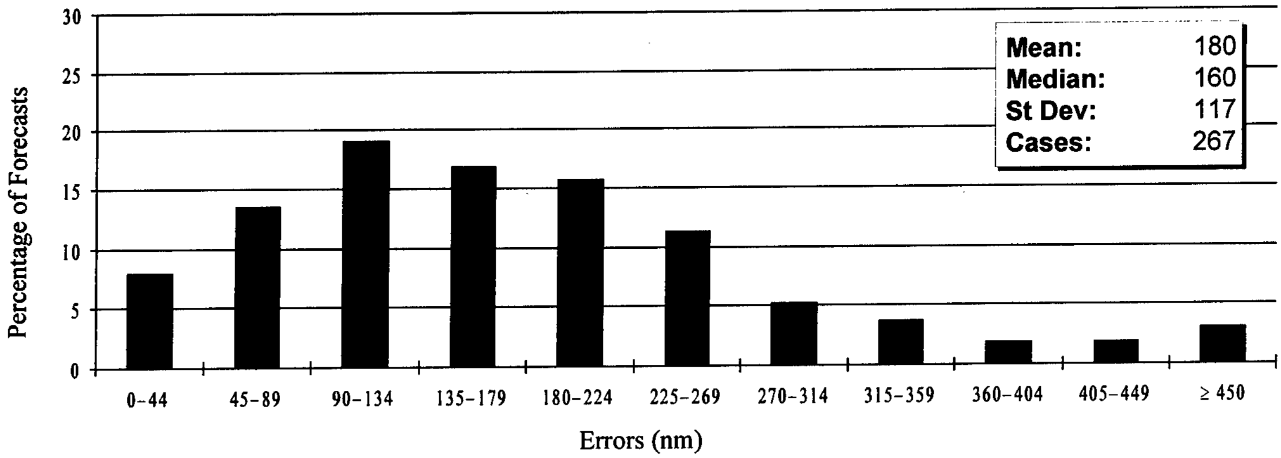

Figure 5-6d Frequency distribution of 36-hour track forecast errors (45-nm increments) for in the South Pacific and South Indian Ocean tropical cyclones in 1996. The largest error, 879 nm, occurred on Tropical Cyclone 21P (Atu).

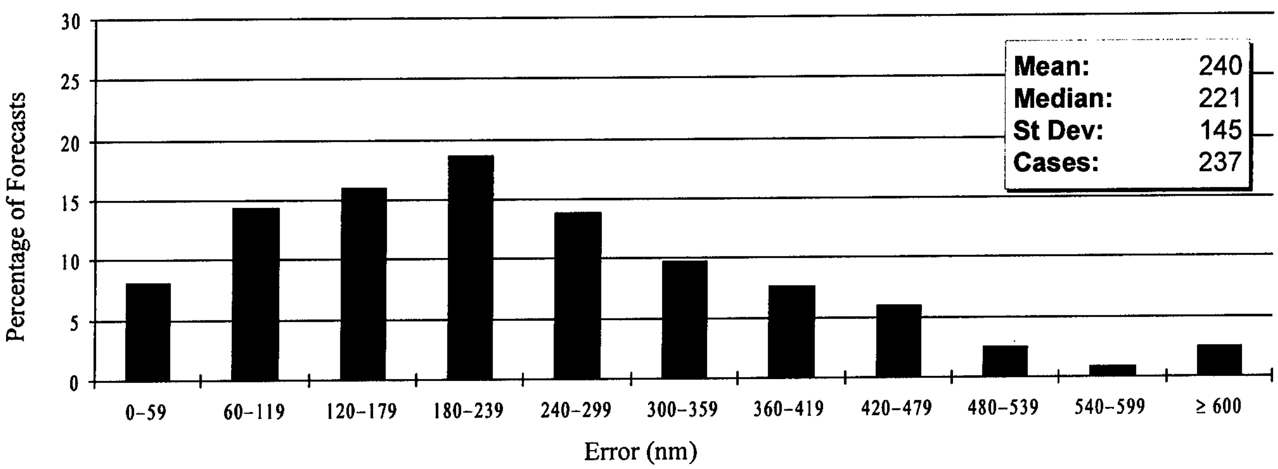

Figure 5-6e Frequency distribution of 48-hour track forecast errors (60-nm increments) for in the South Pacific and South Indian Ocean tropical cyclones in 1996. The largest error, 902 nm, occurred on Tropical Cyclone 28S (Jenna).

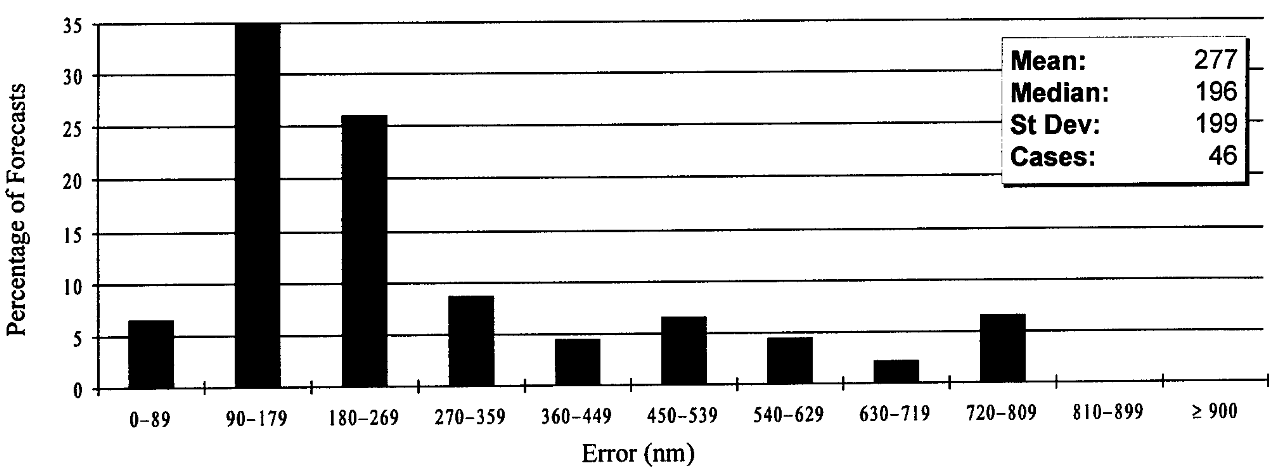

Figure 5-6f Frequency distribution of 72-hour track forecast errors (120-nm increments) for in the South Pacific and South Indian Ocean tropical cyclones in 1996. The largest error, 792 nm, occurred on Tropical Cyclone 04S (Gertie).

Table 5-4 INITIAL POSITION AND FORECAST POSITION ERRORS (NM) FOR THE SOUTHERN HEMISPHERE FOR 1981 - 1996

			24-HOUR				48-HOUR				72-HOUR			
YEAR	NUMBER OF WARNINGS	INITIAL POSITION	NUMBER OF FORECASTS	TRACK	ALONG	CROSS	NUMBER OF FORECASTS	TRACK	ALONG	CROSS	NUMBER OF FORECASTS	TRACK	ALONG	CROSS
1981	226	48	190	165	103	106	140	315	204	201				
1982	275	38	238	144	98	86	176	274	188	164				
1983*	191	35	163	130	88	77	126	241	158	145				
1984	301	36	252	133	90	79	191	231	159	134				
1985*	306	36	257	134	92	79	193	236	169	132				
1986*	279	40	227	129	86	77	171	262	169	164				
1987*	189	46	138	145	94	90	101	280	153	138				
1988*	204	34	99	146	98	83	48	290	246	144				
1989*	287	31	242	124	84	73	186	240	166	136				
1990*	272	27	228	143	105	74	177	263	178	152				
1991*	264	24	231	115	75	69	185	220	152	129				
1992*	267	28	230	124	91	64	208	240	177	129				
1993*	257	21	225	102	74	57	176	199	142	114				
1994*	386	28	345	115	77	68	282	224	147	134				
1995**	245	24	222	108	82	55	175	198	144	108	53	291	169	190
1996	343	24	298	125	90	67	237	240	174	129	46	277	221	133
15-YEAR AVERAGE														
1981-1995	263	33	219	130	89	76	169	248	170	142	53	291	169	190

* These statistics are for JTWC forecasts only. NPMOC statistics are not included.

** JTWC began publishing 72-hour forecast verification in 1995.

Cross-track and along-track errors were adopted by the JTWC in 1986. Right-angle (used prior to 1986) were recomputed as cross-track and along-track after-the-fact to extend the data base.

See Figure 5-1 for the definitions of cross-track and along-track errors.

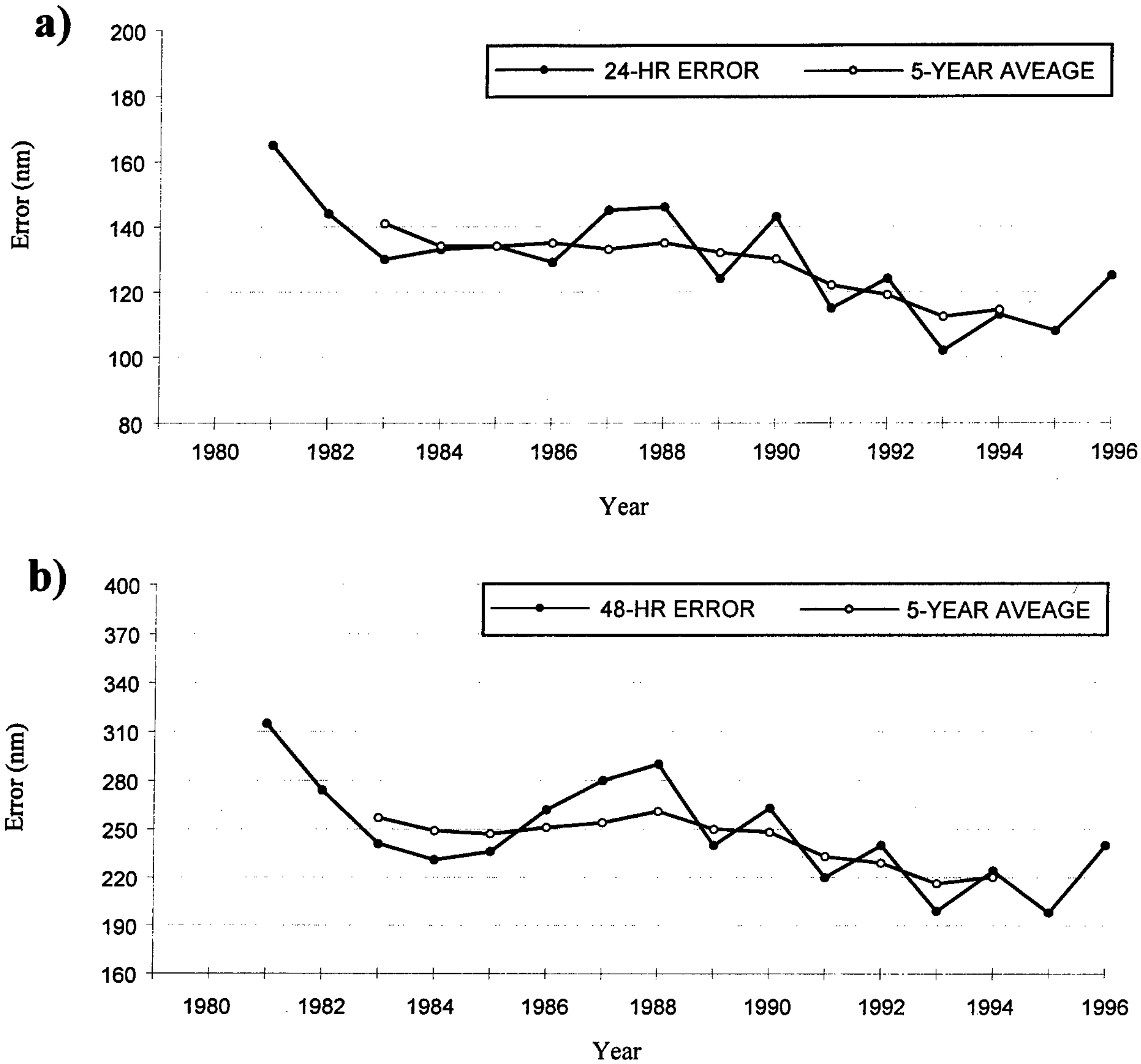

Figure 5-7 Mean track forecast error (nm) and 5-year running mean for a) 24 hours and b) 48 hours for the South Indian Ocean tropical cyclones for the period 1981 to 1996.

5.2 COMPARISON OF OBJECTIVE TECHNIQUES

JTWC uses a variety of objective techniques for guidance in the warning preparation process. Multiple techniques are required, because each technique has particular strengths and weaknesses which vary by basin, numerical model initialization, time of year, synoptic situation and forecast period. The accuracy of objective aid forecasts depends on both the specified position and the past motion of the tropical cyclone as determined by the working best track. JTWC initializes its objective techniques using an extrapolated working best track position so that the output of the techniques will start at the valid time of the next warning initial position.

Unless stated otherwise, all of the objective techniques discussed below run in all basins covered by JTWC's AOR and provide forecast positions at 12-, 24-, 36-, 48-, and 72-hours unless the technique aborts prematurely during computations. The techniques can be divided into six general categories: extrapolation, climatology and analogs, statistical, dynamic, hybrids, and empirical or analytical.

5.2.1 EXTRAPOLATION (XTRP) — Past speed and direction are computed using the rhumb line distance between the current and 12-hour old positions of the tropical cyclone. Extrapolation from the current warning position is used to compute forecast positions.

5.2.2 CLIMATOLOGY and ANALOGS

5.2.2.1 CLIMATOLOGY (CLIM) — Employs time and location windows relative to the current position of the tropical cyclone to determine which historical storms will be used to compute the forecast. The historical data base is 1945-1981 for the Northwest Pacific, and 1900 to 1990 for the rest of JTWC's AOR. Objective intensity forecasts are available from these data bases. Scatter diagrams of expected tropical cyclone motion at bifurcation points are also available from these data bases.

5.2.2.2 ANALOG — A revised Typhoon Analog 1993 (TYAN93) picks the top matches with the basin climatology of historical tropical cyclone best tracks. Matches are based upon the differences between the direction and speed of the superimposed historical best track positions and the past direction and speed of the cyclone. Specifically, the directions and speeds are calculated from the 12-hour old position to the current "fix" position and the 24-hr old position to the "fix" position. Separate comparisons are made for climatology cyclone tracks classified as "straight," "recurver" and "other". There is also a "total" group, that includes the top matches without regard to classification of tracks.

TYAN93 works in the same manner for all basins. The time-window is +/- 35 days from the "fix." The space-window is +/- 2.5 degrees latitude and +/- 5 degrees longitude from the "fix" position on the first pass of each forecast. The maximum-wind-speed window is as follows (for basins with climatology wind speeds): a. If "fix" wind speed is $\leq$ 25 kt, climatology cyclone wind speed must be $\leq$ 30 kt. b. If "fix" wind speed is 30 kt, climatology cyclone wind speed must be in range from 25 to 35 kt. c. If "fix" wind speed is $\geq$ 35 kt, climatology cyclone wind speed must be at least 35 kt. Matching is based upon weighted direction and speed errors. Forecasting is based upon "straight" and "recurver" type climatology tropical cyclones, where the 12-hour and 24-hour best "straight" ("recurver") matches are combined into one set of best matches for "straight" ("recurver").

5.2.3 STATISTICAL

5.2.3.1 CLIMATOLOGY AND PERSISTENCE (CLIPER or CLIP) — A statistical regression technique that is based on climatology, current position and 12-hour and 24-hour past move-

ment. This technique is used as a crude baseline against which to measure the forecast skill of other, more sophisticated techniques. CLIP in the western North Pacific uses third-order regression equations, and is based on the work of Xu and Neumann (1985). CLIPER has been available outside this basin since mid-1990, with regression coefficients recently recomputed by FNMOC based on the updated 1900-1989 data base.

5.2.3.2 COLORADO STATE UNIVERSITY MODEL (CSUM) — A statistical-dynamical technique based on the work of Matsumoto (1984). Predictor parameters include the current and 24-hr old position of the storm, heights from the current and 24-hr old NOGAPS 500-mb analyses, and heights from the 24-hr and 48-hr NOGAPS 500-mb prognoses. Height values from 200-mb fields are substituted for storms that have an intensity exceeding 90 kt and are located north of the subtropical ridge. Three distinct sets of regression equations are used depending on whether the storm's direction of motion falls into "below," "on" or "above" the subtropical ridge categories. During the development of the regression equation coefficients for CSUM, the so-called "perfect prog" approach was used, in which verifying analyses were substituted for the numerical prognoses that are used when CSUM is run operationally. Thus, CSUM was not "tuned" to any particular version of NOGAPS, and in fact, the performance of CSUM should presumably improve as new versions of NOGAPS improve. CSUM runs only in the western North Pacific, South China Sea, and North Indian Ocean basins.

5.2.3.3 JTWC92 or JT92 - JTWC92 is a statistical-dynamical model for the western North Pacific Ocean basin which forecasts tropical cyclone positions at 12-hour intervals to 72 hours. The model uses the deep-layer mean height field derived from the NOGAPS forecast fields. These deep-layer mean height fields are spectrally truncated to wave numbers 0 through 18 prior to use in JTWC92. Separate forecasts are made for each position. That is, the forecast 24-hour position is not a 12-hour forecast from the forecasted 12-hour position.

JTWC92 uses five internal sub-models which are blended and iterated to produce the final forecasts. The first sub-model is a statistical blend of climatology and persistence, known as CLIPER. The second sub-model is an analysis mode predictor, which only uses the "analysis" field. The third sub-model is the forecast mode predictor, which uses only the forecast fields. The fourth sub-model is a combination of 1 and 2 to produce a "first guess" of the 12-hourly forecast positions. The fifth sub-model uses the output of the "first guess" combined with 1, 2, and 3 to produce the forecasts. The iteration is accomplished by using the output of sub-model 5 as though it were the output from sub-model 4. The optimum number of iterations has been determined to be three.

When JTWC92 is used in the operational mode, all the NOGAPS fields are forecast fields. The 00Z and 12Z tropical forecasts are based upon the previous 12-hour old synoptic time NOGAPS forecasts. The 06Z and 18Z tropical forecasts are based on the previous 00Z and 12Z NOGAPS forecasts, respectively. Therefore, operationally, the second sub-model uses forecast fields and not analysis fields.

5.2.4 DYNAMIC

5.2.4.1 NOGAPS VORTEX TRACKING ROUTINE (NGPS/X) —Tropical cyclone vortices are tracked at FNMOC by converting the 1000-mb u and v wind component fields into isogons. The intersection of isogons are either the center of a cyclonic or anticyclonic circulation, or a col. The tracking program starts at the last known location of the cyclone – a warning position. Based on this position and the last known speed and direction of movement, the program hunts for the next cyclonic

center representing the tropical cyclone. Confidence factors are generated within the program and are modified, as required, by a quality control program that formats the data for transmission.

5.2.4.2 GEOPHYSICAL FLUID DYNAMICS - NAVY (GFDN) — This model uses a triple nested movable mesh with 18 sigma levels. The outer mesh domain covers a 75°x75° area with a horizontal resolution of 1° and is fixed for the duration of the model run based on the initial location and movement of the tropical cyclone (TC). The 10°x10° middle and a 5°x5° inner (resolution 1/6°) nested meshes move with the cyclone. Based on the global analysis and an initialization message, the TC is removed from the global analysis, and replaced by a synthetic vortex which has an asymmetric (beta-advection) component added. Boundary conditions are updated periodically from forecast fields generated by a global forecast model. In addition to standard output fields, the model outputs TC track forecasts and maximum isotach swaths indicating the location of maximum winds in relation to the TC track.

5.2.4.3 ONE-WAY (INTERACTIVE) TROPICAL CYCLONE MODEL (OTCM) — This technique is a coarse resolution (205-km grid), three layer, primitive equation model with a horizontal domain of 6400 x 4700 km. OTCM is initialized using 6-hour or 12-hour prognostic fields from the latest NOGAPS run, and the initial fields are smoothed and adjusted in the vicinity of the storm to induce a persistence bias into OTCM's forecast. A symmetric bogus vortex is then inserted, and the boundaries updated every 12 hours by NOGAPS fields as the integration proceeds. The bogus vortex is maintained against frictional dissipation by an analytical heating function. The forecast positions are based on the movement of the vortex in the lowest layer of the model (effectively 850-mb).

5.2.4.4 FNMOC BETA AND ADVECTION MODEL (FBAM) — This model is an adaptation of the Beta and Advection model used by NCEP. The forecast motion results from a calculation of environmental steering and an empirical correction for the observed vector difference between that steering and the 12-hour old storm motion. The steering is computed from the NOGAPS Deep Layer Mean (DLM) wind fields which are a weighted average of the wind fields computed for the 1000-mb to 100-mb levels. The difference between past storm motion and the DLM steering is treated as if the storm were a Rossby wave with an "effective radius" propagating in response to the horizontal gradient of the coriolis parameter, beta. The forecast proceeds in one-hour steps, recomputing the effective radius as beta changes with storm latitude, and blending in a persistence bias for the first 12 hours.

5.2.5 HYBRIDS

5.2.5.1 HALF PERSISTENCE AND CLIMATOLOGY (HPAC) — Forecast positions generated by equally weighting the forecasts given by XTRP and CLIM.

5.2.5.2 BLENDED (BLND) — A simple average of six forecast aids: OTCM, CSUM, FBAM, JT92, CLIP, and HPAC.

5.2.5.3 WEIGHTED (WGTD) — A weighted average of the forecast guidance used to compute BLND: OTCM (29%), CSUM (22%), FBAM (14%), JT92 (14%), HPAC (14%), and CLIP (7%).

5.2.5.4 DYNAMIC AVERAGE (DAVE) — A simple average of all dynamic forecast aids: NOGAPS (NGPS), Bracknell (EGRR), Japanese Typhoon Model (JTYM), JT92, FBAM, OTCM, and CSUM.

5.2.6 EMPIRICAL OR ANALYTICAL

5.2.6.1 DVORAK — An estimation of a tropical cyclone's current and 24-hour forecast intensity is made from the interpretation of satellite imagery (Dvorak, 1984). These intensity estimates are used with other intensity related data and trends to forecast short-term tropical cyclone intensity.

5.2.6.2 MARTIN/HOLLAND — The technique adapts an earlier work (Holland, 1980) and specifically addresses the need for realistic 35-, 50- and 100-kt (18-, 26- and 51-m/sec) wind radii around tropical cyclones. It solves equations for basic gradient wind relations within the tropical cyclone area, using input parameters obtained from enhanced infrared satellite imagery. The diagnosis also includes an asymmetric area of winds caused by tropical cyclone movement. Satellite-derived size and intensity parameters are also used to diagnose internal steering components of tropical cyclone motion known collectively as "beta-drift."

5.2.6.3 TYPHOON ACCELERATION PREDICTION TECHNIQUE (TAPT) — This technique (Weir, 1982) utilizes upper-tropospheric and surface wind fields to estimate acceleration associated with the tropical cyclone's interaction with the mid-latitude westerlies. It includes guidelines for the duration of acceleration, upper limits and probable path of the cyclone.

5.3 TESTING AND RESULTS

A comparison of selected techniques is included in Table 5-5 for all western North Pacific tropical cyclones, Table 5-6 for all North Indian Ocean tropical cyclones and Table 5-7 for the Southern Hemisphere. For example, in Table 5-5 for the 12-hour mean forecast error, 925 cases available for a homogeneous comparison, the average forecast error at 12 hours was 73 nm (135 km) for CSUM and 69 nm (128 km) for FBAM. The difference of 4 nm (7 km) is shown in the lower right. Differences are not always exact, due to computational round-off which occurs for each of the cases available for comparison.

Table 5-5 1996 ERROR STASTISTICS FOR SELECTED OBJECTIVE TECHNIQUES IN THE NORTHWEST PACIFIC
(1 JAN 1996 - 31 DEC 1996)

Number of Cases	X-Axis Technique Error
Y-Axis Technique Error	Error Difference (Y-X)

12-HOUR MEAN FORECAST ERROR (NM)

	JTWC		NGPS		OTCM		GFDN		FBAM		CSUM		CLIP		DAVE	
JTWC	911	64														
	64	0														
NGPS	604	52	657	74												
	72	20	74	0												
OTCM	714	58	555	72	793	120										
	120	62	118	46	120	0										
GFDN	445	51	359	66	395	121	459	77								
	75	24	72	6	73	-48	77	0								
FBAM	856	63	595	72	729	119	429	76	985	70						
	65	2	55	-17	62	-57	55	-21	70	0						
CSUM	823	63	569	72	700	119	414	74	925	69	936	73				
	69	6	59	-13	66	-53	58	-16	73	4	73	0				
CLIP	873	62	608	72	737	119	440	75	965	69	922	72	1003	73		
	68	6	58	-14	65	-54	57	-18	73	4	72	0	73	0		
DAVE	673	65	470	73	567	118	331	78	722	69	692	73	731	73	746	72
	69	4	58	-15	66	-52	58	-20	71	2	71	-2	71	-2	72	0

24-HOUR MEAN FORECAST ERROR (NM)

	JTWC		NGPS		OTCM		GFDN		FBAM		CSUM		CLIP		DAVE	
JTWC	880	105														
	105	0														
NGPS	593	91	641	112												
	110	19	112	0												
OTCM	664	95	523	108	737	183										
	185	90	190	82	183	0										
GFDN	436	86	350	105	375	192	446	113								
	113	27	110	5	109	-83	113	0								
FBAM	829	104	581	109	682	182	422	114	958	116						
	111	7	103	-6	107	-75	103	-11	116	0						
CSUM	801	103	555	110	655	181	408	112	903	115	914	130				
	126	23	118	8	118	-63	115	3	130	15	130	0				
CLIP	846	103	594	110	688	182	432	113	938	115	900	129	976	125		
	120	17	108	-2	112	-70	107	-6	125	10	125	-4	125	0		
DAVE	656	106	462	110	536	181	326	117	706	117	680	130	714	124	729	112
	109	3	99	-11	104	-77	97	-20	112	-5	110	-20	111	-13	112	0

36-HOUR MEAN FORECAST ERROR (NM)

	JTWC		NGPS		OTCM		GFDN		FBAM		CSUM		CLIP		DAVE	
JTWC	822	144														
	144	0														
NGPS	529	125	572	152												
	151	26	152	0												
OTCM	595	132	449	148	664	233										
	235	103	243	95	233	0										
GFDN	416	125	329	160	340	240	427	150								
	148	23	149	-11	146	-94	150	0								
FBAM	774	142	525	152	615	233	407	152	918	167						
	162	20	152	0	158	-75	156	4	167	0						
CSUM	750	142	501	153	590	232	395	152	867	167	878	190				
	187	45	180	27	173	-59	181	29	190	23	190	0				
CLIP	790	141	535	152	619	233	416	150	898	166	864	189	934	183		
	176	35	163	11	165	-68	168	18	183	17	183	-6	183	0		
DAVE	621	146	424	144	489	236	316	156	681	169	659	191	689	182	704	151
	147	1	135	-9	143	-93	138	-18	151	-18	151	-40	151	-31	151	0

Table 5-5 (CONTINUED) 1996 ERROR STASTISTICS FOR SELECTED OBJECTIVE TECHNIQUES
IN THE NORTHWEST PACIFIC
(1 JAN 1996 - 31 DEC 1996)

48-HOUR MEAN FORECAST ERROR (NM)

	JTWC		NGPS		OTCM		GFDN		FBAM		CSUM		CLIP		DAVE	
JTWC	711	178														
	178	0														
NGPS	460	160	512	179												
	177	17	179	0												
OTCM	500	165	379	169	586	290										
	291	126	293	124	290	0										
GFDN	386	160	305	183	306	301	406	191								
	188	28	191	8	186	-115	191	0								
FBAM	672	178	473	179	546	290	387	194	868	218						
	209	31	206	27	208	-82	211	17	218	0						
CSUM	660	178	452	180	524	291	377	193	820	218	831	253				
	247	69	247	67	235	-56	248	55	253	35	253	0				
CLIP	692	177	483	179	550	292	396	191	849	217	817	253	884	247		
	238	61	228	49	230	-62	236	45	248	31	249	-4	247	0		
DAVE	548	181	387	186	437	294	300	201	650	222	631	253	658	246	672	192
	184	3	172	-14	183	-111	179	-22	192	-30	192	-61	192	-54	192	0

72-HOUR MEAN FORECAST ERROR (NM)

	JTWC		NGPS		OTCM		GFDN		FBAM		CSUM		CLIP		DAVE	
JTWC	607	272														
	272	0														
NGPS	375	260	418	267												
	258	-2	267	0												
OTCM	391	249	280	251	439	419										
	414	165	413	162	419	0										
GFDN	198	253	139	268	139	377	209	270								
	268	15	289	21	250	-127	270	0								
FBAM	575	271	392	265	413	419	198	278	752	324						
	311	40	308	43	312	-107	295	17	324	0						
CSUM	568	273	378	270	400	423	195	275	713	323	723	382				
	378	105	387	117	356	-67	384	109	382	59	382	0				
CLIP	591	271	400	267	415	419	206	274	737	322	711	383	769	389		
	382	111	382	115	366	-53	385	111	391	69	390	7	389	0		
DAVE	481	279	321	279	340	426	159	287	570	332	558	379	580	388	590	286
	278	-1	267	-12	276	-150	266	-21	284	-48	286	-93	285	-103	286	0

Table 5-6 1996 ERROR STATISTICS FOR SELECTED OBJECTIVE TECHNIQUES IN THE NORTH INDIAN OCEAN (1 JAN 1996 - 31 DEC 1996)

12-HOUR MEAN FORECAST ERROR (NM)

	JTWC		NGPS		OTCM		FBAM		CLIM		CLIP		HPAC		WGTD	
JTWC	134	81														
	81	0														
NGPS	89	80	91	87												
	87	7	87	0												
OTCM	90	72	72	80	97	107										
	104	32	109	29	107	0										
FBAM	126	79	87	87	94	109	141	88								
	86	7	88	1	84	-25	88	0								
CLIM	124	78	86	87	94	109	134	85	141	99						
	99	21	103	16	98	-11	98	13	99	0						
CLIP	131	80	89	87	95	108	141	88	141	99	148	86				
	83	3	85	-2	81	-27	85	-3	84	-15	86	0				
HPAC	131	80	89	87	95	108	141	88	141	99	148	86	148	90		
	88	8	90	3	85	-23	89	1	88	-11	90	4	90	0		
WGTD	105	79	78	87	81	109	113	84	115	101	115	83	115	88	115	91
	91	12	94	7	88	-21	91	7	91	-10	91	8	91	3	91	0

24-HOUR MEAN FORECAST ERROR (NM)

	JTWC		NGPS		OTCM		FBAM		CLIM		CLIP		HPAC		WGTD	
JTWC	123	134														
	134	0														
NGPS	84	135	87	135												
	135	0	135	0												
OTCM	82	121	68	133	90	186										
	187	66	184	51	186	0										
FBAM	118	133	83	135	88	188	135	152								
	148	15	151	16	145	-43	152	0								
CLIM	116	132	82	136	88	188	128	146	135	164						
	166	34	173	37	169	-19	165	19	164	0						
CLIP	123	134	85	135	89	188	135	152	135	164	142	142				
	139	5	142	7	139	-49	141	-11	139	-25	142	0				
HPAC	123	134	85	135	89	188	135	152	135	164	142	142	142	150		
	148	14	152	17	147	-41	149	-3	147	-17	150	8	150	0		
WGTD	98	134	75	138	77	189	108	146	110	172	110	140	110	150	110	152
	154	20	158	20	151	-38	153	7	152	-20	152	12	152	2	152	0

36-HOUR MEAN FORECAST ERROR (NM)

	JTWC		NGPS		OTCM		FBAM		CLIM		CLIP		HPAC		WGTD	
JTWC	106	187														
	187	0														
NGPS	65	176	73	160												
	154	-22	160	0												
OTCM	67	170	55	154	79	280										
	287	117	263	109	280	0										
FBAM	101	187	69	160	77	285	125	257								
	255	68	277	117	276	-9	257	0								
CLIM	100	186	68	160	77	284	118	254	124	227						
	234	48	224	64	242	-42	231	-23	227	0						
CLIP	106	187	71	159	78	283	125	257	124	227	131	198				
	195	8	181	22	194	-89	197	-60	194	-33	198	0				
HPAC	106	187	71	159	78	283	125	257	124	227	131	198	131	209		
	209	22	195	36	209	-74	210	-47	208	-19	209	11	209	0		
WGTD	84	190	61	162	67	292	99	264	101	235	101	195	101	211	101	264
	275	85	290	128	293	1	266	2	264	29	264	69	264	53	264	0

Table 5-6 (CONTINUED) 1996 ERROR STASTISTICS FOR SELECTED OBJECTIVE TECHNIQUES IN THE NORTH INDIAN OCEAN (1 JAN 1996 - 31 DEC 1996)

48-HOUR MEAN FORECAST ERROR (NM)

	JTWC		NGPS		OTCM		FBAM		CLIM		CLIP		HPAC		WGTD	
JTWC	85	238														
	238	0														
NGPS	50	220	64	190												
	194	-26	190	0												
OTCM	48	219	43	189	64	333										
	330	111	304	115	333	0										
FBAM	80	241	60	191	62	341	115	321								
	322	81	349	158	358	17	321	0								
CLIM	80	241	59	190	62	339	108	325	114	268						
	277	36	275	85	288	-51	275	-50	268	0						
CLIP	85	238	62	188	63	337	115	321	114	268	121	249				
	241	3	234	46	259	-78	248	-73	246	-22	249	0				
HPAC	85	238	62	188	63	337	115	321	114	268	121	249	121	259		
	257	19	249	61	269	-68	261	-60	259	-9	259	10	259	0		
WGTD	68	253	52	193	54	348	92	339	94	280	94	252	94	264	94	311
	334	81	354	161	357	9	314	-25	311	31	311	59	311	47	311	0

72-HOUR MEAN FORECAST ERROR (NM)

	JTWC		NGPS		OTCM		FBAM		CLIM		CLIP		HPAC		WGTD	
JTWC	58	311														
	311	0														
NGPS	29	278	48	241												
	261	-17	241	0												
OTCM	23	234	25	255	36	417										
	427	193	402	147	417	0										
FBAM	54	325	44	244	34	435	92	450								
	500	175	518	274	341	-94	450	0								
CLIM	56	320	43	247	34	430	85	471	91	316						
	289	-31	351	104	353	-77	330	-141	316	0						
CLIP	58	311	46	237	35	426	92	450	91	316	98	315				
	279	-32	320	83	312	-114	317	-133	318	2	315	0				
HPAC	58	311	46	237	35	426	92	450	91	316	98	315	98	333		
	297	-14	341	104	338	-88	336	-114	338	22	333	18	333	0		
WGTD	46	345	38	259	28	463	72	503	74	335	74	326	74	344	74	417
	457	112	532	273	288	-175	424	-79	417	82	417	91	417	73	417	0

Table 5-7 1996 ERROR STASTISTICS FOR SELECTED OBJECTIVE TECHNIQUES IN THE SOUTHERN HEMISPHERE (1 JUL 1995 - 30 JUN 1996)

12-HOUR MEAN FORECAST ERROR (NM)

	JTWC		NGPS		OTCM		FBAM		CLIM		CLIP		HPAC		WGTD	
JTWC	329	68														
	68	0														
NGPS	250	65	388	106												
	103	38	106	0												
OTCM	309	67	358	104	523	80										
	78	11	75	-29	80	0										
FBAM	297	67	357	104	510	79	510	79								
	75	8	74	-30	79	0	79	0								
CLIM	299	67	358	104	513	79	510	79	513	93						
	88	21	83	-21	93	14	93	14	93	0						
CLIP	308	68	357	105	522	80	509	79	512	94	522	89				
	85	17	78	-27	89	9	87	8	87	-7	89	0				
HPAC	309	67	358	104	523	80	510	79	513	93	522	89	523	86		
	81	14	77	-27	86	6	86	7	86	-7	86	-3	86	0		
WGTD	206	65	255	109	348	78	346	77	348	91	348	84	348	83	348	76
	71	6	70	-39	76	-2	76	-1	76	-15	76	-8	76	-7	76	0

24-HOUR MEAN FORECAST ERROR (NM)

	JTWC		NGPS		OTCM		FBAM		CLIM		CLIP		HPAC		WGTD	
JTWC	298	125														
	125	0														
NGPS	232	117	363	151												
	141	24	151	0												
OTCM	277	124	334	149	483	127										
	127	3	123	-26	127	0										
FBAM	275	124	337	149	474	124	487	131								
	129	5	128	-21	128	4	131	0								
CLIM	277	124	338	149	477	124	487	131	490	166						
	163	39	153	4	162	38	166	35	166	0						
CLIP	285	126	337	149	482	126	486	131	489	166	498	151				
	151	25	136	-13	147	21	151	20	151	-15	151	0				
HPAC	286	126	338	149	483	127	487	131	490	166	498	151	499	144		
	145	19	131	-18	140	13	143	12	143	-23	144	-7	144	0		
WGTD	188	123	238	154	322	125	327	129	329	163	329	142	329	139	329	122
	121	-2	116	-38	120	-5	122	-7	122	-41	122	-20	122	-17	122	0

36-HOUR MEAN FORECAST ERROR (NM)

	JTWC		NGPS		OTCM		FBAM		CLIM		CLIP		HPAC		WGTD	
JTWC	267	180														
	180	0														
NGPS	210	173	331	197												
	185	12	197	0												
OTCM	246	177	302	196	442	181										
	177	0	180	-16	181	0										
FBAM	248	178	308	196	435	178	453	194								
	192	14	194	-2	188	10	194	0								
CLIM	250	177	309	196	434	177	449	194	452	230						
	227	50	220	24	229	52	230	36	230	0						
CLIP	257	181	308	196	437	180	448	194	451	230	459	207				
	209	28	195	-1	203	23	206	12	206	-24	207	0				
HPAC	258	181	309	196	438	180	449	194	452	230	459	207	460	202		
	204	23	190	-6	199	19	201	7	201	-29	202	-5	202	0		
WGTD	172	177	219	206	296	180	307	194	306	230	306	200	306	198	309	175
	178	1	173	-33	171	-9	175	-19	174	-56	174	-26	174	-24	175	0

Table 5-7 (CONTINUED) 1996 ERROR STASTISTICS FOR SELECTED OBJECTIVE TECHNIQUES IN THE SOUTHERN HEMISPHERE (1 JUL 1995 - 30 JUN 1996)

48-HOUR MEAN FORECAST ERROR (NM)

	JTWC		NGPS		OTCM		FBAM		CLIM		CLIP		HPAC		WGTD	
JTWC	237	240														
	240	0														
NGPS	188	231	300	243												
	230	-1	243	0												
OTCM	213	229	268	245	401	242										
	235	6	252	7	242	0										
FBAM	222	235	281	242	396	241	422	257								
	254	19	264	22	247	6	257	0								
CLIM	224	235	282	242	399	241	422	257	425	295						
	294	59	287	45	291	50	295	38	295	0						
CLIP	230	239	281	242	400	242	421	258	424	295	431	266				
	268	29	253	11	254	12	266	8	265	-30	266	0				
HPAC	231	240	282	242	401	242	422	257	425	295	431	266	432	263		
	265	25	249	7	252	10	261	4	261	-34	262	-4	263	0		
WGTD	155	238	198	254	268	244	283	257	285	296	285	257	285	255	285	228
	238	0	234	-20	224	-20	229	-28	228	-68	228	-29	228	-27	228	0

72-HOUR MEAN FORECAST ERROR (NM)

	JTWC		NGPS		OTCM		FBAM		CLIM		CLIP		HPAC		WGTD	
JTWC	46	277														
	277	0														
NGPS	41	267	218	353												
	238	-29	353	0												
OTCM	35	246	182	352	308	367										
	413	167	389	37	367	0										
FBAM	44	275	205	360	303	362	348	370								
	384	109	384	24	355	-7	370	0								
CLIM	44	275	206	360	306	361	348	370	351	414						
	452	177	416	56	405	44	414	44	414	0						
CLIP	44	275	205	359	306	362	347	370	350	413	354	394				
	375	100	362	3	367	5	396	26	396	-17	394	0				
HPAC	44	275	206	360	308	367	348	370	351	414	354	394	356	380		
	358	83	348	-12	358	-9	378	8	378	-36	376	-18	380	0		
WGTD	11	216	14	343	13	439	14	489	14	467	14	281	14	204	14	409
	474	258	409	66	404	-35	409	-80	409	-58	409	128	409	205	409	0

6. TROPICAL CYCLONE WARNING VERIFICATION STATISTICS

6.1 GENERAL

Since 1959, JTWC has compiled data on tropical cyclones (TC) within its AOR. In this 38-year period, over 32,000 warnings were verified on 1,800 TCs. The verification data include best tracks (6-hourly positions and associated intensities), JTWC forecasts (12-, 24-, 36-, 48- and 72-hour position, intensity and wind radii), and fixes made from satellite, aircraft, radar, and synoptic data. These data are archived and available upon request.

Efforts are underway to make this information available via anonymous FTP over the Internet, however, until this project is complete JTWC will provide the data by FTP upon request. To request data by Internet, send e-mail to: jtops@npmocw.navy.mil. If the Internet is not an option, data can be copied to 3.5" computer diskettes (that you provide) upon request. Plan for one diskette for each year and ocean basin. Mail them with your request to: NAVPACMETOCCEN WEST /JTWC, PSC 455, Box 12, FPO AP 96540-0051.

6.2 WARNING VERIFICATION STATISTICS

6.2.1 WESTERN NORTH PACIFIC — This section includes verification statistics for each significant TC in the western North Pacific during 1996.

JTWC BEST TRACK, FORECAST TRACK AND INTENSITY ERRORS BY WARNING

TROPICAL DEPRESSION 01W

DTG	WRN NO.	BEST TRACK LAT	LONG	WIND (KT)	POSITION ERRORS 00	12	24	36	48	72	WIND ERRORS 00	12	24	36	48	72
96022306		4.0N	148.7E	20												
96022312		4.0N	148.6E	20												
96022318		4.1N	148.6E	20												
96022400		4.1N	148.5E	20												
96022406		4.2N	148.4E	20												
96022412		4.2N	148.3E	25												
96022418		4.3N	148.2E	25												
96022500		4.3N	148.1E	25												
96022506		4.3N	148.0E	25												
96022512		4.3N	147.5E	25												
96022518		4.8N	146.8E	25												
96022600		5.2N	145.7E	25												
96022606		5.7N	144.4E	25												
96022612		6.1N	143.0E	25												
96022618		6.7N	141.3E	25												
96022700		7.3N	139.5E	25												
96022706		8.0N	137.7E	25												
96022712		8.4N	136.1E	20												
96022718		8.7N	134.5E	20												
96022800		8.9N	133.0E	20												
96022806		9.0N	131.5E	20												
96022812		9.1N	130.0E	25												
96022818		9.3N	128.7E	25												
96022900		9.5N	127.4E	25												

TROPICAL DEPRESSION 01W (CONTINUED)

96022906	1	9.9N	126.3E	30	21	68	127	129			0	5	15	20		
96022912	2	10.1N	125.3E	30	29	90	112	100			0	5	10	20		
96022918	3	10.5N	124.1E	30	21	82	98				0	0	0			
96030100	4	10.7N	122.7E	30	18	60	83				0	0	10			
96030106	5	10.6N	121.4E	30	50	82					0	0				
96030112	6	10.6N	120.4E	30	25	50					0	5				
96030118	7	10.6N	119.6E	30	29						0					
96030200		10.6N	118.8E	25												
		AVERAGE			28	72	106	115								
		# CASES			7	6	4	2								

TROPICAL STORM ANN (02W)

DTG	WRN NO.	BEST TRACK LAT	LONG	WIND (KT)	POSITION ERRORS 00	12	24	36	48	72	WIND ERRORS 00	12	24	36	48	72
96032918		4.0N	150.1E	15												
96033000		4.3N	150.0E	20												
96033006		4.6N	149.9E	20												
96033012		4.9N	149.8E	20												
96033018		5.4N	149.6E	25												
96033100		6.0N	149.2E	25												
96033106		6.6N	148.6E	25												
96033112		7.0N	147.6E	25												
96033118		7.5N	146.6E	25												
96040100		8.0N	145.7E	25												
96040106		8.3N	145.1E	25												
96040112		8.7N	144.5E	30												
96040118		9.0N	143.8E	30												
96040200	1	9.1N	143.0E	35	166	268	373	450	546	854	-10	-5	0	5	10	20
96040206	2	9.2N	142.1E	35	212	269	340	401	445	534	-5	-5	0	5	15	15
96040212	3	9.3N	141.5E	35	215	275	321	347	374	433	-5	-5	0	10	15	10
96040218	4	9.4N	140.8E	35	222	257	300	331	366	446	-5	0	0	15	15	10
96040300	5	9.5N	139.9E	35	196	186	178	235	275	366	0	0	10	20	30	30
96040306	6	9.6N	139.3E	35	186	189	208	269	310	413	0	0	15	20	25	30
96040312	7	9.6N	138.5E	35	183	162	173	193	215	302	0	5	15	15	15	20
96040318	8	9.6N	137.8E	35	198	212	233	254	293	353	0	10	15	10	15	10
96040400	9	9.7N	137.2E	30	206	278	359	441			0	0	0	-10		
96040406		9.7N	136.3E	25												
96040412	10	9.7N	135.5E	25	201	223	237				0	0	-10			
96040418		9.6N	134.7E	25												
96040500	11	9.6N	133.8E	25	142	152	172	177			0	-10	-10	-10		
96040506		9.5N	133.0E	30												
96040512	12	9.5N	132.1E	35	115	128	136	127	138	163	0	5	10	10	15	30
96040518	13	9.5N	130.9E	35	123	128	119	84	91	149	0	5	5	10	20	30
96040600	14	9.6N	129.7E	35	79	70	69	105	170	312	0	5	5	5	15	30
96040606	15	9.7N	128.7E	35	72	58	82	147	232	399	0	0	-5	5	15	25
96040612	16	9.9N	127.7E	35	94	105	102	159	234	378	0	-5	-5	0	10	15
96040618	17	10.2N	126.7E	40	104	131	194	294	399	644	0	-5	0	10	10	25
96040700	18	10.7N	125.7E	40	63	76	152	236	322	490	0	0	5	10	15	25
96040706	19	11.3N	125.0E	40	13	29	79	129	185	316	0	5	10	10	20	25
96040712	20	11.7N	124.3E	40	0	39	79	105	172	299	0	5	10	10	20	30
96040718	21	11.9N	123.8E	35	31	76	132	197	255	318	0	5	0	10	20	30
96040800	22	12.2N	123.4E	35	29	72	137	202	274	364	0	5	0	10	20	30
96040806	23	12.4N	123.1E	30	34	59	117	172	222	304	0	0	0	5	10	20
96040812	24	12.6N	122.8E	30	50	105	166	226	273	355	0	0	0	5	15	20
96040818	25	12.4N	122.5E	30	16	11	26	50	76	142	0	5	5	5	15	20
96040900	26	12.1N	122.3E	30	26	48	68	78			0	5	5	10		
96040906		11.8N	122.1E	25												
96040912	27	11.6N	121.9E	25	108	142	123				0	5	10			
96040918		11.4N	121.7E	20												
96041000		11.3N	121.5E	20												
96041006		11.3N	121.3E	20												
96041012		11.3N	121.1E	15												
96041018		11.4N	120.9E	15												
96041100		11.5N	120.7E	15												
96041106		11.7N	120.5E	15												
96041112		11.9N	120.3E	15												
96041118		12.1N	120.1E	15												
		AVERAGE			115	139	174	217	267	379						
		# CASES			27	27	27	25	22	22						

TROPICAL DEPRESSION 03W

DTG	WRN NO.	BEST TRACK LAT	LONG	WIND (KT)	POSITION ERRORS 00	12	24	36	48	72	WIND ERRORS 00	12	24	36	48	72
96042500		7.7N	113.6E	20												
96042506		7.3N	113.1E	25												
96042512	1	7.2N	112.6E	25	23	35					0	5				
96042518	2	7.1N	112.0E	25	24	24					0	5				
96042600	3	7.2N	111.4E	25	0						0					
96042606	4	7.3N	110.9E	20	0						0					
			AVERAGE		12	30										
			# CASES		4	2										

TYPHOON BART (04W)

DTG	WRN NO.	BEST TRACK LAT	LONG	WIND (KT)	POSITION ERRORS 00	12	24	36	48	72	WIND ERRORS 00	12	24	36	48	72
96050700		6.6N	137.8E	15												
96050706		6.8N	138.0E	15												
96050712		6.9N	138.4E	15												
96050718		7.0N	138.9E	15												
96050800		7.1N	139.2E	15												
96050806		7.1N	139.4E	15												
96050812		7.1N	139.7E	20												
96050818		7.2N	139.9E	20												
96050900		7.4N	139.9E	20												
96050906	1	7.6N	139.7E	25	13	12	56	122	159	169	0	0	0	-5	-5	-5
96050912	2	7.8N	139.3E	25	11	53	136	218	218	150	0	0	5	10	10	10
96050918	3	8.1N	138.7E	30	21	84	172	239	215	163	0	0	0	5	10	10
96051000	4	8.4N	138.0E	35	37	127	223	240	256	252	0	0	0	0	5	5
96051006	5	9.0N	136.9E	35	42	111	162	138	131	133	0	-5	-5	0	5	-5
96051012	6	9.6N	135.9E	40	45	115	106	114	125	133	-5	-5	-10	-10	-10	-35
96051018	7	10.5N	134.7E	45	60	67	35	65	140	330	0	0	5	10	10	-40
96051100	8	11.3N	133.6E	45	66	26	31	30	96	222	0	-5	0	5	0	-55
96051106	9	11.7N	132.5E	50	41	32	47	23	24	72	-5	-5	0	5	-5	-35
96051112	10	11.7N	131.7E	55	18	50	44	17	21	62	0	0	5	5	-5	-20
96051118	11	11.8N	130.8E	55	8	17	21	44	58	45	0	0	5	-5	-20	-15
96051200	12	12.1N	129.7E	60	26	43	42	68	111	196	0	0	0	-5	-25	-20
96051206	13	12.6N	128.9E	60	5	24	13	36	77	154	0	0	-10	-20	-25	-20
96051212	14	13.2N	128.3E	65	8	23	55	91	147	217	0	-5	-20	-35	-20	-20
96051218	15	13.6N	127.9E	65	17	45	96	145	211	244	0	-15	-35	-35	-15	-20
96051300	16	14.1N	127.5E	75	5	39	65	91	130	168	-10	-25	-45	-30	-15	-20
96051306	17	14.5N	127.0E	85	5	34	40	64	68	92	-10	-30	-35	-15	-10	-20
96051312	18	15.0N	126.5E	95	13	30	55	78	90	176	-5	-25	-10	-5	-15	-15
96051318	19	15.4N	126.1E	110	6	26	34	45	62	152	-10	-15	0	5	0	5
96051400	20	15.7N	125.8E	125	5	24	42	32	35	154	0	15	20	5	-5	10
96051406	21	16.1N	125.5E	125	6	34	37	36	22	124	0	10	10	0	-5	10
96051412	22	16.6N	125.2E	120	8	21	57	74	98	71	-5	-15	-25	-40	-40	-20
96051418	23	17.2N	124.9E	115	0	18	34	62	74	199	0	-15	-25	-40	-30	-10
96051500	24	17.7N	124.8E	115	0	11	34	49	84	247	0	0	-5	-15	-10	0
96051506	25	18.2N	124.8E	115	0	34	75	141	181	307	0	-10	-20	-15	-15	-5
96051512	26	18.6N	125.0E	115	11	17	23	67	168	414	0	0	-5	5	0	10
96051518	27	19.1N	125.4E	115	8	45	129	237	363	576	0	0	5	10	10	5
96051600	28	19.4N	125.9E	115	5	39	121	228	303	385	0	10	15	10	15	0
96051606	29	19.6N	126.6E	115	6	34	102	190	245	340	0	20	20	20	20	0
96051612	30	19.9N	127.5E	105	12	78	204	289	320	491	-5	0	-5	-10	-5	-10
96051618	31	20.4N	128.8E	95	21	78	156	222	240		-5	-10	-20	-10	-10	
96051700	32	21.1N	130.2E	85	0	60	113	139	174		-10	-15	-10	-5	-10	
96051706	33	22.2N	131.7E	80	24	82	121	141	255		-10	-5	-5	-5	-10	
96051712	34	23.4N	133.3E	75	6	8	48	101	303		-10	-5	-5	-10	-10	
96051718	35	24.6N	135.1E	65	36	128	192	240			0	0	-5	-10		
96051800	36	25.8N	136.8E	55	12	34	92	294			5	5	-5	-10		
96051806	37	26.7N	138.4E	50	40	86	194				5	0	-10			
96051812	38	27.6N	140.3E	45	8	37	166				0	-10	-15			
96051818	39	28.2N	142.0E	45	0	68					-5	-10				
96051900		28.7N	144.2E	45												
96051906		29.4N	147.2E	45												
96051912		30.4N	151.9E	45												
			AVERAGE		17	49	89	123	154	215						
			# CASES		39	39	38	36	34	30						

TROPICAL STORM CAM (05W)

DTG	WRN NO.	BEST TRACK LAT	LONG	WIND (KT)	POSITION ERRORS 00	12	24	36	48	72	WIND ERRORS 00	12	24	36	48	72
96051600		13.0N	110.9E	15												
96051606		13.2N	111.1E	15												
96051612		13.3N	111.3E	15												
96051618		13.4N	111.5E	15												
96051700		13.5N	111.6E	15												
96051706		13.6N	111.8E	15												
96051712		13.7N	111.9E	15												
96051718		13.9N	112.1E	15												
96051800		14.2N	112.3E	15												
96051806		14.5N	112.5E	20												
96051812		14.8N	112.7E	20												
96051818	1	15.1N	112.9E	25	48	84	141	159	162	256	0	5	5	5	5	-5
96051900	2	15.5N	113.3E	25	66	129	156	179	188	257	0	5	5	5	0	0
96051906	3	15.9N	113.9E	25	56	103	128	141	165	240	0	0	0	0	-5	0
96051912	4	16.4N	114.5E	25	67	96	117	126	164	243	0	0	0	-5	-5	0
96051918	5	16.8N	115.0E	30	74	93	95	130	174	280	0	0	0	-5	0	5
96052000	6	17.1N	115.4E	30	13	37	25	18	24	73	0	0	-5	-5	0	5
96052006	7	17.5N	115.7E	35	20	51	49	41	45	16	0	0	-5	5	10	20
96052012	8	17.9N	116.0E	35	18	48	66	79	84	152	0	0	5	10	10	5
96052018	9	18.1N	116.3E	40	18	49	74	100	130	283	-5	-5	0	5	-5	10
96052100	10	18.4N	116.9E	45	12	59	112	167	225	350	-10	-10	-10	-10	-20	5
96052106	11	18.7N	117.5E	50	20	53	92	143	212		-5	-10	-5	-15	-15	
96052112	12	19.1N	118.2E	50	16	21	24	12	12		-5	-10	-5	-10	-5	
96052118	13	19.4N	118.9E	55	12	23	26	16	42		-10	-10	-20	-15	-5	
96052200	14	19.7N	119.6E	55	6	13	26	29	75		-10	-10	-15	-10	5	
96052206	15	19.9N	120.3E	55	6	32	53	67			-10	-20	-20	-5		
96052212	16	20.2N	121.1E	55	12	26	41	88			-10	-20	-15	5		
96052218	17	20.6N	122.0E	60	18	25	44				-15	-15	-5			
96052300	18	21.0N	122.9E	60	21	25	61				-15	-10	5			
96052306	19	21.5N	123.9E	55	25	28					-10	5				
96052312	20	21.8N	124.9E	50	30	126					-5	10				
96052318	21	22.0N	126.4E	40	32						0					
96052400	22	21.9N	128.0E	30	69						0					
			AVERAGE		30	57	74	94	122	215						
			# CASES		22	20	18	16	14	10						

TYPHOON DAN (06W)

DTG NO.

DTG	WRN NO.	BEST TRACK LAT	LONG	WIND (KT)	POSITION ERRORS 00	12	24	36	48	72	WIND ERRORS 00	12	24	36	48	72
96070312		19.0N	155.6E	15												
96070318		18.9N	154.9E	15												
96070400		18.9N	154.2E	15												
96070406		18.9N	153.4E	15												
96070412		18.9N	152.4E	15												
96070418		19.0N	151.3E	20												
96070500	1	19.1N	150.2E	25	72	90	131	174	201	213	0	5	10	5	5	0
96070506	2	19.3N	149.2E	25	74	91	130	166	187	215	0	5	5	5	0	0
96070512	3	19.5N	148.2E	25	85	124	186	203	217	279	0	5	0	5	5	10
96070518	4	19.8N	147.3E	25	82	92	114	120	127	239		0	0	0	-5	5
96070600	5	20.1N	146.6E	25	8	13	21	39	37	129	0	-5	-5	-5	-15	-15
96070606	6	20.4N	146.0E	30	8	8	12	20	50	201	0	-5	-5	-10	-10	-15
96070612	7	20.6N	145.5E	35	6	12	23	39	50	195	-5	-5	-5	-15	-10	-10
96070618	8	20.9N	144.9E	35	17	57	79	93	64	219	0	0	-5	0	5	10
96070700	9	21.2N	144.2E	40	16	43	35	60	103	332	0	-5	-10	0	0	10
96070706	10	21.6N	143.5E	45	18	24	52	85	174	397	0	-10	-10	-5	0	15
96070712	11	22.1N	142.7E	50	45	73	97	150	254	443	0	-5	5	5	15	20
96070718	12	22.4N	142.0E	60	21	45	69	72	84	223	-5	0	5	10	20	15
96070800	13	22.8N	141.3E	65	8	54	114	187	252	390	0	0	0	10	20	15
96070806	14	23.4N	140.8E	65	16	72	125	174	176	313	0	5	-5	-5	-5	-5
96070812	15	24.0N	140.6E	65	24	65	115	146	142	248	0	-10	-15	-10	-10	-15
96070818	16	24.7N	140.5E	70	36	85	124	131	138	296	-5	-10	-10	-5	-10	-15
96070900	17	25.5N	140.5E	75	13	80	167	234	315	618	0	-5	-5	-5	-10	-15
96070906	18	26.7N	140.6E	75	24	90	155	226	336	559	0	0	0	-5	-5	-15
96070912	19	28.0N	140.7E	75	6	42	67	113	214	266	0	0	0	-5	-5	-10
96070918	20	29.5N	140.8E	70	8	18	53	115	213	144	0	-5	-10	-15	-20	-15
96071000	21	31.0N	141.0E	70	26	36	71	99	96	130	0	-5	-15	-15	-25	-15
96071006	22	32.4N	141.2E	65	20	94	127	161	114	157	0	-5	-10	-15	-25	-15
96071012	23	33.7N	141.8E	65	34	120	259	320	247	253	-10	-15	-20	-25	-25	-5
96071018	24	35.0N	142.9E	65	15	86	225	255	130	169	-15	-20	-25	-25	-20	-5
96071100	25	36.4N	144.2E	65	24	79	124	100	99		-15	-20	-25	-20	-15	

TYPHOON DAN (06W) (CONTINUED)

96071106	26	37.9N	145.8E	60	29	138	232	253	249		-10	-20	-25	-15	-15	
96071112	27	39.8N	147.9E	60	11	166	326	407			-20	-20	-20	-10		
96071118	28	42.0N	149.6E	60	58	211	346	445			-25	-25	-15	-10		
96071200	29	43.9N	150.8E	60	49	194	381	472			0	0	-5	-10		
96071206	30	45.3N	151.6E	60	103	280	469	559			0	0	-5	-5		
96071212		45.8N	152.3E	55												
96071218		45.9N	153.2E	50												
96071300		45.6N	154.7E	45												
96071306		45.2N	157.1E	45												
96071312		45.1N	159.9E	35												
96071318		45.0N	162.1E	35												
96071400		44.9N	164.2E	30												
96071406		45.2N	166.3E	25												
96071412		46.4N	168.1E	25												
96071418		47.7N	169.2E	20												
96071500		49.0N	170.2E	20												
		AVERAGE			32	86	148	188	165	277						
		# CASES			30	30	30	30	26	24						

SUPER TYPHOON EVE (07W)

	WRN	BEST TRACK			POSITION ERRORS						WIND ERRORS					
DTG	NO.	LAT	LONG	WIND (KT)	00	12	24	36	48	72	00	12	24	36	48	72
96071006		19.3N	151.5E	15												
96071012		19.2N	151.0E	15												
96071018		19.1N	150.5E	15												
96071100		19.0N	150.0E	15												
96071106		19.0N	149.5E	15												
96071112		19.0N	148.8E	15												
96071118		19.0N	148.0E	20												
96071200		18.9N	147.3E	20												
96071206		18.9N	146.7E	25												
96071212		18.9N	146.2E	25												
96071218		18.9N	145.7E	25												
96071300		18.9N	145.2E	30												
96071306		19.0N	144.5E	30												
96071312	1	19.2N	143.8E	35	20	34	42	58	77	126	-10	-15	-30	-35	-70	-65
96071318	2	19.6N	142.9E	40	17	26	42	47	49	110	-15	-25	-35	-50	-85	-50
96071400	3	20.1N	142.1E	45	12	28	39	33	50	112	-15	-35	-35	-70	-90	-45
96071406	4	20.5N	141.3E	55	5	27	33	44	62	144	-20	-30	-50	-85	-65	-30
96071412	5	21.0N	140.5E	65	8	24	45	66	95	199	-30	-35	-70	-85	-50	-25
96071418	6	21.5N	139.7E	70	16	33	56	87	128	230	-25	-40	-70	-50	-30	-10
96071500	7	22.0N	138.8E	75	6	6	24	52	86	194	0	-25	-40	0	15	20
96071506	8	22.5N	137.9E	95	6	30	45	61	94	211	-15	-40	-20	5	30	45
96071512	9	22.9N	136.9E	115	8	5	29	60	75	172	0	-10	20	30	40	75
96071518	10	23.4N	136.1E	135	6	17	44	59	63	133	-5	5	20	40	25	85
96071600	11	24.0N	135.3E	140	8	18	48	79	72	191	-10	25	10	15	-5	35
96071606	12	24.7N	134.5E	125	0	12	13	44	99	212	-5	20	20	0	20	40
96071612	13	25.4N	133.7E	115	6	24	38	62	102	174	5	10	10	-15	35	45
96071618	14	26.1N	133.0E	115	16	27	57	92	77	198	5	20	-5	10	35	45
96071700	15	26.9N	132.3E	110	5	24	36	88	54	442	5	5	-10	35	30	30
96071706	16	27.8N	131.6E	100	11	26	66	70	120	545	5	-10	15	30	30	25
96071712	17	28.7N	131.0E	100	6	11	45	54	199	561	0	-15	35	30	30	20
96071718	18	29.5N	130.6E	115	13	19	32	120	217	549	-10	10	30	35	30	25
96071800	19	30.5N	130.4E	115	0	32	24	111	231	474	0	25	25	20	5	5
96071806	20	31.6N	130.7E	90	7	16	64	107	181	438	5	35	30	20	10	0
96071812	21	32.6N	131.0E	65	5	34	36	34	47	59	10	20	20	5	0	-10
96071818	22	33.5N	131.3E	55	0	38	42	37	38	106	5	10	5	5	0	-20
96071900	23	34.0N	131.8E	45	0	34	42	27			-5	-5	-15	-15		
96071906	24	34.2N	132.8E	40	9	27	29				-5	-5	-10			
96071912	25	34.6N	133.9E	35	28	30	15				-5	-10	-10			
96071918	26	34.8N	135.0E	35	15	5	19	59			-5	-5	0	-10		
96072000	27	34.8N	136.0E	35	5	6	43				-5	-5	0			
96072006		34.7N	137.0E	30												
96072012		34.6N	138.0E	30												
96072018		34.3N	139.0E	25												
96072100		33.9N	140.0E	25												
96072106		33.3N	141.0E	30												
96072112		32.9N	141.9E	35												
96072118		32.4N	142.8E	40												
96072200		31.9N	143.8E	40												
96072206		31.5N	144.9E	35												
96072212		31.2N	146.0E	35												
96072218		31.0N	146.9E	30												
96072300		31.2N	147.6E	30												

SUPER TYPHOON EVE (07W) (CONTINUED)

DTG	WRN NO.	LAT	LONG	WIND (KT)	00	12	24	36	48	72	00	12	24	36	48	72
96072306		31.5N	148.4E	30												
96072312		32.1N	149.3E	30												
96072318		33.0N	150.2E	30												
96072400		34.2N	151.2E	30												
96072406		36.0N	153.0E	30												
96072412		37.8N	155.1E	30												
96072418		39.6N	157.3E	30												
96072500		41.4N	159.0E	30												
96072506		42.9N	160.5E	30												
96072512		44.1N	162.6E	30												
96072518		45.3N	164.6E	30												
96072600		46.5N	166.8E	30												
96072606		47.9N	168.4E	30												
96072612		49.5N	170.0E	30												
96072618		51.0N	172.0E	30												
96072700		52.6N	174.5E	30												
96072706		54.0N	178.0E	30												
96072712		55.0N	178.0W	30												
96072718		56.0N	174.0W	30												
		AVERAGE			9	23	39	65	101	254						
		# CASES			27	27	27	24	22	22						

TYPHOON FRANKIE (08W)

	WRN	BEST TRACK			POSITION ERRORS						WIND ERRORS					
DTG	NO.	LAT	LONG	WIND (KT)	00	12	24	36	48	72	00	12	24	36	48	72
96071912		16.9N	114.7E	15												
96071918		16.6N	115.2E	15												
96072000		16.4N	115.7E	15												
96072006		16.0N	115.7E	20												
96072012		16.0N	115.2E	25												
96072018		16.3N	114.5E	25												
96072100	1	16.8N	113.8E	25	18	28	74	111	134	165	0	5	10	-5	-30	-40
96072106	2	17.3N	113.2E	30	5	36	74	94	110	188	-5	0	5	-20	-45	-30
96072112	3	17.7N	112.5E	30	0	39	73	100	140	281	-5	0	0	-25	-60	-15
96072118	4	18.1N	111.7E	35	25	74	102	135	148	290	0	0	-5	-40	-60	-10
96072200	5	18.5N	110.9E	35	20	50	69	96	144	233	0	-5	-25	-55	-35	0
96072206	6	18.7N	110.1E	40	37	53	82	116	194	237	-5	-20	-45	-60	-30	5
96072212	7	19.0N	109.7E	45	38	81	116	142	224	281	-5	-25	-55	-35	-15	10
96072218	8	19.2N	109.1E	50	59	77	91	148	201		-10	-40	-55	-30	-15	
96072300	9	19.5N	108.6E	60	6	16	13	35	84		-10	-35	-5	-10	-5	
96072306	10	19.8N	107.9E	75	5	32	12	49	139		-10	-20	0	0	0	
96072312	11	20.1N	107.2E	90	18	30	53	138	254		-20	0	5	5	5	
96072318	12	20.3N	106.8E	90	8	76	143	207			-5	15	15	10		
96072400	13	20.4N	106.0E	65	12	69	55	49			0	10	5	5		
96072406	14	20.2N	105.1E	55	42	49	17				0	5	5			
96072412		20.2N	104.1E	40												
96072418		20.6N	103.2E	35												
96072500		21.1N	102.3E	25												
96072506		21.7N	101.3E	20												
96072512		22.5N	100.3E	15												
		AVERAGE			21	51	70	110	162	240						
		# CASES			14	14	14	13	11	7						

TYPHOON GLORIA (09W)

	WRN	BEST TRACK			POSITION ERRORS						WIND ERRORS					
DTG	NO.	LAT	LONG	WIND (KT)	00	12	24	36	48	72	00	12	24	36	48	72
96071900		7.1N	136.9E	15												
96071906		7.6N	136.6E	15												
96071912		8.2N	136.2E	15												
96071918		8.7N	135.8E	15												
96072000		9.1N	135.4E	15												
96072006		9.5N	135.0E	15												
96072012		10.0N	134.4E	20												
96072018		10.6N	133.7E	20												
96072100		11.2N	132.8E	20												
96072106		11.8N	131.8E	25												
96072112		12.4N	130.9E	25												
96072118		12.9N	130.1E	30												
96072200	1	13.2N	129.3E	35	51	71	120	133	135	166	-5	-10	-10	-15	-15	-60
96072206	2	13.5N	128.7E	40	53	128	191	186	198	244	-10	-10	-10	-10	-40	-40
96072212	3	13.9N	128.2E	45	18	46	40	25	42	120	-5	-5	-5	-5	-10	5

TYPHOON GLORIA (09W) (CONTINUED)

96072218	4	14.4N	127.8E	45	16	28	12	34	72	165	0	-5	-5	-5	-5	20
96072300	5	14.9N	127.5E	50	18	37	78	85	102	212	0	0	5	-10	0	20
96072306	6	15.5N	126.8E	55	24	82	103	125	146	195	0	0	0	-5	5	20
96072312	7	16.0N	126.0E	60	6	12	25	46	106	166	-5	-5	-10	-5	10	35
96072318	8	16.5N	125.1E	65	21	24	30	66	122	200	-5	-10	-10	0	15	50
96072400	9	16.9N	124.5E	70	23	42	75	140	171	173	-5	-20	-10	0	15	35
96072406	10	17.4N	123.9E	80	0	13	45	105	133	216	-5	-10	0	10	20	45
96072412	11	17.8N	123.4E	90	0	24	16	52	32	236	-15	0	10	25	15	60
96072418	12	18.4N	122.9E	90	6	0	30	36	40	189	0	15	25	10	15	50
96072500	13	19.0N	122.4E	90	12	54	60	32	62		0	15	25	20	25	
96072506	14	19.5N	121.9E	90	23	55	78	20	88		0	15	15	30	30	
96072512	15	19.9N	121.5E	90	12	36	89	54	70		0	15	25	40	45	
96072518	16	20.4N	121.1E	90	18	72	140	149	145		0	15	35	55	55	
96072600	17	21.2N	120.8E	90	6	60	97	149			0	20	40	60		
96072606	18	21.9N	120.8E	90	0	95	222	301			0	5	20	50		
96072612	19	23.4N	120.2E	80	16	113	241				-15	10	20			
96072618	20	24.3N	119.1E	70	12	69	102				0	20	20			
96072700	21	24.8N	117.7E	60	0	33					0	20				
96072706	22	25.1N	116.3E	45	21	67					5					
96072712		25.3N	115.0E	30												
96072718		25.4N	114.0E	20												
			AVERAGE		17	53	90	97	105	191						
			# CASES		22	22	20	18	16	12						

SUPER TYPHOON HERB (10W)

	WRN	BEST TRACK			POSITION ERRORS						WIND ERRORS					
DTG	NO.	LAT	LONG	WIND (KT)	00	12	24	36	48	72	00	12	24	36	48	72
96072106		12.3N	151.6E	15												
96072112		12.5N	151.9E	15												
96072118		12.9N	152.2E	15												
96072200		13.4N	152.4E	15												
96072206		14.1N	152.6E	15												
96072212		14.9N	152.7E	20												
96072218		15.5N	152.7E	25												
96072300		16.1N	152.5E	25												
96072306	1	16.8N	152.0E	25	67	111	163	228	329	566	0	0	0	0	0	-15
96072312	2	17.4N	151.5E	25	106	145	180	271	370	613	0	5	10	10	0	-15
96072318	3	18.0N	150.9E	30	133	145	199	294	419	728	0	0	5	0	-5	-25
96072400	4	18.5N	150.3E	30	103	142	228	292	365	444	0	0	0	-10	-10	-30
96072406	5	19.0N	149.5E	35	24	24	96	172	253	364	0	5	0	-5	-10	-30
96072412	6	19.5N	148.9E	35	24	56	135	192	233	317	0	0	-10	-10	-15	-40
96072418	7	20.0N	147.7E	40	32	107	175	238	281	403	5	0	-5	-10	-15	-25
96072500	8	20.2N	146.4E	45	11	55	68	100	153	321	-5	-10	-10	-15	-20	-25
96072506	9	20.2N	145.0E	55	5	17	45	60	132	318	0	-10	-20	-25	-30	-25
96072512	10	20.2N	143.6E	65	0	28	45	46	21	223	0	0	0	-5	-15	-10
96072518	11	20.5N	142.1E	70	33	105	131	153	91	120	0	-10	-10	-15	-15	-10
96072600	12	20.6N	140.6E	75	12	42	60	84	145	283	0	0	0	-15	-10	-5
96072606	13	20.6N	139.0E	85	21	81	180	246	314	449	0	-10	-10	-15	-10	0
96072612	14	20.4N	137.9E	90	29	96	187	254	308	293	-5	-15	-20	-15	-10	0
96072618	15	20.0N	136.7E	100	58	137	235	340	426	404	0	-5	-10	-5	-5	0
96072700	16	19.7N	135.6E	105	5	29	111	189	238	264	0	-10	0	0	0	-10
96072706	17	19.3N	134.7E	115	8	57	123	185	201	173	0	0	10	0	5	-15
96072712	18	19.0N	133.9E	125	13	26	18	41	92	173	0	10	10	5	5	-15
96072718	19	18.8N	133.2E	125	12	49	90	113	137	199	0	5	5	10	-5	-40
96072800	20	18.6N	132.5E	125	8	16	18	16	27	66	0	0	10	10	-15	-35
96072806	21	18.4N	131.8E	125	8	18	22	61	73	105	0	0	10	5	-20	-30
96072812	22	18.3N	131.1E	125	11	61	91	122	173	196	0	5	5	-10	-25	-40
96072818	23	18.3N	130.5E	125	8	70	92	111	154	174	0	10	5	-15	-35	10
96072900	24	18.7N	129.9E	120	8	32	55	82	97	84	0	5	-10	-15	-35	-10
96072906	25	19.2N	129.3E	115	8	28	46	107	120	88	0	0	-15	-30	-30	15
96072912	26	19.8N	128.7E	115	5	20	55	72	79	91	0	-10	-15	-30	-25	25
96072918	27	20.5N	128.2E	115	0	5	32	52	98	142	0	-15	-25	-30	20	35
96073000	28	21.3N	127.7E	125	11	6	25	54	103	131	-5	-15	-25	-25	0	45
96073006	29	22.0N	127.1E	130	8	30	56	89	125	102	0	-15	-20	30	25	55
96073012	30	22.6N	126.6E	130	0	32	72	133	170	121	0	-15	-15	10	35	55
96073018	31	23.1N	126.1E	140	0	60	121	170	184	127	0	-5	40	35	45	60
96073100	32	23.9N	124.8E	140	6	37	55	37	54		0	0	25	15	5	
96073106	33	24.2N	123.8E	135	6	29	96	159	162		-5	55	0	15	15	
96073112	34	24.8N	122.7E	130	0	44	96	107	65		0	-15	5	10	15	
96073118	35	25.0N	121.4E	75	8	114	154	171	151		0	-5	5	15	10	
96080100	36	25.4N	120.0E	95	0	32	49	67	91		0	0	5	0	0	
96080106	37	26.0N	118.6E	70	5	12	5	23			0	0	5	-5		
96080112	38	26.4N	117.3E	60	16	59	119				0	0	-10			
96080118		26.9N	116.3E	50												

SUPER TYPHOON HERB (10W) (CONTINUED)

DTG	WRN NO.	LAT	LONG	WIND (KT)	00	12	24	36	48	72	00	12	24	36	48	72
96080200		27.5N	115.4E	40												
96080206		28.1N	114.5E	30												
96080212		28.8N	113.8E	30												
96080218		29.5N	113.1E	25												
96080300		30.3N	112.6E	20												
96080306		31.0N	112.1E	20												
96080312		31.7N	111.7E	20												
			AVERAGE		22	57	99	139	179	261						
			# CASES		38	38	38	37	36	31						

TROPICAL STORM IAN (11W)

	WRN	BEST TRACK			POSITION ERRORS						WIND ERRORS					
DTG	NO.	LAT	LONG	WIND (KT)	00	12	24	36	48	72	00	12	24	36	48	72
96072706		11.8N	143.7E	20												
96072712		12.3N	143.9E	25												
96072718		13.1N	144.0E	30												
96072800		13.9N	143.9E	35												
96072806		14.6N	143.6E	35												
96072812	1	15.3N	143.3E	35	62	154	364	484	529	645	-5	0	5	20	35	50
96072818	2	16.2N	142.9E	35	83	231	418	514	610	788	-5	-5	5	25	40	55
96072900	3	17.1N	142.3E	35	55	244	369	462	583	720	0	0	15	30	50	65
96072906	4	19.0N	141.2E	40	62	188	252	355	480	554	-5	0	20	35	50	70
96072912	5	21.1N	140.4E	40	136	229	294	402	498		0	15	30	45	60	
96072918	6	22.8N	139.8E	40	188	234	279	377	420		0	10	20	30	45	
96073000	7	23.9N	139.4E	35	144	159	200	234	222		0	5	5	5	10	
96073006	8	25.0N	139.0E	30	90	128	196	177			0	5	5	10		
96073012		25.9N	138.6E	30												
96073018	9	27.0N	138.2E	25	79	125	119	143			5	5	5	10		
96073106	10	29.3N	137.2E	25	60	125	200				-5	0	0			
96073112		30.0N	136.5E	25												
96073118		30.5N	135.5E	20												
96080100		30.9N	134.4E	20												
96080106		31.2N	133.3E	15												
			AVERAGE		96	182	270	350	478	677						
			# CASES		10	10	10	9	7	4						

TYPHOON JOY (12W)

	WRN	BEST TRACK			POSITION ERRORS						WIND ERRORS					
DTG	NO.	LAT	LONG	WIND (KT)	00	12	24	36	48	72	00	12	24	36	48	72
96072512		19.6N	165.2E	10												
96072518		19.5N	164.6E	10												
96072600		19.4N	164.0E	10												
96072606		19.4N	163.5E	10												
96072612		19.4N	163.0E	15												
96072618		19.4N	162.4E	15												
96072700		19.6N	161.7E	15												
96072706		20.0N	160.7E	15												
96072712		20.6N	159.8E	15												
96072718		21.4N	158.8E	15												
96072800		22.3N	157.8E	15												
96072806		23.1N	156.9E	15												
96072812		24.0N	155.9E	15												
96072818		24.8N	154.8E	20												
96072900		25.8N	153.9E	20												
96072906	1	26.7N	153.4E	25	8	110	223	306	367	441	0	-5	0	20	40	30
96072912	2	27.0N	152.9E	30	23	144	248	345	401	529	0	0	10	20	30	20
96072918	3	26.8N	152.3E	35	62	168	268	338	358	476	-5	0	10	15	25	15
96073000	4	26.4N	152.2E	35	41	142	283	341	359	382	0	5	5	-5	-25	-50
96073006	5	26.2N	152.5E	35	38	52	112	153	189	296	0	10	5	-5	-35	-50
96073012	6	26.2N	152.7E	35	20	30	51	73	93	155	0	5	0	-20	-40	-50
96073018	7	26.3N	153.0E	35	18	26	32	57	83	191	0	0	-5	-30	-45	-50
96073100	8	26.6N	153.2E	35	18	12	33	70	94	226	0	-5	-10	-35	-45	-45
96073106	9	26.9N	153.1E	40	20	69	111	132	140	198	-5	-10	-20	-40	-45	-45
96073112	10	27.5N	152.9E	45	41	70	76	61	63	198	0	-5	-25	-40	-45	-40
96073118	11	28.2N	152.6E	50	55	85	108	121	136	177	-5	-20	-30	-40	-45	-35
96080100	12	28.8N	152.3E	55	12	31	30	66	103	49	0	-5	-5	-15	-25	-25
96080106	13	29.5N	152.0E	65	13	23	56	119	163	64	0	0	0	-15	-25	-10
96080112	14	30.2N	151.9E	70	7	23	82	120	136	115	-5	-5	-10	-15	-25	-10
96080118	15	30.7N	151.9E	75	23	63	112	147	139	136	-10	-5	-10	-15	-20	-5
96080200	16	31.1N	152.0E	75	7	57	105	123	102	155	0	0	-5	-10	-15	0
96080206	17	31.5N	152.4E	75	15	58	93	85	48	46	0	0	-10	-10	-10	-5

TYPHOON JOY (12W) (CONTINUED)

96080212	18	31.8N	153.0E	75	10	16	35	44	65	46	0	5	0	-5	0	5
96080218	19	31.9N	153.6E	75	6	21	7	31	42	109	0	0	5	5	5	5
96080300	20	32.0N	154.2E	70	5	5	10	23	7	124	0	0	5	10	10	10
96080306	21	32.0N	154.9E	70	5	24	64	72	37		0	5	15	15	10	
96080312	22	32.2N	155.1E	65	28	58	119	96	60		0	5	10	10	10	
96080318	23	32.4N	155.3E	60	35	76	79	64	56		-5	0	5	5	5	
96080400	24	32.7N	155.3E	55	16	32	11	68	181		0	5	5	5	5	
96080406	25	33.2N	155.1E	45	7	24	42	191			0	0	0	5		
96080412	26	33.7N	154.9E	40	12	51	78	118			0	5	5	5		
96080418	27	34.1N	154.8E	35	25	92	110				-5	0	5			
96080500		34.5N	155.0E	30												
96080506	28	34.8N	155.3E	30	49	187					0	5				
96080512		36.1N	156.2E	25												
96080518		37.5N	157.1E	25												
96080600		39.0N	157.8E	20												
			AVERAGE		23	63	96	130	143	206						
			# CASES		28	28	27	26	24	20						

TYPHOON KIRK (13W)

	WRN	BEST TRACK			POSITION ERRORS						WIND ERRORS					
DTG	NO.	LAT	LONG	WIND (KT)	00	12	24	36	48	72	00	12	24	36	48	72
96072800		5.3N	155.8E	15												
96072806		5.5N	155.3E	15												
96072812		5.7N	154.7E	15												
96072818		5.9N	154.2E	15												
96072900		6.1N	153.7E	15												
96072906		6.3N	152.9E	15												
96072912		6.5N	152.0E	15												
96072918		6.8N	151.0E	20												
96073000		7.1N	149.7E	20												
96073006		7.4N	1484.E	25												
96073012		7.6N	1473.E	25												
96073018		7.8N	146.2E	25												
96073100		8.0N	145.3E	25												
96073106		8.1N	144.6E	25												
96073112		8.1N	143.9E	20												
96073118		8.2N	143.2E	20												
96080100		8.4N	142.5E	20												
96080106		8.7N	141.6E	20												
96080112		8.9N	140.7E	20												
96080118		9.3N	139.8E	20												
96080200		9.8N	138.9E	20												
96080206		10.4N	138.1E	20												
96080212		11.0N	137.4E	20												
96080218		11.6N	136.7E	20												
96080300		13.1N	135.7E	20												
96080306		15.3N	134.7E	25												
96080312		17.7N	134.0E	25												
96080318	1	20.1N	133.4E	25	30	143	180	196	185	141	0	0	5	15	10	0
96080400	2	22.3N	132.3E	25	17	87	104	91	17	187	0	0	5	5	-5	0
96080406	3	23.8N	131.3E	30	18	113	188	276	354	562	0	5	15	10	10	30
96080412	4	24.9N	130.9E	30	49	142	255	371	506	778	0	5	10	0	5	5
96080418	5	25.8N	130.7E	30	20	44	152	256	392	609	0	5	0	0	5	0
96080500	6	26.4N	130.5E	30	24	41	151	281	420	640	0	0	-10	0	0	-5
96080506	7	27.0N	130.4E	30	50	119	230	369	516	693	0	-10	-10	0	0	-15
96080512	8	27.5N	130.7E	35	19	71	128	187	233	203	-5	-25	-20	-20	-10	-20
96080518	9	27.5N	131.1E	45	36	72	134	193	220	195	-15	-25	-20	-20	-15	-25
96080600	10	27.4N	131.4E	55	7	49	89	136	142	123	-20	-10	-5	0	0	-10
96080606	11	27.1N	131.7E	55	8	24	55	72	77	126	0	10	10	15	5	5
96080612	12	26.7N	132.2E	55	16	49	82	80	68	130	0	0	5	5	-5	-5
96080618	13	26.3N	132.6E	55	13	41	47	64	80	137	0	0	5	-5	-5	-5
96080700	14	25.9N	133.0E	60	20	0	8	21	16	114	0	0	0	-10	-5	-5
96080706	15	25.4N	133.6E	60	5	21	13	37	92	126	0	0	-10	-10	-5	-10
96080712	16	25.1N	133.9E	60	12	29	62	97	123	171	0	-5	-15	-10	-5	-10
96080718	17	24.9N	134.1E	60	6	43	86	121	136	169	-5	-20	-20	-15	-10	-10
96080800	18	24.8N	134.1E	65	8	5	59	123	164	146	-5	-15	-15	-10	-10	-10
96080806	19	24.8N	134.0E	75	12	29	98	139	125	60	-10	-15	-10	-10	-15	-10
96080812	20	24.9N	133.8E	80	0	38	94	117	98	85	-15	-10	-5	0	5	5
96080818	21	25.1N	133.4E	80	8	56	99	107	72	66	-15	-10	-5	-5	5	5
96080900	22	25.1N	132.7E	80	16	52	67	72	84	76	-5	-5	0	5	15	15
96080906	23	25.0N	132.1E	80	16	45	56	54	37	52	0	5	10	15	20	15
96080912	24	24.8N	131.6E	80	24	48	90	118	116	89	0	5	10	15	20	15
96080918	25	24.6N	131.1E	80	10	24	29	52	61	112	0	0	10	15	20	15
96081000	26	24.4N	130.8E	80	8	20	38	47	36	125	-5	-10	0	5	10	10

TYPHOON KIRK (13W) (CONTINUED)

96081006	27	24.3N	130.7E	85	0	5	18	43	60	101	0	5	10	15	10	10
96081012	28	24.2N	130.5E	85	8	30	36	72	60	143	0	5	10	10	10	15
96081018	29	24.3N	130.4E	85	17	47	53	80	47	160	0	5	10	5	10	15
96081100	30	24.5N	130.3E	85	17	39	76	72	52	221	0	0	0	0	5	10
96081106	31	24.8N	130.1E	85	5	33	59	34	48	146	-5	0	-5	0	5	25
96081112	32	25.1N	129.6E	85	8	24	41	48	40	205	-5	-5	-5	0	10	30
96081118	33	25.5N	129.0E	85	6	12	43	70	67	319	-5	-10	-5	0	5	15
96081200	34	25.9N	128.3E	90	0	43	83	107	132	459	-20	-25	-20	-20	-15	20
96081206	35	26.4N	127.8E	95	0	41	84	118	173	489	-20	-20	-15	-10	0	30
96081212	36	26.6N	127.7E	95	0	27	98	147	256	459	-5	0	5	10	25	25
96081218	37	27.2N	127.6E	95	5	42	97	188	333	333	-5	0	0	15	10	-10
96081300	38	27.8N	127.8E	95	0	55	89	180	326	422	-5	0	5	25	25	20
96081306	39	28.5N	128.1E	95	0	52	93	206	282	371	-5	0	10	30	30	20
96081312	40	30.0N	128.8E	95	6	50	57	131	152	149	-5	-5	10	25	5	10
96081318	41	31.1N	129.3E	95	0	34	102	151	111		0	-5	10	15	5	
96081400	42	32.2N	130.2E	95	5	69	95	46	36		0	10	20	10	5	
96081406	43	33.8N	131.6E	85	0	64	72	48	24		0	15	25	10	5	
96081412	44	35.3N	133.7E	70	7	61	74	78	160		0	5	5	0	0	
96081418	45	37.0N	136.5E	65	33	32	47	4			0	0	-5	-5		
96081500	46	38.6N	139.5E	55	11	51	67	190			0	-5	-5	-10		
96081506	47	40.0N	142.3E	50	29	71	162				0	-5	-5			
96081512	48	41.3N	144.9E	45	10	18	127				0	5	-5			
96081518	49	42.4N	147.2E	45	0	104					0	5				
96081600	50	43.7N	150.0E	40	18	107					0	-5				
96081606	51	44.8N	153.5E	40	7						0					
96081612		45.2N	157.0E	40												
			AVERAGE		13	51	89	124	154	248						
			# CASES		51	50	48	46	44	40						

TROPICAL STORM LISA (14W)

DTG	WRN NO.	BEST TRACK LAT	LONG	WIND (KT)	POSITION ERRORS 00	12	24	36	48	72	WIND ERRORS 00	12	24	36	48	72
96080400		15.5N	111.0E	25												
96080406		15.9N	111.7E	25												
96080412		16.4N	112.4E	25												
96080418		16.9N	113.0E	25												
96080500		17.3N	113.4E	25												
96080506	1	17.7N	113.8E	30	72	111	169	243	198		-5	-10	-5	15	20	
96080512	2	18.3N	114.2E	35	39	119	279	343	289		-10	-10	0	15	35	
96080518	3	19.0N	114.8E	40	72	186	311	303	258		-15	-10	5	20	35	
96080600	4	20.1N	115.4E	40	41	146	163	123	102		0	10	25	30	30	
96080606	5	21.4N	116.5E	40	45	87	79	61			0	15	30	30		
96080612	6	22.8N	117.5E	35	55	78	192				0	-5	-5			
96080618	7	24.1N	118.0E	30	28	142	140				0	0	-5			
96080700	8	25.0N	117.6E	30	6	36					0	0				
96080706		25.5N	117.3E	25												
96080712		25.8N	117.0E	20												
96080718		26.1N	116.9E	20												
96080800		26.3N	116.6E	15												
			AVERAGE		45	114	191	215	212							
			# CASES		8	8	7	5	4							

TROPICAL DEPRESSION 15W

DTG	WRN NO.	BEST TRACK LAT	LONG	WIND (KT)	POSITION ERRORS 00	12	24	36	48	72	WIND ERRORS 00	12	24	36	48	72
96081006		29.0N	158.0E	15												
96081012		29.7N	157.8E	15												
96081018		30.4N	157.8E	15												
96081100		31.2N	157.9E	15												
96081106		31.6N	158.1E	15												
96081112		32.1N	158.5E	20												
96081118		32.4N	158.9E	25												
96081200		32.7N	159.2E	30												
96081206	1	32.9N	159.5E	30	18	57	115	169			-5	-5	0	0		
96081212		32.9N	160.0E	30												
96081218	2	32.6N	160.2E	30	18	63	72	85			0	0	0	0		
96081300		32.2N	160.3E	30												
96081306	3	31.8N	160.5E	30	12	54	82	139			0	0	0	0		
96081312		31.6N	161.1E	30												
96081318	4	31.4N	161.6E	30	15	39	58	91			0	0	0	0		
96081400		31.3N	162.0E	30												
96081406	5	31.3N	162.4E	30	13	62	116	178			0	0	0	0		

TROPICAL DEPRESSION 15W (CONTINUED)

DTG	WRN NO.	LAT	LONG	WIND (KT)	00	12	24	36	48	72	00	12	24	36	48	72
96081412		31.5N	163.2E	30												
96081418	6	31.8N	163.8E	30	20	54	80	99			0	0	0	0		
96081500		32.1N	164.5E	30												
96081506	7	32.4N	165.2E	30	13	24	34	60			0	0	-5	5		
96081512		32.7N	165.9E	30												
96081518	8	33.2N	166.5E	30	20	25	54				0	-5	0			
96081600		33.7N	167.1E	30												
96081606	9	34.1N	167.6E	30	13	59	68				-5	5	0			
96081612		34.4N	168.2E	25												
96081618		34.8N	168.7E	20												
96081700		35.6N	169.1E	20												
96081706		36.6N	169.6E	20												
			AVERAGE		16	49	76	118								
			# CASES		9	9	9	7								

TROPICAL STORM MARTY (16W)

	WRN	BEST TRACK			POSITION ERRORS						WIND ERRORS					
DTG	NO.	LAT	LONG	WIND (KT)	00	12	24	36	48	72	00	12	24	36	48	72
96081112		22.9N	108.4E	15												
96081118		22.1N	108.4E	15												
96081200		21.6N	108.3E	20												
96081206		21.3N	108.2E	25												
96081212		21.1N	108.0E	25												
96081218		21.0N	107.7E	25												
96081306	1	20.6N	107.3E	35	25	56	140	220			-10	-25	-10	0		
96081312		20.5N	107.1E	40												
96081318	2	20.3N	106.8E	50	18	68	130	189			-25	-15	0	10		
96081400		20.2N	106.5E	50												
96081406	3	20.2N	106.1E	40	8	28	45				-5	0	0			
96081412		20.1N	105.7E	30												
96081418		20.2N	105.3E	30												
96081500		20.3N	104.9E	25												
96081506		20.3N	104.5E	20												
96081512		20.3N	104.0E	15												
96081518		20.3N	103.6E	15												
96081600		20.3N	103.3E	15												
96081606		20.3N	103.0E	15												
96081612		20.3N	102.7E	15												
96081618		20.4N	102.4E	15												
96081700		20.4N	102.1E	15												
96081418		29.8N	178.9W	25												
96081500		29.4N	178.6W	25												
96081506		29.1N	178.7W	25												
96081512		28.8N	179.0W	25												
96081518		28.3N	179.3W	25												
96081600		27.8N	179.7W	25												
96081606		27.7N	179.7E	25												
96081612		27.5N	179.0E	25												
96081618		27.5N	178.0E	25												
96081700		27.4N	177.1E	25												
			AVERAGE		17	51	105	205								
			# CASES		3	3	3	2								

TROPICAL DEPRESSION 17W

	WRN	BEST TRACK			POSITION ERRORS						WIND ERRORS					
DTG	NO.	LAT	LONG	WIND (KT)	00	12	24	36	48	72	00	12	24	36	48	72
96081312		29.6N	176.5E	25												
96081318		29.8N	177.1E	25												
96081400	1	30.2N	177.9E	30	0	90	126	237			0	5	5	5		
96081412	2	30.0N	179.3W	25	13	80	210	376			0	5	5	5		
96081500		29.4N	178.6W	25												
96081506		29.1N	178.7W	25												
96081512		28.8N	179.0W	25												
96081518		28.3N	179.3W	25												
96081600		27.8N	179.7W	25												
96081606		27.7N	179.7E	25												
96081612		27.5N	179.0E	25												
96081618		27.5N	178.0E	25												
96081700		27.4N	177.1E	25												
			AVERAGE		7	85	168	307								
			# CASES		2	2	2	2								

TYPHOON NIKI (18W)

	WRN	BEST TRACK			POSITION ERRORS						WIND ERRORS					
DTG	NO.	LAT	LONG	WIND (KT)	00	12	24	36	48	72	00	12	24	36	48	72
96081312		8.0N	155.8E	15												
96081318		7.5N	154.3E	15												
96081400		7.0N	152.8E	20												
96081406		7.0N	151.0E	20												
96081412		7.0N	148.8E	20												
96081418		6.5N	147.2E	20												
96081500		6.5N	145.2E	20												
96081506		6.7N	143.4E	20												
96081512		7.0N	142.0E	20												
96081518		7.4N	140.5E	20												
96081600		7.9N	139.0E	20												
96081606		8.5N	137.5E	20												
96081612		10.0N	136.0E	15												
96081618		11.9N	135.3E	25												
96081700		13.5N	134.8E	20												
96081706		14.7N	134.2E	25												
96081712		15.7N	133.3E	25												
96081718		16.4N	132.1E	20												
96081800	1	17.2N	130.8E	30	16	80	157	198	259	382	0	0	5	-5	5	-15
96081806	2	17.6N	129.3E	35	24	79	136	167	244	393	-5	0	-5	-10	-5	-20
96081812	3	17.7N	128.0E	35	33	83	131	222	324	459	-5	0	-15	-5	-15	-20
96081818	4	17.6N	126.8E	35	30	64	126	232	330	474	-5	-10	-20	-15	-30	-35
96081900	5	17.5N	125.5E	35	8	30	69	127	172	210	0	-10	-10	-45	-50	-40
96081906	6	17.5N	124.2E	45	0	12	86	135	152	175	0	-5	-30	-45	-45	-25
96081912	7	17.6N	123.1E	55	5	82	150	173	188	170	0	5	-30	-35	-30	10
96081918	8	17.6N	121.6E	60	23	89	141	144	137	123	0	-20	-30	-35	-30	25
96082000	9	17.5N	120.0E	55	26	45	67	74	87	131	0	-15	-20	-20	-5	45
96082006	10	17.4N	118.4E	65	16	41	62	74	90	132	-10	-20	-25	-25	0	60
96082012	11	17.3N	116.8E	75	13	24	45	64	66	82	0	0	0	10	30	60
96082018	12	17.2N	115.3E	80	31	62	92	100	110		-5	-10	-10	10	35	
96082100	13	17.2N	114.0E	85	5	29	41	62	71		-10	-5	10	5	40	
96082106	14	17.4N	112.7E	90	5	23	38	65	77		0	5	5	25	45	
96082112	15	17.8N	111.4E	90	6	12	33	45	30		0	0	20	45	45	
96082118	16	18.1N	110.3E	95	13	11	29	34			-5	0	25	30		
96082200	17	18.5N	109.2E	85	8	18	36	17			-5	15	15	15		
96082206	18	19.0N	108.2E	80	18	18	16				0	15	30			
96082212	19	19.6N	107.1E	75	21	49	28				0	25	30			
96082218	20	20.2N	106.0E	65	0	41					0	15				
96082300	21	20.6N	104.9E	45	12	30					0	15				
96082306		20.8N	103.9E	30												
96082312		20.8N	103.2E	20												
			AVERAGE		15	44	79	114	156	249						
			# CASES		21	21	19	17	15	11						

TYPHOON ORSON (19W)

	WRN	BEST TRACK			POSITION ERRORS						WIND ERRORS					
DTG	NO.	LAT	LONG	WIND (KT)	00	12	24	36	48	72	00	12	24	36	48	72
96081400		14.8N	1763E	15												
96081406		14.8N	1754E	15												
96081412		14.9N	1743E	15												
96081418		14.9N	1727E	15												
96081500		15.0N	1711E	15												
96081506		15.1N	1696E	15												
96081512		15.2N	1680E	15												
96081518		15.3N	1664E	20												
96081600		15.4N	1648E	20												
96081606		15.5N	1630E	20												
96081612		15.6N	1611E	20												
96081618		15.6N	1593E	20												
96081700		15.4N	1575E	20												
96081706		15.2N	1559E	20												
96081712		15.0N	1541E	20												
96081718		15.0N	1523E	20												
96081800		15.1N	1505E	20												
96081806		15.2N	1492E	20												
96081812		15.4N	1479E	20												
96081818		15.6N	1466E	20												
96081900		16.0N	1453E	20												
96081906		16.6N	1443E	20												
96081912		17.4N	1438E	20												

TYPHOON ORSON (19W) (CONTINUED)

96081918		17.8N	143.6E	20												
96082000		18.2N	143.4E	20												
96082006		18.6N	143.2E	15												
96082012		19.0N	143.0E	15												
96082018		19.7N	142.8E	20												
96082100		20.5N	142.7E	20												
96082106		21.3N	142.8E	20												
96082112		21.7N	142.8E	20												
96082118	1	21.9N	142.8E	25	24	37	32	50	66	193	0	0	-5	-15	-10	-30
96082200	2	22.2N	142.8E	30	25	33	35	63	102	254	0	-5	-10	-15	-10	-50
96082206	3	22.5N	142.7E	30	12	5	26	53	129	338	0	-10	-20	-15	-20	-65
96082212	4	22.9N	142.6E	35	5	28	56	105	198	440	-5	-15	-20	-20	-35	-70
96082218	5	23.2N	142.6E	40	22	25	34	56	113	223	-5	-20	-20	-25	-40	-70
96082300	6	23.4N	142.6E	45	25	24	32	101	203	386	0	-5	0	-20	-40	-45
96082306	7	23.5N	142.6E	55	24	40	115	219	335	540	0	5	0	-10	-40	-30
96082312	8	23.7N	142.7E	55	29	72	158	267	378	527	0	5	-10	-30	-40	-25
96082318	9	23.8N	142.8E	55	22	90	176	276	375	496	0	-5	-15	-45	-40	-20
96082400	10	24.0N	143.3E	55	12	71	158	241	314	411	0	-10	-25	-35	-25	0
96082406	11	24.1N	144.0E	65	13	53	94	133	168	195	0	-10	-40	-35	-20	5
96082412	12	24.2N	144.7E	75	11	65	130	184	221	255	0	-15	-20	-15	0	20
96082418	13	24.2N	145.5E	80	5	44	104	164	183	219	0	-25	-15	-5	10	20
96082500	14	24.4N	146.5E	100	8	17	16	22	52	116	0	-10	-5	10	25	40
96082506	15	24.7N	147.3E	115	10	5	27	29	44	98	0	0	10	25	40	55
96082512	16	24.9N	148.2E	115	5	22	37	46	57	114	0	0	15	30	40	55
96082518	17	25.2N	148.9E	115	12	5	0	24	66	125	0	5	15	30	35	55
96082600	18	25.5N	149.6E	115	8	8	8	42	78	137	0	10	25	30	40	65
96082606	19	25.8N	150.2E	110	5	17	39	67	95	191	-10	0	15	25	45	70
96082612	20	26.0N	150.6E	105	13	36	60	84	122	202	-5	5	15	30	45	70
96082618	21	26.2N	150.9E	100	8	20	50	72	118	190	-5	10	15	35	40	60
96082700	22	26.3N	151.2E	95	6	18	44	66	96	150	0	10	20	35	50	70
96082706	23	26.3N	151.4E	90	12	50	62	84	104	133	0	10	30	35	60	70
96082712	24	26.3N	151.5E	90	8	26	60	120	151	178	0	5	30	45	60	60
96082718	25	26.2N	151.7E	90	5	32	92	174	215	203	0	10	0	15	10	0
96082800	26	26.3N	151.7E	85	8	34	75	97	115	173	5	10	10	15	20	10
96082806	27	26.4N	151.6E	75	5	44	75	83	84	149	0	0	15	10	15	-15
96082812	28	26.4N	151.3E	75	5	48	59	75	87	144	0	10	15	20	5	-15
96082818	29	26.4N	150.8E	75	21	47	63	79	100	172	0	20	15	20	5	-30
96082900	30	26.5N	150.1E	65	13	31	49	64	87	153	0	5	15	0	0	-30
96082906	31	26.8N	149.5E	55	13	18	37	58	99	188	0	0	10	-5	-15	-30
96082912	32	27.0N	148.9E	55	6	18	42	78	109	263	-5	5	-10	-10	-25	-45
96082918	33	27.3N	148.3E	55	8	32	47	72	113	316	-5	0	-10	-25	-40	-40
96083000	34	27.6N	147.7E	45	8	8	39	78	133	381	0	-10	-10	-25	-40	-35
96083006	35	27.9N	147.1E	45	16	27	7	30	79	397	0	-10	-20	-35	-30	-10
96083012	36	28.2N	146.5E	55	5	17	30	69	147	505	-10	-10	-15	-25	-25	0
96083018	37	28.6N	145.8E	55	12	15	39	90	197	427	-10	-20	-30	-25	-20	10
96083100	38	29.0N	145.1E	55	6	15	58	116	183	474	0	-5	-15	-15	-10	15
96083106	39	29.4N	144.4E	65	0	26	68	160	241	543	0	-10	-5	5	5	10
96083112	40	29.8N	143.9E	65	0	36	103	221	371	518	0	-10	-5	10	10	10
96083118	41	30.3N	143.5E	80	13	5	77	151	310	443	-5	0	0	5	10	10
96090100	42	31.0N	143.2E	80	11	49	115	228	297	487	0	0	5	0	5	0
96090106	43	31.6N	143.2E	80	13	62	83	167	180	322	-5	-5	0	5	0	0
96090112	44	32.6N	143.9E	80	23	45	55	132	183	468	-10	-5	-5	0	-5	-10
96090118	45	33.6N	144.8E	75	15	12	149	213	246	529	-10	-10	-5	-10	-10	-10
96090200	46	34.7N	145.8E	70	11	103	171	237	321		-5	-5	0	-5	0	
96090206	47	36.3N	147.1E	65	15	73	79	109	226		-5	0	0	0	0	
96090212	48	38.4N	148.9E	60	0	37	66	139	252		-5	5	0	0	0	
96090218	49	40.0N	151.4E	50	0	32	98	213	330		0	0	0	-5	-10	
96090300	50	41.1N	153.7E	45	4	66	130				0	-5	-5			
96090306	51	42.2N	156.6E	45	12	54	112	167			0	5	5	5		
96090312		42.7N	159.9E	45												
96090318		43.0N	163.3E	40												
96090400		43.4N	167.7E	40												
96090406		43.7N	172.2E	40												
96090412		43.9N	176.7E	40												
96090418		44.3N	178.8W	40												
			AVERAGE		12	36	70	118	173	297						
			# CASES		51	51	51	50	49	45						

TYPHOON PIPER (20W)

DTG	WRN NO.	BEST TRACK LAT	LONG	WIND (KT)	POSITION ERRORS 00	12	24	36	48	72	WIND ERRORS 00	12	24	36	48	72
96081900		20.6N	169.6E	15												
96081906		21.2N	168.1E	15												
96081912		22.2N	166.5E	20												

TYPHOON PIPER (20W) (CONTINUED)

96081918		23.2N	165.0E	20												
96082000		24.4N	163.3E	20												
96082006		25.7N	161.7E	20												
96082012		26.8N	160.3E	20												
96082018		27.9N	158.9E	20												
96082100		28.2N	157.7E	20												
96082106		28.0N	157.0E	20												
96082112		27.5N	156.8E	20												
96082118		26.8N	157.1E	20												
96082200		26.7N	158.0E	25												
96082206		27.0N	158.8E	25												
96082212		27.5N	159.5E	25												
96082218		28.1N	160.0E	25												
96082300	1	28.7N	160.4E	30	20	28	28	42	73	306	0	0	-5	-10	-15	-5
96082306	2	29.5N	160.7E	35	12	26	59	74	126	475	0	0	-5	-10	-10	10
96082312	3	30.3N	160.8E	35	6	47	62	57	51	422	0	-5	-10	-15	-10	-20
96082318	4	30.9N	160.4E	40	35	82	89	69	91	678	-5	-10	-15	-15	-10	-15
96082400	5	31.4N	160.0E	45	18	35	75	132	269		0	-5	-20	-20	-30	
96082406	6	32.0N	159.6E	50	15	45	105	199	388		-5	-10	-20	-20	-25	
96082412	7	32.6N	159.4E	55	13	74	168	324	596		-10	-20	-20	-25	-25	
96082418	8	33.2N	159.1E	60	16	60	196	452	893		-15	-25	-25	-25	-25	
96082500	9	34.2N	158.9E	65	7	64	213	504			0	5	-5	-15		
96082506	10	35.3N	158.6E	65	7	59	235	597			0	5	0	-10		
96082512	11	36.7N	158.5E	60	17	130	393				0	-5	-10			
96082518	12	38.5N	158.8E	60	57	217	584				0	0	-5			
96082600	13	40.7N	159.4E	60	55	179					0	-5				
96082606	14	43.6N	160.3E	55	43	222					0	-5				
96082612		47.5N	161.8E	55												
96082618		52.0N	164.0E	50												
			AVERAGE		23	91	184	246	311	471						
			# CASES		14	14	12	10	8	4						

TROPICAL DEPRESSION 21W

DTG	WRN NO.	BEST TRACK LAT	LONG	WIND (KT)	POSITION ERRORS 00	12	24	36	48	72	WIND ERRORS 00	12	24	36	48	72
96082412		27.0N	155.1E	20												
96082418		27.6N	156.6E	20												
96082500		28.0N	158.0E	20												
96082506		28.6N	159.6E	20												
96082512		29.6N	161.0E	25												
96082518		30.8N	161.8E	25												
96082600	1	31.4N	161.8E	25	5	32	101	161			0	0	0	-5		
96082606		31.7N	161.6E	25												
96082612	2	32.1N	161.2E	25	33	113	170	189			0	0	0	-5		
96082618		32.1N	160.6E	25												
96082700	3	32.2N	159.9E	25	15	54	133	204			0	0	0	0		
96082706		32.5N	159.1E	25												
96082712	4	32.9N	158.3E	25	0	86	179				0	0	-5			
96082718		34.0N	157.3E	25												
96082800		35.5N	156.6E	25												
96082806		37.1N	156.6E	25												
96082812		38.4N	156.9E	25												
96082818		39.5N	157.5E	25												
96082900		40.2N	158.5E	25												
96082906		40.6N	159.5E	25												
96082912		41.1N	160.5E	25												
96082918		41.7N	161.5E	25												
96083000		42.3N	162.6E	25												
			AVERAGE		14	72	146	185								
			# CASES		4	4	4	3								

TROPICAL STORM RICK (22W)

DTG	WRN NO.	BEST TRACK LAT	LONG	WIND (KT)	POSITION ERRORS 00	12	24	36	48	72	WIND ERRORS 00	12	24	36	48	72
96082700		21.5N	168.0E	25												
96082706		22.3N	168.3E	30												
96082712		22.8N	169.0E	35												
96082718		22.9N	169.9E	35												
96082800	1	23.0N	170.8E	35	33	110	193	263			-5	0	0	0		
96082806		23.4N	171.7E	30												
96082812	2	24.0N	172.6E	30	8	5	24	31			-5	0	0	-5		

TROPICAL STORM RICK (22W) (CONTINUED)

DTG	WRN NO.	LAT	LONG	WIND (KT)	00	12	24	36	48	72	00	12	24	36	48	72
96082818		24.8N	173.5E	30												
96082900	3	25.9N	173.9E	30	18	30	85	130			0	-5	-10	-10		
96082906		27.1N	173.8E	30												
96082912	4	28.3N	173.6E	30	130	192	217	250			0	-5	-10	-5		
96082918		29.4N	173.2E	30												
96083000	5	30.3N	173.0E	35	28	109	168	180	188	297	0	0	5	-5	-5	-10
96083006	6	30.7N	172.7E	35	16	31	36	96	155	241	0	5	5	-5	0	-10
96083012	7	31.0N	172.4E	35	46	103	142	185	232		0	5	5	0	5	
96083018	8	31.2N	172.3E	30	31	70	134	222			0	0	-5	0		
96083100	9	31.5N	172.3E	30	17	62	147	252			0	0	-5	0		
96083106		31.9N	172.5E	30												
96083112	10	32.2N	173.1E	30	7	44	69				0	-5	0			
96083118		32.5N	174.0E	30												
96090100		32.9N	175.3E	30												
96090106		33.3N	176.8E	25												
96090112		33.7N	178.6E	25												
96090118		34.5N	179.2W	30												
96090200		35.5N	177.1W	30												
96090206		36.5N	175.0W	30												
96090212		37.8N	173.1W	30												
96090218		39.2N	171.3W	30												
96090300		40.7N	169.6W	30												
			AVERAGE		34	76	122	179	192	270						
			# CASES		10	10	10	9	3	2						

SUPER TYPHOON SALLY (23W)

	WRN	BEST TRACK			POSITION ERRORS						WIND ERRORS					
DTG	NO.	LAT	LONG	WIND (KT)	00	12	24	36	48	72	00	12	24	36	48	72
96090200		8.1N	147.7E	15												
96090206		8.5N	146.7E	15												
96090212		8.9N	145.7E	15												
96090218		9.2N	144.5E	15												
96090300		9.8N	143.1E	15												
96090306		10.5N	141.6E	20												
96090312		11.3N	140.2E	20												
96090318		12.1N	138.4E	20												
96090400		12.6N	137.1E	20												
96090406		13.1N	136.1E	20												
96090412		13.6N	135.4E	25												
96090418		14.0N	134.8E	25												
96090500	1	14.3N	134.2E	25	48	83	132	212	316	546	0	-10	-20	-40	-45	-80
96090506	2	14.6N	133.6E	30	16	52	132	226	375	678	0	-10	-30	-40	-55	-75
96090512	3	15.0N	133.0E	35	18	64	166	274	400	717	-5	-15	-35	-45	-60	-60
96090518	4	15.5N	132.3E	40	8	58	114	232	331	621	-5	-25	-35	-45	-75	-45
96090600	5	16.0N	131.6E	50	33	87	153	224	296	573	0	-15	-15	-20	-30	0
96090606	6	16.7N	130.5E	65	20	57	157	243	364	651	0	-5	-10	-35	-15	25
96090612	7	17.2N	129.3E	75	11	45	116	193	314	613	0	0	-15	-25	-15	40
96090618	8	17.6N	128.2E	80	8	52	97	192	301	529	-5	-10	-40	-20	-10	65
96090700	9	18.1N	126.4E	90	22	18	18	69	128	295	0	-15	-20	-5	15	70
96090706	10	18.6N	124.8E	100	23	18	30	74	144	253	-10	-40	-15	0	30	80
96090712	11	18.9N	123.2E	115	22	40	89	151	207	232	0	-20	0	15	50	85
96090718	12	19.1N	121.5E	140	23	50	101	177	253		0	10	15	30	65	
96090800	13	19.4N	119.7E	135	8	11	35	91	126		-5	5	15	25	45	
96090806	14	19.8N	117.7E	130	5	12	49	102	111		-5	10	20	40	50	
96090812	15	20.2N	115.7E	125	5	35	74	122	103		-5	10	40	50	50	
96090818	16	20.6N	113.7E	120	6	30	90	105			0	20	45	55		
96090900	17	21.0N	111.5E	110	11	40	94	102			-5	5	15	20		
96090906	18	21.5N	109.3E	95	0	43	82				-10	5	15			
96090912	19	22.0N	107.2E	75	0	36	60				-10	10	15			
96090918		22.6N	105.1E	50												
96091000		23.1N	103.5E	35												
96091006		23.4N	102.4E	20												
96091012		23.6N	101.5E	15												
			AVERAGE		15	44	95	165	252	520						
			# CASES		19	19	19	17	15	11						

TROPICAL STORM 24W

	WRN	BEST TRACK			POSITION ERRORS						WIND ERRORS					
DTG	NO.	LAT	LONG	WIND (KT)	00	12	24	36	48	72	00	12	24	36	48	72
96090600		8.3N	148.1E	15												
96090606		9.1N	147.6E	15												

TROPICAL STORM 24W (CONTINUED)

96090612		9.9N	147.1E	15												
96090618		10.7N	146.6E	15												
96090700		11.3N	145.9E	15												
96090706		11.8N	145.1E	15												
96090712		12.3N	144.1E	15												
96090718		12.9N	142.7E	15												
96090800		13.3N	140.9E	15												
96090806		13.8N	139.0E	15												
96090812		14.2N	137.1E	15												
96090818		14.5N	135.0E	15												
96090900		14.7N	133.1E	25												
96090906	1	14.8N	131.2E	25	87	72	145	213	249	321	0	5	10	5	0	-10
96090912	2	14.8N	129.2E	25	36	118	294	257	346	299	0	5	10	5	5	0
96090918	3	14.8N	127.0E	25	46	174	269	284	358	293	0	5	10	5	10	15
96091000	4	15.0N	124.4E	25	75	255	255	331	329	172	0	5	5	5	5	15
96091006	5	15.9N	121.7E	25	198	280	253	312	277	194	0	0	0	0	0	20
96091012	6	16.5N	118.7E	25	103	64	175	209	174	294	0	0	0	0	-5	0
96091018	7	16.8N	117.7E	25	49	120	193	187	206	342	0	-5	0	-10	0	0
96091100	8	16.8N	116.7E	25	39	210	270	247	228	223	0	-5	-10	-5	10	35
96091106	9	16.3N	114.9E	30	117	283	335	339	327	256	0	-5	-10	0	15	35
96091112	10	15.7N	112.9E	30	79	170	195	216			0	-10	-15	-10		
96091118		15.5N	111.5E	35												
96091200	11	15.5N	110.7E	40	26	72	102	125			-10	-15	-10	0		
96091206		15.8N	110.0E	45												
96091212	12	16.2N	109.5E	45	13	34	62	82			-15	-10	0	0		
96091218		16.6N	109.0E	40												
96091300	13	17.0N	108.5E	40	13	21	49	87			-10	-5	-5	0		
96091306		17.4N	108.0E	35												
96091312	14	17.8N	107.5E	30	21	33	74				0	0	5			
96091318		18.1N	107.1E	30												
96091400	15	18.4N	106.8E	30	25	66					0	10				
96091406		18.6N	106.5E	25												
96091412	16	18.7N	106.3E	20	79						0					
			AVERAGE		63	132	191	223	278	267						
			# CASES		16	15	14	13	9	9						

TYPHOON TOM (25W)

	WRN	BEST TRACK			POSITION ERRORS						WIND ERRORS					
DTG	NO.	LAT	LONG	WIND (KT)	00	12	24	36	48	72	00	12	24	36	48	72
96090806		10.9N	161.8E	15												
96090812		10.9N	161.3E	15												
96090818		10.9N	160.5E	15												
96090900		10.9N	159.8E	15												
96090906		10.9N	158.6E	15												
96090912		10.9N	157.5E	15												
96090918		11.1N	156.4E	20												
96091000		11.3N	155.5E	20												
96091006		11.5N	154.7E	20												
96091012		11.9N	153.9E	20												
96091018		12.3N	153.0E	20												
96091100		13.0N	152.0E	20												
96091106		13.6N	151.1E	20												
96091112		14.2N	150.3E	25												
96091118	1	14.8N	149.6E	25	16	21	67	88	84	228	0	0	-5	0	5	5
96091200	2	15.5N	149.0E	25	88	134	160	164	139	237	0	-5	-10	-10	-5	0
96091206	3	16.1N	148.5E	30	24	66	105	131	180	489	0	-5	-5	-5	5	5
96091212	4	16.8N	148.1E	35	5	33	52	97	178	475	0	-5	-5	0	10	5
96091218	5	17.6N	147.6E	40	17	23	18	78	188	508	-5	-5	-5	0	5	0
96091300	6	18.3N	147.1E	45	5	18	37	76	150	286	0	0	0	5	0	-10
96091306	7	18.9N	146.5E	45	12	32	53	79	153	125	0	0	0	-5	-15	-30
96091312	8	19.3N	145.7E	50	6	43	72	122	191	211	0	0	5	0	0	0
96091318	9	19.5N	145.0E	50	20	32	73	144	182	225	0	0	0	0	-5	0
96091400	10	19.6N	144.2E	55	24	45	82	157	162	199	-5	0	-5	-5	-5	5
96091406	11	19.8N	143.6E	55	13	66	118	114	94	72	-5	-5	-5	-10	-5	5
96091412	12	19.9N	143.4E	55	20	49	81	90	156	278	-5	-10	-10	-10	-10	-10
96091418	13	20.1N	143.4E	60	11	82	65	81	140	291	-5	-5	-10	-5	-10	-5
96091500	14	20.3N	143.6E	65	11	75	38	78	133	222	0	0	0	-5	-5	0
96091506	15	20.6N	144.3E	65	12	28	61	85	105	88	0	-5	0	0	0	10
96091512	16	21.0N	144.8E	70	17	73	81	97	108	90	-5	-5	0	5	0	10
96091518	17	21.4N	145.1E	75	22	30	64	100	106	55	-5	0	0	5	5	5
96091600	18	22.0N	145.3E	75	8	40	36	50	44	184	0	0	10	5	10	5
96091606	19	22.3N	146.0E	75	8	18	37	65	129	367	0	0	10	10	15	5
96091612	20	22.6N	146.5E	75	0	18	42	95	178	437	0	5	10	15	15	5
96091618	21	23.1N	146.9E	75	12	30	67	143	251	547	0	5	5	5	-10	-15

TYPHOON TOM (25W) (CONTINUED)

DTG	WRN NO.	LAT	LONG	WIND (KT)	POS 00	POS 12	POS 24	POS 36	POS 48	POS 72	WIND 00	WIND 12	WIND 24	WIND 36	WIND 48	WIND 72
96091700	22	23.6N	147.3E	70	0	18	86	187	330	625	0	-5	0	0	-10	-10
96091706	23	24.1N	147.8E	70	5	29	80	159	285	489	0	0	10	5	0	5
96091712	24	24.7N	148.3E	70	8	29	76	161	251	307	0	10	10	5	-5	0
96091718	25	25.3N	148.9E	65	5	60	111	205	227	194	0	10	10	5	0	0
96091800	26	26.1N	149.6E	60	5	12	65	147	186	249	0	0	-5	-10	-5	-10
96091806	27	27.0N	150.2E	55	0	48	52	90	114	114	0	0	-5	-5	-5	-10
96091812	28	27.9N	151.2E	55	0	30	60	46	44	54	0	0	-5	0	-5	-10
96091818	29	28.8N	152.5E	55	15	88	54	15	53	169	0	0	0	0	-5	-10
96091900	30	30.3N	153.2E	55	43	34	13	19	26		-5	-10	0	-5	-5	
96091906	31	31.7N	154.3E	55	5	57	72	65	41		-15	-10	-5	-5	-10	
96091912	32	32.7N	155.9E	55	20	131	213	281	346		0	5	0	-5	-5	
96091918	33	33.3N	157.6E	50	11	41	132	244	343		0	0	0	-5	-5	
96092000	34	34.1N	159.2E	45	25	34	64	132	172		0	0	-5	-5	-5	
96092006	35	34.9N	160.7E	45	61	87	119				0	0	-5			
96092012		35.7N	162.1E	45												
96092018		36.5N	163.4E	45												
96092100		37.3N	164.5E	45												
96092106		38.0N	165.6E	45												
96092112		38.8N	166.7E	45												
96092118		39.6N	168.2E	45												
96092200		40.7N	170.0E	45												
96092206		42.2N	172.2E	45												
			AVERAGE		16	48	75	115	161	270						
			# CASES		35	35	35	34	34	29						

SUPER TYPHOON VIOLET (26W)

DTG	WRN NO.	BEST TRACK LAT	LONG	WIND (KT)	POSITION ERRORS 00	12	24	36	48	72	WIND ERRORS 00	12	24	36	48	72
96090918		13.3N	138.4E	15												
96091000		14.1N	137.0E	15												
96091006		14.6N	135.9E	15												
96091012		14.9N	134.8E	15												
96091018		15.2N	133.7E	15												
96091100		15.5N	132.9E	20												
96091106		15.7N	132.2E	20												
96091112		15.8N	131.7E	25												
96091118	1	15.9N	131.3E	25	75	77	88	116			0	-5	-10	-45		
96091206	2	16.1N	130.4E	35	11	42	62	93			-5	-5	-40	-55		
96091218	3	16.2N	129.7E	35	5	24	58	37	23	107	0	-30	-35	-45	-45	-75
96091300	4	16.2N	129.5E	45	18	24	24	11	8	29	0	-15	-10	-15	-15	-35
96091306	5	16.3N	129.3E	65	0	17	11	24	29	66	0	0	0	5	10	0
96091312	6	16.3N	129.0E	75	6	23	40	40	51	119	0	10	15	15	5	5
96091318	7	16.4N	128.8E	75	5	31	41	49	74	170	0	0	10	10	-10	15
96091400	8	16.5N	128.7E	80	23	44	64	90	143	275	0	0	5	0	-10	25
96091406	9	16.7N	128.5E	90	16	37	67	110	171	339	0	5	10	-10	0	35
96091412	10	17.1N	128.2E	90	16	53	30	59	118	273	0	0	0	-10	0	40
96091418	11	17.5N	127.8E	95	5	11	20	56	99	202	-5	-5	-15	-5	10	45
96091500	12	17.9N	127.4E	100	0	34	79	109	146	223	0	-10	-15	-5	20	45
96091506	13	18.3N	127.1E	105	8	17	62	115	166	203	0	-20	-10	5	25	35
96091512	14	18.8N	126.8E	115	0	22	79	134	166	212	0	-10	0	25	35	45
96091518	15	19.3N	126.6E	130	0	17	81	150	164	192	-5	0	15	30	35	45
96091600	16	19.8N	126.5E	130	8	53	113	168	175	157	0	5	25	30	35	25
96091606	17	20.2N	126.5E	125	20	71	139	170	158	217	0	10	20	30	25	20
96091612	18	20.6N	126.7E	125	12	62	128	154	182	283	0	20	25	30	35	20
96091618	19	20.9N	127.0E	115	11	30	85	128	158	265	0	10	15	10	10	-20
96091700	20	21.4N	127.7E	105	5	25	42	79	127	300	0	5	0	5	-15	-20
96091706	21	21.8N	128.3E	100	0	5	24	53	109	203	0	10	0	5	-10	-10
96091712	22	22.2N	129.0E	95	5	8	31	36	60	36	0	5	10	-5	-10	-5
96091718	23	22.6N	129.6E	90	8	22	36	69	76	32	0	0	5	-5	-10	0
96091800	24	22.9N	130.0E	90	16	8	8	37	61	29	0	10	-5	-5	-10	0
96091806	25	23.2N	130.5E	90	5	16	30	37	46	27	0	10	-5	-5	-10	0
96091812	26	23.3N	131.0E	80	0	28	33	65	64	63	0	-10	-15	-20	-15	-10
96091818	27	23.7N	131.4E	80	0	39	66	96	99	74	0	-10	-15	-20	-10	-5
96091900	28	23.9N	131.6E	90	8	30	30	31	58	128	0	-5	-15	-15	-10	-10
96091906	29	24.0N	131.8E	90	6	13	8	16	21	282	0	-5	-15	-10	-10	-15
96091912	30	24.2N	132.0E	90	5	20	17	13	42	366	0	0	-5	-5	-5	-10
96091918	31	24.6N	132.1E	90	6	37	54	54	57	338	0	0	0	-5	0	-5
96092000	32	25.0N	132.2E	90	0	34	62	105	87	187	0	0	0	0	-5	0
96092006	33	25.5N	132.3E	90	5	58	84	135	181	335	0	0	-5	0	-15	-5
96092012	34	26.1N	132.9E	85	17	36	56	42	84	187	0	-5	-5	-10	-15	0
96092018	35	26.7N	133.5E	80	17	54	59	14	51	194	0	-5	0	-15	-10	5
96092100	36	27.3N	134.2E	80	20	39	31	57	76	263	0	0	-5	-10	-5	10
96092106	37	28.2N	135.0E	80	8	43	67	78	68	277	0	5	-10	-5	0	15
96092112	38	29.2N	136.2E	75	12	64	131	158	114	329	0	-5	-10	-5	0	15

SUPER TYPHOON VIOLET (26W) (CONTINUED)

96092118	39	30.9N	137.9E	70	0	23	38	48	46	111	0	-10	-5	0	5	20
96092200	40	32.5N	139.3E	75	0	83	137	97	68	150	0	0	5	10	10	20
96092206	41	34.9N	140.9E	80	5	56	79	63	71		0	5	10	15	15	
96092212	42	37.1N	142.7E	75	0	42	50	55	66		0	5	10	15	15	
96092218	43	39.3N	144.6E	70	18	14	16	48	119		0	10	15	20	20	
96092300	44	41.5N	146.7E	65	0	66	141	163			0	10	15	15		
96092306		43.0N	148.1E	60												
96092312		44.5N	149.6E	55												
96092318		45.8N	151.1E	50												
96092400		46.7N	152.4E	45												
96092406		47.6N	154.3E	40												
96092412		48.4N	156.2E	40												
96092418		48.9N	158.3E	35												
96092500		49.2N	160.6E	35												
			AVERAGE		10	36	60	79	95	191						
			# CASES		44	44	44	44	41	38						

TYPHOON WILLIE (27W)

DTG	WRN NO.	BEST TRACK LAT	LONG	WIND (KT)	POSITION ERRORS 00	12	24	36	48	72	WIND ERRORS 00	12	24	36	48	72
96091600		18.7N	107.2E	15												
96091606		18.5N	107.5E	15												
96091612		18.3N	107.8E	15												
96091618		18.1N	108.1E	20												
96091700		17.8N	108.4E	25												
96091706		17.5N	108.7E	25												
96091712		17.3N	109.2E	35												
96091718	1	17.2N	109.7E	40	31	74	168	246	274	360	-15	-20	-15	-30	-25	-15
96091800	2	17.2N	110.2E	45	16	69	145	197	223	334	-5	0	0	-5	0	10
96091806	3	17.3N	110.8E	50	13	90	164	189	223	326	0	5	-5	0	0	15
96091812	4	17.9N	111.4E	50	12	39	84	147	248	414	0	-5	-5	0	5	15
96091818	5	18.6N	111.7E	50	21	34	79	164	266	426	0	-15	-5	0	5	5
96091900	6	19.3N	111.8E	55	16	25	16	24	38	51	0	0	-15	-15	-15	0
96091906	7	19.9N	111.5E	65	6	17	18	47	62	115	0	5	-10	-15	-10	0
96091912	8	20.1N	111.3E	65	13	18	17	33	35	64	0	0	-5	-10	-5	-10
96091918	9	20.2N	111.1E	65	8	46	71	86	91	146	0	0	-5	-5	-15	10
96092000	10	20.2N	110.6E	65	11	18	16	46	77	95	0	5	15	30	25	30
96092006	11	20.1N	110.1E	65	16	12	40	63	108	122	0	5	20	15	-5	10
96092012	12	20.0N	109.5E	60	8	12	56	102	131	83	0	5	20	0	-20	10
96092018	13	20.0N	108.9E	60	16	75	158	202	205		0	15	-5	-20	-20	
96092100	14	19.8N	108.4E	60	5	12	45	69	64		0	10	-5	-20	0	
96092106	15	19.6N	108.0E	55	5	17	40	36	47		0	0	-5	0	0	
96092112	16	19.4N	107.6E	55	25	64	72	38	61		0	5	-15	10	5	
96092118	17	19.3N	107.2E	65	5	11	33	87			0	5	5	10		
96092200	18	19.2N	106.8E	60	0	16	74	134			-5	-10	20	15		
96092206	19	19.0N	106.3E	60	17	58	108				-5	10	20			
96092212	20	18.8N	105.7E	60	25	74	163				-10	15	10			
96092218	21	18.2N	104.8E	40	34	95					0	10				
96092300	22	17.5N	104.0E	20	34	82					10	10				
96092306		17.1N	103.0E	20												
96092312		16.5N	101.7E	15												
			AVERAGE		16	44	79	107	135	212						
			# CASES		22	22	20	18	16	12						

SUPER TYPHOON YATES (28W)

DTG	WRN NO.	BEST TRACK LAT	LONG	WIND (KT)	POSITION ERRORS 00	12	24	36	48	72	WIND ERRORS 00	12	24	36	48	72
96091706		8.0N	175.7W	15												
96091712		8.1N	176.9W	15												
96091718		8.2N	178.2W	15												
96091800		8.3N	179.6W	15												
96091806		8.4N	178.9E	15												
96091812		8.5N	177.4E	15												
96091818		8.7N	175.9E	20												
96091900		8.8N	174.3E	20												
96091906		8.9N	172.8E	25												
96091912		9.0N	171.3E	25												
96091918		9.1N	169.8E	25												
96092000		9.3N	168.4E	25												
96092006		9.5N	167.2E	25												
96092012		9.7N	166.0E	25												

SUPER TYPHOON YATES (28W) (CONTINUED)

96092018		10.0N	165.0E	25												
96092100		10.6N	164.2E	25												
96092106		11.2N	163.5E	25												
96092112		11.9N	163.0E	25												
96092118		12.6N	162.4E	25												
96092200		13.4N	161.8E	25												
96092206		14.3N	160.9E	25												
96092212		15.1N	159.8E	30												
96092218	1	15.5N	158.6E	35	21	11	66	138	204	290	0	-25	-50	-40	-45	-40
96092300	2	15.9N	157.3E	55	11	64	145	211	283	393	0	-50	-40	-35	-40	-25
96092306	3	16.2N	156.1E	80	8	20	72	138	197	319	-15	-40	-35	-40	-40	-25
96092312	4	16.4N	154.9E	115	0	36	84	158	239	292	-10	0	5	0	0	-10
96092318	5	16.4N	153.8E	115	0	17	55	141	231	301	-5	0	0	0	0	0
96092400	6	16.3N	152.7E	115	0	12	29	79	158	305	0	0	-5	5	10	25
96092406	7	16.2N	151.5E	115	11	31	41	47	106	271	0	-5	-5	5	10	20
96092412	8	16.1N	150.3E	120	0	5	34	109	157	182	-10	-20	-5	5	10	15
96092418	9	16.0N	149.1E	125	0	0	44	111	144	206	-15	-15	-5	5	20	15
96092500	10	15.9N	147.8E	130	0	21	64	97	102	205	0	10	5	0	5	-10
96092506	11	15.9N	146.6E	130	0	42	89	108	130	214	0	10	5	10	0	-10
96092512	12	16.0N	145.7E	125	0	16	31	38	64	368	0	5	5	10	-5	-10
96092518	13	16.2N	144.8E	125	6	29	29	12	94	359	0	5	15	5	-5	-5
96092600	14	16.5N	144.0E	125	0	12	37	43	96	310	-5	-5	5	-10	-10	-10
96092606	15	17.0N	143.2E	125	11	18	16	90	167	282	0	10	5	-5	-10	0
96092612	16	17.5N	142.4E	125	12	13	28	94	171	187	0	10	-5	-5	-10	0
96092618	17	18.1N	141.7E	115	6	5	66	126	189	209	0	-10	-20	-25	-25	-15
96092700	18	18.8N	141.0E	115	12	48	103	162	177	140	-10	-20	-20	-25	-20	0
96092706	19	19.6N	140.3E	120	13	60	108	135	140	90	-5	-10	-10	-10	-5	5
96092712	20	20.2N	139.6E	125	5	42	111	124	138	11	-10	-10	-15	-10	0	10
96092718	21	20.6N	139.0E	125	17	79	113	137	128	39	-15	-15	-15	-5	0	15
96092800	22	21.0N	138.6E	125	6	24	24	52	31	177	0	0	-5	0	10	20
96092806	23	21.4N	138.2E	125	0	21	62	84	123	247	0	5	0	0	5	5
96092812	24	21.9N	137.9E	125	5	60	136	251	406	654	0	0	5	10	10	5
96092818	25	22.7N	137.9E	120	5	30	12	72	155	357	0	10	10	15	15	5
96092900	26	23.4N	138.2E	120	0	0	35	42	80	245	0	15	20	20	20	10
96092906	27	24.3N	138.6E	110	11	43	78	128	174	327	5	0	0	-5	-10	-15
96092912	28	25.3N	139.1E	105	13	58	72	117	120	306	0	5	5	0	-10	-15
96092918	29	26.7N	139.6E	100	5	30	91	136	189	319	0	5	5	0	-15	-15
96093000	30	28.3N	140.4E	90	0	97	258	315	417	456	0	10	10	0	-10	-10
96093006	31	29.9N	141.7E	85	8	131	215	299	380	528	0	0	0	-15	-10	-10
96093012	32	31.4N	144.0E	80	6	51	98	237	376	607	0	5	0	-10	-15	-15
96093018	33	32.7N	146.7E	75	7	83	168	276	385		0	0	-5	-15	-20	
96100100	34	33.6N	149.7E	70	0	18	125	240	321		0	0	0	-15	-15	
96100106	35	34.3N	152.3E	65	23	90	189	302			0	-10	-10	-15		
96100112	36	34.9N	155.2E	65	38	157	299	426			-10	-15	-20	-20		
96100118	37	35.4N	158.6E	65	39	106	151				-20	-20	-25			
96100200		35.9N	162.3E	60												
96100206		36.6N	165.7E	60												
96100212		37.3N	169.2E	60												
96100218		38.4N	172.1E	60												
96100300		39.3N	175.3E	55												
96100306		40.5N	178.5E	55												
96100312		41.7N	177.5W	55												
			AVERAGE		8	43	92	147	191	288						
			# CASES		37	37	37	36	34	32						

TYPHOON ZANE (29W)

	WRN	BEST TRACK			POSITION ERRORS						WIND ERRORS					
DTG	NO.	LAT	LONG	WIND (KT)	00	12	24	36	48	72	00	12	24	36	48	72
96092018		5.7N	153.6E	15												
96092100		5.7N	152.7E	15												
96092106		5.7N	151.6E	15												
96092112		5.7N	150.5E	15												
96092118		5.7N	149.1E	15												
96092200		5.7N	147.7E	15												
96092206		5.8N	146.3E	15												
96092212		6.4N	145.4E	15												
96092218		7.4N	144.9E	15												
96092300		8.4N	144.5E	15												
96092306		9.2N	143.9E	20												
96092312		10.1N	142.9E	20												
96092318		11.5N	141.4E	25												
96092400	1	13.1N	139.8E	30	72	47	77	45	37	85	0	0	0	-10	-20	-20
96092406	2	14.7N	138.1E	30	29	54	96	92	116	137	0	0	0	-15	-25	-10
96092412	3	15.6N	136.9E	35	0	53	45	81	132	185	0	0	-15	-25	-25	-10

TYPHOON ZANE (29W) (CONTINUED)

96092418	4	16.2N	135.5E	40	17	75	92	129	162	204	0	-5	-25	-35	-30	-20
96092500	5	16.6N	134.0E	45	25	29	95	148	210	394	0	-20	-30	-30	-25	-20
96092506	6	17.0N	132.5E	50	13	72	117	152	165	216	0	-20	-30	-25	-10	-15
96092512	7	17.6N	131.3E	70	24	79	130	159	173	246	-20	-30	-30	-25	-10	-15
96092518	8	18.3N	130.3E	80	20	36	82	117	156	338	-15	-25	-15	5	5	5
96092600	9	19.0N	129.4E	90	5	23	24	39	110	234	-15	-15	-10	10	5	0
96092606	10	19.6N	128.4E	100	13	26	42	88	104	206	-10	0	20	25	10	0
96092612	11	20.1N	127.7E	100	0	16	24	77	131	268	0	0	20	15	10	5
96092618	12	20.6N	127.0E	105	13	45	62	102	189	268	0	20	20	10	5	15
96092700	13	21.0N	126.4E	105	5	12	16	68	150	201	0	10	0	0	-5	20
96092706	14	21.4N	125.9E	95	8	16	12	89	128	107	-5	-15	-20	-25	-25	-10
96092712	15	21.8N	125.5E	95	0	24	63	131	123	136	0	-15	-15	-20	-20	0
96092718	16	22.3N	125.4E	105	0	12	71	99	66	99	0	5	5	-5	0	10
96092800	17	22.9N	125.3E	110	8	48	116	124	81	165	0	5	5	5	15	15
96092806	18	23.5N	125.2E	110	0	56	92	55	10	63	0	5	5	15	15	15
96092812	19	24.4N	125.5E	110	5	45	62	22	30	199	0	5	10	25	20	15
96092818	20	25.4N	125.9E	110	5	53	127	184	192	125	0	-5	0	5	5	5
96092900	21	26.3N	126.3E	110	8	83	160	190	181	192	0	0	15	10	10	5
96092906	22	26.9N	126.5E	110	6	42	73	78	83	132	0	10	15	15	5	-5
96092912	23	27.3N	126.7E	105	8	41	71	112	136	202	0	10	10	15	5	-5
96092918	24	27.2N	127.1E	95	8	51	100	140	148	217	0	5	10	10	5	-10
96093000	25	27.2N	128.1E	85	6	48	111	166	204	238	0	-5	-5	-15	-20	-25
96093006	26	27.2N	129.2E	85	0	44	108	147	204	321	0	5	0	-10	-20	-20
96093012	27	27.5N	130.6E	80	0	30	36	62	145	56	0	5	-5	-10	-20	-20
96093018	28	27.9N	132.2E	75	11	31	31	62	103		-5	-5	-5	-20	-25	
96100100	29	28.5N	134.1E	70	0	10	47	80	118	377	0	-5	-5	-25	-30	-15
96100106	30	28.9N	136.2E	70	6	13	70	101	131		0	0	-5	-15	-15	
96100112	31	29.3N	138.3E	70	15	36	30	24	47		0	-5	-10	-20	-15	
96100118	32	29.5N	140.5E	65	12	55	74	86	146		-5	-10	-20	-20	-15	
96100200	33	29.5N	142.8E	65	12	39	26	86	244		-5	-10	-20	-15	-10	
96100206	34	29.8N	145.2E	65	5	0	20	118	266		0	-5	-5	-5	0	
96100212	35	30.3N	147.6E	65	11	15	81	223	318		0	-5	0	0	5	
96100218	36	30.7N	149.8E	65	5	36	146	292	363		0	-5	-5	0	0	
96100300	37	31.1N	151.8E	65	61	178	154	174	290		0	0	0	5	5	
96100306	38	31.7N	154.1E	60	0	40	140	167			0	0	0	5		
96100312	39	32.4N	156.5E	55	50	161	192	167			0	0	5	5		
96100318		32.9N	159.4E	50												
96100400		33.1N	162.4E	45												
96100406		33.3N	165.0E	40												
96100412		33.4N	166.7E	35												
96100418		32.9N	168.2E	35												
96100500		32.0N	169.4E	30												
96100506		30.8N	170.3E	25												
96100512		29.5N	170.8E	25												
96100518		28.4N	171.0E	15												
96100600		27.3N	171.0E	15												
			AVERAGE		13	46	80	115	152	201						
			# CASES		39	39	39	39	37	28						

TROPICAL STORM ABEL (30W)

	WRN	BEST TRACK			POSITION ERRORS						WIND ERRORS					
DTG	NO.	LAT	LONG	WIND (KT)	00	12	24	36	48	72	00	12	24	36	48	72
96100906		12.0N	133.0E	15												
96100912		12.8N	131.7E	15												
96100918		13.5N	130.6E	20												
96101000		13.9N	129.6E	20												
96101006		14.2N	128.6E	20												
96101012		14.5N	127.6E	25												
96101018		14.8N	126.6E	25												
96101100	1	15.0N	125.6E	25	61	133	196	189	133	81	0	5	10	-5	-5	20
96101106	2	15.2N	124.6E	25	89	173	213	187	165	59	0	5	0	-10	-5	20
96101112	3	15.4N	123.7E	25	104	159	188	199	190	119	0	5	-15	-5	0	20
96101118	4	15.8N	122.7E	25	70	143	199	224	193	198	0	-5	-15	-5	0	25
96101200	5	16.3N	121.7E	25	186	138	126	133	165	266	0	-20	-10	5	15	15
96101206	6	17.1N	120.6E	35	129	99	78	140	246	494	-5	-20	-10	5	0	-5
96101212	7	17.7N	119.5E	50	16	70	78	25	145	517	-20	-10	0	15	25	0
96101218	8	18.2N	118.6E	50	12	67	41	63	191	566	-20	-10	0	15	30	0
96101300	9	18.8N	117.6E	45	11	28	72	168	313	606	-15	-5	5	15	15	0
96101306	10	19.4N	116.7E	45	18	71	153	275	450		-15	-10	-5	0	-5	
96101312	11	19.6N	116.0E	40	18	90	198	378	534		-5	10	20	5	-5	
96101318	12	19.6N	115.5E	40	36	115	236	426	582		0	10	20	5	-5	
96101400	13	19.4N	114.9E	35	6	25	66	140	198	199	0	-5	0	-5	-5	-5
96101406	14	19.1N	114.3E	35	24	63	152	236	337	452	0	5	0	0	-5	-5
96101412	15	18.6N	113.7E	35	12	82	170	254	312	383	0	5	0	0	-5	0

TROPICAL STORM ABEL (30W) (CONTINUED)

DTG	WRN NO.	LAT	LONG	WIND (KT)	POS 00	POS 12	POS 24	POS 36	POS 48	POS 72	WIND 00	WIND 12	WIND 24	WIND 36	WIND 48	WIND 72
96101418	16	18.0N	113.2E	30	12	87	161	225			0	0	0	-5		
96101500		17.2N	112.8E	30												
96101506	17	16.3N	112.4E	30	18	48	94	104			0	0	0	-5		
96101512		15.5N	111.9E	30												
96101518	18	14.7N	111.4E	30	21	58	115	178			0	0	-5	-5		
96101600		14.0N	111.1E	30												
96101606	19	13.7N	110.9E	30	11	55	109				0	0	5			
96101612		13.6N	110.7E	30												
96101618	20	13.6N	110.5E	30	25	75					0	5				
96101700		13.7N	110.3E	25												
96101706	21	13.8N	110.1E	25	11						0					
96101712		13.9N	109.9E	20												
			AVERAGE		43	89	140	197	277	329						
			# CASES		21	20	19	18	15	12						

TROPICAL DEPRESSION 31W

DTG	WRN NO.	BEST TRACK LAT	LONG	WIND (KT)	POSITION ERRORS 00	12	24	36	48	72	WIND ERRORS 00	12	24	36	48	72
96101000		8.9N	158.4E	20												
96101006		9.0N	157.3E	20												
96101012		9.2N	156.2E	20												
96101018		9.4N	155.3E	20												
96101100		9.7N	154.4E	20												
96101106		10.2N	153.8E	20												
96101112		11.0N	153.0E	20												
96101118		11.7N	152.3E	20												
96101200		12.2N	151.8E	20												
96101206		12.8N	151.4E	20												
96101212		13.4N	151.1E	20												
96101218		14.0N	150.8E	20												
96101300		14.4N	150.5E	25												
96101306	1	14.8N	149.8E	25	13	58	106	143	142	233	0	5	10	20	30	45
96101312	2	15.2N	149.0E	25	104	169	223	263	283	234	0	5	10	20	30	45
96101318	3	15.6N	148.3E	25	24	68	116	104	164	243	0	0	5	10	20	30
96101400	4	16.0N	147.6E	25	21	42	36	78	145	296	0	0	5	10	20	30
96101406	5	16.5N	146.9E	25	5	29	51	66	102	212	0	5	10	15	25	40
96101412	6	16.9N	146.2E	25	0	29	34	42	68	109	0	5	10	15	25	40
96101418	7	17.5N	145.3E	25	20	52	66	82			0	0	0	0		
96101500		17.5N	144.3E	25												
96101506	8	17.8N	143.5E	25	5	87	135	235			0	0	0	0		
96101512		18.7N	142.7E	25												
96101518	9	19.5N	142.3E	25	69	104	176	262	319		5	5	10	15	15	
96101600	10	20.2N	141.7E	25	33	83	128	226			0	0	0	-5		
96101606		20.8N	141.2E	25												
96101612	11	21.5N	140.9E	25	50	57	110	215			0	0	0	5		
96101618		22.4N	140.7E	25												
96101700	12	23.2N	140.5E	25	18	105	211				0	0	5			
96101706		23.8N	140.3E	25												
96101712	13	24.3N	139.8E	25	22	76					0	5				
96101718		24.7N	139.2E	25												
96101800		25.8N	138.7E	20												
96101806		27.0N	138.5E	15												
			AVERAGE		30	74	116	156	175	222						
			# CASES		13	13	12	11	7	6						

TYPHOON BETH (32W)

DTG	WRN NO.	BEST TRACK LAT	LONG	WIND (KT)	POSITION ERRORS 00	12	24	36	48	72	WIND ERRORS 00	12	24	36	48	72
96100712		10.9N	162.2E	15												
96100718		11.0N	161.1E	15												
96100800		11.0N	160.0E	15												
96100806		11.1N	158.7E	15												
96100812		11.2N	157.4E	15												
96100818		11.5N	156.2E	15												
96100900		11.9N	154.8E	15												
96100906		12.3N	153.5E	15												
96100912		13.0N	152.1E	15												
96100918		13.6N	150.8E	15												
96101000		14.1N	149.5E	15												
96101006		14.5N	148.6E	15												
96101012		14.7N	147.6E	15												
96101018		14.8N	146.7E	15												

TYPHOON BETH (32W) (CONTINUED)

96101100		14.8N	145.7E	20												
96101106		14.7N	144.6E	20												
96101112		14.2N	143.8E	25												
96101118		14.0N	142.7E	25												
96101200		14.0N	141.6E	25												
96101206		14.2N	140.3E	25												
96101212		14.6N	139.2E	25												
96101218		15.0N	138.1E	25												
96101300		15.4N	136.5E	25												
96101306		15.5N	134.8E	25												
96101312	1	15.6N	133.8E	25	35	115	203	280	352	418	0	5	10	10	20	10
96101318	2	15.7N	133.0E	30	26	82	171	257	313	379	0	5	5	10	15	5
96101400	3	15.9N	132.2E	30	13	50	108	142	132	101	0	0	0	10	10	0
96101406	4	16.0N	131.6E	30	18	59	91	98	90	91	0	0	5	10	10	-10
96101412	5	16.4N	131.1E	35	42	91	119	114	122	120	-5	-5	5	5	5	-20
96101418	6	17.0N	130.4E	40	49	60	48	37	18	16	-10	-10	-5	-5	-5	-15
96101500	7	17.3N	130.0E	45	26	24	33	20	20	160	-10	0	-5	-5	0	-15
96101506	8	17.5N	129.5E	45	13	33	56	46	11	184	-5	-5	-10	-10	-5	-15
96101512	9	17.6N	129.0E	45	23	39	45	45	34	128	-5	-10	-15	-15	-15	-20
96101518	10	17.6N	128.2E	50	16	33	37	37	23	126	-5	-10	-15	-15	-15	-20
96101600	11	17.6N	127.4E	55	21	18	20	58	120	167	-10	-10	-10	-30	-15	-20
96101606	12	17.6N	126.6E	60	0	5	12	86	145	201	-10	-10	-10	-30	-15	-20
96101612	13	17.6N	125.9E	65	18	52	37	43	108	174	-5	-5	-10	-15	-20	-10
96101618	14	17.6N	125.1E	70	0	13	34	70	132	145	-5	-10	-10	-15	-20	0
96101700	15	17.7N	124.0E	75	13	49	74	130	153	140	-5	-5	-5	0	15	60
96101706	16	17.7N	123.4E	80	8	18	42	100	121	62	0	0	-5	-5	0	30
96101712	17	17.7N	122.8E	90	8	16	48	91	100	121	0	10	-10	-5	5	40
96101718	18	17.6N	122.1E	90	0	45	96	122	124	237	0	-5	-10	-5	15	45
96101800	19	17.8N	121.4E	75	0	30	82	101	131	291	10	-10	-10	0	25	50
96101806	20	18.2N	120.5E	75	0	21	39	57	69	190	0	-10	-10	10	30	50
96101812	21	18.4N	120.2E	80	8	88	136	186	258	350	0	5	15	35	40	50
96101818	22	18.8N	119.3E	80	30	90	128	199	271	337	0	5	25	40	45	50
96101900	23	18.9N	118.3E	80	0	25	63	60	77	158	0	10	35	45	50	50
96101906	24	18.9N	117.4E	80	5	34	88	95	77	204	0	20	40	45	55	45
96101912	25	18.7N	116.6E	75	13	79	109	143	143	263	0	25	35	45	45	30
96101918	26	18.4N	115.6E	65	24	81	90	89	128	343	0	15	25	30	30	15
96102000	27	17.6N	114.8E	55	16	73	123	133	104		0	10	15	20	20	
96102006	28	17.1N	113.7E	50	5	34	36	72	141		0	5	10	10	10	
96102012	29	16.9N	112.6E	45	6	43	67	135	244		0	10	10	5	10	
96102018	30	16.5N	111.5E	40	13	18	85	175	325		5	15	10	5	10	
96102100	31	16.1N	110.5E	35	0	33	116	261			0	0	-5	0		
96102106	32	15.8N	109.8E	30	21	83	128	208			0	0	0	5		
96102112		15.2N	109.2E	30												
96102118	33	14.5N	108.9E	30	60	123					-5	-5				
96102200		13.9N	108.7E	30												
96102206		13.4N	109.0E	25												
96102212		13.1N	109.7E	20												
		AVERAGE			16	51	81	116	137	197						
		# CASES			33	33	32	32	30	26						

TYPHOON CARLO (33W)

	WRN	BEST TRACK			POSITION ERRORS						WIND ERRORS					
DTG	NO.	LAT	LONG	WIND (KT)	00	12	24	36	48	72	00	12	24	36	48	72
96101700		17.0N	168.0E	15												
96101706		16.2N	167.3E	15												
96101712		15.7N	166.4E	15												
96101718		15.3N	165.2E	15												
96101800		15.1N	164.1E	15												
96101806		15.1N	163.0E	15												
96101812		15.1N	161.6E	15												
96101818		15.1N	160.5E	10												
96101900		15.4N	158.7E	15												
96101906		15.8N	156.9E	20												
96101912		16.4N	155.2E	20												
96101918		16.8N	153.7E	20												
96102000		17.0N	152.2E	20												
96102006		17.3N	151.5E	20												
96102012		17.7N	150.8E	20												
96102018		18.0N	150.3E	20												
96102100	1	18.4N	149.8E	25	36	39	74	103	90	105	0	-5	-10	-15	-20	-50
96102106	2	18.8N	149.3E	30	30	48	69	72	84	98	0	-10	-10	-15	-30	-50
96102112	3	19.0N	148.8E	35	21	55	96	98	131	318	0	-5	-10	-15	-35	-25
96102118	4	19.1N	148.5E	45	29	55	71	89	122	407	0	0	-5	-20	-35	-10
96102200	5	19.2N	148.0E	45	29	33	62	54	172	572	0	-5	-10	-25	-35	-5

TYPHOON CARLO (33W) (CONTINUED)

DTG	WRN NO.	LAT	LONG	WIND (KT)	POS 00	POS 12	POS 24	POS 36	POS 48	POS 72	WIND 00	WIND 12	WIND 24	WIND 36	WIND 48	WIND 72
96102206	6	19.3N	147.6E	50	0	25	33	53	215	683	5	0	-15	-35	-35	-5
96102212	7	19.4N	147.1E	55	0	28	45	176	347	772	0	-5	-25	-35	-25	0
96102218	8	19.7N	146.3E	60	0	23	94	197	318	688	0	-15	-30	-30	-10	10
96102300	9	20.0N	145.5E	65	12	91	118	202	283	479	0	-20	-30	-20	-15	0
96102306	10	20.2N	145.2E	80	20	66	175	291	398	508	-15	-30	-30	-10	-5	0
96102312	11	20.7N	145.0E	90	12	40	76	106	157	250	0	-5	10	20	20	0
96102318	12	21.5N	144.9E	100	5	10	24	49	37	113	-10	-5	15	10	5	-5
96102400	13	22.6N	144.8E	105	0	24	44	129	157	179	0	10	15	20	5	0
96102406	14	23.8N	144.9E	105	5	34	60	109	102		0	20	25	25	5	
96102412	15	25.2N	145.1E	95	0	27	86	131	214		-10	-10	5	0	0	
96102418	16	26.8N	145.4E	85	11	20	77	140	195		-10	0	10	-5	0	
96102500	17	28.4N	146.0E	80	13	98	200	279	356		-5	15	10	5	5	
96102506	18	30.1N	146.9E	70	0	46	61	109			5	0	-15	-15		
96102512	19	31.9N	148.7E	60	8	14	7	36			5	0	-5	-10		
96102518	20	33.6N	150.4E	55	11	46	40				0	-10	-10			
96102600	21	35.1N	152.3E	55	9	61	130				-5	-5	0			
96102606	22	36.7N	154.4E	55	7	97					0	5				
96102612	23	38.2N	157.4E	50	15	79					0	10				
96102618	24	39.9N	160.5E	45	25						0					
96102700		41.9N	163.6E	40												
			AVERAGE		13	47	79	128	199	398						
			# CASES		24	23	21	19	17	13						

TROPICAL DEPRESSION 34W

DTG	WRN NO.	BEST TRACK LAT	LONG	WIND (KT)	POSITION ERRORS 00	12	24	36	48	72	WIND ERRORS 00	12	24	36	48	72
96102412		10.5N	121.0E	15												
96102418		9.7N	120.0E	15												
96102500		9.3N	118.7E	15												
96102506		8.9N	117.5E	15												
96102512		8.7N	116.2E	15												
96102518		8.4N	114.9E	15												
96102600		8.1N	113.7E	15												
96102606		7.7N	112.8E	15												
96102612		7.4N	112.1E	15												
96102618		7.0N	111.5E	15												
96102700		6.6N	110.9E	20												
96102706		6.3N	110.3E	25												
96102712		5.9N	109.6E	30												
96102718		5.8N	108.7E	30												
96102800		5.7N	107.7E	25												
96102806		5.8N	106.6E	25												
96102812		6.0N	105.5E	25												
96102818		6.5N	104.4E	25												
96102900		7.5N	103.7E	25												
96102906	1	8.6N	103.2E	25	24	102	114	83			-5	0	5	5		
96102912		9.5N	102.8E	25												
96102918	2	10.4N	102.3E	25	29	35	40	57			0	5	0	0		
96103000		11.0N	101.6E	25												
96103006	3	11.2N	100.7E	20	8	85	83	125			0	-5	-5	10		
96103012		11.4N	99.6E	15												
96103018	4	11.7N	98.3E	20	79						-5					
96103100		12.4N	97.3E	25												
96103106		13.4N	96.7E	25												
96103112		14.6N	97.2E	20												
96103118		15.7N	97.9E	15												
			AVERAGE		36	75	79	89								
			# CASES		4	3	3	3								

TROPICAL STORM 35W

DTG	WRN NO.	BEST TRACK LAT	LONG	WIND (KT)	POSITION ERRORS 00	12	24	36	48	72	WIND ERRORS 00	12	24	36	48	72
96103106		10.8N	120.8E	15												
96103112		10.8N	120.1E	20												
96103118		10.9N	119.4E	20												
96110100		11.0N	118.5E	20												
96110106		11.2N	117.7E	20												
96110112		11.5N	116.9E	25												
96110118		11.9N	116.0E	25												
96110200	1	12.6N	114.4E	30	49	118	271	394	432		-5	-10	0	15	30	
96110206	2	13.2N	112.7E	35	83	176	303	378	327		-10	-10	5	20	10	

TROPICAL STORM 35W (CONTINUED)

DTG	WRN NO.	LAT	LONG	WIND (KT)	00	12	24	36	48	72	00	12	24	36	48	72
96110212	3	13.6N	111.2E	40	98	206	297	291			-10	0	10	5		
96110218	4	14.0N	109.3E	40	106	163	180				-10	0	-5			
96110300	5	14.4N	107.2E	35	6	24	88				-5	-5	0			
96110306	6	14.7N	105.3E	30	11	60	219				-5	-5	-5			
96110312		14.8N	103.8E	30												
96110318		15.4N	102.6E	25												
96110400		16.4N	102.2E	20												
96110406		17.3N	102.2E	20												
			AVERAGE		59	125	227	355	380							
			# CASES		6	6	6	3	2							

SUPER TYPHOON DALE (36W)

DTG	WRN NO.	BEST TRACK LAT	LONG	WIND (KT)	POSITION ERRORS 00	12	24	36	48	72	WIND ERRORS 00	12	24	36	48	72
96110200		9.1N	154.0E	15												
96110206		9.1N	153.7E	15												
96110212		9.1N	153.4E	15												
96110218		9.1N	152.9E	15												
96110300		9.2N	152.5E	15												
96110306		9.4N	152.2E	20												
96110312		9.7N	152.1E	25												
96110318		9.9N	152.2E	25												
96110400		9.9N	151.9E	25												
96110406	1	10.0N	152.0E	30	21	58	114	152	142	198	-5	-5	-5	-10	-15	-25
96110412	2	9.9N	151.9E	35	43	61	113	123	126	146	-10	-5	-5	-5	-10	-25
96110418	3	10.1N	151.9E	35	64	97	123	122	145	162	-5	0	0	-5	-5	0
96110500	4	10.2N	152.0E	35	71	146	143	95	115	72	-5	-5	-5	-10	-10	0
96110506	5	10.5N	152.1E	35	87	128	100	64	126	106	-5	-10	-15	-15	-15	0
96110512	6	10.7N	152.3E	40	48	78	106	59	41	72	0	-5	-15	-15	-20	5
96110518	7	10.9N	152.0E	45	42	85	82	51	72	48	0	-10	-15	-15	-15	-5
96110600	8	11.3N	151.1E	50	48	76	76	58	99	74	-5	-10	-10	-15	0	0
96110606	9	11.5N	150.2E	60	76	102	64	113	128	81	-5	-5	-5	0	10	-10
96110612	10	11.6N	149.1E	65	42	79	123	155	236	251	-5	-5	-15	0	10	-20
96110618	11	11.5N	148.4E	70	34	106	94	145	159	161	-5	-10	-15	0	0	-20
96110700	12	11.1N	148.0E	75	11	16	18	64	59	137	-10	-20	-15	0	-15	-20
96110706	13	11.3N	147.7E	80	8	63	72	58	26	99	-5	0	15	15	0	-15
96110712	14	11.7N	146.1E	90	0	45	109	100	88	119	0	10	25	10	-5	-15
96110718	15	11.4N	144.5E	90	12	84	105	125	115	200	0	10	15	-5	-5	-15
96110800	16	11.6N	143.3E	90	0	67	78	123	155	201	0	10	0	-15	-5	5
96110806	17	11.4N	142.4E	90	0	58	114	198	240	280	0	-5	-15	-15	-5	5
96110812	18	11.7N	141.5E	90	18	88	144	228	230	287	0	-10	-25	-15	-5	5
96110818	19	12.3N	140.0E	100	18	72	156	220	244	371	0	-15	-20	-10	-5	10
96110900	20	12.8N	138.9E	115	8	66	148	162	228	473	-10	-25	-20	-10	5	20
96110906	21	13.7N	137.8E	130	0	32	64	111	225	562	0	-10	-15	-20	-10	5
96110912	22	14.5N	136.6E	140	0	68	90	162	237	515	5	15	20	10	-10	15
96110918	23	15.7N	135.2E	140	21	36	83	176	253	626	10	15	20	10	-5	15
96111000	24	16.8N	133.8E	140	0	92	162	228	286	555	5	5	5	0	5	5
96111006	25	17.5N	132.8E	140	0	64	152	212	264	736	0	0	5	5	5	15
96111012	26	18.3N	132.1E	140	11	74	149	197	324	924	0	10	5	15	15	25
96111018	27	19.3N	131.6E	140	11	65	94	129	275	907	0	10	10	10	5	20
96111100	28	20.5N	131.3E	130	5	20	76	192	388	1048	0	-5	5	0	0	20
96111106	29	21.7N	131.3E	130	5	22	87	201	463	1129	0	-5	-5	-10	5	15
96111112	30	22.7N	131.4E	130	0	29	91	220	345		0	5	5	0	0	
96111118	31	23.7N	131.8E	125	0	17	120	244	393		0	0	-5	5	0	
96111200	32	24.9N	132.5E	115	0	59	236	425	612		0	0	0	10	0	
96111206	33	26.1N	133.8E	115	0	106	257	450	692		0	-5	0	5	0	
96111212	34	27.8N	136.4E	105	44	164	246	267			0	10	10	10		
96111218	35	29.5N	139.3E	105	37	191	272	352			0	20	25	15		
96111300	36	31.2N	143.9E	90	87	129	153				0	15	10			
96111306	37	32.9N	148.7E	80	40	9	91				0	5	10			
96111312	38	34.9N	154.3E	70	15	27					-5	0				
96111318	39	37.4N	160.6E	65	61	181					0	5				
96111400		40.7N	167.1E	60												
			AVERAGE		26	76	122	171	229	364						
			# CASES		39	39	37	35	33	29						

TROPICAL STORM ERNIE (37W)

DTG	WRN NO.	BEST TRACK LAT	LONG	WIND (KT)	POSITION ERRORS 00	12	24	36	48	72	WIND ERRORS 00	12	24	36	48	72
96102900		7.0N	155.0E	15												
96102906		7.0N	154.5E	15												

TROPICAL STORM ERNIE (37W) (CONTINUED)

96102912		7.0N	154.0E	15												
96102918		7.0N	153.5E	15												
96103000		7.0N	153.0E	15												
96103006		7.0N	152.5E	15												
96103012		7.0N	152.0E	15												
96103018		7.0N	151.5E	15												
96103100		7.0N	151.0E	15												
96103106		6.9N	150.4E	15												
96103112		6.8N	149.7E	15												
96103118		6.6N	148.8E	15												
96110100		6.4N	147.7E	15												
96110106		6.1N	146.2E	15												
96110112		5.9N	144.7E	15												
96110118		5.7N	143.2E	15												
96110200		5.6N	142.0E	15												
96110206		5.5N	141.0E	15												
96110212		5.5N	140.2E	15												
96110218		5.4N	139.4E	15												
96110300		5.2N	138.3E	15												
96110306		5.0N	137.1E	15												
96110312		4.9N	136.0E	20												
96110318		5.1N	134.9E	20												
96110400		5.3N	133.4E	20												
96110406		5.5N	132.2E	20												
96110412	1	6.0N	131.2E	25	29	127	215	274	353	412	0	5	5	0	0	0
96110418	2	6.6N	130.2E	25	51	134	187	223	285	332	0	10	10	10	0	-10
96110500	3	7.4N	129.2E	25	26	48	49	108	130	107	0	5	5	5	0	-5
96110506	4	8.1N	128.3E	25	25	36	29	74	105	91	0	5	0	0	-5	-5
96110512	5	8.7N	127.2E	30	16	18	71	112	101	108	0	0	0	0	-5	-5
96110518	6	9.1N	126.3E	30	23	24	96	117	85	136	0	-5	-5	-5	-5	0
96110600	7	9.5N	125.3E	35	24	93	96	85	88	234	-5	-10	-10	-10	-5	15
96110606	8	10.3N	124.7E	40	43	96	109	85	113	274	-5	-10	-15	-10	-5	20
96110612	9	11.2N	123.8E	40	18	84	104	90	70	193	0	-5	-5	0	5	30
96110618	10	11.7N	122.8E	45	18	101	88	83	81	191	0	-5	0	5	20	35
96110700	11	12.0N	121.3E	45	21	78	144	182	225	260	0	0	0	5	25	30
96110706	12	12.1N	120.2E	50	8	103	183	237	291	381	0	5	15	25	40	50
96110712	13	12.3N	119.8E	50	64	146	209	300	365	479	0	5	15	30	40	30
96110718	14	12.5N	119.5E	50	105	148	175	233	298	381	0	5	20	35	35	30
96110800	15	12.7N	119.3E	50	16	197	243	295	369	403	0	0	15	25	20	20
96110806	16	13.4N	118.9E	50	30	90	216	259	311	308	0	5	20	20	20	20
96110812	17	14.1N	118.6E	50	13	64	139	172	149	64	0	10	20	15	20	20
96110818	18	14.8N	118.4E	45	25	96	127	164	146	90	0	15	15	15	20	20
96110900	19	16.0N	118.3E	40	24	120	171	182	186	186	-5	0	-10	-15	-15	-15
96110906	20	17.3N	117.7E	35	20	36	63	123	144	193	0	-10	-15	-15	-15	-5
96110912	21	17.9N	117.7E	35	75	160	232	264			-5	-15	-15	-15		
96110918		18.5N	117.8E	40												
96111000	22	19.2N	117.9E	45	0	34	102	118	138	215	-5	-5	-5	0	0	15
96111006	23	19.6N	118.0E	45	0	28	73	164	193	279	-5	-5	-5	0	10	15
96111012	24	19.8N	118.0E	45	30	43	135	194	239	350	-5	-5	-15	-20	-10	-10
96111018	25	20.0N	118.1E	45	47	94	181	229	254	423	0	0	0	15	15	20
96111100	26	20.2N	118.1E	45	0	102	184	224	232	467	0	0	0	15	15	15
96111106	27	19.8N	118.5E	45	5	80	148	165	120	234	0	0	10	15	15	15
96111112	28	19.4N	119.2E	45	12	72	110	75	81	276	0	-5	0	0	0	-5
96111118	29	19.3N	120.0E	45	39	79	104	125	187	343	0	5	0	-5	-5	-10
96111200	30	19.0N	120.6E	45	0	64	123	187	281	414	0	5	-5	-10	-15	-10
96111206	31	18.4N	121.0E	35	34	62	99	174	266	357	0	0	-5	-10	-15	-10
96111212	32	17.6N	121.1E	35	5	102	179	255	321	350	0	0	-5	-15	-10	0
96111218	33	16.7N	120.4E	35	18	89	129	182	205	300	0	-5	-10	-15	-5	5
96111300	34	16.2N	119.3E	35	8	53	120	188	213	244	0	-5	-10	-10	-10	-5
96111306	35	15.8N	118.2E	35	8	23	21	59	96	159	0	-5	-10	-5	-10	-5
96111312	36	15.5N	117.3E	35	0	61	122	185	212	339	0	-10	-10	0	0	5
96111318	37	14.9N	116.2E	35	21	72	107	154	172	243	0	-5	0	0	5	0
96111400	38	14.1N	115.1E	40	0	8	42	50	67	56	0	5	10	10	10	5
96111406	39	13.6N	113.9E	40	0	46	105	128	143	95	0	10	10	5	0	5
96111412	40	13.0N	112.8E	40	8	58	82	90	93	34	0	10	10	5	0	5
96111418	41	12.3N	112.3E	35	21	43	54	77	75	21	0	0	5	0	0	0
96111500	42	11.4N	111.6E	35	8	56	63	67	82	173	0	-5	0	-5	0	-5
96111506	43	11.0N	110.8E	35	13	32	29	18	36	129	0	0	0	0	0	0
96111512	44	10.8N	110.1E	35	0	29	51	45	23		0	0	0	0	0	
96111518	45	10.4N	109.2E	30	16	46	71	69	35		0	0	5	0	0	
96111600	46	10.0N	108.3E	30	0	13	61	84			0	0	0	0		
96111606		9.7N	107.3E	30												
96111612	47	9.4N	106.3E	30	0	42	67	131			0	0	0	0		
96111618		9.4N	105.0E	25												
96111700	48	9.5N	103.9E	25	8	23	84				0	0	-5			
96111706		9.6N	102.8E	25												
96111712		9.8N	101.8E	25												

TROPICAL STORM ERNIE (37W) (CONTINUED)

DTG	WRN NO.	LAT	LONG	WIND (KT)	00	12	24	36	48	72	00	12	24	36	48	72
96111718		10.1N	100.8E	25												
96111800		10.4N	100.0E	25												
		AVERAGE			21	72	117	152	175	246						
		# CASES			48	48	48	47	44	42						

TROPICAL STORM 38W

	WRN	BEST TRACK			POSITION ERRORS						WIND ERRORS						PLATFORM
DTG	NO.	LAT	LONG	WIND (KT)	00	12	24	36	48	72	00	12	24	36	48	72	
96110406		21.4N	175.1E	25													
96110412		22.4N	174.9E	35													
96110418		23.1N	174.3E	40													
96110500		23.5N	173.7E	50													
96110506		23.6N	173.1E	50													
96110512		23.6N	172.5E	45													
96110518		23.7N	172.1E	40													
96110600		24.0N	171.8E	35													
96110606	1	24.3N	171.8E	35	8	68	158	145			-5	-5	-5	-10			
96110612		24.5N	172.0E	35													
96110618	2	24.7N	172.2E	35	21	32	115	87			-5	-5	-5	-10			
96110700		25.0N	172.3E	35													
96110706	3	25.4N	172.4E	35	49	39	112	190			-5	-5	-5	-5			
96110712		26.7N	171.8E	35													
96110718	4	27.6N	170.5E	35	32	121	196	275			-5	-10	-5	-5			
96110800		27.0N	169.0E	35													
96110806	5	26.6N	169.3E	35	34	166	282				-10	-10	-10				
96110812		26.5N	169.8E	30													
96110818		26.5N	170.2E	30													
96110900		26.3N	170.4E	25													
96110906		26.0N	170.6E	25													
96110912		25.6N	170.7E	25													
96110918		25.1N	170.6E	25													
96111000		24.5N	170.7E	25													
96111006		24.0N	171.0E	25													
96111012		24.0N	171.9E	30													
96111018		23.9N	173.1E	30													
96111100		23.8N	174.4E	30													
96111106		23.7N	175.8E	25													
96111112		23.3N	177.3E	25													
96111118		22.8N	178.8E	25													
96111200		22.2N	179.1W	25													
		AVERAGE			29	86	173	175									
		# CASES			5	5	5	4									

TROPICAL DEPRESSION 39W

	WRN	BEST TRACK			POSITION ERRORS						WIND ERRORS					
DTG	NO.	LAT	LONG	WIND (KT)	00	12	24	36	48	72	00	12	24	36	48	72
96110612		13.8N	125.4E	15												
96110618		14.5N	125.4E	20												
96110700		15.2N	125.2E	20												
96110706		15.8N	124.8E	25												
96110712		16.3N	124.3E	25												
96110718		16.8N	123.6E	25												
96110800		17.3N	122.8E	30												
96110806	1	17.8N	121.6E	30	47	70	120	162			-5	-5	0	5		
96110812		18.1N	120.3E	30												
96110818	2	18.7N	119.7E	30	48	135	188				-5	-5	-10			
96110900		19.2N	119.0E	30												
96110906	3	19.8N	118.5E	30	65	135					-5	-5				
96110912		20.4N	118.0E	30												
96110918		19.8N	117.6E	25												
96111000		19.2N	117.9E	25												
		AVERAGE			54	114	154	163								
		# CASES			3	3	2	1								

TROPICAL DEPRESSION 40W

DTG	WRN NO.	BEST TRACK LAT	LONG	WIND (KT)	POSITION ERRORS 00	12	24	36	48	72	WIND ERRORS 00	12	24	36	48	72
96112300		8.0N	151.0E	15												
96112306		8.2N	150.8E	15												
96112312		8.6N	150.4E	15												
96112318		9.2N	149.7E	15												
96112400		10.0N	148.6E	15												
96112406		10.9N	147.4E	15												
96112412		11.6N	146.1E	20												
96112418		12.3N	144.8E	20												
96112500	1	13.4N	143.6E	20	30	155	213	251	278	294	0	0	10	20	30	55
96112506	2	14.9N	142.9E	20	87	167	199	225	253	241	0	0	10	20	30	50
96112512	3	16.1N	142.4E	25	86	58	38	29	75	236	-5	0	10	20	35	45
96112518	4	17.0N	141.7E	25	90	90	82	115	167	113	5	10	15	25	40	50
96112600	5	17.5N	141.0E	25	90	145	223	333	428	384	5	10	15	15	10	5
96112606	6	17.8N	140.3E	25	100	136	176	236	296	272	0	5	15	15	5	5
96112612	7	18.1N	139.6E	25	125	171	206	309	354	359	0	5	20	15	5	5
96112618	8	18.3N	139.0E	25	154	203	276	376	397	411	0	5	15	10	5	0
96112700	9	18.3N	138.5E	25	5	42	149	188			0	5	5	0		
96112706		18.1N	138.1E	25												
96112712	10	17.7N	137.7E	20	26	111	161				5	0	-10			
96112718		17.0N	137.0E	20												
96112800		16.1N	135.9E	20												
96112806		15.7N	134.5E	25												
96112812		15.8N	133.2E	25												
96112818		16.0N	132.1E	25												
96112900	11	15.9N	131.2E	25	181	193	256	339			5	5	5	5		
96112906		15.3N	130.6E	25												
96112912	12	14.5N	130.4E	25	180	232	306	391			0	0	0	0		
96112918		14.0N	129.9E	25												
96113000	13	13.7N	129.3E	25	150	201	277				0					
96113006		13.4N	128.6E	25												
96113012	14	13.1N	127.8E	25	234	322	440				0	5	0			
96113018		12.7N	127.0E	25												
96120100	15	12.0N	126.3E	20	35	164					5					
96120106		11.0N	126.0E	20												
96120112		10.0N	125.8E	20												
96120118		9.2N	125.7E	15												
96120200		8.5N	125.6E	10												
			AVERAGE		105	160	215	254	281	289						
			# CASES		15	15	14	11	8	8						

TROPICAL DEPRESSION 41W

DTG	WRN NO.	BEST TRACK LAT	LONG	WIND (KT)	POSITION ERRORS 00	12	24	36	48	72	WIND ERRORS 00	12	24	36	48	72
96121218		4.2N	103.7E	15												
96121300		4.2N	104.3E	15												
96121306		4.2N	104.9E	20												
96121312		4.2N	105.5E	20												
96121318		4.2N	106.1E	20												
96121400		4.2N	106.6E	25												
96121406	1	4.2N	107.1E	25	119	216	306	391			0	5	0	-5		
96121412		4.1N	107.4E	25												
96121418	2	3.9N	107.7E	25	83	170	268	394			0	5	0	-5		
96121500		3.8N	107.9E	25												
96121506	3	3.6N	108.2E	25	17	73	91	78			0	5	5	5		
96121512		3.5N	108.4E	25												
96121518	4	3.3N	108.7E	25	50	64	33	69			0	5	5	-5		
96121600		3.2N	109.3E	25												
96121606	5	3.3N	109.7E	25	40	69	128	155			0	0	-5	-5		
96121612		3.5N	110.1E	25												
96121618	6	4.0N	110.5E	25	42	67	80	75			0	-5	-5	-5		
96121700		4.4N	110.3E	30												
96121706	7	4.5N	110.1E	30	8	8	26	43			0	0	0	5		
96121712		4.6N	109.8E	30												
96121718	8	4.6N	109.6E	30	43	78	117	153			0	0	5	5		
96121800		4.6N	109.5E	30												
96121806	9	4.6N	109.3E	30	0	13	16	41			0	5	0	0		
96121812		4.7N	109.1E	30												
96121818	10	4.8N	109.0E	25	0	13	42				0	0	0			
96121900		4.9N	108.8E	25												
96121906	11	4.9N	108.5E	25	17	60	126	185			0	0	0	5		

DTG	WRN NO.	LAT	LONG	WIND (KT)	00	12	24	36	48	72	00	12	24	36	48	72
96121912		4.8N	108.2E	25												
96121918	12	4.8N	107.7E	25	36	91	139				0	0	0			
96122000		4.8N	107.0E	25												
96122006	13	4.9N	106.4E	25	72	104					0	0				
96122012		5.0N	105.8E	20												
96122018		5.1N	105.3E	20												
96122100		5.2N	104.8E	20												
		AVERAGE			41	79	115	159								
		# CASES			13	13	12	10								

TYPHOON FERN (42W)

DTG	WRN NO.	BEST TRACK LAT	LONG	WIND (KT)	POSITION ERRORS 00	12	24	36	48	72	WIND ERRORS 00	12	24	36	48	72
96121712		5.2N	151.3E	20												
96121718		5.4N	150.8E	20												
96121800		5.5N	150.3E	20												
96121806		5.6N	149.5E	20												
96121812		5.7N	148.8E	20												
96121818		5.9N	148.1E	20												
96121900		6.1N	147.4E	20												
96121906		6.3N	146.7E	20												
96121912		6.5N	146.0E	25												
96121918		6.8N	145.4E	25												
96122000		7.4N	144.3E	25												
96122006		7.5N	143.5E	25												
96122012		7.6N	142.6E	25												
96122018		7.8N	142.2E	25												
96122100		7.9N	142.0E	25												
96122106		8.0N	141.8E	30												
96122112		8.2N	141.6E	35												
96122118	1	8.3N	141.4E	40	101	124	155	175	207	260	-10	-10	5	20	25	20
96122200	2	8.5N	141.2E	45	50	69	96	131	173	276	-5	5	25	35	30	25
96122206	3	8.6N	141.1E	45	55	61	96	141	180	284	0	10	25	30	25	20
96122212	4	8.7N	141.0E	45	66	77	97	115	150	240	0	10	15	10	5	5
96122218	5	8.8N	140.8E	40	53	59	85	120	142	192	0	5	5	0	0	-5
96122300	6	8.8N	140.6E	35	21	42	97	122	162	222	0	0	-5	-15	-10	-30
96122306	7	8.8N	140.4E	35	30	72	118	143	175	208	0	-5	-10	-15	-10	-40
96122312	8	8.7N	140.1E	35	51	105	118	138	149	176	0	-10	-15	-15	-15	-45
96122318	9	8.5N	139.6E	40	85	119	137	147	163	166	-5	-15	-15	-15	-20	-45
96122400	10	8.5N	139.0E	45	78	72	84	101	96	141	-10	-20	-15	-20	-25	-45
96122406	11	8.6N	138.7E	50	13	24	47	64	49	113	-5	-5	0	-5	-20	-25
96122412	12	8.8N	138.5E	55	17	30	60	80	90	193	0	5	5	0	-5	-5
96122418	13	9.0N	138.3E	55	8	31	76	83	121	246	0	5	0	-5	-5	-5
96122500	14	9.2N	138.2E	55	5	47	69	51	104	204	0	-5	-10	-15	-20	-20
96122506	15	9.4N	138.2E	55	11	47	59	55	109	171	0	-10	-15	-15	-15	-20
96122512	16	9.8N	138.3E	60	6	6	23	24	86	98	-5	-10	-15	-10	0	-5
96122518	17	10.1N	138.4E	65	13	8	37	83	117	68	0	-10	-15	-10	-15	-20
96122600	18	10.6N	138.5E	70	12	18	35	88	99	6	-5	-15	-10	-5	-5	10
96122606	19	11.3N	138.7E	75	5	48	75	107	86	78	0	-5	5	5	5	30
96122612	20	11.7N	138.8E	80	11	32	71	86	38	84	-5	5	20	20	10	35
96122618	21	12.0N	138.8E	80	11	39	59	74	87	120	0	15	25	20	10	40
96122700	22	12.4N	138.8E	80	24	51	43	49	33	349	0	10	15	10	20	40
96122706	23	13.0N	138.7E	75	0	8	34	41	97	493	-5	0	5	5	25	40
96122712	24	13.6N	138.8E	75	0	23	26	108	255	687	-5	0	-5	5	20	30
96122718	25	14.3N	139.1E	75	0	31	57	74	193	689	0	0	-5	15	25	35
96122800	26	14.8N	139.7E	75	21	38	54	178	371	955	0	-5	5	25	30	40
96122806	27	15.8N	140.6E	75	30	42	114	263	475	1102	-5	-10	10	25	30	40
96122812	28	16.2N	141.6E	75	24	69	165	313	520	1112	0	10	25	30	35	35
96122818	29	16.8N	142.6E	75	29	93	216	408	714		0	20	30	35	40	
96122900	30	17.1N	143.6E	60	53	130	260	484	834		10	30	35	40	40	
96122906	31	17.2N	144.6E	50	66	115	195	375	528		10	25	30	40	35	
96122912	32	17.2N	145.5E	40	107	149	211	335	390		15	20	25	25	20	
96122918	33	17.2N	146.2E	35	107	129	234	336			15	20	25	20		
96123000	34	17.2N	146.7E	30	0	46	173	230			15	15	10	5		
96123006	35	17.2N	147.1E	25	11	111	206				5	10	5			
96123012		17.1N	147.2E	20												
96123018		16.7N	146.7E	15												
96123100		16.7N	146.3E	15												
96123106		16.9N	146.3E	15												
96123112		17.0N	146.5E	15												
		AVERAGE			34	62	106	157	219	320						
		# CASES			35	35	35	34	32	28						

TROPICAL STORM GREG (43W)

DTG	WRN NO.	BEST TRACK LAT	LONG	WIND (KT)	POSITION ERRORS 00	12	24	36	48	72	WIND ERRORS 00	12	24	36	48	72
96122106		7.8N	110.0E	15												
96122112		8.0N	110.1E	15												
96122118		8.0N	110.5E	15												
96122200		8.0N	110.7E	15												
96122206		7.9N	110.9E	15												
96122212		7.8N	111.1E	15												
96122218		7.7N	111.3E	15												
96122300		7.6N	111.4E	20												
96122306		7.5N	111.5E	25												
96122312		7.4N	111.6E	25												
96122318		7.3N	111.8E	25												
96122400		7.3N	112.1E	25												
96122406	1	7.3N	112.4E	30	17	64	101	109			0	-10	-15	-15		
96122412		7.2N	112.9E	35												
96122418	2	6.9N	113.4E	40	61	107	152	320			-10	-15	-15	0		
96122500	3	6.6N	113.9E	45	0	24	93	239	414		-5	-5	0	-5	-5	
96122506	4	6.5N	114.4E	45	13	49	143	329	474		-5	-5	5	-5	0	
96122512	5	6.5N	114.9E	45	16	124	329	516			-5	5	5	0		
96122518	6	6.6N	115.8E	45	37	205	425	573			-5	10	5	5		
96122600	7	6.7N	117.3E	35	29	176	303				0	0	5			
96122606	8	5.8N	119.2E	30	48	174	261				0	0	5			
96122612		5.5N	121.3E	30												
96122618	9	4.9N	123.4E	30	29	166					0	10				
96122700		4.1N	125.0E	25												
96122706	10	3.3N	126.1E	20	0						5					
			AVERAGE		26	121	226	348	444							
			# CASES		10	9	8	6	2							

6.2.2 NORTH INDIAN OCEAN — This section includes verification statistics for each warning in the North Indian Ocean during 1996.

JTWC BEST TRACK, FORECAST TRACK AND INTENSITY ERRORS BY WARNING

TROPICAL CYCLONE 01B

DTG	WRN NO.	BEST TRACK LAT	LONG	WIND (KT)	POSITION ERRORS 00	12	24	36	48	72	WIND ERRORS 00	12	24	36	48	72
96050106		7.5N	91.5E	20												
96050112		7.9N	91.4E	25												
96050118		8.4N	91.3E	25												
96050200		8.9N	91.2E	25												
96050206		9.4N	91.2E	25												
96050212		9.9N	91.1E	25												
96050218		10.5N	91.1E	25												
96050300		11.0N	91.0E	25												
96050306		11.5N	90.9E	25												
96050312		12.1N	90.8E	25												
96050318		12.5N	90.6E	25												
96050400		12.9N	90.3E	25												
96050406		13.3N	90.0E	25												
96050412		13.6N	89.6E	25												
96050418		13.9N	89.3E	25												
96050500		14.2N	89.0E	25												
96050506		14.6N	88.7E	25												
96050512		14.9N	88.5E	25												
96050518		15.4N	88.3E	25												
96050600		15.9N	88.2E	25												
96050606		16.6N	88.2E	25												
96050612		17.3N	88.3E	25												
96050618		17.8N	88.5E	30												
96050700	1	18.3N	88.9E	30	47	96	198	321			0	0	0	15		
96050706	2	18.8N	89.3E	30	58	130	254	389			0	-5	5	20		
96050712	3	19.5N	89.9E	35	0	52	113				-5	-5	10			

TROPICAL CYCLONE 01B (CONTINUED)

DTG	WRN NO.	LAT	LONG	WIND (KT)	00	12	24	36	48	72	00	12	24	36	48	72
96050718	4	20.4N	90.9E	40	8	35	68				-5	0	0			
96050800	5	21.3N	92.1E	40	17	60					-5	5				
96050806	6	22.2N	93.4E	35	25	138					0	0				
96050812		23.0N	94.8E	30												
96050818		23.7N	96.2E	25												
			AVERAGE		26	86	159	356								
			# CASES		6	6	4	2								

TROPICAL CYCLONE 02A

	WRN	BEST TRACK			POSITION ERRORS						WIND ERRORS					
DTG	NO.	LAT	LONG	WIND (KT)	00	12	24	36	48	72	00	12	24	36	48	72
96060900		16.6N	62.7E	15												
96060906		16.9N	62.4E	15												
96060912		17.1N	62.0E	15												
96060918		17.3N	61.6E	20												
96061000		17.5N	61.1E	25												
96061006		17.7N	60.6E	25												
96061012		17.9N	60.0E	30												
96061018		18.2N	59.3E	35												
96061100	1	18.6N	58.7E	40	83	127	173	168			-10	5	15	20		
96061106	2	19.2N	58.0E	40	110	222	271				0	0	10			
96061112	3	20.1N	57.6E	35	0	71	151				0	0	10			
96061118	4	20.7N	57.2E	35	0	182					0	5				
96061200		21.0N	56.5E	30												
96061206		21.0N	55.9E	20												
96061212		21.0N	55.4E	15												
			AVERAGE		49	151	199	169								
			# CASES		4	4	3	1								

TROPICAL CYCLONE 03B

	WRN	BEST TRACK			POSITION ERRORS						WIND ERRORS					
DTG	NO.	LAT	LONG	WIND (KT)	00	12	24	36	48	72	00	12	24	36	48	72
96061100		8.2N	87.8E	15												
96061106		8.5N	87.7E	20												
96061112		8.8N	87.6E	20												
96061118		9.3N	87.4E	20												
96061200		9.9N	86.9E	25												
96061206	1	10.4N	86.2E	30	42	121	214	265	260	196	0	-5	0	10	20	40
96061212	2	10.9N	85.5E	35	0	148	213	212	175	81	0	-10	-5	0	10	20
96061218	3	11.5N	84.6E	40	26	97	116	98	40	75	-10	-10	-5	0	10	10
96061300	4	12.2N	83.7E	45	31	42	77	179	317		0	10	15	-5	-15	
96061306	5	12.8N	82.9E	45	79	37	24	66	105	94	5	5	-20	5	-20	-20
96061312	6	13.4N	82.3E	45	0	86	128	198	230		0	10	15	-5	-15	
96061318	7	13.9N	81.9E	45	0	148	258	335	388		0	-5	-5	-10	-15	
96061400	8	14.1N	81.8E	45	0	133	218	280			0	0	-10	-20		
96061406	9	14.5N	81.8E	45	0	118	178	182	141	74	0	0	0	-5	-15	-5
96061412	10	15.1N	82.1E	45	82	179	241	267	245	161	0	-5	-5	-10	-15	-5
96061418	11	15.8N	82.6E	45	138	220	266	266	228	168	0	-5	-5	-10	-10	0
96061500	12	16.4N	83.0E	45	0	91	110				0	-20	-25			
96061506	13	16.8N	83.3E	45	0	46	46	17	42		0	0	-10	-15	-10	
96061512	14	17.2N	83.6E	45	11	13	67	131	182		0	0	-10	-10	-10	
96061518	15	17.5N	83.7E	45	0	43	110	182	207		0	-5	-5	-5	-5	
96061600	16	17.8N	83.7E	45	12	65	130	189			0	-10	-10	-10		
96061606	17	18.0N	83.5E	45	51	133	229				-5	-10	-5			
96061612	18	18.2N	83.1E	45	61	111	152				-5	-5	-5			
96061618	19	18.3N	82.7E	40	20	18	13				0	0	-5			
96061700	20	18.4N	82.2E	35	0	45					0	-10				
96061706		18.5N	81.6E	30												
96061712		18.8N	81.2E	30												
96061718		19.3N	81.0E	25												
96061800		19.8N	80.9E	25												
96061806		20.4N	80.8E	25												
96061812		21.3N	80.7E	25												
96061818		22.1N	80.7E	25												
			AVERAGE		28	95	147	192	197	122						
			# CASES		20	20	19	15	13	7						

TROPICAL CYCLONE 04A

DTG	WRN NO.	BEST TRACK LAT	LONG	WIND (KT)	POSITION ERRORS 00	12	24	36	48	72	WIND ERRORS 00	12	24	36	48	72
96061500		15.6N	72.0E	15												
96061506		15.9N	72.0E	15												
96061512		16.2N	71.9E	15												
96061518		16.5N	71.8E	15												
96061600		16.8N	71.7E	25												
96061606		17.2N	71.4E	20												
96061612		17.4N	71.0E	20												
96061618		17.5N	70.5E	25												
96061700		17.5N	69.6E	25												
96061706		17.6N	69.1E	25												
96061712		18.1N	69.1E	30												
96061718	1	18.4N	69.5E	35	0	97	179	267	371	507	0	-5	-20	-5	20	30
96061800	2	18.8N	69.9E	40	48	128	194	290	366	439	-5	-15	-15	5	25	35
96061806	3	19.2N	70.3E	45	18	50	105	139	137	42	-5	-20	-5	15	10	5
96061812	4	19.7N	70.6E	55	21	34	84	97	45		-15	-15	0	5	5	
96061818	5	20.3N	70.8E	65	12	16	29	43			-25	-15	0	0		
96061900	6	21.0N	70.9E	60	23	60	77	97			-20	-10	0	0		
96061906	7	22.0N	71.1E	55	55	118	163	186			-10	0	-5	0		
96061912	8	23.0N	71.4E	45	42	61	71	134			0					
96061918		23.8N	71.7E	35												
96062000		24.5N	72.0E	30												
96062006		25.1N	72.2E	30												
96062012		25.6N	72.4E	25												
96062018		26.0N	72.6E	25												
96062100		26.3N	72.9E	25												
96062106		26.6N	73.2E	25												
96062112		26.9N	73.5E	25												
96062118		27.1N	73.8E	25												
96062200		27.3N	74.1E	25												
96062206		27.5N	74.4E	25												
96062212		27.7N	74.8E	25												
96062218		27.9N	75.1E	25												
96062300		28.1N	75.4E	20												
96062306		28.3N	75.8E	20												
96062312		28.5N	76.1E	20												
96062318		28.7N	76.4E	20												
96062400		28.9N	76.7E	20												
96062406		29.1N	77.0E	20												
96062412		29.2N	77.3E	15												
96062418		29.4N	77.7E	15												
96062500		29.5N	78.1E	15												
96062506		29.6N	78.6E	15												
96062512		29.7N	79.2E	15												
			AVERAGE		28	71	113	157	230	330						
			# CASES		8	8	8	8	4	3						

TROPICAL CYCLONE 05A

DTG	WRN NO.	BEST TRACK LAT	LONG	WIND (KT)	POSITION ERRORS 00	12	24	36	48	72	WIND ERRORS 00	12	24	36	48	72
96101400		9.1N	91.7E	15												
96101406		9.5N	90.5E	15												
96101412		10.0N	89.2E	15												
96101418		10.6N	87.9E	15												
96101500		11.3N	86.6E	15												
96101506		11.9N	85.4E	15												
96101512		12.4N	84.4E	15												
96101518		12.9N	83.7E	15												
96101600		13.3N	83.2E	15												
96101606		13.4N	82.7E	20												
96101612		13.4N	82.3E	20												
96101618		13.3N	82.0E	20												
96101700		13.1N	81.7E	20												
96101706		12.9N	81.3E	20												
96101712		12.8N	80.8E	20												
96101718		12.9N	80.4E	20												
96101800		13.0N	80.1E	15												
96101806		13.0N	79.8E	15												
96101812		13.0N	79.5E	15												
96101818		13.0N	78.8E	15												
96101900		13.0N	78.1E	15												

TROPICAL CYCLONE 05A (CONTINUED)

96101906		13.0N	77.5E	15												
96101912		13.0N	76.9E	15												
96101918		13.0N	76.3E	15												
96102000		13.1N	75.4E	15												
96102006		13.2N	74.4E	15												
96102012		13.2N	73.2E	20												
96102018		13.2N	72.1E	20												
96102100		13.3N	71.3E	20												
96102106		13.5N	70.7E	25												
96102112		13.7N	70.3E	25												
96102118		13.8N	70.0E	25												
96102200		13.9N	69.8E	30												
96102206		14.0N	69.7E	35												
96102212	1	14.2N	69.6E	40	34	82	143	201	249	280	-5	-15	-20	-20	-10	5
96102218	2	14.3N	69.7E	45	13	58	139	204	255	248	-10	-20	-25	-15	-10	10
96102300	3	14.5N	69.9E	50	31	95	175	236	268	243	-10	-20	-15	-10	0	20
96102306	4	15.0N	70.1E	55	58	138	200	250	260	240	-5	-10	0	-5	0	20
96102312	5	15.8N	70.2E	60	21	90	150	180	156	34	-5	0	5	10	15	25
96102318	6	16.8N	70.2E	65	12	51	77	140	238	417	-10	5	5	10	15	10
96102400	7	17.6N	70.0E	60	34	71	124	182	280	472	-5	5	0	0	0	-10
96102406	8	18.3N	69.9E	55	8	43	50	37	73	147		5	5	10	10	-10
96102412	9	19.0N	69.9E	55	30	47	49	51	96	144	-5	0	10	10	10	-20
96102418	10	19.5N	70.0E	55	37	49	51	90	133	191	-5	5	15	15	5	-15
96102500	11	19.8N	70.1E	50	20	53	131	220	305	436	0	10	10	10	-5	-10
96102506	12	20.0N	70.1E	45	37	87	168	257	345		5	5	10	0	-15	
96102512	13	20.1N	69.9E	40	32	77	126	194			0	10	10	-5		
96102518	14	20.0N	69.7E	35	45	72	117				0	10	-5			
96102600	15	19.8N	69.7E	30	16	41					0	0				
96102606		19.6N	69.7E	25												
96102612		19.4N	69.7E	25												
96102618		19.0N	69.6E	30												
96102700		18.4N	69.3E	35												
96102706		17.8N	69.0E	40												
96102712		17.0N	68.6E	45												
96102718		16.2N	68.1E	40												
96102800	16	15.5N	67.5E	35	54	41	21	41	58		0	0	0	0	-5	
96102806	17	15.0N	67.0E	35	34	45	80	121	172		0	0	0	0	-5	
96102812	18	14.8N	66.6E	35	5	18	58	96	138	172	0	0	0	0	-5	-5
96102818	19	14.5N	66.0E	35	32	58	111	156	184	168	0	0	0	-5	-5	0
96102900	20	14.3N	65.1E	35	68	140	184	247	266	233	0	0	0	-5	0	0
96102906	21	14.1N	64.1E	35	49	102	139	160	162		0	0	-5	-5	0	
96102912	22	13.9N	62.8E	35	33	33	29	18	75		0	-5	-5	-5	-5	
96102918	23	13.7N	61.6E	35	41	31	11	18	63		0	-5	-10	-5	-5	
96103000	24	13.7N	60.6E	35	29	52	103	119	106		0	0	0	-5	-5	
96103006	25	13.7N	59.4E	35	34	60	88	103	116		0	0	0	0	-5	
96103012	26	13.7N	58.3E	35	0	40	70	87			0	0	0	0		
96103018	27	13.6N	57.6E	35	34	64	78	93			0	0	5	0		
96103100	28	13.5N	56.7E	30	36	76	100				0	0	5			
96103106	29	13.3N	56.1E	30	33	88	167				0	5	0			
96103112	30	13.0N	55.4E	30	51	133					-5	0				
96103118		12.3N	54.8E	25												
96110100		11.8N	54.3E	25												
96110106		10.9N	53.8E	25												
96110112		10.1N	53.3E	25												
96110118		9.3N	52.8E	25												
96110200		8.5N	52.4E	20												
96110206		7.7N	51.9E	20												
		AVERAGE			33	68	105	141	182	245						
		# CASES			30	30	28	25	22	14						

TROPICAL CYCLONE 06B

DTG	WRN NO.	BEST TRACK LAT	LONG	WIND (KT)	POSITION ERRORS 00	12	24	36	48	72	WIND ERRORS 00	12	24	36	48	72
0696102118		91N	932E	20												
96102200		9.5N	93.1E	25												
96102206		9.9N	93.0E	25												
96102212		10.2N	92.9E	25												
96102218		10.5N	92.8E	25												
96102300		10.7N	92.6E	25												
96102306		10.9N	92.2E	25												
96102312		10.9N	91.7E	25												
96102318		11.0N	90.9E	25												
96102400		11.2N	90.0E	25												
96102406		11.4N	89.3E	25												

TROPICAL CYCLONE 06B (CONTINUED)

DTG	WRN NO.	LAT	LONG	WIND (KT)	00	12	24	36	48	72	00	12	24	36	48	72
96102412		11.6N	88.7E	25												
96102418		11.8N	88.2E	25												
96102500		12.0N	87.8E	25												
96102506	1	12.2N	87.4E	30	26	58	81	128	155	230	0	0	5	10	15	-10
96102512	2	12.4N	87.0E	30	71	129	155	186	235	393	0	0	0	10	0	-10
96102518	3	12.6N	86.6E	35	175	290	393	483			0	5	-10	-20		
96102600	4	12.9N	86.2E	35	152	205	281	367	491		0	0	-10	-15	-20	
96102606	5	13.2N	85.7E	40	170	221	285	378	501		-5	0	-10	-15	-20	
96102612	6	13.6N	85.4E	45	56	58	103	203	343		0	5	10	15	-5	
96102618	7	14.2N	85.3E	45	64	62	126	235	371		0	5	10	15	0	
96102700	8	14.7N	85.3E	45	13	58	142	244	367		0	5	15	20	25	
96102706	9	15.5N	85.4E	45	21	75	167	291	447		0	5	10	20	30	
96102712	10	16.2N	85.7E	45	33	87	189	326			0	5	10	25		
96102718	11	17.0N	86.2E	45	52	112	221	375			0	5	15	30		
96102800	12	18.0N	86.8E	45	58	158	309				0	5	25			
96102806	13	19.1N	87.5E	45	82	188	346				0	5	20			
96102812	14	20.4N	88.2E	45	95	188					0	15				
96102818	15	21.9N	88.9E	40	23	76					5	15				
96102900	16	23.7N	89.6E	30	54						5					
96102906		14.1N	64.1E	35												
			AVERAGE		72	132	216	293	364	312						
			# CASES		16	15	13	11	8	2						

TROPICAL CYCLONE 07B

	WRN	BEST TRACK			POSITION ERRORS						WIND ERRORS					
DTG	NO.	LAT	LONG	WIND (KT)	00	12	24	36	48	72	00	12	24	36	48	72
96110100		15.0N	97.3E	15												
96110106		15.7N	96.5E	15												
96110112		15.9N	96.0E	15												
96110118		16.2N	95.2E	15												
96110200		16.4N	94.3E	15												
96110206		16.4N	93.5E	15												
96110212		16.4N	92.9E	15												
96110218		16.2N	92.1E	15												
96110300		16.1N	91.4E	20												
96110306		16.0N	90.8E	20												
96110312	1	16.0N	90.2E	25	26	30	62	108	142	116	0	0	-5	-20	-25	-80
96110318	2	16.0N	89.5E	25	33	30	37	62	93	93	0	-5	-15	-25	-35	-80
96110400	3	16.0N	88.8E	30	18	5	29	60	104	128	0	-5	-20	-30	-50	-60
96110406	4	16.0N	88.3E	35	11	29	49	73	128	181	0	-5	-10	-20	-80	-30
96110412	5	16.1N	87.7E	40	0	18	32	62	67	26	-5	-15	-20	-35	-80	-10
96110418	6	16.0N	87.0E	50	13	21	24	13	33	83	-5	-15	-30	-50	-80	0
96110500	7	16.0N	86.3E	60	23	26	13	29	54		-5	-10	-25	-50	-45	
96110506	8	16.0N	85.6E	65	5	12	49	97	120		0	-10	-40	-50	-20	
96110512	9	16.0N	84.9E	75	0	11	50	90	101		-10	-30	-40	-20	0	
96110518	10	16.0N	84.1E	85	5	16	62	96			-10	-30	-40	0		
96110600	11	16.0N	83.6E	100	18	67	104	118			-30	-45	-35	-5		
96110606	12	16.2N	82.9E	115	11	30	74	85			0	10	15	10		
96110612	13	16.5N	82.4E	120	13	33	62				-5	20	35			
96110618	14	16.8N	81.7E	115	12	82	132				5	50	45			
96110700	15	17.3N	80.8E	80	0	33					10	25				
96110706	16	17.5N	79.6E	50	11	58					30	35				
96110712		17.6N	78.8E	30												
96110718		17.8N	77.7E	20												
			AVERAGE		12	32	56	75	94	105						
			# CASES		16	16	14	12	9	6						

TROPICAL CYCLONE 08B

	WRN	BEST TRACK			POSITION ERRORS						WIND ERRORS					
DTG	NO.	LAT	LONG	WIND (KT)	00	12	24	36	48	72	00	12	24	36	48	72
96112612		8.9N	92.3E	20												
96112618		9.2N	91.3E	20												
96112700		9.4N	90.3E	25												
96112706		9.6N	89.2E	25												
96112712		10.0N	87.9E	25												
96112718		10.4N	86.8E	25												
96112800		11.1N	85.9E	30												
96112806	1	11.7N	85.3E	35	18	64	129	258	431	593	-5	-5	-5	0	-5	-25
96112812	2	12.4N	84.9E	35	16	29	107	280	468	595	-5	-10	-5	0	-15	-25
96112818	3	13.0N	84.6E	40	0	29	151	334	494	575	-5	-5	0	0	-15	-20
96112900	4	13.6N	84.4E	45	8	58	233	402	501	548	0	5	10	-5	-15	-20

TROPICAL CYCLONE 08B (CONTINUED)

96112906	5	14.1N	84.4E	45	29	141	319	473	522	563	0	5	5	-5	-15	-15
96112912	6	14.6N	84.8E	45	70	233	397	462	457	511	0	5	0	-5	-15	-15
96112918	7	15.0N	85.7E	45	104	233	322	325	358	602	0	0	0	-5	-5	-5
96113000	8	15.3N	86.9E	45	88	170	267	386	535	875	0	-5	-5	-5	-5	-30
96113006	9	15.3N	87.9E	50	50	119	252	370	487	694	-5	-10	-10	-5	-5	-35
96113012	10	15.1N	88.8E	55	49	159	300	436	578	780	0	0	-10	-10	-10	-40
96113018	11	14.7N	89.2E	55	72	163	258	355	464	666	0	0	-5	-5	-15	-20
96120100	12	14.3N	89.0E	55	62	162	255	323	357	382	0	0	5	10	0	0
96120106	13	14.0N	88.6E	55	13	18	37	54	79	109	0	0	0	-5	-15	-20
96120112	14	13.9N	88.1E	55	13	33	66	87	133	253	0	0	0	-10	-20	-50
96120118	15	13.9N	87.6E	50	13	24	37	66	130	214	0	0	-5	-20	-15	-50
96120200	16	13.9N	87.1E	50	13	30	56	116	154	242	0	5	-10	-15	-15	-50
96120206	17	13.9N	86.6E	45	0	11	52	99	163	293	0	-5	-20	-15	-25	-40
96120212	18	13.9N	86.1E	45	0	13	18	46	105	272	0	-10	-20	-15	-40	-40
96120218	19	14.0N	85.5E	50	11	16	34	94	161	276	-5	-15	-10	-20	-40	-35
96120300	20	14.1N	84.9E	55	39	76	136	210	295	366	0	0	10	-25	-40	-30
96120306	21	14.2N	84.3E	60	11	26	73	137	213	334	0	10	5	5	-20	-20
96120312	22	14.2N	83.8E	60	5	34	87	153	220	365	0	10	-5	-15	-20	-15
96120318	23	14.3N	83.3E	55	18	24	62	113	185	358	0	-10	-15	-10	-15	-5
96120400	24	14.4N	82.9E	55	26	65	122	175	252	375	0	-15	-10	-15	-20	-5
96120406	25	14.5N	82.6E	65	46	94	156	222	283	344	0	-5	0	-10	-15	5
96120412	26	14.5N	82.3E	75	52	104	171	238	296	325	-5	0	-10	-15	-15	10
96120418	27	14.5N	82.2E	75	73	122	162	212	274		0	10	-5	-10	-5	
96120500	28	14.5N	82.0E	75	54	105	149	221	270		0	5	-10	-10	-5	
96120506	29	14.4N	81.8E	65	8	30	56	103	117		-10	-5	-5	0	5	
96120512	30	14.2N	81.5E	60	18	34	42	50			-5	-10	-10	-5		
96120518	31	14.0N	81.3E	55	23	36	60	109			0	-5	0	5		
96120600	32	13.8N	81.1E	55	8	26	94	208			0	0	5	10		
96120606	33	13.5N	80.8E	50	5	42	141				0	10	15			
96120612	34	13.0N	80.5E	45	23	89	173				0	5	5			
96120618	35	12.5N	79.8E	35	18	107					0	5				
96120700		12.2N	78.8E	30												
96120706		12.1N	77.5E	20												
96120712		11.9N	76.3E	15												
		AVERAGE			31	78	147	223	310	443						
		# CASES			35	35	34	32	29	26						

7. TROPICAL CYCLONE (TC) SUPPORT SUMMARY

7.1 COMBINED SSM/I- AND IR-DERIVED RAINRATES FOR THE TROPICS

J.F. Turk and J.D. Hawkins
Naval Research Laboratory
Monterey, CA 93943

Infrared (IR) derived rainrate techniques focus on the cloud-top temperatures to infer rain. These IR techniques typically associate colder cloud tops with higher rainrates. However, there are a number of incorrect assumptions associated with this underlying methodology and a number of alternative explanations have been proposed. The method proposed here takes advantage of the superior rainrate measuring capabilities of the DMSP SSM/I sensor and combines it with the advantages of the frequent updates of infrared geostationary imagery and the associated wide synoptic coverage of geostationary imagery.

The technique basically merges the SSM/I imagery and the IR geostationary imagery by a histogram type matching program after collocating geostationary data that has been mapped to the SSM/I type resolutions (in this case 28 km). The rainrates from the SSM/I are matched with the brightness temperatures from the IR imagery when the SSM/I data are available. A data base is created that serves as a reference table for converting IR temperatures to rainrates over a much larger domain than the swath width of the SSM/I pass.

The technique improves when the number of matches between the SSM/I rainrates and the brightness temperatures from the IR imagery in the reference data base is large. The results have been enhanced recently by the fact there are now four (4) operational SSM/Is available. Thus, for each IR image, the method is applied and a rainrate product is created. The resulting image of rainrates can be used for several purposes: a) a snapshot of current rain over a large domain; b) as input to numerical models using the reverse physical initialization technique; and c) to accumulate the rain over time to give a time series of rainrates for a given TC.

The snapshot rainrate picture and a time series animation of the individual images are very informative about the rain in and around a TC. The rainbands and their evolution are the main features displayed. This helps to augment the SSM/I 85-GHz imagery that is the focus of a study on TC structure and intensity. Preliminary results incorporating these rainrates into NOGAPS via physical initialization (Gregg Rohaly) are very promising and are currently undergoing tests.

Accumulation images are enlightening due to the fact that the images readily depict the diurnal maximums associated with the IR signature of TCs. This type of data may help determine which TCs are wet versus dry and alert forecasters to those TCs that can be particularly troublesome from the standpoint of flooding when they reach landfall. Verification studies are ongoing with P-3 airborne radar data in the Atlantic Ocean and with limited NEXRAD sites in the Northwest Pacific Ocean.

7.2 THE AUTOMATED TC FORECASTING SYSTEM

C.R. Sampson and A.J. Schrader
Marine Meteorology Division
Naval Research Laboratory, Monterey CA

The Automated Tropical Cyclone Forecasting (ATCF) System, developed by NRL Monterey, is a computer based application designed to automate and optimize the forecasting process at operational Navy TC

warning centers. ATCF was initially installed on PC DOS-based computers at the JTWC in 1988. ATCF version 3.1, installed at JTWC during 1997, is UNIX-based with an X-Windows interface similar to what is seen in Windows 95 applications. This X-Windows interface has markedly simplified navigation through the system, thereby reducing the time required to generate forecasts. Another significant improvement is that ATCF now allows users to track and forecast many storms concurrently. ATCF continues to attract a great deal of interest and has upgrades scheduled for the next few years. Major highlights for these upgrades include integration of satellite derived products such as cloud and water vapor tracked winds, and a redesign of the tropical cyclone database to allow 120-hour track forecasts and wind radii quadrants.

7.3 GEOPHYSICAL FLUID DYNAMICS-NAVY (GFDN) TC MODEL

M.A. Rennick
FNMOC
Monterey, CA 93943

In May, 1996, FNMOC started running the Navy implementation of the Geophysical Fluid Dynamics Laboratory (GFDL) TC model, GFDN, in support of JTWC. The GFDN is a triple-nested movable mesh model, including initialization, forecast, and diagnostic sections. Some key features include: three computational nests with resolution 1°, 1/3°, and 1/6°, convective adjustment, surface fluxes, second order turbulence, infrared and solar radiation, a bulk subsurface layer, and parameterization of surface features by vegetation type.

The model is initialized from the NOGAPS analysis and the TCBOGUS message issued by JTWC. The TC component is removed from the global analysis, and replaced by a synthetic vortex generated by an axi-symmetric version of the forecast model constrained by the structure indicated by the TCBOGUS message. An asymmetric (beta-advection) component is also added to the synthetic vortex. Boundary conditions are updated periodically from NOGAPS forecast fields.

FNMOC ran GFDN on the off time (06/18Z) watches whenever a TCBOGUS for a western Pacific TC was received. The model applied the highest priority off time TCBOGUS to the off time NOGAPS analyses (available ~ 1015/2215Z) and used the forecast fields from the previous real time (00/12Z) NOGAPS for boundary conditions. These forecasts were available to JTWC by about 1130/2330Z, in time for their subsequent 12/00Z warnings. Beginning 11 September 1996, if JTWC issued more than one western North Pacific TCBOGUS, the second priority message was applied to the preliminary NOGAPS off time analysis (available ~ 0745/1945Z). These forecasts were available by about 0845/2045Z.

The GFDN provided high quality tropical cyclone track guidance in the western Pacific basin. It had excellent detection capability, especially for cyclones of tropical storm intensity or greater. Mean track error decreased with cyclone intensity, while the forecast intensity error increased. Due to its perceived positive impact on the official forecasts, FNMOC now runs GFDN in all basins within JTWC's area of responsibility.

7.4 SSM/I-DERIVED TC STRUCTURE

J.D. Hawkins, J.C. Sandidge, D.A. May, R.J. Holyer, and M.J. Helveston
Naval Research Laboratory
Monterey, CA 93943

Monitoring TC structure, structure change and intensity via visible and infrared

imagery is inherently limited due to upper-level cloud obscuration and the subjective nature of the current Dvorak rules for low-end systems before an eye takes shape. Thus, the satellite analyst has a difficult task of accurately determining the TC structure, structure changes and the associated intensity. This statement is even more true at night, when visible data is not available to assist the analyst and coarse resolution infrared (IR) data is the only consistent data set for utilization.

The Special Sensor Microwave/Imager (SSM/I) is a passive microwave imager onboard the Defense Meteorological Satellite Program (DMSP) platforms. The frequencies utilized by the SSM/I have the ability to penetrate many upper-level clouds allowing for a clearer view of the mid- and lower-level structure within a TC. This is crucial to removing one of the main barriers for effective use of visible/IR imagery. The 85-GHz channel on the SSM/I is of particular interest since the spatial resolution is still fair (12-15 km) and is oversampled, meaning the inherent resolution is superior to 15 km.

The Naval Research Lab in Monterey, California (NRL-MRY) has taken advantage of the 85-GHz channel and the associated sampling pattern by adopting a mapping routine developed by Gene Poe at NRL-DC. This mapping routine can accurately map 85-GHz data at resolutions as fine as 1-2 km. In addition, the mapping routine allows the user to map the SSM/I data to the same resolution as coincident visible/IR data from the Operational Linescan System (OLS) on the DMSP or the corresponding geostationary data at nadir. Our studies reveal the remapped 85-GHz data agrees remarkably well with the features one can analyze in the visible/IR data, when clear cut items are in view (e.g., mesoscale convective clusters, eye, eyewall, and rainbands).

The 85-GHz imagery is able to map the rainbands, eyewall and eye very well since it responds to scattering due to both raindrops and ice particles by virtue of dramatically lowered brightness temperatures. Thus, although cirrus type clouds will preclude an analyst from seeing many or all spiral banding features of interest, the 85-GHz data can clearly depict these dominant items that are necessary for understanding the TC's structure and their changes over time. Time histories of 85-GHz data for a given TC clearly map the evolution of the rainbands, eyewall and eye as the storm develops, matures and then decays.

Of particular interest is the ability to map eyewall cycles. These cycles manifest themselves when the original eye becomes very small and intense. The TC forms a secondary eyewall further out, the circulation supporting the inner eye is cut off and the inner eye collapses. The outer eye then takes over and gradually shrinks in diameter as the storm regains its original structure. Intensity changes are linked to this internal process.

Since the SSM/I can map the TC structure so well, we have developed an automated technique to analyze the 85-GHz imagery and output an estimated TC maximum sustained wind speed. This has been done via a neural network approach where the SSM/I images are represented by Empirical Orthogonal Functions (EOF). Thus, the patterns (e.g., rainbands, eyewall) in the 85-GHz images are contained within the EOFs.

Considerable effort has been expended to create a data base of 85-GHz images of TCs of varying intensity in order to train and validate the neural net. The current data base has over 500 high quality SSM/I images, with which the neural net has used ~ 450 for training and ~ 50 for validation. Earlier efforts suffered from a small data base and limited EOFs that could be used before the neural net encountered memorization problems. In addition, earlier studies revealed that typical RMS errors were > 20 kt when no a priori information was used.

Numerous methods were studied using a priori data in the form of best track intensities (6 or 12 hours before SSM/I image) or the warning intensity at the time of the image. Results improved dramatically as one might expect and RMS errors were 4 and 7 kt respectively.

The latest neural net runs using the expanded 500-set data base now indicate that we can get below the 20-kt RMS error with no a priori knowledge. These results likely indicate that we are approaching the statistical accuracy of the western Pacific best track intensity data base since it is largely based on Dvorak values. We estimate that the limit using this data base is ~ 15 kt.

Work is ongoing to focus on those Atlantic TCs with aircraft reconnaissance and the limited Pacific cases that have high confidence due to additional observations (e.g., islands, ships) being available. These data sets are now being updated in a semi-automated manner during the 1997 season. The SSM/I data are now finding more use for intensity and location related efforts as the capabilities of the 85-GHz data are becoming better understood.

7.5 OPERATIONAL USE OF SCATTEROMETER DATA FOR TCs

J.D. Hawkins, W.L. Jones, L. Rice, and M.J. Helveston
Naval Research Laboratory
Monterey, CA 93943
and
R.T. Edson
Joint Typhoon Warning Center, Guam

Scatterometer surface wind vectors from both ERS-2 and more recently from the NASA Scatterometer (NSCAT) are utilized by JTWC for mapping the ocean surface wind field in and around tropical cyclones (TCs) in a quasi-real-time mode. Scatterometer data continued to show good potential for identifying the early potential of developing TCs and gave JTWC an initial estimate of minimum intensity observed within the system. While both ERS-2 and NSCAT are active sensors, NSCAT offered some potentially superior capabilities due to its inherently better resolution of 25 km versus 50 km for ERS-2 and its two 600-km swaths, instead of the single 500-km swath for the ERS satellites. (Unfortunately the satellite carrying the NSCAT sensor stopped transmitting 30 June 1997).

The double swath coverage afforded daily and sometimes twice daily coverage for all TCs, versus the occasional hit with ERS. Thus, the potential to use the data had grown considerably. During the evaluation, questions related to the frequency differences between the two sensors and how the wind directions are derived were investigated.

NSCAT operated at ~ 15 GHz instead of ~ 5 GHz for ERS and thus was susceptible to heavy rain. Under light wind conditions, heavy rain produced anomalously high wind retrievals; while under strong winds, heavy rain caused lighter than normal winds to be produced. Thus, the user needed to know when rain contamination was occurring. NRL-MRY is continuing to investigate several methods to resolve this issue using both SSM/I and geostationary IR data sets for future NSCAT launches.

The SSM/I produces rainrates over its 1400-km swath that are physically based and have undergone extensive validation in the Precipitation Intercomparison Projects (PIP) efforts. It should be noted several of these cases also included TC-type conditions. However, one rarely gets a reasonable matchup with SSM/I overpasses and NSCAT data. Thus, we have produced a rainfall method that incorporates both SSM/I data and the more frequent geostationary IR data.

Through this method we will be able to identify NSCAT values that are contaminated by rainfall, and then to accurately specify the contamination over each NSCAT cell so as to apply a rainrate correction factor for each wind value.

Selecting wind directions for scatterometers is also difficult, since the current retrieval algorithms produce 2-4 possible vectors. Various methods exist to dealias, or select, one wind direction. This usually involves the first guess from a global model, which is a problem, since most global models do not have the resolution needed to resolve the inner circulation of a TC. A number of techniques are under study to determine how best to dealias the NSCAT data with as little dependence from models as possible.

7.6 CONTINUED STUDY OF WIND DISTRIBUTION FORECAST CAPABILITIES AT JTWC

C. P. Guard
ONR-sponsored Research at University of Guam
Mangilao, Guam 96923

While US and international TC warning centers have performed forecast verifications for decades, the verifications have primarily been limited to the forecast position and intensity. There has been a reluctance to-date by the warning centers to validate the predicted distribution of the over-water gale-, storm-, and hurricane-force near-surface winds. This reluctance has resulted in little formal documentation of the extent of the ability of the centers to forecast the surface wind distribution. A study was initiated in 1995 to ascertain the characteristics of JTWC TC wind distribution forecasts. The study was continued in 1996, and in addition, a preliminary evaluation of the wind distribution output of the GFDN model. The research has revealed several interesting and important characteristics of the wind distribution forecasts.

The operational warning time wind distribution was found to be of insufficient quality to use as the verification source. This required a comprehensive reanalysis of the actual wind field data in order to develop a validation data base. Several sources of data were used, and the analyses were checked both for spatial and temporal consistency. JTWC hand-plotted surface-gradient composite analyses, sectional charts, hand-plotted time sections, and raw data messages were the primary sources of conventional data. Also, Doppler radar, scatterometer, and microwave imager remote-sensing data were used.

A statistical breakdown of the data sources used to verify the 35- and 50-kt (17- and 26-m/sec) wind revealed that the most common data source for verification of 35-kt winds (17-m/sec) was ship data and for 50-kt (26-m/sec) winds was land observations. In 1995, ERS-1 scatterometer data were evaluated as a validation source and was found to be very good. As a result, scatterometer became a major source of over-water validation data. To put the wind distribution errors in perspective with the total forecast, wind distribution errors were compared with the average annual JTWC track forecast errors for the various forecast periods. The 1996, results were similar to the 1995 results. Major findings are summarized below:

a. Absolute wind distribution errors

An accurate initial analysis is highly favorable for an accurate subsequent wind distribution forecast; in the < 24-hour forecast periods, the total wind distribution forecast error is comprised nearly equally from track forecast error and error in determining the extent of the winds; at 72-hr, the track forecast error contributes 6-8 times more to the total error than does the 72-hr wind analysis error;

and, thus, after 24 hours, the track error becomes the greatest contributor to the overall wind distribution error.

b. Average wind distribution forecast error (bias)

In general, the bias shows that in 1995, JTWC under-analyzed and under-forecast the strong sector wind distribution and over-analyzed and over-forecast the weak sector wind distribution, thus under-forecasting the asymmetry. In 1996, there was a tendency to under-analyze and under-forecast both sectors for 35-kt (17 m/sec) wind distribution. For the 50-kt (26 m/sec) wind distribution, the tendency was to under-forecast both sectors, even though the weak sector winds were over analyzed.

7.7 A PRELIMINARY STUDY OF GFDN-GENERATED WIND DISTRIBUTION FORECASTS

C. P. Guard
ONR-sponsored Research at University of Guam
Mangilao, Guam 96923

The GFDN, the Navy adaptation of the GFDL high resolution hurricane model, provides a graphic display of the wind distribution predicted by the model. A preliminary study was conducted to assess the accuracy of the GFDN wind distribution predictions. The validation data base was taken from the study on JTWC wind distribution forecast capabilities. The absolute and average forecast errors were compared with those of the JTWC. The preliminary findings of the study are: (1) the model significantly under-forecast the strong sector winds and over-forecast the weak sector winds (to a lesser extent) for 35-kt (17 m/sec) winds, thus under-forecasting the asymmetry; (2) for 50-kt (26-kt m/sec) winds, both the strong and weak sectors were under forecast. The study also revealed that there were some boundary problems with the output that have since been corrected.

7.8 PROGRESS ON A RESEARCH QUALITY, CONFIDENCE-BASED TC INTENSITY DATA BASE

C.P. Guard and M.A. Lander
ONR-sponsored Research at University of Guam
Mangilao, Guam 96923

Work continued on the confidence-based TC intensity data base (IDB). This data base is needed because, in general, TC best-track (BT) IDBs are not of sufficient quality to be used as validation data for TC intensity research. There are several reasons for this shortfall, the most basic reason being that there is no way to discern the quality of the data on which a specific BT intensity is based. Different data platforms provide intensity data of varying accuracy, and from this knowledge, one can infer a certain level of confidence in that data.

a. Methodology of data base development

After determining the need for improving the JTWC IDB, a list of reasons for the needed changes was compiled. Examples of these are: landfall data not originally available, re-analysis of aircraft data, etc. Then, various data types were assessed for their accuracy in providing surface wind speeds, and each type was assigned a relative confidence value. Next, the JTWC "fix files" were reassessed and corrected where possible. Landfall data are being obtained from other countries, and these are being incorporated into the fix data base from which the IDB is developed. Translation speed, stability considerations, intensity spin up-spin down considerations, and appropriate wind-pressure relationships are also being used to make corrections.

b. Proposed Format and Availability

Once modifications are made, they will be put into a new data base, modified slightly from that of the preexisting JTWC BT data base. In addition to the data available in the JTWC format, the modified format includes the updated intensity value, the magnitude of the change, the coded reason for the change, and the relative accuracy or confidence of the intensity value. Initially, the data base will include data from the 1990s. Eventually, it will be expanded to the 1980s, 1970s, and earlier periods. The data base will reside on a web page in late 1997, and will be periodically updated as new data becomes available.

7.9 A WIND-PRESSURE RELATIONSHIP FOR MIDGET TCs IN THE WESTERN NORTH PACIFIC

C.P. Guard and M.A. Lander
ONR-sponsored Research at University of Guam
Mangilao, Guam 96923

A new wind-pressure relationship (WPR) that relates maximum sustained surface winds in TCs to the minimum central pressure has been developed for western North Pacific (WNP) midget TCs. Midget TCs have a high intensity inner core where the outer winds are from the inertial spin down of the belt of maximum winds. There is no outer core. The WPR was based primarily on carefully selected data of midget TCs making landfall on islands and coastal areas of the WNP. Some aircraft data were used where the small TC size could be confirmed and where it was clear that the aircraft was in the strong sector of the TC. The new WPR indicates that these small TCs can have the same winds as larger TCs, but with a 10-17 mb higher central pressure, which corresponds to a 10-20-kt difference in wind speed. It also indicates that as the intensity approaches 130 kt (62 m/sec), the WPR converges with the WPR used for more normal sized TCs. This is because the midget TC usually acquires outer core characteristics.

The regression equation for the new WPR (for WNP midget TCs) is:

$$\mathrm{Vmax} = 17.548(\mathrm{Pn}-\mathrm{Pc})^{0.4345}$$

Table 7-1 relates the maximum sustained wind with the minimum central pressure given by the new WPR (with Pn = 1010 mb) and that given by the Atkinson-Holliday WPR (Atkinson and Holliday 1977).

Table 7-1 A comparison of the maximum sustained winds (Vmax) with the minimum central pressure (Pc) in millibars for (a) midget TCs (new WPR) and (b) normal-sized TCs (Atkinson-Holliday WPR) (A & H).

Vmax	Pc midget	Pc A & H	Vmax	Pc midget	Pc A & H
30		1000	**105**	949	939
35		997	**110**	943	934
40	1003	994	**115**	935	928
45	1002	991	**120**	928	922
50	1000	988	**125**	919	916
55	994	984	**130**	910	910
60	992	980	**135**	904	904
65	989	976	**140**	898	898
70	986	972	**145**	892	892
75	982	968	**150**	886	886
80	978	964	**155**	879	879
85	972	959	**160**	872	872
90	965	954	**165**	865	865
95	960	949	**170**	858	858
100	955	944			

7.10 A STUDY OF TC INTENSITY CHANGES USING THE DIGITAL DVORAK ALGORITHM

M. A. Lander
ONR-sponsored research at University of Guam
Mangilao, Guam 96923

One of the utilities installed in the JTWC's MIDDAS satellite image processing equipment is an automated routine for computing Dvorak "T" numbers for tropical cyclones that possess eyes. The routine, developed by Zehr (personal communication), adapts the rules of the Dvorak technique as subjectively applied to enhanced infrared imagery (Dvorak 1984) in order to arrive at an objective T number, or "digital Dvorak" T number (hereafter referred to as DD numbers). Infrared imagery is available hourly from the GMS satellite, and hourly DD numbers were calculated for all of the typhoons of 1996 (and for some of the typhoons of 1995).

A preliminary study of the time series of the DD numbers shows that, in some cases, they differ substantially from the warning intensity and also from the subjectively determined T numbers obtained from application of Dvorak's technique. The output of the DD algorithm, when performed hourly, often undergoes rapid and large fluctuations. If the DD numbers truly represented rapid (on the order of 3 to 6 hours) intensity fluctuations with magnitudes (30-40 kt) as large as seen with some typhoons, there are two topics for further research: (1) how are the extremely rapid fluctuations of estimated intensity, if they are genuine, to be incorporated into the warning? And, (2) how can the best tracks, having had these rapid fluctuations removed, be used to study the processes governing what may prove to be real intensity fluctuations of the magnitude indicated by the DD numbers?

Another characteristic of the time series of the DD numbers emerges for most of the very intense typhoons: the DD numbers rise more quickly, and peak earlier, than do the subjectively determined T numbers. Also, within 24 hours of the peak, the DD numbers rapidly decrease to values as low as two T numbers below their peak value. A recovery is then observed before the DD numbers fall once again as the TC recurves and becomes extratropical. The cause of the rapid drop of the DD numbers after peaking is identifiable in nearly all cases of this phenomenon as the result of the formation of concentric eye wall clouds. A relatively precipitation-free moat forming between the concentric wall clouds causes the DD algorithm to yield a greatly reduced T number. When the outer wall cloud contracts and the inner wall cloud dissipates, the DD numbers rise. The behavior of the DD numbers may serve to highlight processes (such as eye wall replacement) and lead to a better understanding of them.

7.11 A LOOK AT GLOBAL TC ACTIVITY DURING 1995: CONTRASTING HIGH ATLANTIC ACTIVITY WITH LOW ACTIVITY IN OTHER BASINS

M.A. Lander and C.P. Guard
ONR-sponsored research at University of Guam
Mangilao, Guam 96923

The 19 named TCs in the North Atlantic (NAT) during 1995 were nearly a record for that basin. During the past three decades, only the year 1969 — with its 18 TCs of at least tropical storm intensity — was nearly as prolific. During 1995 and 1969 (two years that have been designated herein as "prolific" years in the NAT), the annual number of TCs in most of the other TC basins was well-below normal (to such an extent that even the annual global number of TCs during these two years

was below normal). Despite the strong reduction of the annual number of TCs in most basins during the aforementioned NAT prolific years, there is no overall correlation between the annual number of TCs in the NAT and the annual number of TCs in any other major TC basin [i.e., the western North Pacific (WNP), eastern North Pacific (ENP), and Southern Hemisphere (SH)]. In fact, the only statistically significant correlations of annual numbers of TCs are weak positive correlations between the WNP and the ENP, between the SH and the WNP, and between the SH and the ENP. These weak positive correlations act to increase the variance of the annual global number of TCs.

There are only two large-scale atmospheric phenomena [i.e., ENSO and the Quasi-Biennial Oscillation (QBO)] that have been documented to have an effect on the annual number of TCs in the NAT and within the other TC basins. It has been shown that only within the NAT are the magnitude of these relationships strong. In all other major basins, the ENSO and the QBO have little, if any, effect on the annual number of TCs (although the formation regions of TCs within the WNP and the SH are shifted quite markedly by ENSO).

The global distribution of TCs during the NAT prolific years of 1969 and 1995 stands quite apart from the long-term relationships noted between the annual number of TCs in the NAT with the annual number of TCs in the other major TC basins. The ENSO and QBO can not alone account for the unusual distribution of TCs during 1969 and 1995. In fact, 1969 is considered by some to have been an El Niño year, while the global climatic anomalies during 1995 were considered by some to be representative of the cold phase of ENSO (i.e., La Niña). The only apparent commonality between 1969 and 1995 was that the QBO was in a westerly phase, a large-scale atmospheric condition experienced approximately once every two years.

The NAT prolific year of 1995 need not herald the return to a higher number of NAT TCs such as has been documented to have occurred during the decades of the 1940s through 1960s. In fact, the NAT prolific year of 1969 was, in retrospect, a "herald" of lower NAT TC activity during the 1970s through the 1980s. It is hypothesized that NAT prolific years such as 1995 and 1969 will always be a characteristic of the NAT time series, regardless of inter-decadal changes in the average annual number of TCs in the NAT.

That the NAT prolific year of 1995 was a signal of global climate change is unlikely, considering that the phenomenon has occurred in the past, and that the global distribution of TCs during the previous NAT prolific year —1969 — was so strikingly similar. Based on the peculiar similarities between the global TC distribution of 1969 and 1995, it is hypothesized that the phenomenon of NAT prolific years (accompanying "meager" years in other basins) has its roots in a specific (but infrequent) state of the global atmosphere which does not appear to be related to ENSO, the QBO, inter-decadal changes in the annual number of TCs in the NAT, or long-term global climate change. Its mechanism remains a mystery.

7.12 UPDATING TC SATELLITE-DERIVED POSITION CODE NUMBER CRITERIA USED BY JTWC

T.R. Crume
Satellite Operations, Nimitz Hill, Guam
and
M.A.. Lander
ONR-sponsored research at University of Guam
Mangilao, Guam 96923
and
R.T. Edson
Joint Typhoon Warning Center, Guam

In order to construct an accurate track history of a given TC from the many fixes obtained, it is desirable to have a methodology for determining not only the position, but also the reliability of that position. The Special Projects Section of Detachment 1, First Weather Wing (1WW) developed and published such a methodology in Pamphlet 105-10 (1WWP 105-10) entitled, Tropical Cyclone Position and Intensity Analysis Using Satellite Data (Arnold and Olsen 1974). One of the terms introduced in 1WWP 105-10 was Position Code Number (PCN). The PCN indicates the expected accuracy of the reported position. There are six PCNs: TCs with eyes (PCN 1 and 2); well defined circulation centers (CC) (PCN 3 and 4); and, poorly defined CC (PCN 5 and 6). Odd-numbered PCNs indicate geographical navigation of the gridding. Even-numbered PCNs indicate the gridding was based on satellite ephemerides alone.

Given the advances in technology, both in terms of image processing capabilities and the addition of new spectral windows, the process of assigning PCNs to TC fixes needs to be updated and improved. Specifically, the following recommendations are offered:

(1) the guidance currently available for determining PCNs should be updated to reflect changes in advances in technology and the decrease in the relative numbers of PCNs 3 and 4,

(2) a systematic categorization of fix types linked to specific PCNs (this includes concise documentation of the cloud features, sensor types, and specific image processing methodologies used to make the fix), should be made and

(3) the relative accuracy of the fixes from the new image categories requires validation.

Satellite Operations is currently using a newly developed list of PCN categories. After a year, the error statistics of the PCN categories will be examined.

7.13 A TECHNIQUE FOR ESTIMATING THE INTENSITY OF TCs WHICH ARE UNDERGOING EXTRATROPICAL TRANSITION

D.W. Miller
Satellite Operations, Nimitz Hill, Guam
and
M.A. Lander
ONR-sponsored research at University of Guam
Mangilao, Guam 96923

A review of western North Pacific synoptic data from 1994 through 1996 revealed that the intensity estimates of a significant number of typhoons that became extratropical were underestimated by the tropical satellite reconnaissance network using Dvorak's (1975, 1984) techniques. Occasional use of Hebert and Poteat's (H&P) (1975) technique for estimating the intensity of subtropical cyclones on these recurving typhoons also resulted in intensity estimates which were too low.

The application of Dvorak's techniques to TCs undergoing extratropical transition resulted in the intensity being underestimated by as much as three T numbers below the actual intensity as verified by synoptic data (good examples of this problem are described in Seth's summary in the 1994 ATCR; and in Dan's (06W) summary in this ATCR).

A technique to address the underestimation of the intensity of TCs which are undergoing extratropical transition (XT) was developed. The XT technique borrows from both Dvorak and H&P in the application of the log10 spiral to the primary outer cloud band, and, as in H&P, an incorporation of the effects of excess translational speed. Additional factors include: the degree of organization of the central and peripheral low- and mid-level clouds, and the extent of any resid-

ual or regenerative deep convection between the LLCC and the primary outer cloud band. These four factors are evaluated for wind speed contributions in the final determination of the "XT" number. The XT technique is an additive process whereby the TC intensity is derived from the addition of contributions from each of the applicable factors. There is a direct equivalence of Dvorak T numbers and XT numbers. The XT technique should be used until the satellite imagery indicates that the system has completed its transition into an extratropical cyclone. At that point it is recommended that a technique developed by Smigielski and Mogil (1992) for the estimation of the central SLP of extratropical cyclones be used if continued analysis is warranted. Further details of the XT technique are found in Miller and Lander (1997).

7.14 ON THE ABILITY OF OPERATIONAL DYNAMIC MODELS TO PREDICT TC INTENSITY

M.A.. Lander
ONR-sponsored research at University of Guam
Mangilao, Guam 96923

For many years, operational dynamic models have been used to predict TC motion. In this area, the dynamic models generally out-perform baseline statistical measures of skill (e.g., CLIPER), and a steady improvement in their skill has been observed. More recently, increases in the spatial resolution, better physics, and (in some cases) improved bogussing techniques have rendered them capable of simulating TCs with realistic horizontal and vertical structure (e.g., a small region of very low pressure accompanied by high winds close to the low pressure center, and an outdraft cyclonic circulation in the upper troposphere). These dynamic models also have shown realistic genesis and development of TCs such as the deepening of tropical depressions to typhoons within credible time spans. The intensity diagnoses and intensity forecasts of TCs in the western North Pacific (WNP) during 1996, made by several operational dynamic models (for which the analyzed and forecast intensity of TCs was routinely available at the JTWC, Guam), are evaluated with respect to the final best-track intensities produced by the JTWC. Dvorak (1975, 1984) observed that, on average, TCs intensify at a rate of one so-called "T" number per day. Each rise of a T number represents a 10-15-mb increase of intensity at the lower T numbers, to increases of approximately 30 mb per T number at the higher T numbers. Dvorak also categorized fast and slow development as an increase of 1.5 T numbers per day and 0.5 T numbers per day respectively. Additional categorizations of TC rates of intensification are rapid deepening (Holliday and Thompson 1979) and explosive deepening (Dunnavan 1983); these are 24-hr central pressure drops of at least 1.75 mb/hr for at least 12 hours and 2.75 mb /hr for at least 6 hours respectively. The results presented herein are based upon a preliminary examination of the dynamic model's (and JTWC's) ability to predict the 24-, 48- and 72-hour intensities of several of the WNP TCs of 1996. The only statistic evaluated was a simple comparison of the models' intensity trends with the intensity trends derived from the JTWC best tracks. Intensity trends were evaluated in a permutation of several forecast intervals: 0 to 24 hours, 0 to 48 hours, 24 to 48 hours, etc. A model's intensity prediction was scored as correct if its trend was in the same direction as the best track; even if the model changed by only 1 mb in the right direction and the best track changed by 70 mb. A model's intensity prediction was scored as incorrect if the trend was against the best track; no change in model intensity was scored as incorrect if the best track exhibited

any change. Examination of the intensity output of the various dynamic models also reveals some general characteristics. At the 0- to 24-hour forecast interval and the 0- to 48-hour forecast interval, most of the models have only modest skill over a random choice. At the extended forecast period of 48 to 72 hours, most of the models show no skill over a random choice. In fact, most of them are more often incorrect than correct. There are also large differences of skill from one TC to another.

Upon closer examination of the behavior of the model predictions of intensity, it is seen that the global spectral models have very small magnitudes of intensity change, while the regional models (e.g., GFDN), with their finer resolution and different physics packages, exhibit magnitudes of intensity change that are realistic. Also, the regional models have consistently higher skill over the global models at all permutations of forecast intervals. Further research is warranted to see if the models have any skill in flagging deviations of intensification from normal rates (e.g., rapid deepening, explosive deepening, and non-developing). A complete study of objective prediction of TC intensity must also include statistical intensity prediction schemes.

7.15 WATER VAPOR AND HIGH RESOLUTION VISUALLY TRACKED WINDS FOR TC APPLICATIONS

T.L. Olander
S.T. Wanzong
C.S. Velden
Cooperative Institute for Meteorological Satellite Studies, University of Wisconsin
Madison, Wisconsin
and
J.D. Hawkins
Naval Research Laboratory
Monterey, CA 93943
and
R.T. Edson
Joint Typhoon Warning Center, Guam

Upper-level water vapor winds (Velden et al. 1997) and low-level cloud motion winds from high-resolution visible satellite imagery were derived and evaluated. These winds are derived from sequences of GMS-5 imagery accessed through the Bureau of Meteorology in Australia. Water vapor wind data sets were produced nominally at 12-hour intervals (00 and 12Z). However, during TC events, the frequency was increased to 6 hourly. The data sets were provided via Internet to JTWC for real time analysis. The data sets were also provided to FNMOC for inclusion into the operational NOGAPS model beginning in late July. Indications are the winds have made an immediate impact (improvement) on the NOGAPS upper-level analyses over the western North Pacific.

Special water vapor wind data sets were also produced over the Indian Ocean region during Naval exercises. These data sets were helpful in forecasting conditions for both the exercises, and TC monitoring in that region.

In 1996, UW-CIMSS began experimenting with a new product derived from sequences of high-resolution GMS visible imagery. Fields of high density, low-level cloud-tracked winds were derived and disseminated to JTWC for their evaluation. The fields were produced in the genesis region surrounding Guam at 00Z daily. However, during TC events the data set center was programmed to "float" with the center of the TC to provide coverage in the immediate TC environment. While several minor problems were discovered with the product, the winds show promise with further R&D to provide information on both TC genesis and size.

BIBLIOGRAPHY

Arakawa, H., 1952: Mame Taifu or midget typhoon (small storms of typhoon intensity). *Geophysical Magazine*, **24**, pp 463-474.

Arnold, C.P., and C.C. Olsen, 1974: Tropical cyclone position and intensity analysis using satellite data. First Weather Wing Pamphlet 105-10, 97 pp.

Atkinson, G.D., and C.R. Holliday, 1977: Tropical cyclone minimum sea-level pressure and maximum sustained wind relationship for the western North Pacific. *Mon. Wea. Rev.*, **105**, No. 4, pp 421-427 (also Fleet Weather Central/JTWC Technical Note 75-1).

Black, P.G., 1983: Tropical storm structure revealed by stereoscopic photographs from Skylab. Adv. Space Res., 2, pp 115-124.

______, and F.D. Marks, Jr., 1987: Environmental interactions associated with hurricane supercells. Proc. 17th Conf. on Hurricanes and Tropical Meteor., Miami, Amer. Meteor. Soc., pp 416-419.

______, and F.D. Marks, 1991: The structure of an eye wall meso-vortex in Hurricane Hugo (1989). Preprints, 19th Conf. on Hurricanes and Tropical Meteor., AMS, Miami, FL, pp 357-358.

______, ______, and R.A. Black, 1986: Supercell structure in tropical cyclones. Proc. 23d Conf. on Radar Meteor., Snowmass, Colorado, Amer. Meteor. Soc., pp 255-259

Brand, S., 1972: Very large and very small typhoons of the western North Pacific Ocean. *J. Meteor. Soc. Japan*, **50**, pp 332-341.

Carr, L.E., and R.L. Elsberry, 1994: Monsoonal interactions leading to sudden tropical cyclone track changes. *Mon. Wea. Rev.*, **123**, pp 265-289.

______, and ______, 1994: Systematic and integrated approach to tropical cyclone track forecasting, Part I: Description of basic approach. Naval Postgraduate School publication NPS-MR-002. Naval Postgraduate School, Monterey, CA 93943. 65 pp. plus figs. and append.

______, M.A. Boothe, S.R. White, C.S. Kent, and R.L. Elsberry, 1995: Systematic and integrated approach to tropical cyclone track forecasting. Part II: Climatology reproducibility, and refinement of meteorological knowledge base. Naval Postgraduate School, Monterey, CA 93943, 96 pp.

Climate Prediction Center, 1996: Monthly 850-mb and 200-mb wind anomalies. Climate Diagnostics Bulletin. U.S. Prediction Center Dept of Commerce, Washington, D.C. monthly bulletins.

Crume, T.R., and M.A. Lander, 1997: Updating tropical cyclone satellite-derived Position Code Number criteria. JTWC/SATOPS Technical Note 97-001.

Davidson, N.E., and G.J. Holland, 1987: A diagnostic analysis of two intense monsoon depressions over Australia. *Mon. Wea.. Rev.*, **115**, pp 380-392.

Desai, B.N., and Koteswaram, P., 1951: Air masses and fronts in the monsoon depressions in India. Indian J. Meteorol. Geophys. 2, pp 250-265.

Dunnavan, G.M., 1981: Forecasting intense tropical cyclones using 700-mb equivalent potential temperature and central sea-level pressure. NOCC/JTWC Technical Note 81-1, 12 pp.

Dvorak, V.F., 1975: Tropical Cyclone intensity analysis and forecasting from satellite imagery. *Mon. Wea. Rev.*, **103**, pp 420-430.

______, 1984: Tropical Cyclone intensity analysis using satellite data. NOAA Tech. Rep. NESDIS 11. US Dept. of Commerce, 46 pp.

Ebert, E.E., and G.J. Holland, 1992: Observations of record cold cloud-top temperatures in Tropical Cyclone Hilda (1990). *Monthly Weather Review*, **120**, 2240-2251.

Emanuel, K.A., 1988: The maximum intensity of hurricanes. J. Atmos. Sci., 45, pp 1143-1155.

Glass, M., and G.W. Felde, 1990: Tropical storm structure analysis using SSM/I and OLS data. 5th Intl. Conf. on Interactive and Info. Processing Systems for Meteor., Oceanogr. and Hydrol., Anaheim, CA, Amer. Meteor. Soc., pp 432-437.

Gray, W.M., 1978: Hurricanes: their formation, structure and likely role in the tropical circulation. Meteorology over the tropical oceans, Roy. *Meteor. Soc.*, pp 155-218.

Hebert, P.H., and K.O. Poteat, 1975: A satellite classification technique for subtropical cyclones. NOAA Technical Memorandum NWS SR-83, 25 pp.

Holland, G.J., 1980: An analytical model of wind and pressure profiles in hurricanes. *Mon. Wea. Rev.*, 108, No. 8, pp 1212-1218.

______, **1987:** [Tropical cyclone] mature structure and structure change. A Global View of Tropical Cyclones. R.L. Elsberry, Ed. [Limited edition publication sponsored by the U.S. Navy, Office of Naval Research].

______, **and M.A. Lander, 1993:** The meandering nature of tropical cyclone tracks. *J. Atmos. Sci.*, **50**, 1254-1266.

Holliday, C.R., and A.H. Thompson, 1979: Climatological characteristics of rapidly intensifying typhoons. *Mon. Wea. Rev.*, **107**, No 8, pp 1022-1034.

JMA, 1976: The north-oriented track type. Forecasting Manual for Typhoons, [English version], Available in English or Japanese from the Japan Meteorological Agency, 1-3-4 Ote-machi, Chiyoda-ku, Tokyo, Japan, pp 194-197.

JTWC, 1993: Illustration of the cloud distribution in a monsoon depression. 1993 Annual Tropical Cyclone Report, JTWC, p 130. [NTIS AD A285097].

Keen, R.A. 1982: The role of cross-equatorial tropical cyclone pairs in the Southern Oscillation. *Mon. Wea. Rev.*, 110, pp 1405-1416.

______, **1988:** Equatorial westerlies and the Southern Oscillation. *Proceedings of the U.S. TOGA workshop on western Pacific air-sea interaction, U.S. TOGA Report No. 8*, UCAR, Boulder, CO, 207pp.

Kepert, J.D., and C.W. Fairall, 1993: The impact of sea spray on the tropical cyclone boundary layer. Paper presented at *The Fourth Internation Conf. on S. Hemisphere Meteor. and Oceanog.*, Hobart, Australia.

Laing, A.K., 1994: Features of marine wind fields over New Zealand waters from ERS-1 scatterometer data. *NZ J. Mar. Freshwater Res.*, **28**, pp 365-378.

______, **and E. Brenstrum, 1996:** Scatterometer observations of low-level wind jets over New Zealand coastal waters. *Weather and Forecasting*, **11**, 458-475.

Lander, M.A., 1990: Evolution of the cloud pattern during the formation of tropical cyclone twins symmetrical with respect to the equator. *Mon. Wea. Rev.*, **118**, No. 5, pp 1194-1202.

______, **1994a:** Description of a monsoon gyre and its effects on the tropical cyclones in the western North Pacific during August 1991. *Weather and Forecasting*, **9**, pp 640-654.

______, **1994b:** An exploration of the relationships between tropical storm formation in the Western North Pacific and ENSO, *Mon. Wea. Rev.*, **122**, No. 4, pp 636-651.

______, **1996:** Specific tropical cyclone track types and unusual tropical cyclone motions associated with a reverse-oriented monsoon trough in the western North Pacific. *Weather and Forecasting*, 11, No. 2, pp 170-186.

______, **and G.J. Holland, 1993:** On the interaction of tropical-cyclone scale vortices. I: Observations. *Quart. J. Roy. Meteor. Soc.*, **119**, pp 1347-1361.

Lighthill, J., G. J. Holland, W. M. Gray, C. Landsea, G. Craig, J. Evans, Y. Kurihara, and C. P. Guard, 1994: Global Climate Change and Tropical Cyclones. *Bull. Amer. Meteor. Soc.*, **75**, pp 2147-2157.

Luther, D.S., D.E. Harrison, and R.A. Knox, 1983: Zonal winds in the central equatorial Pacific and El Niño. *Science*, **222**, pp 327-330.

Marks, F.D. Jr., and R.A. Houze Jr., 1984: Airborne Doppler radar observations in Hurricane Debby. *Bull. Amer. Meteor. Soc.*, **44**, pp 1296-1317.

Matsumoto, C.R., 1984: A statistical method for one- to three-day tropical cyclone track prediction. Department of Atmospheric Science Paper No. 379, Colorado State University, Fort Collins, CO 80523, 201 pp.

Meighan, P.J., 1987: Radar observations of tropical cyclones. M.S. thesis, Melbourne University, 297 pp. [Available from the author at Bureau of Meteorology, PO Box 1289K, Melbourne, Vic, 3001, Australia.]

Merrill, R.T., 1984: A comparison of large and small tropical cyclones. *Mon. Wea. Rev.*, **112**, pp 1408-1418.

Miller, D.W., and M.A. Lander, 1997a: Intensity estimation of tropical cyclones during extratropical transition. JTWC/SATOPS Technical Note 97-002.

______, **and** ______, **1997b:** Tropical cyclone positioning using Microwave Imagery. JTWC/SATOPS Technical Note 97-002.

Morrissey, M.L., 1988: An evaluation of COADS ship reports in the western North Pacific, *J. Climate.*

Mundell, D.B., 1990: Prediction of tropical cyclone rapid intensification events. Thesis for fulfillment of Master's degree submitted to Colorado State University, Fort Collins, CO 80523, 186 pp.

OFCM, 1993: National Hurricane Operations Plan, U.S. Dept. of Commerce, Washington, D.C., p E-1.

Orville, R.E., and R.W. Henderson, 1986: Global distribution of midnight lightning, September 1977 to August 1978. *Mon. Wea. Rev.*, 114, pp 2640-2653.

Quilfen, Y., 1992: Validation and quality of ERS-1 data: Scatterometer wind data. *Proc. the ERS-1 Geophysical Validation Workshop*, Penhors, France, European Space Agency, pp 107-112.

Ramage, C.S., 1971: Monsoon Meteorology. Academic Press, 296 pp.

______, 1974: The typhoons of October 1970 in the South China Sea: Intensification, decay and ocean interaction. *J. Appl. Meteor.*, **13**, pp 739-751.

______, 1986: El Nino. *Scientific American,* May Issue, pp 77-84.

Ramanathan, K.R., and Ramakrishnan, K.P., 1932: The Indian southwest monsoon and the structure of depressions associated with it. *Mem. India Meteorol. Dept.,* **26**, pp 13-36.

Ramaswamy, C., 1969: The Problem of the Indian Southwest Monsoon. Indian Geophys. Union, Hyderabad, India.

Sadler, J.C., 1967: The tropical upper tropospheric trough as a secondary source of typhoons and a primary source of trade wind disturbances. Final Report, contract No. AF 19(628)-3860, HIG Report 67-12, Hawaii Institute of Geophysics, University of Hawaii, Honolulu, HI 96822, 44 pp.

______, 1975: The upper circulation over the global tropics. UHMET Pub. 75-05. Department of Meteorology, University of Hawaii, Honolulu, HI 96822.

______, 1976: A role of the tropical upper tropospheric trough in early season typhoon development. *Mon. Wea. Rev.*, 104, pp 1266-1278.

______, 1978: Mid-season typhoon development and intensity changes and the tropical upper tropospheric trough. *Mon. Wea. Rev.*, **106**, pp 1137-1152.

______, M.A. Lander, A.M. Hori, and L.K. Oda, 1987: Tropical Marine Climatic Atlas, Vol II, Pacific Ocean. UHMET 87-02, Department of Meteorology, University of Hawaii, Honolulu, HI 96822, 14 pp.

Shanghai Typhoon Institute, 1990: *Climatological Atlas for Northwest Pacific Tropical Cyclones.* China Meteorological Press, 316 pp.

Shoemaker, D.N., 1991: Characteristics of tropical cyclones affecting the Philippine Islands. NOCC/JTWC Technical Note 91-01, 35 pp.

Smigielski, F.J., and H.M. Mogil, 1992: A Systematic Satellite Approach For Estimating Central Pressures Of Mid-Latitude Oceanic Storms. NOAA Technical Report. NESDIS 63. U.S. Department of Commerce.

Stewart, S.R., and S.W. Lyons, 1996: A WSR-88D radar view of Tropical Cyclone Ed. *Weather and Forecasting*, **11**, pp 115-135.

______, J. Simpson, and D. Wolff, 1997: Convectively-induced mesocyclonic vortices in the eyewall of tropical cyclones as seen by WSR-88D Doppler radars. Preprints,22nd Conf. on Hurricanes and Tropical Meteor., AMS, Ft. Collins, CO.

Taiwan Central Weather Bureau. 1982: Methods of Typhoon Forecasting in Taiwan Republic of China. Central Weather Bureau, Taipei, Taiwan, 27pp.

Tsui, T. L. and R. J. Miller, 1988: Evaluation of western North Pacific tropical cyclone objective forecast aids. *Weather and Forecasting*, **3**, No. 1, pp 76-85.

Velden, C.S., C.M. Hayden, S.J. Nieman, W.P. Menzel, S. Wanzong and J.S. Goerss, 1997: Upper tropospheric winds derived from geostationary satellite water vapor observations. February issue of *Bull. Amer. Meteor. Soc.*

Wakimoto, R.M., and P.G. Black, 1993: Damage survey of Hurricane Andrew and its relationship to the radar-detected eyewall. Proc. 20th Conf. Hurr. and Trop. Meteor., San Antonio, Texas, Amer. Meteor. Soc., pp 54-57.

Weir, R.C., 1982: Predicting the acceleration of northward-moving tropical cyclones using upper-tropospheric winds. NOCC/JTWC Technical Note 82-2, 40 pp.

Willoughby, H.E., 1990: Temporal changes in the primary circulation in tropical cyclones. *J. Atmos. Sci.*, **47**, pp 242-264.

______, J.A. Clos, and M.G. Shoreibah, 1982: Concentric eye walls, secondary wind maxima, and the evolution of the hurricane vortex. J. Atmos. Sci., 39, pp 395-411.

Xu, Y., and C.J. Neumann, 1985: A statistical model for the prediction of western North Pacific tropical cyclone motion. NOAA Technical Memorandum NWS NHC 28, 30 pp.

Zehr, R.M., 1992: Tropical cyclogenesis in the western North Pacific. NOAA Technical Report, NESDIS 61, U.S. Dept. of Commerce, Washington DC, 181 pp.

APPENDIX A
DEFINITIONS

BEST TRACK - A subjectively smoothed path, versus a precise and very erratic fix-to-fix path, used to represent tropical cyclone movement, and based on an assessment of all available data.

BINARY INTERACTION - A mutual cyclonic orbit of two tropical cyclones around their centroid. Lander and Holland (1993) showed that the behavior of most binary tropical cyclones consists of an approach, sudden capture, then a period of steady cyclonic orbit followed by a sudden escape or (less frequently) a merger (see Figure A-1).

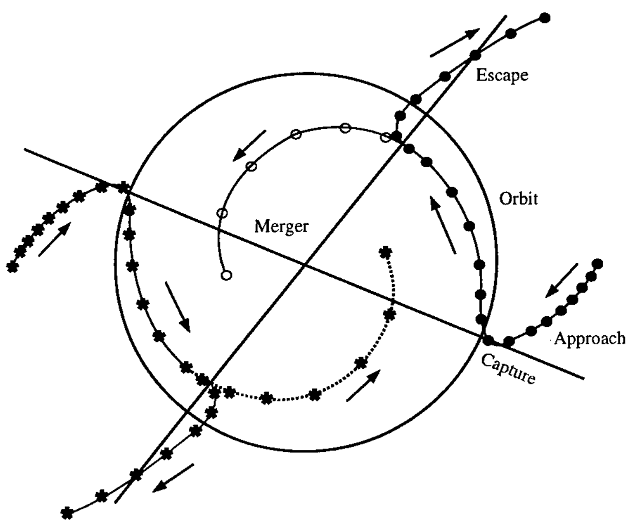

Figure A-1 Model of binary interation of two tropical cyclones that contain the major elements of approach and capture, followed by mutual orbit, then escape, or merger.

CENTER - The vertical axis or core of a tropical cyclone. Usually determined by cloud vorticity patterns, wind and/or pressure distribution.

EPHEMERIS - Position of a body (satellite) in space as a function of time; used for gridding satellite imagery. Since ephemeris gridding is based solely on the predicted position of the satellite, it is susceptible to errors from vehicle wobble, orbital eccentricity, the oblateness of the Earth, and variation in vehicle speed.

EXPLOSIVE DEEPENING - A decrease in the minimum sea-level pressure of a tropical cyclone of 2.5 mb/hr for at least 12 hours or 5 mb/hr for at least six hours (Dunnavan 1981).

EXTRATROPICAL - A term used to indicate that a cyclone has lost its "tropical" characteristics. The term implies both poleward displacement from the tropics and the conversion of the cyclone's primary energy source from the release of latent heat of condensation to baroclinic processes. In the XT technique (Miller and Lander 1997a) a tropical cyclone is defined as having completed extratropical transition when the circulation center has moved poleward of the polar jet maximum or when water vapor imagery clearly indicates the system has become entirely cold-core. It is important to note that cyclones can become extratropical and still maintain winds of typhoon or storm force.

EYE - The central area of a tropical cyclone when it is more than half surrounded by wall cloud.

INTENSITY - The maximum sustained 1-minute mean surface wind speed, typically within one degree of the center of a tropical cyclone.

MAXIMUM SUSTAINED WIND - The highest surface wind speed averaged over a 1-minute period of time. (Peak gusts over water average 20 to 25 percent higher than sustained winds).

MEI-YU FRONT - The Term "mei-yu" is the Chinese expression for "plum rains". The mei-yu front is a persistant east-west zone of disturbed weather during spring which is quasi - stationary and stretches from the east China coast, across Taiwan, and eastward into the Pacific south of Japan.

MONSOON DEPRESSION - A tropical cyclonic vortex characterized by: 1) its large size, the outer-most closed isobar may have a diameter on the order of 600 nm (1000 km); 2) a loosely organized cluster of deep convective elements; 3) a low-level wind distribution which features a 100-nm (200-km) diameter light-wind core which may be partially surrounded by a band of gales; and, 4) a lack of a distinct cloud system center. Note: most monsoon depressions which form in the western North Pacific eventually acquire persistent central convection and accelerated core winds marking its transition into a conventional tropical cyclone.

MONSOON GYRE - A mode of the summer monsoon circulation of the western North Pacific characterized by: 1) a very large nearly circular low-level cyclonic vortex that has an outer-most closed isobar with diameter on the order of 1350 nm (2500 km); 2) a cloud band rimming the southern through eastern periphery of the vortex/surface low; 3) a relatively long (two week) life span - initially, a subsident regime exists in its core and western and northwestern quadrants with light winds and scattered low cumulus clouds; later, the area within the outer closed isobar may fill with deep convective cloud and become a monsoon depression or tropical cyclone; and, 4) the large vortex cannot be the result of the expanding wind field of a preexisting monsoon depression or tropical cyclone. Note: a series of small or very small tropical cyclones may emerge from the "head" or leading edge of the peripheral cloud band of a monsoon gyre (JTWC 1993; Lander 1994a).

RAPID DEEPENING - A decrease in the minimum sea-level pressure of a tropical cyclone of 1.75 mb/hr or 42 mb for 24-hours (Holliday and Thompson 1979).

RECURVATURE - The turning of a tropical cyclone from an initial path toward the west and poleward to east and poleward, after moving poleward of the mid-tropospheric subtropical ridge axis.

REVERSE-ORIENTED MONSOON TROUGH - The distinguishing characteristics of a reverse-oriented monsoon trough in the western North Pacific are a SW-NE (i.e., reverse) orientation of the trough axis with respect to the normal NW-SE orientation of the trough axis, and the penetration of the trough axis into subtropical areas normally the province of easterly flow.

SIGNIFICANT TROPICAL CYCLONE - A tropical cyclone becomes "significant" with the issuance of the first numbered warning by the responsible warning agency.

SIZE - The areal extent of a tropical cyclone, usually measured radially outward from the center to the outer-most closed isobar. Based on an average radius of the outer-most closed isobar, size categories in degrees of latitude follow: $< 2°$ = very small, 2° to 3° = small, 3° to 6° = medium (average), 6° to 8° = large, and 8° or greater = very large (Brand 1972 and a modification of Merrill 1982).

STRENGTH - The average wind speed of the surrounding low-level wind flow, usually measured within a one to three degree annulus of the center of a tropical cyclone (Weatherford and Gray 1985).

SUBTROPICAL CYCLONE - A low pressure system that forms over the ocean in the subtropics and has some characteristics of a tropical circulation, but not a central dense overcast. Although of upper cold low or low-level baroclinic origins, the system can transition to a tropical cyclone.

SUPER TYPHOON - A typhoon with maximum sustained 1-minute mean surface winds of 130 kt (67 m/sec) or greater.

TROPICAL CYCLONE - A non-frontal, migratory low-pressure system, usually of synoptic scale, originating over tropical or subtropical waters and having a definite organized circulation.

TROPICAL DEPRESSION - A tropical cyclone with maximum sustained 1-minute mean surface winds of 33 kt (17 m/sec) or less.

TROPICAL DISTURBANCE - A discrete system of apparently organized convection, generally 100 to 300 nm (185 to 555 km) in diameter, originating in the tropics or subtropics, having a non-frontal, migratory character and having maintained its identity for 12- to 24-hours. The system may or may not be associated with a detectable perturbation of the low-level wind or pressure field. It is the basic generic designation which, in successive stages of development, may be classified as a tropical depression, tropical storm, typhoon or super typhoon.

TROPICAL STORM - A tropical cyclone with maximum 1-minute mean sustained surface winds in the range of 34 to 63 kt (18 to 32 m/sec), inclusive.

TROPICAL UPPER-TROPOSPHERIC TROUGH (TUTT) - A dominant climatological system and a daily upper-level synoptic feature of the summer season, over the tropical North Atlantic, North Pacific and South Pacific Oceans (Sadler 1979). Cold core lows in the TUTT are referred to as cells, or TUTT cells.

TYPHOON (HURRICANE) - A tropical cyclone with maximum sustained 1-minute mean surface winds of 64 to 129 kt (33 to 66 m/sec). West of 180° E longitude they are called typhoons and east of 180° E longitude hurricanes.

WALL CLOUD - An organized band of deep cumuliform clouds that immediately surrounds the central area of a tropical cyclone. The wall cloud may entirely enclose or partially surround the center.

WESTERLY WIND BURST - A short-duration low-level westerly wind event along and near the equator in the western Pacific Ocean (and sometimes in the Indian Ocean) (Luther et al. 1983). Typically, a westerly wind burst (WWB) lasts several days and has westerly winds of at least 10 kt (5 m/sec) (Keen 1988). Most WWBs occur during the monsoon transition months of April-May, and November-December. They show some relationship to the ENSO phenomenon (Luther et al. 1983; Ramage 1986). Some WWBs are even more energetic, with wind speeds of 30 kt (15 m/sec) observed during well-developed systems. These intense WWBs are associated with a large cluster of deep-convective cloud along the equator. An intense WWB is a necessary precursor to the formation of tropical cyclone twins symmetrical with respect to the equator (Keen 1982; Lander 1990).

APPENDIX B
NAMES FOR TROPICAL CYCLONES IN THE WESTERN NORTH PACIFIC OCEAN AND SOUTH CHINA SEA

Column 1		Column 2		Column 3		Column 4	
ANN	*AN*	**ABEL**	*A-bel*	**AMBER**	*AM-ber*	**ALEX**	*AL-x*
BART	*BART*	**BETH**	*BETH*	**BING**	*BING*	**BABS**	*BABS*
CAM	*KAM*	**CARLO**	*KAR-lo*	**CASS**	*KASS*	**CHIP**	*CHIP*
DAN	*DAN*	**DALE**	*DAY-l*	**DAVID**	*DAY-vid*	**DAWN**	*DAWN*
EVE	*EEV*	**ERNIE**	*ER-nee*	**ELLA**	*EL-la*	**ELVIS**	*EL-vis*
FRANKIE	*FRANK-ee*	**FERN**	*FERN*	**FRITZ**	*FRITZ*	**FAITH**	*FAITH*
GLORIA	*GLOR-ee-uh*	**GREG**	*GREG*	**GINGER**	*JIN-jer*	**GIL**	*GIL*
HERB	*HERB*	**HANNAH**	*HAN-nah*	**HANK**	*HANGK*	**HILDA**	*HIL-dah*
IAN	*EE-an*	**ISA**	*EE-sah*	**IVAN**	*I-van*	**IRIS**	*I-ris*
JOY	*JOY*	**JIMMY**	*JIM-ee*	**JOAN**	*JONE*	**JACOB**	*JAY-kob*
KIRK	*KIRK*	**KELLY**	*KEL-lee*	**KEITH**	*KEETH*	**KATE**	*KATE*
LISA	*LEE-sah*	**LEVI**	*LEEV-eye*	**LINDA**	*LIN-dah*	**LEO**	*LEE-o*
MARTY	*MAR-tee*	**MARIE**	*mah-REE*	**MORT**	*MORT*	**MAGGIE**	*MAG-gee*
NIKI	*NI-kee*	**NESTOR**	*NES-tor*	**NICHOLE**	*nik-KOL*	**NEIL**	*NEEL*
ORSON	*OR-son*	**OPAL**	*O-pel*	**OTTO**	*OT-tow*	**OLGA**	*OL-gah*
PIPER	*PI-per*	**PETER**	*PEE-ter*	**PENNY**	*PEN-nee*	**PAUL**	*PAUL*
RICK	*RICK*	**ROSIE**	*RO-zee*	**REX**	*REX*	**RACHEL**	*RAY-chel*
SALLY	*SAL-lee*	**SCOTT**	*SKOT*	**STELLA**	*STEL-lah*	**SAM**	*SAM*
TOM	*TOM*	**TINA**	*TEE-nah*	**TODD**	*TOD*	**TANYA**	*TAHN-yah*
VIOLET	*VI-uh-let*	**VICTOR**	*vik-TOR*	**VICKI**	*VIK-kee*	**VIRGIL**	*VER-jil*
WILLIE	*WIL-lee*	**WINNIE**	*WIN-nee*	**WALDO**	*WAL-do*	**WENDY**	*WEN-dee*
YATES	*YATES*	**YULE**	YOU-l	**YANNI**	*YAN-ni*	**YORK**	*YORK*
ZANE	*ZANE*	**ZITA**	*ZEE-tah*	**ZEB**	*ZEB*	**ZIA**	*ZEE-uh*

NOTE 1: Assign names in rotation, alphabetically, starting with (ANN) for first tropical cyclone of 1996. When the last name in Column 4 (ZIA) has been used, the sequence will begin again with the first name in Column 1 (ANN).

NOTE 2: Pronunciation guide for names is italicized.

SOURCE: CINCPACINST 3140.1W

APPENDIX C
CONTRACTIONS

AB Air Base

ABW Air Base Wing

ABIO Significant Tropical Weather Advisory for the Indian Ocean

ABPW Significant Tropical Weather Advisory for the Western Pacific Ocean

ACCS Air Control Center Squadron

ACFT Aircraft

ADEOS Japanese Advanced Earth Observing Satellite

ADP Automated Data Processing

AFB Air Force Base

AFDIS Air Force Dial-In System

AFGWC Air Force Global Weather Central

AIREP Aircraft (Weather) Report

AJTWC Alternate Joint Typhoon Warning Center

AMOS Automated Meteorological Observing Station

AOR Area of Responsibility

ARC Automated Remote Collection (system)

ARGOS (International Service for Drifting Buoys)

ARQ Automated Response to Query

ATCF Automated Tropical Cyclone Forecast (system)

ATCR Annual Tropical Cyclone Report

AUTODIN Automated Digital Network

AVHRR AdvancedVery High Resolution Radiometer

AWDS Automated Weather Distribution System

AWN Automated Weather Network

BLND Blended (Hybrid Aid)

BRAC Base Realignment and Closure

CDO Central Dense Overcast

CI Current Intensity

CIMSS Cooperative Institute for Meterological Satellite Studies

CIV Civilian

CLD Cloud

CLIM Climatology

CLIP or **CLIPER** Climatology and Persistence Technique

CM Centimeter(s)

C-MAN Coastal-Marine Automated Network

CMOD Compact Meteorological and Oceanographic Drifter (buoy)

COMNAVMETOCCOM or CNMOC Commander Naval Meteorology and Oceanography Command

CPA Closest Point of Approach

CPHC Central Pacific Hurricane Center

CSC Cloud System Center

CSUM Colorado State University Model

CW Continuous Wave

DAVE Dynamic Average

DD Digital Dvorak

DDN Defense Data Network

DEG Degree(s)

DFS Digital Facsimile System

DISN Defense Information Systems Network

DMS Defense Messaging System

DMSP Defense Meteorological Satellite Program

DOD Department of Defense

DSN Defense Switched Network

DTG Date Time Group

EGRR Bracknell Model

ENSO El Niño-Southern Oscillation

ERS European Remote Sensing Satellite

FBAM FNMOC Beta and Advection Model

FI Forecast Intensity (Dvorak)

FLENUMMETOCCEN or FNMOC Fleet Numerical Meteorology and Oceanography Center

FT Foot/Feet

FTP File Transfer Protocol

GCA Great Circle Arc

GFDN Geophysical Fluid Dynamics - Navy

GMS Japan Geostationary Meteorological Satellite

GMT Greenwich Mean Time

GOES Geostationary Operational Environmental Satellite

GSRS Geostationary Satellite Receiving System

GTS Global Telecommun-ications System

HIRS High Resolution Infrared Sounder

hPa Hectopascal

HPAC Mean of XTRP and CLIM Techniques (Half Persistence and Climatology)

HF High Frequency

HR Hour(s)

HRPT High Resolution Picture Transmission

ICAO International Civil Aviation Organization

INIT Initial

INST Instruction

IP Internet Protocol

IR Infrared

JGSM Japanese Global Spectral model

JTWC Joint Typhoon Warning Center

JTWC92 or JT92 Statistical-Dynamical Objective Technique

JTYM Japanese Typhoon Model

KM Kilometer(s)

KT Knot(s)

LAN Local Area Network

LAT Latitude

LLCC Low-Level Circulation Center

LONG Longitude

LUT Local User Terminal

LVL Level

M Meter(s)

MAX Maximum

MB Millibar(s)

MBAM Medium Beta and Advection Model

MCAS Marine Corps Air Station

MCS Mesoscale Convective System

MET Meteorological

METEOSAT European Meteorological Satellite

MIDDAS Meteorological Imagery, Data Display, and Analysis System

MIN Minimum

MINI-MET Mini-Meteorological (buoy)

MISTIC Mission Sensor Tactical Imaging Computer

MM Millimeter(s)

MOVG Moving

MSLP Minimum Sea-level Pressure

MSU Microwave Sounding Unit

NARDAC Naval Regional Data Automation Center

NAS Naval Air Station

NASA National Aeronautics and Space Administration

NAVPACMETOCCEN or NPMOC Naval Pacific Meteorology and Oceanography Center (Hawaii)

NAVPACMETOCCEN WEST or NPMOCW Naval Pacific Meteorology and Oceanography Center West (Guam)

NCEP National Centers for Environmental Prediction

NEDN Naval Environmental Data Network

NESDIS	National Environmental Satellite, Data, and Information Service
NESN	Naval Environmental Satellite Network
NEXRAD	Next Generation (Doppler Weather) Radar (WSR-88D)
NGDC	National Geophysical Data Center
NHC	National Hurricane Center
NIPRNET	Non-secure Internet Protocol Router Network
NM	Nautical Mile(s)
NMC	National Meteorological Center (now NCEP)
NOAA	National Oceanic and Atmospheric Administration
NODDES	Naval Oceanographic Data Distribution and Expansion System
NODDS	Naval Oceanography Data Distribution System
NOGAPS or NGPS	Navy Operational Global Atmospheric Prediction System
NORAPS or NRPS	Navy Operational Regional Atmospheric Prediction System
NPS	Naval Postgraduate School
NR	Number
NRL	Naval Research Laboratory
NRL-MRY	Naval Research Laboratory at Monterey, CA
NSCAT	NASA Scatterometer
NSDS-G	Naval Satellite Display System - Geostationary
NTWP	Naval Telecommunications Area Master Station, Western Pacific
SIPRNET	Secret Internet Protocol Router Network
NWP	Northwest Pacific
NWS	National Weather Service
OBS	Observations
OLS	Operational Linescan System
ONR	Office of Naval Research
OSS	Operations Support Squadron
OSB	Ocean Sciences Branch
OTCM	One-Way (Interactive) Tropical Cyclone Model
PACAF	Pacific Air Force
PACMEDS	Pacific Meteorological Data System
PACOM	Pacific Command
PAGASA	Philippine Atmospheric, Geophysical, and Astronomical Services Administation
PC	Personal Computer
PCN	Position Code Number
PDN	Public Data Network
PIREP	Pilot Weather Report(s)
QBO	Quasi-Biennial Oscillation
RADOB	Radar Observation
RECON	Reconnaissance
RECR	Recurve (Forecast Aid)
RMSE	Root mean square error
ROCI	Radius of outer-most closed isobar
SAT	Satellite
SCS	South China Sea
SDHS	Satellite Data Handling System
SEC	Second(s)
SFC	Surface
SGDB	Satellite Global Data Base
SIPRNET	Secret Internet Protocol Router Network
SLP	Sea-Level Pressure
SPAWARSYSCOM	Space and Naval Warfare Systems Command
SPIDR	Space Physics Interactive Data Resource
SSM/I	Special Sensor Microwave/Imager
SST	Sea Surface Temperature
SSU	Stratosphere Sounding Unit
ST	Subtropical
STNRY	Stationary

STR Subtropical Ridge

STRT Straight (Forecast Aid)

STY Super Typhoon

SWDIS Satellite Weather Data Imaging System

TAPT Typhoon Acceleration Prediction Technique

TC Tropical Cyclone

TCFA Tropical Cyclone Formation Alert

TD Tropical Depression

TDA Typhoon Duty Assistant

TDO Typhoon Duty Officer

TELEFAX Telephone Facsimile

TESS Tactical Environmental Support System

TIFF Tagged Image File Format

TIROS-N Television Infrared Observational Satellite-Next Generation

TOGA Tropical Ocean Global Atmosphere

TOVS TIROS Operational Vertical Sounder

TS Tropical Storm

TUTT Tropical Upper-Tropospheric Trough

TY Typhoon

TYAN Typhoon Analog (Forecast Aid)

ULCC Upper-Level Circulation Center

US United States

USAF United States Air Force

USCINCPAC Commander-in-Chief Pacific (AF - Air Force, FLT - Fleet)

USN United States Navy

VIS Visual

WAN Wide Area Network

WESTPAC or WNP Western (North) Pacific

WGTD Weighted (Hybrid Aid)

WMO World Meteorological Organization

WRN or WRNG Warning(s)

WSD Wind Speed and Direction

WSR-88D Weather Surveillance Radar - 1988 Doppler

WVTW Water Vapor Tracked Winds

WWB Westerly Wind Burst

WWW World Wide Web

XT Extratropical

XTRP Extrapolation

Z Zulu time (Greenwich Mean Time/Universal Coordinated Time)

APPENDIX D

PAST ANNUAL TROPICAL CYCLONE REPORTS

Copies of the past Annual Tropical Cyclone Reports for DOD agencies or contractors can be obtained through:

Defense Technical Information Center (DTIC)
DTIC-BR (Reference & Retrieval Division)
8725 John J. Kingman Road
Suite 0940
Ft. Belvoir, VA 22060-6218

Phone: comm (703) 767-8274
DSN 427-9070
Fax: comm (703) 767-9070
DSN 427-9070

Copies for non-DOD agencies or users can be obtained from:

National Technical Information Service
5285 Port Royal Road
Springfield, VA 22161

Phone: (703) 487-4650
Fax: (703) 321-8547

Refer to the following numbers when ordering:

Year	Acquisition Number	Year	Acquisition Number	Year	Acquisition Number
1959	AD 786147	1972	AD 768334	1984	AD A153395
1960	AD 786148	1973	AD 777093	1985	AD A168284
1961	AD 786149	1974	AD 010271	1986	AD A184082
1962	AD 786128	1975	AD A023601	1987	AD A191883
1963	AD 786208	1976	AD A038484	1988	AD A207206
1964	AD 786209	1977	AD A055512	1989	AD A232469
1965	AD 786210	1978	AD A070904	1990	AD A239910
1966	AD 785891	1979	AD A082071	1991	AD A251952
1967	AD 785344	1980	AD A094668	1992	AD A274464
1968	AD 785251	1981	AD A112002	1993	AD A285097
1969	AD 785178	1982	AD A124860	1994	AD A301618
1970	AD 785252	1983	AD A137836	1995	AD A321611
1971	AD 768333				

APPENDIX E
DISTRIBUTION LIST

1 COPY

ACCU-WEATHER, INC.
AMERICAN EMBASSY, NEW DEHLI
ANALYSIS & PROCESSING CENTER, INDONESIA
ARNOLD ASSOCIATES
ASIAN DISASTER PREPAREDNESS CENTER, BANGKOK, THAILAND
ATMOSPHERIC DIV LIBRARY, NEW ZEALAND
BARRETT CONSULTING GROUP
BRUNEI SHELL PETROLEUM CO
CATHOLIC UNIVERSITY OF AMERICA
CAF WEATHER CENTRAL, TAIWAN
CENTRAL MET OBSERVATORY, BEIJING
CENTRAL METEOROLOGICAL OFFICE, SEOUL
CHULALONGKORN UNIVERSITY, BANGKOK
CHUNG CHENG INSTITUTE, TAIWAN
CITY POLYTECHNIC OF HONG KONG
CIUDAD UNIVERSITARIA, MEXICO
CIVIL DEFENSE, CHUUK
CIVIL DEFENSE, MAJURO
CIVIL DEFENSE, PALAU
CIVIL DEFENSE, POHNPEI
CIVIL DEFENSE, SAIPAN
CIVIL DEFENSE, YAP
CINCPACFLT
CNN, ATLANTA, GA
CNO, WASHINGTON, D.C.
COMNAVMETOCCOM
COLORADO STATE UNIVERSITY LIBRARY
COMMONWEALTH NORTHERN MARIANA ISLANDS
COMNAVMARIANAS
COMNAVSURFPAC, SAN DIEGO
COMPHIBGRU ONE
COMSCWESTPAC GU
COMSEVENTHFLT
COMSPAWARSYSCOM
COMSUBGRU SEVEN
COMTHIRDFLT
COMUSNAVCENT
CONGRESSIONAL INFORMATION SERVICE, MD
DCA GUAM
DET 2, 5WS CAMP HUMPHREYS, KOREA
DET 3, 5WS CAMP CASEY, KOREA
DISASTER CONTROL OFFICE, SAIPAN
ECONOMIC COUNCIL SAIPAN
EDMUNDS COLLEGE SOCIAL SCIENCE DEPT
ENVIRONMENTAL QUALITY PROTECTION BOARD, PALAU
FEDERAL EMERGENCY MANAGEMENT AGENCY, GUAM
FIJI METEOROLOGICAL SERVICE
FLENUMMETOC DET, ASHEVILLE
GEOLOGICAL FLUID DYNAMICS LAB, PRINCETON, NJ
GEOLOGICAL SURVEY, GUAM
GEOPHYSICS LAB
GIFU METEOROLOGICAL OFFICE, JAPAN
GODDARD SPACE FLIGHT CENTER
GUAM COMMUNITY COLLEGE
GUAM POWER AUTHORITY
GUAM PUBLIC LIBRARY
HORIZON MARINE, INC
HQ AIR COMBAT COMMAND/OSW
HQ AMC TACC/WXC
HQ AWS
HQ US STRATCOM/J3615
HQ USAF/XOWO
INDIA METEOROLOGICAL DEPT.
INDIAN INSTITUTE OF TROPICAL MET
INSTITUO DE GEOFISICA, MEXICO
INTERNATIONAL CENTER FOR DISASTER MITIGATION, TOKYO
JAPAN AIR LINES
JCS ENV SERVICES DIV, PENTAGON
JET PROPULSION LAB, PASADENA
KOREAN METEOROLOGICAL ADMIN FORECAST BUREAU
LEND FOUNDATION
LISD CAMP SPRINGS CENTER, MD
MARATHON OIL CO, TX
MAURITIUS METEOROLOGICAL SERVICE
MASS INST OF TECH
MCAS FUTENMA
MCAS IWAKUNI
MCAS KANEOHE BAY, HI
MERCANTILE AND GENERAL REINSURANCE, AUSTRALIA
METEOROLOGICAL DEPARTMENT, PAKISTAN
METEOROLOGICAL OFFICE, BRACKNELL
METEOROLOGICAL SERVICE, MADAGASCAR
METEOROLOGICAL SERVICE, MAURITIUS
METEOROLOGICAL SERVICE, NEW ZEALAND
METEOROLOGICAL SERVICE, REUNION
MIL ASST ENV SCI (R & AT / E &LS)
MOBIL OIL GUAM, INC
NASA
NATIONAL CLIMATIC DATA CENTER LIBRARY, ASHEVILLE, NC
NATIONAL METEOROLOGICAL CENTER
NATIONAL METEOROLOGICAL LIBRARY, BRACKNELL, UK

NATIONAL TAIWAN UNIVERSITY
NATIONAL TECHNICAL INFORMATION SERVICE
NATIONAL WEATHER SERVICE, CHUUK
NATIONAL WEATHER SERVICE, MAJURO
NATIONAL WEATHER SERVICE, PALAU
NATIONAL WEATHER SERVICE, PAPUA NEW GUINEA
NATIONAL WEATHER SERVICE, POHNPEI
NATIONAL WEATHER SERVICE, SAIPAN
NATIONAL WEATHER SERVICE, YAP
NAVAL CIVIL ENG LAB PORT HUENENE, CA
NAVAL POSTGRADUATE SCHOOL LIBRARY
NAVAL RESEARCH LAB
NAVCENTMETOCFAC, BAHRAIN
NAVEURMETOCCEN, ROTA
NAVHISTCEN
NAVICECEN, SUITLAND
NAVLANTMETOCCEN, NORFOLK
NAVLANTMETOCFAC, JACKSONVILLE
NAVOCEANO
NAVPACMETOC DET, ATSUGI
NAVPACMETOC DET, KADENA
NAVPACMETOC DET, SASEBO
NAVPACMETOCFAC, SAN DIEGO
NAVPACMETOCFAC, YOKOSUKA
NAVTRAMETOC DET, NEWPORT
NEW ZEALAND INSURANCE
NOAA/ACQUISITION SECTION, ROCKVILLE, MD
NOAA/AOML, HRD, MIAMI, FL
NOAA/HYDROMETEOROLOGY BR, SILVER SPRINGS, MD
NOAA/NESDIS, HONOLULU, HI
NOAA/PMEL, SEATTLE, WA
NOAA ENVIRONMENTAL RESEARCH LAB
NOAA LIBRARY, SEATTLE, WA
NOBEL DENTON
NRL ATMOSPHERIC DIRECTORATE
OCEANROUTES, INC, JOLIMENT, WEST AUSTRALIA
OCEANROUTES, INC, SINGAPORE
OCEANROUTES, INC, SUNNYVALE, CA
OCEANWEATHER, INC
OFFICE OF FEDERAL COORDINATOR MET
OFFICE OF NAVAL RESEARCH
OFFICE OF THE NAVAL DEPUTY, NOAA
PACIFIC STARS & STRIPES
PACNAVFACENGCOM
PAGASA FORECAST SECTION
PAGASA LIBRARY
PENNSYLVANIA STATE UNIVERSITY
QUEENS COLLEGE, DEPT OF GEOLOGY
REUNION METEOROLOGICAL SERVICE
RUCH WEATHER SERVICE, INC
SAINT LOUIS UNIVERSITY
SAT APPL LAB, NOAA/NESDIS, WASHINGTON, DC
SHANGHAI TYPHOON INSTITUTE
SOUTHSIDE WEATHER SERVICE AUSTRALIA
SRI LANKA METEOROLOGICAL SOCIETY
TAO PROJECT OFFICE
TEXAS A & M UNIVERSITY
UNIV OF COLORADO, ATMOS SCIENCE
UNIVERSITY OF CHICAGO
UNIVERSITY OF GUAM, BIOLOGY DEPT
UNIVERSITY OF HAWAII LIBRARY
UNIVERSITY OF WASHINGTON
USCCC SCOTT AFB, IL
USCINCPAC
USCINCPAC REP GUAM
USNA (OCEANOGRAPHY DEPT/LIBRARY)
USS ABRAHAM LINCOLN (CVN 72)
USS AMERICA (CV 66)
USS BELLEAU WOOD (LHA-3)
USS BOXER (LHD-4)
USS BLUE RIDGE (LCC 19)
USS CARL VINSON (CVN 70)
USS CONSTELLATION (CV 64)
USS EISENHOWER (CVN 69)
USS ESSEX (LHD-2)
USS GEORGE WASHINGTON (CVN 73)
USS GUAM (LPH-9)
USS INDEPENDENCE (CV 62)
USS JOHN C. STENNIS (CVN 74)
USS J. F. KENNEDY (CV 67)
USS KEARSARGE (LHD-3)
USS KITTY HAWK (CV 63)
USS NASAU (LHA-4)
USS NEW ORLEANS (LPH 11)
USS NIMITZ (CVN 68)
USS PELELIU (LHA 5)
USS SAIPAN (LHA-2)
USS TARAWA (LHA 1)
USS T. ROOSEVELT (CVN 71)
USS WASP (LHD 1)
VANUATU METEOROLOGICAL SERVICE
WORLD DATA CENTER B1, MOSCOW
AFGWC/WFM OFFUTT AFB, NE
607WS WS/CC YONGSAN AIN KOREA
8 OSS/OSW KUNSAN AB, KOREA
15 OSS/OSW
18 OSS/OSW KADENA AB, JAPAN
35 OSS/OSW
36 ABW ANDERSEN AFB, GUAM
36 OSS/OSW ANDERSEN AFB, GUAM
53 WRS KEESLER AFB, MS
334 TTS/TTMV KEESLER AFB, MS
374 OSS/DOW YOKOTA AB, JAPAN
375 OG/WXF SCOTT AFB, IL
432 OSS/OSW MISAWA AB, JAPAN

603 ACCENS/WE OSAN AB, KOREA
36 OSS/OSW ANDERSEN AFB, GU
815 WS (AFRES), KEESLER AFB, MS

2 COPIES
AEROMET INC., KWAJALEIN
AFGWC/WFMP
AWS TECH LIBRARY
BUREAU OF METEOROLOGY, BRISBANE
BUREAU OF METEOROLOGY, DARWIN
BUREAU OF METEOROLOGY LIBRARIAN, MELBOURNE
BUREAU OF METEOROLOGY, PERTH
BUREAU OF PLANNING, GUAM
CIVIL DEFENSE, GUAM
DEFENSE TECHNICAL INFORMATION CENTER
DEPARTMENT OF COMMERCE
ECMWF, BERKSHIRE, UK
ESCAP LIBRARY, BANGKOK
FLENUMMETOCCEN MONTEREY, CA
FLORIDA STATE UNIVERSITY
HQ AWS GROUP, ATC & WX WING JASDF, TOKYO
INSTITUTE OF PHYSICS, TAIWAN
MET RESEARCH INST LIBRARY, TOKYO
MICRONESIAN RESEARCH CENTER UOG, GUAM
NATIONAL CLIMATIC DATA CENTER
NATIONAL DATA BUOY CENTER
NATIONAL HURRICANE CENTER, MIAMI
NATIONAL WEATHER SERVICE, HONOLULU
NAVPACMETOCCEN
NAVPACMETOC DET, DIEGO GARCIA
NAVPACMETOC DET, MISAWA
NOAA CENTRAL LIBRARY GUAM
NORA 1570 DALLAS, TX
NWSO, GUAM
OKINAWA METEOROLOGY OBSERVATORY
SAT APPL LAB, NOAA/NESDIS, CAMP SPRINGS, MD
TYPHOON COMMITTEE SECRETARIAT, MANILA
UNIVERSITY OF PHILIPPINES
US ARMY, FORT SHAFTER
WORLD DATA CENTER A, NOAA
73 WEATHER GROUP, ROK AF

3 COPIES
BUREAU OF METEOROLOGY, DIRECTOR, MELBOURNE, AUSTRALIA
CENTRAL WEATHER BUREAU, TAIWAN
INDIA METEOROLOGICAL DEPT
INOSHAC, DDGM (WF), INDIA
JAPAN METEOROLOGICAL AGENCY
KOREAN METEOROLOGY ADMINISTRATION PLANNING BUREAU
NATIONAL WEATHER ASSOCIATION
NAVPGSCOL DEPT OF METEOROLOGY
NOAA CORAL GABLES LIBRARY
NRL, MONTEREY
PACAF/DOW
UNIVERSITY OF HAWAII, METEOROLOGY DEPT
WEATHER CENTRAL, CAF

REPORT DOCUMENTATION PAGE

Form Approved
OMB No. 0704-0188

1A. REPORT SECURITY CLASSIFICATION
UNCLASSIFIED

1b. RESTRICTIVE MARKINGS

2a. SECURITY CLASSIFICATION AUTHORITY

2a. SECURITY CLASSIFICATION AUTHORITY

3. DISTRIBUTION/AVAILABILITY OF REPORT
AS IT APPEARS IN THE REPORT/
DISTRIBUTION UNLIMITED

4. PERFORMING ORGANIZATION REPORT NUMBER(S)

5. MONITORING ORGANIZATION REPORT NUMBER(S)

6a. NAME OF PERFORMING ORGANIZATION
NAVPACMETOCCENWEST/JTWC

6b. OFFICE SYMBOL
(If applicable)

7a. NAME OF MONITORING ORGANIZATION
NAVPACMETOCCENWEST/JTWC

6c. ADDRESS (City, State and Zip Code)
PSC 455, BOX 12
FPO AP 96540-0051

7b. ADDRESS (City, State and Zip Code)
PSC 455, BOX 12
FPO AP 96540-0051

8a. NAME OF FUNDING/SPONSORING ORGANIZATION
NAVPACMETOCCENWEST/JTWC

8b. OFFICE SYMBOL
(If applicable)

9. PROCUREMENT INSTRUMENT IDENIFICATION NUMBER

8c. ADDRESS (City, State and Zip Code)
PSC 455, BOX 12
FPO AP 96540-0051

10. SOURCE OF FUNDING NUMBERS

PROGRAM ELEMENT NO.	PROJECT NO.	TASK NO.	WORK UNIT ACCESSION NO.

11. TITLE (Include Security Classification)

1996 ANNUAL TROPICAL CYCLONE REPORT

12. PERSONAL AUTHOR(S)

13a. TYPE OF REPORT	13b. TIME COVERED	14. DATE OF REPORT(Year, Month, Day)	15. PAGE COUNT
ANNUAL	FROM JAN 96 TO DEC 96	1996	331 plus i - vi

16. SUPPLEMENTARY NOTATION

17. COSATI CODES

FIELD	GROUP	SUB-GROUP
04	02	

18. SUBJECT TERMS (Continued on reverse if necessary and identify by block number)
TROPICAL CYCLONES
TROPICAL DEPRESSIONS
TROPICAL CYCLONE RESEARCH
TROPICAL STORMS
TYPHOONS/SUPER TYPHOONS
METEOROLOGICAL SATELLITES

19. ABSTRACT (Continued on reverse if necessary and identify by block number)

ANNUAL PUBLICATION SUMMARIZING TROPICAL CYCLONE ACTIVITY IN THE WESTERN NORTH PACIFIC, BAY OF BENGAL, ARABIAN SEA, WESTERN SOUTH PACIFIC AND SOUTH INDIAN OCEANS. A BEST TRACK IS PROVIDED FOR EACH SIGNIFICANT TROPICAL CYCLONE. A BRIEF NARRATIVE IS GIVEN FOR ALL TROPICAL CYCLONES IN THE WESTERN NORTH PACIFIC AND NORTH INDIAN OCEANS. ALL FIX DATA USED TO CONSTRUCT THE BEST TRACKS ARE PROVIDED UPON REQUEST ON DISKETTES. FORECAST VERIFICATION DATA AND STATISTICS FOR THE JOINT TYPHOON WARNING CENTER (JTWC) ARE SUBMITTED.

20. DISTRIBUTION/AVAILABILITY OF ABSTRACT
[x] UNCLASSIFIED/UNLIMITED [x] SAME AS RPT. [ ] DTIC USERS

21. ABSTRACT SECURITY CLASSIFICATION
UNCLASSIFIED

22a. NAME OF RESPONSIBLE INIVIDUAL	22b. TELEPHONE (Include Area Code)	22c. OFFICE SYMBOL
FRANK H. WELLS	(671) 349-5286	JTWC

DD FORM 1473, JUN 86

Previous editions are obsolete.

SECURITY CLASSIFICATION OF THIS PAGE
UNCLASSIFIED

BLOCK 18 (CONTINUED)

RADAR
AUTOMATED METEOROLOGICAL OBSERVING STATIONS
SYNOPTIC DATA
TROPICAL CYCLONE INTENSITY
TROPICAL CYCLONE BEST TRACK
TROPICAL CYCLONE FORECASTING
TROPICAL CYCLONE RECONNAISSANCE
TROPICAL CYCLONE STEERING MODELS
OBJECTIVE FORECASTING TECHNIQUES
TROPICAL CYCLONE FIX DATA
MICROWAVE IMAGERY
DRIFTING BUOYS

BACK COVER: From its location on Guam, JTWC monitors an area of responsibility that stretches from 180° east longitude westward across the Western Pacific and Indian Oceans to the eastern coast of Africa.

1996 Tropical Cyclone Tracks